BUILDING A RATIONAL MODEL FOR THE IDENTIFICATION OF ALLOSTERIC SITES

Camille Roxane Chevalier Indey

2016

Supervised by Professor Nicholas C. O. Tomkinson

Department of Pure and Applied Chemistry

A thesis submitted to the University of Strathclyde in part fulfilment of regulations for the degree of Doctor of Philosophy in Chemistry.

Declaration of copyright

This thesis is the result of the author's original research. It has been composed by the author and has not been previously submitted for examination which has led to the award of a degree.

Signed: Date:

Acknowledgements

First of all, I would like to acknowledge Professor Nick Tomkinson for welcoming me as his student and trusting me with this challenging but great project. He was always here to give advice and steer me in the right direction. He also let me take ownership of the project and trusted me in the decisions I took. He always encouraged me and helped me see the bright side of things. I would like to thank him for making the workspace always fun and full of laughter brought by his (sometimes weird) jokes. He encouraged us to be a united group and made us discover Scotland by bringing us on group walks. I can't thank him enough.

Of course, I would also like to acknowledge everyone in TG627 past and present: Jim, Heulyn, Mike, Julian, Tom, Kevin, Lola, Andrei, Carla, Stuart, Jayde and Steven. A special thanks to Jim, Heulyn and Kevin who had the great opportunity to proof read my thesis and all my other reports during my PhD. Everyone in the lab have made it a fun environment to work in and have been helpful and present when needed. I would like to thank Lola, my PhD sister, with whom we have shared a common interest in medicinal chemistry. We have worked and suffered together and were able to be there for each other in times of crisis and doubt. I also want to especially thank Jim and Heulyn with whom we have become very close friends and have shared great moments away.

I would like to say thank you to various members of SIPBS who have been of great help to me. Professor Simon Mackay was of great help by bringing all his knowledge of medicinal chemistry in this project. He has invested time and money for this project to move forward and I am very grateful. Giacomo was a very helpful postdoc that helped me send compounds for testing and has guided me in my research throughout the last year of my project. I also want to thank Dr Johnston, Murray Robertson and Tony Vassileiou who have been of enormous help regarding pharmacophore generation, virtual screening and teaching me how to use Pipeline pilot as well as GOLD. They have all helped bring in their knowledge in this project.

A special thanks to the staff the staff in the department that were always helpful throughout my project: Pat for her advice and help regarding the LC/MS and Craig for his NMR expertise.

I also want to acknowledge Dr Meijer for his generosity and enthusiasm. He provided us with a sample of L41 and has kindly agreed to carry out some biological testing on our analogues in a parasite cellular assay.

Last but not least, I would like to thank the important people in my life. First of all my family for their endless support and who have always been present in my life. They have helped me become who I am today and I will always be grateful to them. Maman, Papa, Nico et Jojo je vous aime. I also want to thank my in-laws, Arlette and Bernard who have been so helpful and encouraging throughout this whole process. I want to acknowledge my friends back in France: Julien, Paul, Victor, Claire, Patrick who have brought good laughs, great support and have encouraged me from far away. Most importantly, I want to say a big thank you to my husband Benoit who has always believed in me. He has encouraged me during hard times and has been my rock throughout this whole experience. Merci beaucoup mon amour de croire en moi, je t'aime !

Table of Contents

Abstract

Allostery is the regulation of protein function, structure and/or flexibility that is induced by the binding of a ligand at a site distinct from the orthosteric site.[1, 2] Interaction of a small molecule with these sites can bring greater selectivity as they are not conserved within a family and therefore could lead to new opportunities in drug discovery. Unfortunately, no definitive technique has yet been identified to distinguish these allosteric sites. Al-Shar'i developed a new technique using a combination of fluctuation analysis, cross correlation, simple intrasequence difference (SID) and energy analysis.[3] A potential site has been determined for the protein kinase DYRK2 using this technique. The potential allosteric pocket was studied through a virtual screen which gave a hit that was successfully prepared and showed good selectivity for DYRK2 over DYRK1A by Differential Scanning Fluorimetry (DSF). This oxyamidine hit was further investigated through a structure activity relationship (SAR) which enabled the synthesis of three compounds that showed a higher stabilization than the initial hit (T_m > 1.2 °C). A second library was synthesized based on the same core, but with an amide functionality instead of an oxyamidine. From this new library, a SAR study was also carried out. This led to the synthesis of five analogues that have shown great binding activity (IC_{50} < 240nM) and selectivity for DYRK2.

Abbreviations

$[E_o]$:	Initial concentration of enzyme
[I]:	Concentration of inhibitor
µW:	Microwave irradiation
ADP:	Adenosine diphosphate
Ala:	Alanine
AMBER:	Assisted model building with energy refinement
Arg:	Arginine
Asn:	Asparagine
Asp:	Aspartic acid
ATP:	Adenosine triphosphate
ATR:	Attenuated total reflectance
Bu:	Butyl
c	Cyclic
CAMK:	Calmodulin/Calcium regulated kinases
Cat:	Catalytic
Cbz:	Carboxybenzyl
CDI	Carbonyldiimidazole
CDK	Cyclin-dependent kinase
CK	Creatine kinase
CRO:	Contract research organization
Cy:	Cyclohexyl
Decomp:	Decomposition
DIAD:	Diisopropyl azodicarboxylate
DMF:	Dimethylformamide
DMSO:	Dimethyl sulfoxide
DNA:	Deoxyribonucleic acid
DSF:	Differential scanning fluorimetry
DYRK:	Dual specificity tyrosine-regulated kinase
E:	Enzyme
Equiv.:	Equivalent

Et:	Ethyl
Et_3N:	Triethylamine
EWG:	Electron-withdrawing group
FDA:	US food and drug administration
GC/MS:	Gas chromatography mass spectrometry
Gln:	Glutamine
Glu:	Glutamic acid
Gly:	Glycine
HATU:	*O*-(7-Azabenzotriazol-1-yl)-*N*,*N*,*N′*,*N′*-tetramethyluronium hexafluorophosphate
HBA:	H bond acceptor
HBD:	H bond donor
HF:	Hit finder
HTS:	High throughput screening
Hünig's base:	*N*,*N*-Diisopropylethylamine
Hz:	Hertz
^{i}Bu:	isobutyl
IC_{50}:	Half maximal inhibitory concentration
Ile:	Isoleucine
^{i}Pr:	Isopropyl
K_m:	Michaelis-Menten constant
KNF:	Koshland, Némethy and Filmer
LC/MS:	Liquid chromatography mass spectrometer
Leu:	Leucine
LT:	Life Technologies
Lys:	Lysine
m-CPBA:	*Meta*-chloroperoxybenzoic acid
MD:	Molecular dynamics
Met:	Methionine
MW:	Molecular weight
MWC:	Monod, Wyman and Changeux
NAM:	Negative Allosteric Modulator

NBS	*N*-bromosuccinimide
NMR:	Nuclear magnetic resonance
NOESY:	Nuclear Overhauser effect spectroscopy
PAM:	Positive Allosteric Modulator
PDB:	Protein database
PE:	Petroleum ether
Ph:	Phenyl
Phe:	Phenylalanine
pKa:	Acid dissociation constant
PKA:	Protein kinase A
ppm:	Parts per million
Pr:	Propyl
Pro:	Proline
PSA:	Polar surface area
p-TSA:	*Para* toluene sulfonic acid
PyBOP:	Benzotriazol-1-yl-oxytripyrrolidinophosphonium hexafluorophosphate
R:	Relaxed
RF:	Random forest
RT:	Reverse-transcriptase
Rt:	Room temperature
S:	Substrate
SAR:	Structure activity relationship
SEDG:	Strong electron-withdrawing group
Ser:	Serine
SGC:	Structura genomic consortium
SID:	Simple intrasequence difference
SIPBS:	Strathclyde institute of pharmacy and biomedical sciences
SMILES:	Simplified molecular-input line-entry system
Sta:	Staurosporine
STE:	homologs of yeast
T:	Tensed

THF:	Tetrahydrofuran
Thr:	Threonine
Thr:	Threonine
TK:	Tyrosine kinase
TKL:	Tyrosine kinase like
TLC:	Thin layer chromatography
T_m:	Melting temperature
Tyr:	Tyrosine
Val:	Valine
V_{max}:	Maximum velocity
v_o:	Initial velocity
VS:	Virtual screen
WEDG:	Weak electron-withdrawing group
ΔG_u:	Gibbs free energy of unfolding

Chapter 1: Introduction

I. Proteins

Proteins are essential macromolecules of life, as they perform various pivotal functions within living organisms. They act as catalysts, transporters and store other molecules, and control growth and differentiation among numerous other functions.[4]

1. Protein structure

The function of the protein is dependent on its structure and each protein has a unique fold determined by its amino acid sequence. A protein is represented by four degrees of structural order: primary, secondary, tertiary and quaternary which are represented in **Figure 1**.

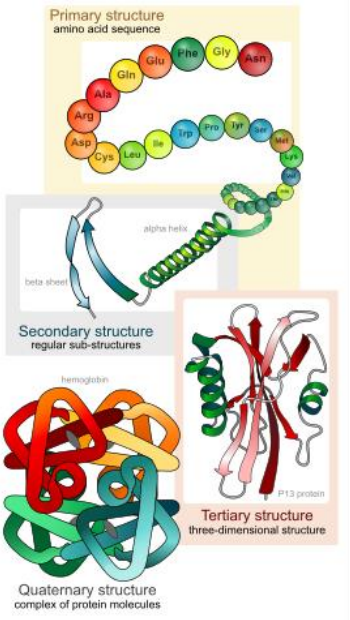

<u>Figure 1:</u> Four different levels of structural order representing a protein: primary, secondary, tertiary and quaternary structures.[5]

The primary structure of a protein is its amino acid sequence from the amino end (*N*-terminus) to the carboxyl end (*C*-terminus). The secondary structure is formed by hydrogen bonding between amino and carbonyl functionalities at the backbone level.

It can bring about two different major types of folding depending on the hydrogen bond network between the amino acids: the α-helix and the β-sheet, **Figure 2**.

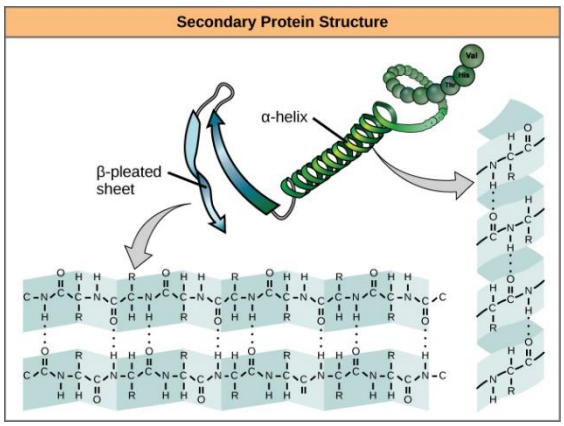

<u>Figure 2:</u> α-helix and β-sheet H-bonding network.[6]

An α-helix is a spiral conformation that is enabled by hydrogen bonding at the backbone level between the NH of one amino acid and the carbonyl of another amino acid that is four residues further along the primary sequence (*i* and *i*+4). β-sheets, on the contrary, are formed by chains of amino acids in a fully extended conformation. These chains are held together by a hydrogen network at the backbone level between the NH of an amino acid on one β-sheet with the carbonyl of another amino acid of a second β-sheet, and can be in a parallel or antiparallel orientation.

The tertiary structure is the 3-D shape of the folded polypeptide chain where secondary motifs and distant amino acids in the primary chain are brought together *via* hydrogen bonds, disulfide bonds, ionic and hydrophobic interactions.

The quaternary structure is the arrangement of multiple protein tertiary conformations when they come together.[4]

2. **Protein kinases**

There are 518 protein kinase genes that have been identified to date, which represents 1.7% of all human genes.[7] Most of these proteins belong to a superfamily: the eukaryotic protein kinase and are represented by a phylogenetic tree, as shown in **Figure 3**.

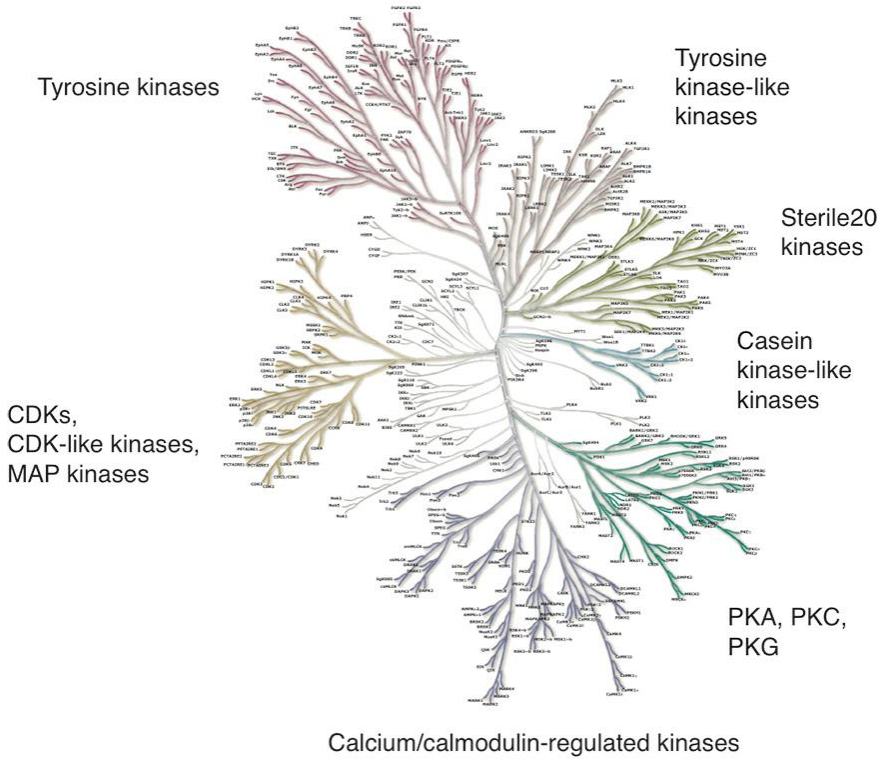

<u>Figure 3:</u> Protein kinase family tree.[8]

These kinases are grouped into seven families (TK, CDK, CAMK, PKA, CK1, STE, and TKL) and each family contains subfamilies. These have been characterised according to their sequence homology, structural similarities and their biological function.[7]

Protein kinases enable the transfer of the terminal phosphate group of ATP **1** to a specific hydroxyl group of their protein substrate for serine/threonine (Ser)/(Thr) and tyrosine (Tyr) kinases. **Figure 4** is a schematic representation of the functionality of protein kinases. The ATP **1** binds into the orthosteric pocket with the adenine ring buried in the hydrophobic pocket and the phosphate orientated outwards towards the solution making it more accessible, **Figure 9**. The protein substrate then binds to the active site where the phosphate is then transferred to the protein substrate. The substrate is then released from the kinase and ADP release occurs afterwards. These processes can markedly change the conformation and functionality of the substrate protein.

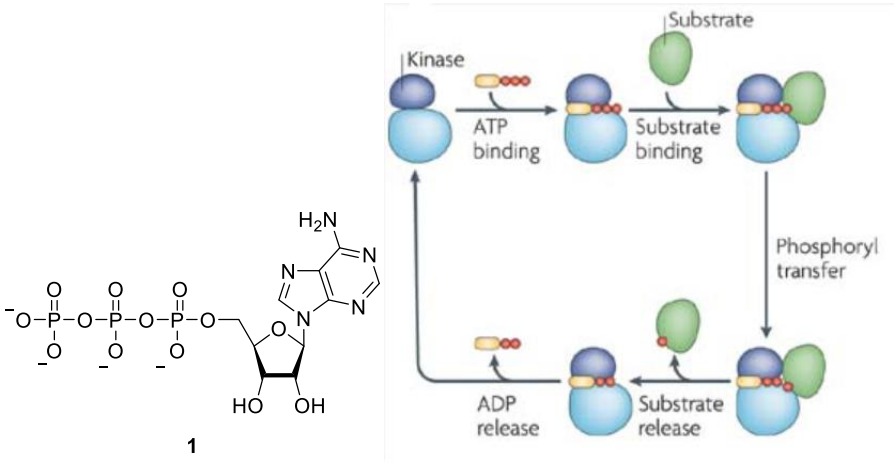

Figure 4: ATP and representation of the catalytic role of kinases.[9]

This catalytic transfer is performed through either of the following amino acids of the protein substrate: serine (Ser), threonine (Thr) or tyrosine (Tyr) **Figure 5**.[10] Each of these amino acids contains a hydroxyl group on their side chain which facilitates the transfer of the terminal phosphate group to the protein substrate.

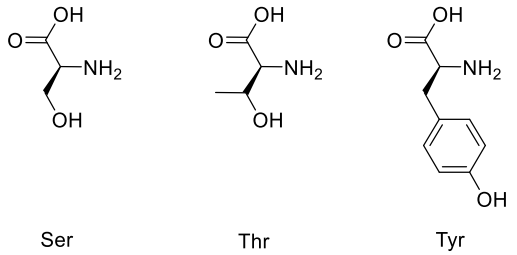

Figure 5: Amino acid residues involved in catalytic phosphorylation.

Protein kinases can either be serine/threonine kinases or tyrosine kinases. In some cases dual specific kinases can phosphorylate serine/threonine as well as tyrosine.[10, 11]

Protein phosphorylation plays an important role in the process of cellular signal transduction. Therefore, protein kinases influence cellular growth, differentiation, metabolism and apoptosis which makes them an interesting target for drug discovery research.[7]

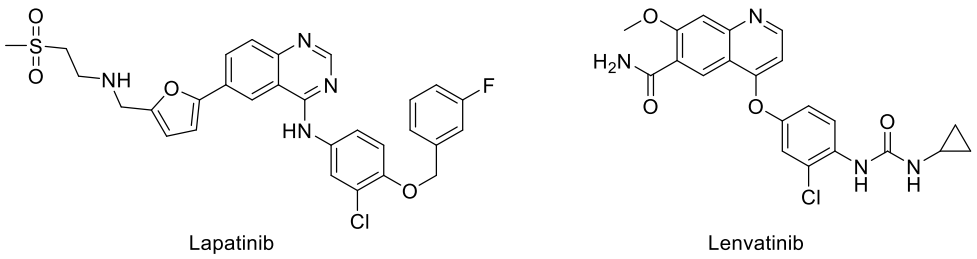

Figure 6: Two of the 28 US FDA approved kinase inhibitors.

258 kinase inhibitors are currently undergoing clinical trials most of which target tyrosine kinases with indications in cancer.[12] To date, 28 small-molecules that target kinases have been approved by the US FDA.[13] For example, lapatinib from GSK was approved in 2007 for breast cancer by inhibiting EGFR (epidermal growth factor receptor).[14] Most recently, lenvatinib from Eisai was approved for thyroid cancer in 2015 and inhibits VEGFR2 and VEGFR3,[15] **Figure 6**.

3. Understanding the protein kinase structure

In order to target a protein kinase, one must understand the structure and binding motif of the protein kinase. A considerable amount of research has been aimed at understanding the biological structure of these proteins.

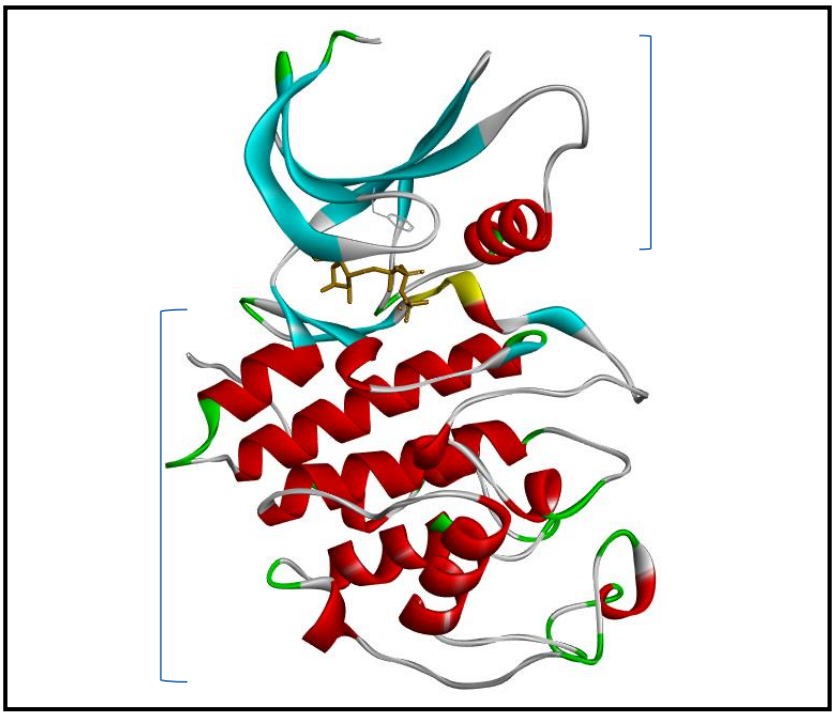

Figure 7: CDK2 with ATP (PDB: 1QMZ altered).

Each protein kinase contains a bilobal fold with the catalytic active site between these two lobes, **Figure 7**. The *N*-terminal lobe generally consists of 5 antiparallel β-sheets (in blue) and an α-helix (in red). The *C*-terminal loop, on the contrary, consists mainly of α-helices. These two lobes are connected via a loop called the hinge region. A deep cleft is generated between these two lobes which constitutes the active site or orthosteric site where the natural substrate ATP **1** (orange) binds.[16]

Protein kinases are highly flexible and the opening and closing of the kinase domain (*aka* orthosteric pocket) is regulated by the activation loop. This flexible activation loop is situated in the *C*-terminal lobe and consists of 20-30 amino acids depending on the protein kinase. There is a highly conserved motif at the start of the loop: aspartic acid (Asp), phenylalanine (Phe) and glycine (Gly). This is known as the DFG motif and is represented in yellow, **Figure 7**.[17] Generally, this activation loop is the key for the regulation of the protein kinase. Upon phosphorylation, the loop departs from the active site allowing the possibility of a readily accessible ligand to interact with the pocket. When the protein kinase is dephosphorylated, the loop occupies and blocks the active site. Therefore, the activation loop functions as a 'phosphorylation-sensitive switch'.[18] Nevertheless, this does not apply to all protein kinases to explain the inactive and active states of protein kinases.

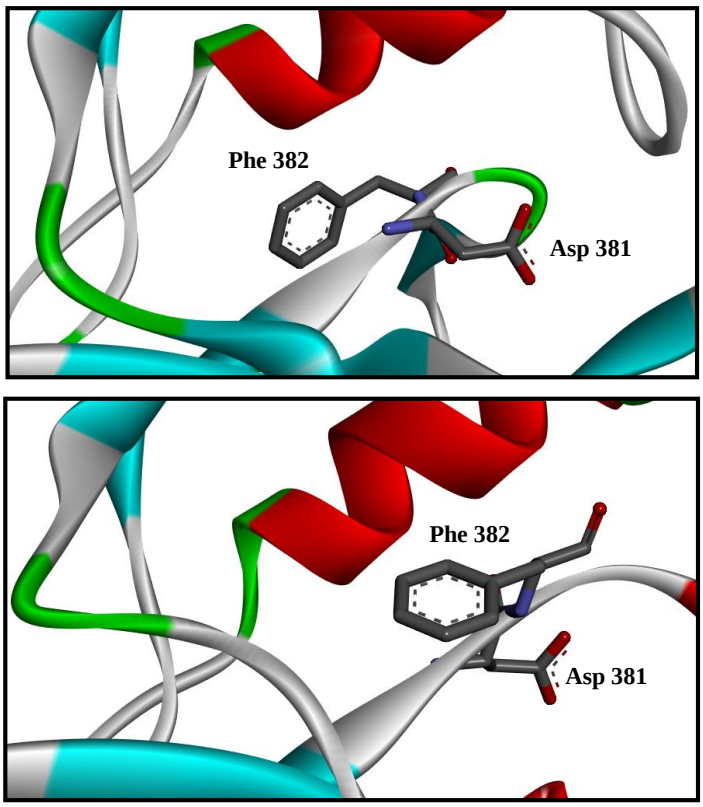

Figure 8: a. c-Abl (2GQG) in active state; b. c-Abl (1IEP) in inactive state.

Figure 8 represents c-ABL, a protein kinase, in its active (**a.**) and inactive (**b.**) form. When the protein is activated, the loop displays an open conformation and phenylalanine (Phe 382) of the DFG motif points inwards towards the active site and the aspartic acid (Asp 381) points outside the active site. This conformation allows the ATP **1** substrate to bind and allows the necessary amino acids to carry out the phosphate transfer. This is known as DFG-in conformation (activated kinase). Moreover, a change in the orientation of the α-helix in the *N*-lobe can be observed and is orientated inwards, towards the active site. When the protein is inactive (DFG-out), the activation loop adopts a flipped conformation and noth amino acid flip by nearly 90° compared to the activated form. This leads to an incompetent state for ATP **1** binding but opens an allosteric pocket adjacent to the ATP pocket, which will be explained later. All known protein kinases adopt the DFG-in and DFG-out conformation but can differ in their conformation according to their amino acid sequence.

4. **Binding mode**

a. ATP binding in the active site

Within the protein kinase family, the catalytic domain is highly conserved as they all have ATP **1** as their natural substrate.

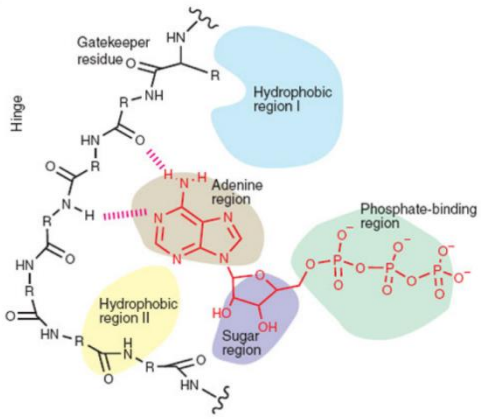

Figure 9: ATP binding mode in a protein kinase.[19]

Due to the conserved nature of the catalytic domain, a similar type of binding is observed, with the adenine ring of ATP forming key hydrogen bonds with the amine/carbonyl groups of the amino acids in the hinge region, **Figure 9**. Mg^{2+} cofactors bind to the phosphate unit in order to counteract the negative charges and are essential for the catalytic process. Two hydrophobic regions can be observed in the binding complex for each kinase, above and underneath the adenine ring.[19] The gatekeeper residue controls the access to hydrophobic region I (**Figure 9**) and varies according to the kinase.[17]

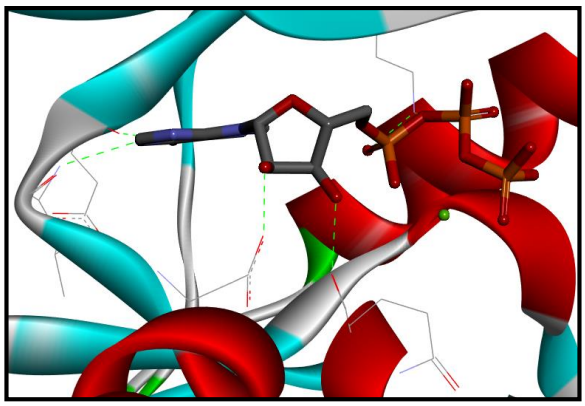

Figure 10: CDK2 ATP binding pose in active site (2GQG).

Figure 10 is an example of ATP **1** bound in the CDK2 active site. The adenine ring forms key hydrogen bonds with the carbonyl of glutamic acid (Glu 81) and the amine of leucine (Leu 83) from the hinge region. The sugar moiety of ATP forms hydrogen bonds with aspartic acid (Asp 86) and glutamine (Gln 131) and finally the phosphate region forms a hydrogen bond with lysine (Lys 33). A Mg^{2+} cofactor, in green, can be observed in the phosphate region.

b. Inhibitors

Most of the molecules that inhibit kinases have targeted the ATP binding site and are therefore in competition with the natural substrate. However, throughout the years new types of inhibitors have been discovered. Four different types of inhibitors have been reported to date:[17, 19]

- Type I inhibitors: target the ATP binding site where the adenine ring lies. The protein needs to be in its activated form in order for the inhibitor to complete its function. These inhibitors generally form 1−3 hydrogen bond(s) with the hinge region and can gain selectivity by targeting the other regions described previously, e.g. the hydrophobic pocket behind the gatekeeper residue.
- Type II inhibitors: target the hydrophobic pocket adjacent to the ATP binding site that opens up when the protein kinase is in its inactive form (DFG out). Certain inhibitors only target this new pocket (allosteric pocket) or also extend into the adenine pocket.
- Type III inhibitors: are not ATP competitive and target specifically an adjacent allosteric pocket to the active site. In contrast to Type I they do not form any hydrogen bonding with the hinge region. These inhibitors induce a conformational change in the kinase.
- Type IV inhibitors: interact with any allosteric site that is distant from the orthosteric site. They induce a conformational change which will be explained in more detail later.

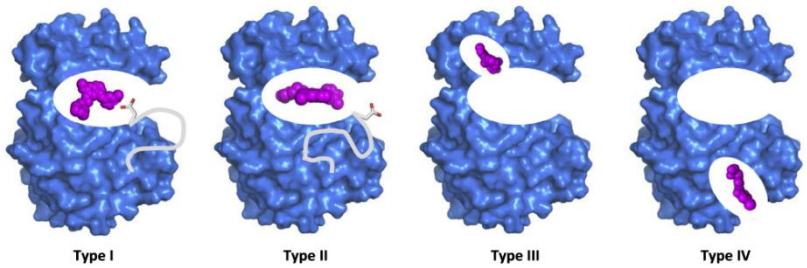

Figure 11: Schematic representation of the four types of inhibitors.[13]

Figure 11 is a schematic representation of the four different types of inhibitors found to date. Most of the kinase inhibitors that are on the market, like lapatinib and lenvatinib previously seen in **Figure 6** are Type II and target the inactive state (DFG out) of the kinase.

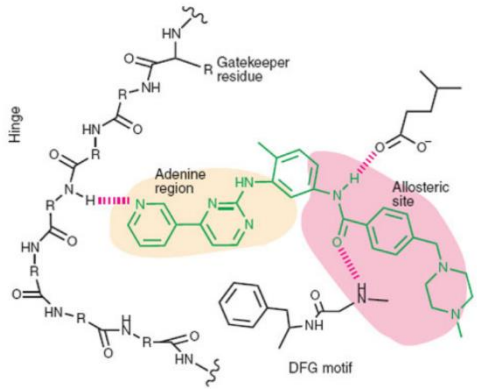

Figure 12: Schematic representation of Type II inhibitor imatinib.[19]

Figure 12 is a schematic representation of the binding of imatinib which is a Type II inhibitor to its kinase target and which will be described later. When bound to the inactive state of the kinase, the pyridine and pyrimidine groups are in the adenine region of the orthosteric site and an H-bond interaction is observed between the pyridine nitrogen and the NH of an amino acid in the hinge region. The piperazine moiety and the phenyl amide are in the allosteric site that opens up when the protein is inactive. This leads to two H-bond interactions between the amide and two amino acids, one being part of the DFG motif. Therefore, all Type II inhibitors will adopt a similar conformation when bound in the kinase.

Only one marketed kinase drug is a Type III inhibitor: trametinib, **Figure 13**. This drug targets MEK1 and MEK2 kinases that are expressed in metastatic melanoma.

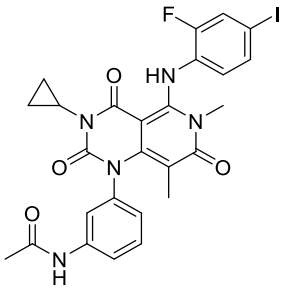

Trametinib

<u>Figure 13:</u> Trametinib the only Type III kinase inhibitor marketed to date.[13]

In summary, several possibilities are available for drug discovery programmes targeting protein kinases. Type IV inhibitors have not yet reached the market due to the difficulty of finding these allosteric sites. Accordingly, we were interested in Type IV inhibitors, also known as allosteric inhibitors.

II. Allosterism

1. Definition

The word allosteric originates from the greek *allos*, other and *stereos*, object/solid; implying that an allosteric site is a site distinct from an orthosteric/active site.[20] This concept was first introduced by Monod and Changeux in 1961 when they were looking at the biological process of regulating protein function.[21, 22] They observed that the binding of a regulatory effector at a topographically distinct site (allosteric site) affected the function of the protein either *via* a conformational or dynamical change yet to be determined.[21] Therefore, allostery can be defined as the regulation of protein function, structure and/or flexibility that is induced by the binding of a ligand at a site distinct from the orthosteric site, which is called an allosteric site.[1, 2]

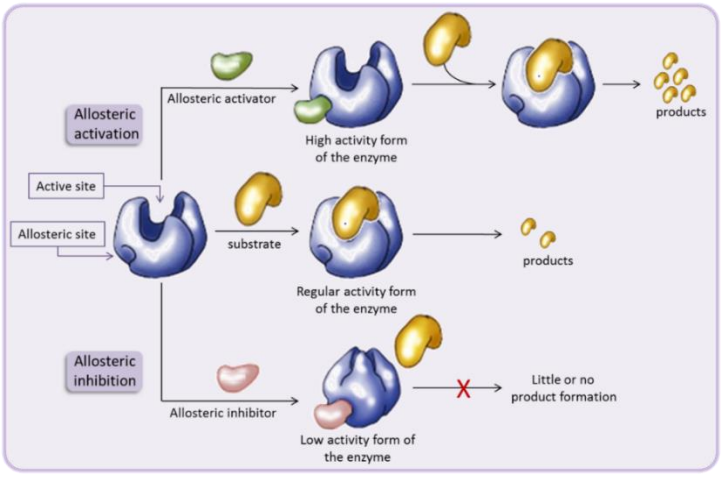

Figure 14: Schematic representation of allosteric regulation.[3]

Allosteric effectors can be small molecules or macromolecules. This can then either activate, or inhibit a proteins function by either increasing or decreasing the activity or affinity towards its natural substrate. This is referred to as allosteric regulation and a schematic representation of this regulation is shown in **Figure 14**. An allosteric modulator that enhances the protein's function is called a positive allosteric modulator (PAM). When the molecule binds to an allosteric site and inhibits its function it is called a negative allosteric modulator (NAM).[23]

A good example to demonstrate fully this phenomenon would be the metalloprotein haemoglobin. This metalloprotein is found in red blood cells and enables the transport of oxygen from the lungs to the rest of the body. On one hand, the first oxygen molecule that binds to haemoglobin is an allosteric activator or PAM as it enhances the affinity towards other oxygen molecules through conformational change.[24] By contrast, when 2,3-bisphosphoglycerate, present in red blood cells, binds to haemoglobin the metalloprotein is stabilized in its inactive state imparting a loss in affinity for oxygen.[25] Accordingly, this substrate would be considered an allosteric inhibitor or NAM.

2. Models

a. Established views on allosterism

Two models were proposed in the late 1960's in order to understand the process of allosteric regulation on proteins that were oligomeric, i.e. with a finite number of subunits; a subunit being a single protein molecule within the protein complex. They both stipulated that the protein's subunits existed in two freely interconvertible conformational states, tensed (T) or relaxed (R).[22, 26, 27] These models essentially differ in how the subunits interact with each other in order to explain this conformational change.

The first model was the MWC (Monod, Wyman and Changeux model), also known as the concerted model.[22] This view suggested that all the subunits of the protein exist in the same conformational state either T or R. Therefore, if an allosteric modulator binds then the change in one subunit will imply a change in all other subunits.[22, 24, 27] The second model, KNF (Koshland, Némethy and Filmer model), relies on a sequential model, where the ligand binds through an induced fit mechanism and thus affects the structure of the neighbouring subunits.[24, 26, 27]

These models have shown that allosterism implies a change in conformation in multidomain proteins.

b. Contemporary views on allosterism

Nowadays, with significant amounts of research into this field, researchers have shown that allosteric behaviour can be seen in single domain proteins as well as multidomain proteins.[1, 28]

Recently it has been shown that proteins should be considered as an ensemble of conformers in their native state, therefore as something dynamic.[28, 29] These different conformations have distinct energy landscapes, with one conformation predominantly present at equilibrium. When an allosteric modulator binds to one of these pre-existing conformers, it perturbs the equilibrium and there is a shift towards a new set of conformers. This is known as the population shift.[24, 28, 30]

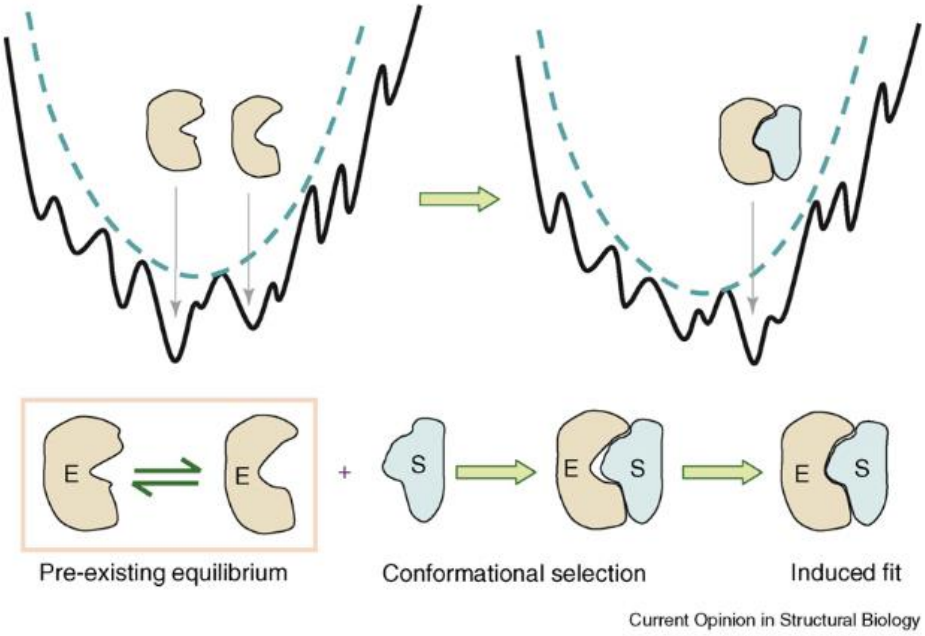

<u>Figure 15:</u> a. Energy landscape of enzyme before and after presence of substrate; b. Enzyme conformers native state and with substrate.[31]

Figure 15 explains this phenomenon. Part **a.** shows the energy landscape of the different conformations of the protein in its native state with some conformations of low energy being more predominant, as seen in part **b.** When the substrate is present, it selects the conformer(s) of the protein that enables an optimal interaction (conformational selection). Further rearrangement by induced fit occurs in order to obtain the most stable final complex (part **b.**). Once the substrate is bound to the protein, a different energy landscape is observed from the native protein (part **a.**) inducing a population shift towards the conformer that binds to the substrate.

Studies have shown that allosterism does not have to imply a conformational change at the backbone level. Allostery can be seen as a thermodynamic process involving an enthalpic and entropic contribution. This indicates that any change in the activity of a protein occurs *via* a dynamic fluctuation, whilst an allosteric modulator is bound. Allostery can therefore be categorised into three types:[32]

- Type 1: Governed by entropy with a subtle change in the structural backbone
- Type 2: Governed by entropy and enthalpy with minor conformational change
- Type 3: Governed by enthalpy with large or local conformational change

Therefore, if no real conformational change is needed for a protein to be considered allosteric, it can be considered that any protein can potentially be allosteric.

This new research on allostery has shown that proteins exist as an ensemble of conformers and that allosterism relies on a thermodynamic process involving enthalpy and entropy. Most importantly, a lack of conformational change does not imply that a protein is non-allosteric therefore implying that all proteins can be considered allosteric.

3. Industrial implications

Traditionally, pharmaceutical companies have focused their drug discovery on orthosteric sites of proteins, either in the active or inactive state of the protein. Many drawbacks can arise from this focus including drug resistance and selectivity. Allosteric modulators offer new opportunities in drug discovery by providing unique advantages and new classes of compounds.

First of all, allosteric modulators can bring greater selectivity than orthosteric drugs. In general, the orthosteric site is highly conserved throughout a protein family (*e.g.* kinases).[33] An allosteric site is generally considered to be remote from the orthosteric site and is often unique in its sequence and structure. Thus, an allosteric modulator can more selectively target the protein of interest amongst the protein kinases and even subfamilies.[24, 34, 35] By gaining selectivity this would potentially diminish side effects of drugs as it would selectively target the protein of interest without interfering with other proteins that may have similar topologies in their orthosteric sites. Furthermore, in the case of kinases, allosteric modulators would not compete with ATP **1**, the endogenous ligand that is present in high concentration in cells between 1–10 mM.[36] Allosteric modulators exhibit little intrinsic activity as they enhance or inhibit the action of the endogenous ligand leading to the preservation of the natural physiological signalling.[35] Last, but not least, allosteric modulators could potentially be used in combination therapies. For example, combining an allosteric modulator that enhances the activity of the protein with an orthosteric agonist could be an interesting combination. This modulator would increase the efficacy of the orthosteric drug, which could reduce the incidence of adverse effects.[35]

Allosteric modulators can therefore bring a lot of advantages to drug discovery research. The main challenge is identifying the allosteric site and subsequently designing an allosteric effector that binds to it efficiently.

4. Identifying allosteric sites

Most of the allosteric drugs on the market have been found by serendipity.[8] For example, imatinib **2**, shown in **Figure 16**, is a tyrosine-kinase Type II allosteric inhibitor for several kinases and is used in the treatment of multiple cancers.[11]

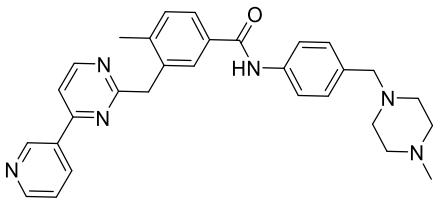

2

<u>Figure 16:</u> Imatinib 2, Type II inhibitor marketed by Novartis.

Imatinib **2** was initially considered an ATP-competitive inhibitor of Bcr-Abl as the kinetic result suggested. However, with further investigation and a co-crystal structure (1IEP) it was shown that **2** binds to a site near the ATP active site of the inactive form of Abl without competing with ATP **1**, **Figure 12**.[11] Imatinib **2** was found to be a Type II inhibitor and started a new interest in the field of kinase inhibition.[17]

Figure 17 represents imatinib **2** bound to the inactive state of the protein kinase. The pyridine moiety of the compound is in the adenine region where the nitrogen of the pyridine ring forms a hydrogen bond with the NH at the backbone level of methionine (Met 318). Additionally one of the nitrogen atom from the pyrimidine ring interacts with the hydroxyl group of threonine (Thr 315). The rest of the molecule is situated in the new allosteric pocket that opens in the inactive state. The NH of the amide interacts with glutamic acid (Glu 286) from the α-helix of the *N*-lobe and the carbonyl with asparagine (Asp 381) from the DFG motif. This is linked to the schematic representation of imatinib **2** described previously, **Figure 12**.

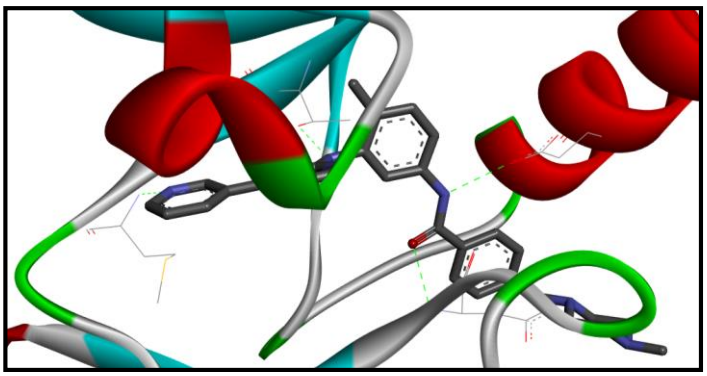

Figure 17: Imatinib 2 in active site of c-ABL (1IEP) in the inactive state.

Other allosteric sites have been found by using High Throughput Screening (HTS) and X-ray crystallography. This method requires very rigorous kinetic studies in order to determine the ligand's mode of inhibition before the crystallographic study can be done.[37] This method has been used frequently and resulted in the discovery of new allosteric sites. A good example of this method was the discovery of an allosteric site of HIV-1 reverse-transcriptase. Through this method, three allosteric inhibitors are now commercially available: efavirenz, nevirapine, and delavirdine.[37]

5. Guidelines

In 2014, Van Westen *et. al.* carried out a study attempting to discover trends in allosteric modulators. During this study they examined specific chemical and target properties of known allosteric inhibitors.[38] Using ChEMBL (a manually curated chemical database of bioactive molecules with annotated physicochemical properties) as their dataset they searched for key words; in total they retrieved 1002 papers which formed their allosteric data set. Analysing this literature they looked for trends in the target compounds, which were compared to non-allosteric modulators, **Figure 18**.

They observed that there were no distinct differences at the protein type level between the two classes. Nevertheless, when they investigated protein family and compared both allosteric and non-allosteric modulators (**a.** and **b.**) clear differences were observed. For example, class C GPCRs, here referred to as 7TM3, nuclear receptors and ligand-gated ion channels were enriched in the allosteric set. These results show the trends according to the literature and that some allosteric modulators for kinases already exist.

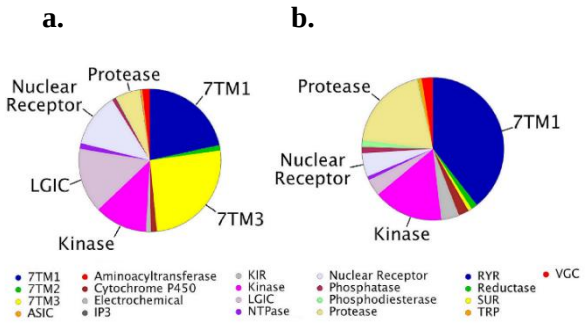

Figure 18: c. Distribution of protein family for allosteric modulators; d. distribution of protein family for non-allosteric modulators.[38]

In terms of physicochemical properties of the associated compounds, they examined various factors, and once more compared allosteric and non-allosteric subsets, **Figure 19**. Analysis of molecular weight (MW) and Log D in accordance to Lipinski rule of 5 for both libraries (scattered plot (**a.**)), showed that allosteric modulators have a narrower range of molecular weight and a less broad Log D when compared to orthosteric ligands. From these results, allosteric modulators adhered better to Lipinski's rule of five due to the fact that there are no known allosteric modulators far from drug-like space.

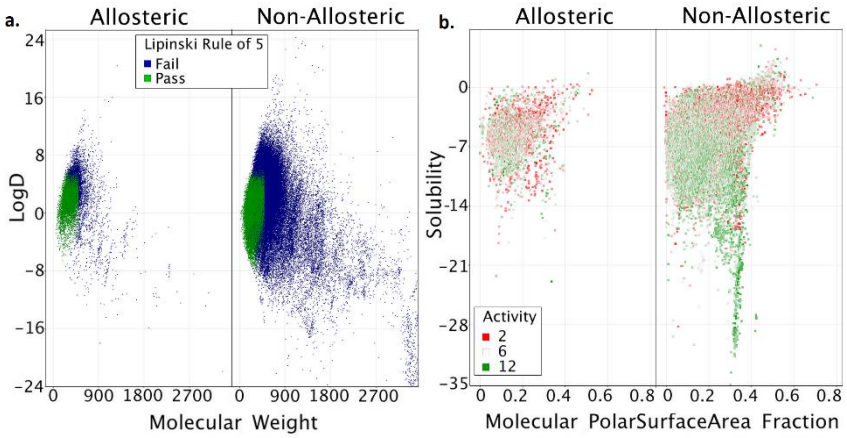

Figure 19: Scatter plot showing allosteric and non-allosteric modulators: a. MW *vs* log D and adherence to Lipinski rule of 5, b. Molecular PSA fraction *vs* solubility and activity.[38]

Furthermore, they explored the differences in terms of normalized activity between the two subsets (**b.**), the relative molecular polar surface area (PSA) and solubility. It was observed that allosteric modulators showed a more restricted subset in terms of physicochemical properties than non-allosteric modulators and that the

physicochemical properties of the molecules depended equally on the target in question.[38]

III. Predicting an allosteric site

To date there is no clear technique to identify rationally and reliably allosteric sites. Elsewhere in our laboratories, Al-Shar'i developed a model based on molecular dynamics to identify allosteric sites.[3] His model focused on the protein kinases JNK1 and CDK2 which have known allosteric sites. Within this project we decided to apply his model to DYRK2 which has no known allosteric inhibitors and an interesting biological profile.[39]

1. DYRK2 our test protein

Recent research has shown that DYRK (Dual specificity tyrosine-(Y)-phosphorylation regulated kinase) proteins are involved in key signalling pathways that are critical for processes such as brain development, cell homeostasis and regulation of splicing.[39, 40] DYRK2 has been found to be overexpressed in lung adenocarcinoma as well as oesophageal carcinoma.[41] Moreover, DYRK2 is an effector kinase for Ser 46 of p53 which leads to DNA damage-induced apoptosis.[41] Therefore, this target is highly interesting as it is involved in the regulation of cancer cells and neurodegenerative diseases.

DYRK2 is part of the DYRK subfamily and within the CDK family. This family consists of dual specificity kinases that phosphorylate on serine and threonine and autophosphorylate on tyrosine residues (**Figure 5**).[39]

Within the family there is a high degree of conservation in the catalytic domain. They differ mainly in the *C*-terminal and *N*-terminal extensions.[39] Therefore, it is difficult to target selectively DYRK2 in the catalytic domain because of this high degree of similarity, as is the case for many kinases. For example the ATP binding site of DYRK1A and DYRK2 only have 3 residues that differ and a common gatekeeper phenylalanine (Phe). It is still possible to gain selectivity within the two isoforms as

has been observed by Soundararajan *et. al.* when they screened a panel of kinase inhibitors.[40]

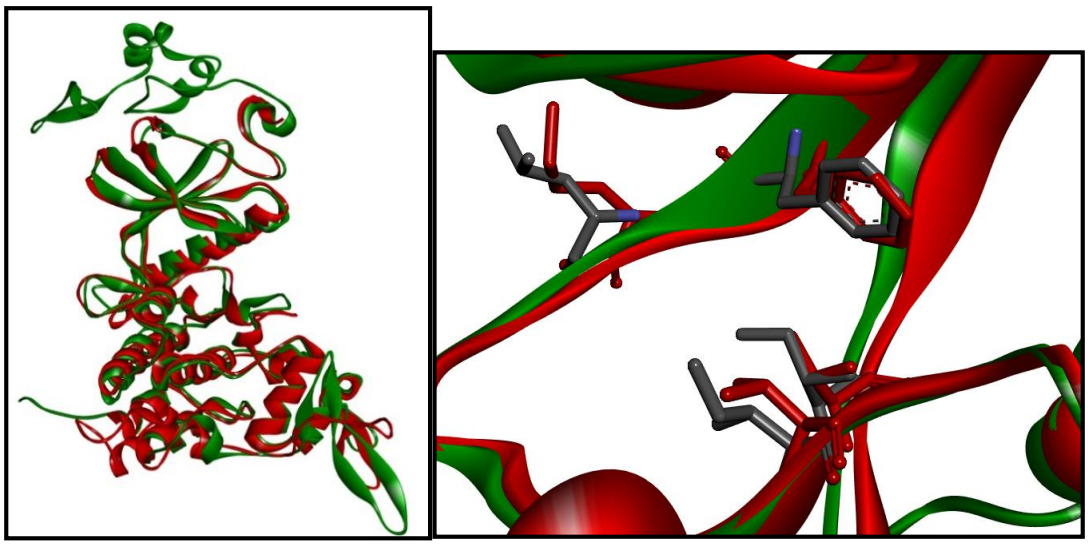

Figure 20: a. DYRK1A (red) and DYRK2 (green) superimposition; b. Close up of orthosteric site.

Figure 20 shows the superimposition of DYRK1A (4MQ1), in red, and DYRK2 (3K2L), in green, in the overall fold of the protein (**a.**) and a close up of the orthosteric pocket (**b.**). DYRK1A has a valine residue (Val 222) which is replaced by an isoleucine (Ile 212) in DYRK2, while in the hinge region methionine (Met 240) on DYRK1A is a leucine (Leu 230) in DYRK2 which slightly decreases the hydrophobicity of the pocket thus opening it more. The last residue that differs precedes the DFG motif and is Val 306 in DYRK1A which is replaced by Ile 294 in DYRK2, which results in a significant change in the hydrophobic contact surface.[12] This change in residue seems to be the most important. These small changes that influence hydrophobicity have led to the possibility of gaining selectivity between the two isoforms.

Figure 21 shows a co-crystal structure of DYRK2 (PDB file: 4AZF) with **L41** which is a competitive inhibitor found by Meijer *et. al.*[12] **L41**, shown in **Figure 22**, is a Leucettamine B derivative and has shown promising results with an unusual multi-target selectivity of kinases.[12]

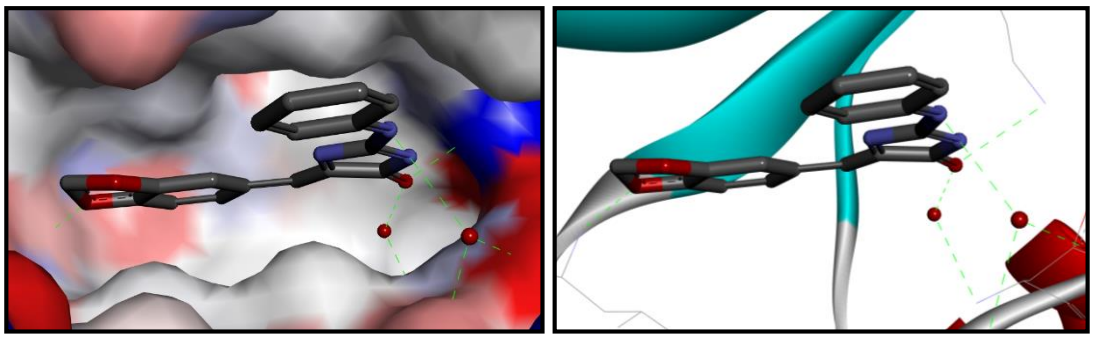

Figure 21: DYRK2 protein (4AZF) with L41 with and without the surface.[12]

In order to get more insight into how **L41** binds, it was co-crystalized with DYRK2 as well as DYRK1A, CLK3, PIM1 and GSK-3*β*. This made it possible to determine the key hydrogen bonding interactions between **L41** and the ATP binding pocket of DYRK2 with the following amino acids playing a primary role: Leu 231, Lys 178, Asp 295 (aspartic acid) and Asn 280 (asparagine). The two latter interactions are possible through an extended hydrogen bonding network involving water molecules.[12]

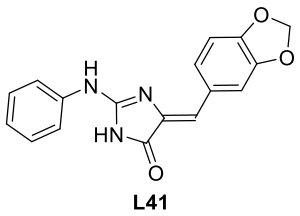

L41

Figure 22: L41 molecule.[12]

Meijer and co-workers have shown that this family of compounds derived from leucettamine is a promising family of neurodegenerative inhibitors. In our case, compound **L41** has been chosen to compare our biology results with this competitive inhibitor, which has shown an IC_{50} of 70 nM for DYRK2 and 10 nM for DYRK1A.[12] It is therefore a non-selective inhibitor of these two isoforms of DYRK which will provide a benchmark for our biological assay. Meijer generously provided us with a sample of **L41**.

The work that will be presented until the end of this Chapter is work that was carried out by Al-Shar'i during his PhD.

2. **Allosteric site identification**

The following analysis were applied to DYRK2 in order to predict an allosteric pocket within the protein.

a. **Fluctuation analysis**

The first part of the process was to look at how the protein moves over time. This gave an insight into the dynamic fluctuation of the protein for each individual residue. Once the highly flexible terminal loops were edited out, a potential site was found where flexibility of the protein was shown as well as stability.[3]

b. **Cross-correlation motion**

This analysis enabled examination of which residues move together during a conformational change with a two dimensional heat map. This gave an insight into the location of a potential allosteric site, similar to the previous analysis, that is linked to the catalytic site *via* residue motion.[3]

c. **SID analysis**

Simple Intrasequence Difference (SID) analysis is a bioinformatic tool developed by Dufton *et. al.* which has enabled the understanding of the properties of protein fold topology.[42] This study was used to identify the major interfaces that might be involved in allosteric modulation for DYRK2. This tool scored the residues of the protein with the highest score indicating vulnerability to conformational change. This correlated well with the previous analyses (**a.** and **b.**) and pointed towards the same potential allosteric site.

d. **Energy correlation**

A protein is in a continuous exchange of energy with its surroundings within the cell and this affects the protein function. This energy exchange does not diffuse randomly within the protein and follows a specific pathway.[43] This analysis enabled Al-Shar'i to find the interconnectivity of the protein and the energy pathways that affect the function of the protein.

In summary, the combination of all these analyses enabled Al-Shar'i to identify a putative allosteric site for DYRK2.

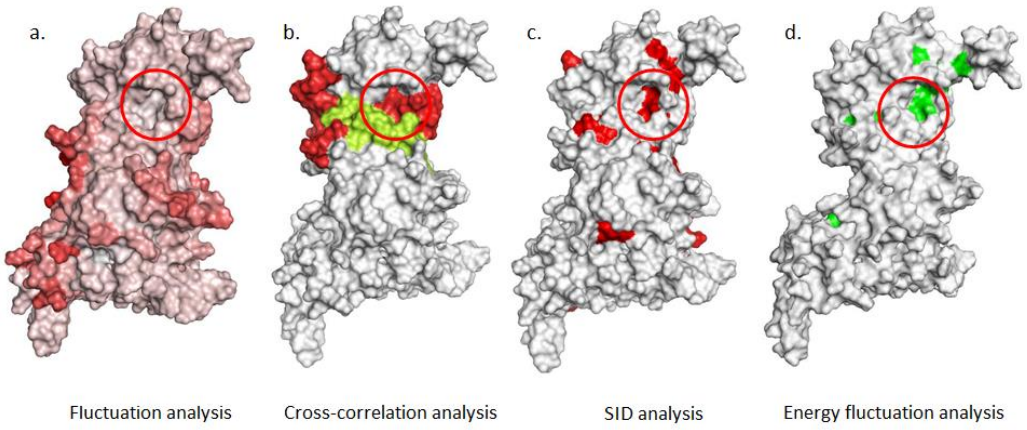

Figure 23: Summary of all 4 analysis tools used for identifying a putative allosteric site.

Figure 23 shows the overall results of the study: **a.** the fluctuation analysis where the colouring shows flexibility (red being highly flexible), **b.** the cross-correlation with the two different coloured segments correlated to each other, **c.** represents the SID analysis where red corresponds to the interfaces with the most potential towards conformational change and finally **d.** represents the energy fluctuation with the energy gates to the interaction pathways represented in green. Based on all of the above, the red circle highlights the allosteric site considered for the project.

3. **Potential allosteric site**

The potential allosteric site, circled, was remote and on the opposite side from the catalytic site of the protein, with a volume of 60 $Å^3$. **Figure 24** represents DYRK2 protein kinase with the allosteric site in red and the ATP site in orange. We can observe that the putative allosteric site is situated in the *C*-lobe on the opposite face from the ATP site and distant from it.

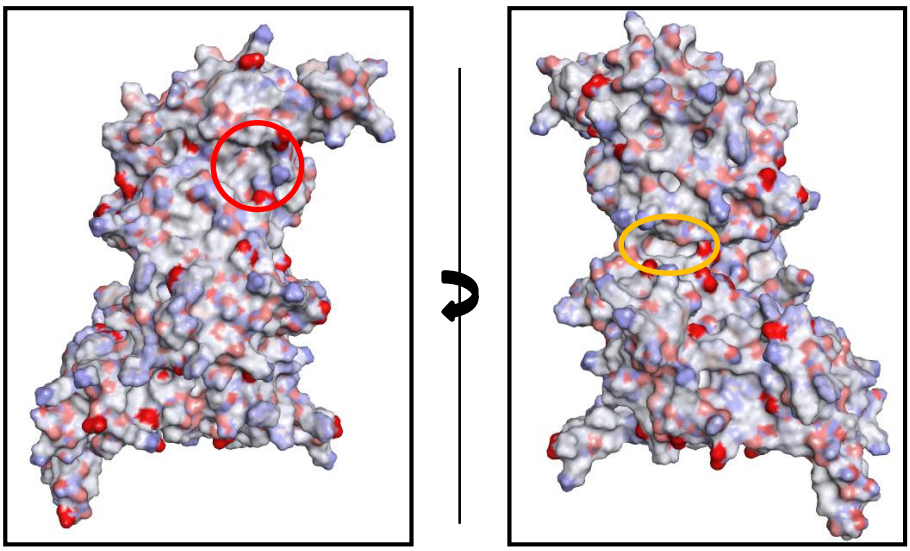

Figure 24: DYRK2 protein kinase 3K2L.

The following residues were present in the putative allosteric site: glutamic acid (Glu 156), arginine (Arg 88), tyrosine (Tyr 45 and Tyr 89), lysine (Lys 110), phenylalanine (Phe 158) and threonine (Thr 159), as seen in **Figure 25**.

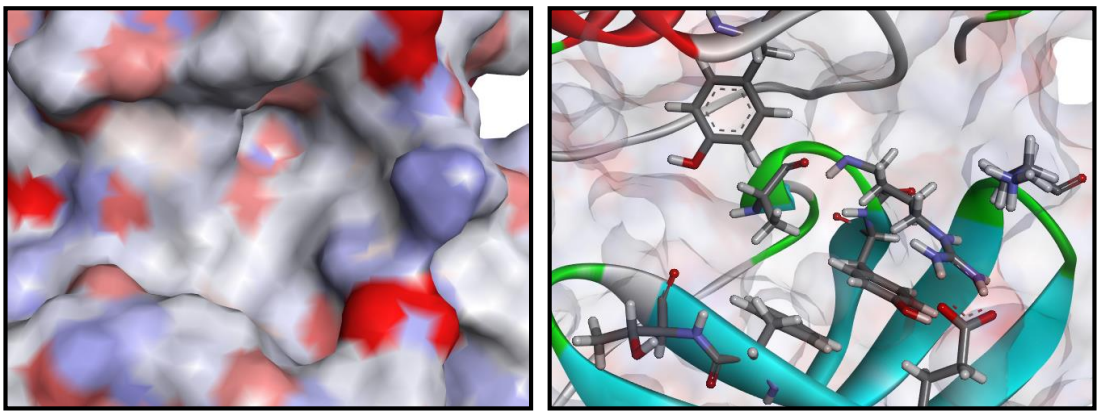

Figure 25: Close up of putative allosteric pocket with and without surface.

In summary, a putative allosteric site was identified and was explored by chemical probe simulation and virtual screening.

4. Chemical probe simulation

In order to know if the site identified using Al-Shar'i's methods[3] could potentially be an allosteric site, it was important to simulate virtually the effect of ligand binding to this site and observe if any conformational change of the protein occurred.

Al-Shar'i started by designing a chemical probe that would be small, easily accessible and most importantly, pick up hydrogen bond interactions with the residues within this pocket. Chemical probe **3a** showed good predicted binding poses with two proposed hydrogen bond interactions with Lys 110 and Thr 159. Several other probes were also designed in order to explore the hydrophobic region of the binding site by modifying the substituents on the pyridine ring as shown in **Figure 26**. He also looked into using chlorine as a substituent by either placing it *ortho* **3b**, *meta* **3c** with respect to the nitrogen of the pyridine ring or incorporating two chlorines **3d**. Methylated derivatives were also designed with the *ortho* **3f**, the *meta* **3e** and two methyl substituents **3g** to the nitrogen in the pyridine ring. These analogues were designed to enhance potential lipophilic interactions with residues in the pocket such as Phe 158 or Tyr 45/89. Finally, he also designed a fused ring system **3i** and a thiophane derivative **3h**.

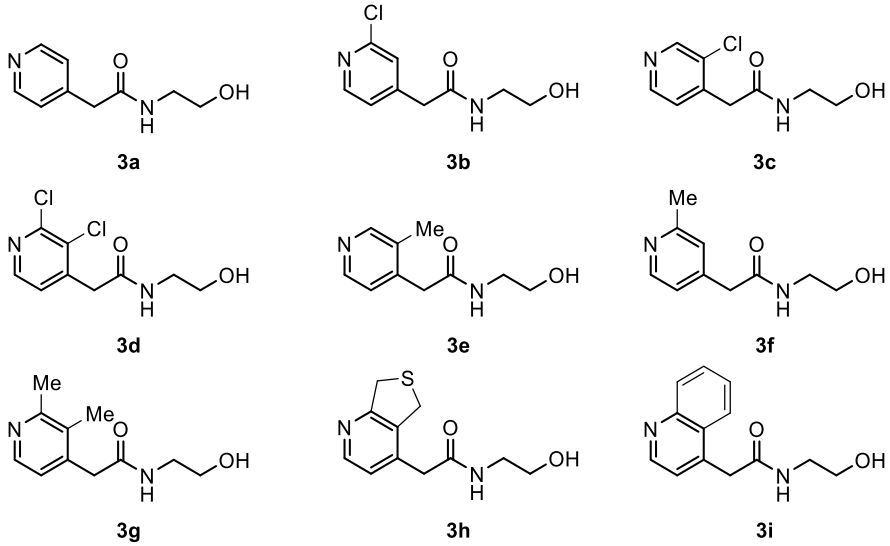

<u>Figure 26:</u> Designed virtual chemical probes.

The probes were docked in the putative allosteric pocket using the software GOLD.[44] Probe **3g** showed the best binding mode in this pocket with two putative interactions. The nitrogen from the pyridine ring showed a potential interaction with the hydrogen of the amine side chain of Lys 110 and the hydrogen from the hydroxyl group interacted with the oxygen of Thr 159 as initially predicted, **Figure 27**.

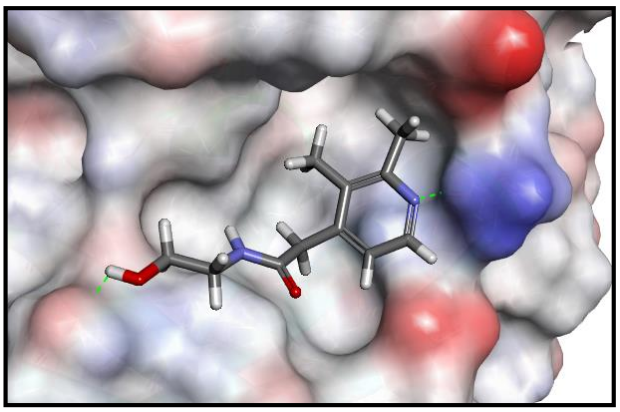

Figure 27: Dock pose of probe 3g in the allosteric pocket.

This chemical probe was therefore used to run all the analyses described previously. The residual fluctuation analysis showed that there was a restraint in flexibility near the ATP binding site upon binding of the probe. The cross-correlation map showed attenuation in the magnitude of the correlation with binding of the probe. As for the energy correlation, it showed that binding of the probe disrupted some of the energetic pathways found in the native protein.[3]

All these positive results were encouraging and lead to the next step of screening a library of small molecules targeting this potential allosteric binding site.

5. Virtual screening

a. Pharmacophore

In order carry out a virtual screening (VS) of a database, it was important to construct a pharmacophore that would pick up the key chemical functionalities that appear to be important for effective binding. Al-Shar'i used the Interaction General protocol which uses a LUDI algorithm to generate an interaction map with all the features that could be used in order to get reasonable interaction with the protein. The initial pharmacophore generated had seven features which made it too selective when it was used for screening of the Maybridge database, delivering only two hits. Therefore, it was decided that it would be fragmented into three pharmacophores that complemented each other and the initial pharmacophore, **Figure 28**.

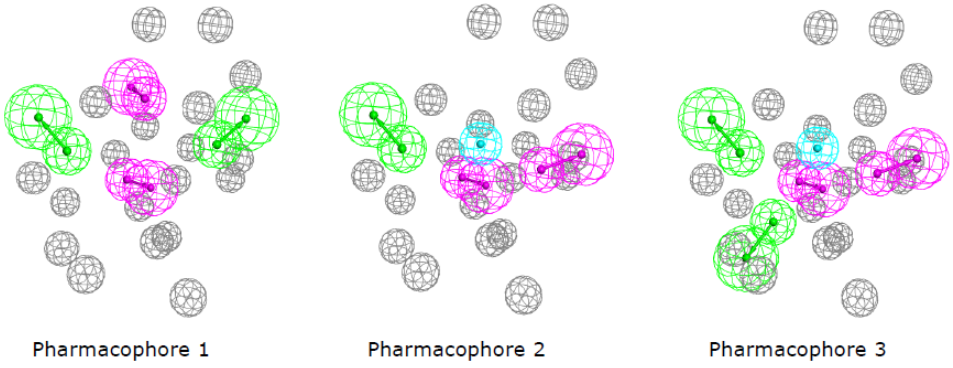

<u>Figure 28:</u> 2D pharmacophores generated with hydrogen donors (magenta), hydrogen acceptors (green), hydrophobic feature (blue) and excluded volumes (grey).

Pharmacophore 1 has four key features with two hydrogen bond acceptors (shown in green) and two donors (shown in magenta). Pharmacophore 2 is composed of one hydrogen bond acceptor, two donors and a hydrophobic feature (shown in blue). Finally, Pharmacophore 3 has two hydrogen bond acceptors, two donors and one hydrophobic feature. All of these three pharmacophores have the same excluded volumes (shown in grey).

b. Maybridge screening

The Maybridge 2009 database was screened against the three pharmacophores shown in **Figure 29**.[45] More than 56,000 compounds were virtually screened and only the ligands that mapped one of the three pharmacophores were returned as hits.

<u>Figure 29:</u> Pipeline protocol to retrieve 116 hit compounds.

An output of 2,987 compounds was observed for the three combined pharmacophores. Several filters were used in order to retrieve the best possible ligands: Lipinski's rule of five (551 hits removed) and a fit value higher than 2, which corresponds to how well the hit maps the pharmacophore (2,297 removed), brought the total number of

hits down to 139. Finally, the duplicates were removed as only one was necessary to get to the final hits. 116 hits were therefore retrieved from this screening.

c. Molecular docking

All 116 compounds were docked using GOLD version 5 by using GoldScore as the scoring function. Only the best ligands that showed strong predicted binding interactions with residues in the proposed allosteric pocket and reasonable chemical structure (easy access) were selected. 48 compounds were selected and bought from the vendor for experimental evaluation.[3]

6. Experimental analysis

a. Differential scanning fluorimetry (DSF)

Differential scanning fluorimetry (DSF) is a rapid and inexpensive way of screening and identifying low-molecular weight ligands that stabilize proteins. An increase in the signal from a fluorescence dye, with affinity for hydrophobic parts of the protein, is observed when the protein unfolds.[46] It is a first analysis to know if ligands interact in any way with the protein. It does not however give any indication as to where and how the ligand binds to the protein.

A protein's stability is linked to its Gibbs free energy of unfolding (ΔG_u) which is temperature related. By increasing the temperature, a protein destabilizes which results in unfolding. When ΔG_u becomes zero at equilibrium (concentration of folded and unfolded protein are equal), the temperature is considered a melting temperature T_m. If a molecule binds to the protein, making it more stable, ΔG_u increases, as well as T_m. It has been shown that the stabilizing effect of a compound bound to a protein is proportional to the concentration and affinity of the ligand.[46]

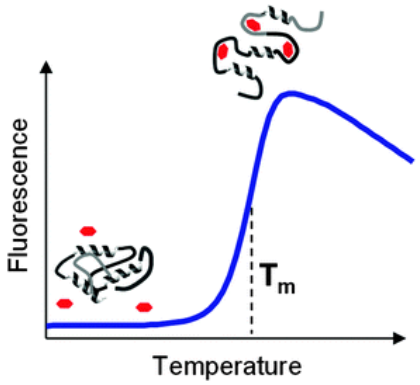

Figure 30: DSF assay representation.[47]

Figure 30 is a representation of a DSF curve. At low temperature the protein, embodied in black, is stable in the mixture with the fluorophore, in red. As the temperature increases, the protein unfolds, leading to the hydrophobic parts being accessible for the fluorophore resulting in the emission of light. With this curve, it is possible to determine the T_m.

The DSF assay was applied to the 48 compounds, at the Structural Genomics Consortium (SGC) in Oxford, purchased from the Maybridge library. This assay was run at a concentration of 12.5 µM for each compound using dimethylsulfoxide (DMSO) as a reference. Only four of the compounds tested in this assay stabilized DYRK2, as shown in **Figure 31**.

In **Figure 31** the blue line represents the thermal shift of the protein with no bound ligand, which is the reference. The other lines purple, red, green and light blue represent the thermal shifts of DYRK2 in the presence of **D05**, **C10**, **C04** and **C03** respectively. These compounds show good thermal shifts ranging from 1.7 °C to 3.4 °C as compared to the reference. The degree to which the temperature shifts is proportional to the affinity of the ligand for a given protein.[48] Vedadi *et. al.* have shown that T_m shifts of 4 °C in general give IC_{50} values of 1 µM,[48] therefore it can perhaps be inferred that the putative hits generated from virtual screening have activity in the micromolar range.

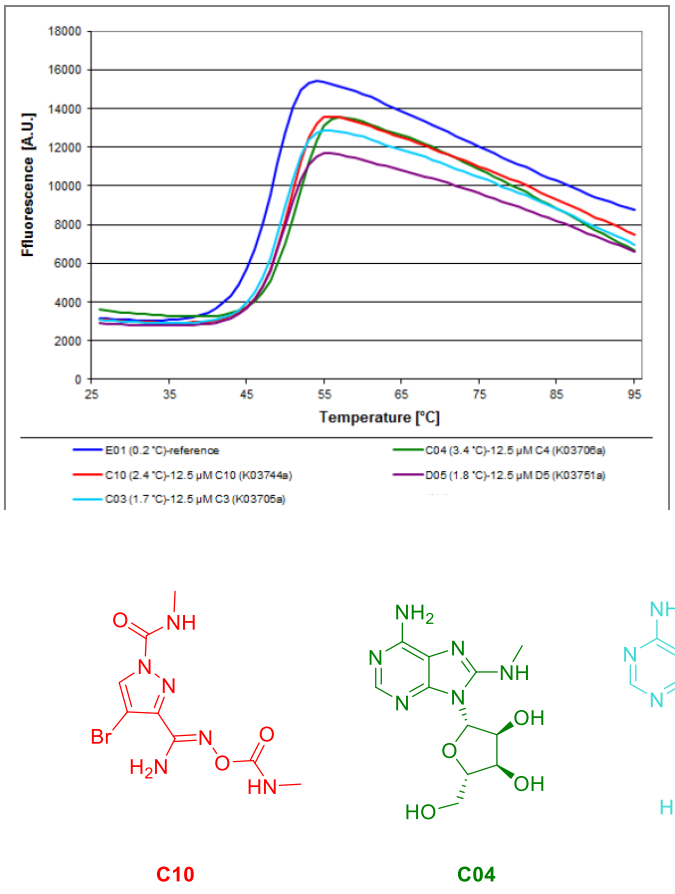

Figure 31: DSF results for the four most active compounds and their structures.

It was thought that **C04** and **C03** would be potential ATP binding site ligands when compared to ATP **1** (**Figure 4**). The four compounds were therefore docked in the putative allosteric site and the ATP binding site. Whilst looking at the conformations, the number and type of interaction(s) of the compounds with the protein suggested that only **D05** and **C10** showed promise as allosteric modulators.[3]

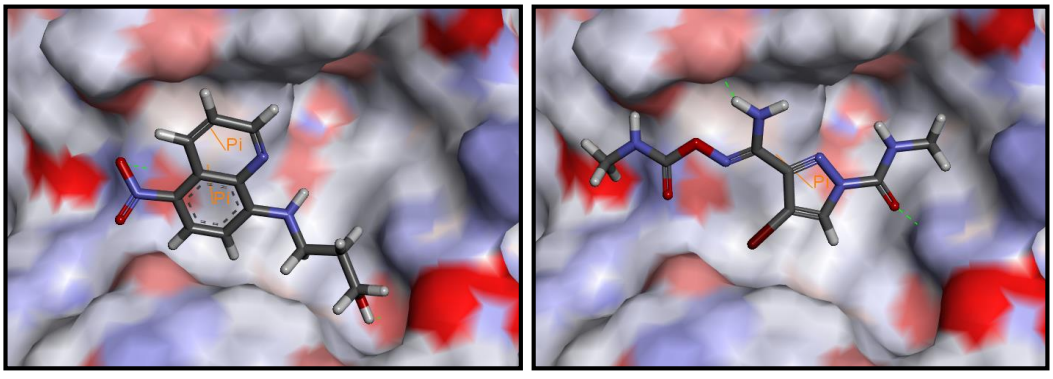

Figure 32: Docked poses of D05 and C10 in putative allosteric pocket.

Figure 32 depicts the two hits **D05** and **C10** docked in the putative allosteric pocket. Both analogues seemed to fit nicely in the pocket by making key interactions with amino acids. **D05** is involved in π-π stacking with Tyr 45 as well as two H-bond interactions: the nitro group with Tyr 45 and the hydroxyl with Tyr 89. **C10** is also involved in a π-π interaction with Tyr 45 and interacts with Arg 88 through the carbonyl urea, and with Ser 44 through the amine and amide of the oxyamidine moiety by H-bonding. With these promising poses, both ligands were taken forward for kinetic studies.

b. **Kinetic studies**

- Background

IC_{50} is the inhibitory concentration that causes 50% of maximal enzymatic activity. This can be determined by a concentration-response plot with varying inhibitor concentration while fixing the concentration of the enzyme and substrate. A curve is obtained by plotting the fractional enzyme activity (Y axis) as a function of the concentration of the inhibitor (X axis). The IC_{50} can then be determined directly from this plot. In order to be accurate, it is necessary to perform this assay with a wide range of concentrations.

- Results

The assay was run in Strathclyde with a DYRK2 Cyclex screening kit. Before doing any testing, control tests were run. First, it was necessary to determine the K_m (Michaelis-Menten constant) and compare it to the one stipulated in the manual of K_m = 4.6 µM in order to confirm the accuracy and reproducibility of the assay. This was done by screening ATP at various concentrations against DYRK2 and gave K_m = 3.8 µM which is comparable to the stipulated constant. Then, as a control, the non-selective orthosteric kinase inhibitor staurosporine was tested for DYRK2 activity.

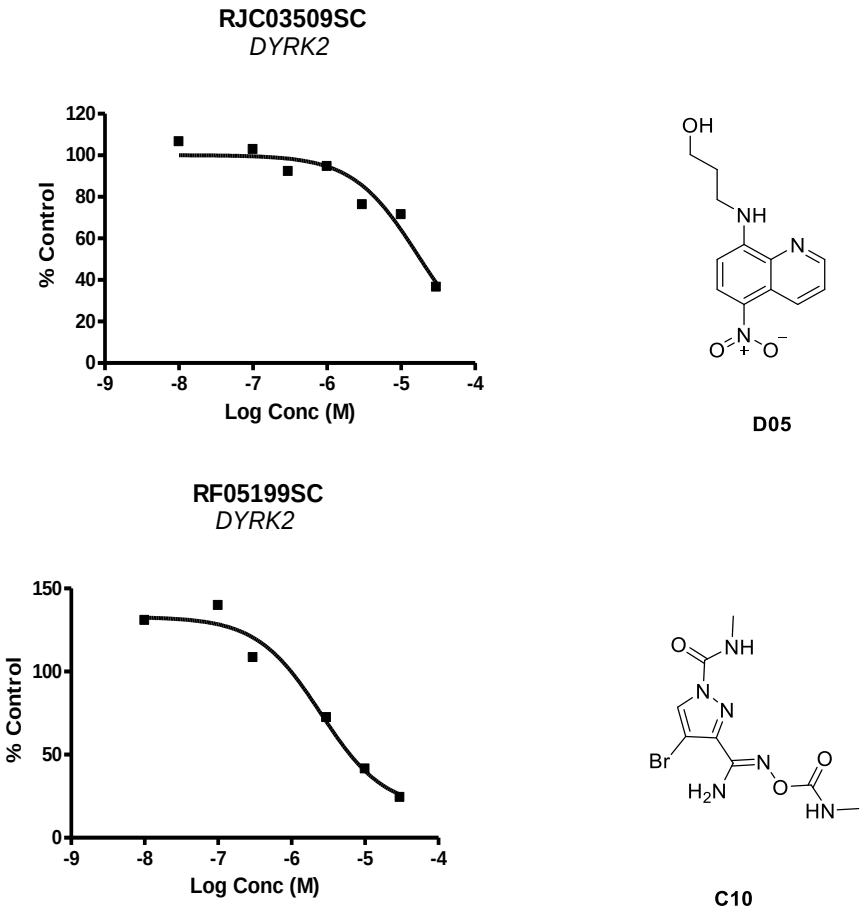

Figure 33: Enzymatic activity according to concentration plots for D05 and C10.

Finally, both compounds **C10** and **D05** were tested. Both compounds displayed positive hits with IC_{50} values of 2.5 µM and 16 µM respectively, **Figure 33**.

c. Mode of inhibition with enzyme kinetics

This analysis did not give an insight on the mode of inhibition which would be necessary to determine if they were acting as allosteric modulators.

- Background

Enzyme kinetics involves the study of enzyme-catalysed chemical reactions. This is carried out by measuring the reaction rate and determining the effects whilst varying the conditions. The data will therefore give insight into the catalytic mechanism, how the activity is controlled and how an agonist or antagonist might inhibit an enzyme.

Enzyme assays enable the measurement of the rate at which an enzyme catalyses a reaction. In most cases, the initial velocity (v_o) of the reaction is proportional to the initial concentration of the enzyme [E_o], as only small amounts of enzyme are necessary. When the substrate concentration is increased, with a fixed enzyme concentration, the initial velocity eventually reaches a maximum V_{max}. This is due to the fact that the enzyme is saturated with the substrate. **Figure 34** shows a typical saturation curve with the X-axis being the concentration of the substrate and the Y-axis the rate. The Michaelis-Menten constant, K_m, can be determined from the graph as it is equal to the concentration of substrate at half the maximum rate.

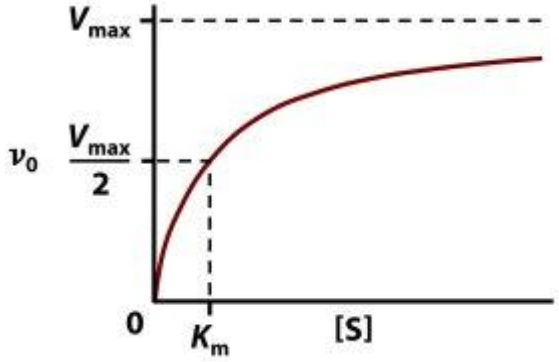

Figure 34: Curve plot of concentration against rate.[49]

The most well-known and fundamental equation of enzyme kinetics is the Michaelis-Menten equation from 1913, which is based on the reaction shown in **Scheme 1**.[27, 28]

Scheme 1: Michaelis-Menten enzyme reaction scheme.

Within the reaction E is the free enzyme and S the substrate. An important part of this theory is that a specific enzyme-substrate complex (ES) is formed during the catalysis before the release of the product P and the enzyme E. The rate constant of each step is represented by k_1, k_{-1} and k_2. With this reaction, Michaelis and Menten were able to describe, with the following equation, the dependence of the initial rate on substrate concentration:

$$v = \frac{V_{max} \times [S]}{K_m + [S]}$$

with $V_{max} = k_2 \times [E]_{tot}$ and $K_m = \frac{k_2 + k_{-1}}{k_1}$

Equation 1: Michaelis-Menten equation.

Equation 1, is the Michaelis-Menten equation, where K_m is the Michaelis-Menten constant.[50, 51] Both V_{max} and K_m are constants and K_m can be numerically determined with the graph, shown in **Figure 34**, as it is equal to the concentration of substrate at half the maximum rate.

As it is difficult to read precisely from the curved line a straight line version of the Michaelis-Menten equation was derived, which is referred to as a Lineweaver-Burk plot, **Figure 35**.[52]

$$\frac{1}{v_o} = \frac{K_m}{V_{max} \times [S]} + \frac{1}{V_{max}}$$

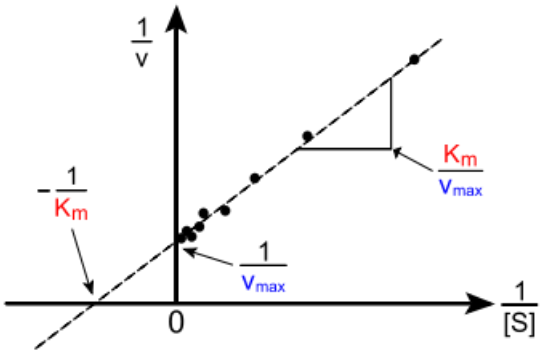

Figure 35: Lineweaver-Burk plot.[53]

Using the Lineweaver-Burk plot it is easier to determine the K_m and V_{max} from the intercept at each axis as shown in **Figure 35**.

In order to determine the mode of inhibition of an enzyme (competitive, non-competitive or uncompetitive), the reaction needs to be monitored at different concentrations of the inhibitor [I]. According to the mode of inhibition different profiles can be seen with the Lineweaver-Burk plot as shown in **Figure 36**.

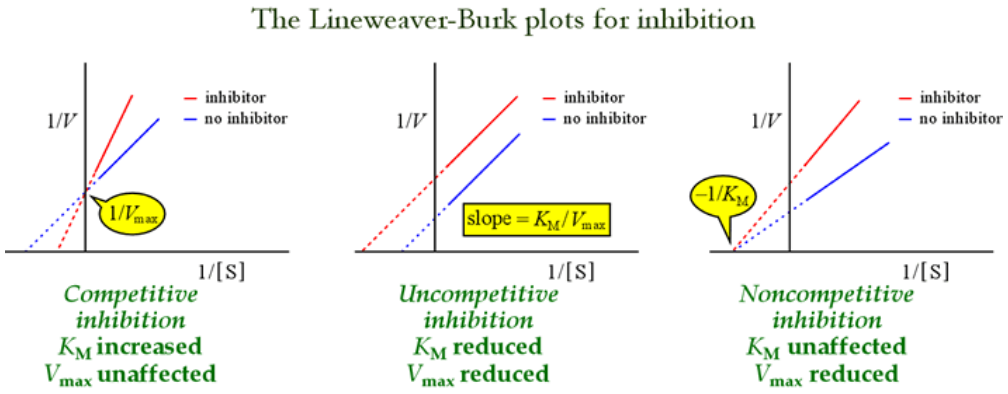

Figure 36: Lineweaver-Burk plot profile for different inhibition process.[54]

Competitive inhibition occurs when the natural substrate and the inhibitor compete to access the active site of an enzyme.[55] This mode of inhibition does not affect the maximum velocity V_{max} and increases the Michaelis-Menten constant K_m. In our case, this would be the profile if our compound was competing with ATP. Non-competitive inhibition occurs when the substrate and the inhibitor do not compete to access the active site as the inhibitor interacts with a different site and reduces the activity of the enzyme without disturbing binding of the substrate.[55] This mode of inhibition does not affect K_m and reduces V_{max}. Finally, uncompetitive inhibition occurs when the inhibitor binds to the enzyme-substrate complex.[56] This inhibition results in reduced values for K_m and V_{max}.

- Results for hits

C10 was the inhibitor that was chosen for the kinetic study of DYRK2 as it showed higher binding affinity towards the protein target. This was performed with five different concentrations of the inhibitor for eight different ATP concentrations. With the results from this study, saturation plots were drawn and the following data was obtained (**Table 1**).

Table 1: Kinetic parameters obtained from the curve plots.

C10 [Conc] µM	V_{max} µM.s^{-1}	K_m µM
0	0.1778	4.002
0.1	0.1506	7.583
1	0.1435	21.70
2.5	0.1153	41.34
5	0.0468	20.95
10	0.0429	24.02

This data shows that K_m increases whilst increasing the concentration of the inhibitor whereas V_{max} decreases. Moreover, K_m decreases again once the concentration of the inhibitor is above 5 µM whereas V_{max} remains the same. This experimental data has shown that **C10** seems to be a mixed inhibitor and therefore could potentially be involved in an allosteric mechanism with DYRK2. This project describes the process by which we attempted to validate this (see section **IV** in this Chapter).

c. Biochemical assay

In order to improve the throughput of compound assessment for the molecules synthesized, rather than use the in-house method using the Cyclex kit (both expensive and labour-intensive), we performed an initial screen using the DSF protocol (section **6a** in this Chapter). Our most promising compounds were then sent to Life Technologies (LT), a CRO that specializes in kinase assays, amongst other products and services.

- Lanthascreen assay for DYRK2.

For the DYRK2 kinase a Lanthascreen kinase binding assay was used on our analogues.

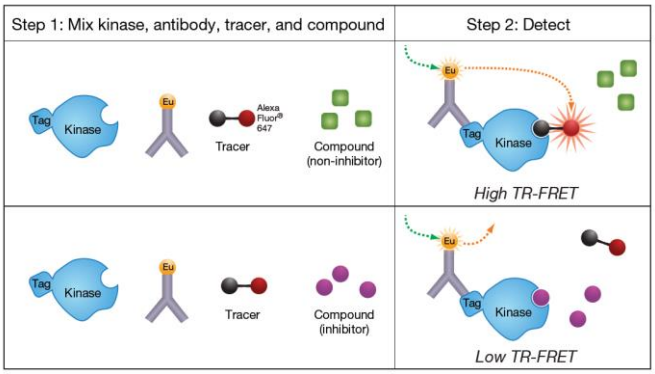

Figure 37: Schematic representation of Lanthascreen binding assay.

This assay is a quick and easy method to assess the binding affinity of a compound to its protein target. The assay works by mixing the kinase that recognises the europium labelled anti-tag antibody, an ATP competitive tracer that is detected by the antibody and the compound of interest, **Figure 37**. When the compound does not inhibit the protein a high TR-FRET is observed. In contrast, when the compound is competing and displacing the tracer a loss of the TR-FRET is observed. From this description one would think that this assay would only be useful for ATP-competitive (Type I) inhibitors. Accordingly, Invitrogen tested the ability of this Lanthascreen assay to see if the assay could detect Type III inhibitors. They have found that the results from this assay and the reported activity assay results matched.[57] It was therefore decided that we would use this assay to determine the binding affinity of our compounds for DYRK2.

Only this assay was available for the protein target DYRK2.

- Z'Lyte assay for DYRK1A

For the DYRK1A kinase, Life Technologies use a different type of assay: Z'LYTE, **Figure 38**. This biochemical assay is based on a fluorescence tag and the difference in sensitivity between phosphorylated and non-phosphorylated proteins to cleavage.

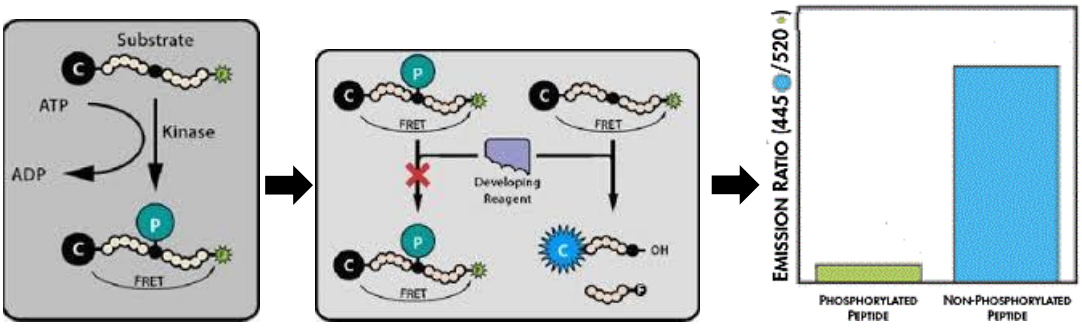

Figure 38: Schematic representation of Z'LYTE assay.

The first step is the reaction of the FRET-protein with ATP and the substrate of interest. After the reaction in solution there is ADP, the phosphorylated FRET-protein as well as some non-phosphorylated FRET-protein. The next step consists of adding a developing agent which is a protease that recognises and cleaves non-phosphorylated FRET-proteins. When cleavage occurs this disrupts the FRET between the donor (coumarin) and the fluorophore (fluorescein) due to the presence of two distinct protein sequences. In contrast, the phosphorylated protein still conserves FRET. The solution is then excited at 400 nm and an emission ratio is determined, **Equation 2**.

$$Emission\ ratio = \frac{Coumarin\ emission\ (445\ nm)}{Fluorescein\ (520\ nm)}$$

Equation 2: Emission ratio equation.

The cleaved and uncleaved FRET-proteins both contribute to the fluorescence signals. In order to determine the relative extent of phosphorylation the emission ratio (ER) is calculated. The lower the ER the less active the substrate (phosphorylated FRET-protein in high concentration indicates no kinase inhibition) and the higher the ER the more active the compound (non-phosphorylated FRET-protein in high concentration indicates kinase inhibition). After some calculations it is possible to determine the % inhibition of the substrate of interest.

This assay was used for all analogues tested against DYRK1A to establish whether they were selective for DYRK2.

IV. Summary

Protein kinases play a pivotal role in cellular signal transduction (*e.g.* cellular growth and apoptosis among other functions) which make them interesting targets in drug discovery. Unfortunately, due to the fact that ATP is the natural substrate for all 518 kinases it can prove difficult to gain selectivity while targeting the orthosteric pocket. Allosteric modulators of kinases could enable the regulation of protein function by binding to a site distinct from the ATP site. Therefore, by generating an allosteric inhibitor greater selectivity could be achieved and hence less side effects potentially observed. However, no definitive technique has been established to identify allosteric sites and use this to generate an allosteric modulator. Providing a model which enables the identification of these sites could revolutionize drug discovery.

V. Project aims

The project aims were two-fold:

- Establish whether Al-Shar'i, had identified an allosteric pocket in DYRK2 by synthesizing analogues of the initial Maybridge hit **C10** to generate a structure-activity relationship (SAR) for the binding site.
- Generate a potent and selective inhibitor of DYRK2 that could be used to probe its biological function (in comparison with DYRK1A), and potentially form the basis of a DYRK2 drug discovery programme.

Analogues of compound **C10** would be synthesized and optimized for potency by initially testing in our DSF assay to determine if they stabilize DYRK2. If so, they would then be tested in the Lanthascreen assay at a single point concentration (1 μM) to see if they inhibited DYRK2. If the compound showed over 40% inhibition at 1 μM, a full IC_{50} curve would be determined. If the compound was potent (< 100 nM), it would be assessed for selectivity over DYRK1A, and a kinetic analysis performed to establish whether the mode of inhibition was competitive or not. Ultimitaley, we would only be able to establish whether our most active compound inhibited *via* an allosteric

mechanism using the pocket predicted by Al-Shar'i by obtaining a crystal structure of the compound bound to the protein.

Chapter 2: Oxyamidine pyrazole series

I. C10 Hit

1. Synthesis

Pyrazole oxyamidine **C10**, **Figure 39**, was purchased from Maybridge and used for kinetic studies. It was not analysed for purity or confirmation of structure prior to biological evaluation. Therefore, it was decided that **C10** would be synthesized and biological evaluation carried out. It was hoped that this would provide us with a genuine hit molecule that could be used as a starting point for probe development.

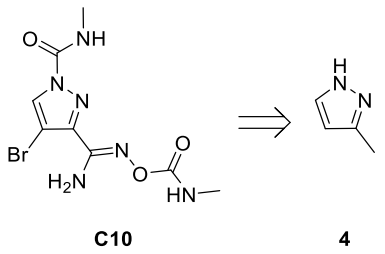

Figure 39: Pyrazole hit.

The structure of **C10** is unusual with the compound possessing a number of heteroatoms, intriguing functionalities and few hydrogen atoms. Our initial thoughts for the synthesis of **C10**, was to start with methyl pyrazole **4**, **Figure 39**. Oxidation of **4** would lead to carboxylic acid **5** which could then be brominated to give **6**. Formation of the primary amide **7**, followed by dehydration would lead to nitrile **8** which could then be treated with hydroxylamine to afford oxyamidine **9**. Finally **C10** would be generated from **9** using a methyl isocyanate derivative, **Scheme 2**.

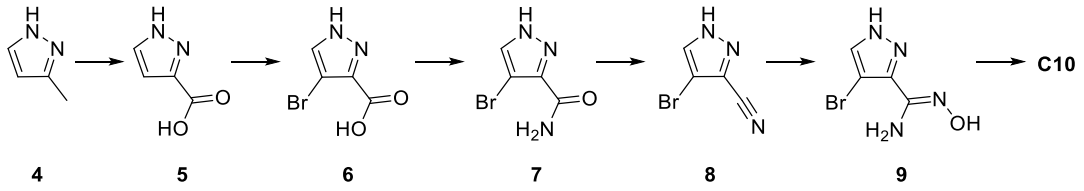

Scheme 2: Forward synthesis of C10.

Based upon this forward synthesis, we began by oxidising 3-methyl pyrazole **4** with potassium permanganate in water at reflux for 67 h. No purification was needed as the

product crystallised upon addition of HCl (pH = 2) at 0 °C. This proceeded smoothly and afforded carboxylic acid **5** in 51% yield, **Scheme 3**.[58] Traces of starting material were observed in the water layer, as well as some product by LC/MS, indicating an incomplete oxidation reaction and recovery of product. Adding more equivalents of oxidant could potentially push the reaction further but this optimization was not carried out.

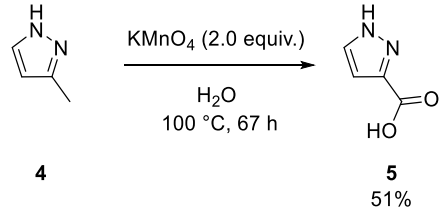

Scheme 3: Pyrazole 4 to carboxylic acid 5.

For the bromination of **5** our first thought was to use *N*-bromosuccinimide (NBS) in slight excess, **Scheme 4**.[59] The isolation of brominated compound **6** proved to be quite tricky, as traces of succinimide **10** were still present after purification by column chromatography.

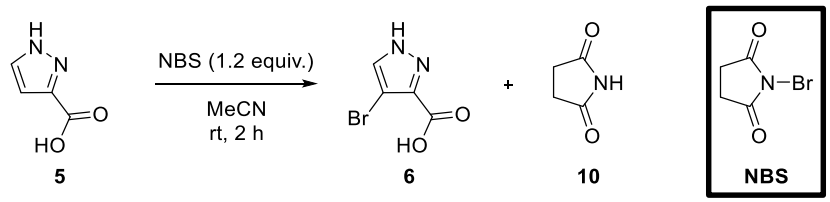

Scheme 4: Bromination of carboxylic acid 5 with NBS.

Performed on a large scale, the reaction mixture was filtered removing excess succinimide **10** and concentrating the filtrate gave the crude bromide **6**. This was divided into four portions in order to test different isolation processes to eliminate co-product **10**. For the first batch, the crude was dissolved in diethyl ether and washed with water. The second batch was dissolved in ethyl acetate and again washed with water. The third batch was dissolved in diethyl ether and the organic layer was treated with a 1 M NaOH solution. The aqueous phase was then treated with 1 M HCl solution and the compound extracted with diethyl ether. Finally, the fourth batch was dissolved in water and the compound extracted with ethyl acetate. The organic layer was then

washed with 1 M HCl solution. Unfortunately none of these techniques resolved the problem and traces of **10** were present in each sample.

Therefore, different conditions were examined for the bromination. Compound **5** was treated with bromine in acetic acid for 16 hours at room temperature and brominated acid **6** was isolated cleanly after work up in 61% yield, **Scheme 5**.[60]

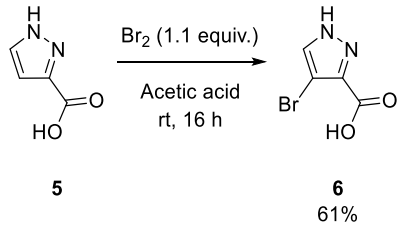

Scheme 5: Bromination of 5 with bromine.

The next step was the isolation of intermediate **7** before dehydration to nitrile **8**. The acid chloride was obtained by heating **6** in neat thionyl chloride for 3 hours at 90 °C before removal of excess thionyl chloride under reduced pressure. This crude intermediate was then treated with an ammonia solution (0.4 M) in THF at room temperature for 18 h to afford primary amide **7** in 84% yield after removal of solvent and excess ammonia.[61] Dehydration of **7** was performed by treatment with phosphorus oxychloride in anhydrous acetonitrile in the presence of sodium chloride for 19 hours at 80 °C.[62] Nitrile **8** was isolated by column chromatography in 74% yield, **Scheme 6**.

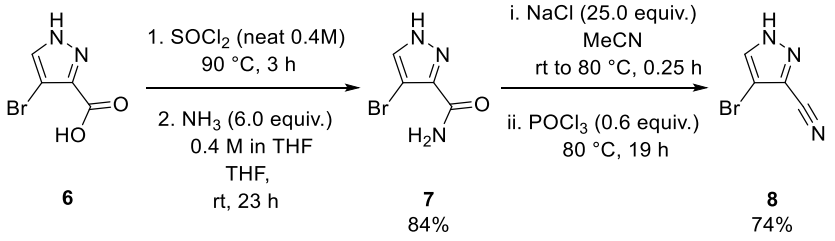

Scheme 6: Preparation of nitrile 8 from carboxylic acid 6.

Nitrile **8** was further treated with hydroxylamine hydrochloride under basic conditions in water at 70 °C for 22 hours, **Scheme 7**.[63] After work-up, oxyamidine **9** was isolated in 80% without the need for further purification.

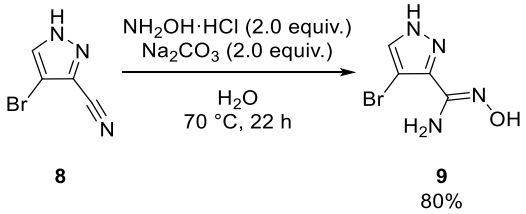

Scheme 7: Formation of oxyamidine 9.

Methyl isocyanate **11** could be used to introduce the desired carbamate/urea functionality of **C10**. However, due to its toxicity a substitute for methyl isocyanate was sought. Duspara *et. al.* reported that the methylamine adduct of 1,1-carbonyldiimidazole (CDI) **12** could serve as a suitable substitute for **11**, **Figure 40**.[64]

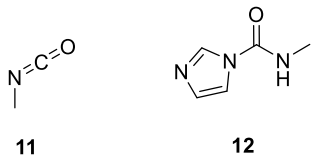

Figure 40: Methyl isocyanate 33 and a substitute 34.

Therefore, it was necessary to synthesize **12.** The reaction of CDI **13** with methylamine hydrochloride in a 3:1 MeCN:DMF solution for 2.5 hours at room temperature afforded **12** in 88% yield after column chromatography, **Scheme 8**.[64]

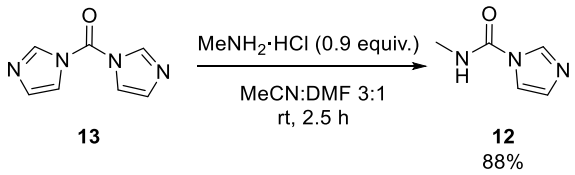

Scheme 8: Synthesis of substitute 12.

It was hoped that the final two functionalities of **C10** could be installed in a one-pot procedure. The reaction was performed by following the method of Duspara, by reacting oxyamidine **9** with **12** in CH_2Cl_2 in the presence of Et_3N for 18 hours at room temperature, **Scheme 9**.[64]

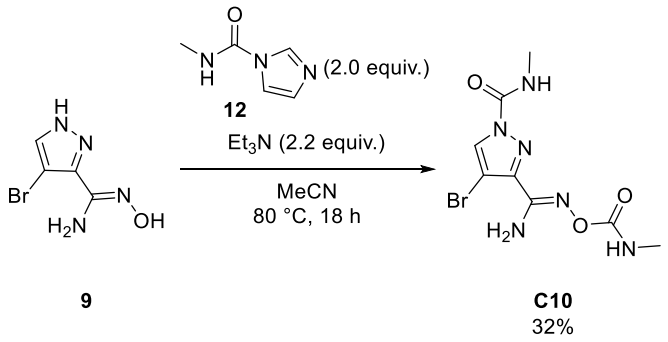

Scheme 9: Last step in the synthesis of C10.

The reaction was followed by LC/MS and did not go to completion; an intermediate, with only one methyl isocyanate equivalent, and the product could be observed. Carbamoylimidazole substitutes for isocyanates have been shown to react at elevated temperatures with less reactive nucleophiles.[65] Therefore, the reaction was repeated in MeCN at 80 °C for 18 h. **C10** was isolated in 32% yield after two columns, which were necessary due to the presence of unidentified impurities that had similar affinities to silica, **Scheme 9**.

2. Analysis

To confirm the structure of **C10**, crystals were grown by vapour diffusion in MeOH and petroleum ether (PE) for X-ray analysis (**Figure 41**).

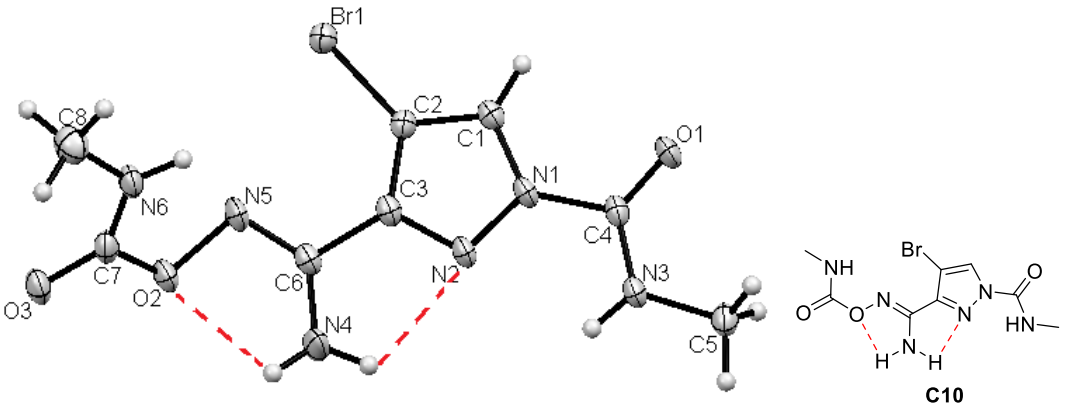

Figure 41: X-ray structure of pyrazole C10 and ChemDraw representation.

The X-ray structure confirmed that pyrazole **C10** was indeed isolated and had an extended conformation in the solid-state, **Figure 41**. In this conformation, the two protons from the primary amine were hydrogen bonding with the nitrogen from the

pyrazole ring and with the oxygen of the oxyamidine functionality. We also observed the *trans* configuration of the oxyamidine moiety.

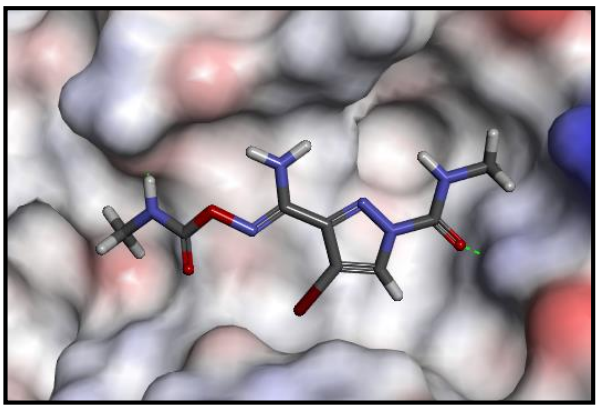

Figure 42: C10 predicted docked pose with GOLD in the putative allosteric pocket.

Figure 42, shows the highest Gold scoring pose in the putative allosteric site. Two hydrogen bonding interactions can be observed in the predictive model between the carbonyl of the urea functionality with Arg 88 and the hydrogen from the amide functionality with Ser 44. This predicted docked pose had a similar conformation to the X-ray structure obtained for the free ligand.

3. DSF results

All the analogues synthesized in this thesis were screened in a DSF assay against DYRK1A and DYRK2 at the Structural Genomics Consortium (SGC) in Oxford. The assay was run more than twice (unless otherwise stated) at a final concentration of 10 µM with DYRK2 and 100 µM with DYRK1A for each compound. The difference in concentration between the two protein kinases was to see if at higher concentration stabilization could be observed for DYRK1A. It has been shown that the stabilizing effect of compounds upon binding is proportional to the concentration of the ligand.[46] The results shown are an average of all runs.

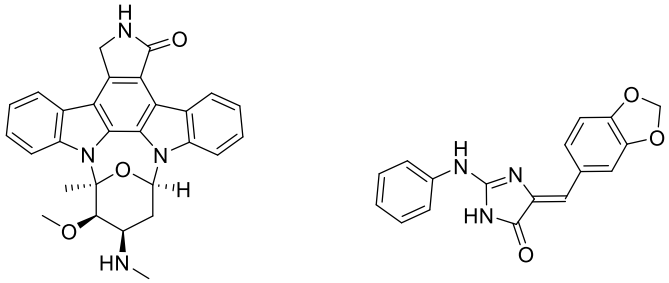

Figure 43: Staurosporine and L41.

The assay was screened against two references: staurosporine and **L41** (**Figure 43**). Staurosporine is a well-known natural product that is an ATP-competitive kinase inhibitor which binds to many kinases with high affinity and little selectivity.[66] **L41** is a known non-selective competitive inhibitor of DYRK2 and DYRK1A previously described (**Figure 22**).[12]

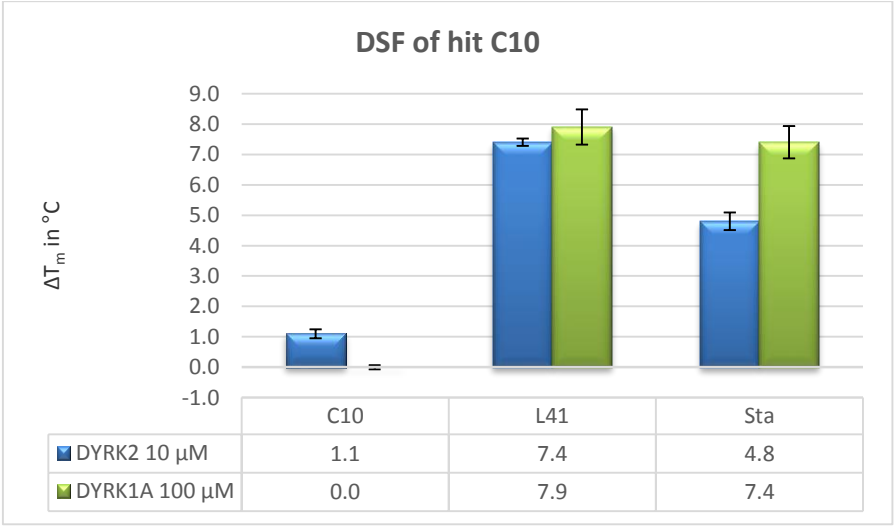

Graph 1: Bar graph representation of the T_m of compounds C10, L41 and staurosporine against DRYK2 and DYRK1A.

Graph 1 represents the T_m of hit compound **C10**, staurosporine and **L41** for DYRK2 and DYRK1A with the error bar associate to each compound. From this graph we can see that our two references, staurosporine and **L41**, have a high T_m and are both non-selective for the two DYRK isoforms. Compound **C10** showed a T_m of 1.1 °C for DYRK2. This T_m for **C10** was less than when the compound was first screened originally. This is likely due to the screening procedure being different with regards to

concentration. Nonetheless, these results were very encouraging, as they showed an encouraging degree of selectivity towards DYRK2 over DYRK1A.

4. Biochemical assay results

The Maybridge sample of **C10** was previously analysed in a dose response assay with a Cyclex kit and gave an IC_{50} = 2.5 µM. We decided to submit our synthetic **C10** to Life Technologies to determine the % displacement at single point concentration for DYRK2 and DYRK1A. We also submitted our reference test compound **L41** in this assay, **Table 2**.

Table 2: % displacement of analogues single point concentration at 1 µM.

	DYRK2	DYRK1A
C10	19 ± 3%	2 ± 0%
L41	101 ± 1%	ND

We can see that **C10** inhibits DYRK2 at 19% at 1 µM and 2% for DYRK1A at the same concentration. We observed selectivity in this assay (although without associated potency) which confirmed our DSF results. **L41** as expected gave full displacement at 1 µM for DYRK2.

The IC_{50} for **L41** was determined for DYRK2 (**Figure 44**) and DYRK1A (**Figure 45**) to act as a reference for our future compounds.

IC50 (nM)	Hillslope	R^2 Value	Conc of Compound (nM)	% Displacement Point 1	% Displacement Point 2
45.0	0.76	0.9904	10000	97	99
45.0	0.76	0.9904	3330	115	112
45.0	0.76	0.9904	1110	117	113
45.0	0.76	0.9904	370	105	109
45.0	0.76	0.9904	123	77	88
45.0	0.76	0.9904	41.2	60	64
45.0	0.76	0.9904	13.7	35	38
45.0	0.76	0.9904	4.57	28	26
45.0	0.76	0.9904	1.52	14	27
45.0	0.76	0.9904	0.500	3	5

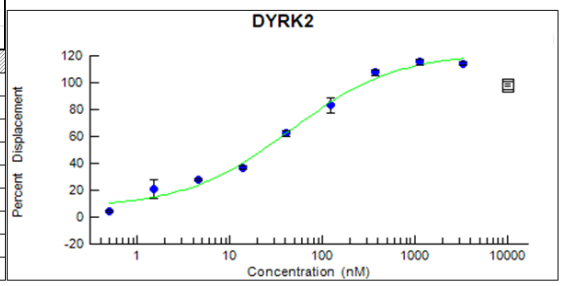

Figure 44: IC_{50} determination for L41 for DYRK2.

L41 displayed an IC_{50} = 45 nM for DYRK2 and IC_{50} = 49 nM for DYRK1A. This showed that our reference compound was non-selective between the two isoforms.

IC50 (nM)	Hillslope	R^2 Value	Conc of Compound (nM)	% Displacement Point 1	% Displacement Point 2
48.7	0.84	0.9942	30000	94	99
48.7	0.84	0.9942	10000	98	101
48.7	0.84	0.9942	3330	99	100
48.7	0.84	0.9942	1110	97	96
48.7	0.84	0.9942	370	86	84
48.7	0.84	0.9942	123	63	64
48.7	0.84	0.9942	41.2	59	43
48.7	0.84	0.9942	13.7	22	27
48.7	0.84	0.9942	4.57	9	10
48.7	0.84	0.9942	1.49	8	4

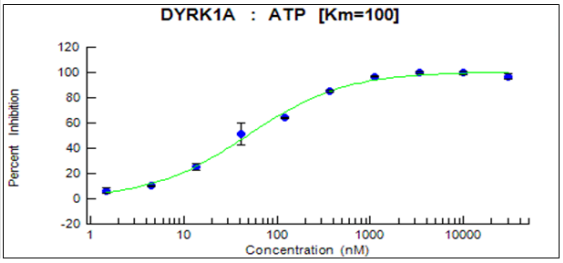

Figure 45: IC_{50} determination for L41 for DYRK1A.

The IC_{50} for **C10** was determined to compare it to all our future results to determine gain in activity if any.

IC50 (nM)	Hillslope	R^2 Value	Conc of Compound (nM)	% Displacement Point 1	% Displacement Point 2
3220	1.33	0.9985	90000	94	93
3220	1.33	0.9985	30000	102	91
3220	1.33	0.9985	10000	78	77
3220	1.33	0.9985	3330	56	49
3220	1.33	0.9985	1110	34	18
3220	1.33	0.9985	370	6	15
3220	1.33	0.9985	123	9	8
3220	1.33	0.9985	41.2	11	12
3220	1.33	0.9985	13.7	10	6
3220	1.33	0.9985	4.50	3	12

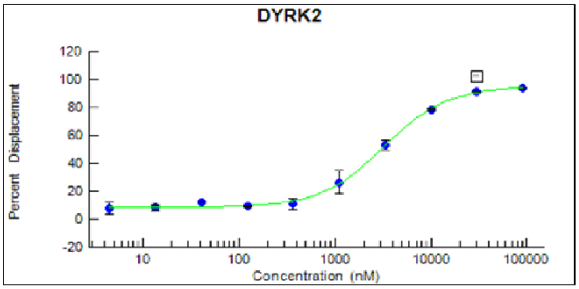

Figure 46: IC_{50} determination for C10.

Figure 46 represents the inhibition curve of **C10** for DYRK2 which gave an IC_{50} = 3.22 µM. The objective now was to generate more active compounds, ideally in the nM region while maintaining the selectivity observed over DYRK1A.

II. C10 SAR analogues

Following on from the promising results seen with **C10**, it was decided that other derivatives would be explored.

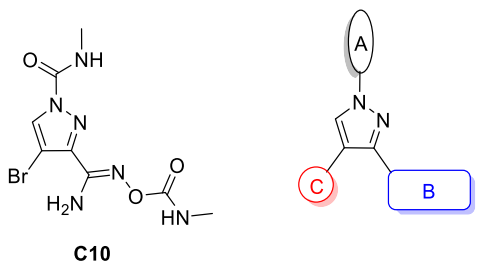

C10

Figure 47: SAR exploration of pyrazole C10.

In order to generate a structure activity relationship (SAR) profile, different moieties at positions A, B and C of the central pyrazole scaffold were explored, as shown in **Figure 47**.

1. **Exploration of Part C**

The first question we sought to answer was the importance of the bromine atom. In order to explore this question, it was decided that the bromine atom would be replaced with a proton and a phenyl group.

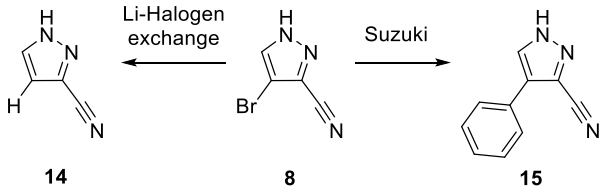

Scheme 10: Proposed synthesis from nitrile intermediate 8: lithium-halogen exchange for intermediate 14 and Suzuki coupling for intermediate 15.

In order to install these functionalities, it was decided that from nitrile **8** the derivatives could be easily accessible by lithium-halogen exchange with a proton source to give intermediate **14** and by a Suzuki coupling for intermediate **15**, **Scheme 10**.

a. **Synthesis of proton analogue 17**

Lithium-halogen exchange can be achieved by the addition of *n*-BuLi followed by a proton source.[67]

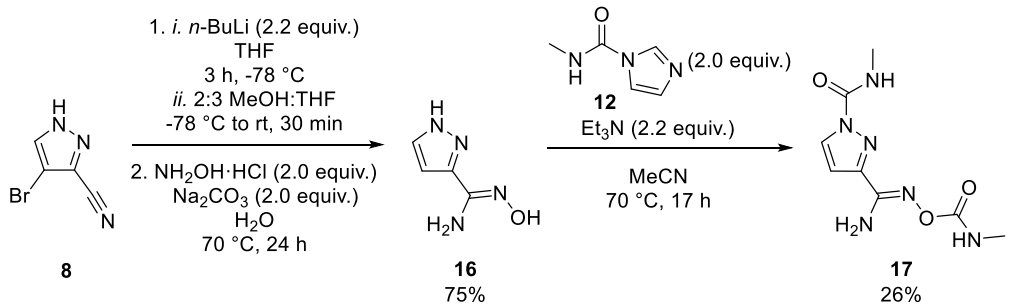

Scheme 11: Synthesis of 17 from nitrile 8.

Nitrile **8** was treated with *n*-BuLi followed by a MeOH:THF solution, which afforded nitrile **14** which was directly treated with hydroxylamine to afford oxyamidine **16** in

75% yield over two steps.[67] The acylation of oxyamidine **16** was achieved under similar conditions to those developed previously to deliver the target compound **17** in 26%, **Scheme 11**. The fairly low yield was due to a tricky purification involving two columns and a recrystallization by vapour diffusion in MeOH with PE. As the crystals were small, it was not possible to get an X-ray structure for analogue **17**.

b. Synthesis of phenyl analogue 20

The Suzuki-Miyaura cross coupling reaction is a well-known method for the formation of a biaryl compound. Numerous conditions have been developed to bring about this procedure with various palladium sources, ligands, solvents, and bases having been reported, **Scheme 12**.

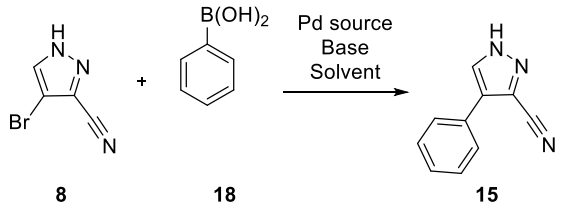

Scheme 12: Synthesis of 15 *via* a Suzuki cross coupling reaction.

A series of different reaction conditions were examined, varying the palladium source, base and solvent, shown in **Table 3**.

Table 3: Conditions tried for Suzuki coupling.

Entry	Pd source	Base (equiv.)	Solvent	Heating	15*
1	$PdCl_2(PPh_3)_2$	Na_2CO_3 (0.7 equiv.)	Toluene	90 °C, 20 h	6%
2	$Pd(dppf)Cl_2$	Cs_2CO_3 (5.5 equiv.)	Dioxane	µW, 140 °C, 0.25 h	0%
3	$Pd(dppf)Cl_2$	Na_2CO_3 (2.2 equiv.)	1:2 H_2O:Dioxane	120 °C, 23 h	51%

*isolated yields

The first attempt, entry **1**, with $PdCl_2(PPh_3)_2$ in the presence of Na_2CO_3 in toluene only provided 6% of the desired product **15**. When using microwave irradiation with $Pd(dppf)Cl_2$ and Cs_2CO_3 in dioxane, entry **2**, only starting material **8** was observed by ^1H NMR spectroscopy.[68] By using $Pd(dppf)Cl_2$ and Na_2CO_3 in 1:2 H_2O:1,4-dioxane at 120 °C overnight, nitrile intermediate **15** was isolated in 51% yield following column chromatography.

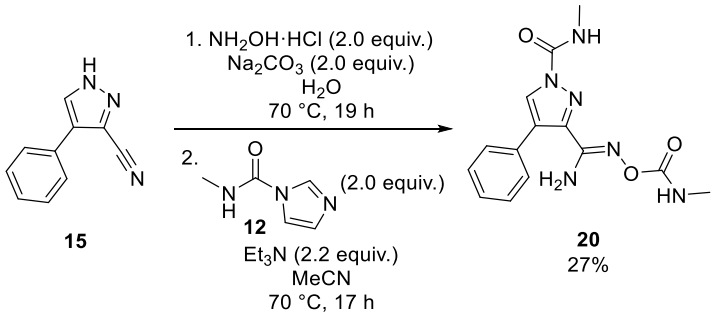

Scheme 13: Synthesis of phenyl derivative 19 from phenyl nitrile 15.

The final steps were carried out as developed previously to afford target compound **20** in 27% yield over two steps, **Scheme 13**.

An X-ray structure was obtained for phenyl derivative **20** by vapour diffusion in MeOH and PE.

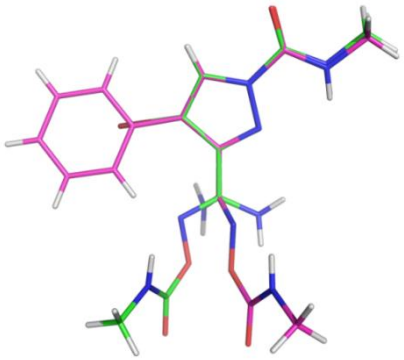

Figure 48: Superimposition of C10 X-ray structure (green) and phenyl derivative 20 (pink) with Pymol.

When superimposing the hit **C10**, in green, and **20**, in pink, we can see that in addition to the phenyl group, the major change in conformation involves the oxyamidine side chain of the molecule, **Figure 48**. It would appear that the bulky phenyl group in **20** disrupts the hydrogen bonding matrix between the amine of the oxyamidine functionality and the pyrazole ring in the solid state.

c. DSF assay

We were interested in exploring a smaller group with **17**, to see if we could still maintain stabilization, and whether the larger Ph group (**20**) would disrupt stabilization

due to a variation in conformation in the solid state and the enforced rotation of a potential hydrogen bonding group with the binding site.

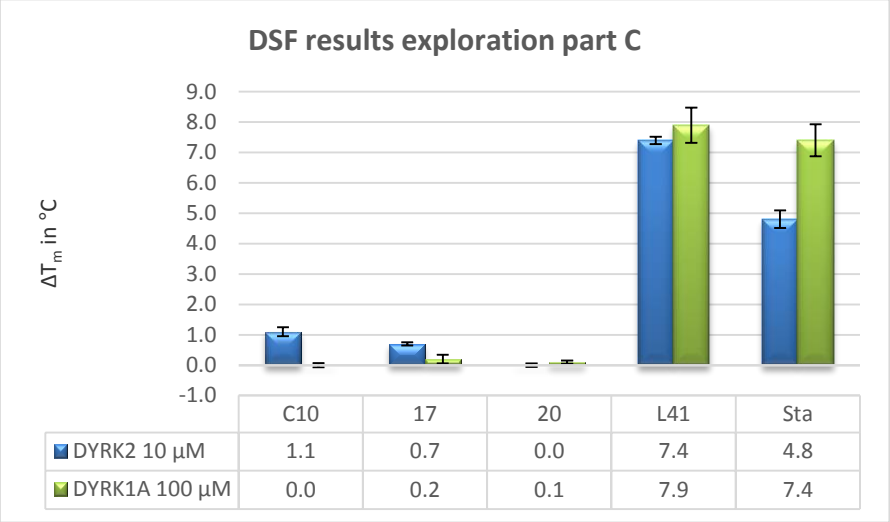

<u>Graph 2:</u> Bar graph representation of the T_m of compounds C10, 17, 20, L41 and staurosporine against DRYK2 and DYRK1A.

Graph 2, represents the T_m observed by DSF assay with the two derivatives **17** and **20**, as well as **C10** and the two references staurosporine and **L41**. These results showed that the bromine did help stabilize the protein. If a phenyl group was present (**20**) the protein was no longer stabilized whereas when it was an unsubstituted (**17**) it displayed some modest stabilization with a T_m of 0.7 °C and selectivity towards DYRK2.

It was decided that all compounds synthesized further on in this Chapter would be docked in the allosteric pocket by using GOLD and Gold score as the scoring function. The protein used was provided by Al-Shar'i which consisted of an average conformation of MD simulation of the protein 3K2L. The advantage was that chemical probe **3g** (see p25) was docked in the putative allosteric site which therefore did not require to indicate coordinates for docking. The author carried out the docking by asking the program to deliver only the three best predicted scoring conformations and analysing them individually. It was observed that sometimes the highest score did not necessarily indicate an optimal conformation of the compound. Therefore, the predicted pose shown throughout this Chapter has been chosen from a set of three to the best judgement of the author.

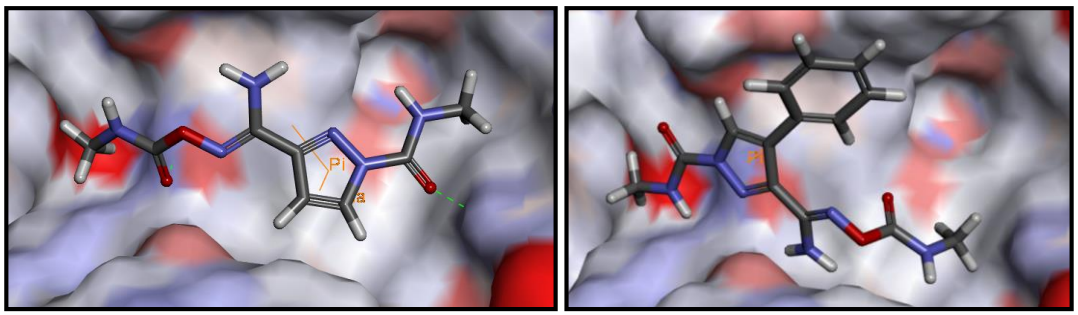

Figure 49: GOLD docked poses of hydrogen derivative 17 and phenyl derivative 20 in the allosteric pocket in Discovery Studio.

When docked in the putative allosteric pocket, **Figure 49**, unsubstituted derivative **17** was predicted to adopt a similar pose to **C10** and picked up two H-bond interactions: the carbonyl from the urea functionality with Arg 88 and the carbonyl from the oxyamidine with Tyr 45. Moreover, two π interactions can be observed regarding the pyrazole ring with Ala 86 as a π-σ interaction and with Tyr 45 as a π-π interaction. On the other hand, phenyl derivative **20**, was predicted to adopt a completely different conformation than the initial hit **C10** and did not pick up any H-bond interaction and only a π-π interaction with Tyr 45. This could be a possible explanation for the fact that this derivative does not stabilize the protein.

It was decided that, for now, the bromine would be kept as part of the structure for the preparation of subsequent analogues.

2. **Exploration of Parts A and B simultaneously**

It was proposed that an easy way to explore both substituents A and B simultaneously, was by reacting a range of acyl chlorides or isocyanates with oxyamidine **9**. This provided a rapid way of gaining some useful SAR data.

a. **Carbamate analogues**

We wanted to keep the carbamate functionality of the initial hit but explore the chain length and steric bulk as well as the necessity of the NH present for protein stabilization.

➢ Synthesis

The carbamate analogues were synthesized by treating oxyamidine **9** with ethyl and isopropyl isocyanate (**Scheme 14**). This gave the desired ethyl **21** and isopropyl **22** carbamates in moderate yields of 42% and 67%, respectively.

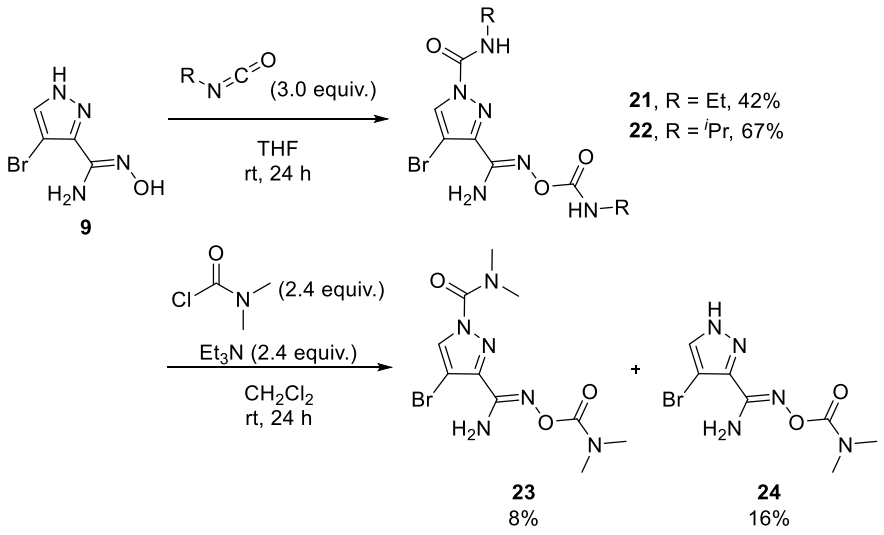

Scheme 14: Synthesis of carbamate analogues 21−24.

For dimethyl analogue **23**, 3.7 equiv. of *N*,*N*-dimethyl carbamoyl chloride was used in CH_2Cl_2 for 24 h. The mono **24** and disubstituted **23** compounds were isolated in 16% and 8%, respectively, as the reaction did not reach completion, **Scheme 14**. However, each product was isolated in sufficient quantity and purity for biological evaluation.

➢ DSF results

These carbamate analogues, **Figure 50**, were synthesised to gain more insight into this pocket, specifically the importance of the NH for hydrogen bonding with compound **23**. We also wanted to see if extending the carbamate chain, **21**, or increasing the steric demand of the ligand, **22**, could be tolerated.

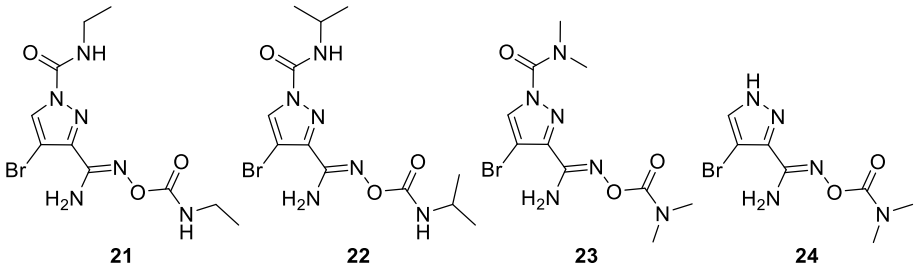

Figure 50: Synthesis of carbamate analogues 21–24.

Graph 3, shows a bar graph of the T_m of these compounds against DYRK2 and DYRK1A.

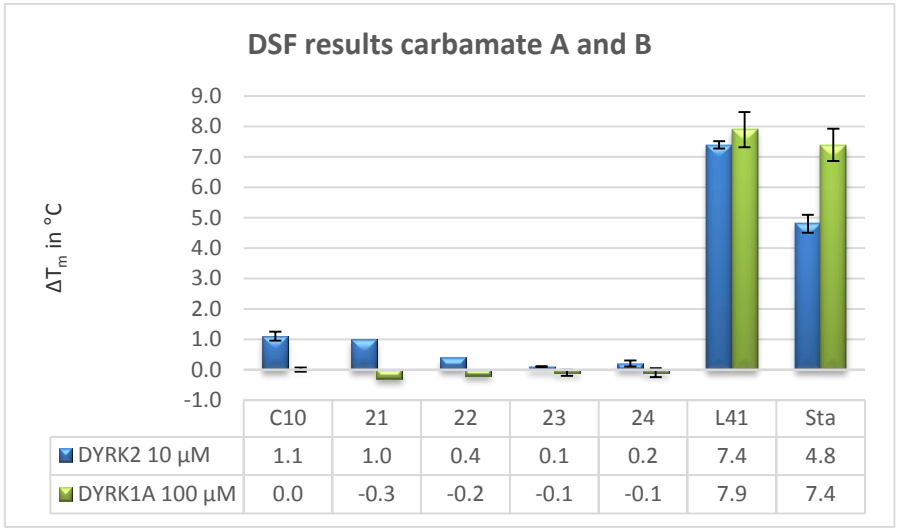

Graph 3: Bar graph representation of the T_m of compounds C10, 21–24, L41 and staurosporine against DRYK2 and DYRK1A.

From the screening, we discovered the importance of the NH group, as both dimethyl derivatives **23** and **24** showed no stabilization. The isopropyl group from **22** appeared too big to be tolerated by the receptor. The ethyl derivative **21** showed a T_m of 1.0 °C, comparable to that of **C10**. No error bars can be observed for analogues **21** and **22** as the assay was only ran once for these compounds. Therefore, it was difficult to consider these results as accurate.

These analogues were docked in the putative allosteric site and compared to hit **C10**.

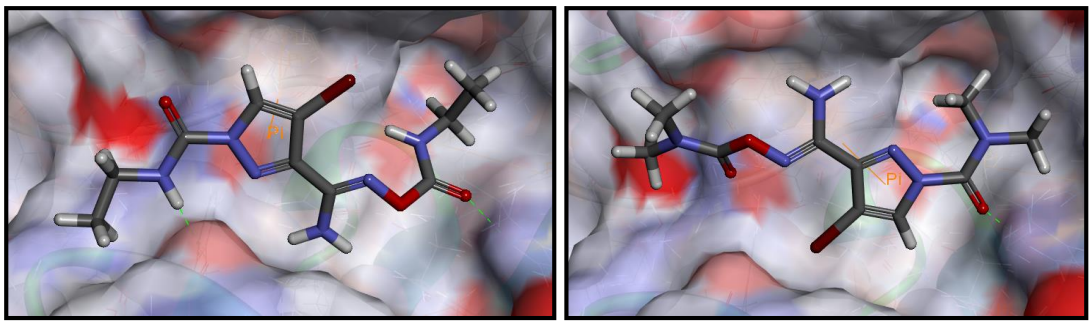

<u>Figure 51:</u> Docked poses of 21 and 23 in the putative allosteric pocket.

Figure 51, represents the predicted poses of ethyl derivative **21** and dimethyl derivative **23**. Surprisingly, **21** was predicted to adopt a different conformation with the oxyamidine moiety now facing the other side of the pocket. Two H-bond interactions were still observed between the NH of the urea with Thr 159 and the oxyamidine carbonyl with Arg 88 as well as a π-π interaction of the pyrazole ring with Tyr 45. As for **23**, a similar pose was envisaged to adopt but this time only the carbonyl group of the urea was involved in H-bonding with Arg 88, as well as a π-π interaction of the pyrazole ring with Tyr 45.

b. Carbonate analogues

We decided to continue to explore the necessity of the carbamate by changing to a carbonate series. The oxygen could be involved in binding through its H-bond acceptor functionality. This would enable us to assess if losing the H-bond donor acceptor of the molecule influences stabilization.

- Synthesis

For the carbonate series, a range of chloroformates available from the laboratory were used to acylate common intermediate **9**.

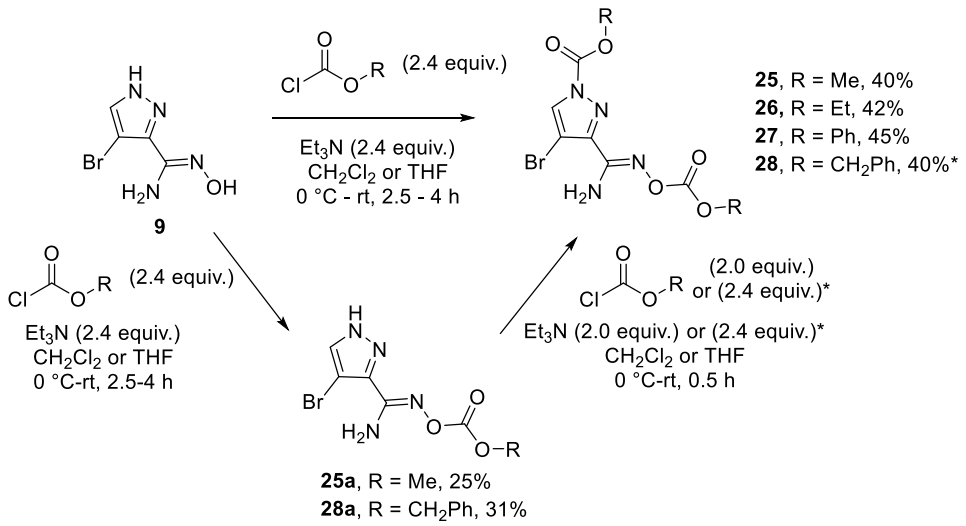

Scheme 15: Acylation of oxyamidine 9 with acyl chlorides.

Oxyamidine **9** was treated with the appropriate chloroformate at 0 °C in the presence of Et_3N to afford desired compounds **26** and **27** in 42% and 45% yield. When treated with methyl and benzyl chloroformate, only the monosubstituted compounds **25a** and **28a** were observed by ^1H NMR under the conditions used. These monosubstituted compounds were isolated and further treated with 2.0 equiv. of the chloroformate to give desired compounds **25** and **28** both in 40% yield, **Scheme 15**.

- DSF results

The carbonate analogues were synthesized in order to explore the pocket, **Figure 52**.

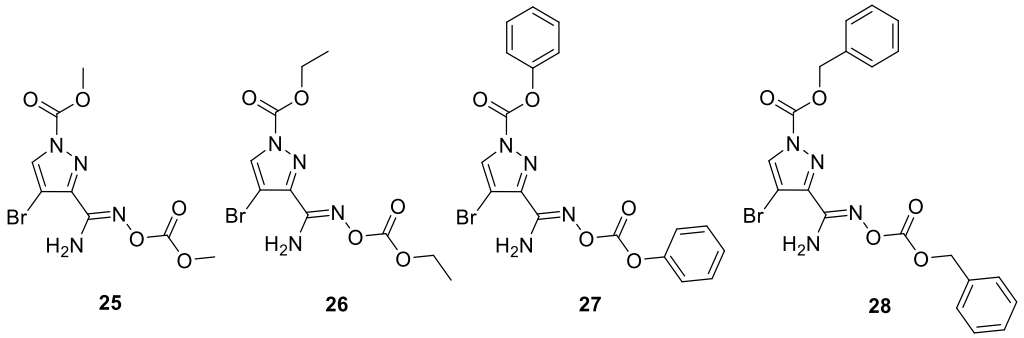

Figure 52: Carbonate analogues synthesized.

Compound **25** was synthesized in order to directly compare with hit **C10** and to see if it was important to have an H-bond donor in both positions. We were also interested in extending the carbonate chain (**26**), as well as having a phenyl ring to increase π-π interactions (**27** and **28**).

Again, the same procedure was undertaken for these derivatives for DYRK1A and DYRK2. **Graph 4**, shows the T_m observed for DYRK1A and DYRK2 for carbonate derivatives **25**–**28**.

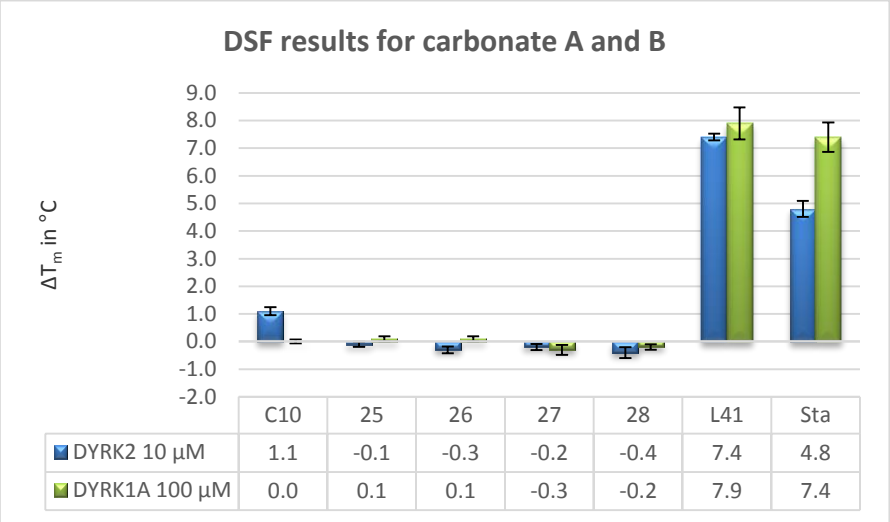

	C10	25	26	27	28	L41	Sta
DYRK2 10 µM	1.1	-0.1	-0.3	-0.2	-0.4	7.4	4.8
DYRK1A 100 µM	0.0	0.1	0.1	-0.3	-0.2	7.9	7.4

<u>Graph 4:</u> Bar graph representation of the T_m of compounds 25–28, L41 and staurosporine against DRYK2 and DYRK1A.

None of the carbonate analogues synthesized stabilized DYRK2 or DYRK1A providing valuable SAR information on our target. It appeared a H-bond donor was necessary at both positions in order for stabilization to occur.

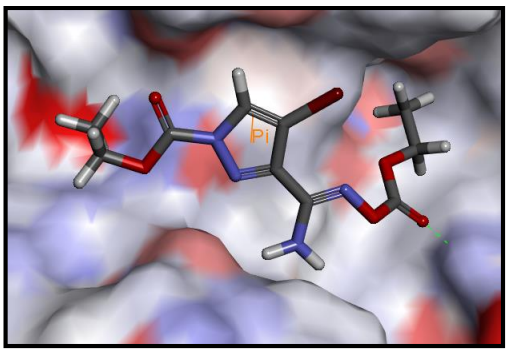

<u>Figure 53:</u> Predicted docked pose of ethyl carbonate 26 in putative allosteric site.

In **Figure 53**, carbonate **26** was predicted to adopt a different conformation in comparison to initial hit **C10**. This only provided one H-bond interaction with Arg 88 through the carbonyl of the carbonate functionality and a π-π interaction with Tyr 45 from the pyrazole ring.

c. **Alkyl and aryl analogues**

To complete the full set of SAR for the exploration of Parts A and B simultaneously, it was decided that we would look into having aryl and alkyl analogues to explore hydrophobic and π interactions. These would again assess the need for H-bond donors in these regions of the molecule

- Synthesis

Compounds **29**–**33** were prepared in moderate yields ranging from 21–54%, by the reaction of **9** with a series of available acyl chlorides in the presence of Et_3N, **Scheme 16**.

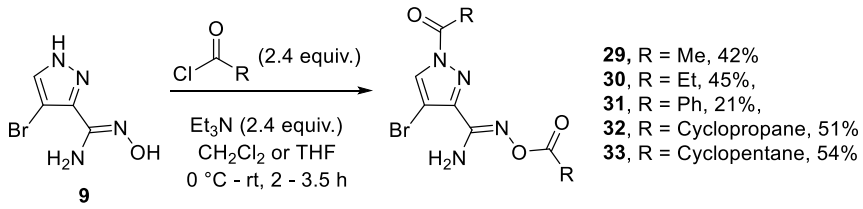

Scheme 16: Acylation conditions used for the synthesis of 29–33.

- DSF results

Figure 54 shows the acylated analogues **29**–**33** that were isolated from the available acyl chlorides, for our DSF assay.

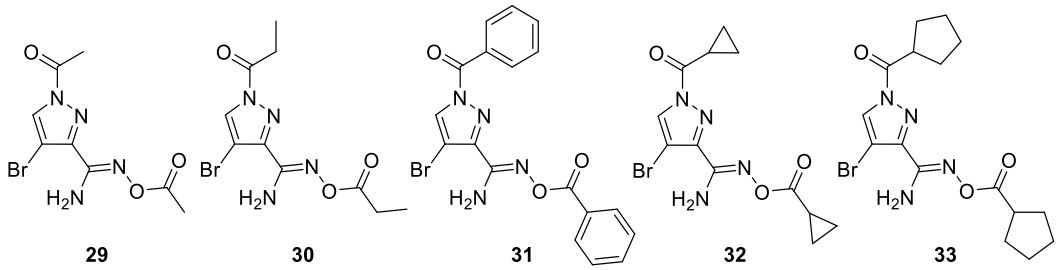

Figure 54: Acylated compounds 29–33.

Analogue **30** would help us compare with the initial hit **C10** and see if having an alkyl chain is sufficient to maintain stability. A shorter chain with methyl analogue **29** was also explored. We were also intrigued by how enhancing 3-dimensional shape of our compound through the presence of cyclopropane **32** and cyclopentane **33** moieties would influence protein stabilization. Finally, we wanted to have an analogue with a phenyl ring to increase potential π-π stacking (analogue **31**).

Graph 5, shows the T_m observed for DYRK1A and DYRK2 for derivatives **29**–**33**.

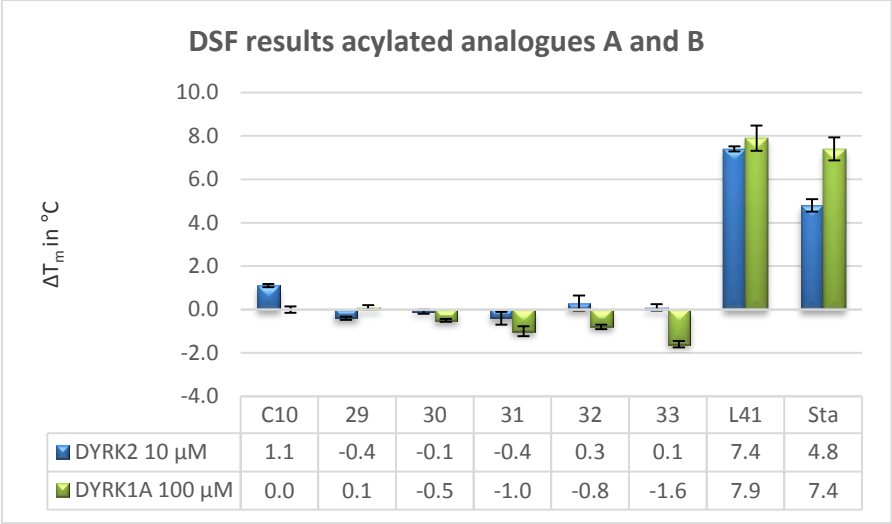

	C10	29	30	31	32	33	L41	Sta
DYRK2 10 µM	1.1	-0.4	-0.1	-0.4	0.3	0.1	7.4	4.8
DYRK1A 100 µM	0.0	0.1	-0.5	-1.0	-0.8	-1.6	7.9	7.4

<u>Graph 5:</u> Bar graph representation of the T_m of compounds 29–33, L41 and staurosporine against DRYK2 and DYRK1A.

None of the compounds, **29**–**33**, showed any stabilization of DYRK2 or DYRK1A, again underlying the importance of the H-bond donor of NH at these positions for stabilization.

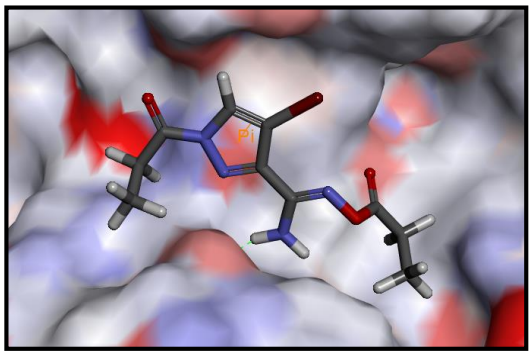

<u>Figure 55:</u> Predicted docked pose of ethyl analogue 30 in the putative allosteric site.

When ethyl analogue **30** was docked in the putative site, **Figure 55**, no H-bonding was predicted, only interaction arising from the usual π-π interaction with Tyr 45. This might provide a possible reason for the complete loss in stabilization for DYRK2 with these analogues.

In summary, exploration of Parts A and B simultaneously showed that none of the derivatives stabilized the protein to a greater extent than **C10**. This indicated the necessity of one or two H-bond donors with NH for stabilization.

3. **Exploration of Part B**

With the previous results in mind, it was decided that we would first only vary Part B and keep the urea functionality in Part A constant, **Figure 47**. This was explored with various alkyl, aryl, and carbamate groups.

a. **Alkyl exploration**

Our initial synthesis consisted of acylating nitrile **8** prior to forming oxyamidine **34**. This would give a common intermediate that could then be diversified at a late stage, **Scheme 17**.

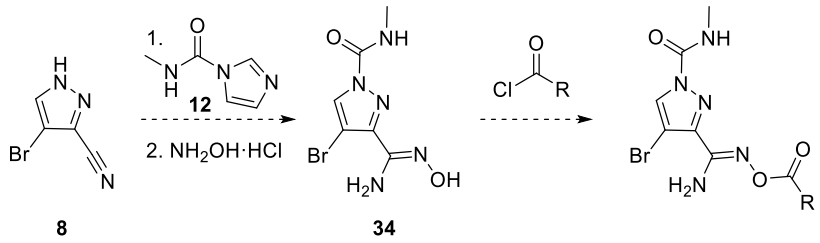

Scheme 17: Initial synthesis plan.

Nitrile **8** was acylated with compound **12** to give the desired nitrile **35** in 39% yield, which was then treated with hydroxylamine and sodium carbonate to give oxyamidine **34** in 47% yield. We were also able to isolate the nitrile **8** in a 20% yield resulting from the urea being cleaved under basic conditions, **Scheme 18**. The oxyamidine intermediate **34** was then treated with ethyl chloroformate to get compound **36** (27%) and propionyl chloride to prepare compound **37** (27%).

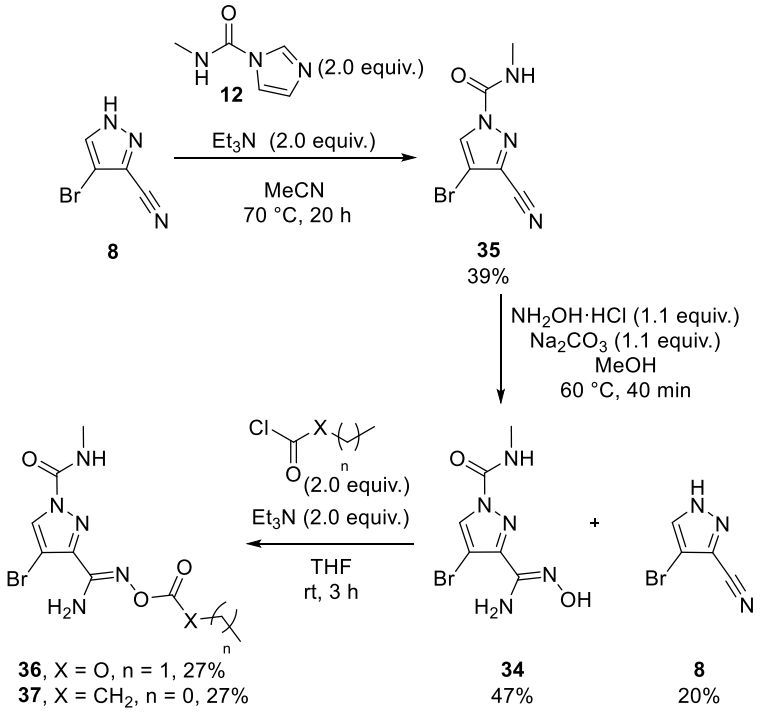

Scheme 18: Initial synthesis of compounds 36 and 37.

Our first synthetic strategy had shown some disadvantages: low yields and formation of nitrile **8** as an unwanted co-product. For these reasons, an alternative route was explored.

- Second synthesis

The second strategy involved coupling oxyamidine **9** with the desired carboxylic acid in the presence of PyBOP and Hünig's base (*N*,*N*-diispropylethylamine) followed by acylation with **12**. It was thought that this could be performed in a one-pot two-step procedure to save both time and effort, **Scheme 19**.

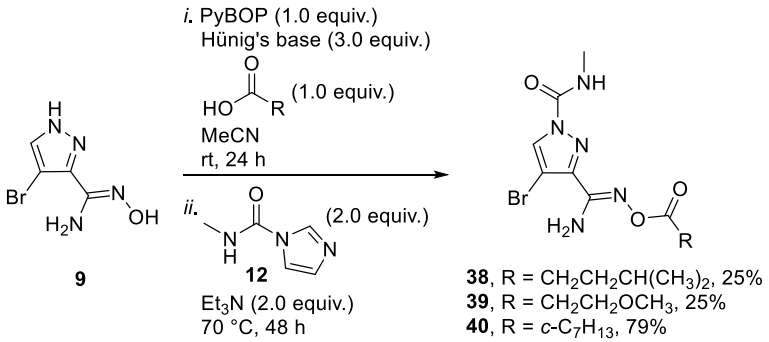

Scheme 19: One-pot two-step synthesis.

Oxyamidine **9** was treated with PyBOP and carboxylic acid in the presence of Hünig's base for 24 hours at room temperature. After that time, compound **12** and Et_3N were then added and the reaction left to stir for 48 h at 70 °C. This gave the desired analogues **38–40** in yields ranging from 25–79% after purification by column chromatography.

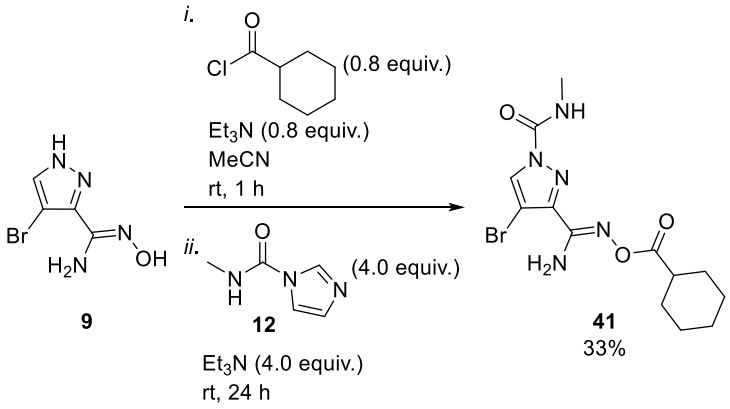

<u>Scheme 20:</u> Synthesis conditions for analogue 40.

For cyclohexyl derivative **41**, a different approach was used to synthesize it as only the carbonyl chloride was available in house. Therefore, oxyamidine **9** was treated with 0.8 equiv. of the desired carbonyl chloride in the presence of Et_3N for 1 hour before adding **12** and Et_3N and stirring for a further 24 hours at room temperature. The reaction enabled the isolation of cyclohexyl analogue **41** in 33% yield, **Scheme 20**.

- DSF results

The alkyl derivatives prepared were submitted to the DSF assay, **Figure 56**.

The importance of the carbamate functionality was explored with the preparation of derivative **37**. In addition, a longer alkyl chain was explored to determine if the ligand could establish any hydrophobic interactions further away in the pocket with derivative **38**. Adding a methoxy group at the end of an alkyl chain with derivative **39** was also explored for a potential H-bond interaction. A carbonate derivative **36** was prepared as the oxygen could provide an extra interaction due to its H-bond acceptor character. Derivatives **36** and **37** could be compared directly with compounds **26** and **30** and would underline the importance of the urea functionality on that side of the ligand. Moreover, we wanted to add more shape to our analogue by having cyclic alkyls with a 6- (**40**) and 7- (**41**) membered ring.

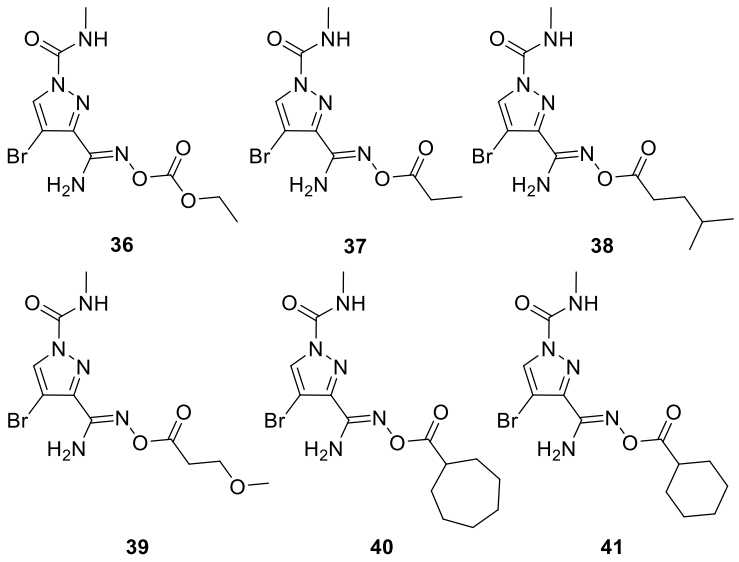

Figure 56: Alkyl analogues 36–41 synthesized.

The alkyl derivatives **36**–**41** were submitted to the DSF assay with the results represented in **Graph 6**.

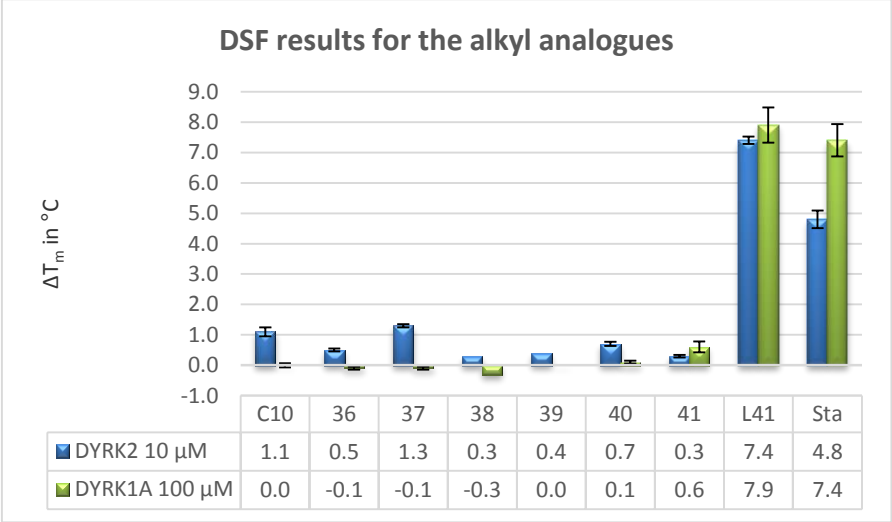

Graph 6: Bar graph representation of the T_m of compounds 36–41, L41 and staurosporine against DRYK2 and DYRK1A.

Of all the alkyl analogues synthesized, **37** was the only compound that showed a similar shift to **C10** in this series with a shift of 1.3 °C. This again suggested that the carbamate at the end of the oxyamidine functionality was not essential for stabilization, however the urea functionality was important. Carbonate **36**, as well as alkyl derivatives **38**−**41**, showed no significant stabilization of DYRK2.

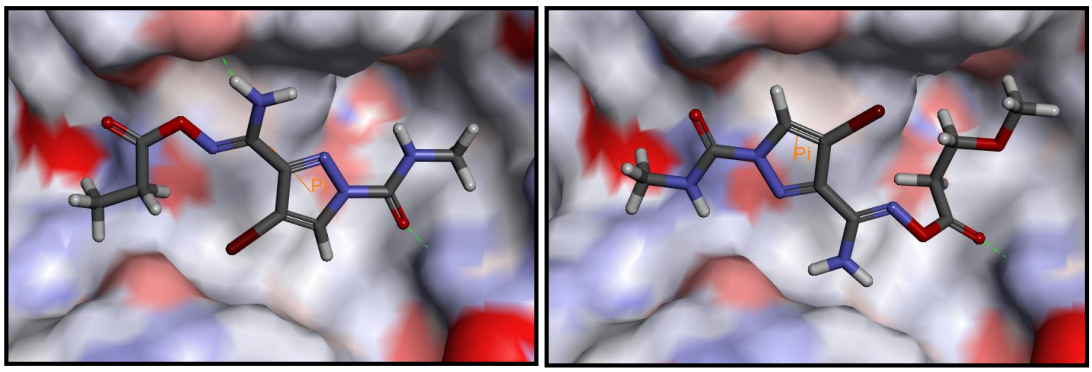

<u>Figure 57:</u> Predicted docked poses of 37 and 39 in the putative allosteric site.

When docked in the allosteric site, **Figure 57**, **37** was predicted to adopt a similar pose to **C10** with two H-bond interactions between the amine and Ser 44 as well as the carbonyl group and Arg 88. A π-π interaction was alos predicted between the pyrazole ring and Tyr 45. In contrast, **39** was predicted to adopt a different conformation to **C10** which suggested only one H-bond interaction with the carbonyl group and Arg 88 was possible.

b. **Aryl analogues**

- First synthesis

In a similar way to the alkyl derivatives, we first tried to synthesize these analogues by reacting oxyamidine **34** with PyBOP and the desired carboxylic acid in the presence of Hünig's base at room temperature, **Scheme 21**.

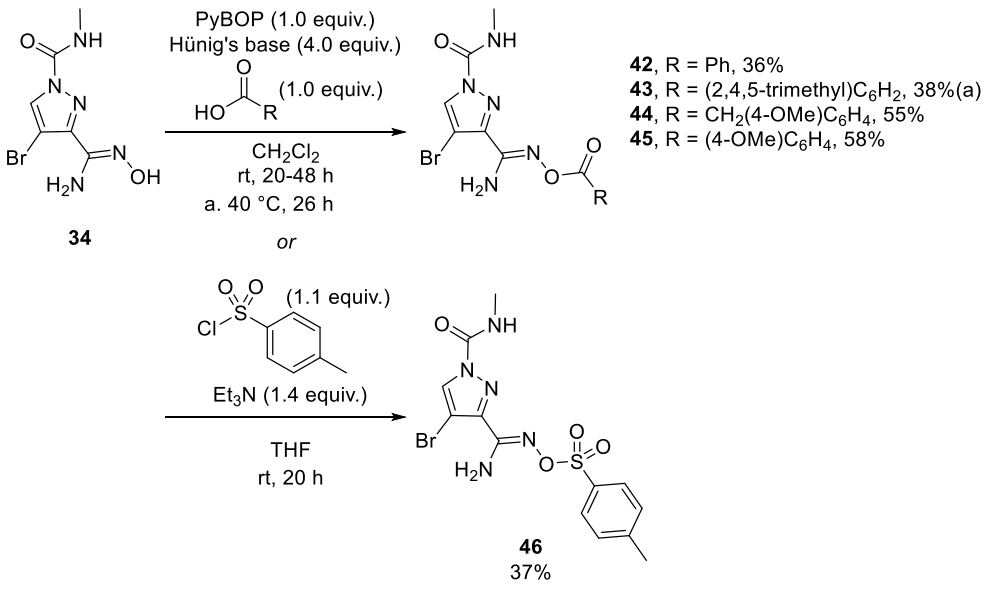

<u>Scheme 21:</u> Synthesis for aryl analogues 42–46.

This gave the desired hits **42**–**45** in moderate yields ranging from 36–58%. For analogue **43**, due to the steric hindrance of the trimethylphenyl group, heat was required to get the reaction to go to completion and the compound was isolated in 38%. We also reacted **34** with *p*-toluenesulfonyl chloride in the presence of Et_3N to access sulfone derivative **46** in 37% yield. This synthesis had similar drawbacks to those observed previously so it was decided to examine the one-pot two step synthesis.

- Second synthesis

In a similar way to the alkyl derivatives, oxyamidine **9** was treated with PyBOP and the desired carboxylic acid in the presence of Hünig's base for 24 hours. Compound **12** was then added in the presence of Et_3N and stirred for 48 h at 70 °C. The aryl derivatives **47**–**51** were successfully isolated in 17–50% yields, **Scheme 22**.

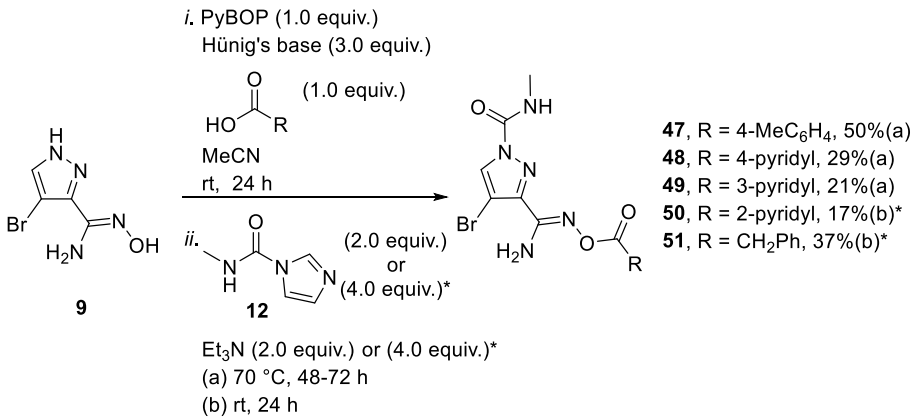

Scheme 22: PyBOP coupling followed by acylation of oxyamidine 9.

As we only had the acyl chlorides for certain derivatives in house, we decided to couple them with oxyamidine **9** in slight excess in the presence of Et_3N for 1 hour before adding **12** with Et_3N. They were isolated in moderate yields from 33−46% for derivatives **52**−**55**, **Scheme 23**.

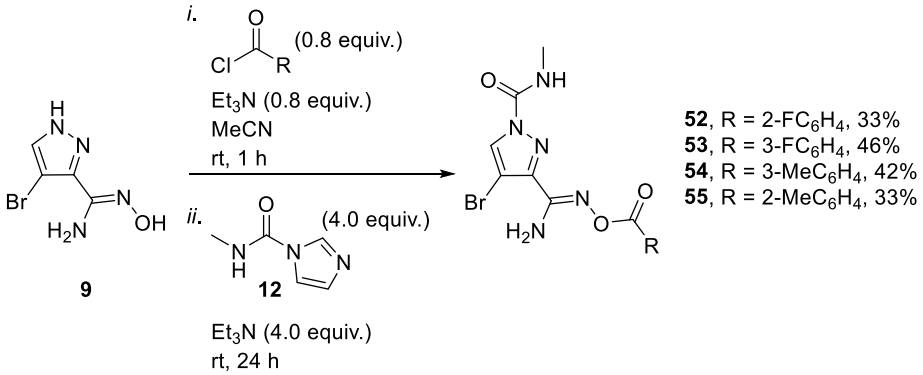

Scheme 23: Synthesis of analogues 52–55.

➢ DSF results

Aryl analogues **42**–**55** were examined through the DSF assay.

- Aromatic pyridine

Our first set included the aromatic pyridine analogues **48**–**50** and analogue **42**, **Figure 58**.

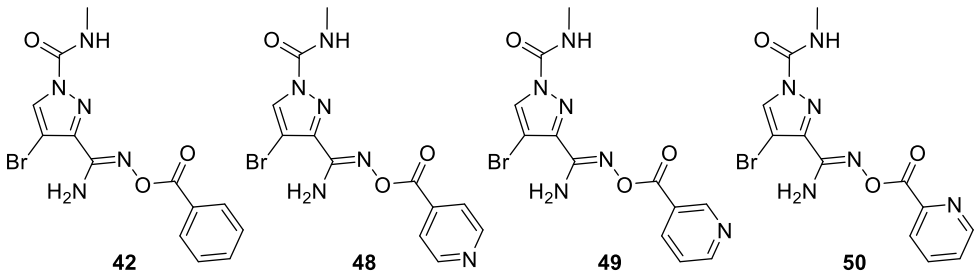

Figure 58: Exploring the ring with analogues 42 and 48–50.

We were intrigued to know if first of all an aryl ring, **42**, could be tolerated and the influence of having a nitrogen within the ring. We analysed the influence of the position of the nitrogen on the ring with 4-pyridyl (**48**), 3-pyridyl, (**49**) and 2-pyridyl (**50**) on stabilization.

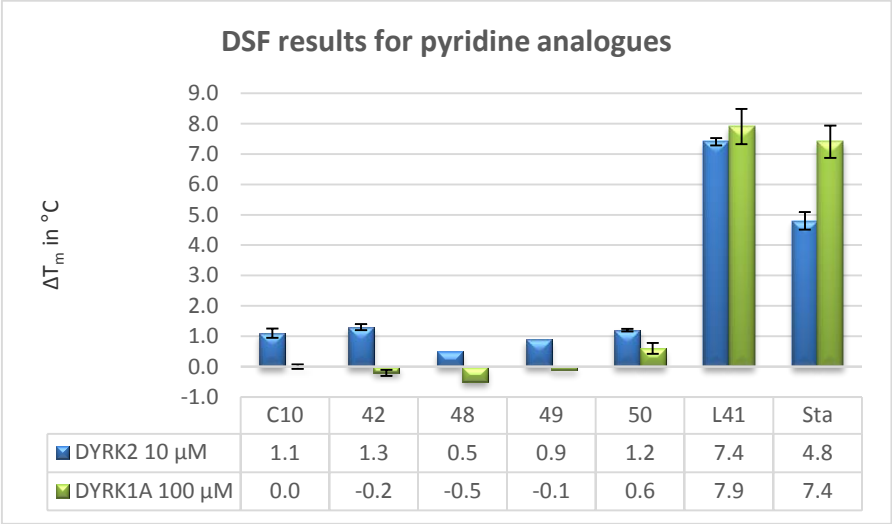

Graph 7: Bar graph representation of the T_m of compounds 42 and 48–50, L41 and staurosporine against DRYK2 and DYRK1A.

Graph 7, clearly showed that an aryl ring, **42**, still stabilises the protein to the same extent as **C10**. This further suggested that the carbamate NH was not necessary for stabilization and that a planar aromatic ring, as opposed to more bulky cyclohexyl ring (**41**) could be accommodated in the binding site. We observed a similar trend for the 2-pyridyl (**50**) and 3-pyridyl (**49**) analogues with a T_m of 1.2 and 0.9 °C, respectively for DYRK2. Compound **50** still showed a minimum stabilization of DYRK1A (0.6 °C) which suggested less selectivity than **49**, **42** or **C10** (< 0.0 °C). In contrast, a 4-pyridyl group (**48**) was not favoured for stabilization. It must be observed that analogues **48** and **49** were only run once in the assay indicating low accuracy.

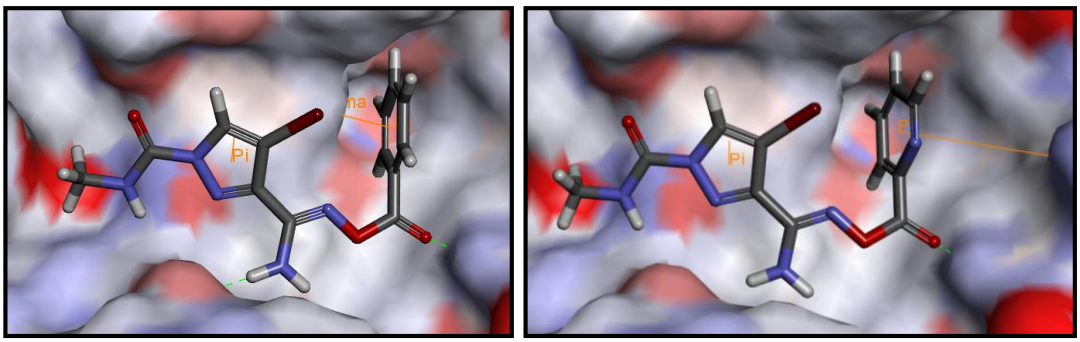

Figure 59: Predicted docked poses for derivatives 42 and 50.

When derivatives **42** and **50** were docked in the allosteric site, **Figure 59**, they both were predicted to adopt a similar pose and were different to **C10**. These analogues both had a π-π interaction between the pyrazole ring and Tyr 45 as well as an H-bond interaction between the carbonyl and Arg 88. They differed in their π interaction of the phenyl/pyridyl ring and an extra H-bond interaction was present for **42** between the amine and Thr 159. For **42**, the phenyl ring was predicted to interact through a π-σ interaction with Tyr 45 whereas the 2-pyridyl analogue (**50**) was envisaged to interact through a π-π interaction with Lys 110.

- Aromatic substitution

Our next set of compounds examined the substitution on the aryl ring with Me and F groups, **Figure 60**.

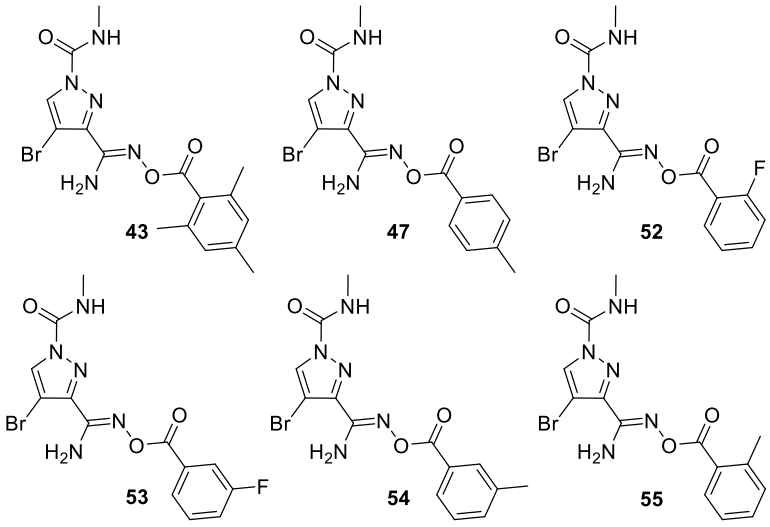

Figure 60: Exploring the phenyl ring with analogues 43, 47, 52−55.

With this set, we were interested in exploring hydrophobicity by adding a Me group to the ring in the *para* (**47**), *meta* (**54**), and *ortho* positions of the ring, (**55**). This also increased the electron density of the ring. Adding some 3-dimensional shape to the derivative with the trimethyl group **43** would give insight into the space of the pocket and might disrupt stabilization. Introducing a fluorine atom in drugs can increase potency as it can affect lipophilicity and hydrophobic interactions.[69] Fluorine is approximately the same size as a hydrogen atom but a C-F bond has increased polarizability relative to a C-H bond due to the electronegativity of F.[70] Fluorine is an isostere of H, which is why 2-fluoro (**52**) and 3-fluorophenyl (**53**) analogues were synthesized and compared to the aryl analogue **42**. Bioisoteres can bring about greater selectivity, improve potency, decrease toxicity and improve pharmacokinetics which explains the necessity to explore them.[71-76]

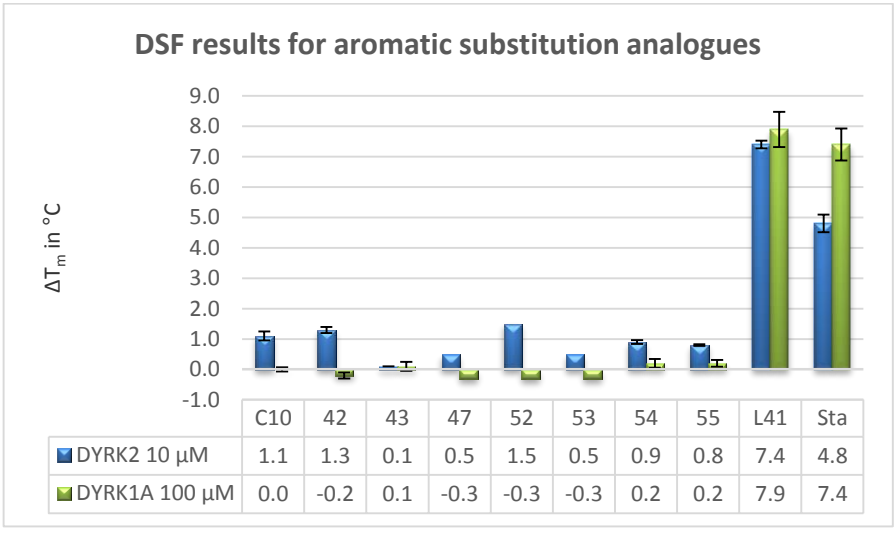

	C10	42	43	47	52	53	54	55	L41	Sta
DYRK2 10 µM	1.1	1.3	0.1	0.5	1.5	0.5	0.9	0.8	7.4	4.8
DYRK1A 100 µM	0.0	-0.2	0.1	-0.3	-0.3	-0.3	0.2	0.2	7.9	7.4

<u>Graph 8:</u> Bar graph representation of the T_m of compounds 42, 43, 47, 52−55, L41 and staurosporine against DRYK2 and DYRK1A.

Graph 8, shows us that having a Me group at the *ortho* position (**55**) and *meta* position, (**54**) gave similar T_m shifts to **C10** (0.8 and 0.9 °C, respectively) but did not bring more stabilization than aryl analogue **42**. This suggested that the Me groups did not bring more hydrophobic interactions at these positions. When the Me group was in the *para* position (**47**) the stabilization was reduced (0.5 °C) whereas introducing greater bulkiness to the compound with derivative **43**, clearly abrogated the stabilization of DYRK2. It must noted that analogues **47**, **52** and **53** were only run once and are considered less accurate than the other analogues tested.

Interestingly, compound **52**, with the fluorine atom in the *ortho* position, showed a T_m of 1.5 °C which was the best stabilization we had seen retaining selectivity. In contrast, with the fluorine atom at the *meta* position (**53**) we observed a decrease in stabilization (0.5 °C) compared to **42**.

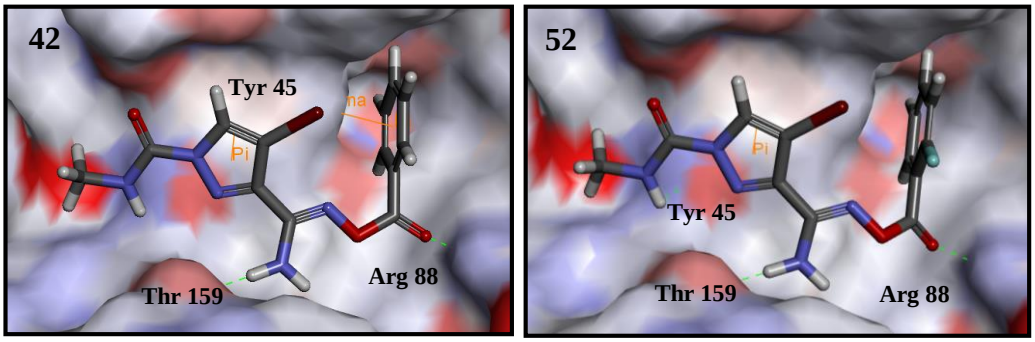

Figure 61: Docked poses of 42 and 52 in the allosteric pocket.

From the docked pose of **42** and **52**, we observed that although we lost a π-σ interaction with **52** we gained an extra H-bond interaction between the NH of the amide and Tyr 45, **Figure 61**. This might be a reason for the increase in stabilization.

- Electron-rich aryl and sulfone

Figure 62 represents the analogues submitted for the DSF assay. We wanted to have electron rich rings with a methoxy group in the *para* position (**45**) and by extending to a benzyl group (**44**). Compound **51** was also synthesized to understand how the stabilization was affected by extending the phenyl ring further into the pocket than **42**. The sulfone derivative **46** was prepared in order to increase hydrogen bonding as well as hydrophobic interactions. It has been showed by Bissantz and co-workers that sulfonyl tend to have a dual character: HBA and hydrophobic interaction.[77] One would consider a sulfonyl group only as a HBA. However, by screening the PDB for crystal structures with ligands containing sulfonyl groups, van der Waals interactions with nonpolar atoms as well as weak hydrogen bond interactions with Cα-H donors at the backbone level were observed for certain proteins.[77] This would help us compare it to **47** with the carbonyl moiety being more involved in H-bonding if this were the case.

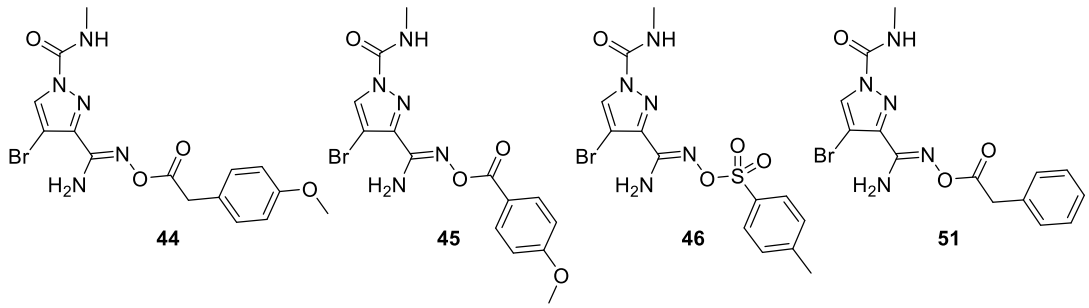

Figure 62: Exploring electron rich rings and sulfone derivatives 44−46 and 51.

All these analogues **44**−**46** and **51**, were put through the DSF assay against DYRK2 and DYRK1A, **Graph 9**.

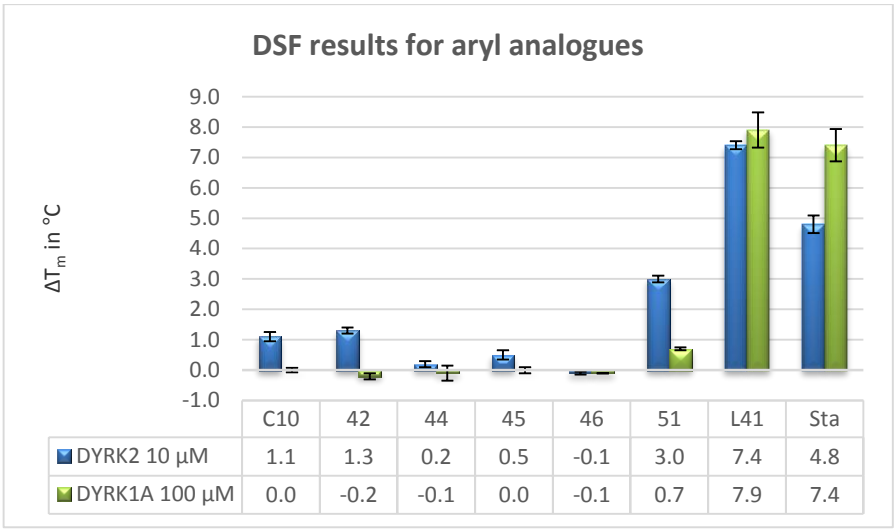

Graph 9: Bar graph representation of the T_m of compounds C10, 42, 44−46, 51, L41 and staurosporine against DRYK2 and DYRK1A.

From these results we observed that the sulfone derivative, (**46**) abrogated stabilization completely compared to its carbonyl homologue **47** (T_m = 0.5 °C). Adding a methoxy group (**45**) and extending the derivative to a benzyl (**44**) did not stabilize the protein compared to phenyl analogue **42**. Most significantly, derivative **51** showed the highest increase in stabilization of the series, with a 3.0 °C shift for DYRK2. It did show a small degree stabilization of DYRK1A which was quite minimal when compared to the shift of DYRK2.

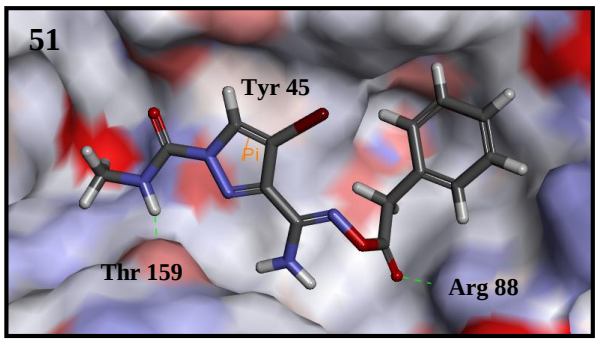

Figure 63: Predicted docked pose of 51 in the allosteric site.

We docked **51** in an attempt to potentially understand the increase in stabilization, **Figure 63**. The predicted pose was different to **C10** but still had the same potential number of interactions. It was observed from the prediction that the NH of the amide was H-bonding with Thr 159 and the carbonyl group of the oxyamidine with Arg 88. The pyrazole ring interacted with Tyr 45 through a π-π interaction.

- Biochemical assay

Analogue **51** showed the most promising results from the DSF assay with a T_m = 3.0 °C. It was therefore sent for a single pint concentration assay at 1 µM against DYRK2.

Table 4: % displacement of analogue 51 at 1 µM against DYRK2.

Compound	DYRK2
C10	19 ± 3%
51	23 ± 3%

Table 4 represents the % inhibition of analogues **C10** and **51** at 1 µM. Both analogues showed similar inhibition with **C10** at 19% and **51** at 23%. Even though stabilization was doubled there was no clear difference in binding activity at the single concentration examined in the assay.

c. **Carbamate derivatives**

➢ Synthesis

It was important to also explore Part B as a different carbamate group to Part A. The synthesis was completed in a two-step procedure to allow the isolation of the desired analogues, **Scheme 24**.

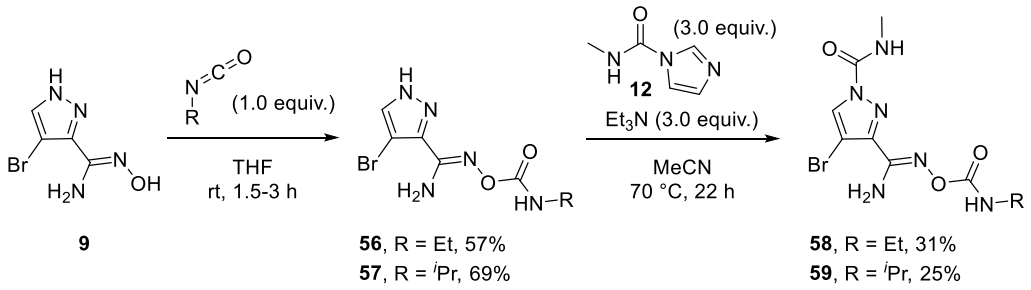

Scheme 24: Synthesis of carbamate analogues 58 and 59.

Oxyamidine **9** was reacted with the desired isocyanate and led to the isolation of ethyl derivative **56** and isopropyl derivative **57** in 57% and 69% yields respectively. They were both treated with compound **12** in the presence of Et_3N to give ethyl derivative **58** in 31% and isopropyl derivative **59** in 25% yield.

➢ DSF assay

By synthesizing these two analogues we were interested in knowing if we could extend into the pocket with **57** and observe the effects of adding steric bulk (**58**), **Figure 64**.

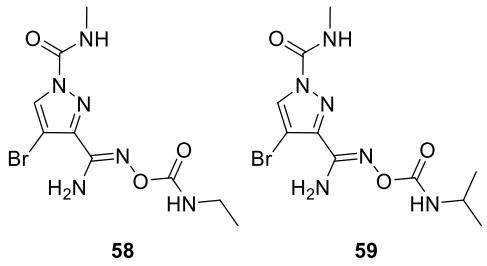

Figure 64: Exploring the carbamate chain with analogues 58 and 59.

Moreover, this would help establish whether it was necessary to have the carbamate functionality to gain stability of DYRK2 compared to the previous aryl and alkyl derivatives.

Carbamates **58** and **59** were examined in the DSF assay, **Graph 10**.

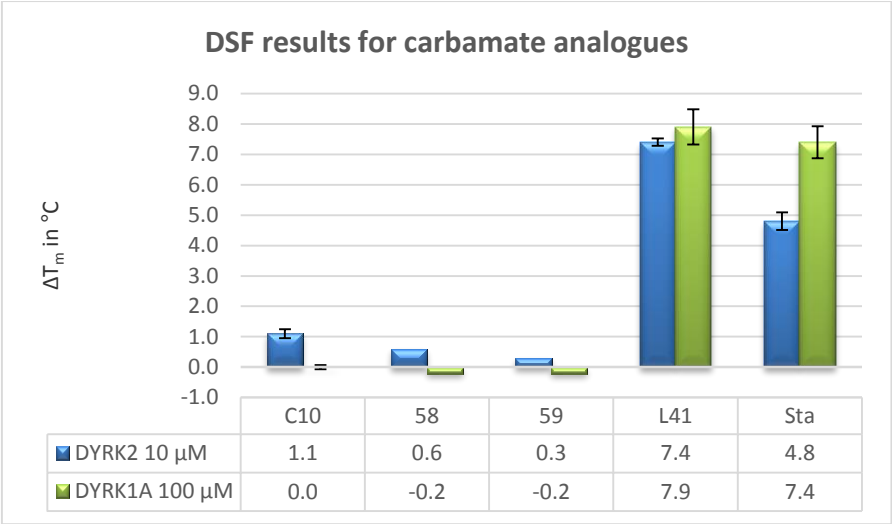

<u>Graph 10:</u> Bar graph representation of the T_m of compounds C10, 58, 59, C10, L41 and staurosporine against DRYK2 and DYRK1A.

The carbamate derivatives **58** and **59**, showed very low T_m shifts indicating that introducing steric bulk or extending the side-chain of the carbamate oxyamidine did not improve stabilization. It must be noted that analogues **58** and **59** were only ran once in this assay rendering the results less accurate. Moreover, this functionality was not necessary as more stabilization was gained with alkyl derivative **37** and aryl derivatives **42**, **51**, **50**, and **52**, **Figure 65**, and confirmed that an H-bond donor at this position of the molecule was not needed.

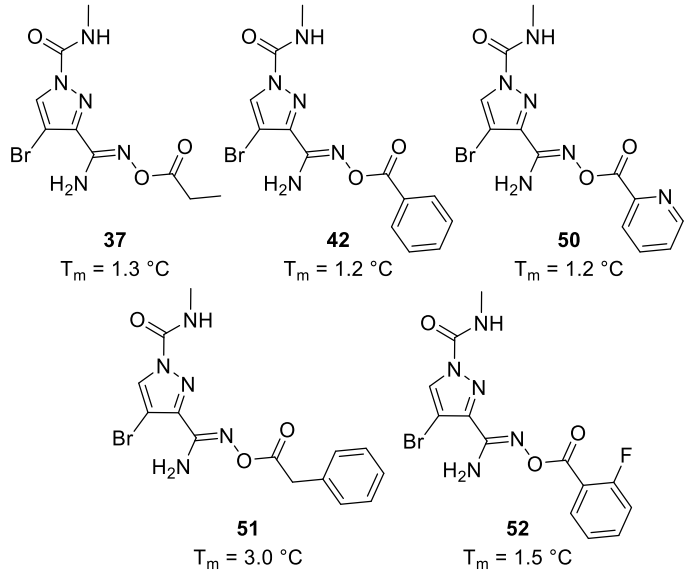

<u>Figure 65:</u> Analogues that have shown T_m shifts ≥ C10.

In summary, we observed that alkyl derivative **37** was the only alkyl compound that showed similar stabilization to **C10**. As for the aryl derivatives, three compounds displayed similar or higher stabilization than **C10** with 2-pyridyl, **50**, the 2-fluoro, **52** and phenyl **42**, derivatives, **Figure 65**. Derivative **51**, exhibited the best stabilization to date with a T_m = 3.0 °C for DYRK2.

4. Exploration of Part A and B

With the results observed previously, we decided to explore both part A and B simultaneously.

a. Synthesis

The first step was to prepare ethyl derivative **60** and isopropyl derivative **61** by treatment of CDI **13** with the corresponding amine salt, **Scheme 25**. The desired derivatives **60** and **61** were isolated in 77% and 67% yields respectively.

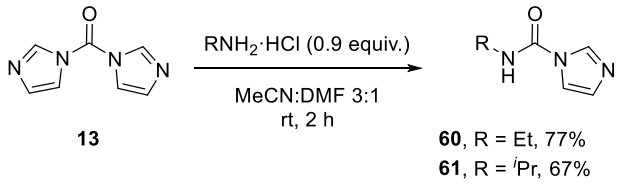

Scheme 25: Synthesis of CDI derivatives 60 and 61.

Oxyamidine **9** was coupled with the required carboxylic acids in the presence of PyBOP and Hünig's base, and the intermediates **62** and **63** were isolated in 25–29% yields. These were further treated with compounds **60** or **61**, at room temperature. This enabled the isolation of analogues **64–67** in 17–36% yields. For derivatives **64**, **66** and **67** an additional 1.5 hours of heating at 40 °C was required to drive the reaction to completion, **Scheme 26**.

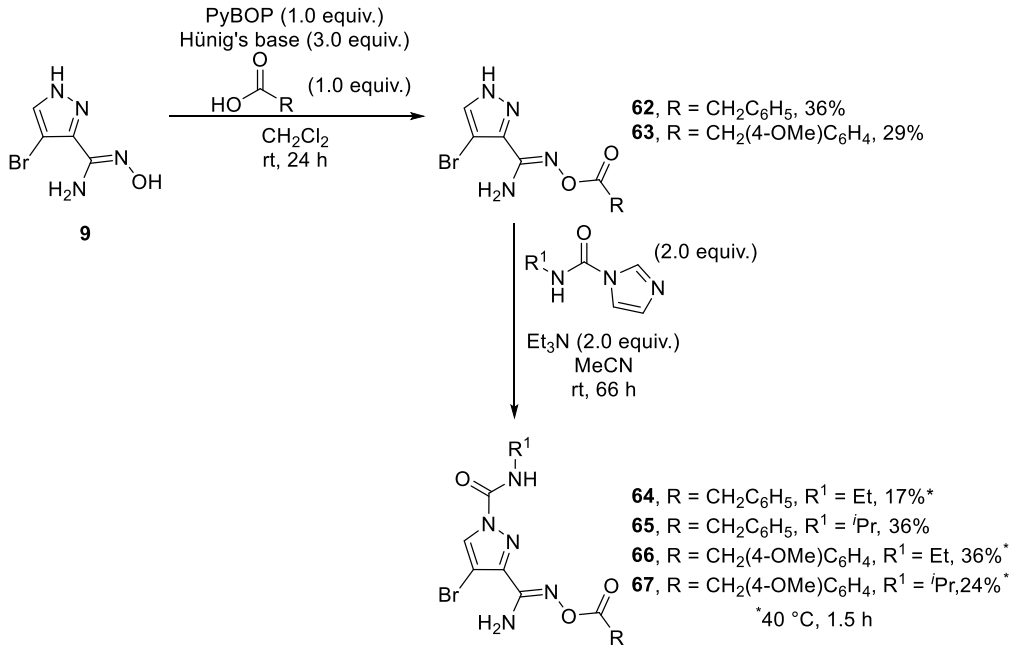

Scheme 26: Synthesis for exploration of part A and B.

For dimethyl analogue **68**, intermediate **62** was treated with 3 equiv. of dimethyl carbamoyl chloride in the presence of Et_3N for 22 h at 40 °C. Analogue **68** was isolated in 60% after purification. For analogue **69**, intermediate **63** was treated with the same reagents, heating the reaction mixture at 40 °C for 18 h. This gave the desired analogue **69** in 50% yield, **Scheme 27**.

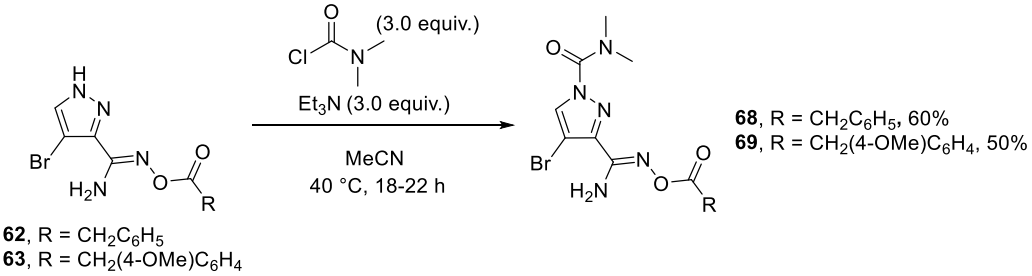

Scheme 27: Dimethyl analogues 68 and 69 synthesis.

b. DSF results

Compounds **64**–**69** were tested in the DSF assay and are separated into groups to compare the results.

➢ Benzyl derivative

Analogues **64** and **65** were targeted to discover if extension of the carbamate group would give insight into whether bulkier (**65**) and longer (**64**) chains were tolerated with a benzyl group at the oxyamidine moiety, **Figure 66**. As for analogue **69**, we wanted to confirm the necessity of having the urea NH for stabilization by synthesizing this dimethyl analogue.

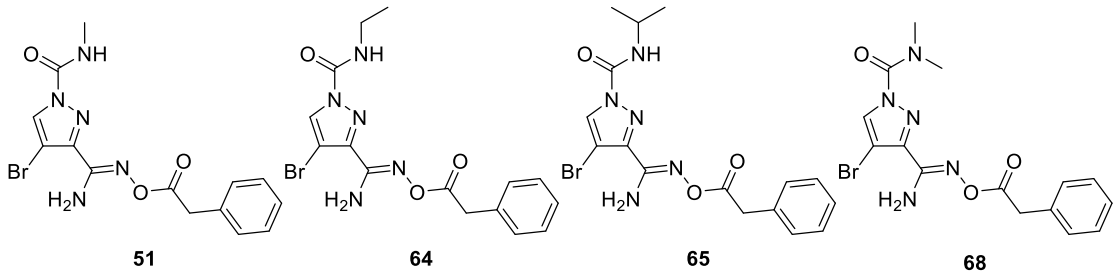

Figure 66: Exploring urea functionality with benzyl derivatives 51, 64, 65 and 69.

Each compound was examined within the DSF assay screen to determine to what extent they stabilized the protein, **Graph 11**.

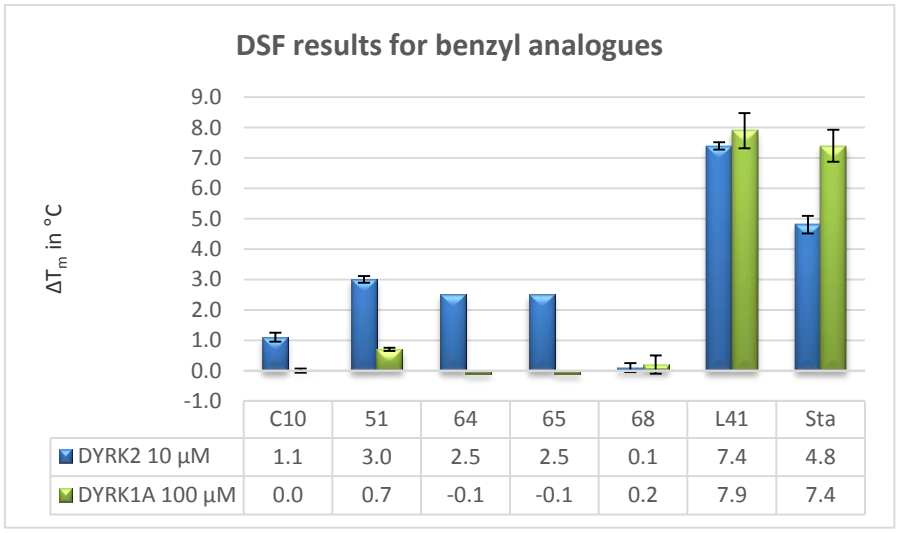

	C10	51	64	65	68	L41	Sta
DYRK2 10 µM	1.1	3.0	2.5	2.5	0.1	7.4	4.8
DYRK1A 100 µM	0.0	0.7	-0.1	-0.1	0.2	7.9	7.4

Graph 11: Bar graph representation of the T_m of compounds C10, 51, 64−65, L41 and staurosporine against DRYK2 and DYRK1A.

We observed that derivatives **65** and **64** had the same temperature shifts of 2.5 °C which was pretty similar to the methyl analogue **51**. The advantage of these two compounds was that they showed no stabilization of DYRK1A. This suggested that by

extending (**64**) or adding bulkiness (**63**) stabilization was conserved but selectivity was improved for DYRK2 over DYRK1A compared to **51**. We clearly observed that dimethyl analogue (**68**) abrogated stabilization of the protein. It must be noted that analogues **64** and **65** were only ran once in the assay rendering the results less accurate. These results corroborated what had previously been seen: the NH of the urea was of great importance for stabilization.

- *p*-methoxy benzyl derivatives

Although we had seen that *p*-methoxy benzyl analogue **44** did not help stabilization, the following analogues were synthesized before the biological results were received. As previously, we wanted to look into probing the alkyl group on the amine atom of the urea functionality (**66**) adding bulkiness (**67**) and the importance of the NH of the urea with **69**, **Figure 67**.

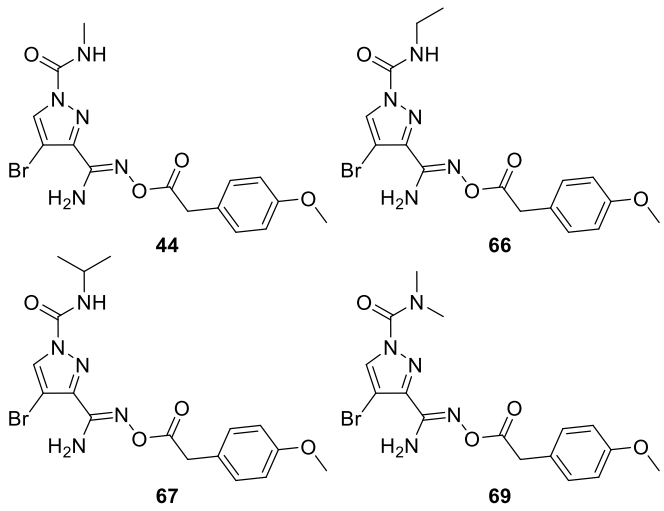

Figure 67: Exploring the urea functionality with *p*-methoxy benzyl derivatives 44, 66−67 and 69.

These analogues were screened against DYRK2 and DYRK1A in the DSF assay, **Graph 12**.

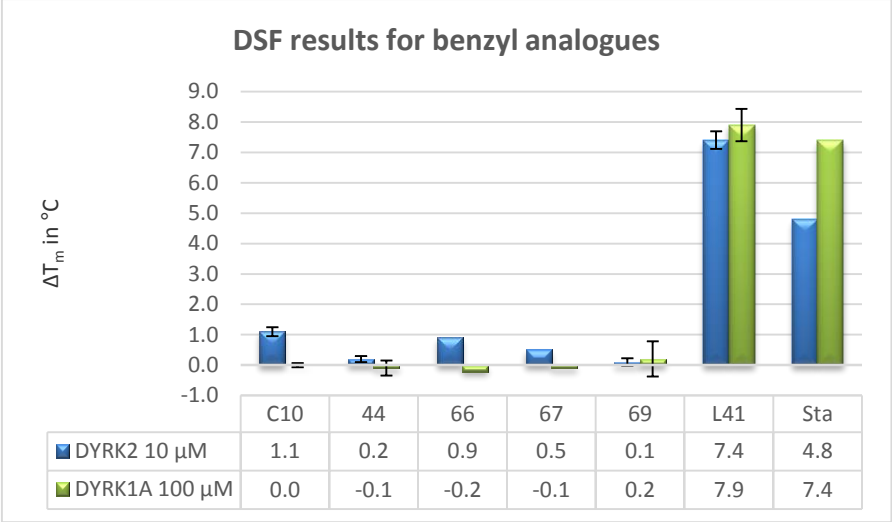

	C10	44	66	67	69	L41	Sta
DYRK2 10 µM	1.1	0.2	0.9	0.5	0.1	7.4	4.8
DYRK1A 100 µM	0.0	-0.1	-0.2	-0.1	0.2	7.9	7.4

<u>Graph 12:</u> Bar graph representation of the T_m of compounds C10, 44, 66, 67, 69, L41 and staurosporine against DRYK2 and DYRK1A.

The results indicated that by extending the alkyl chain of the urea functionality, **66** stabilized DYRK2 to a greater extent than methyl analogue **44** with a T_m = 0.9 °C. This was only seen for this series of compounds when changing the urea. When bulkiness was added (**67**) a slight increase was observed compared to **44** but not to a great extent. The dimethyl analogue **69**, followed the trend seen by previous analogues **23**, **24** and **68** of not stabilizing the protein. Either the the presence of an electron-donating methoxy substituent on the aromatic ring or sterics reduced stabilization when compared with the equivalent unsubstituted series (**51**, **64** and **65**).

III. Conclusion

The oxyamidine series has explored the pocket and generated some interesting SAR. **Figure 68**, is an overall picture of what was tolerated or not for stabilization.

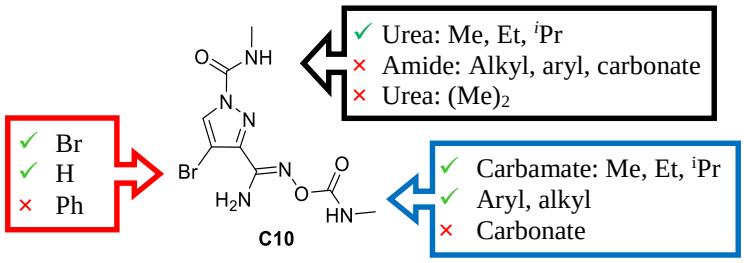

<u>Figure 68:</u> Overall SAR study of C10.

Part C indicated that hydrogen was tolerated but gave less stabilization of DYRK2 than with bromine. When a phenyl group was present, the overall conformation of **C10** in the solid state changed which likely lead to the stabilization of DYRK2 being abrogated. Part B of the hit was explored and it was observed that carbonates were not tolerated. Aryl and alkyl groups increased or retained stabilization depending on the substituents. Carbamates were tolerated but with the Me being more favourable for stabilizing DYRK2. Finally Part A was also explored and clearly showed that the NH of the urea was important for stabilization. Moreover, extending or adding some bulkiness to the alkyl chain did not completely attenuate the stabilization of the protein.

A library of 44 compounds was successfully generated and biologically tested. Due to the long synthesis needed to get to these derivatives, it was decided to explore amides in Part B as an alternative higher throughput synthetic strategy.

Chapter 3: Amide pyrazole series

The synthetic sequence to obtain derivatives of **C10** was long. We were interested in designing amides after analysing the allosteric pocket and hypothesised that they could be an interesting alternative to the oxyamidine series. It was therefore decided that Part B of the hit compound **C10** would be explored with an amide functionality instead of the oxyamidine moiety. The synthesis of these derivatives would be shorter, allowing for SAR studies to be carried out quickly.

I. First amide analogues to test hypothesis.

1. Synthesis

It was envisaged that the amide analogues could be prepared in two steps from the known intermediate **6**: first by HATU coupling of acid **6** with an amine, followed by acylation with **12**, leading to the target molecule **70**, **Scheme 28**.

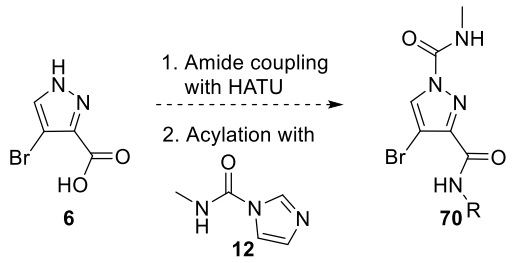

Scheme 28: Proposed synthesis of amide analogues.

a. Two steps with isolation of intermediate

It was first decided to carry out each step individually, and isolate the intermediates to facilitate the exploration of Part A with the urea functionality.

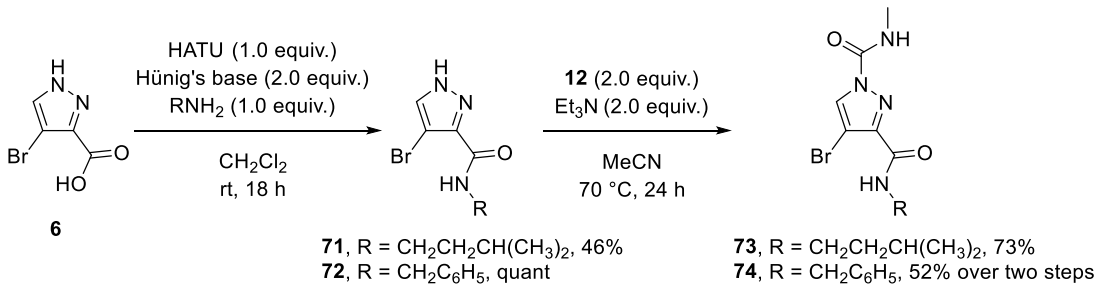

Scheme 29: Amide synthesis.

Treatment of carboxylic acid **6** with HATU in the presence of Hünig's base and an amine at room temperature for 18 h gave the desired intermediates **71** and **72** ranging from 46% to quantitative yield. The intermediates were further treated with **12** in the presence of Et_3N at 70 °C for 24 h to provide the desired amide analogues **73** and **74** in 73% and 52% yield, respectively, **Scheme 29**.

b. One-pot two-step synthesis

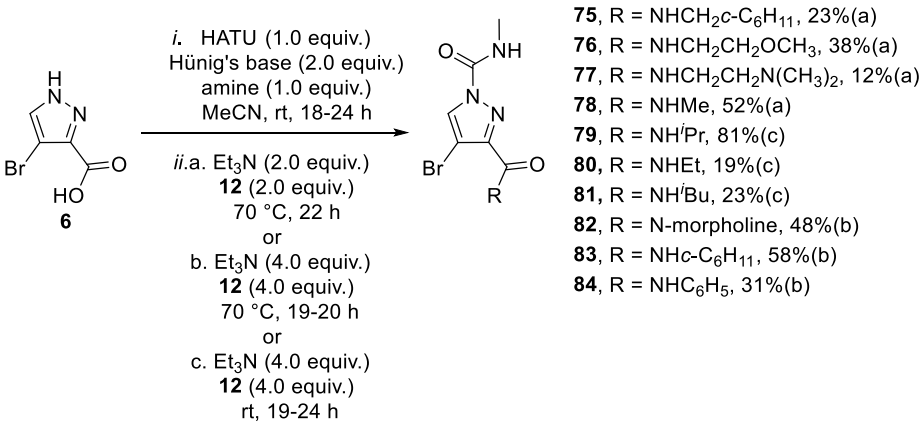

Scheme 30: Amide derivatives synthesized.

It was considered that the two steps could be carried out sequentially, which would avoid a purification step. This one-pot procedure was examined for cyclohexyl analogue **75** to give the product in 23% yield compared to 19% using the two-step protocol. Therefore, this two-step one-pot process was carried out by treating carboxylic acid **6** in anhydrous MeCN in the presence of Hünig's base and an amine for 18−24 h at room temperature. Compound **12** and Et_3N were then added and further stirring carried out at 70 °C for 19−22 h. It was observed that by adding more

equivalents of **12** and stirring it at room temperature the reaction gave better yields. The conditions used for the isolation of amide analogues **75−84** in 12−58% yield are presented in **Scheme 30**.

2. **DSF assay**

The first amide synthesized was **73**, which was designed and discussed with Prof Mackay by observing the putative allosteric pocket. It was thought that the long alkyl chain could lie in the small side pocket and interact through hydrophobic interactions with Phe 158 and Tyr 89. An encouraging T_m of 0.8 °C meant that **73** was the starting point for our SAR study on the amide scaffold.

a. **Alkyl chains**

We were first interested in varying the alkyl chain of the amide, **Figure 69**.

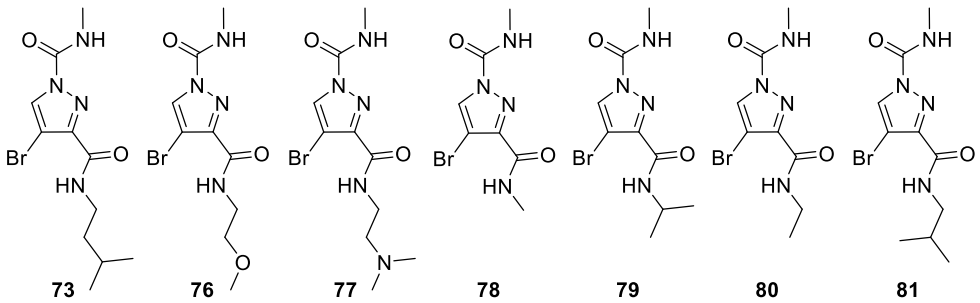

Figure 69: Alkyl chain analogues 73, 76−81.

By making analogue **77**, we were interested in determining if the nitrogen could pick up an additional interaction with the protein. The amide chain was reduced to a methyl, **78**, and we decided to examine if the chain length would influence the stabilization of DYRK2 with ethyl amide **80**, or the protein could tolerate steric bulk with isopropyl **79** and isobutyl **81** analogues. We also examined the effect of having an H-bond acceptor with ethyl methoxy amide **76**.

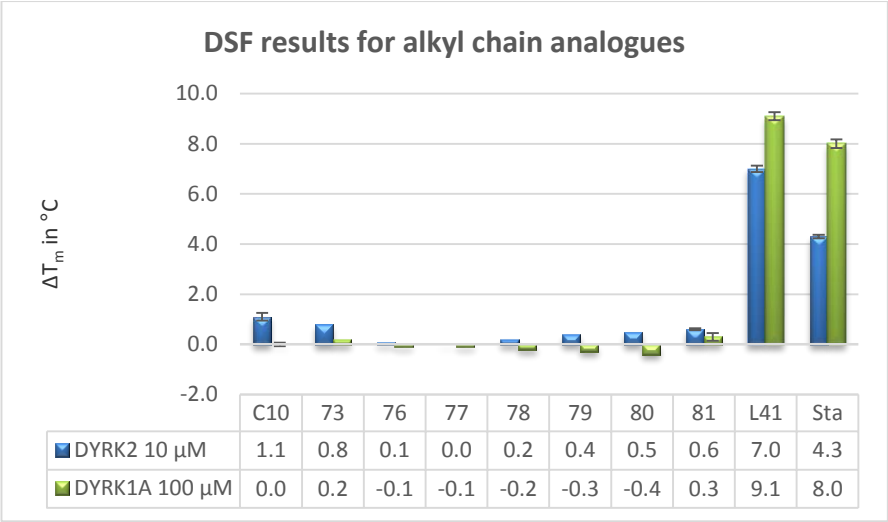

	C10	73	76	77	78	79	80	81	L41	Sta
DYRK2 10 µM	1.1	0.8	0.1	0.0	0.2	0.4	0.5	0.6	7.0	4.3
DYRK1A 100 µM	0.0	0.2	-0.1	-0.1	-0.2	-0.3	-0.4	0.3	9.1	8.0

Graph 13: Bar graph representation of the T_m of alkyl analogues 73, 76−81, L41 and staurosporine against DRYK2 and DYRK1A.

The analogues were submitted to the DSF assay, **Graph 13**. The first amide derivative **73** gave a T_m of 0.8 °C which was comparable to hit **C10**. Unfortunately none of the other alkyl chain derivatives showed an increase in stabilization of the protein. It must be noted that analogues **73** and **76−80** were tested only once in the DSF assay rendering their results less accurate.

b. Cyclic and aromatic amides

A series of cyclic and aromatic amides were prepared to explore the binding site further, **Figure 70**.

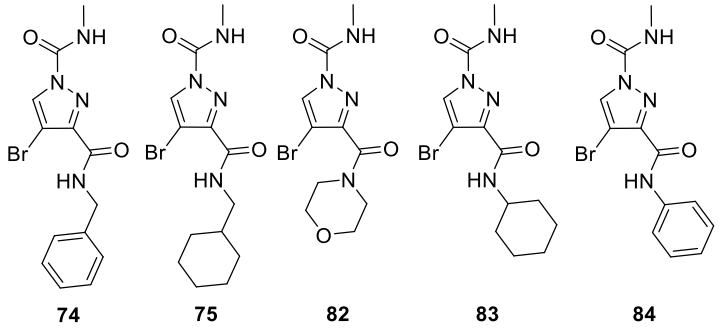

Figure 70: Cyclic and aromatic analogues 74, 75 and 82−84.

We were interested in having an aliphatic ring with cyclohexyl analogue **83** and seeing how varying the carbon chain length (**75**) might affect stability of the protein. We also wanted to add a cyclic tertiary amide to our set with morpholine amide **82** to investigate

whether a tertiary amide would be tolerated. Finally, we wanted to explore having an aromatic ring (**84**) as well as extending the space between the aromatic ring and the amide group (**74**). This could add additional π-π stacking and theoretically help increase stabilization.

These cyclic and aromatic analogues were submitted to our DSF assay, **Graph 14**.

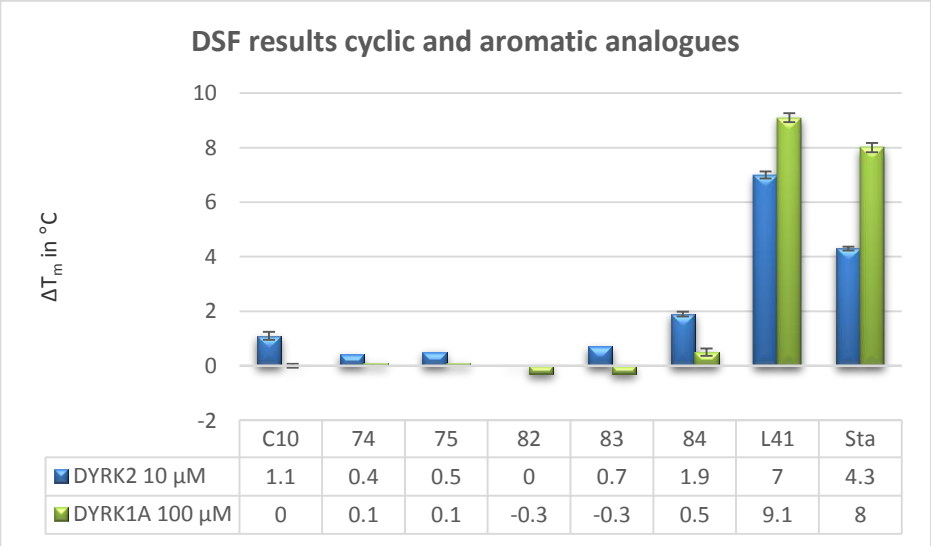

	C10	74	75	82	83	84	L41	Sta
DYRK2 10 µM	1.1	0.4	0.5	0	0.7	1.9	7	4.3
DYRK1A 100 µM	0	0.1	0.1	-0.3	-0.3	0.5	9.1	8

<u>Graph 14:</u> Bar graph representation of the T_m of compounds 74, 75, 82−84, L41 and staurosporine against DRYK2 and DYRK1A.

The best result was obtained with compound **84**, the aniline derived amide, which resulted in a T_m of 1.9 °C for DYRK2 and a T_m of 0.5 °C for DYRK1A. Addition of an extra carbon (**74**) abrogated stabilization of DYRK2 (T_m = 0.4 °C). It must be noted that analogues **74−75** and **82−83** were tested only once in the DSF assay rendering their results less accurate.

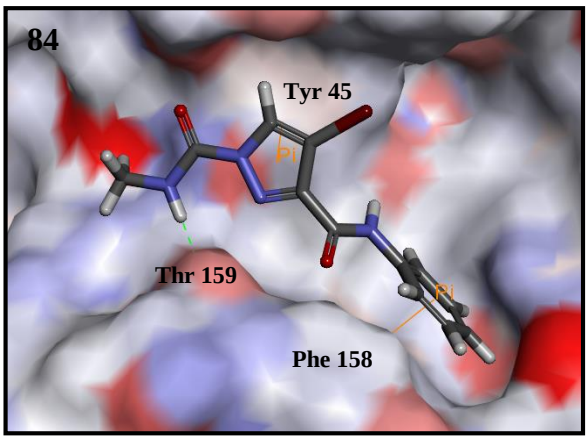

Figure 71: Predicted aniline amide 84 pose in putative allosteric site.

Figure 71, shows a predicted docked pose of amide **84** in the proposed allosteric pocket which gave a T_m of 1.9 °C. The NH from the urea functionality was predicted to interact with Thr 159 and two π-π interactions could be observed between the pyrazole ring and Tyr 45 and the phenyl ring with Phe 158.

3. **Biochemical assay**

With **84** showing an increase in stabilization of DYRK2 relative to **C10**, we decided to obtain more insight into the binding affinity of this analogue. Compound **84** was sent for a single point concentration at 1 µM for DYRK2 and DYRK1A, **Table 5**.

Table 5: % displacement of 84 and C10 at single point concentration of 1 µM.

Compound	DYRK2	DYRK1A
C10	19 ± 3%	2 ± 0%
84	13 ± 4%	4 ± 1%

While a displacement of 13 ± 4% **84** showed similar activity at a single point concentration to **C10** and had potential for further improvement. We also obtained a binding affinity for our initial amide hit **84** to see how future compounds would compare to this initial active amide. **Figure 72** shows the table and graph representation of concentration against percent displacement.

IC50 (nM)	Hillslope	R^2 Value	Conc of Compound (nM)	% Displacement Point 1	% Displacement Point 2
15500	1.19	0.9915	30000	59	52
15500	1.19	0.9915	10000	29	33
15500	1.19	0.9915	3330	12	10
15500	1.19	0.9915	1110	9	5
15500	1.19	0.9915	370	7	-2
15500	1.19	0.9915	123	4	-4
15500	1.19	0.9915	41.2	7	1
15500	1.19	0.9915	13.7	4	2
15500	1.19	0.9915	4.57	-3	1
15500	1.19	0.9915	1.50	0	5

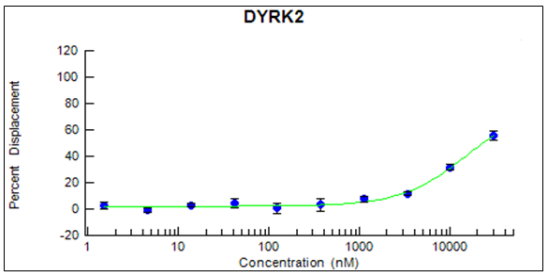

Figure 72: IC_{50} of amide 84 for DYRK2.

Even though the inhibition did not reach 100%, the binding affinity of amide **84** was extrapolated to be IC_{50} = 15.5 µM for DYRK2. This indicated that analogue **84** was less active than **C10**. Nevertheless, this could still potentially be improved by investigating the scaffold with an SAR study.

II. SAR study of amide 84 region by region

In a similar manner to **C10**, we wanted explore the importance of the urea functionality with Part A, as well as the importance of the bromine with Part C. Finally, the phenyl amide functionality was to be explored with Part B, **Figure 73**.

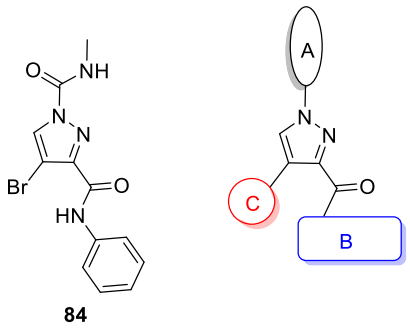

Figure 73: Amide analogue 84 and possible directions of SAR study.

1. Exploring Part A

a. Synthesis

The same one-pot two-step synthesis described previously in **Scheme 30** was carried out. Coupling of carboxylic acid **6** with aniline in the presence of Hünig's base and HATU was performed for 19–24 h in MeCN. The desired isocyanate or thioisocyanate

(1.2, 2.0 or 3.0 equiv.) was then added to the reaction with Et_3N.The analogues (**85–92**) were isolated in 12–58%, **Scheme 31**.

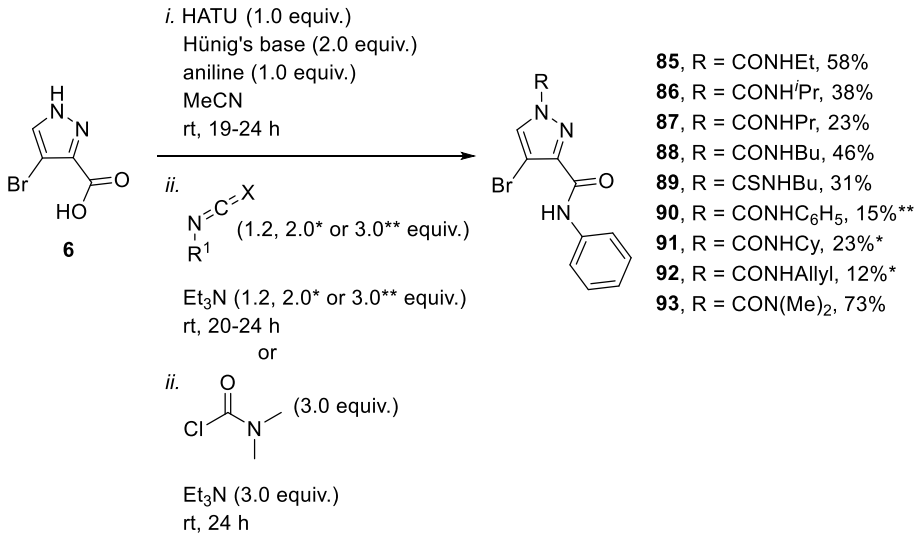

Scheme 31: Synthesis of analogues 85–93 for the exploration of part A.

For dimethyl analogue **93**, *N*,*N*-dimethylcarbamoyl chloride was used to acylate the pyrazole core. This lead to the isolation of analogue **93** in 73% after column chromatography.

We were interested to know what structure these amide analogues adopted in the solid-state. We therefore grew crystals of analogue **86** by vapour diffusion with MeOH and PE, **Figure 74**.

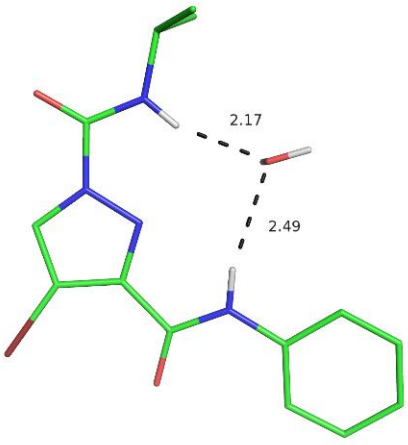

Figure 74: X-ray structure of analogue 86.

From this crystal structure, it was observed that the NH of the urea and the amide H-bond to a molecule of water. There was no evidence of the analogue adopting a similar predicted pose in the putative allosteric pocket of the protein of interest DYRK2. This might suggest that our amide analogues could interact in another binding site, like the orthosteric site, of the protein.

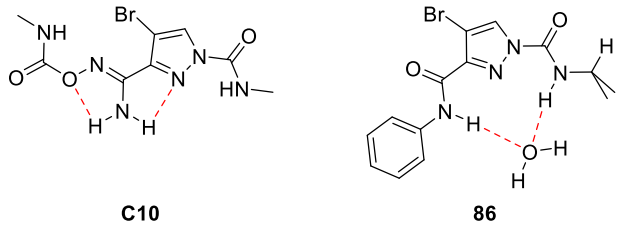

Figure 75: Solid−state conformations of C10 and 448

This analysis was of interest to us to see how the solid-state of the amide analogues differed from the oxyamidine series, **Figure 75**. We observed from these two analogues that the pyrazole nitrogen of amide analogue **86** was not involved in the H-bonding network compared to **C10**.

b. **DSF assay**

Our first interest was on the urea functionality, with respect to chain length and substitution, **Figure 76**. The first question that arose was whether we could increase stabilization by adding a longer alkyl chain with analogues **85**, **87** and **88**, or by making it bulkier with **86**. We also wanted to investigate if changing to a thiourea (**89**) would influence stabilization. Moreover, changing to a phenyl substituted urea (**90**) could potentially increase π–π interactions as well as hydrophobic features. By introducing a cyclohexyl group (**91**) we removed some planarity from our compound, which could possibly influence stabilization. As we had the allylisocyanate already in- house, we decided it would provide an additional analogue with a longer alkyl chain bearing an alkene at the end that could be involved in some π-π interactions (**92**). Finally, we were still interested in the importance of the urea NH and its role in stabilization which is why **93** was synthesized.

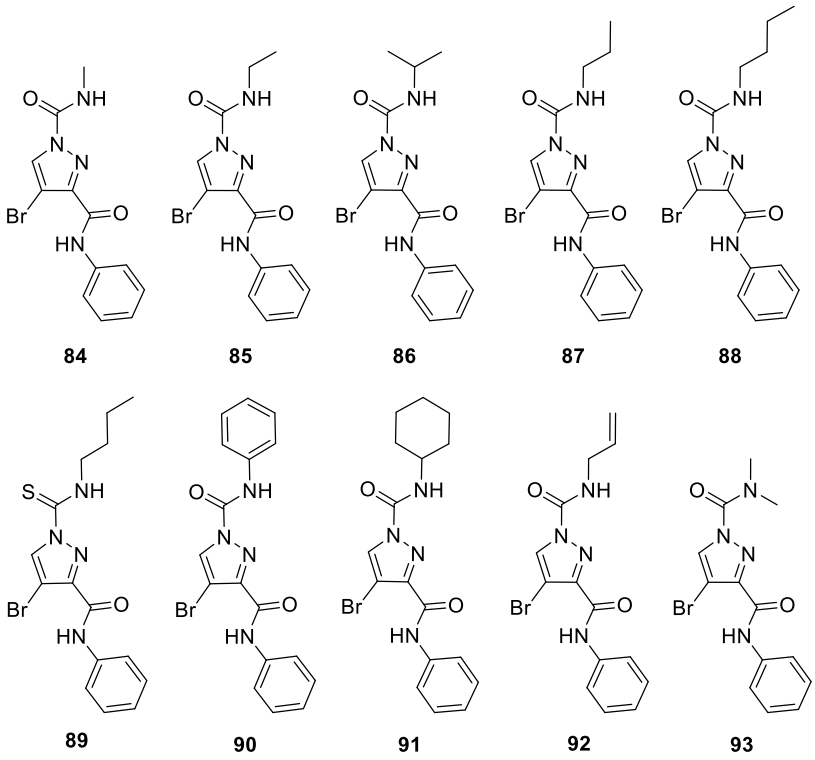

Figure 76: Analogues 84–93 to explore our putative allosteric pocket.

The analogues prepared **85−93** were subjected to the DSF screen. The assay was run at 10 µM for DYRK2 and DYRK1A. This concentration for both proteins was adopted in the DSF assay for the remainder of the investigation. The results are collated in **Graph 15**.

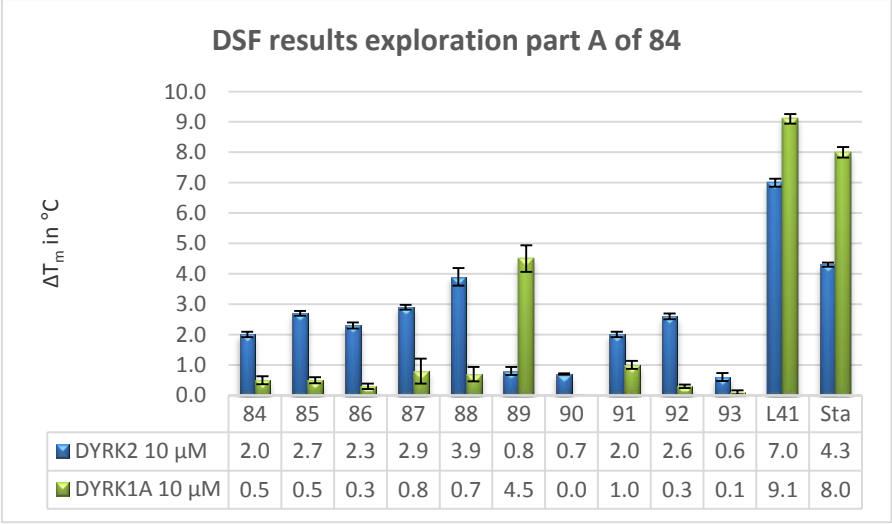

	84	85	86	87	88	89	90	91	92	93	L41	Sta
DYRK2 10 µM	2.0	2.7	2.3	2.9	3.9	0.8	0.7	2.0	2.6	0.6	7.0	4.3
DYRK1A 10 µM	0.5	0.5	0.3	0.8	0.7	4.5	0.0	1.0	0.3	0.1	9.1	8.0

Graph 15: Bar graph representation of the T_m of compounds 84−93, L41 and staurosporine against DRYK2 and DYRK1A.

This data allowed us to determine the important substitution pattern regarding stabilization in this region of the ligand. Extending the alkyl chain of the urea functionality showed considerable increase from the ethyl (**85**), to the propyl (**87**) and finally the butyl analogue (**88**) with T_m = 2.7 °C, T_m = 2.9 °C and T_m = 3.9 °C respectively. As previously seen in the oxyamidine series, the *N*,*N*-dimethyl urea **93**, showed loss of stabilization. The most interesting data from this series was the difference between butylurea **88** and butylthiourea, **89**. We observed a complete switch in selectivity towards the DYRK isoforms and high T_m shifts. The precise origin of this intriguing switch was not apparent but was certainly a particularly interesting observation.

c. **Biochemical assay**

With the exciting results from the DSF assay, we were eager to bring some analogues forward for further testing, **Figure 77**.

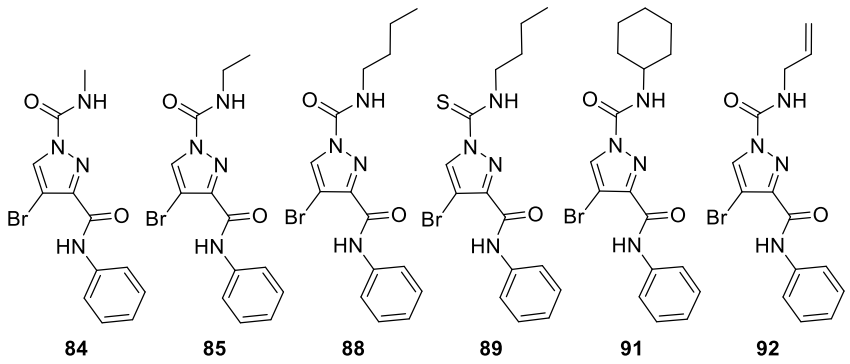

<u>Figure 77:</u> Compounds sent for single point concentration assay.

Selected analogues were evaluated by single point displacement at 1 μM for DYRK2 and/or DYRK1A, **Table 6**.

Table 6: **% displacement of analogues at single point concentration at 1 µM for DYRK2 and DYRK1A.**

Compound	DYRK2	DYRK1A
84	13 ± 4%	4 ± 1%
85	5 ± 3%	ND
88	31 ± 1%	3 ± 1%
89	4 ± 1%	5 ± 2%
91	7 ± 0%	ND
92	9 ± 3%	ND

These results were interesting as they did not always correlate with the DSF results observed. In terms of binding activity, having a longer chain (**85**), an allyl group (**92**) or a cyclohexyl group (**91**) did not influence the % inhibition for DYRK2 when compared to **84**. In contrast, butyl urea analogue **88** showed an increase in activity with 31% displacement and maintained selectivity. Thiourea analogue **89**, showed no activity against both DYRK isoforms. This result indicated that a minor change, from a urea to a thiourea, altered the binding activity towards the same protein. In addition, the surprising DSF result obtained with **89** in terms of DYRK2 *vs* DYRK1A selectivity was not supported with this biochemical assay.

Out of curiosity, we decided to generate a graph to compare our two biological assays and assess if a trend could be observed, **Graph 16**.

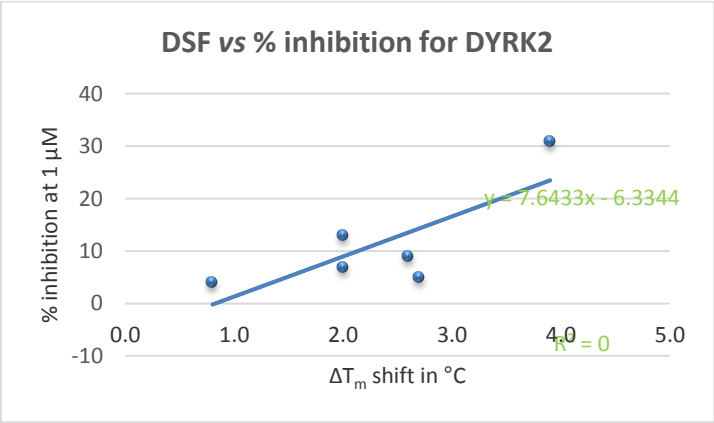

Graph 16: **DSF results *vs* % inhibition at 1 µM for DYRK2.**

From the graph we could distinguish a slight trend between the DSF and % inhibition for this series of compounds. However, from the DSF results we were unable to determine a theoretical % inhibition with confidence, as no direct significant correlation existed.

d. **Docked poses**

It was decided that we would dock some of the synthesized analogues in the putative allosteric pocket and the orthosteric site of DYRK2. For the allosteric site docking, the average minimum conformation of the protein 3K2L was used which had been generated by Al-Shar'i.[3] For the orthosteric site, protein kinase DYRK2 4AZF from the PDB was used, as it already had an ATP-competitive ligand bound in the pocket. The software GOLD was used for docking and GoldScore was applied as the scoring function for consistency.[44] The author carried out the docking by asking the program to deliver only the three best predicted scoring conformations and analysing them individually. It was observed that sometimes the highest score did not necessarily indicate an optimal conformation of the compound. Therefore, the predicted pose shown throughout this Chapter has been chosen from a set of three to the best judgement of the author. Moreover, only the predicted docked poses of compounds showing crucial differences in the biochemical analysis are reported.

From the inhibition results, we wanted to rationalize the loss in activity between urea analogue **88** and thiourea analogue **89**. We docked the analogues in the allosteric pocket, **Figure 78**.

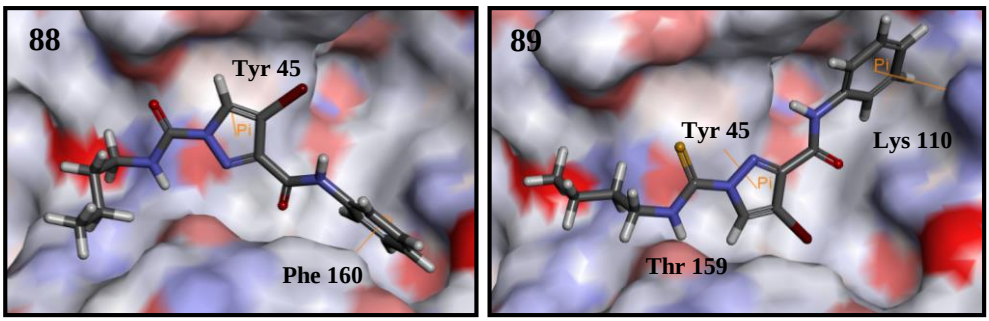

Figure 78: Predicted docked poses of 88 (left) and 89 (right) in the allosteric pocket.

The two analogues were predicted to adopt completely different conformations when docked in the putative allosteric pocket. Urea **88** envisaged to adopt a similar conformation to amide **84** with two π-π interactions between the phenyl ring with Phe 160 and the pyrazole ring with Tyr 45. In contrast, thiourea **89** was predicted to adopt a different conformation with respect to the pyrazole amide region of the molecule. The bromine was facing down and the amide facing the top right hand side of the pocket in **Figure 78**. The pyrazole ring was foretold to be involved in a π-π interaction whereas the phenyl ring was now interacting with Lys 110 through a π-σ bond. An H-bond interaction was predicted between the NH of the amide and Thr 159. From these virtual poses, there was no clear evidence to explain the differences in activity between analogues **88** and **89** apart from a change in conformation We also docked these compounds in the ATP site to determine if a more obvious conclusion could be drawn, **Figure 79**.

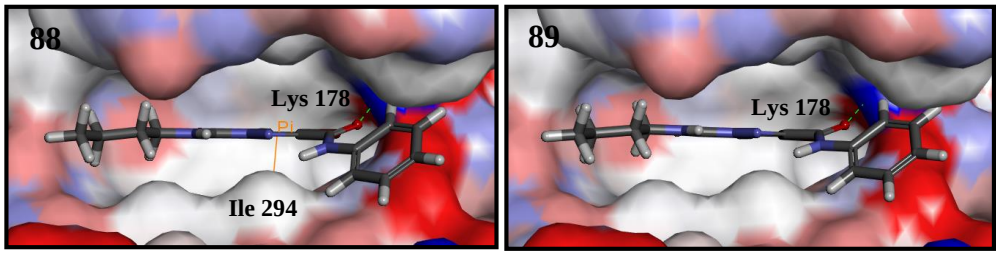

Figure 79: Predicted docked poses of 88 (left) and 89 (right) in the orthosteric site.

Both analogues adopted very similar predicted poses in the orthosteric site, with the carbonyl group of the amide H-bonding with Lys 178. Only **88** adopted a pose where the pyrazole ring could potentially interact with Ile 294 through a π-σ bond. There was again no clear explanation from our modelling studies to account for the difference in activity between urea **88** and thiourea **89**. Unable to use modelling studies to guide our investigation, we continued to explore the binding pocket with substitution at Part B.

2. **Exploring Part B**

Part B of the scaffold was investigated with various substitution patterns, electron withdrawing groups and electron donating groups incorporated on the amide functionality. These analogues are assembled according to their relevance in order to compare the results obtained.

a. **Importance of amide NH**

➢ Synthesis

Ester **94** was synthesized as shown in **Scheme 32**.

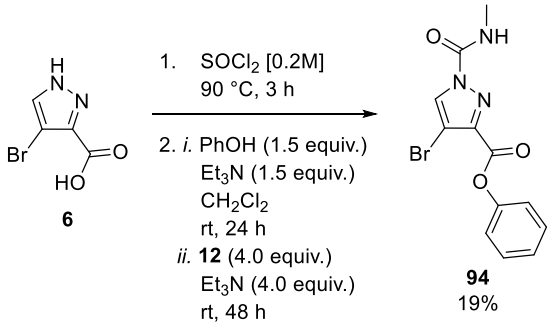

Scheme 32: Synthesis of ester analogue 94.

Carboxylic acid **6** was treated with thionyl chloride for 3 h at 90 °C. After the removal of excess thionyl chloride, the acyl chloride intermediate was treated with excess phenol and Et_3N in anhydrous CH_2Cl_2. After completion of the reaction as determined by LC/MS, **12** and Et_3N were added and stirring continud for a further 48 h at room temperature. After recrystallization from EtOAc, ester **94** was isolated in 19% yield.

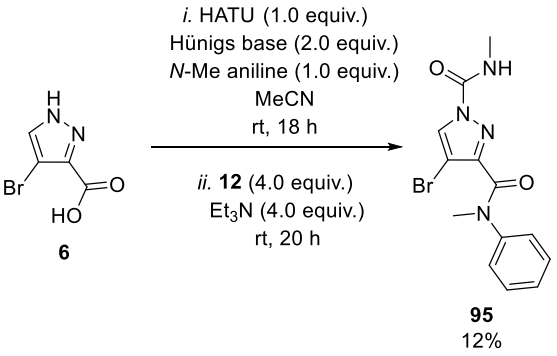

Scheme 33: Synthesis for tertiary amide analogue 95.

For *N*-methyl amide **95**, the amide coupling protocol previously described (**Scheme 30**) was used. Acid **6** was treated with HATU in the presence of Hünig's base followed by addition of *N*-methyl aniline. Compound **12** and Et_3N were added after completion of the amide synthesis. We were able to isolate **95** in 12% yield after purification by column chromatography, **Scheme 33**.

➢ DSF assay

The start of our investigation on the SAR associated with Part B was focused on the importance of the amide NH bond. To answer this question the corresponding ester **94** was synthesized, along with the *N*-Me amide analogue **95**.

The analogues were screened in the DSF assay and the results presented in **Graph 17**.

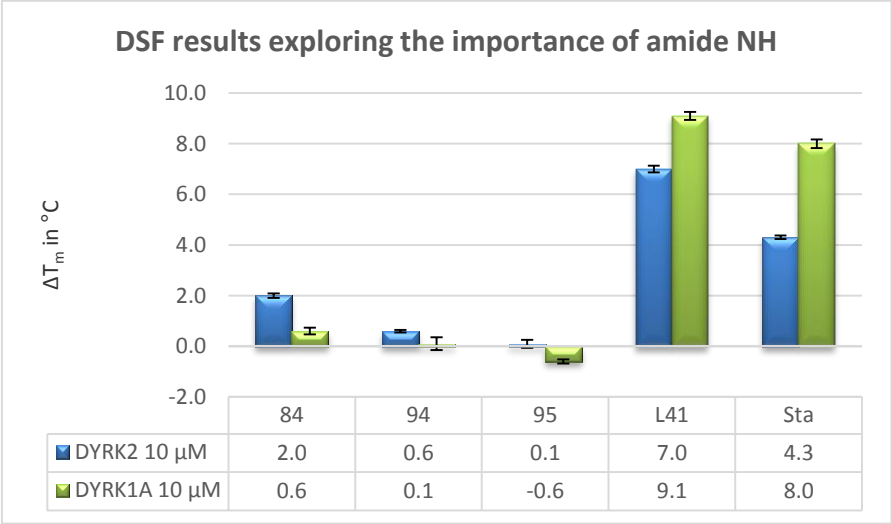

Graph 17: Bar graph representation of the T_m of compounds 94, 95, L41 and staurosporine against DRYK2 and DYRK1A.

From these results, it was concluded that the amide NH was essential for the stabilization of DYRK2, as both of the analogues **94** and **95** gave low T_m shifts ($T_m \leq 0.6$ °C) relative to **84** ($T_m = 2.0$ °C).

➢ Biochemical assay

We were interested to get further data on ester **94** and compare it to **84**, **Table 7**.

Table 7: % displacement of 94 and 84 at single point concentration at 1 µM for DYRK2 and DYRK1A.

Compound	DYRK2
84	13 ± 4%
94	7 ± 5%

Analogue **94** was slightly less active than **84** with 7 ± 5% displacement at 1 µM. The high error did not necessarily confirm the conclusion that the NH of the amide was

important for activity. Nevertheless, a secondary amide would still be kept throughout the SAR study.

b. **Pyridine amide analogues**

As with the oxyamidine series, we were intrigued in synthesizing pyridyl amides for this scaffold.

- Synthesis

To gain access to the three regioisomeric pyridine amide analogues the following synthesis was followed, **Scheme 34**.

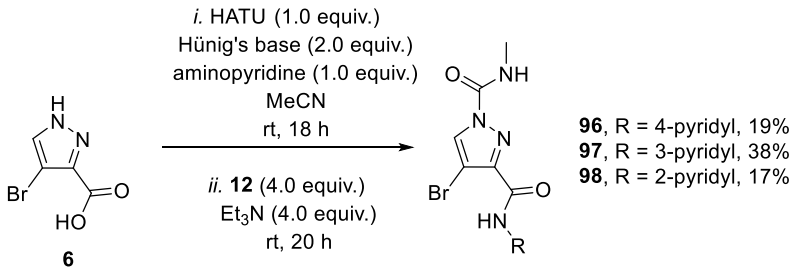

<u>Scheme 34:</u> Synthesis of pyridine amide analogues.

Treatment of acid **6** with HATU in the presence of Hünig's base was carried out followed by addition of the required amino pyridine. Acylation with **12** led to the desired pyridyl amides **96**, **97** and **98** in 19%, 38% and 17% yield respectively.

- DSF results

These derivatives were of particular interest as the nitrogen from the pyridine ring could pick up an additional H-bond interaction. A specific question that arose was whether the position of the nitrogen would influence stabilization. As such, these analogues were synthesized, **Figure 80**.

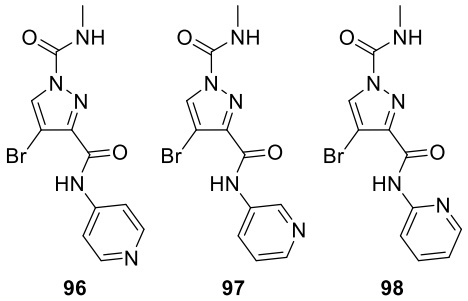

Figure 80: Pyridine analogues 96−98.

Compounds **96−98** were subjected to the DSF assay and the results obtained are collected in **Graph 18**.

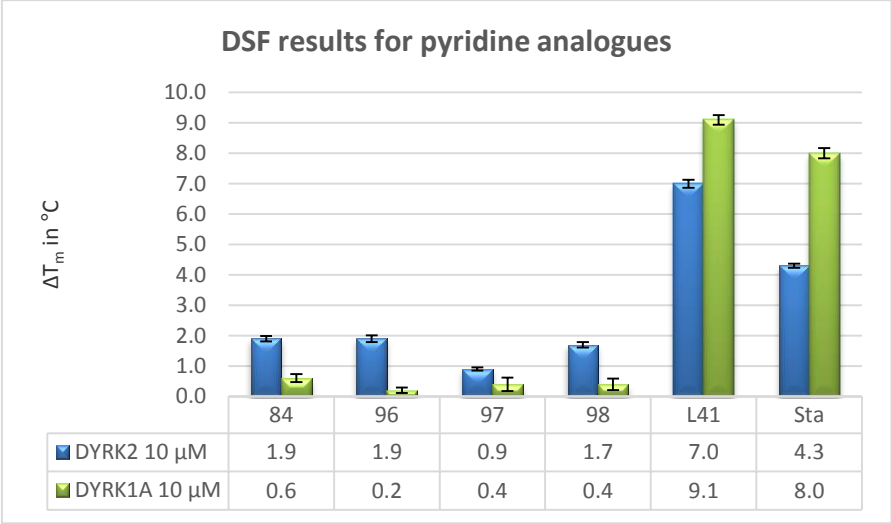

Graph 18: Bar graph representation of the T_m of compounds 96−98, L41 and staurosporine against DRYK2 and DYRK1A.

It was observed that the 4-pyridyl substituent (**96**) maintained stabilization of DYRK2 but was more selective (DYRK1A T_m = 0.2 °C) compared to phenyl amide **84** (DYRK1A T_m = 0.6 °C). Moreover, 2-pyridyl analogue **98** showed similar stabilization to **96** whereas 3-pyridyl analogue **97** showed a loss in stabilization.

- Biochemical assay

We were interested in investigating how the pyridine series would affect the binding affinity. Therefore, they were tested at a single point concentration of 1 µM against DYRK2, **Table 8**.

Table 8: % displacement of 84, 96−98 at 1 µM against DYRK2.

Compound	DYRK2
84	13 ± 4%
96	26 ± 1%
97	0 ± 3%
98	31 ± 2%

Analogue **97** (3-pyridyl) was completely inactive with 0% displacement at 1 µM. In contrast, the 4-pyridyl (**96**) and 2-pyridyl (**98**) analogues showed an increase in activity compared with amide **84**, with a displacement of around 30%. These results suggested that an interaction between the nitrogen and the protein was possible at positions 2 and 4 of the aromatic ring rendering these positions highly favourable for further investigation.

As we had previously looked into generating a graph to compare DSF results and % displacement, we also examined this series of analogues, **Graph 19**.

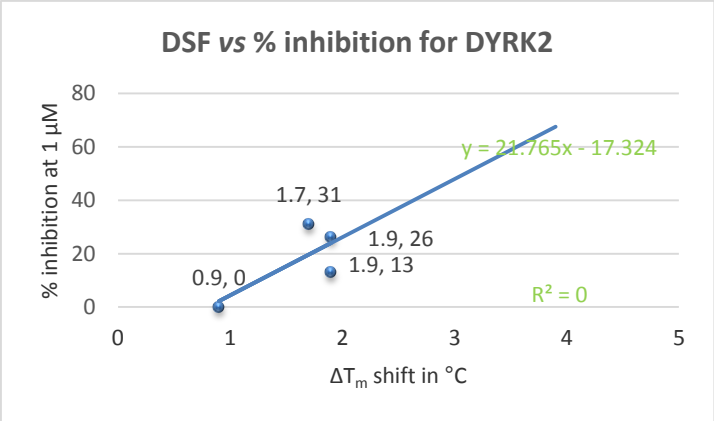

Graph 19: Graph representing DSF results *vs* % displacement at 1 µM for DYRK2 for pyridine series.

Disappointingly, the graph demonstrated how the % inhibition could not be accurately predicted using the DSF results, as no clear trend could be observed for this series.

- Docked poses

With the 3-pyridyl analogue **97** being completely inactive compared to 2-pyridyl compound **98**, we wanted to have a logical explanation to rationalize this important

observation. By docking each compound in the allosteric site, we hoped a plausible explanation would emerge, **Figure 81**.

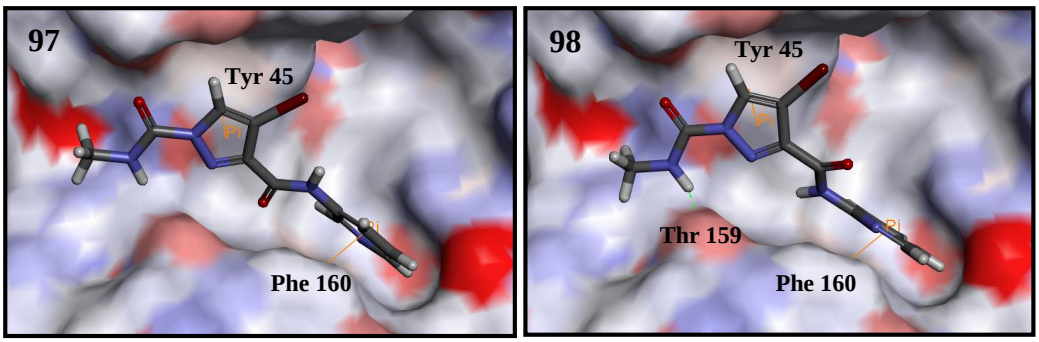

Figure 81: Predicted docked poses of 97 (left) and 98 (right) in the allosteric pocket.

Both analogues (**97** and **98**) were predicted to adopt a similar conformation in the allosteric pocket. The pyrazole ring and the phenyl rings of both **97** and **98** were foreseen to be involved in π-π stacking with Tyr 45 and Phe 160 respectively. Only **98** had an H-bond interaction between the NH of the urea and Thr 159. The nitrogen atom from the pyridine ring did not seem to be involved in any interaction from these predicted poses. The analogues were also docked in the orthosteric site to see if significant differences could be observed, **Figure 82**.

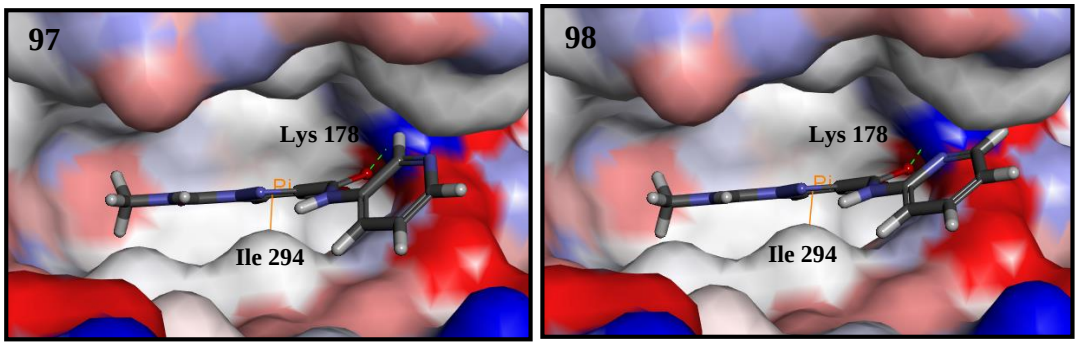

Figure 82: Predicted docked poses of 97 (left) and 98 (right) in the orthosteric site.

Both analogues, **97** and **98**, were also predicted to adopt a similar conformation when docked in the orthosteric site. They both displayed potential interactions with the same amino acids in the pocket: the pyrazole ring with Ile 294 through a π-σ interaction and the carbonyl group of the amide with Lys 178 through an H-bond interaction. Again, the nitrogen from the pyridine ring was not involved in an H-bond interaction from

these predicted poses. In both of these modelling studies, no clear predictive model helped us account for the complete loss of activity seen with **97**.

c. Amides with an electron withdrawing group

Altering the electron density on a ring by varying substituents around it is a strategy to probe for electron distribution effects on stabilization.

- Synthesis

The compounds were synthesized with the same conditions used for all of our previous amide analogues, **Scheme 35**, the products being isolated in 19−38% yield.

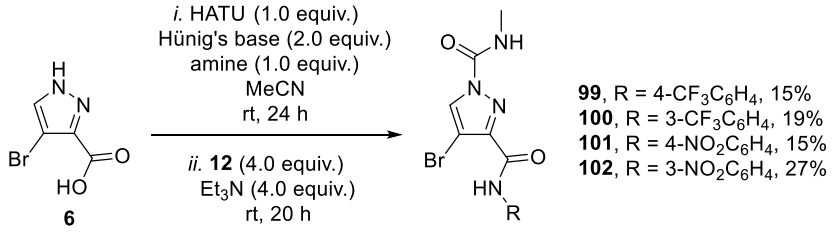

Scheme 35: Synthesis for analogues with EWG.

- DSF results

The following electron-deficient analogues were synthesized, **Figure 83**.

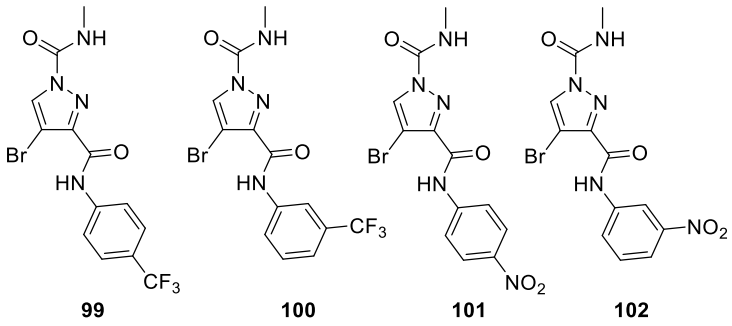

Figure 83: EW analogues.

The trifluoromethyl group was an interesting group to incorporate as it is a bioisostere of chlorine and methyl groups. This would enable comparison with further compounds prepared. Moreover, it was also a highly electronegative group due to the polarization induced by the fluorine atoms. We therefore decided to synthesize the 4-CF_3 (**99**) and 3-CF_3 (**100**) analogues to compare the substitution pattern regarding stabilization. By preparing the nitro analogues (4-NO_2, **101** and 3-NO_2, **102**) we could

potentially have access to the corresponding aniline through reduction. This would enable us to investigate electronic effects in protein stabilization.

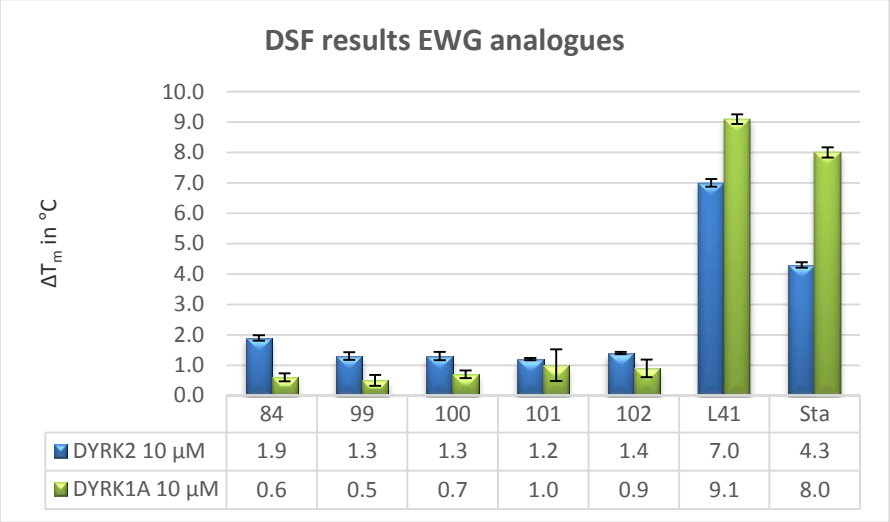

	84	99	100	101	102	L41	Sta
DYRK2 10 µM	1.9	1.3	1.3	1.2	1.4	7.0	4.3
DYRK1A 10 µM	0.6	0.5	0.7	1.0	0.9	9.1	8.0

<u>Graph 20:</u> Bar graph representation of the T_m of compounds 84, 99−102, L41 and staurosporine against DRYK2 and DYRK1A.

From the results shown in **Graph 20**, we concluded that having an EWG on the ring reduced stabilization of DYRK2 for the analogues examined. Nevertheless, we did observe a rise in stabilization for DYRK1A for these analogues, especially with 4-NO_2 (**101**) and 3-NO_2, (**102**) analogues, which showed a T_m of 1.0 and 0.9 °C shift, respectively which suggested no selectivity between the two isoforms.

The EWG proved quite deceiving as they did not help gain stabilization and the compounds prepared showed no selectivity towards the desired protein. However, at this stage our conclusions that EWG on the phenyl were not favourable.

d. Amides with strong electron donating groups (SEDG)

Due to a lack of initial success through the incorporation of EWG's on the aromatic ring, we went on to explore electron donating groups. We were therefore interested in investigating the difference in the donating capacity of these groups as well as their H-bonding abilities.

- Synthesis

For methoxy analogue **105**, we did not have the desired aniline in house. Therefore, we reduced 4-nitroanisole **103** in the presence of ammonium chloride and iron in a 2:1

acetone:H_2O solution for 3 h at 60 °C. This gave the aniline **104** in 93% yield that was directly used in the amide synthesis, **Scheme 36**.

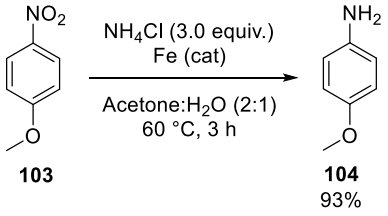

Scheme 36: Reduction of 4-nitroanisole 103.

With the other amines in house, acid **6** was treated with HATU and Hünig's base and the appropriate aniline. After 24 h, acylation was carried out by the addition of **12** in the presence of Et_3N, **Scheme 37**. This gave the amide analogues **105−111a** in 12−42% yield after purification by column chromatography.

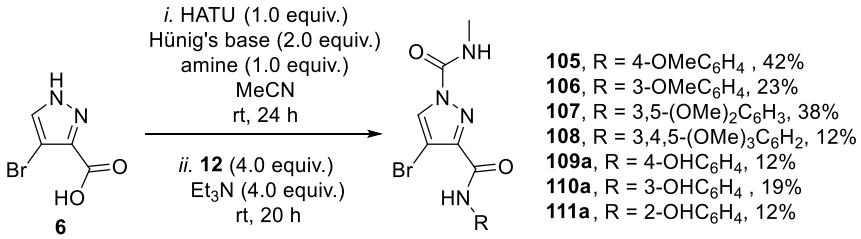

Scheme 37: Amide synthesis for analogues 105−111a.

For hydroxyl analogues **109a**, **110a** and **111a**, we were also able to isolate the carbamate derivatives **109b**, **110b** and **111b**. Due to the excess of reagent **12** (4.0 equiv.), the phenol group also reacted to give co-products **109b**, **110b** and **111b** in 4%, 8% and 4% yield, respectively, **Figure 84**.

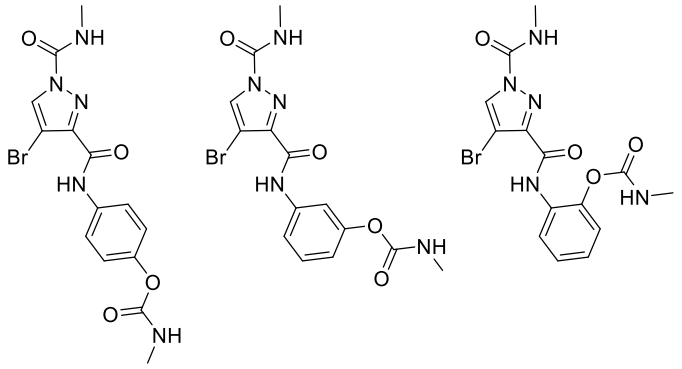

Figure 84: Co-products 109b, 110b and 111b.

Straightforward access to amine analogues **112** and **113**, was through reduction of nitro analogues **101** and **102**, respectively, **Scheme 38**.

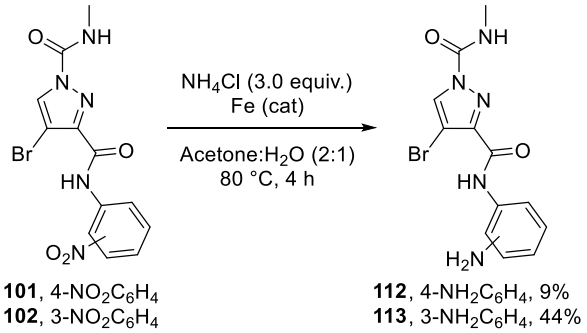

Scheme 38: Reduction of nitro compounds 456 and 474.

The reduction was carried out with ammonium chloride and iron in a 2:1 acetone:H_2O solution. The solution was heated at 80 °C for 4 hours to give the desired 4-amino amide product **112** in 9% and the 3-amino amide **113** in 44% yield.

- DSF results

The amides prepared with SEDG are presented in **Figure 85**.

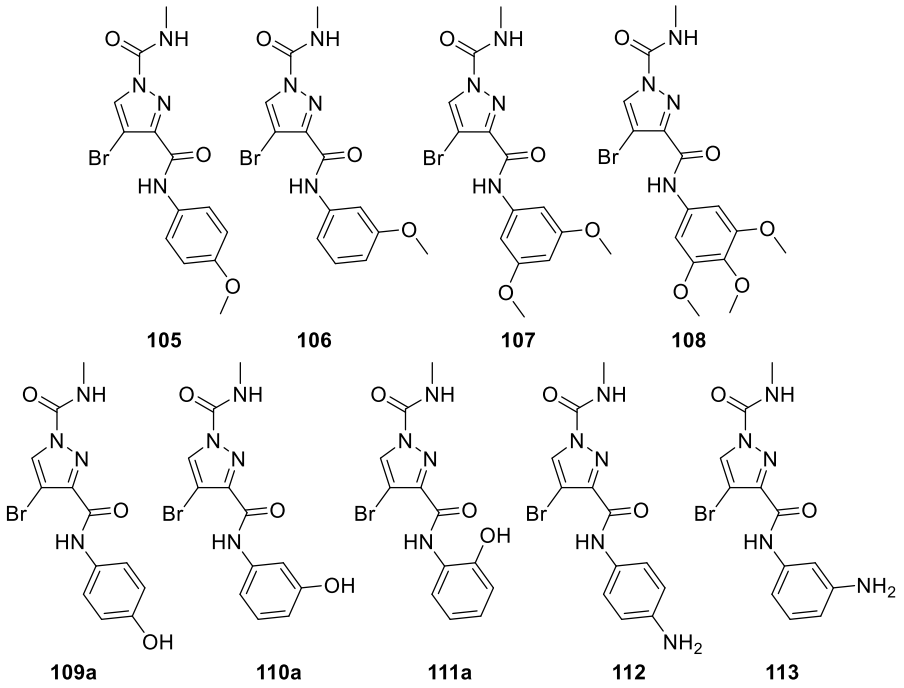

Figure 85: Analogues 105−113 with a SEDG on amide ring.

Analogues **105**, with 4-OMe and **106**, with 3-OMe, could potentially pick up an H-bond interaction through the lone pair of the oxygen. We also wanted to see how multiple methoxy groups could influence stabilization of the protein (**107** and **108**). Furthermore, the hydroxyl containing analogues **109a**, **110a** and **111a** could act as both H-bond donors and acceptors through the proton and the oxygen respectively. We also wanted to investigate the effect of having a free aniline group with analogues **112** and **113**. A direct comparison could be carried out between these analogues and their nitro derivatives **101** and **102**.

The compounds prepared were submitted to the DSF assay against DYRK2 and DYRK1A and the results are presented in **Graph 21**.

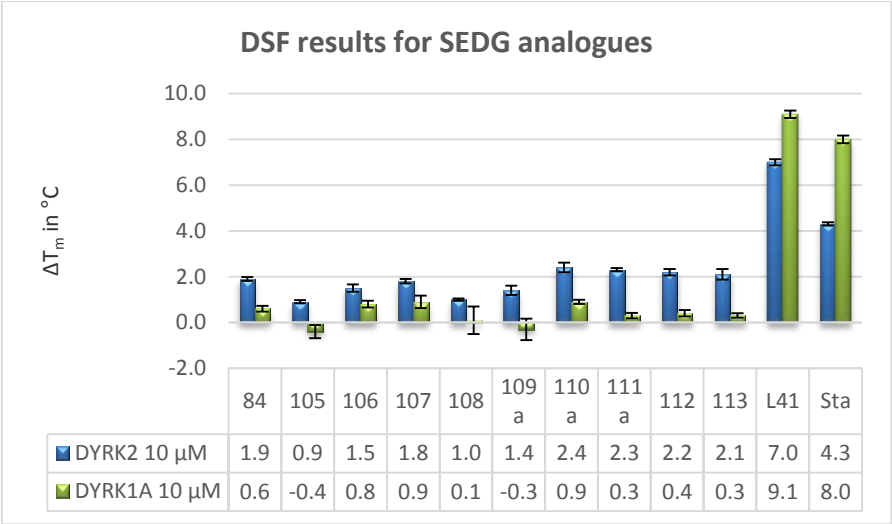

	84	105	106	107	108	109 a	110 a	111 a	112	113	L41	Sta
DYRK2 10 µM	1.9	0.9	1.5	1.8	1.0	1.4	2.4	2.3	2.2	2.1	7.0	4.3
DYRK1A 10 µM	0.6	-0.4	0.8	0.9	0.1	-0.3	0.9	0.3	0.4	0.3	9.1	8.0

Graph 21: Bar graph representation of the T_m of compounds 84, 105−113, L41 and staurosporine against DRYK2 and DYRK1A.

From the set of results in **Graph 21**, only phenol analogues (**110a** and **111a**) and amine analogues (**112** and **113**) showed an increase in stabilization of DYRK2 albeit slight. Phenol analogue **110a**, with the hydroxyl in the *meta* position, showed an increase in stabilization with a T_m of 2.4 °C for DYRK2 and still showed acceptable selectivity with a shift of 0.9 °C for DYRK1A. When the hydroxyl was in the *ortho* position, (**111a**) similar stabilization to **110a** was observed, but greater selectivity over DYRK1A was obtained with a shift of 0.3 °C. Finally, the position of the amine group (*meta* or *para*, **113** and **112**, respectively) did not appear to influence the shift, which suggested that they did not pick up an additional specific interaction. Moreover, we had previously seen that when the nitro group (**101** or **102**) was present no selectivity was observed, whereas the anilines were more selective for DYRK2. Overall this series of compounds provided some interesting trends in the data. We therefore continued to probe the effect of EDG on stabilization.

e. Amides with a weak electron donating groups (WEDG)

We also decided to look into WEDG like vinyl, methyl (Me) and phenyl (Ph) groups.

- Synthesis

In order to introduce a phenyl group onto our aniline ring, we had to synthesize the desired amine **115**, **Scheme 39**. We therefore reacted 4-bromoaniline **114** with phenyl

boronic acid **18** in a ligand free Suzuki reaction developed by Leadbeater *et al.* under microwave irradiation.[78] After 5 min of irradiation at 150 °C, the desired 4-aminobiphenyl **115** was isolated after column chromatography in 60% yield.

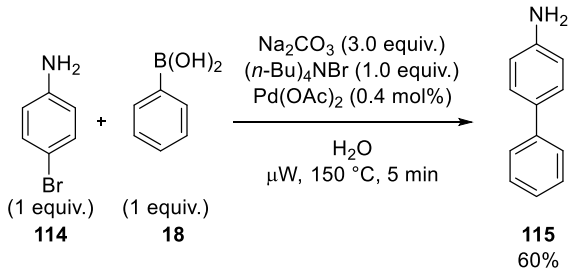

Scheme 39: Synthesis of biphenyl amine 115 by Suzuki coupling.[78]

With all the desired anilines available, the coupling of these amines with carboxylic acid **6** was carried out with the same protocol as previously described. This enabled the isolation of amide analogues **116−119** in 31−62% yield after purification by column chromatography, **Scheme 40**.

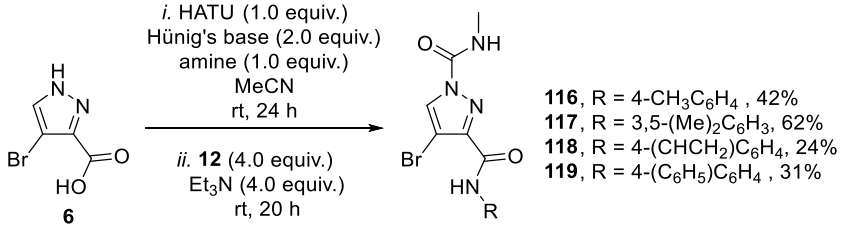

Scheme 40: Amide coupling for the synthesis of analogues 116−119.

- DSF results

The following analogues were prepared to explore how WEDG affected stabilization, **Figure 86**.

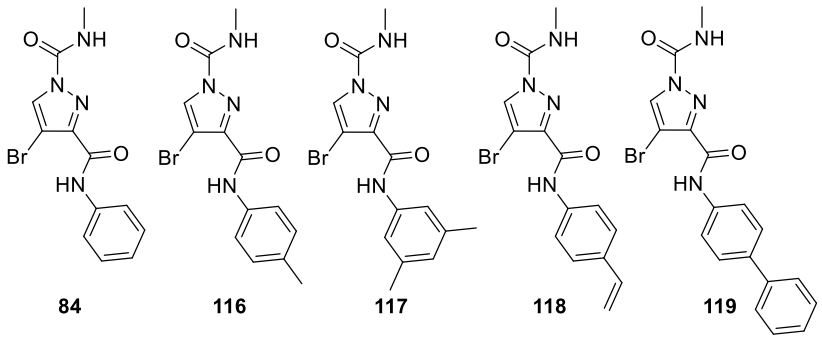

Figure 86: Weak electron donating groups for analogues 116−119.

We looked into having a Me group at the *para* position with analogue **116**, which could increase hydrophobic interactions. It could also be directly compared to the trifluoromethyl bioisostere **99**. We were also interested in having a Me group at both *meta* positions with analogue **117** which could again increase hydrophobic contact. Our vinyl analogue **118** could increase the potential for π-interactions due to the presence of the alkene. Finally, the biphenyl analogue **119** could allow access to further π-interactions.

These analogues were submitted to the DSF assay for DYRK2 and DYRK1A, **Graph 22**.

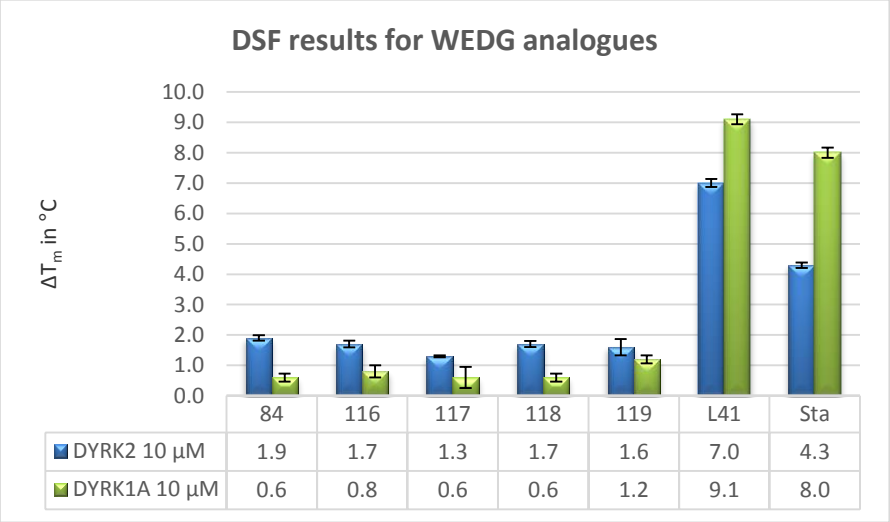

	84	116	117	118	119	L41	Sta
DYRK2 10 µM	1.9	1.7	1.3	1.7	1.6	7.0	4.3
DYRK1A 10 µM	0.6	0.8	0.6	0.6	1.2	9.1	8.0

<u>Graph 22:</u> Bar graph representation of the T_m of compounds 84, 116−119, L41 and staurosporine against DRYK2 and DYRK1A.

No analogues from this series showed an increase in stabilization of DYRK2 relative to initial hit **89**. Interesting results regarding biphenyl analogue **119** were obtained which showed no selectivity towards the two DYRK isoforms. Moreover, no change in stabilization between 4-Me analogue **116** and its 4-CF_3 isostere (**99**) was observed.

We saw from this series that adding hydrophobic or π-electron rich features on this scaffold did not increase stabilization or selectivity relative to **84**.

f. **Halogen substitution on phenyl ring**

To continue our exploration on the effect of functionality on the aromatic ring we elected to incorporate halogen atoms onto the amide scaffold to see how this could influence the biological results.

➢ Synthesis

For the synthesis of analogues **120** and **121**, the conditions outlined in **Scheme 41** were followed.

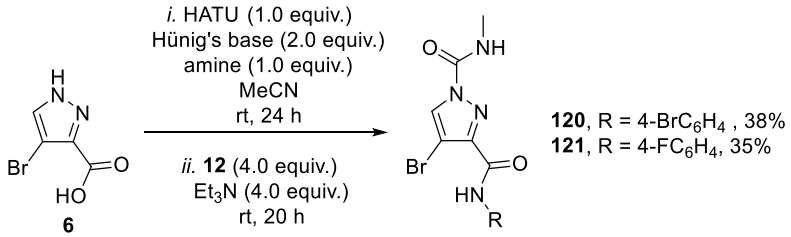

Scheme 41: Synthesis of halogenated analogues 120 and 121.

After standard coupling, purification of the crude reaction mixture gave analogues **120** and **121** in 38% and 35% yield respectively.

➢ DSF results

Halogens can introduce steric requirements as well as specific interactions. We were therefore interested in exploring the effect of these substituents on the scaffold, **Figure 87**.

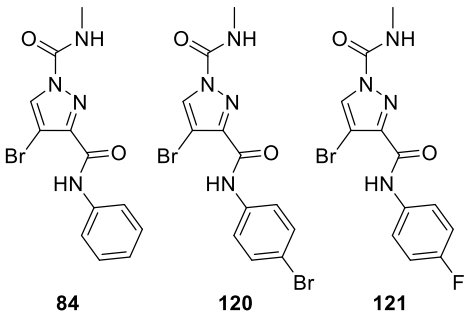

Figure 87: Halogenated analogues 120 and 121.

Fluorine is an isostere for hydrogen and is very electronegative, introducing a highly polarized C-F bond.[70] Moreover, fluorine increases lipophilicity and hydrophobic interactions which is why 4-F analogue **121** was prepared. Bromine can induce a steric

change and can act as a Lewis acid to an electron donor generating what is known as a halogen bonding interaction,[79] which led to the preparation of 4-Br analogue **120**. Compounds **120** and **121** were examined in the DSF assay, **Graph 23**.

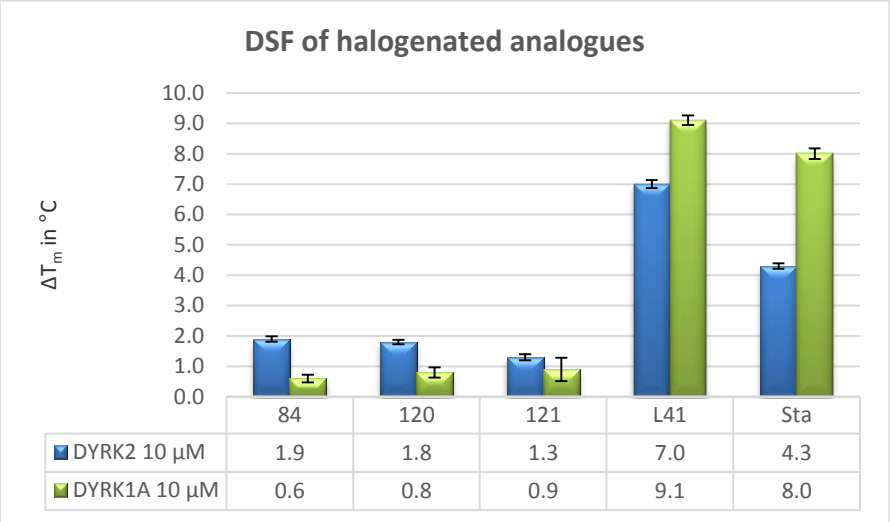

	84	120	121	L41	Sta
DYRK2 10 µM	1.9	1.8	1.3	7.0	4.3
DYRK1A 10 µM	0.6	0.8	0.9	9.1	8.0

Graph 23: Bar graph representation of the T_m of compounds 84, 120, 121, L41 and staurosporine against DRYK2 and DYRK1A.

Adding a halogen to the *para* position of the phenyl amide did not help increase stabilization of the protein of interest. In contrast, improved DYRK1A stabilization was observed for these analogues.

Therefore, halogen substitution had led to a decrease in selectivity between the isoforms and no significant increase in stabilization, suggesting this substitution was not appropriate for further investigation.

g. Disubstituted amides with different electronic effects

Having had no clear steer on SAR using mono-substituted aromatic rings we decided to investigate how the presence of two substituents with different electronic effects could influence stabilization of the protein.

- Synthesis

Amide coupling was carried out with a similar protocol with the required anilines, **Scheme 42**.

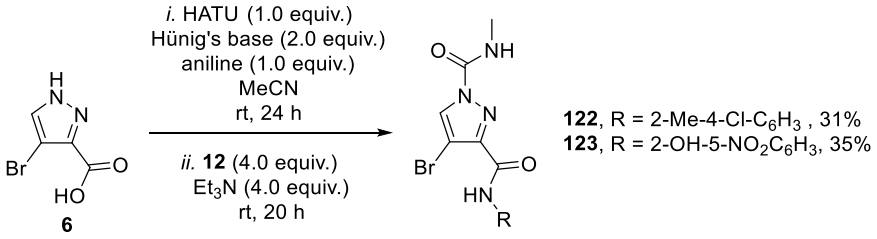

Scheme 42: Synthesis for analogues 122 and 123.

Analogue **122** was isolated and purified by column chromatography in 31% yield. Analogue **123**, precipitated out of solution overnight in H_2O and was filtered. No purification was needed and **123** which was isolated in 35% yield.

- DSF results

Disubstituted analogues **122** and **123** were synthesized to explore electronic patterns on stabilization, **Figure 88**.

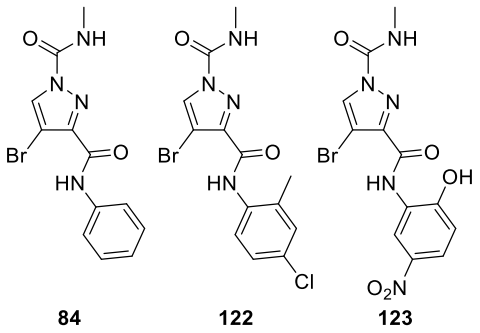

Figure 88: Disubstituted amide analogues 122 and 123.

Analogue **122** was of interest as the chlorine could be involved in halogen bonding with an electron donor as well as influence hydrophobicity. Analogue **123** was of particular interest as the nitro group and hydroxyl could both be involved in H-bonding. Moreover, the electron withdrawing effect of the nitro group would lower the pKa of the phenol, which could influence stabilization. This analogue could be directly compared to hydroxyl analogue **111a** (T_m = 2.3 °C) and nitro analogue **102** (T_m = 1.4 °C) which would allow interpretation of the importance of each substituent amide **123**. Results from the DSF assay are outlined in **Graph 24**.

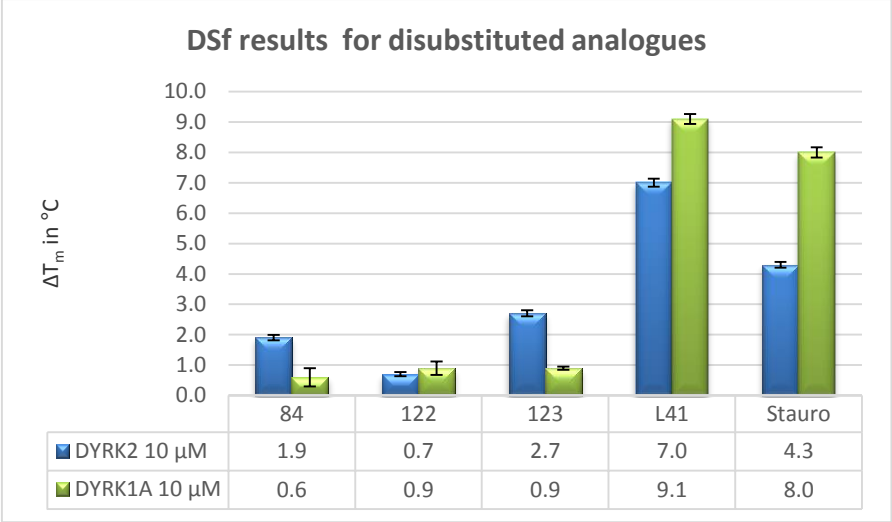

<u>Graph 24:</u> Bar graph representation of the T_m of compounds 84, 122, 123, L41 and staurosporine against DRYK2 and DYRK1A.

Analogue **122** was not selective and stabilized both protein isoforms weakly. In contrast, analogue **123** showed a significant increase in protein stabilization with a T_m = 2.7 °C for DYRK2. It also showed a minimum stabilization of 0.9 °C for DYRK1A but could still be considered selective. This was an important breakthrough in this series and our first important increase.

- Biochemical assay

Analogue **123** showed a high temperature shift in the DSF assay, which could suggest an important interaction with the receptor. The compound was tested in the Lanthascreen assay against DYRK2 and DYRK1A at 1 µM, **Table 9**. Hydroxyl analogue **111a** and nitro analogue **102** were also examined to compare their activity with **123**.

<u>Table 9:</u> % displacement of analogues at 1 µM against DYRK2 and DYRK1A.

Compound	DYRK2	DYRK1A
84	13 ± 4%	4 ± 1%
102	5 ± 3%	ND
111a	24 ± 1%	ND
123	64 ± 0%	-13 ± 0%

Analogue **123** showed 64% displacement at 1 µM for DYRK2 and showed complete selectivity between the two isoforms (DYRK1A = -13%). It was interesting to see that when the hydroxyl was present on the ring (**111a**) only 24% displacement was observed and when only the nitro group was present (**102**) only 5% inhibition was observed. Therefore, the combination of these two substituents resulted in a significant increase in activity. By using a predictive pKa calculation, nitrophenol **123** has a pKa = 6.4 for the phenol whereas phenol analogue **111a** has a pKa = 8.8.[80] This reduction in pKa of the phenol could explain this observation. For DYRK1A inhibition, we had no clear reason for the negative result of -13% and assumed it to be 0% at that concentration. With this important increase in activity of **123**, a full inhibitory curve was carried out by LT.

IC50 (nM)	Hillslope	R^2 Value	Conc of Compound (nM)	% Displacement Point 1	Point 2
1450	0.78	0.9996	30000	99	102
1450	0.78	0.9996	10000	88	91
1450	0.78	0.9996	3330	74	76
1450	0.78	0.9996	1110	55	57
1450	0.78	0.9996	370	37	35
1450	0.78	0.9996	123	22	25
1450	0.78	0.9996	41.2	15	21
1450	0.78	0.9996	13.7	13	14
1450	0.78	0.9996	4.57	15	12
1450	0.78	0.9996	1.50	12	13

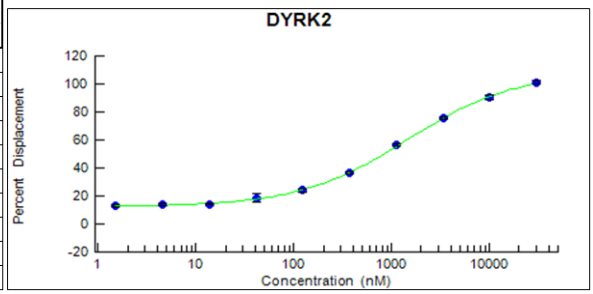

Figure 89: IC_{50} curve for 123.

The IC_{50} curve obtained in **Figure 89** indicated an IC_{50} = 1.45 µM for **123**. This was an important breakthrough as we had increased the activity by 10 fold compared to **84**. Nevertheless, we were still eager to get more active compounds and continued our exploration around this scaffold.

- Docked poses

With a 10 fold increase in activity between **84** and **123**, we wanted to generate a potential explanation through modelling.

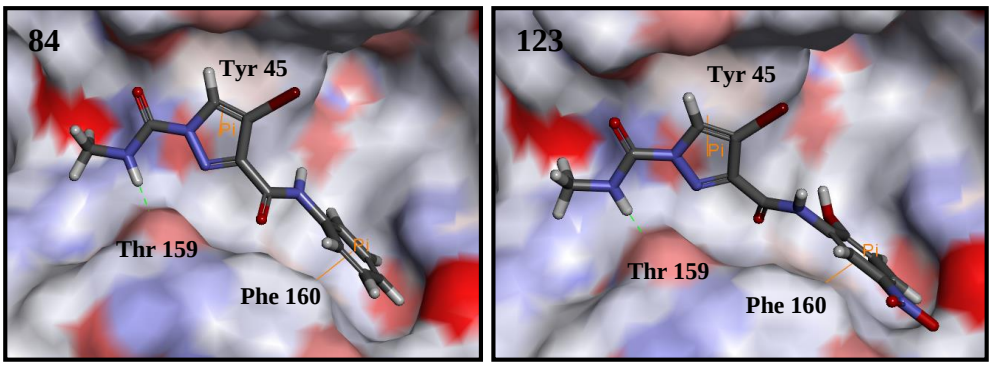

Figure 90: Predicted docked poses of 84 (left) and 123 (right) in the allosteric pocket.

The predicted poses of both **84** and **123** adopted a similar conformation and were involved in the same potential interactions when docked in the allosteric pocket, **Figure 90**. The pyrazole ring and the phenyl ring were foreseen to be involved in π-π stacking with Tyr 45 and Phe 160 respectively. Moreover, the NH of the urea interacted with Thr 159 through H-bonding. From these predicted poses there was no clear evidence as to why **123** was 10 times more active than **84** although the phenol moiety was potentially pointing into the binding site no specific interaction with the enzyme was observed. We decided to follow up by docking these compounds in the orthosteric site of DYRK2, **Figure 91**.

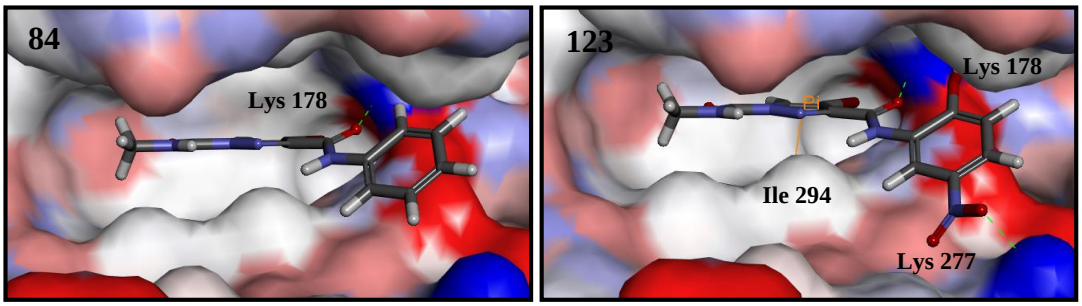

Figure 91: Predicted docked poses of 84 (left) and 123 (right) in the orthosteric site.

A clear difference was observed between the two predicted poses of the analogues when they were docked in the orthosteric site. As previously discussed, **84** was foreseen to only be involved in one H-bond interaction between the carbonyl group of the amide and Lys 178. Within this predicted model, **123** was involved in two H-bond interactions between the carbonyl group and Lys 178 as well as the oxygen of the nitro group with Lys 277. The pyrazole ring also was expected to interact with Ile 294 through a π-σ bond interaction. These differences could explain the 10 fold increase in

activity which would suggest that our analogues might bind in the orthosteric site rather than the allosteric site.

h. **Bicyclic aromatic amides: naphthalene and quinoline series**

A parallel series of compound examined the introduction of a bicyclic aromatic amide.

- Synthesis

To investigate the effect of a bicyclic aromatic ring we examined 1-aminonaphthalene and aminoquinoline partners.

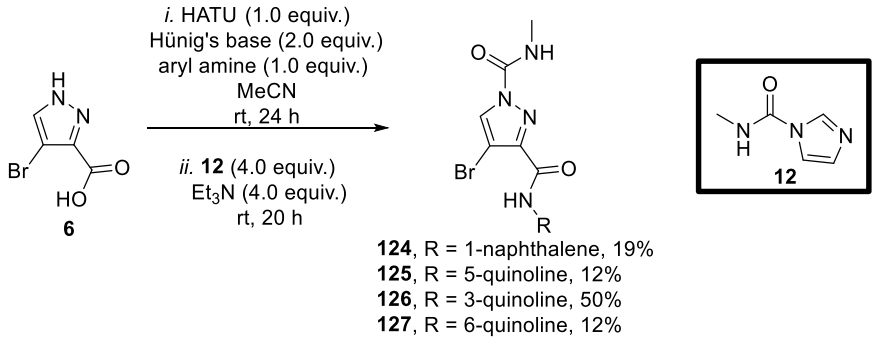

<u>Figure 92:</u> Synthesis of bicyclic aromatic analogues 124−127.

To synthesize the desired bicyclic aromatic analogues, carboxylic acid **6** was treated with HATU and Hünig's base followed by the appropriate aryl amine. The reaction was stirred for 24 h before acylation with reagent **12**. The amide analogues **124−127** were isolated in 12−50% yield, **Figure 92**.

- DSF results

These compounds would enable us to determine if the pocket could tolerate larger conformationally fixed groups, **Figure 93**.

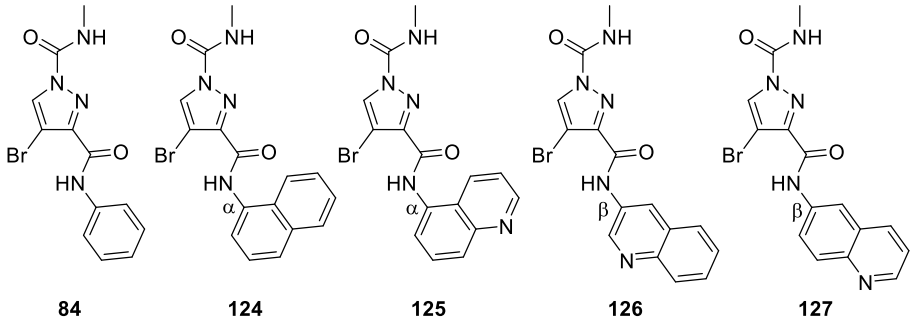

Figure 93: Naphthalene and quinoline derivatives 124−127.

We first examined having a naphthalene ring with analogue **124** to see how this would affect stabilization. We then went on to investigate 5-aminoquinoline (**125**) to see if the nitrogen could be involved in H-bonding and therefore increase stabilization. We also explored 3-aminoquinoline (**126**) and 6-aminoquinoline (**127**) to see how the ring position (α or β to the fused ring system) as well as the nitrogen position could influence stabilization.

These analogues were examined in the DSF assay for DYRK2 and DYRK1A stabilization with the results presented in **Graph 25**.

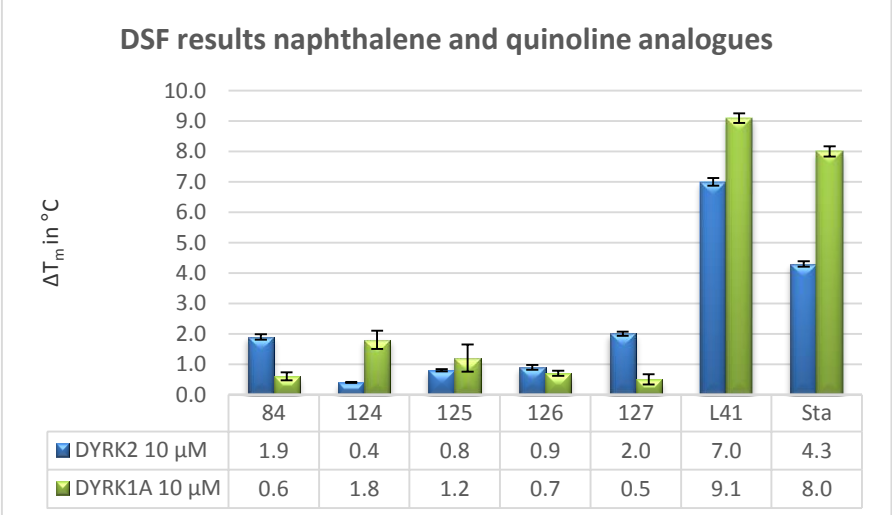

Graph 25: Bar graph representation of the T_m of compounds 84, 124−127, L41 and staurosporine against DRYK2 and DYRK1A.

The results for this series revealed no increase in stabilization of DYRK2 but still showed interesting results compared to previous lead compounds. With naphthalene analogue **124**, we observed a complete switch of selectivity compared to our previous

series. It stabilized DYRK1A with a shift of 1.8 °C and did not stabilize DYRK2 (T_m = 0.4 °C). When a quinoline was present β to the fused ring system, a different result was obtained depending on the position of the nitrogen. With 3-aminoquinoline (**126**) no selectivity was observed and the compound barely stabilized both proteins. In contrast, with 6-aminoquinoline (**127**) an increase in stabilization of DYRK2 was observed when compared to the other analogues of this series with a T_m = 2.0 °C. This compound also retained selectivity. In hindsight, it would have been interesting to examine the β-naphthalene analogue but due to perceived difficulties in synthesizing the starting aniline, it was not investigated. From this series we were unable to increase stability with a bicyclic aromatic 6-membered ring system.

- Biochemical assay

As we observed a switch in selectivity for analogue **124** in the DSF assay, we decided to see if the same results could be observed in the Lanthascreen assay.

Table 10: % displacement of 84 and 124 at 1 µM against DYRK2 and DYRK1A.

Compound	DYRK2	DYRK1A
84	13 ± 4%	4 ± 1%
124	9 ± 1%	5 ± 1%

The results from this assay indicated that naphthalene analogue **124** was inactive for both proteins and was not selective for DYRK1A. This suggested that we needed to acknowledge once again that T_m shifts were not providing an accurate and reliable reflection on activity.

i. Bicyclic aromatic amides: indole series

Another intriguing bicyclic core was the indole. This would be a smaller ring system than the previous bicyclic aromatic rings which could be favourable.

- Synthesis

Aminoindoles were expensive to buy from suppliers. This led us to gain access to these amines through reduction of their nitro precursors, **Scheme 43**.

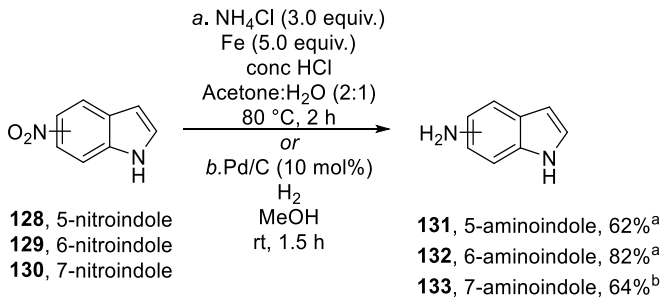

Scheme 43: Reduction of nitroindoles 128−130 to desired aminoindoles 131−133.

We first applied the reduction conditions from a patent to 5-aminoindole **131** and 6-aminoindole **132**.[81] The nitroindoles were reduced with NH_4Cl and iron in a 2:1 acetone:H_2O solution for 2 h at 80 °C. This gave **131** and **132** with no further purification in 62% and 82% yield respectively. It was decided that hydrogenation would be applied for the reduction of 7-nitroindole **130** as the work up was easier.[82] Simple filtration of the reaction mixture through celite followed by washing with MeOH gave the 7-aminoindole **133** in 64% yield after trituration.

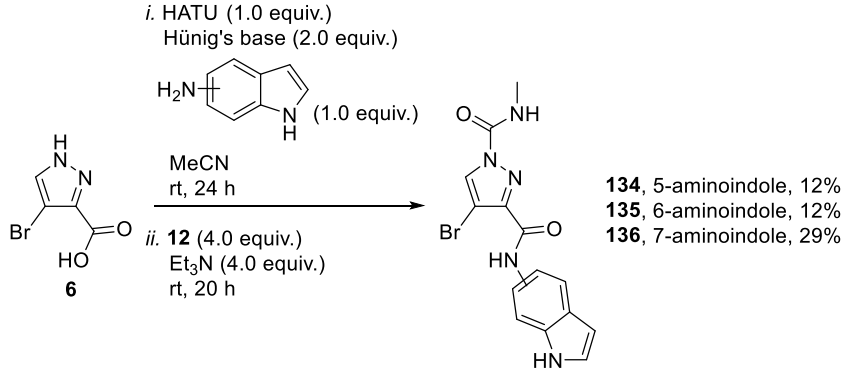

Scheme 44: Synthesis for indole amide analogues 134−136.

The next step was to synthesize the amide analogues by coupling the pyrazole ring, **Scheme 44**. The aminoindole analogues **134−136** were isolated after column chromatography in 12−29% yield.

- DSF results

Tryptophan is an amino acid that has an indole side chain and indoles are known to be important scaffolds in numerous drug molecules.[83] We therefore decided to synthesize a series of indole amides by varying the position of the amide link, **Figure 94**.

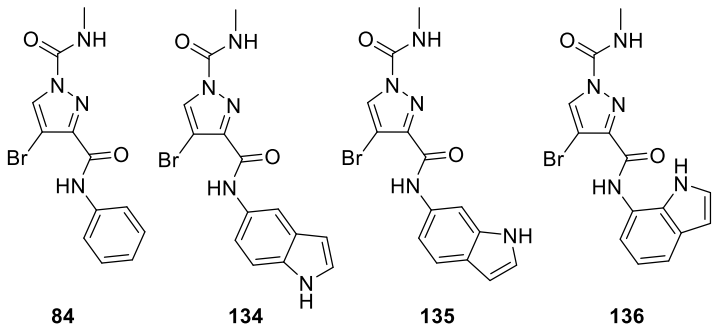

Figure 94: Indole amide analogues 134−136.

Analogues **134** and **135** would allow us to investigate how stabilization was influenced with regard to the position of the H-bond donor amine. Given the activity associated with phenol **123**, this alternative HBD with **136** could provide additional insight.

The indole amide series was tested in the DSF assay against DYRK2 and DYRK1A and the results presented in **Graph 26**.

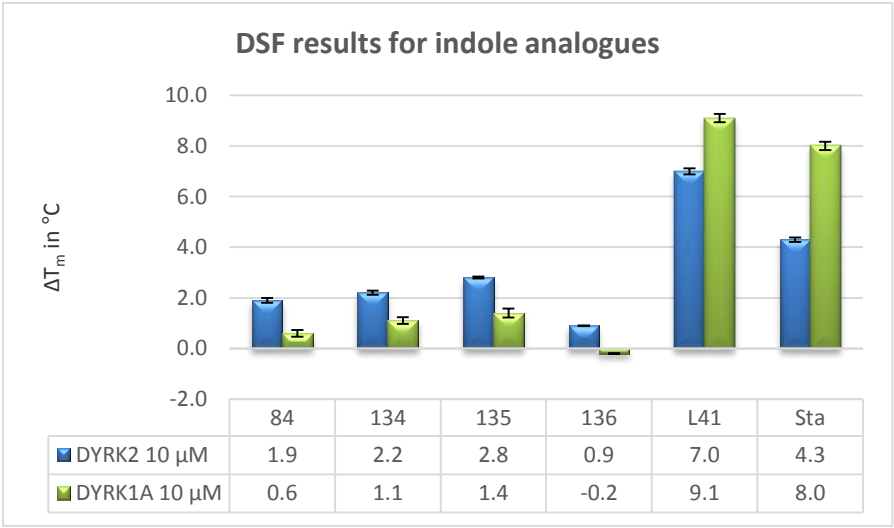

	84	134	135	136	L41	Sta
DYRK2 10 µM	1.9	2.2	2.8	0.9	7.0	4.3
DYRK1A 10 µM	0.6	1.1	1.4	-0.2	9.1	8.0

Graph 26: Bar graph representation of the T_m of compounds 84, 134−136, L41 and staurosporine against DRYK2 and DYRK1A.

Analogues **134** and **135** showed an increase in stabilization for DYRK2 with a T_m of 2.2 and 2.8 °C, respectively relative to **84**. Unfortunately, they were less selective and showed a similar level of stabilization of DYRK1A. In contrast, analogue **136** showed more selectivity towards DYRK2 but did not stabilize this protein to a comparable extent (T_m = 0.9 °C) to that of **84**.

➢ Biochemical assay

Indole analogues **135** and **136** were sent for a single point concentration assay at 1 µM on DYRK2 with the results shown in **Table 11**.

Table 11: % displacement of analogues at 1 µM against DYRK2.

Compound	DYRK2
84	13 ± 4%
135	24 ± 2%
136	4 ± 6%

The results corroborate the trend observed in the DSF assay. Analogue **135** showed more activity than **84** towards DYRK2 at 1 µM with 24% inhibition. Analogue **136** displayed 4 ± 6% inhibition at the same concentration which suggested either the same activity as **84** or inactivity. Nonetheless, this indicated that the position of the NH was crucial for activity. Once again we had obtained a clear indication of the potential of an H-bonding interaction between the aromatic ring of the amide and the target protein. It was also clear that the vector of this H-bond was important and should be the focus of our attention

➢ Docked poses

We wondered if the subtle differences in activity could be explained through modelling analogues **135** ad **136** in the allosteric site, **Figure 95**.

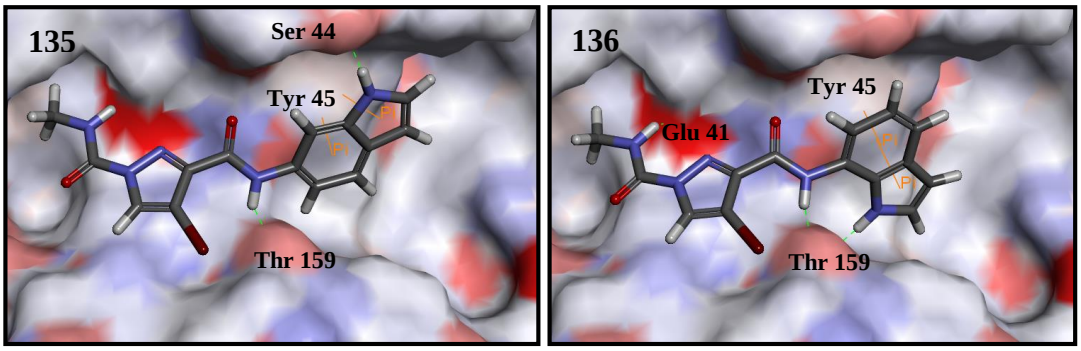

Figure 95: Predicted docked pose of 135 (left) and 136 (right) in the allosteric pocket.

Analogue **135** showed two H-bond interactions between the NH of the amide with Thr 159 and the NH of the indole with Ser 44 in this predictive pose. The aromatic

π-system of the indole was expected to be involved in π-π stacking with Tyr 45. We observed that the predicted pose of analogue **136** had four H-bond interactions with the NH of the amide and the NH of the indole with Thr 159. The carbonyl group of the amide formed an H-bond interaction with Tyr 45 and the NH of the urea with Glu 41. The indole ring was also foressen to be involved in π-π stacking with Tyr 45 in a similar manner to compound **135**. From these observations, it would suggest that analogue **136** was more active than **135**, which did not agree with the experimental results. As such, we decided to dock the amides in the orthosteric site of DYRK2, **Figure 96**.

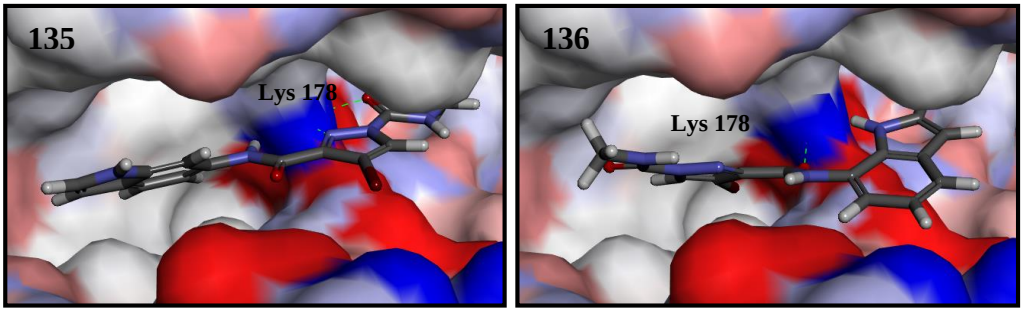

Figure 96: Predicted docked pose of 135 (left) and 136 (right) in the orthosteric site.

The analogues adopted different predicted conformations when docked in the orthosteric site. Compound **135**, had the indole in the ATP site and the urea in the adjacent side pocket in this virtual prediction. This led to the nitrogen from the pyrazole ring and the carbonyl group involved in H-bonding interaction with Lys 178. The predicted docked conformation of compound **136** had the pyrazole and urea functionality in the active site and the indole pointing into the adjacent pocket. Only the carbonyl group of the amide was close enough to be involved in a potential H-bond interaction. These observations on the predicted poses would explain the difference in activity between both analogues. This suggested that **135** and **136** might interact with the protein through the ATP site.

j. Bicyclic aromatic amides: benzoxazole series

Benzoxazole is a heterocyclic group that has shown extensive biological activities.[84] We therefore elected to synthesize a series of benzoxazole amide analogues in order

to test this group against DYRK2, with both nitrogen and oxygen being able to pick up an H-bonding interaction with the protein.

- Synthesis

Aminobenzoxazoles were expensive reagents to buy and as such, these monomers synthesized from less expensive starting materials. The required aminonitrophenol **137**−**139** was treated with triethylorthoformate in the presence of a catalytic amount of *p*-toluenesulfonic acid in toluene. The reaction was irradiated in the microwave for 10 minutes at 120 °C whereupon the nitrobenzoxazole precipitated upon cooling to -10 °C and isolated by filtration.[85] This lead to the isolation of 4-nitrobenzoxazole **140** in 64%, 5-nitrobenzoxazole **141** in 81% and 6-nitrobenzoxazole **142** in 57%. These intermediates were then reduced to their amine derivatives in the presence of NH_4Cl and iron in a 2:1 acetone:H_2O solution at 90 °C for 3 hours. The aminobenzoxazoles **143**−**145** were isolated in 46−88% yield, **Scheme 45**.

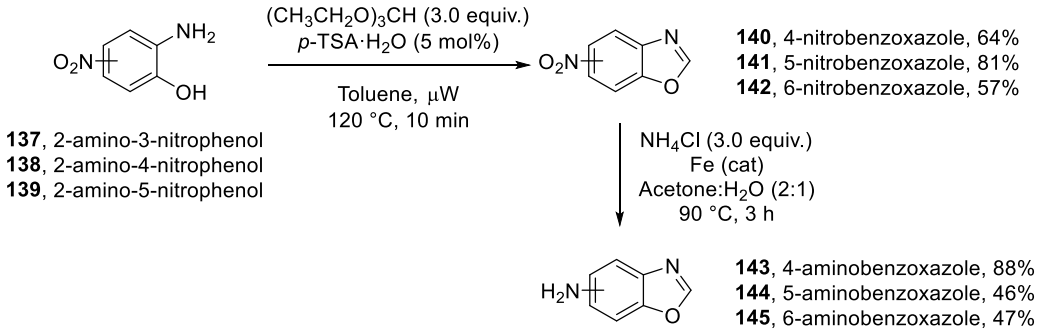

Scheme 45: Synthesis of aminobenzoxazoles 143−145.

We also wanted to prepare 2-methyl-4-aminobenzoxazole **147**. The synthesis involved treating 2-amino-3-nitrophenol **137** with triethylorthoacetate at 100 °C for 16 hours under solvent free conditions.[86] This led to the isolation of nitrobenzoxazole **146** in 88%, which was then reduced in the presence of iron for 3 hours at 70 °C.[86] 2-Methyl-4-aminobenzoxazole **147** was isolated in 67% yield, **Scheme 46**.

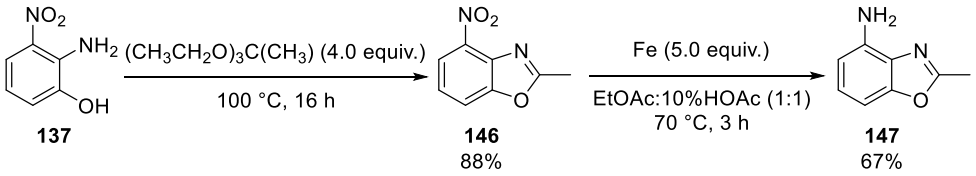

Scheme 46: Synthesis of 2-methyl-4-aminobenzoxazole 147.

With each aryl amine prepared, the next step consisted of synthesizing their amide analogues, **Scheme 47**.

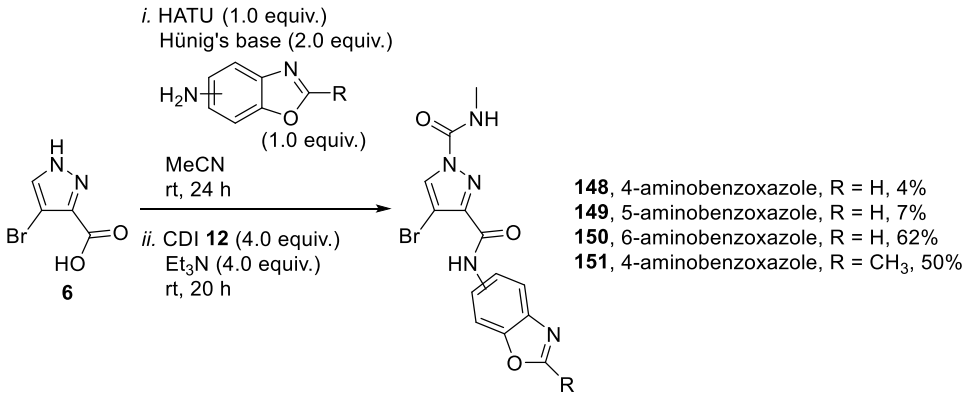

Scheme 47: Synthesis of benzoxazole analogues 148−151.

The same amide coupling conditions discussed previously was applied to carboxylic acid **6** and the appropriate aniline followed by acylation with **12**. The analogues **148−151** were isolated in 4−62% yield after purification. For analogue **151**, the compound precipitated directly from solution which, after filtration, led to the isolation of the compound in 50% yield. LC/MS showed a product that did not require further purification. Low recovery for analogues **148** and **149** was due to both reactions not reaching completion. For analogue **148**, purification was difficult due to impurities with a similar R_f which led to a final purification through crystallization by vapour diffusion with CH_2Cl_2, MeOH and PE. This enabled us to obtain an X-ray structure for the benzoxazole amide **148**, **Figure 97**.

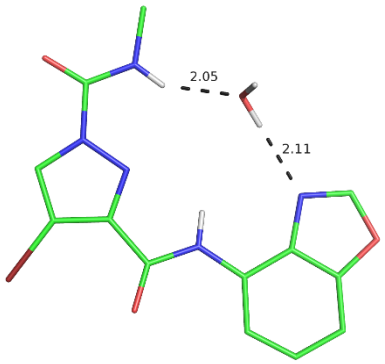

Figure 97: X-ray structure of analogue 148.

In the solid-state the benzoxazole ring of **148** was pointing towards the pyrazole ring and the urea. This conformation enabled an H-bond network between the nitrogen of the benzoxazole, a molecule of H_2O and the NH of the urea, and retains the same conformation of the other amides in the series examined by crystallography.

- DSF results

Benzoxazoles are interesting heterocycles as they are capable of both hydrophobic and π-interactions. Moreover, they have two H-bond acceptors with the oxygen and nitrogen within the scaffold. That is why each of the analogues were synthesized, **Figure 98**.

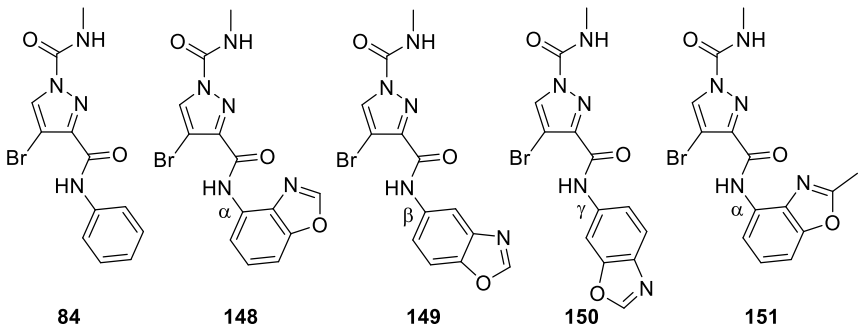

Figure 98: Benzoxazole amide analogues 148−151.

We elected to explore the ring by varying the position of the amide: α-position relative to the fused ring (**148**) along with the β (**149**) and γ (**150**) positions. These different analogues would provide more insight into the position of the H-bond acceptors needed for stabilization and activity. Methyl benzoxazole analogue **151** was also prepared to determine the tolerance of substitution along this vector.

The benzoxazole derivatives were examined in the DSF assay against DYRK2 and DYRK1A and the results are shown in **Graph 27**.

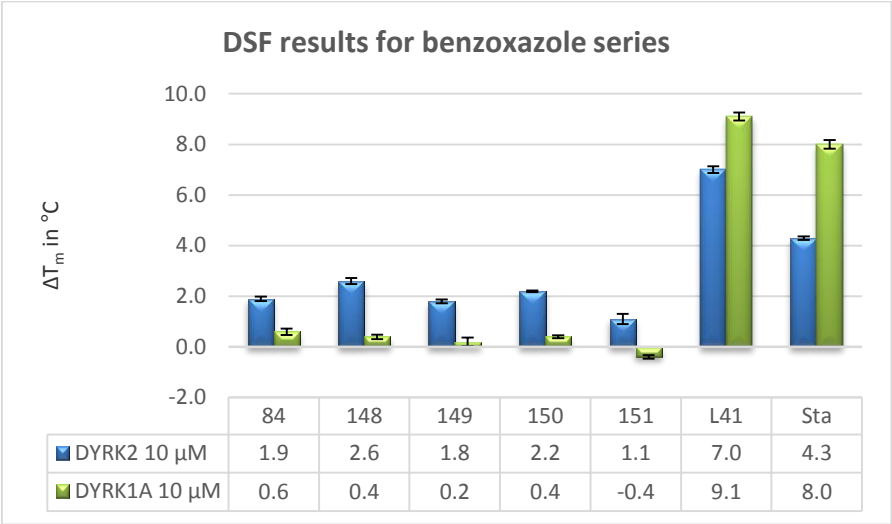

<u>Graph 27:</u> Bar graph representation of the T_m of compounds 84, 148−151, L41 and staurosporine against DRYK2 and DYRK1A.

Analogue **148** showed the best results in this series with an increase in stabilization with T_m = 2.6 ℃ for DYRK2 compared to the other benzoxazole amides. The compound also displayed excellent selectivity for DYRK1A in this assy.

- Biochemical assay

We decided to test all of these analogues in LT's single point concentration assay for DYRK2.

<u>Table 12:</u> % displacement of benzoxazole analogues at 1 µM against DYRK2.

Compound	DYRK2
84	13 ± 4%
148	43 ± 3%
149	11 ± 0%
150	26 ± 3%
151	27 ± 3%

Analogue **148** showed 43% inhibition at 1 µM for DYRK2 which was very encouraging. Compound **150** inhibited the protein to 26% at the same concentration

and analogue **149** was as active as initial hit **84** with 11% inhibition. This result showed how important the position of an HBA was in order to gain activity. The most surprising result from this assay was analogue **151** which showed similar inhibition to **150** whilst showing no stabilizing effect in the DSF assay. This observation led us to generate a graph to compare both assays, **Graph 28**. No trend could be detected within this series, which was particularly frustrating.

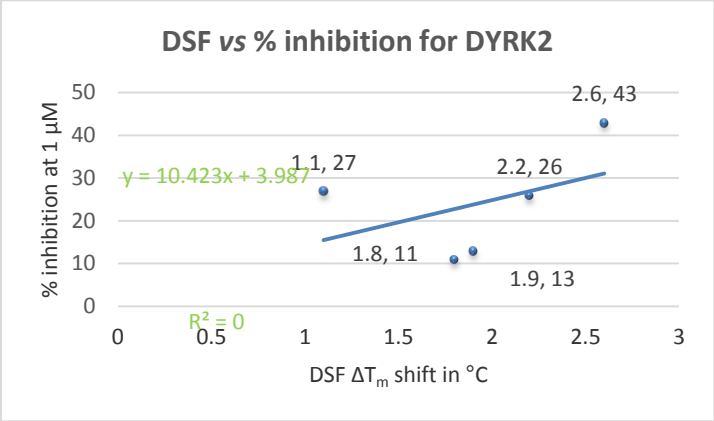

<u>Graph 28:</u> Graph representing DSF results *vs* % displacement at 1 µM for DYRK2 for benzoxazole series.

With benzoxazole analogue **148** giving such high displacement, an IC_{50} curve was generated for the inhibition of DYRK2, **Figure 99**.

IC50 (nM)	Hillslope	R^2 Value	Conc of Compound (nM)	% Displacement Point 1	% Displacement Point 2
1710	2.38	0.9877	90000	72	68
1710	2.38	0.9877	30000	79	77
1710	2.38	0.9877	10000	73	75
1710	2.38	0.9877	3330	56	68
1710	2.38	0.9877	1110	14	17
1710	2.38	0.9877	370	12	-5
1710	2.38	0.9877	123	-2	4
1710	2.38	0.9877	41.2	-1	-17
1710	2.38	0.9877	13.7	1	-21
1710	2.38	0.9877	4.50	-7	5

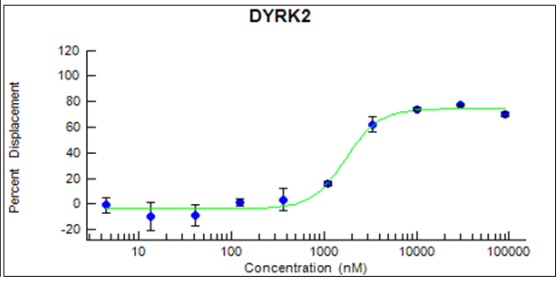

<u>Figure 99:</u> IC_{50} curve of 148.

The inhibitory effect of analogue **148** was determined to be 1.71 µM. This was an increase on initial hit **84**, but was similar to that of nitrophenol **123**. Nevertheless, a different curve shape to that of **123** was observed. Their hillslopes were highly different with **148** showing positive cooperative binding (once a ligand is bound to the enzyme, its affinity for other ligan molecues increases) whereas **123** showed negative

cooperativity. There was still potential to gain access to a more active compound, and once again we considered the importance of an H-bond to be central to gaining this activity.

- Docked poses

A significant loss in activity was observed between analogues **148** and **149**. We therefore docked them in the allosteric pocket to try and rationalize this result, **Figure 100**.

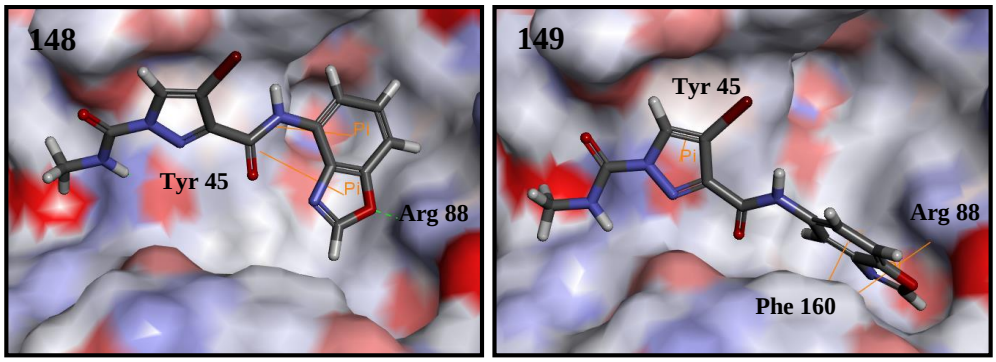

Figure 100: Predicted docked poses of 148 (left) and 149 (right) in the allosteric site.

The predicted conformations of analogues **148** and **149** in the allosteric pocket were different. Compound **148** was expected to sit at an unusual angle, with the oxygen of the benzoxazole ring involved in H-bonding with Arg 88. Even though it seemed that the benzoxazole ring was far from Tyr 45, potential π-π stacking was still observed. Analogue **149** was predicted to sit well in the allosteric pocket with the benzoxazole ring involved in some π-π stacking between the aromatic rings and Phe 160 as well as a π-cation interaction between the heterocycle and Arg 88. Due to the unclear nature of our modelling we also examined these analogues in the orthosteric site, **Figure 101**.

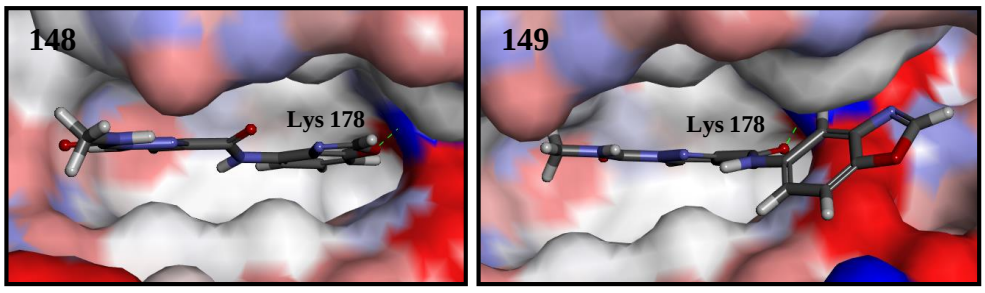

Figure 101: Predicted docked pose of 148 (left) and 149 (right) in the orthosteric site.

Analogue **148** was predicted to adopt an optimal conformation in the orthosteric site and was involved in an H-bond interaction between Lys 178 and the oxygen of the benzoxazole ring. Analogue **149**, however, was foreseen to adopt a conformation where its benzoxazole was pointing out of the active site and was more solvent exposed. The carbonyl group of the amide was involved in H-bonding with Lys 178. The former observation made regarding the predicted conformation of **149** in the orthosteric pocket might be an indication as to why it was less active than **148**.

k. Conclusion

At this point we had explored Part B of the amide analogue scaffold **84**. We examined electron-withdrawing groups, strong electron-donating groups, weak electron-donating groups, disubstituted rings and bicyclic rings.

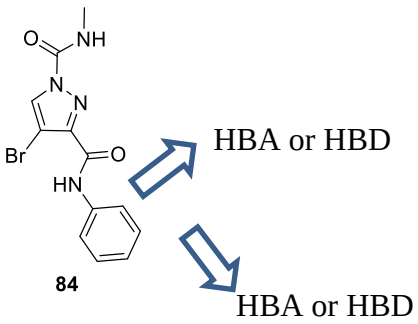

Figure 102: Exploring Part B of amide analogue 84.

We had discovered that an HBD or HBA in the *ortho* position of the phenyl ring was needed for increased activity. Moreover, we discovered that when a bicyclic aromatic system was present an HBA or HBD was needed in the *meta* position of the phenyl ring in order to gain activity, **Figure 102**. Although the activity of our compound fell short of where we wanted to be it was clear that our ligands showed potential for further optimization.

It is important to note that the majority of the data presented in this Thesis is in chronological order with regards to the synthesis of compounds. However, up to this point we had obtained no biochemical data and the evolution of the project had been directed through results from the DSF assay. At this stage, because of confusing data we decided to obtain supporting biochemical data from Life Technologies. We also obtained biochemical data of selected historical compounds from the project, the

results for which have been included at appropriate places to support discussion up to this point. It was clear that the DSF data was not accurate enough for our requirements and simply provided a crude screen prior to obtaining more reliable biochemical analysis. For the remainder of the Thesis, DSF data will be presented, however, due to our loss of confidence in the assay, this will not be discussed in detail.

It is also important to note that during the project is was difficult to carry out a SAR study based on modelling. With no clear evidence of allosteric inhibition our study was carried out by SAR based only on activity rather than being protein structure-based with an underlying hypothesis of the need for an HBA/HBD on the amide substituent. Throughout the study when results were obtained, modelling was carried out for both allosteric and orthosteric pockets for each analogue. It was rare that a clear explanation could be provided for the difference in activity between certain analogues. Therefore, we will no longer discuss the modelling results to a great extent. Thus from this point onwards our investigations were guided by activity based upon the biochemical assay.

3. Exploring Part C

Similar to the oxyamidine series, exploring the influence of the bromine atom on the pyrazole ring for activity was carried out.

a. Synthesis

From the oxyamidine series, we already had access to carboxylic acid **5** but we did not have access to chlorine analogue **153**. We therefore carried out the synthesis of this intermediate from methylpyrazole **4**, **Scheme 48**.

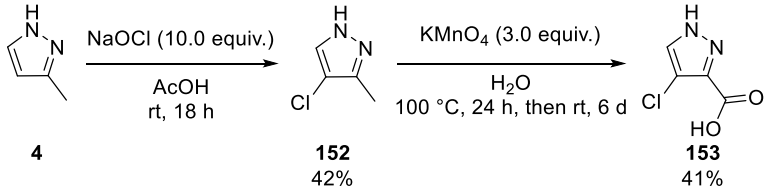

Scheme 48: Synthesis of 4-chloro-pyrazole-3-carboxylic acid 153.

Methylpyrazole **4** was treated with sodium hypochlorite in a large excess in acetic acid for 18 h at room temperature. After neutralizing the solution, chloro pyrazole **152** was

extracted and isolated in 42% yield with no need for further purification.[87] Carboxylic acid **153** was obtained after treating **152** with potassium permanganate in H_2O for 24 h at 100 °C followed by stirring for 6 days at room temperature.[60] After filtration of the manganese dioxide, the water layer was evaporated and acidified to pH = 2 and the precipitate filtered. This enabled the isolation of carboxylic acid **153** in 41% yield.

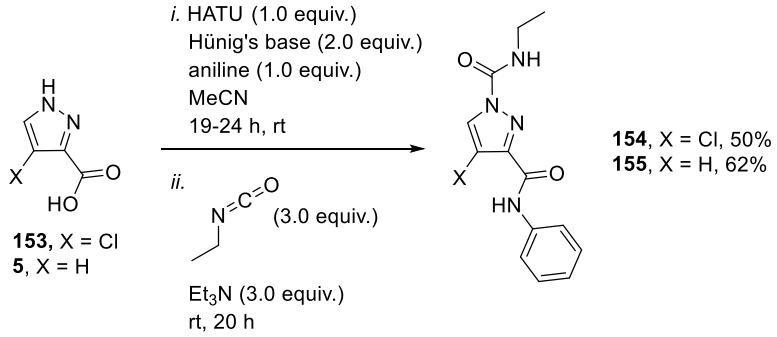

Scheme 49: Synthesis of analogues 154 and 155.

With the desired carboxylic acids prepared, the amide coupling was carried out with HATU, Hünig's base and aniline followed by acylation with ethylisocyanate. The chlorine analogue **154** was isolated in 50% yield and unsubstituted analogue **155** in 62% yield after column chromatography.

b. DSF and biochemical assay results

That following analogues were prepared to probe the importance of the bromine atom for activity, **Figure 103**.

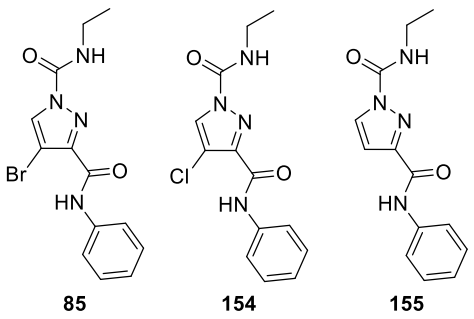

Figure 103: Probing the importance of the bromine atom with analogues 154 and 155.

Analogues **154** and **155** were submitted to the DSF assay and the results presented in **Graph 29**.

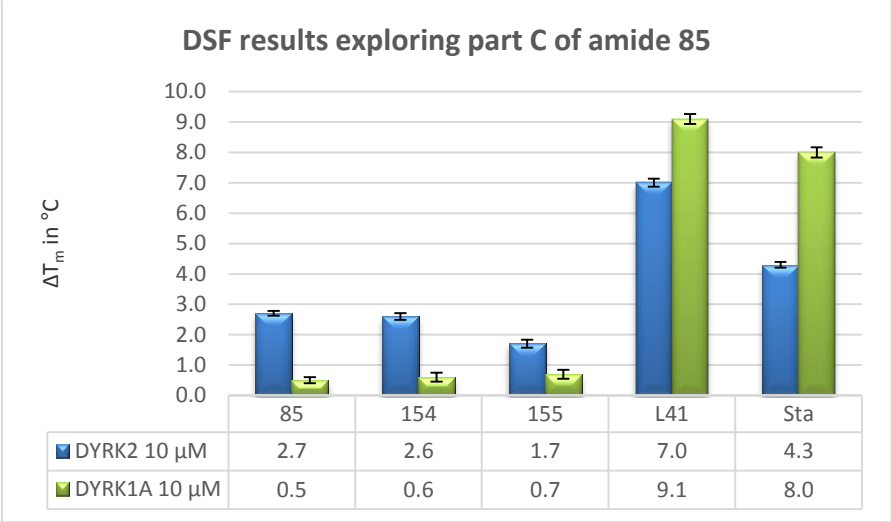

Graph 29: Bar graph representation of the T_m of compounds 85, 154, 155, L41 and staurosporine against DRYK2 and DYRK1A.

Both analogues (**154** and **155**) were tested in the single point concentration assay to determine how active they were compared to compound **85**. The results of the LT screen are shown in **Table 13**.

Table 13: % displacement of analogues at 1 µM against DYRK2.

Compound	DYRK2
84	13 ± 4%
85	5 ± 3%
154	8 ± 8%
155	11 ± 3%

From this analysis, unsubstituted analogue **155** had shown a marginal increase in activity compared to the chloro and bromo analogues (**154** and **155**). The error was high for analogue **154** which did not enable a conclusive result. Nevertheless, it was decided to maintain the bromine atom in the scaffold due to the amount of **6** prepared and the SAR data generated with this compound to date. Only if a compound showed outstanding activity would the chloro and unsubstituted derivatives be synthesized in the future.

4. Conclusion

We explored the pyrazole amide scaffold sequentially and discovered what influenced each region (Parts A, B and C) of the molecule.

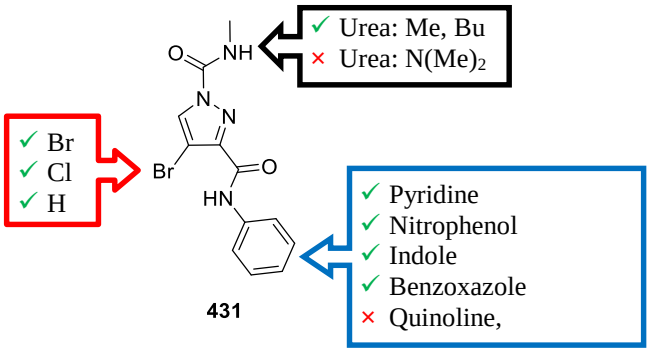

Figure 104: SAR study part by part.

From the LT results, only a small increase was observed when the bromine atom was varied to a chloro and a hydrogen atom in Part C. Exploration of Part A showed that the NH of the urea was involved in a H-bonding interaction as the *N*,*N*-dimethyl analogue attenuated activity and that extending the alkyl chain to a butyl group improved activity. Finally, with Part B, we observed that activity increased when a pyridyl amide, a nitrophenol, indole or benzoxazole amide was present. Larger bicyclic rings like naphthalene and quinoline were not well tolerated in this portion of the ligand.

Two analogues showed a near 10 fold increase from initial hit **84**: nitrophenol amide **123** with an IC_{50} = 1.45 µM and benzoxazole derivative **148** with an IC_{50} = 1.71 µM, **Figure 105**.

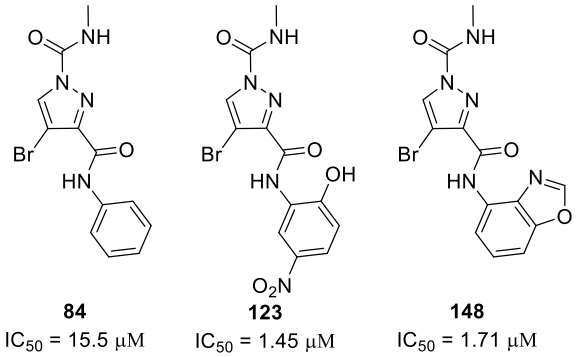

Figure 105: Best hits from SAR study starting from 84.

We decided to continue exploring this scaffold to increase activity, through investigation of the phenol amide **110a** and **111a**, the nitrophenol **123**, the pyridyl (**97**) and the benzoxazole **148** series.

III. Exploring phenol amide analogues

1. Exploring the phenol functionality with a bioisostere

a. Synthesis

N-Oxide amine **157** was prepared, **Scheme 50**.

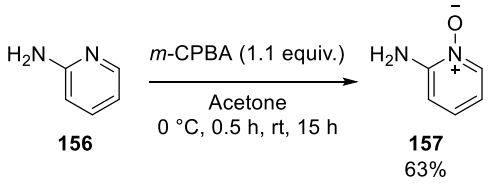

Scheme 50: Synthesis of pyridine-*N*-oxide 157.

2-Aminopyridine **156** was treated with *m*-CPBA at 0 °C for 0.5 h before leaving the reaction to stir overnight at room temperature in acetone.[88] The *N*-oxide **157** was isolated following column chromatography in 63% yield.

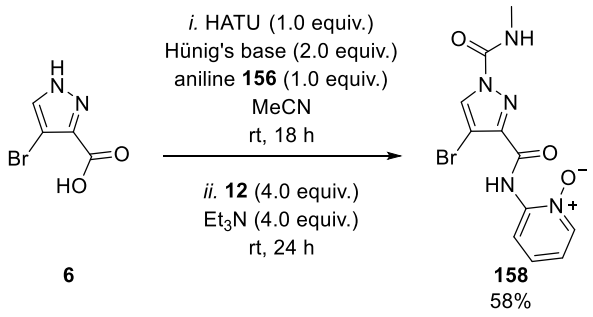

Scheme 51: Amide coupling conditions for *N*-oxide analogue 158.

To gain access to **158**, carboxylic acid **6** was treated with HATU and Hünig's base, followed by *N*-oxide aniline **156**. The reaction mixture was stirred for 18 h at room temperature and the precipitate filtered and dried to give analogue **158** in 58% yield, **Scheme 51**.

b. DSF and biochemical assay results

Analogue **158** was prepared to investigate the effect of a bioisostere of **111a** on activity, **Figure 106**. Bioisosteres are groups that have similar physicochemical properties and can produce a similar biological effect. Bioisosteric groups can introduce greater selectivity and reduce side-effects, as they can alter in size and H-bonding ability amongst other variables.[75]

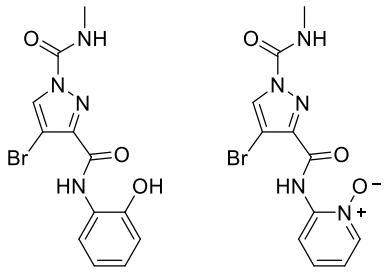

Figure 106: Bioisostere of phenol amide 111a.

Both analogues (**111a** and **158**) were submitted to the DSF assay and thermal shifts are presented in **Graph 30**.

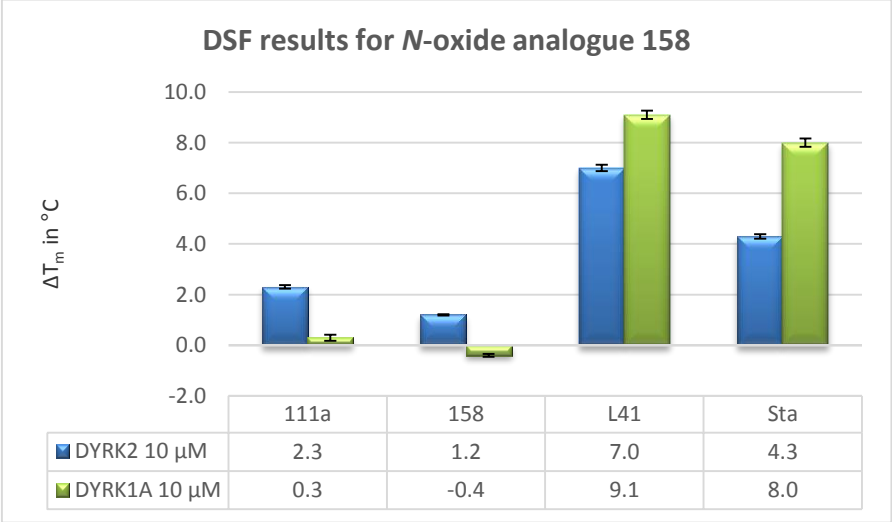

Graph 30: Bar graph representation of the T_m of compounds 111a, 158, L41 and staurosporine against DRYK2 and DYRK1A.

We were intrigued to know if this trend in the DSF assay was also applied to the binding affinity. Analogues **111a** and **158** were submitted to a single point concentration assay at Life Technologies, **Table 14**.

Table 14: % displacement of 111a and 158 at 1 µM against DYRK2.

Compound	DYRK2
84	13 ± 4%
111a	24 ± 3%
158	8 ± 1%

Hydroxyl derivative **111a**, with a binding affinity of 24% at 1 µM showed an increase in activity compared to initial hit **84**. In contrast, bioisostere **158** led to a reduced activity.

2. **Diverting to carboxylic acid derivatives**

a. **Synthesis**

As a primary step in our synthesis was the coupling of an amine with a carboxylic acid, we had to protect the carboxylic acid present on an aniline ring in order to introduce this functionality into our ligand.

- Bn protecting group

The initial synthesis consisted of protecting the carboxylic acid with a benzyl group. It was previously observed in the oxyamidine series that the urea functionality could be cleaved under basic reaction conditions. The benzyl group could easily be removed under neutral hydrogenation conditions, which should not affect the urea functionality.

Therefore, the first step was to generate the benzyl protected carboxylic acid **160** through a Mistunobu reaction, **Scheme 52**.

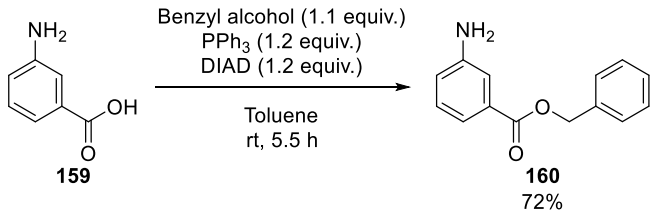

Scheme 52: Mitsunobu reaction to obtain Bn protected aniline 160.

Carboxylic acid **159** was treated with benzyl alcohol and triphenylphosphine in toluene under anhydrous conditions. The drop-wise addition of DIAD (diisopropyl azodicarboxylate) brought about the reaction, and the mixture was stirred for 5.5 h at room temperature. After column chromatography, **160** was isolated in 72% yield.

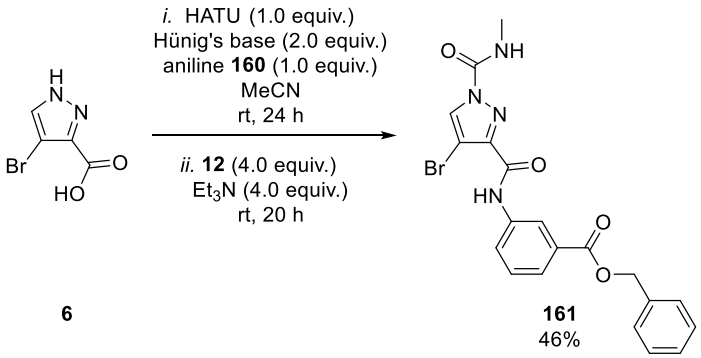

Scheme 53: Synthesis of protected carboxylic acid analogue 527.

Standard conditions for the preparation of the amide were applied to aniline **160**. The precipitate obtained was filtered and washed with a minimum amount of MeCN. This enabled the isolation of compound **161** in 46% yield without the need for further purification.

The final step to obtain the desired carboxylic acid analogue was to remove the benzyl group, **Scheme 54**.

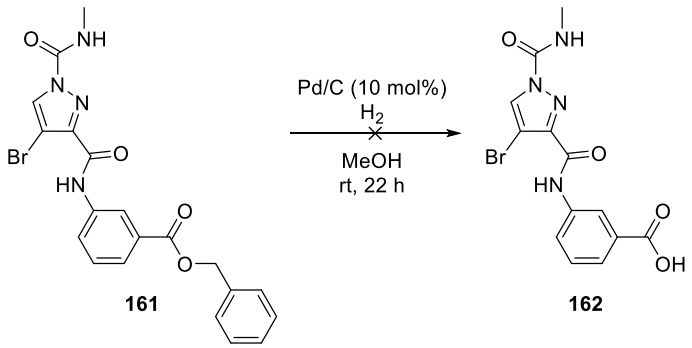

Scheme 54: Attempted synthesis of carboxylic acid analogue 162.

Unfortunately, with the conditions used (Pd/C 10 mol%, H_2, MeOH, rt) only starting material **161** was recovered, possibly because **161** was poorly solubilized in MeOH. Instead of examining alternative conditions, we decided to adopt a new strategy.

➢ Ethyl ester protecting group

Forming an ethyl ester to protect carboxylic acid **159** was our next solution. Of course, to deprotect the ester a hydrolysis was to be performed either under acidic or basic conditions, which could lead to the removal of the urea functionality. For ease of synthesis it was decided that the carboxylic acid derivative would be synthesized without the urea functionality.

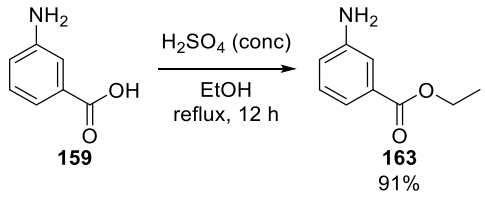

Scheme 55: Esterification of amino carboxylic acid 159.

We esterified carboxylic acid **159** in the presence of sulfuric acid and ethanol. The reaction was stirred for 12 h at reflux.[89] After purification by column chromatography, aniline **163** was isolated in 91% yield, **Scheme 55**.

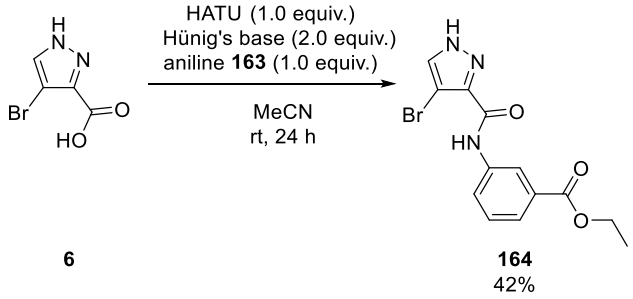

Scheme 56: Synthesis of analogue 164.

With the desired aniline prepared, we examined the amide coupling, **Scheme 56**, which gave the amide analogue **164** in 42% yield.

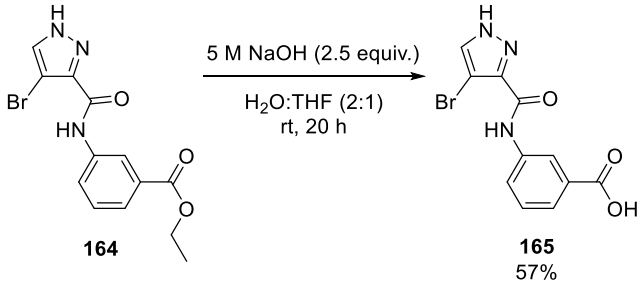

Scheme 57: Hydrolysis of 164 to give carboxylic acid analogue 165.

Finally, ester **164** was hydrolysed under basic conditions using 5 M NaOH in a 2:1 H_2O:THF solution for 20 h at room temperature.[90] After work up, the acid was recrystallized from hot H_2O and filtered which led to the isolation of carboxylic acid **165** in 57% yield.

b. DSF and biochemical assay results

Carboxylic acids can introduce acidity to a compound and can also be involved in strong electrostatic interactions as well as H-bonding. The big drawback related to this functional group is the fact that the molecule is unlikely to be able to pass the blood brain barrier.[91] However, as we were primarily interested in validating our allosteric model, the decision was made to generate a carboxylic acid analogue along with the ester analogues to explore how this would influence the biochemical data, **Figure 107**.

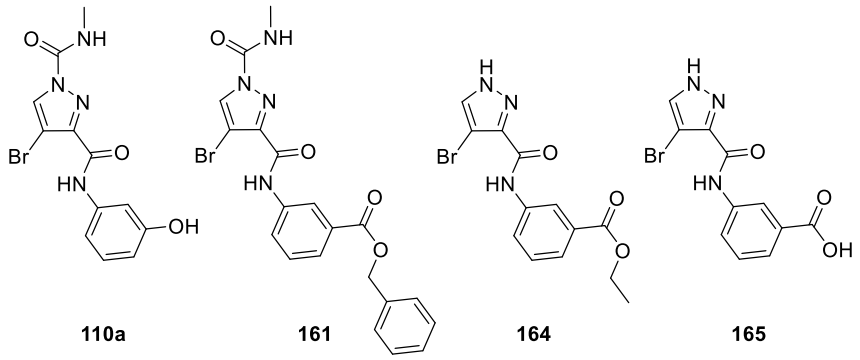

Figure 107: Esters and carboxylic acid analogues 161, 164 and 165.

Analogues **161**, **164** and **165** were all submitted to the DSF assay and the results obtained are presented in **Graph 31**.

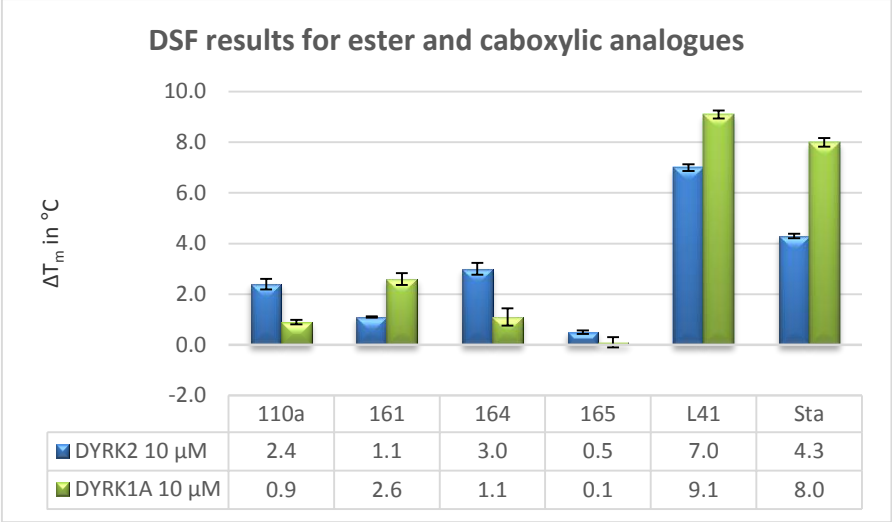

<u>Graph 31:</u> Bar graph representation of the T_m of compounds 110a, 161, 164, 165, L41 and staurosporine against DRYK2 and DYRK1A.

With the DSF results showing a significant difference in stabilization between ester **164** and carboxylic acid **165**, these analogues were submitted for a single point concentration assay at 1 µM against DYRK2, **Table 15**.

<u>Table 15:</u> % displacement of analogues at 1 µM against DYRK2.

Compound	DYRK2
84	13 ± 4%
164	44 ± 1%
165	38 ± 4%

A considerable increase in inhibition was observed with both analogues (**164** and **165**). The binding affinities for ester (**164**) and acid (**165**) were 44% and 38% respectively. The similar inhibition of these analogues suggested that it was not the electrostatic capability of the carboxylic acid that brought activity but the H-bonding capacity.

3. Conclusion

In this series, we successfully isolated two promising analogues: ester **164** and carboxylic acid **165**. These compounds both showed good binding affinities (44% ad 38%) at 1 µM. However, due to more interesting results obtained for another set of analogues, this series was not pursued further.

IV. Exploring nitrophenol amide analogue 123

Nitrophenol analogue **123** showed promising results with an IC_{50} = 1.45 µM. This led to further investigation in order to improve activity.

1. Exploring Part C of nitrophenol analogue 123

Initially we examined variation of Part C to study the effect on activity.

a. Synthesis

The desired chlorine and unsubstituted analogues of **123** were prepared using the standard protocol outlined in **Scheme 58**, providing the target amides **166** and **167** in 24% and 18% isolated yields, respectively.

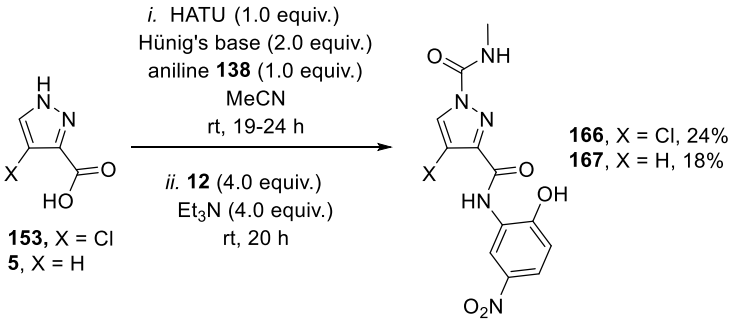

Scheme 58: Synthesis of nitro analogues 166 and 167.

b. DSF and biochemical assay results

Both analogues (**166** and **167**) were prepared to further probe the importance of the bromine atom on activity, **Figure 108**.

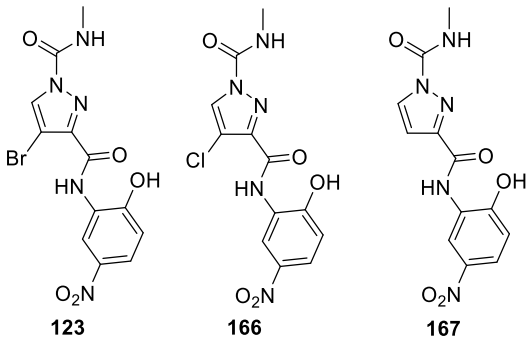

Figure 108: Analogues of 123 exploring Part C.

Analogues **166** and **167** were submitted to the DSF assay and the results obtained presented in **Graph 32**.

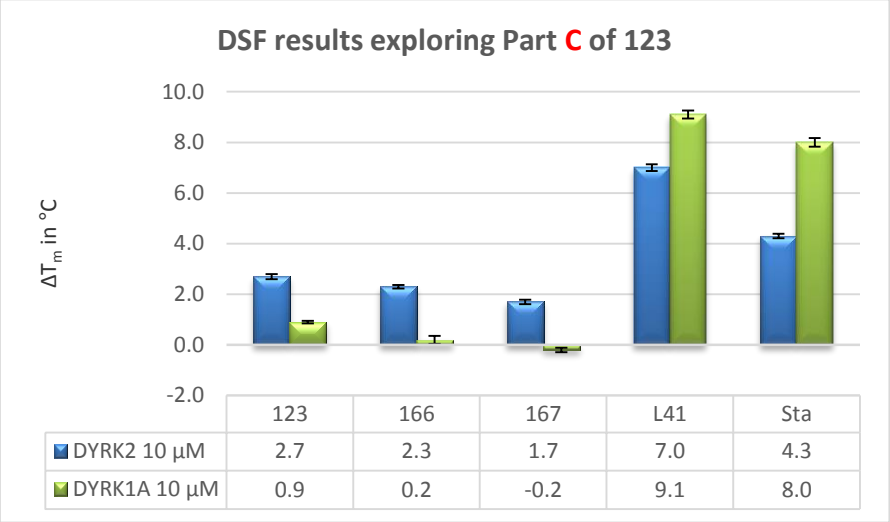

Graph 32: Bar graph representation of the T_m of compounds 123, 166, 167, L41 and staurosporine against DRYK2 and DYRK1A.

Further biological evaluation was carried out to determine binding affinity. A single point concentration assay was applied to analogues **166** and **167** against DYRK2 and DYRK1A, **Table 16**.

Table 16: % displacement of analogues at 1 µM against DYRK2.

Compound	DYRK2	DYRK1A
123	64 ± 0%	-13 ± 0%
166	50 ± 2%	ND
167	45 ± 3%	7 ± 2%

Bromo analogue **123** proved more active with 64% inhibition followed by chlorine analogue **166** with 50% inhibition. Unsubstituted analogue **167** showed similar activity with 45% inhibition for DYRK2 with an error of ± 3%. Nevertheless, selectivity was still maintained when the halogen atom was altered: unsubstituted analogue **167** inhibited DYRK1A at 7% at 1 µM. This was a different result to what was observed with the phenyl amide analogues (**154** and **155**). In the previous series unsubstituted analogue **155** was more active than the chloro (**154**) and bromo (**85**) derivatives.

Therefore, depending on the substitution pattern on the phenyl ring, different trends were observed concerning the substitution of the pyrazole ring.

With analogue **166** showing 50% inhibition, we obtained full IC_{50} data, **Figure 109**.

IC50 (nM)	Hillslope	R^2 Value	Conc of Compound (nM)	% Displacement Point 1	% Displacement Point 2
1080	0.89	0.9947	90000	108	108
1080	0.89	0.9947	30000	109	107
1080	0.89	0.9947	10000	104	104
1080	0.89	0.9947	3330	82	86
1080	0.89	0.9947	1110	55	51
1080	0.89	0.9947	370	33	38
1080	0.89	0.9947	123	11	16
1080	0.89	0.9947	41.2	12	7
1080	0.89	0.9947	13.7	2	8
1080	0.89	0.9947	4.50	3	-8

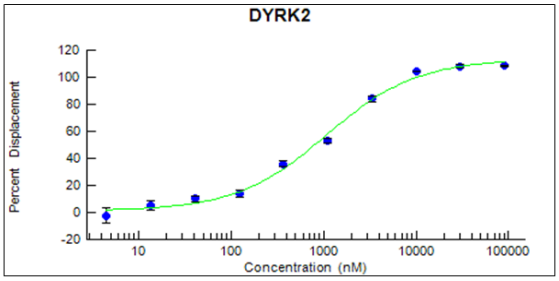

Figure 109: IC_{50} curve for 166.

Compound **166** dispayed similar activity to **123** within the full biochemical assay with an IC_{50} = 1.08 µM (**123**; IC_{50} = 1.45 µM).

Analogue **167** was also of interest to us and therefore a full activity curve was obtained, **Figure 110**.

IC50 (nM)	Hillslope	R^2 Value	Conc of Compound (nM)	% Displacement Point 1	% Displacement Point 2
2500	1.02	0.9953	90000	98	97
2500	1.02	0.9953	30000	91	91
2500	1.02	0.9953	10000	80	82
2500	1.02	0.9953	3330	56	62
2500	1.02	0.9953	1110	31	26
2500	1.02	0.9953	370	15	12
2500	1.02	0.9953	123	8	13
2500	1.02	0.9953	41.2	4	-6
2500	1.02	0.9953	13.7	13	-4
2500	1.02	0.9953	4.50	-3	0

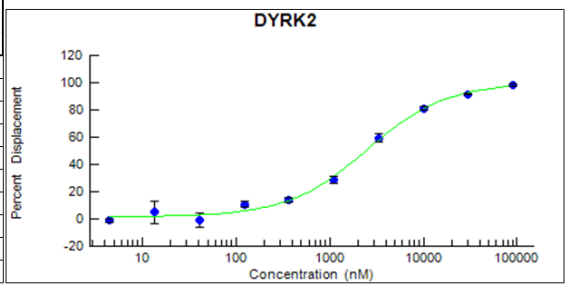

Figure 110: IC_{50} curve for 167.

Surprisingly, unsubstituted analogue **167** showed less activity than expected with an IC_{50} = 2.5 µM.

In conclusion, for this nitrophenol series, chlorine analogue **166** showed the best activity followed by bromine analogue **123** and unsubstituted analogue **167** suggesting that further optimization should also be possible for this portion of the molecule. Nevertheless, it was decided to maintain the bromine atom in the scaffold due to the amount of **6** prepared and the SAR data generated with this compound to date. Only if

a compound showed outstanding activity would the chloro and unsubstituted derivatives be synthesized in the future.

2. Exploring Part A of nitrophenol analogue 123

The next point of interest was the presence of the urea functionality on analogue **123**. To date we had a series of data suggesting activity could be modulated through increasing alkyl chain length of the urea. However, later results also indicated that this functionality was not essential for activity. We therefore elected to investigate this phenomenon further.

a. Synthesis

Within this series to gain access to the free pyrazole, no acylation after amide coupling was required, **Scheme 59**.

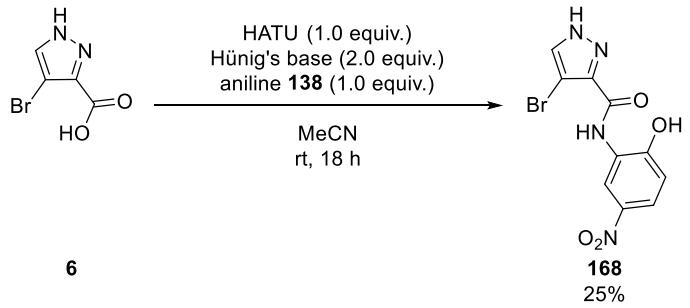

Scheme 59: Synthesis for analogue 168.

Carboxylic acid **6** was treated with HATU and Hünig's base before the addition of aniline **138**. The reaction mixture was stirred for 18 h at room temperature whereupon the compound precipitated. Following filtration and washing with MeCN, **168** was isolated without the need for further purification in 25% yield

b. DSF and biochemical assay results

The analysis of **123** was continued by generating free pyrazole **168** to determine the necessity of the urea functionality towards activity, **Figure 111**.

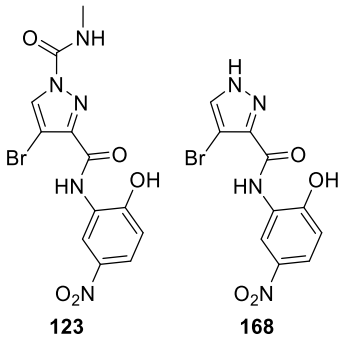

Figure 111: Probing the necessity of the urea functionality with analogue 168.

Analogue **168** was submitted to the DSF assay against DYRK2 and DYRK1A, **Graph 33**.

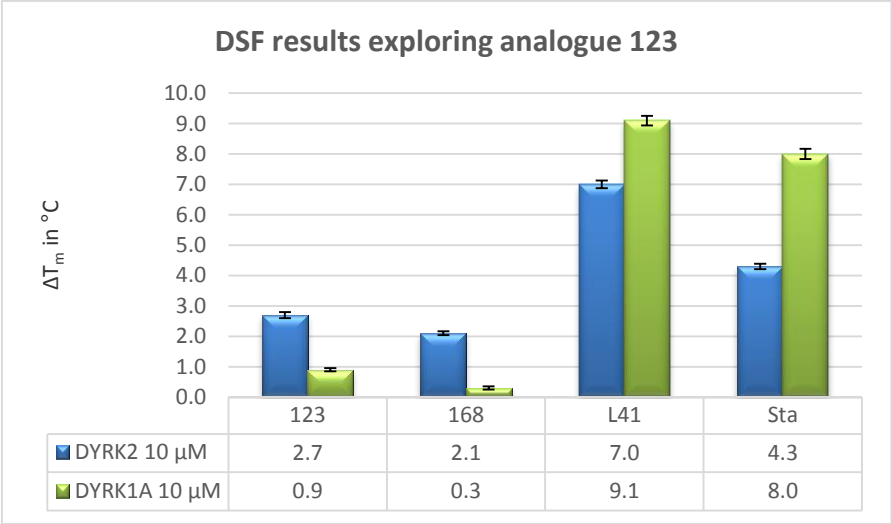

Graph 33: Bar graph representation of the T_m of compounds 123, 168, L41 and staurosporine against DRYK2 and DYRK1A.

Analogue **168** was further tested in a single point concentration assay at 1 µM against DYRK2 and DYRK1A, **Table 17**.

Table 17: % displacement of 123 and 168 at 1 µM against DYRK2.

Compound	DYRK2	DYRK1A
123	64 ± 0%	-13 ± 0%
168	51 ± 3%	8 ± 1%

Analogue **168** showed 51% inhibition at 1 µM for DYRK2 which suggested good activity. Moreover, selectivity was conserved with only 8% displacement at the same concentration for DYRK1A.

A full inhibition curve for analogue **168** was obtained to more accurately compare activity to analogue **123**, **Figure 112**.

IC50 (nM)	Hillslope	R^2 Value	Conc of Compound (nM)	% Displacement Point 1	% Displacement Point 2
1110	0.85	0.9995	90000	93	92
1110	0.85	0.9995	30000	88	96
1110	0.85	0.9995	10000	84	82
1110	0.85	0.9995	3330	70	70
1110	0.85	0.9995	1110	51	46
1110	0.85	0.9995	370	32	27
1110	0.85	0.9995	123	13	16
1110	0.85	0.9995	41.2	11	4
1110	0.85	0.9995	13.7	8	1
1110	0.85	0.9995	4.50	0	6

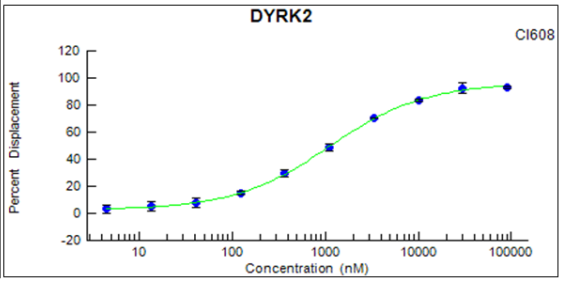

Figure 112: IC_{50} curve for 168.

Free pyrazole **168** was slightly more active with an IC_{50} = 1.11 µM when compared to analogue **123** (IC_{50} = 1.45 µM). Therefore, we concluded that the urea functionality was not essential for activity. This was an important and useful observation since it shortened the synthesis of our target molecules and increased ligand efficiency.

3. Exploring the importance of the OH of nitrophenol analogue 168

In the next analysis, we wanted to explore the importance of the phenol group on activity.

a. Synthesis

Standard conditions were applied to the synthesis of **170**, **Scheme 60**, the amide being isolated in 25% yield after column chromatography.

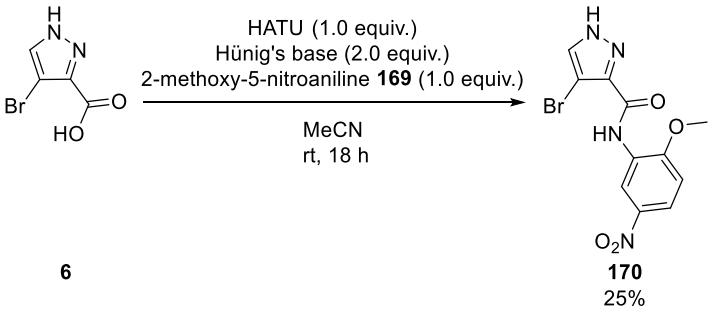

Scheme 60: Synthesis of analogue 170.

b. DSF and biochemical assay results

To determine if the phenol moiety in **168** was acting as an HBD, **170** was prepared and examined in the DSF assay against DYRK2 and DYRK1A, **Graph 34**.

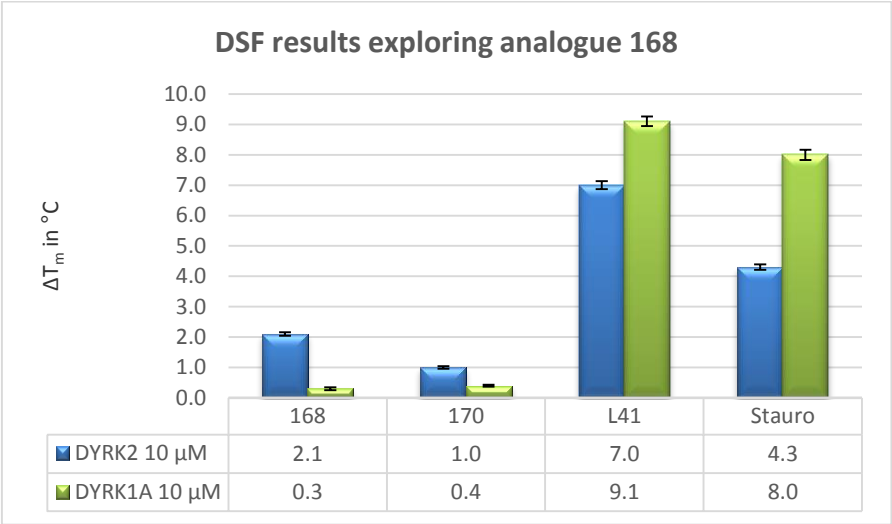

Graph 34: Bar graph representation of the T_m of compounds 168, 170, L41 and staurosporine against DRYK2 and DYRK1A.

To confirm the inactivity of analogue **170**, the compound was tested at a single concentration assay against DYRK2 and DYRK1A, **Table 18.**

Table 18: % displacement of 168 and 170 for DYRK2 and DYRK1A.

Compound	DYRK2 1 µM	DYRK2 3 µM	DYRK1A 1 µM
168	51 ± 3%	ND	8 ± 1%
170	-24 ± 4%	-14 ± 2%	5 ± 1%

The assay displayed a negative displacement for **170** (-24%) against DYRK2 at 1 µM. We decided to change the concentration to see how the result would be influenced. At 3 µM, **170** showed -14% displacement for the same protein. With no clear evidence of what this could mean, we interpreted this result as **170** being inactive towards DYRK2. Moreover, the compound showed little affinity towards DYRK1A, with 5% inhibition at 1 µM.

From these results, we concluded that the hydroxyl moiety of **168** was crucial for activity, and a potential HBD should be incorporated into this position of the phenyl amide.

4. Exploring the importance of the nitro group in analogue 168

Previous results had noticed that the nitro group had a marked influence on activity. We hypothesized this was due to moderation of the pKa of the phenol. We proposed to investigate this interesting observation further.

a. Synthesis

The first step in the synthesis of the initial target compound was the reduction of 2-nitro-4-(trifluoromethyl)phenol **171**, **Scheme 61**.

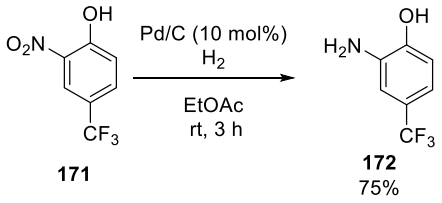

171 **172** 75%

<u>Scheme 61</u>: Reduction of nitro phenol X.

Hydrogenation of nitro phenol **171** was carried out in the presence of Pd/C in EtOAc for 3 h at room temperature.[92] After filtering the resulting suspension through celite and trituration with chloroform and PE, we were able to isolate aniline **172** in 75% yield.

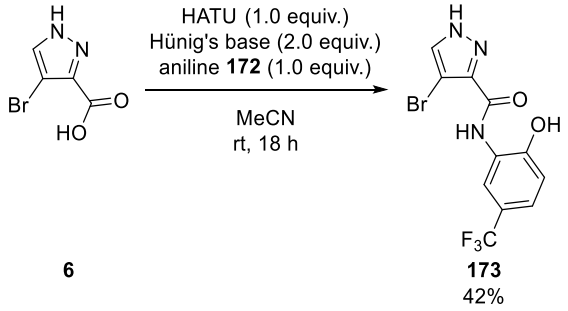

Scheme 62: Synthesis of analogue 173.

With the desired aniline **172** prepared, it was coupled to carboxylic acid **6** under standard conditions. Analogue **173** was isolated following column chromatography in 42% yield, **Scheme 62**.

b. DSF and biochemical assay results

A trifluoromethyl group is less electron withdrawing than a nitro group. This meant that the trifluoromethyl analogue **173** would have a higher pKa than nitro derivative **168**. The same pKa calculation were carried out on **168** and **173** and gave pKa = 6.4 and 8.6 respectively.[80] Having a trifluoromethyl group does not influence to a great extent the pKa of the phenol when compared to analogue **111a** (pKa = 8.8). We wanted to discover how this change would affect activity towards DYRK2, **Figure 113**.

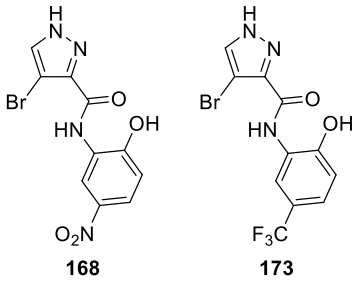

Figure 113: Exploring the influence of the nitro group with analogues 168 and 173.

Analogues **173** was submitted to the DSF assay against DYRK2 and DYRK1A, **Graph 35**.

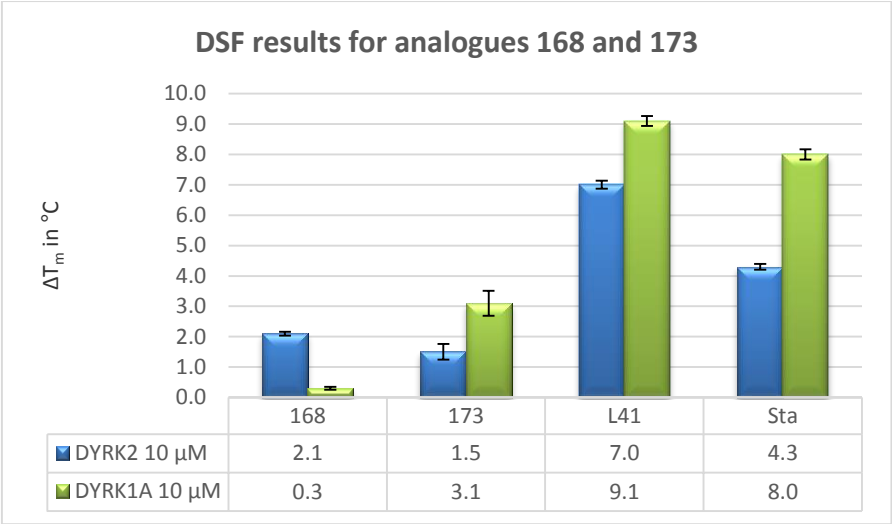

Graph 35: Bar graph representation of the T_m of compounds 168, 173, L41 and staurosporine against DRYK2 and DYRK1A.

With the DSF results showing a complete switch in selectivity, the LT single point concentration assay at 1 µM was carried out for analogues **168** and **173** against both isoforms, **Table 19**.

Table 19: % displacement of 168 and 173 at 1 µM against DYRK2 and DYRK1A.

Compound	DYRK2	DYRK1A
168	51 ± 3%	8 ± 1%
173	34 ± 2%	8 ± 2%

From these results, analogue **173** was shown to be moderately active against DYRK2 with 34% inhibition at 1 µM. It also showed inactivity against DYRK1A with 8% inhibition, an identical value to that obtained with analogue **168**.

From the preparation of **178** we were able to confirm the hypothesis that the pKa of the phenol did influence activity and the more acidic the phenol (**168**) resulted in a more active ligand.

5. Conclusion

We successfully prepared 5 analogues which probed the importance of the urea functionality in Part A, of the bromine atom in Part C and the importance of the acidity of the phenol in Part B.

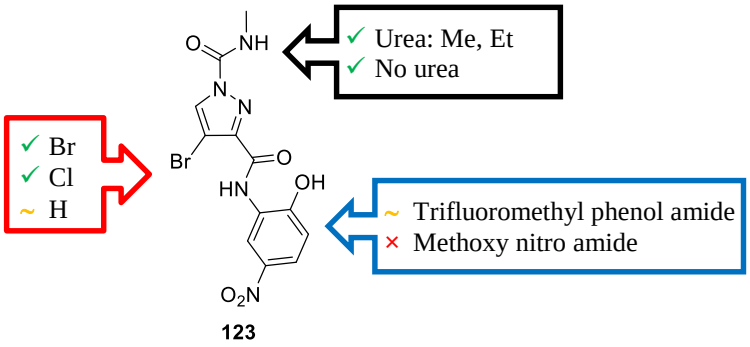

Figure 114: SAR summary of analogue 123.

When exploring Part C of this series, we concluded that chloro analogue **166** was the most active derivative (IC_{50} = 1.08 µM). We also discovered that the urea functionality was not crucial for activity, as free pyrazole **168** was revealed to be more active (IC_{50} = 1.11 µM) than analogue **123** (IC_{50} = 1.45 µM), **Figure 115**.

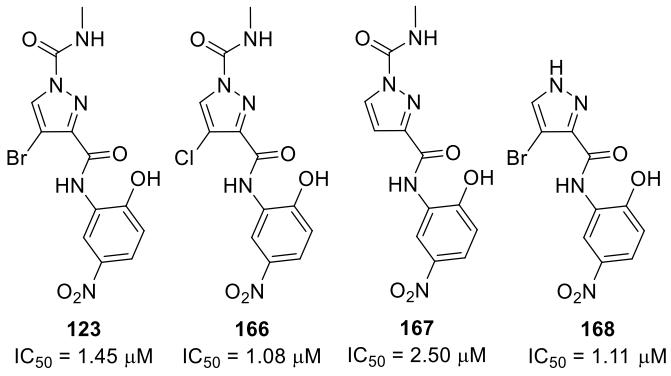

Figure 115: Nitrophenol series most active analogues.

Moreover, we probed the necessity of the hydroxyl for activity as methoxy analogue **170** was completely inactive. Finally, we discovered that the pKa of the phenol was relevant for optimal activity as the trifluoromethyl derivative **173** showed a decrease in activity. This clear trend in activity opened a number of avenues for further optimization of the ligand.

V. Exploring pyridyl amide analogues

We had previously explored introduction of pyridyl moiety and studied the influence of the position of the nitrogen atom on activity. We decided to explore this phenomenon further by synthesizing fluoropyridyl derivatives.

1. Synthesis

To access the fluoropyridyl analogues the standard amide protocol was adopted, **Scheme 63**, to give the target compounds **174** and **175** in 15% and 19% isolated yields respectively.

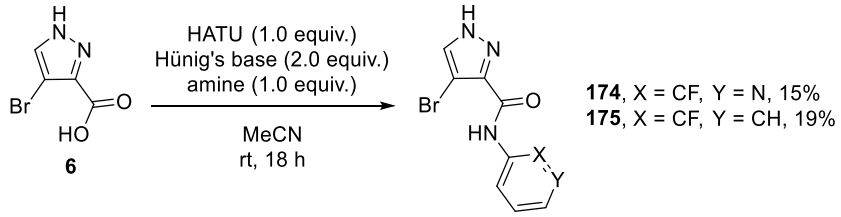

Scheme 63: Synthesis for analogues 174 and 175.

2. DSF and biochemical assay results

We explored fluoropyridyl analogue **174** and fluorine derivative **175** to understand the influence of the polarised C-F bond on activity, **Figure 116**.

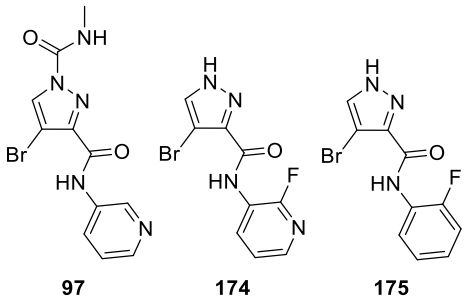

Figure 116: Exploring the influence of polarised C-F bond with 174 and 175.

Analogues **174** and **175** were submitted to the DSF assay, **Graph 36**.

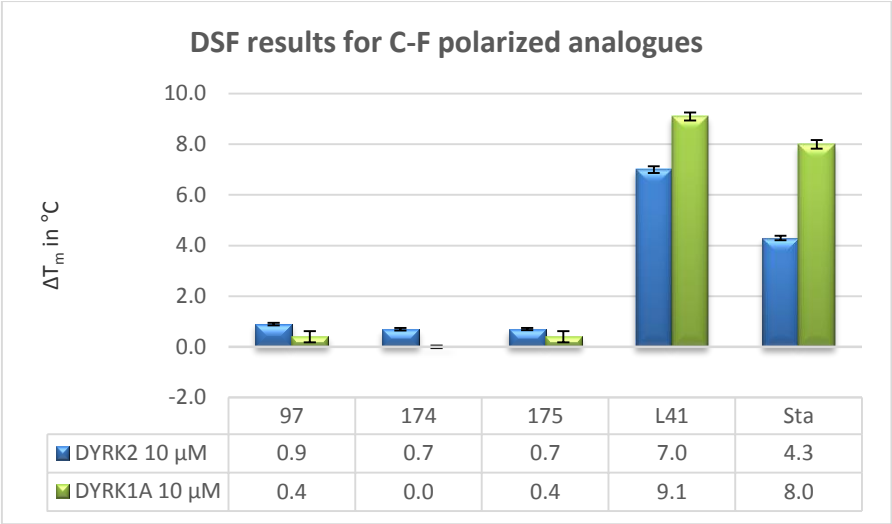

<u>Graph 36:</u> Bar graph representation of the T_m of compounds 97, 174, 175, L41 and staurosporine against DRYK2 and DYRK1A.

Further biochemical analysis was carried out on these analogues with the LT single point concentration assay at 1 µM against DYRK2, **Table 20**.

<u>Table 20:</u> % displacement of analogues at 1 µM against DYRK2.

Compound	DYRK2
84	13 ± 4%
97	0 ± 3%
174	37 ± 3%
175	8 ± 4%

It was previously seen that 3-pyridyl analogue **97** was inactive against DYRK2 with 0% inhibition at 1 µM. Interestingly, when we added a fluorine atom in the *ortho* position, analogue **174** inhibited the protein to 37% at the same concentration. In contrast, when only a fluorine atom was present in the *ortho* position of the phenyl ring (**175**) activity was similar to that of **84** when error was taken into consideration. The difference in activity between pyridyl analogue **97** and its fluorine derivative **174** could be explained through pKa. A pyridine ring has a pKa = 5.2 and the basicity of pyridine decreases when a fluorine substituent is present due to its electron withdrawing effects, with 2-fluoropyridyl pKa = -0.44.[93]

3. Conclusion

In this series, we observed that position and polarized C-F bond on the phenyl ring was important to increase activity. With sufficient analysis on this series, we decided to abandon this series of analogues and focus on the benzoxazole family where there was opportunity for the introduction of good diversity.

VI. Exploring the benzoxazole amide analogue 148

Benzoxazole analogue **148** showed promising results with IC_{50} = 1.71 µM. We decided to explore this series further to improve activity.

1. Benzimidazole analogues

Our interest resided in the importance of the benzoxazole ring by preparing benzimidazole derivatives.

a. Synthesis

A similar protocol to the synthesis of the amino benzoxazole was applied for the preparation of 4-aminobenzimidazole **178**, **Scheme 64**.

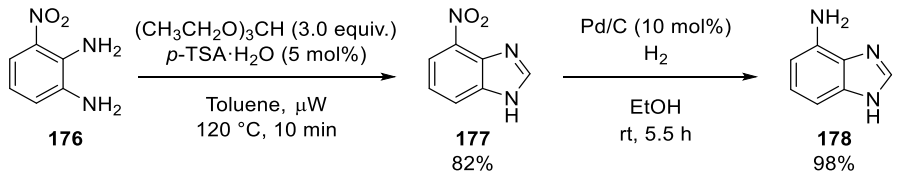

Scheme 64: Synthesis of 4-amino benzimidazole 178.

To form the benzimidazole ring, 3-nitrophenylenediamine **176** was treated with triethylorthoformate in the presence of a catalytic amount of *p*-toluenesulfonic acid in toluene. The reaction was irradiated for 10 minutes at 120 °C.[85] After filtration, benzimidazole **177** was isolated in 82% yield. Nitro benzimidazole **177** was then hydrogenated in the presence of Pd/C to give aniline **178** in 98% yield.

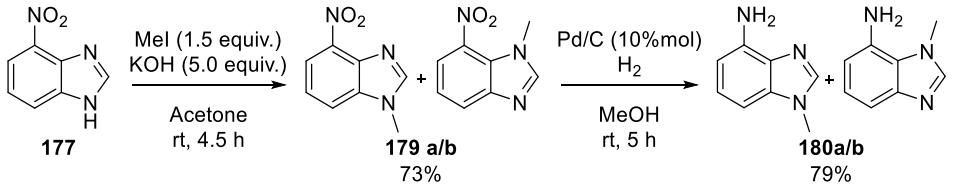

Scheme 65: ***N*-Methyl-4-amino benzimidazole 180 synthesis.**

We also wanted to explore the necessity of the NH of the imidazole ring by introducing a methyl group. Benzimidazole **177** was treated with MeI in the presence of KOH in a large excess.[94] A near 1:1 mixture of regioisomers **179** was isolated that were not separable by column chromatography. The mixture of regioisomers was reduced in the presence of H_2 and Pd/C to isolate regioisomers **180** in 79% yield (1:1 ratio).

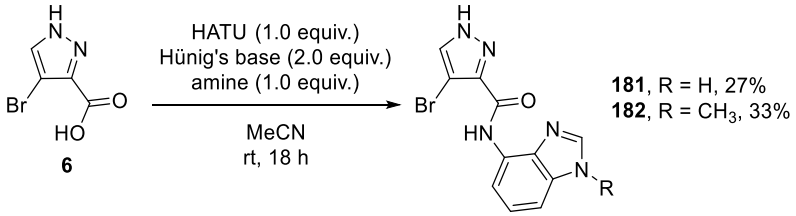

Scheme 66: **Amide synthesis of analogues 181 and 182.**

These anilines were coupled to carboxylic acid **6** in the presence of HATU and Hünig's base. Products from each reaction precipitated and were filtered and washed with a minimum amount of MeCN. Free benzimidazole analogue **181** was isolated in 27% with no further purification required. *N*-Methylated benzimidazole amide was isolated as a single regioisomer **182**, as confirmed by a 2D NOESY experiment (**Appendix 1**). The second possible regioisomer was not obtained, most likely due to the increased steric requirements of the reactive aniline disfavouring coupling. Analogue **182** was recrystallized and isolated in 33% yield.

b. DSF and biochemical assay results

Altering the benzoxazole ring led to the isolation of benzimidazole analogues **181** and **182**, **Figure 117**.

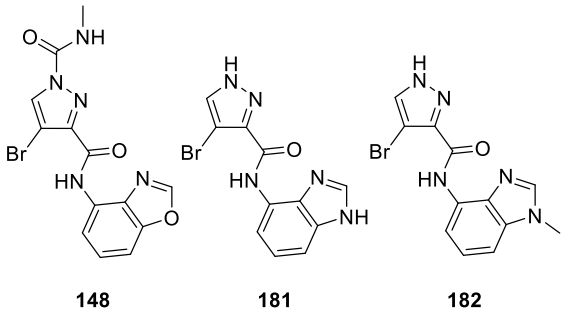

Figure 117: Benzoxazole and benzimidazole analogues 148, 181 and 182.

Both analogues (**181** and **182**) were submitted to the DSF assay against DYRK1A and DYRK2 are shown in **Graph 37**.

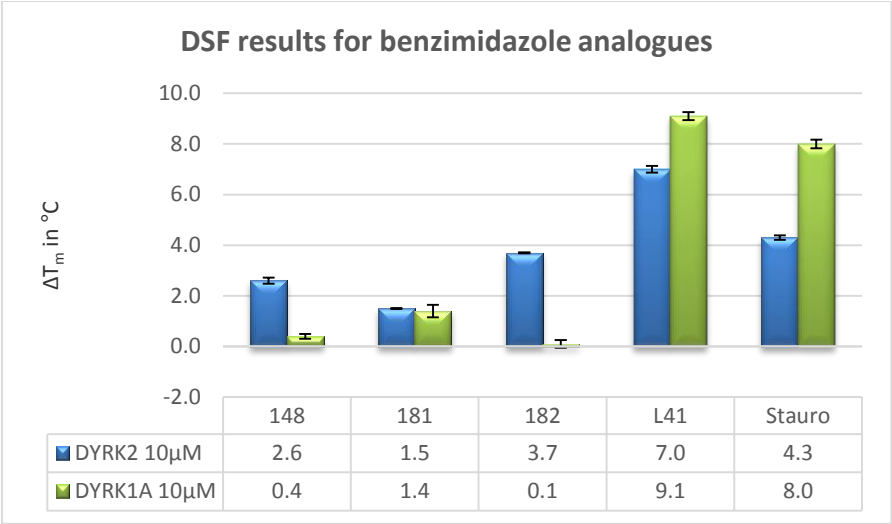

Graph 37: Bar graph representation of the T_m of compounds 148, 181, 182, L41 and staurosporine against DRYK2 and DYRK1A.

With both analogues, particularly **182**, showing interesting results we were eager to determine their binding affinities towards both protein isoforms in LT's single point concentration assay, **Table 21**.

Table 21: % displacement of analogues at 1 µM against DYRK2 and DYRK1A.

Compound	DYRK2	DYRK1A
148	43 ± 3%	ND
181	68 ± 1%	0 ± 1%
182	77 ± 0%	0 ± 2%

We were pleased to discover that both of these analogues showed excellent results with 68% and 77% inhibition of DYRK2 for analogues **181** and **182** respectively. Moreover, both analogues were selective with no inhibitory effect recorded for DYRK1A.

A full inhibitory curve was carried out for analogue **181** against DYRK2 to determine to what extent it was active, **Figure 118**

IC50 (nM)	Hillslope	R^2 Value	Conc of Compound (nM)	% Displacement Point 1	% Displacement Point 2
223	1.30	0.9866	30000	76	70
223	1.30	0.9866	10000	82	83
223	1.30	0.9866	3330	83	80
223	1.30	0.9866	1110	69	70
223	1.30	0.9866	370	52	58
223	1.30	0.9866	123	26	32
223	1.30	0.9866	41.2	20	4
223	1.30	0.9866	13.7	12	15
223	1.30	0.9866	4.57	4	11
223	1.30	0.9866	1.50	4	-2

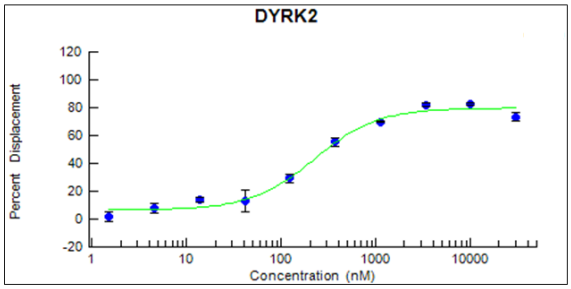

Figure 118: IC_{50} curve of analogue 181.

Analogue **181** had a binding affinity of IC_{50} = 223 nM which showed an important increase in activity compared to **148** (IC_{50} = 1.71 µM).

Given this exciting result, analogue **182** was sent to LT to establish a binding affinity towards DYRK2, **Figure 119**.

IC50 (nM)	Hillslope	R^2 Value	Conc of Compound (nM)	% Displacement Point 1	% Displacement Point 2
140	1.44	0.9895	30000	-35	-34
140	1.44	0.9895	10000	33	36
140	1.44	0.9895	3330	62	74
140	1.44	0.9895	1110	76	74
140	1.44	0.9895	370	70	71
140	1.44	0.9895	123	36	39
140	1.44	0.9895	41.2	24	18
140	1.44	0.9895	13.7	15	13
140	1.44	0.9895	4.57	5	8
140	1.44	0.9895	1.50	15	-1

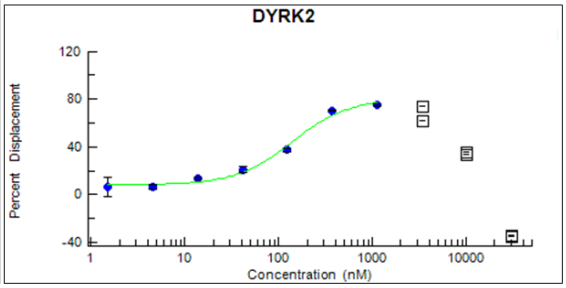

Figure 119: IC_{50} curve of analogue 182.

We observed that above 3.33 µM of **182**, the % inhibition was inconclusive. This was explained by the compound precipitating and therefore no longer being able to inhibit the protein. Nonetheless, analogue **182** was the most active compound synthesized to date with an IC_{50} = 140 nM. This provided a 100 fold increase in activity from the initial amide analogue **84** and a 10 fold increase from benzoxazole analogue **148**.

2. Exploring benzimidazole analogues

The benzimidazole analogues **181** and **182** were the most active analogues synthesized to date. Further SAR around this scaffold was still possible specifically with respect to the free NH pyrazole with Part A, the importance of the bromine atom in Part C and finally the alkyl chain of the benzimidazole ring with Part B.

a. Alkylating the pyrazole core

Our first interest was the importance of the free NH pyrazole by exploring various alkyl chains in Part A.

- Synthesis

A more laborious synthesis was carried out to gain access to the desired alkyl analogues. The first step consisted of preparing pyrazole methyl ester **183**, **Scheme 67**.

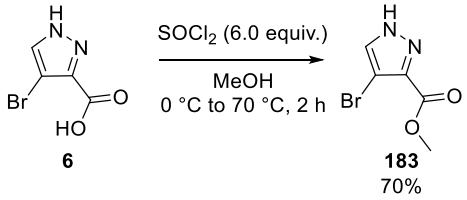

Scheme 67: Esterification of acid 6.

Carboxylic acid **6** was treated with thionyl chloride in MeOH at reflux for 2 h. After neutralizing the reaction mixture with saturated $NaHCO_3$, the product precipitated and was filtered.[95] Ester **183** was isolated in 70% yield with no further purification required.

The alkylation of pyrazole **183** was then carried out with various alkyl halides followed by hydrolysis to gain access to the requisite carboxylic acid, **Scheme 68**.

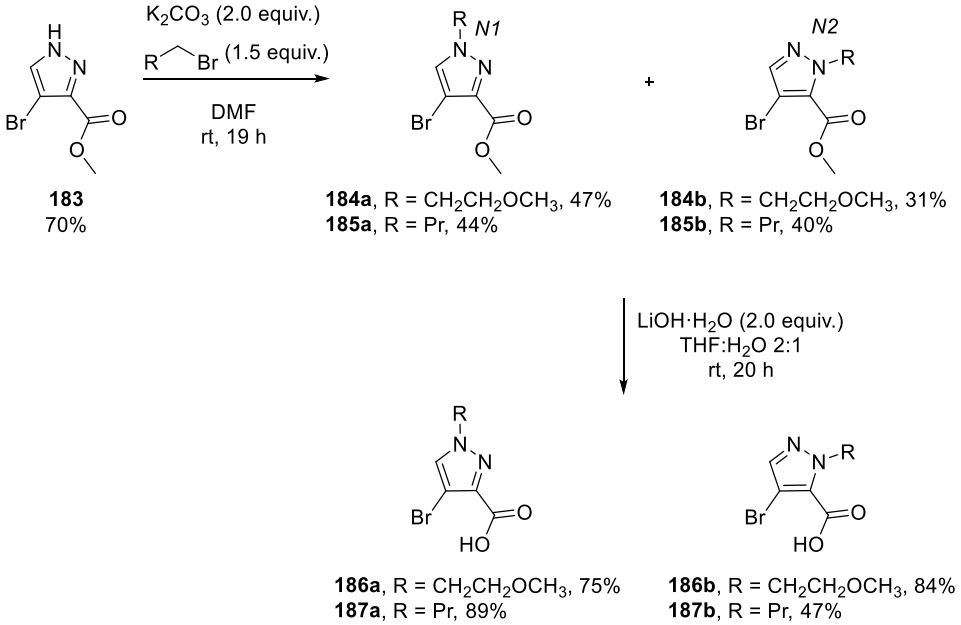

Scheme 68: Alkylation and subsequent hydrolysis of ester 183.

Alkylation was carried out in anhydrous DMF in the presence of an excess of the alkyl halide and K_2CO_3.[95] The reaction mixture was stirred for 19 h at room temperature leading to a crude mixture consisting of two regioisomeric pyrazoles. Separation of the two regiosisomers by column chromatography was achieved in both examples. The desired *N1* regioisomers **184a** and **185a** were isolated in higher yields (44−47%) than the *N2* regiosiomers **184b** and **185b** (31−40%) most probably due to steric reasons. Regioisomers **184a**/**184b** and **185a**/**185b** were determined by a 2D NOESY experiment (**Appendix 2** and **Appendix 3** respectively). The *N1* alkylated esters were hydrolysed in the presence of LiOH in a 2:1 THF:H_2O solution.[95] This led to the isolation of the carboxylic acids **186a** and **187a** in respectable yields (70−89%). We also elected to hydrolyse the *N2* regioisomers under the same conditions to gain access to carboxylic acids **186b** and **187b** in 47−84% yield.

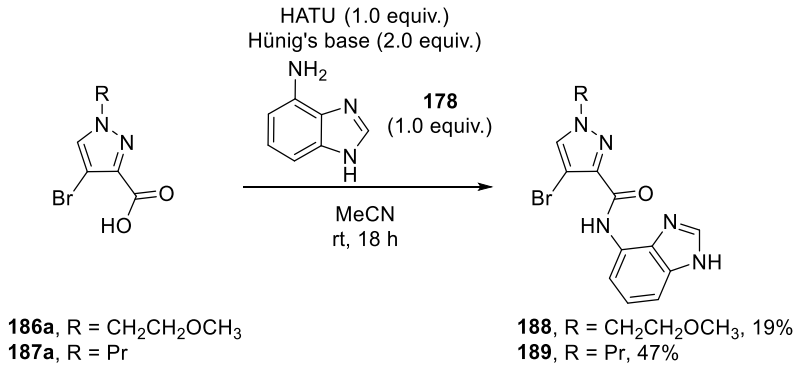

Scheme 69: Synthesis of alkylated analogues 188 and 189.

With the required carboxylic acids prepared, the final step was to synthesize the amide analogues, **Scheme 69**. Acids **186a** and **187a** were treated with HATU and Hünig's base before the addition of aniline **178** in MeCN. The crude mixture was purified by column chromatography to isolate the desired analogues (**188** and **189**) in acceptable yields ranging from 19−47%.

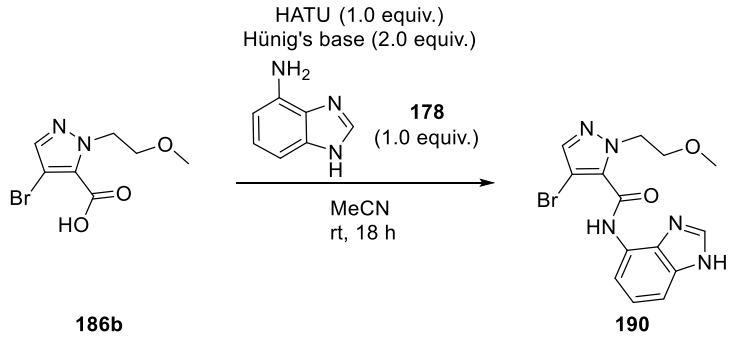

Scheme 70: Synthesis of *N*2 regioisomer amide 190.

We also prepared the *N2* regioisomeric amide analogue **190** in 42% yield, **Scheme 70**.

- DSF and biochemical assay results

Analogue **181** gave very promising results (IC_{50} = 223 nM) leading to further exploration of Part A of the molecule through alkylation, **Figure 120**.

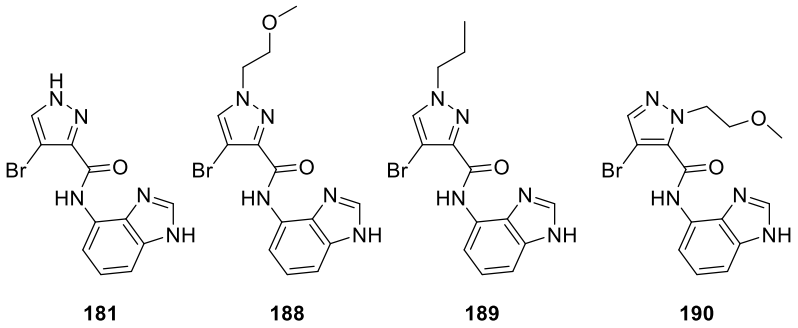

Figure 120: Alkylated benzimidazole analogues 188−190.

These analogues (**188−190**) were submitted to the DSF assay, **Graph 38**.

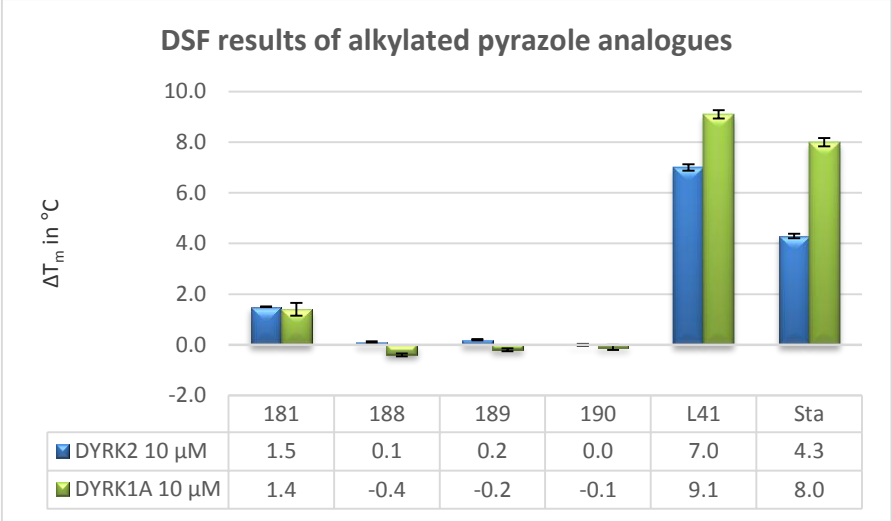

Graph 38: Bar graph representation of the T_m of compounds 181, 188−190, L41 and staurosporine against DRYK2 and DYRK1A.

The DSF results showed no stabilization, however, the analogues were sent to LT for a single point concentration at 1 µM against DYRK2, **Table 22**.

Table 22: % displacement of alkylated analogues at 1µM against DYRK2.

Compound	DYRK2
181	68 ± 1%
188	6 ± 6%
190	-6 ± 2%
189	-4 ± 3%

A clear conclusion was drawn from the biochemical assay results: no substitution was tolerated on the pyrazole ring. This suggested that an H-bond donor or acceptor was needed in that position in order to maintain or gain activity.

b. **Exploring part A of benzimidazole 641**

- Synthesis

N-Methylbenzimidazole **179** was synthesized as a mixture of regioisomers, **Scheme 65**. We wanted to improve the synthesis and isolate the desired regioisomer **191** by adopting Milata's procedure.[96]

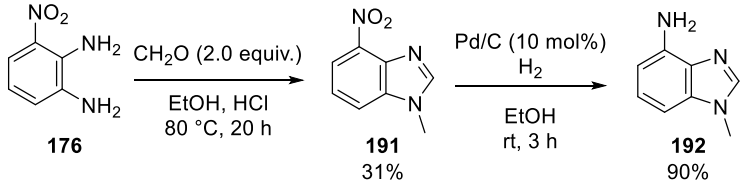

Scheme 71: Synthesis of single regioisomer 192.

Treatment of diamine **176** with formaldehyde in the presence of EtOH and concentrated HCl (3:1) at reflux for 20 h resulted in a precipitate, which was isolated by filtration. After recrystallization, the desired *N*-methyl nitrobenzimidazole **191** was isolated in 31% yield. Reduction was then carried out under standard conditions using Pd/C and hydrogen, whereupon amine **192** was isolated in 90% yield, **Scheme 71**. The position of the methyl group was determined by a 2D NOESY experiment which showed a cross correlation between the methyl group and the protons of the phenyl ring (**Appendix 4**).

For urea analogue **193**, acid **6** was coupled with aminobenzimidazole **192** in the presence of HATU and Hünig's base for 24 h. After that time compound **12** and Et_3N were added and the mixture stirred for a further 20 h. The precipitate formed was isolated and washed with a minimum volume of MeCN. This led to the isolation of analogue **193** in 31% yield with no further purification required, **Scheme 72**.

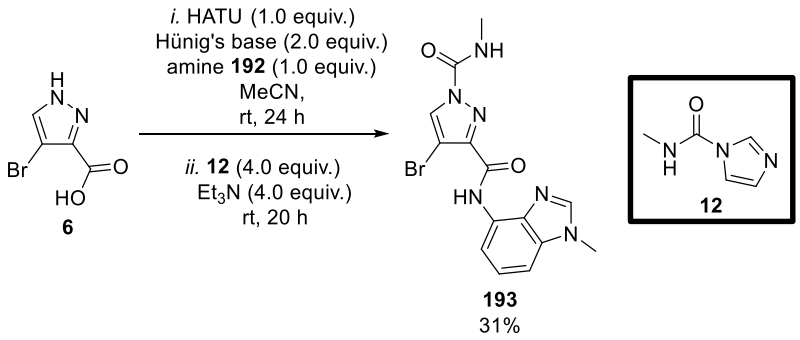

Scheme 72: Synthesis of analogue 193.

For the isolation of analogue **196** a different strategy was adopted. Ester **183** was alkylated with MeI in the presence of Cs_2CO_3 for 20 h at room temperature.[97] After purification by column chromatography, two regioisomers **194a** and **194b** were isolated in 32% and 17% yield respectively. The connectivity of both regioisomers was determined by 2D NOESY experiment (**Appendix 5**), showing the *N1* regioisomer to be **194a** and *N2* the minor isomer **194b**, **Scheme 73**.

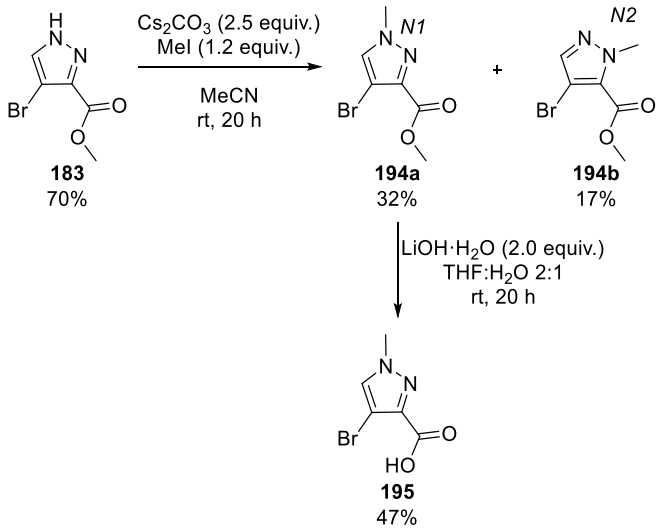

Scheme 73: Alkylation of ester 183 followed by hydrolysis.

Only regioisomer **194a** was hydrolysed with LiOH in a 2:1 THF:H_2O solution for 20 h at room temperature to give carboxylic acid **195** in 47% yield, **Scheme 73**.

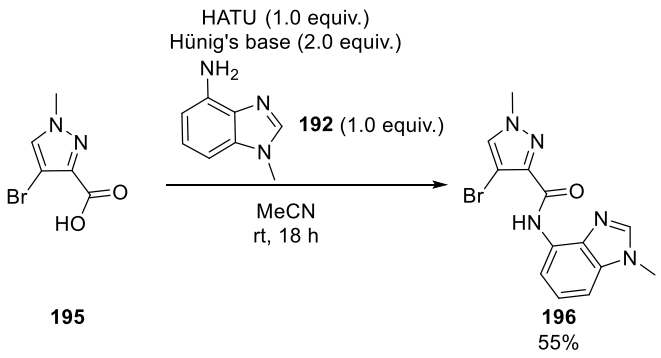

Scheme 74: Synthesis of analogue 196.

Acid **195** was treated with HATU and Hünig's base followed by the addition of aminobenzimidazole **192**. After 18 h, analogue **196** was isolated in 55% yield, **Scheme 74**.

- DSF and biochemical assay results

To answer the hypothesis that an HBD or HBA was required for activity, a urea (**193**) and methylated (1**96**) derivative of **182** were prepared, **Figure 121**.

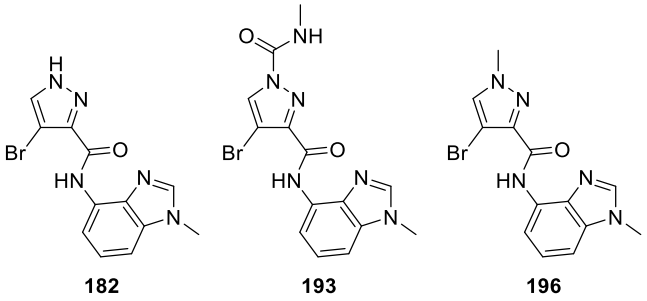

Figure 121: Exploring the necessity of an HBA or HBD.

The compounds (**193** and **196**) were submitted to the DSF assay to gain stability data, **Graph 39**.

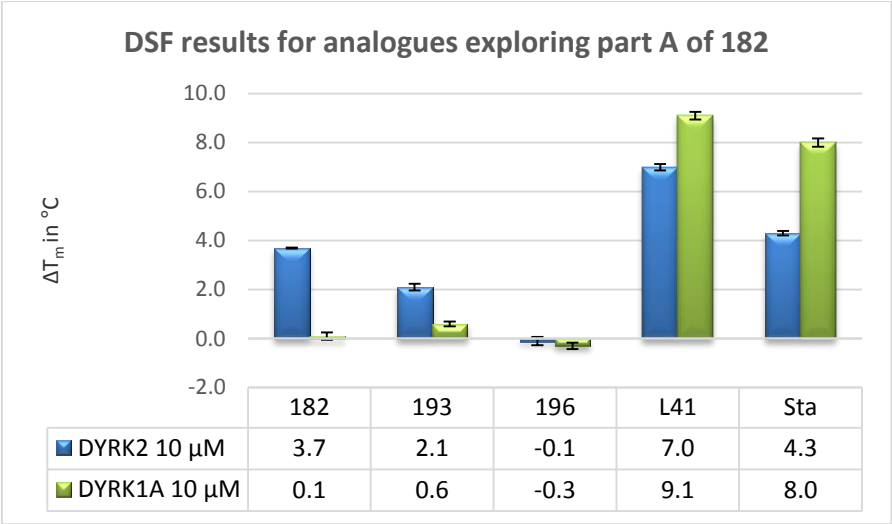

Graph 39: Bar graph representation of the T_m of compounds 182, 193, 196, L41 and staurosporine against DRYK2 and DYRK1A.

To gain access to the analogues binding affinity, they were sent for further analysis in a single point concentration assay at 1 µM for DYRK2, **Table 23**.

Table 23: % displacement of analogues at 1 µM against DYRK2.

Compound	DYRK2	DYRK1A
182	77 ± 0%	0 ± 2%
193	81 ± 3%	8 ± 0%
196	3 ± 1%	ND

Both analogues **182** and **193** were equally active and completely selective for DYRK2. In contrast, *N*-methyl analogue **196** was completely inactive against DYRK2. We continued the conclusion from the previous section that an HBD or HBA was required on the pyrazole ring for activity.

A full inhibition curve was obtained for analogue **193** due to the promising activity, **Figure 122**.

IC50 (nM)	Hillslope	R^2 Value	Conc of Compound (nM)	% Displacement Point 1	% Displacement Point 2
70.1	0.80	0.9870	30000	-16	-12
70.1	0.80	0.9870	10000	35	37
70.1	0.80	0.9870	3330	76	76
70.1	0.80	0.9870	1110	86	80
70.1	0.80	0.9870	370	82	78
70.1	0.80	0.9870	123	52	59
70.1	0.80	0.9870	41.2	29	39
70.1	0.80	0.9870	13.7	22	28
70.1	0.80	0.9870	4.57	2	11
70.1	0.80	0.9870	1.50	1	5

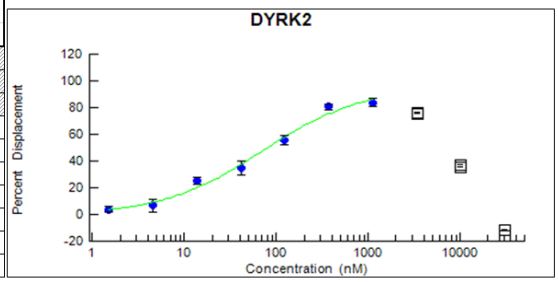

Figure 122: IC_{50} curve of analogue 193.

A similar trend to **182** was observed when analogue **193** was present above 3.33 µM. The compound precipitated from solution leading to inconclusive results. It was still possible to determine the binding activity of **193**, giving an extrapolated IC_{50} = 70 nM. Even though the urea functionality did not help with solubility, it increased the activity by 2 fold relative to **182**.

c. Exploring Part C of benzimidazole

In this series, we decide to explore Part C of analogue **182** with a chloro (**197**) and indazole (**199**) derivative.

➢ Synthesis

At this stage we had access to the required reagents from previous work.

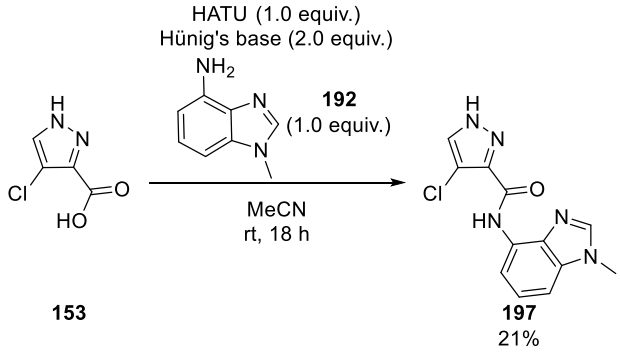

Scheme 75: Synthesis of chlorine analogue 197.

Carboxylic acid **153** was coupled to aminobenzimidazole **192**. The reaction mixture was stirred overnight at room temperature in MeCN. After purification by column chromatography, **197** was isolated in 21% yield, **Scheme 75**.

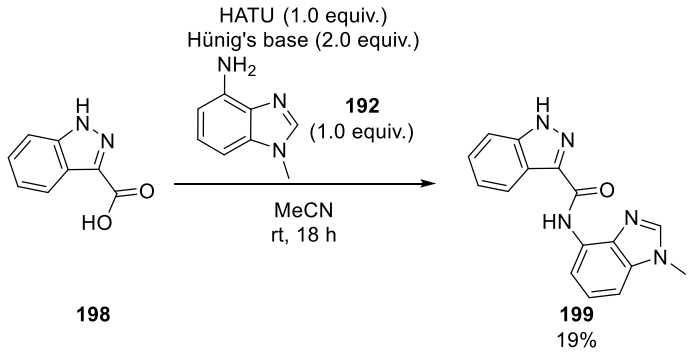

Scheme 76: Synthesis of indazole analogue 199.

For indazole analogue **199** the same protocol was applied to carboxylic acid **198**. This led to the isolation of **199** in 19% yield after column chromatography, **Scheme 76**.

- DSF and biochemical assay results

The following analogues were prepared to probe the importance of the bromine atom on analogue **182**, **Figure 123**.

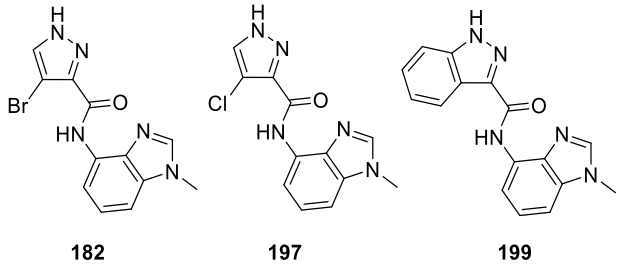

Figure 123: Exploration of Part C of analogue 182.

Both analogues (**197** and **199**) were submitted to the DSF assay against both protein isoforms, **Graph 40**.

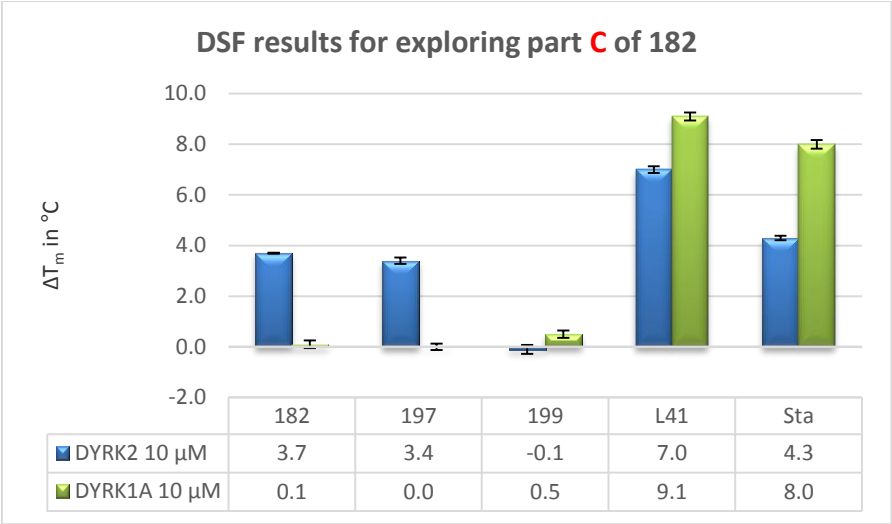

Graph 40: Bar graph representation of the T_m of compounds 182, 197, 198, L41 and staurosporine against DRYK2 and DYRK1A.

We decided to gain further biochemical data for analogues **197** and **199** by submitting them to a single point concentration assay at 1 µM against DYRK2, **Table 24**.

Table 24: % displacement of analogues at 1 µM against DYRK2.

Compound	DYRK2	DYRK1A
182	77 ± 0%	0 ± 2%
197	78 ± 2%	5 ± 1%
199	1 ± 10%	ND

Similar activity was observed for chloro (**197**) and bromo (**182**) analogues with 78% and 77% inhibition at 1 µM, respectively. Indazole analogue **199** displayed 1 ± 10% inhibition at that concentration. The error associated with that compound was very high, however, that inhibition still being low the data suggested that a halogen atom was highly preferable to a rigid aromatic group on the pyrazole ring.

With chloro analogue **197** showing high % inhibition at 1 µM, we decided to carry out a full inhibition curve, **Figure 124**.

IC50 (nM)	Hillslope	R^2 Value	Conc of Compound (nM)	% Displacement	
				Point 1	Point 2
106	0.75	0.9856	30000	-40	-4
106	0.75	0.9856	10000	32	35
106	0.75	0.9856	3330	68	72
106	0.75	0.9856	1110	87	77
106	0.75	0.9856	370	73	77
106	0.75	0.9856	123	52	45
106	0.75	0.9856	41.2	29	31
106	0.75	0.9856	13.7	28	18
106	0.75	0.9856	4.57	0	9
106	0.75	0.9856	1.50	5	3

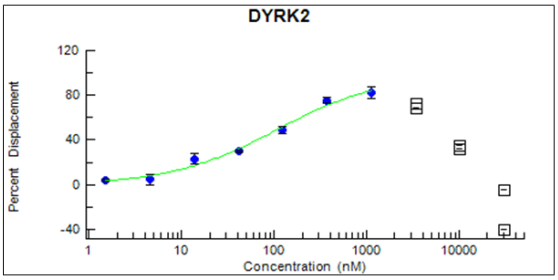

Figure 124: IC_{50} curve of analogue 197.

Consistent with previous observations of compound precipitation over 3.33 µM analogue **197** was also insoluble at these concentrations. It was still possible to determine the binding activity of **197** with an extrapolated IC_{50} = 106 nM. Chloro analogue **197** did increase activity without increasing solubility.

d. Exploring the chain length of benzimidazole

The final SAR carried out in this study explored the length of the alkyl chain on the benzimidazole ring of **182**.

- Synthesis

With 1-bromopropane available, we decided to use it to extend the side-chain of the benzimidazole ring. Nitrobenzimidazole **177** was treated with 1-bromopropane in the presence of K_2CO_3 in anhydrous DMF for 19 h at room temperature. Two regioisomers were observed by ^1H NMR spectroscopy and TLC analysis showed two separable products. After column chromatography, *N1* regioisomer **200a** was isolated in 51% yield and regioisomer *N3* **200b** in 23%, **Scheme 77**. The regiochemistry of the two products was determined by 2D NOESY experiments (**Appendix 6**). The difference in yield of the isomers was attributed to the steric influence of the nitro group.

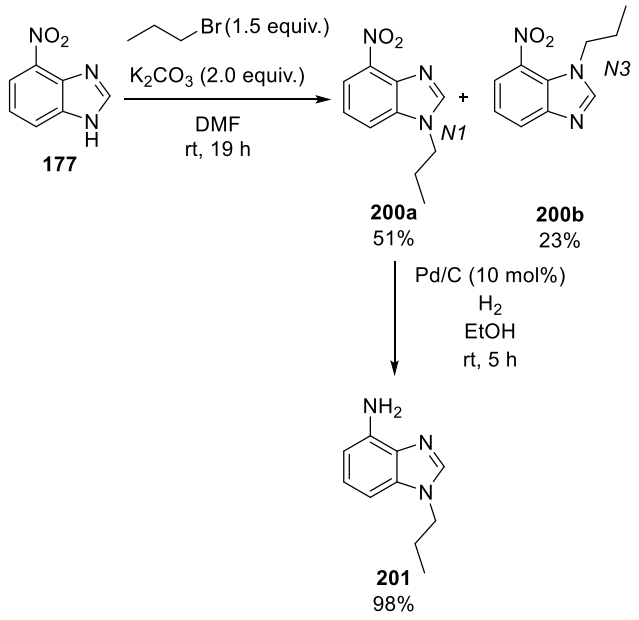

Scheme 77: Synthesis of *N*-propyl benzimidazole amine 201.

Only the reduction of alkylated benzimidazole **200a** was carried out with Pd/C under a H_2 atmosphere for 5 h at room temperature. After filtration through celite, the aminobenzimidazole **201** was isolated in 98% yield, **Scheme 77**.

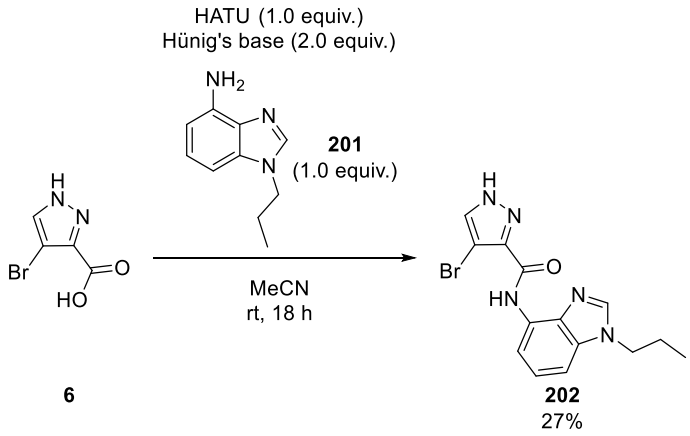

Scheme 78: Synthesis of analogue 202.

With aminobenzimidazole **201** prepared, amide formation was carried out, **Scheme 78**, to give the final compound **202** in 27% yield.

- DSF and biochemical assay results

In this final set, we wished to establish if increasing the side-chain of the benzimidazole ring a change in both activity and solubility could be observed, **Figure 125**.

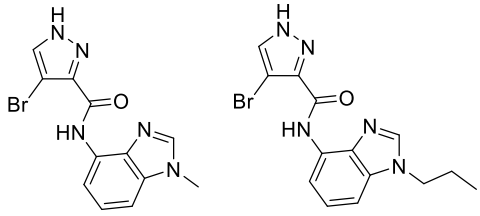

Figure 125: Exploring the chain length of the benzimidazole moiety.

Analogue **202** was submitted for testing in the DSF assay against DYRK2 and DYRK1A, **Graph 41**.

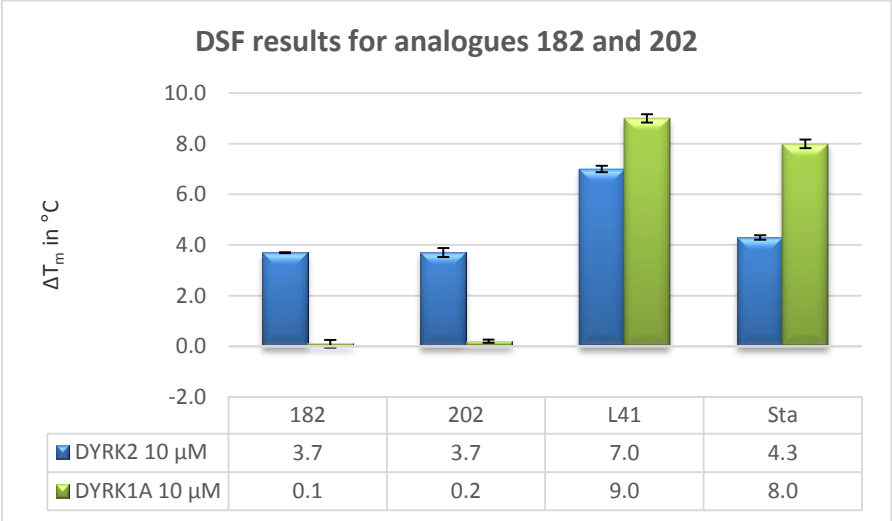

Graph 41: Bar graph representation of the T_m of compounds 182, 202, L41 and staurosporine against DRYK2 and DYRK1A.

Further biochemical analysis was carried out for analogue **202** with the single concentration assay at 1 µM against both protein isoforms, **Table 25**.

Table 25: % displacement of 182 and 202 at 1 µM against DYRK2.

Compound	DYRK2	DYRK1A
182	77 ± 0%	0 ± 2%
202	87 ± 1%	8 ± 1%

An increase in activity with analogue **202** was observed with 87% inhibition at 1 µM. Further analysis involved the full inhibition curve to determine the IC_{50} of analogue **202**, **Figure 126**.

IC50 (nM)	Hillslope	R^2 Value	Conc of Compound (nM)	% Displacement Point 1	% Displacement Point 2
62.0	1.25	0.9968	30000	103	105
62.0	1.25	0.9968	10000	109	115
62.0	1.25	0.9968	3330	109	113
62.0	1.25	0.9968	1110	107	138
62.0	1.25	0.9968	370	96	103
62.0	1.25	0.9968	123	76	82
62.0	1.25	0.9968	41.2	55	43
62.0	1.25	0.9968	13.7	24	24
62.0	1.25	0.9968	4.57	8	16
62.0	1.25	0.9968	1.50	20	8

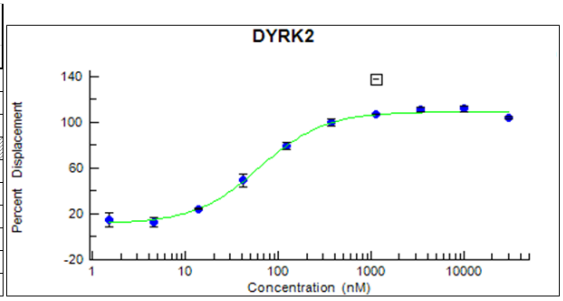

Figure 126: IC_{50} curve of analogue 202 against DYRK2.

We only observed one point that was erroneous and inconclusive for **202**. The compound inhibited to 100% and was soluble at high concentrations. The binding affinity was determined: IC_{50} = 62 nM. Analogue **202** was the most active compound which suggested that by adding a longer hydrophobic tail to the benzimidazole ring of the molecule was advantageous to both activity and solubility.

We deemed it necessary to get a full inhibition curve of **202** against DYRK1A to establish selectivity of the compound between the two isoforms, **Figure 127**.

IC50 (nM)	Hillslope	R^2 Value	Conc of Compound (nM)	% Displacement Point 1	% Displacement Point 2
>30000	1.14	0.494	30000	0	4
>30000	1.14	0.494	10000	-4	2
>30000	1.14	0.494	3330	-3	-1
>30000	1.14	0.494	1110	0	-8
>30000	1.14	0.494	370	-3	-5
>30000	1.14	0.494	123	-1	-3
>30000	1.14	0.494	41.2	-7	1
>30000	1.14	0.494	13.7	-5	-1
>30000	1.14	0.494	4.57	-4	-2
>30000	1.14	0.494	1.49	0	2

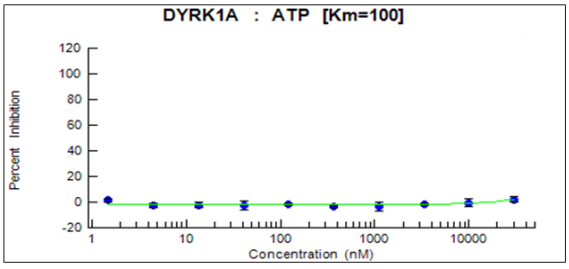

Figure 127: IC_{50} curve of analogue 202 against DYRK1A.

Analogue **202** was completely inactive against DYRK1A with and IC_{50} > 30 µM from the inhibition curve. Therefore, we concluded that analogue **202** was more than 500 fold selective for the protein of interest DYRK2 over DYRK1A.

e. Docked poses

We wished to understand the selectivity of analogue **202** between the two isoforms. With no clear knowledge of where the compound bound in DYRK2 we decided to dock the compound (**202**) in the proposed allosteric and the orthosteric pockets.

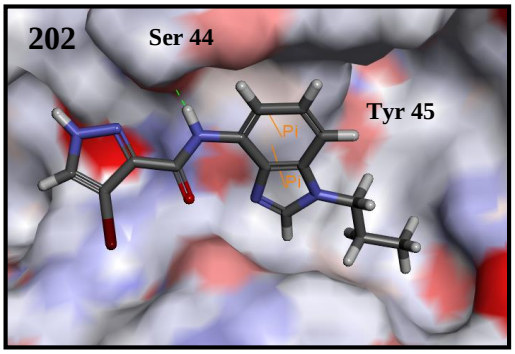

Figure 128: Predicted docked pose 202 in the allosteric pocket.

Figure 128 represents the potential conformation analogue **202** might adopt in the allosteric site. The NH of the amide was predicted to be involved in an H-bond interaction with Ser 44 and the benzimidazole interacted with Tyr 45 through π-π stacking. The propyl chain was foreseen to be 'buried' in the small pocket on the right hand side of the binding site and could be involved in hydrophobic contact.

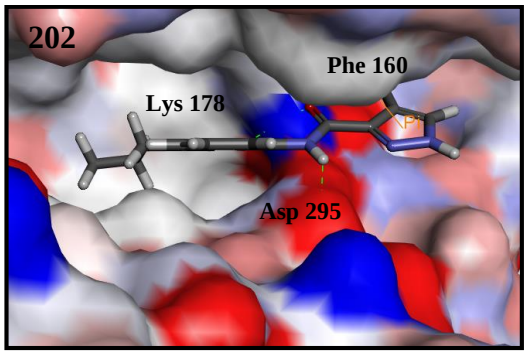

Figure 129: Predicted docked pose of 202 in the orthosteric pocket.

When analogue **202** was docked in the orthosteric site, we observed that the predicted conformation indicated that the pyrazole ring was shifted to a small adjacent pocket,

Figure 129. The non-alkylated nitrogen and carbonyl group were both foressen to be involved in H-bonding with Lys 178 and the NH of the amide with Asp 295. A π-π stacking interaction was observed between the pyrazole ring and Phe 160. Moreover, the benzimidazole ring fitted nicely into the hydrophobic pocket of the ATP site.

From both of these predicted poses (allosteric and orthosteric site), it was difficult to determine what was the most likely site analogue **202** was interacting with. Only further biological evaluation would enable us to determine by which site this analogue interacted with the protein (*e.g*: mode of inhibition).

With **202** being selective between the two isoforms we decided to dock the compound in DYRK1A (PDB: 3ANR) to comprehend this observation, **Figure 130**.

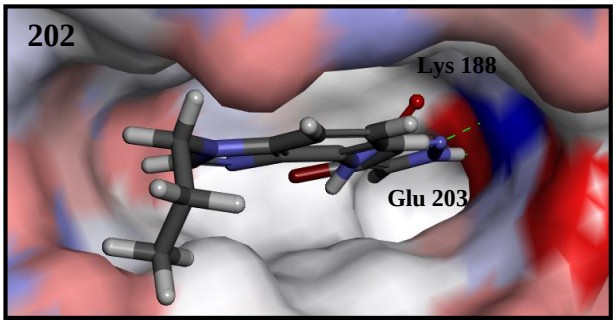

Figure 130: Predicted pose of 202 in the orthosteric site of DYRK1A.

The predictive conformation of analogue **202** placed the pyrazole ring deep in the ATP binding pocket. This enabled the NH and the nitrogen from this ring to potentially H-bond with Glu 203 and Lys 188, respectively. The alkyl chain from the benzimidazole ring was predicte to be exposed to solvent. This could provide a reason why analogue **202** was inactive for DYRK1A.

3. Conclusion

The SAR study carried out on the benzoxazole series led to the preparation of 8 benzimidazole derivatives starting off with analogue **181**, **Figure 131**.

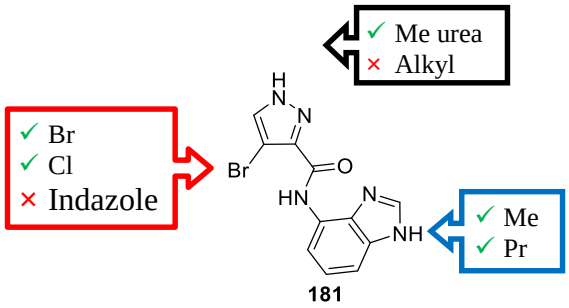

Figure 131: SAR summary of benzimidazole 181.

We discovered that more rigid and sterically demanding indazole (**199**) was not tolerated in Part C. In contrast, halogen derivatives (**182** and **197**) were highly active. For Part A, it was necessary to have an HBD or HBA by either having the free pyrazole or the urea functionality to gain activity. When an alkyl group was present activity was abrogated for the target protein. Finally, we showed that an alkyl chain on the benzimidazole ring increased activity: the longer the chain the more active the compound. Our best analogue in this series was **202** which possessed a *N*-propyl group on the benzimidazole ring, **Figure 132**.

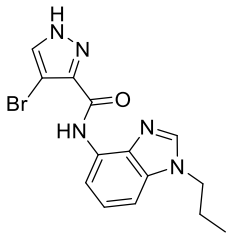

Figure 132: Best analogue synthesized to date: 202.

VII. Conclusion

A library of 90 analogues were synthesized while exploring the amide functionality. Phenyl analogue **84** was our starting point for our SAR investigation with three regions explored: Part A with the urea functionality, Part B with the phenyl amide and Part C with the halogen substitution, Error! Reference source not found..

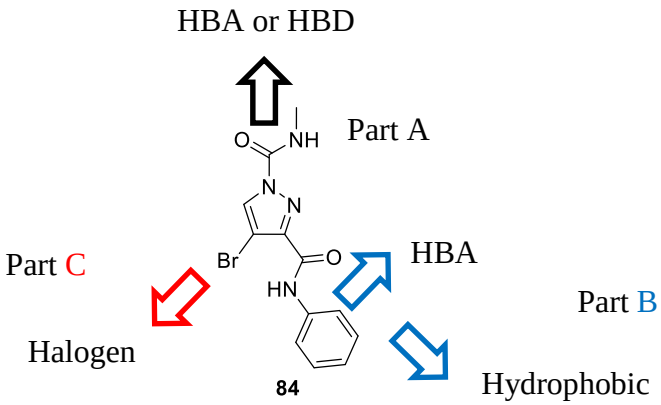

Figure 133: SAR study aroud analogue 84.

We observed that an HBA or HBD, in Part A, including the carbonyl group of the urea or the NH of the urea or of the free pyrazole was crucial for activity. Moreover, in Part B we observed that in the *ortho* position of the phenyl amide an HBA was needed for the analogue to be active. A bicyclic core such as benzimidazole was considered optimal as it could easily deliver a hydrophobic feature in a perpendicular direction to the HBA.

Throughout the study, 10 compounds showed good to excellent binding activity, **Figure 134**.

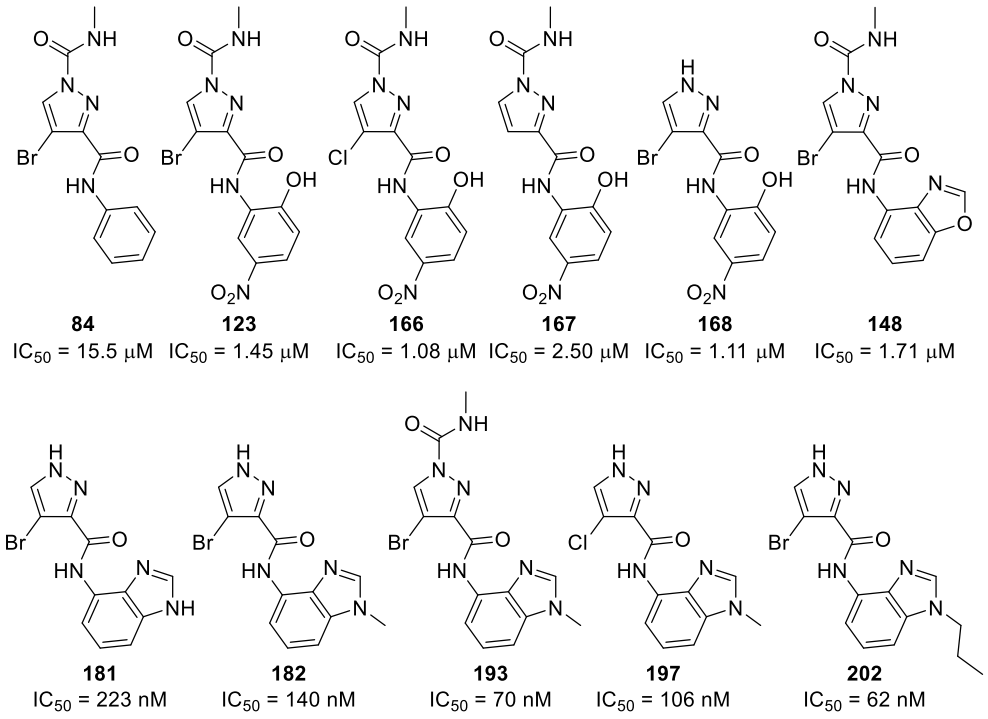

Figure 134: Active analogues with dose-response curves.

We were able to gain a 250 fold increase through the SAR analysis between initial hit **84** (IC_{50} = 15.5 μM) and lead analogue **202** (IC_{50} = 62 nM) through several iterations of investigation.

Chapter 4: Determination of allosteric modulation

A wide range of analogues were synthesized throughout this project. Some have shown excellent activity, whilst others were partially or completely inactive. Nevertheless, the biological assays that were used only revealed stabilization or activity. At this stage we had not been able to show if they interacted with the allosteric or orthosteric site.

I. Mode of inhibition

1. Background

We previously described how to determine the mode of inhibition of a compound, **Figure 36** (p 35). To perform a mode of inhibition assay, the compound of interest should be screened at various concentrations (inhibition curve) while varying the concentration of the natural substrate. This provided a series of inhibition curves at different concentrations of natural substrate. The results obtained indicate if the compound is competitive or non-competitive against ATP.

Two examples from the literature will be discussed to outline what is to be expected: an ATP-competitive inhibitor and a non-ATP competitive inhibitor.

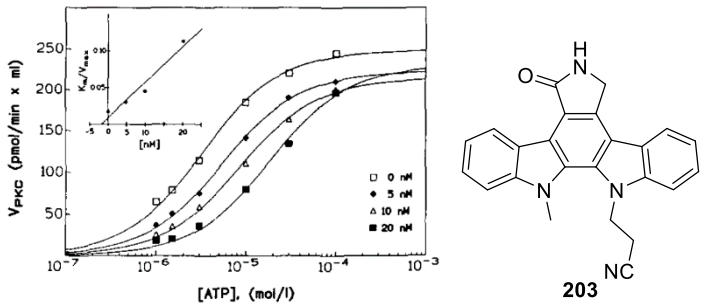

Figure 135: Competitive PKC inhibitor.

In 1993, Martigny-Baron *et al.* examined the selectivity and mode of inhibition of **203** against PKC isoforms.[98] They screened **203** at different concentrations and at different ATP concentrations, **Figure 135**. From this data it was apparent that when the concentration of **203** was increased a significant change was observed in the inhibition curve. This indicated that the inhibitor was competing with ATP to carry out its function.

Qui *et al.* discovered a potent non-ATP-competitive inhibitor of kinase protein MK2.[99] In order to determine the mode of inhibition, three inhibition curves were obtained with the enantiomer of interest (**204**), **Figure 136**. Three ATP concentrations were examined within this assay: 1 µM, 10 µM and 100 µM.

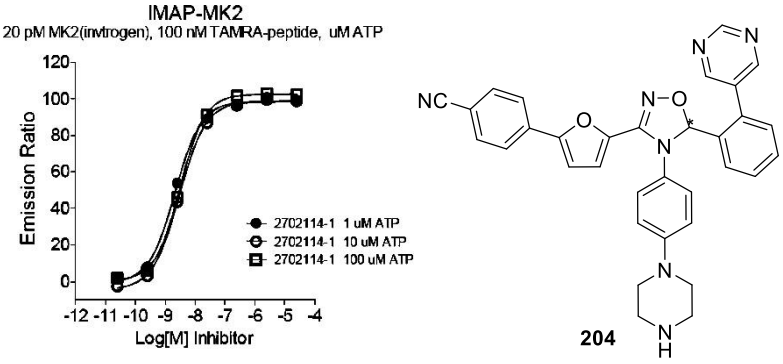

Figure 136: Non-ATP-competitive inhibitor mode of inhibition assay.

When the ATP concentration was increased, the IC_{50} of the compound did not vary. This indicated that the compound did not compete with ATP to carry out its function rendering **204** as a non-ATP-competitive inhibitor.

Analogue **202** was tested at various ATP concentrations to determine the mode of inhibition.

2. **Assay**

In the initial Lanthascreen assay for DYRK2, an ATP like tracer was present in solution, **Figure 37**. In order to determine the mode of inhibition, ATP needs to be present during the kinase reaction. Therefore, a different assay needed to be used to determine if analogue **202** was competitive or non-competitive. Life Technologies has such an assay for DYRK2 in a Z'LYTE assay (**Figure 38** p 37). This biochemical assay was based on a fluorescence tag and the difference in sensitivity between phosphorylated and non-phosphorylated proteins to cleavage.

3. **Results**

Substrate **202** was examined at a single point concentration of 1 µM at three different ATP concentrations: 10 nM, 100 nM and 1 µM. In order to compare the results **L41**, a known competitive inhibitor, was also tested at the same concentrations of ATP.

Table 26: Variation of ATP concentration for L41 and 202 against DYRK2.

[ATP] in nM	L41	202
10	76 ± 3%	75 ± 0%
100	42 ± 1%	38 ± 1%
1000	8 ± 1%	5 ± 2%

The results obtained from this assay revealed that analogue **202** had a similar profile to **L41**, **Table 26**. When the concentration of ATP was increased, the activity of **L41** decreased. **L41** loses its activity as it can no longer bind to the orthosteric site when ATP is present in high concentration, which suggests competitive behaviour. The same observation can be made with analogue **202** indicating a competitive behaviour.

Although the original aim of this project was to prepare an allosteric modulator of DYRK2, results suggested we had prepared a selective (between the two DYRK isoforms) orthosteric DYRK2 modulator.

II. Selectivity panel

In the development of a probe compound and within a drug discovery programme an understanding of selectivity is critical. This enables an understanding of interaction with alternative proteins and a greater knowledge of a mechanism of action for any phenotype observed. This is called a kinase selectivity panel.

a. Targets

Hit compound **202** was tested against 41 other kinases. The choice of the kinases was based on 5 factors:

- Isoforms of DYRK
- Other family members
- Most investigated kinases that are clinically relevant[100]
- Literature targets that are hit by other inhibitors including DYRK2[12, 101, 102]
- Known kinase targets to avoid

The kinases chosen are collected in **Figure 137** by family and assay type. Analogue **202** was obviously screened against the five isoforms of DYRK: DYRK2, DYRK1A, DYRK1B, DYRK3 and DYRK4. Additional members of the CMGC family were chosen as some have shown cross inhibition in other kinase profiling panels: HIPK (1, 2 and 4), CLK (1−4), GSK (α and β), ICK and MAPK1.[12, 103] The CDKs (1, 2 and 9) were selected as they have been highly pursued as potential cancer drug targets. In the TK family, the selected kinases have all shown important clinical relevance. ABL is a known driver of malignant transformation which makes it an important target to test. EGFR is a kinase that has been seen to be overexpressed in a plethora of cancers and particularly in breast and lung cancer. JAK2 has been a target in oncology rendering it an important target to examine within the screen. The activating mutation of MET can cause a 'hereditary papillary renal carcinoma' and has been seen to be implicated in other malignancies. Finally, SRC kinases have been shown to play an important role in cell proliferation and survival. They also have been overexpressed in a variety of different cancers.

CMGC Family	Assay
DYRK2	Lanthascreen
DYRK1A	Z'LYTE
DYRK1B	Z'LYTE
DYRK3	Z'LYTE
DYRK4	Z'LYTE
HIPK1	Z'LYTE
HIPK2	Z'LYTE
HIPK4	Z'LYTE
CLK1	Z'LYTE
CLK2	Z'LYTE
CLK3	Z'LYTE
CLK4	Lanthascreen
GSK α	Z'LYTE
GSK β	Z'LYTE
CDK1/Cyclin B	Z'LYTE
CDK2/Cyclin A	Z'LYTE
ICK	Lanthascreen
CDK9/Cyclin T1	Z'LYTE
MAPK1 (ERK2)	Z'LYTE

TK Family	Assay
EGFR	Z'LYTE
ABL1	Z'LYTE
MET (cMET)	Z'LYTE
SRC	Z'LYTE
JAK2	Z'LYTE

AGC Family	Assay
ROCK1	Z'LYTE
AKT1 (PKB α)	Z'LYTE

CAMK Family	Assay
PIM1	Z'LYTE
PIM2	Z'LYTE
MAP2K2 (MEK2)	Z'LYTE
CHEK1 (Chk1)	Z'LYTE

TKL Family	Assay
AKL	Z'LYTE
BRAF	Z'LYTE
IRAK1	Adapta

STE Family	test
PAK1	Z'LYTE
SLK	Lanthascreen

CK1 Family	Assay
CSNK2A1 (CK2 α1)	Z'LYTE
CSNK1A1 (CK1 α1)	Z'LYTE

Other	Assay
Aurora A	Z'LYTE
Aurora B	Z'LYTE
PLK1	Z'LYTE
Wee1	Lanthascreen
Haspin	Adapta

Atypical kinases	Assay
FRAP1 (mTOR)	Z'LYTE

Figure 137: Kinase profile list of targets and LT assay.

In the AGC family, ROCK1 is involved in gene transcription, proliferation, apoptosis and oncogenic transformation and should therefore be avoided.[104] AKT1 is an important pharmacological target as it was found to be up-regulated in a number of cancers and has been shown to be important for tumour growth.[100] In the CAMK family, the PIMs have been found to cross inhibit with the DYRK family for certain

inhibitors.[12, 101] CHEK1 is an important target as it is a central component of DNA response. It enables the regulation of cell cycle through checkpoints to prevent the entry of DNA damaged cells into mitosis rendering it a very interesting target.[105] Finally, MAP2K2 is an important target as it is actually a cascade reaction of several kinases (RAS-RAF-MEK-ERK) *aka* the mitogen activated protein kinase (MAPK) cascade. It is involved in numerous processes such as cell cycle progression, differentiation, apoptosis and transformation to the cancerous state.[106] In the TKL family, AKL and BRAF have been shown to be of great pharmacological relevance. AKL is a kinase in which 'translocation drives anaplastic lymphoma'.[100] BRAF plays a pivotal role in cell proliferation and a BRAF mutation was responsible for the development of melanomas and other cancers. IRAK1 has shown cross inhibition with DYRK2.[103] In the STE family, PAK1 is an important effector associated with ROCK1 and SLK has been shown to promote apoptosis and is involved in a cascade pathway with p38 and JNK1.[107] In the CK family, CK1 and CK2 have shown cross inhibition with DYRK2 for Leucettamine derivatives.[12] As for other kinases, Aurora A and B are important kinases in mitosis and were the first kinases pursued in oncology. PLK1 is also involved in mitosis making it an interesting target. Haspin is a histone kinase that is critical in mitosis by favouring chromosome cohesion, metaphase alignment as well as progression through the cycle.[108] Wee1 is a key regulator of cell cycle progression and influences cell size by inhibiting CDK1. Finally, the last kinase chosen was mTOR which is part of the PI3K kinase family (lipid kinases) which is involved in cell growth, survival and differentiation.[100]

b. **Assays**

Three different assays were run depending on the chosen kinase. One binding assay called Lanthascreen, discussed previously, and two activity assays: Z'LYTE and Adapta. Z'LYTE was described in detail on p 37. The Adapta assay is outlined below.

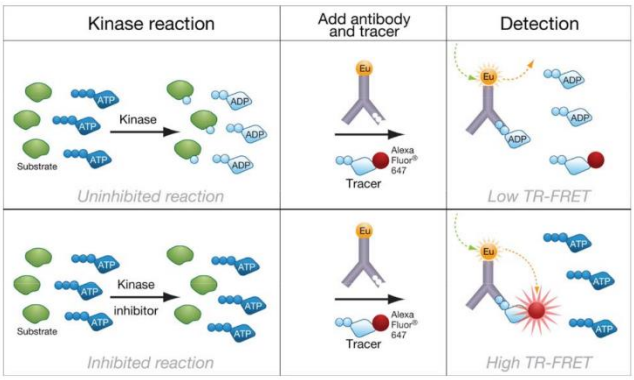

Figure 138: Schematic representation of Adapta assay.

The Adapta assay relies on a two-step reaction, **Figure 138**. The first reaction consists of mixing the analogue of interest with ATP and the kinase. The reaction is then allowed to incubate before the addition of EDTA (to stop the kinase reaction) as well as a detection solution of a Europium-labelled anti-ADP antibody and a labelled ADP tracer. The ADP that was formed by the kinase reaction displaces the ADP tracer from the antibody resulting in a lower TR-FRET signal. When an inhibitor is present, less ADP is formed which leads to the ADP tracer interacting with the antibody instead resulting in a higher TR-FRET signal. The higher the TR-FRET the more active the inhibitor.

c. Results

Analogue **202** was therefore tested at a single point concentration of 1 µM for each kinase chosen, **Figure 139**.

CMGC Family	% inhibition
DYRK2	87 ± 1%
DYRK1A	8 ± 1%
DYRK1B	7 ± 0%
DYRK3	12 ± 3%
DYRK4	1 ± 0%
HIPK1	3 ± 2%
HIPK2	2 ± 0%
HIPK4	5 ± 0%
CLK1	-1 ± 1%
CLK2	-3 ± 0%
CLK3	3 ± 1%
CLK4	32 ± 4%
GSK α	3 ± 0%
GSK β	5 ± 3%
CDK1/Cyclin B	4 ± 2%
CDK2/Cyclin A	1 ± 1%
ICK	2 ± 0%
CDK9/Cyclin T1	-2 ± 6%
MAPK1 (ERK2)	6 ± 1%

TK Family	% inhibition
EGFR	-5 ± 2%
ABL1	-3 ± 1%
MET (cMET)	-1 ± 1%
SRC	14 ± 1%
JAK2	-16 ± 2%

AGC Family	% inhibition
ROCK1	-8 ± 0%
AKT1 (PKB α)	1 ± 2%

CAMK Family	% inhibition
PIM1	-4 ± 1%
PIM2	-6 ± 3%
MAP2K2 (MEK2)	5 ± 1%
CHEK1 (Chk1)	-2 ± 8%

TKL Family	% inhibition
ALK	6 ± 3%
BRAF	-1 ± 4%
IRAK1	0 ± 14%

STE Family	% inhibition
PAK1	15 ± 9%
SLK	3 ± 0%

CK1 Family	% inhibition
CSNK2A1 (CK2 α1)	-1 ± 2%
CSNK1A1 (CK1 δ1)	-3 ± 0%

Other	% inhibition
Aurora A	1 ± 5%
Aurora B	-11 ± 4%
PLK1	6 ± 2%
Wee1	2 ± 0%
Haspin	24 ± 5%

Atypical kinases	% inhibition
FRAP1 (mTOR)	-2 ± 0%

Legend
< 20%
20% - 60%
≥ 60%

Figure 139: Kinase profiling results with analogue 709.

Analogue **202** displayed outstanding selectivity over the panel of kinases chosen. It showed modest activity towards CLK4 with 32 ± 4% inhibition, Haspin with 19 ± 5% inhibition and potentially PAK1 with 15 ± 9% inhibition. Nevertheless, it has shown higher selectivity towards Haspin than reference compound **L41** (75%), **Table 27**.

Table 27: % inhibition for L41 and 202 at 1 µM against DYRK2 and Haspin.

	L41	202
DYRK2	101 ± 1%	87 ± 1%
Haspin	75 ± 3%	19 ± 5%

From all of these results, we can conclude that analogue **202** has shown an excellent selectivity for the panel of kinases chosen over reference compound **L41** (screening carried out by Meijer).[12]

III. Co-crystallization

In order to determine how the analogues bind in the ATP pocket of DYRK2, the SGC carried out a co-crystallization with the best hits. Analogues **181**, **182**, **193**, **197**, and **202** were sent to try and crystallize each analogue with DYRK2 as they showed good binding activity (< 240 nM), **Figure 140**.

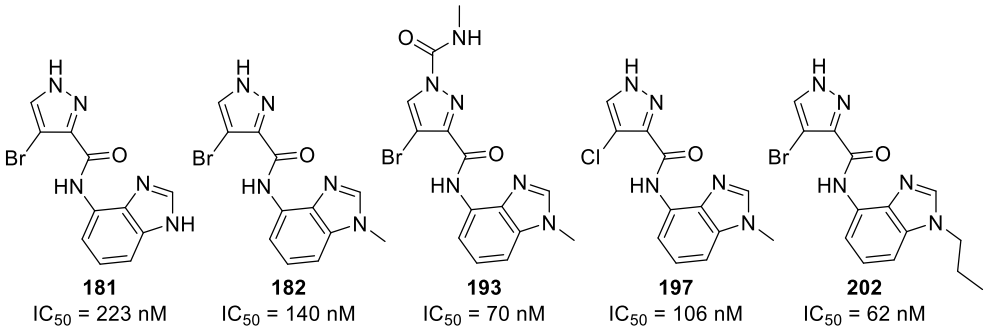

Figure 140: Hits sent for co-crystallization.

The crystals were grown with the following conditions: 10−18% PEG 8000, 0.1 M Citrate, pH = 5.0−6.0, 0.1−0.2 M NaCl. The crystals obtained did not diffract well with **181** and **202**, giving 3.2 Å resolution. However, we managed to get some structural understanding of these compounds in the ATP pocket. The full structure determination is ongoing and only pictures of the compounds bound in the orthosteric site have been provided.

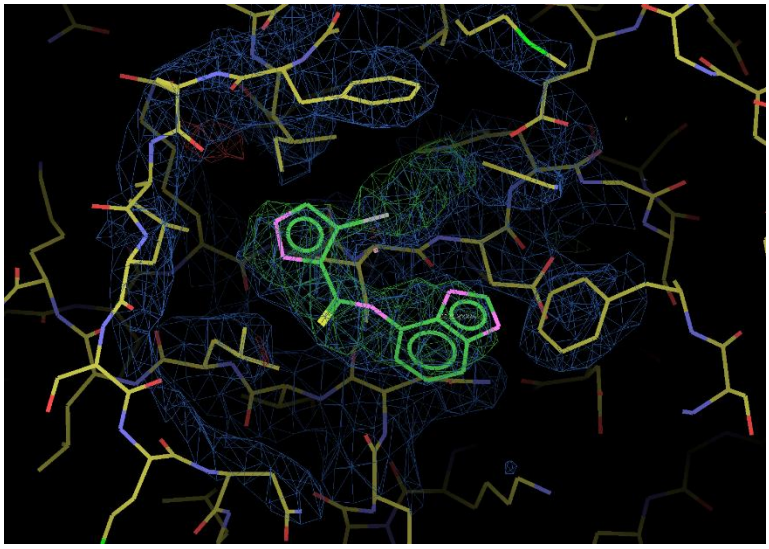

Figure 141: Analogue 181 co-crystallised with DYRK2.

Analogue **181** showed a binding pose in the ATP site of DYRK2, **Figure 141**. From this structure determination it was not clear yet what interactions were involved that rendered this molecule active. The bromine and the small imidazole ring were pointing in the hydrophobic pocket. Moreover, the pyrazole ring appeared to be a hinge-binder. It is interesting to note that during the development of the amide scaffold a number of single crystals of the pyrazole were obtained (**86** p 87 and **148** p 121).

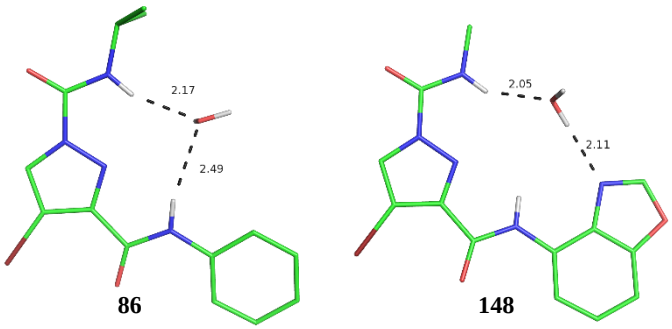

Figure 142: Single crystal structures obtained of analogues 86 and 148.

When amide analogue **86** and **148** were crystallised, a hydrogen bonding network was observed which led to the NH of the amide pointing in the same direction as the nitrogen of the pyrazole ring, **Figure 142**. A 180 ° rotation was observed, at that level, when it was bound in the orthosteric site.

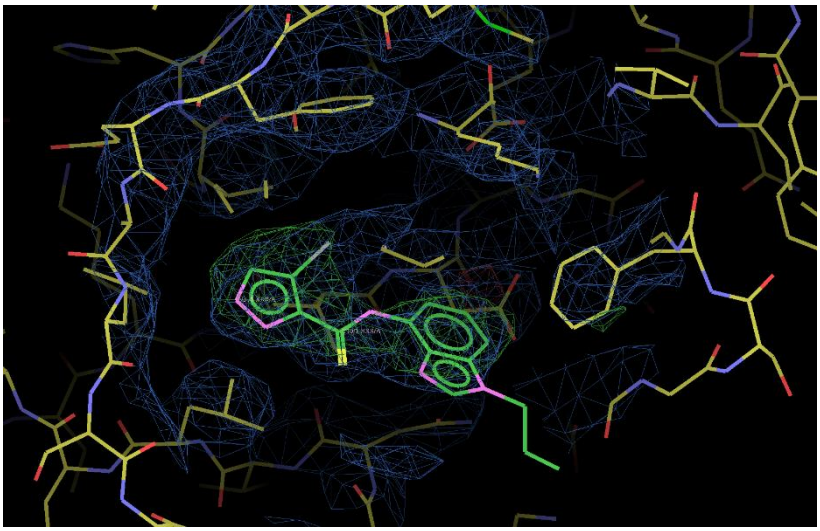

Figure 143: Analogue 202 co-crystallised with DYRK2.

Analogue **202** showed a different binding pose to **181** in the orthosteric site. The bromine was still pointing towards the hydrophobic region of the site but there was a switch regarding the benzimidazole ring: presumably the *N*-propyl group is too large to occupy the back of the pocket and necessitated a rotation towards the solvent exposed region. No clear interactions were determined to explain high potency. Structure refinement is ongoing from collaborators and data will be available once it has been provided.

We observed that the binding pose provided by the crystal structure of analogue **202** was different to the predicted modelling studies.

IV. Conclusion

The most active analogue **202** had shown great potency for the target of interest DYRK2. **202** was shown to be ATP-competitive and have high selectivity against a panel of 40 kinases. Moreover, two analogues, **181** and **202**, were co-crystallised with DYRK2 revealing the binding pose adopted within the ATP pocket. Modifications to the hit compounds can be carried out based upon this crystal structure once it has been fully refined.

Chapter 5: Refined model developed

Al-Shar'i's initial model, which identified allosteric pockets, was based on a protein set of two kinase proteins with known allosteric inhibitors and consisted of four different analyses. This model was then applied to the protein DYRK2, where one pocket in the *N*-lobe was identified as a potential allosteric pocket.

When my research as a graduate student began, Antony Vassileiou also began a PhD project developing a more refined model to identify allosteric sites in proteins. To date, his model consists of 60 test proteins exploring 120 variables.

I. Model

This new model was developed by Antony using a machine learning algorithm called Random Forest (RF) which was first introduced by Breiman in 2001.[109]

RF was used to develop predictive models either for classification or regression problems. A classification problem is one where a category is predicted, whereas a regression problem is one where numerical data is desired. For our model, a classification problem was of interest as we wanted to know if an amino acid was considered to be involved in an allosteric site or not. The ideal output given at the end would be a list of the amino acids of the protein of interest with a true (allosteric) or false (non-allosteric) response.

To produce the RF dataset, 60 proteins with known allosteric regulators were selected, of which 14 were protein kinases. A 50 ns trajectory of molecular dynamics was simulated for each protein using the ff12SB forcefield in AMBER.[110] For each trajectory, a series of analytical methods which produced residue properties were applied. For example, the residue fluctuation, the accessible surface area and the SID score,[42] amongst other were analysed. A final column of data was then created marking each residue as either part of an allosteric binding site or not.

Table 28 is an example of the dataset, where A, B, C were the variables obtained from each residue of each protein. The final column was then added to say if the residue was true or false. The dataset was therefore ready to be trained.

Table 28: Example of dataset for training set.

Protein	AA	A	B	C	D	…	T/F
	Q	0.18	-3.1	2.3	0.002	…	T
	E	0.02	-2.4	2.5	0.023	…	F
	R	0.06	-0.5	1.8	0.123	…	F
	P	0.11	-1.1	0.9	-0.027	…	T
…	…	…	…	…	…	…	…
	G	0.08	0.1	3.0	-0.156	…	F

The dataset obtained was then analysed by the RF algorithm. For each decision tree:

1. A portion of the dataset (example 2/3 rows) was picked at random.
2. A subset of variables (columns, the square root of the total) was chosen at random.
3. For each variable chosen in 2, RF choosed the optimum splitting threshold.
4. It split the data into two nodes based on the best variable from within the random subset.
5. Repeated 2−4 on each node until they contain only a single class (T or F).

These two sources of randomness (at 1 by varying the rows and at 2 varying the columns) forced each tree to base its decisions on different criteria. The process was then repeated and the model created 1000 trees.

Figure 144 is a schematic representation of how RF works, where red represents the data that is unused due to non-optimal splitting, green represents the splitting nodes and orange the single class terminal nodes.

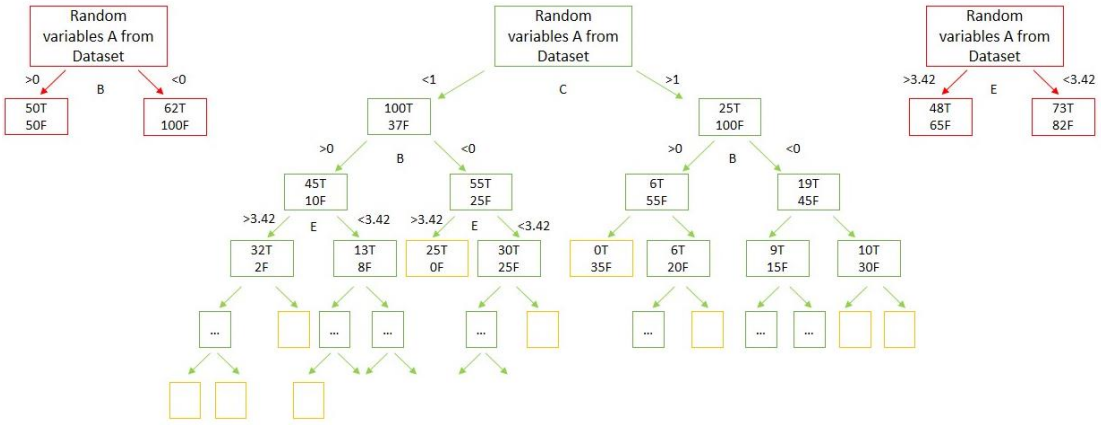

<u>Figure 144:</u> Schematic representation of RF for the first tree.

Once the model was established, it was used to predict the amino acids that could be considered allosteric in an unknown protein. Similar to the training set, a 50 ns trajectory was simulated for the test protein which was then put through the RF predictive model. Each amino acid was individually put through every tree in the model. A 'vote' was then cast on its classification based on the terminal node it reached in each tree. For example amino acid Leu 231 went through the tree shown in **Figure 144**. Leu 231 would first be analysed by variable C and would go in one of the two pools depending on the number generated by the trajectory. It would then continue the journey down the tree until it had reached one pool with a perfect split: 100 true or false. Leu 231 would then go on to the next tree of this forest which would also say if it was true or false. In the end the majority of true or false would determine if the amino acid could be considered allosteric or not. This was then done on each amino acid of the protein sequence.

II. Results

The model was applied to DYRK2 by Antony to determine what the new model would predict as an allosteric site, **Figure 145**.

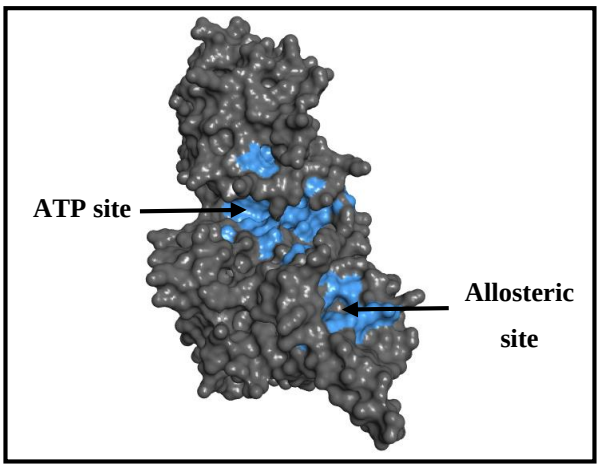

Figure 145: DYRK2 protein after Vassileiou's model with false in grey and true in blue.

The model provided a true/false statement regarding each amino acid and its possibility of being involved in an allosteric site. In **Figure 145**, the blue represents the amino acid that are predicted to be true whereas the grey are the amino acids that are false. We observed that the model has picked up the ATP site as well as a new allosteric site situated in the *C*-lobe of the protein.

Closer inspection of the pocket revealed that it is a deeper and narrower pocket than the predicted pocket by Al-Shar'i's model, **Figure 146**.

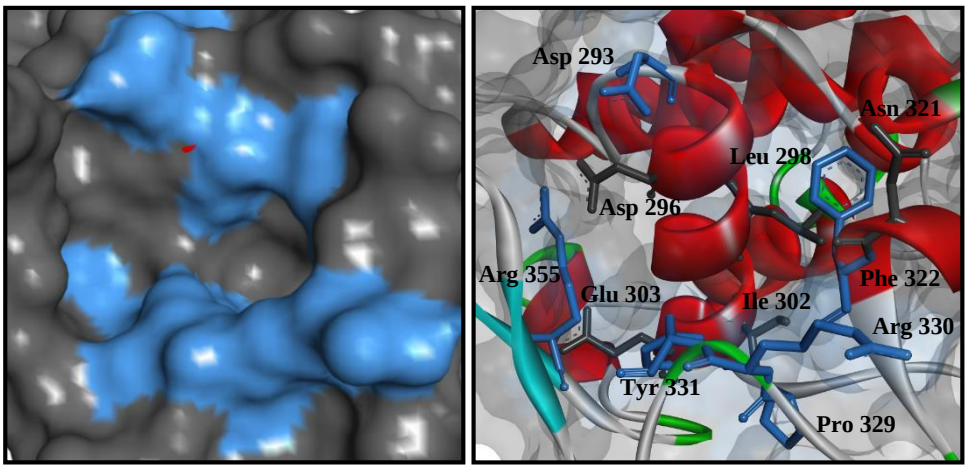

Figure 146: Close up allosteric pocket with refined model (blue amino acids are true, grey are false).

The amino acids involved in this allosteric pocket are highlighted in **Figure 146**, with blue representing residues that are considered true and the grey residues which are false. The pocket was composed of six 'true' amino acids: Asp 293, Phe 322, Pro 329,

Arg 330, Tyr 331 and Arg 355. It also contained the following amino acids to complete the allosteric pocket: Asp 296, Leu 298, Ile 302, Glu 303 and Asn 321. A wide range of amino acids with different properties are represented: hydrophobic, polar and electronically charged.

III. Virtual screening

The first putative pocket found was analysed by generating a pharmacophore through the LUDI algorithm and then a virtual screen of the Maybridge library was performed (section **5a** and **b**, p 26 and 27). Maybridge compounds are expensive, with 2 mg of an analogue costing around £45. This increases the cost to carry out biological testing to see if a hit can be extracted. We had access to 14,390 compounds from the Maybridge library thanks to Louise Young from SIPBS at the University of Strathclyde. This library will be referred to as Hitfinder (HF).

1. First attempt

a. Pharmacophore generation and VS

The work presented here on out was carried out by the author unless otherwise stated. From this pocket, generated a pharmacophore utilising the LUDI algorithm in Discovery Studio providing an interaction map. After close inspection and some optimisation, we were able to generate the pharmacophore shown in **Figure 147**.

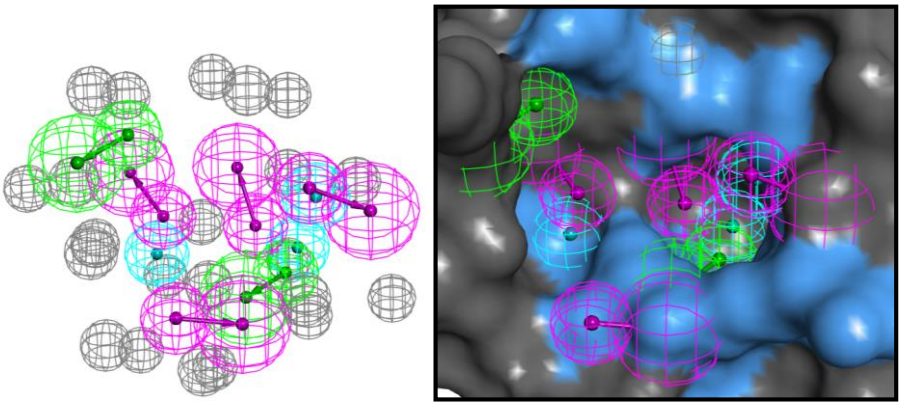

Figure 147: Pharmacophore of the second allosteric pocket in 2D.

The pharmacophore had 22 exclusion spheres and 9 key features: 3 hydrophobic, 4 donor and 2 acceptor. While the new pharmacophore had a lot of key features, it was possible to ask the programme to map a minimum of features when the library was screened against a pharmacophore. Therefore, even if the pharmacophore had a number of key features, the programme only needed to hit the minimum number of features desired by the user. This provided a filtering option that could be reduced or increased according to the results obtained. We noticed that when the pharmacophore was screened against the HF library no hits surfaced even when asking the library to fit only one feature. This was an odd result that we could not explain and was highly unlikely to happen. Therefore we decided to screen the Maybridge library against the pharmacophore and for the compounds to hit minimum 2 features. With those results obtained, Murray Robertson from SIPBS, then used Pipeline Pilot to extract and see which compounds were present in the HF library based on the code associated to each analogue. This led to 1,941 compounds that we had access to and needed to filter, **Figure 148**.

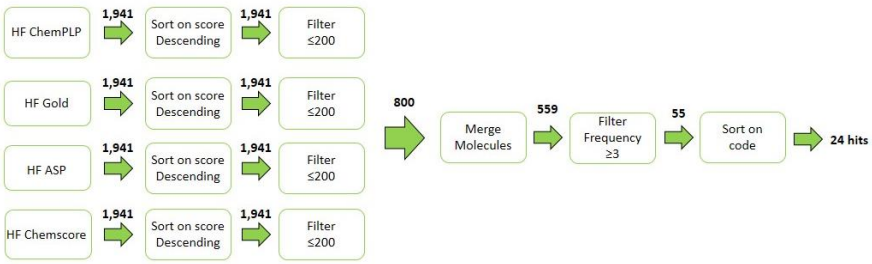

<u>Figure 148:</u> Pipeline Pilot protocol.

All of these compounds were docked in the new allosteric site of protein 3K2L provided by Vassileiou with the following coordinates: XYZ 9.5, 30.5 and -2.0. The four different scoring functions were used which provided four different HF library results for all 1941 compounds. These results were then sorted according to the scoring function chosen in a descending order to have the highest scoring analogue first. Compounds were then filtered to allow only 200 analogues with the highest scores to be carried through. This was carried out for all four scoring functions and provided 800 analogues in total. When libraries were merged according to the SMILES, only 559 were unique. Finally, this list was filtered by frequency as we wanted the analogue to be present in at least 3 of the 4 scoring functions. This led to 55 analogues present

in at least three sets of scoring function. Furthermore, we regrouped the molecules by their Maybridge code and ended up with 24 virtual hits.

b. **Compounds**

From these 24 compounds, only 11 were chosen for testing, due to their docked pose and also availability from the HF library. In addition, some of the analogues that were on the list were not available.

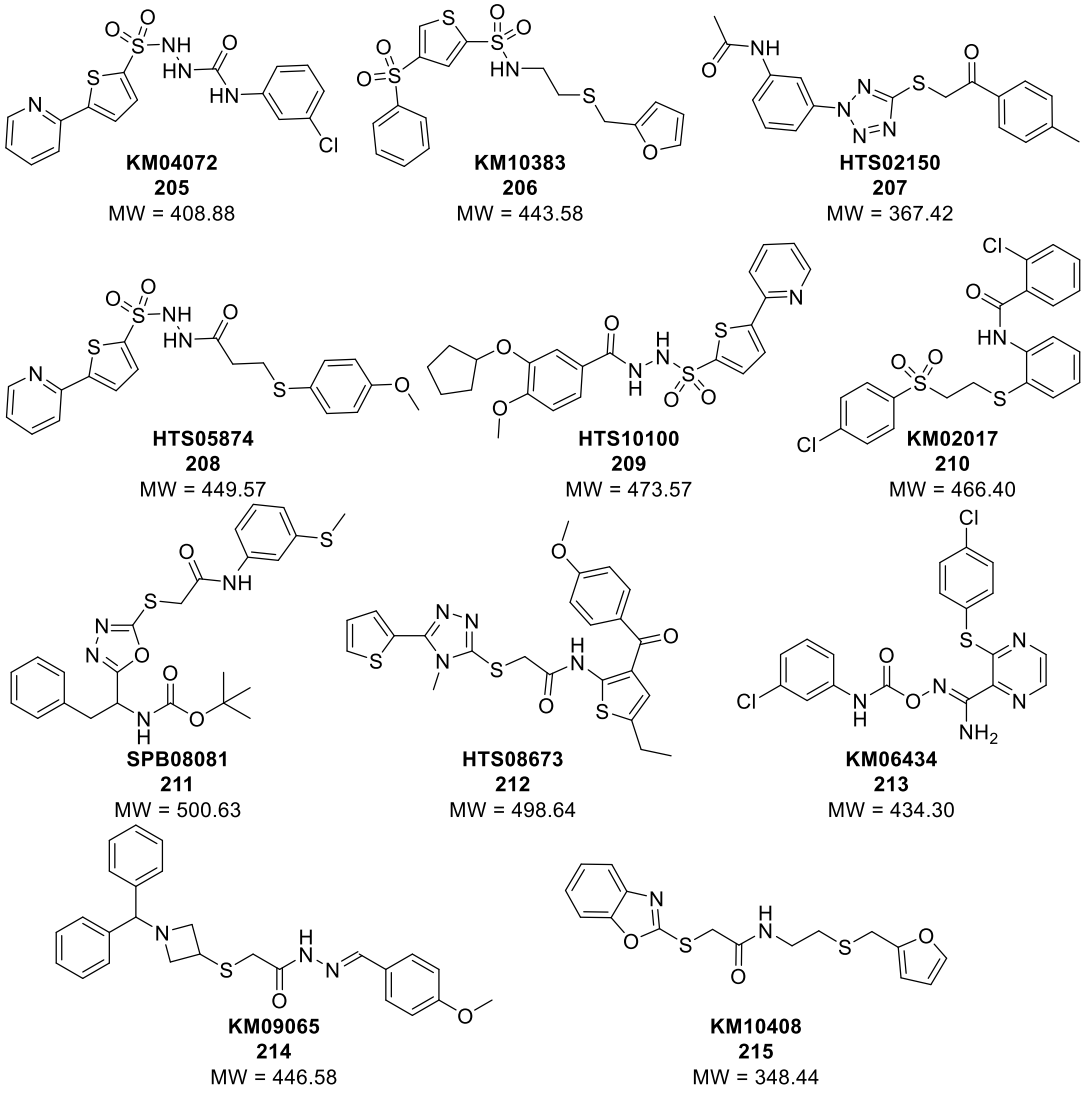

<u>Figure 149:</u> Analogues chosen for DSF testing from protocol.

Figure 149 represents the compounds available chosen from our first protocol. Some of these compounds have high molecular weights (MW) and have a number of

heteroatoms. A wide range of compounds were chosen with different chemical properties, rigidity, and shape.

c. DSF results

We were sceptical that these compounds could fit in the pocket, knowing that we had a smaller allosteric site than the initial one examined. Nevertheless, they were sent for testing at the SGC to see if any of the analogues could be considered a hit. The DSF results of the analogues screened against DYRK2 and DYRK1A are shown in **Graph 42**.

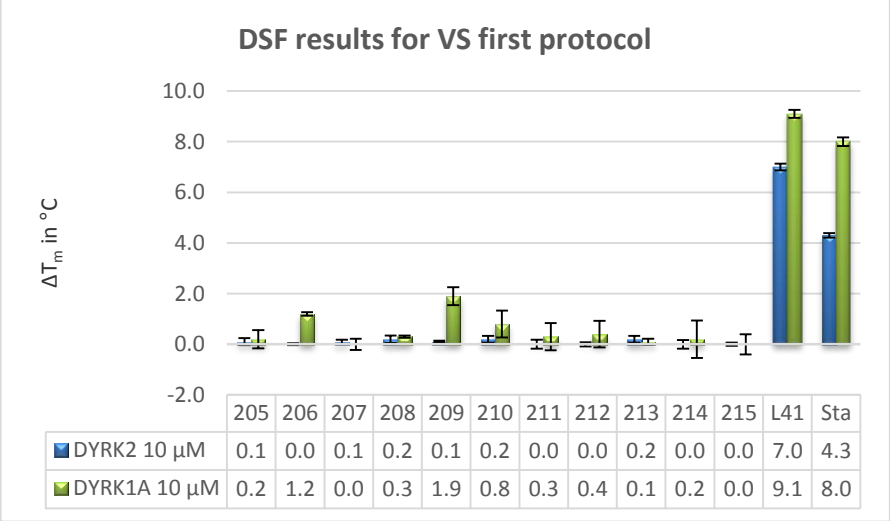

	205	206	207	208	209	210	211	212	213	214	215	L41	Sta
DYRK2 10 µM	0.1	0.0	0.1	0.2	0.1	0.2	0.0	0.0	0.2	0.0	0.0	7.0	4.3
DYRK1A 10 µM	0.2	1.2	0.0	0.3	1.9	0.8	0.3	0.4	0.1	0.2	0.0	9.1	8.0

Graph 42: Bar graph representation of DSF results of VS analogues first protocol.

From the results, we can observe that none of the analogues from the VS stabilize the protein target DYRK2 with all $T_m \leq 0.2$ °C. However, two have shown some stability towards DYRK1A: **206** (**KM10383**) with a $T_m = 1.2$ °C and **209** (**HTS10100**) with $T_m = 1.9$ °C. It must be noted that the error bars for screening analogues against DYRK1A are very high.

2. Second protocol

With the disappointing DSF results, a new strategy had to be put in place to find an alternative method to analyse the new putative allosteric pocket. For this new strategy, no pharmacophore was used to screen the HF library. It was observed that some analogues showed unrealistic conformations while trying to fit certain features.

Therefore, all 14,390 compounds from the HF library were docked in the pocket of interest with the same coordinates used previously. The scoring function that was first used was ChemPLP and then the compounds were rescored with three other scoring function (Gold, ASP and Chemscore). This consisted of using the established docked pose and rescoring it with the new scoring function algorithm. Therefore the whole library was scored in the four scoring functions available in Gold.

a. **Analysis protocol**

The Pipeline Pilot protocol used in this second attempt was developed by the author and is outlined in **Figure 150**.

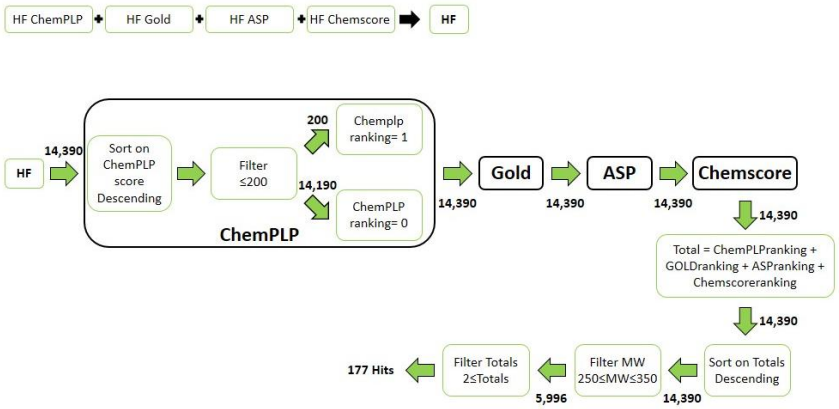

<u>Figure 150:</u> Pipeline pilot protocol second attempt.

The first step consisted of merging all the different files associated with the HF library for each scoring function. One common file with all the data generated was therefore used, referred to as HF in this protocol. We first decided to sort the library according to the ChemPLP scoring function by sorting them in descending order. We then decided to keep the first 200 analogues and gave them an Index A of 1. This meant that they were of interest to us for this scoring function. The other 14,190 compounds were indexed as 0. The whole library of 14,390 compounds was merged again to carry out the same protocol for each scoring function. A compound might have a high scoring function within ChemPLP but a poor score in ASP. Therefore, it was important to carry out the same analysis on all scoring functions. We then elected to sum the indexes of all four scoring functions. If a compound was present in the 200 best compounds for each scoring function than the total would be of 4. If it was present in

none of the 200 best than the final total would be of 0. Compounds were then sorted according to that total in a descending order, and filtered according to their MW. We have previously seen that allosteric modulators tend to have a lower MW than orthosteric ligands (section **5**, p 17). Therefore, we only examined analogues that had a MW between 250 and 350 g mol^{-1}. Finally, only the compounds that showed a total of indexes of 2 or above were selected. This gave 177 compounds to analyse within Discovery Studio.

b. **Compounds**

We did not want to over use our access to the HF library and send 177 compounds for testing. Moreover, we wanted to be more selective in the compounds chosen.

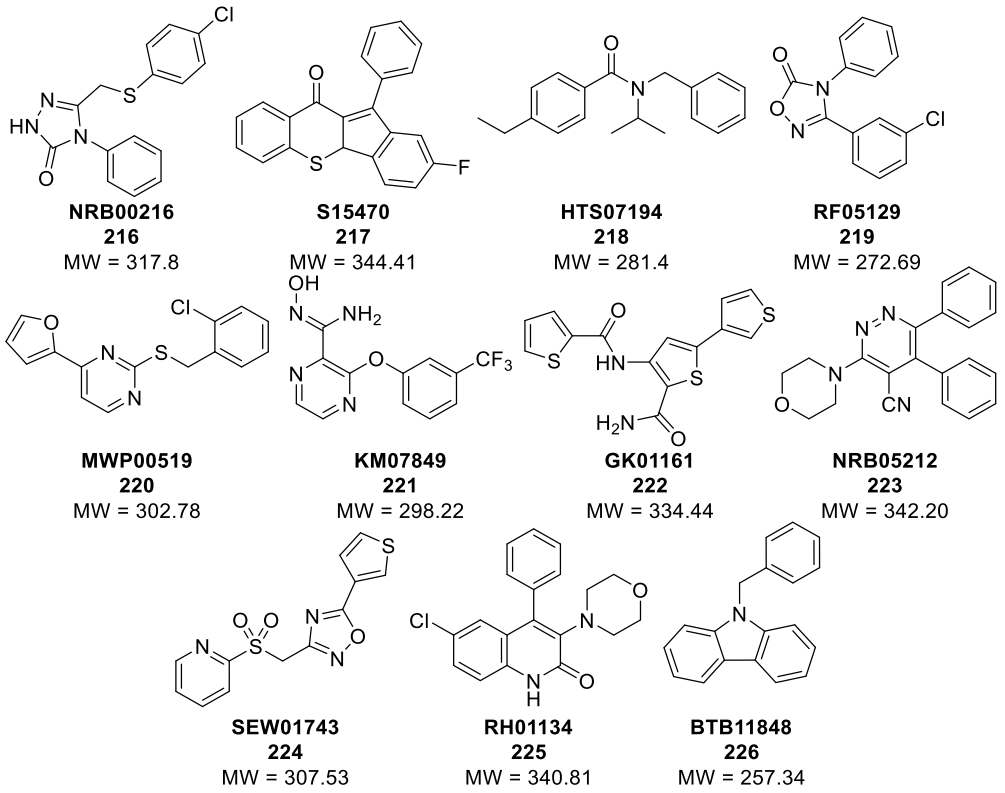

<u>Figure 151:</u> Analogues selected from second protocol part 1.

22 compounds were selected out of the set which are split into 2 sets for ease of analysis, **Figure 151** and **Figure 152**. A wide variety of compounds were chosen with various substitution patterns, shape and rigidity.

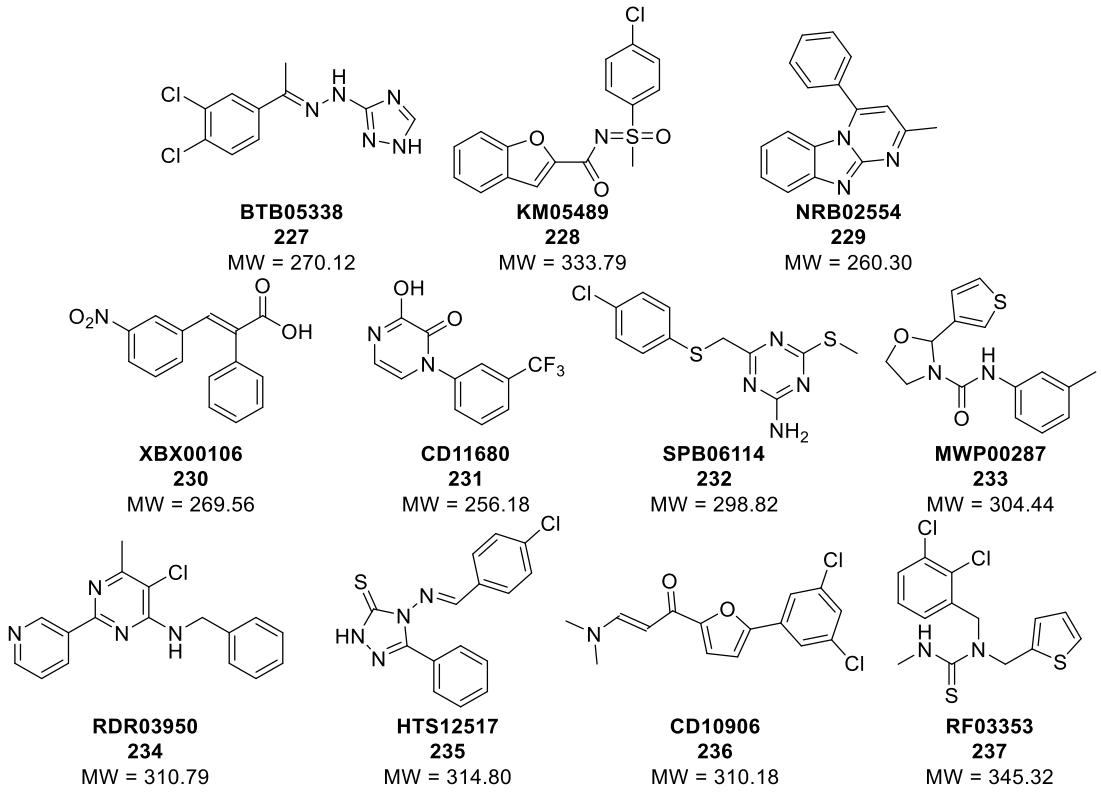

<u>Figure 152:</u> Analogues selected from second protocol part 2.

c. DSF results

All analogues were screened in the DSF assay against DYRK2 and DYRK1A. With 22 compounds in all, the results are shown in two different graphs.

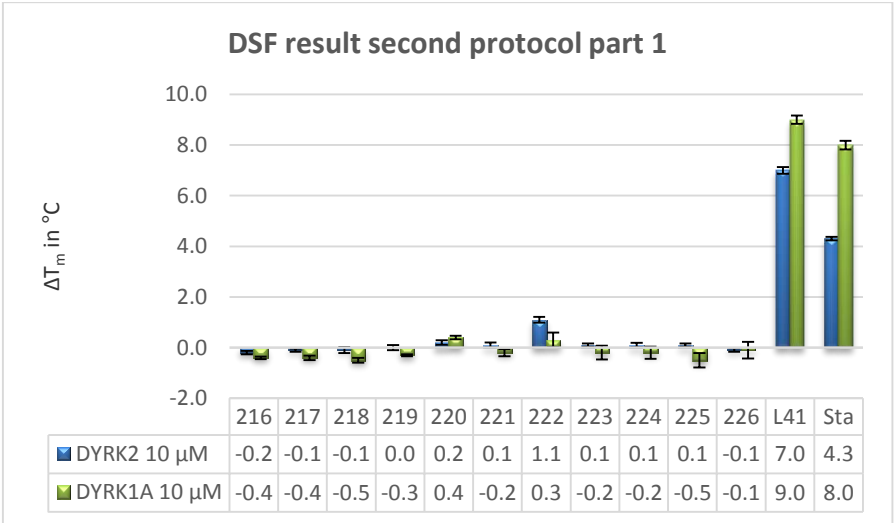

	216	217	218	219	220	221	222	223	224	225	226	L41	Sta
DYRK2 10 µM	-0.2	-0.1	-0.1	0.0	0.2	0.1	1.1	0.1	0.1	0.1	-0.1	7.0	4.3
DYRK1A 10 µM	-0.4	-0.4	-0.5	-0.3	0.4	-0.2	0.3	-0.2	-0.2	-0.5	-0.1	9.0	8.0

<u>Graph 43:</u> Bar graph representation of DSF results for 2nd protocol analogues part 1.

The first batch of 11 compounds, showed that only one analogue had displayed a slight stabilization of DYRK2, **Graph 43**. **222** (**GK01161**) had a T_m = 1.1 °C for DYRK2 and showed selectivity which could be a potential candidate for an SAR study.

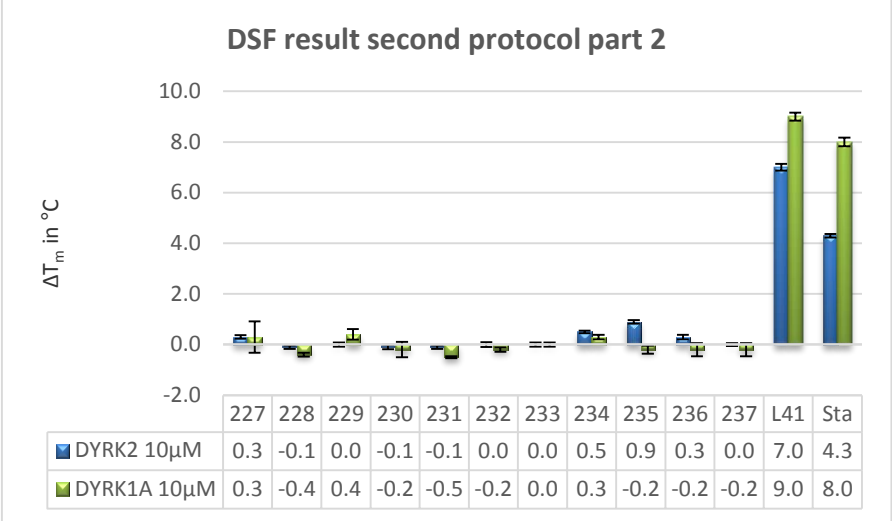

	227	228	229	230	231	232	233	234	235	236	237	L41	Sta
DYRK2 10µM	0.3	-0.1	0.0	-0.1	-0.1	0.0	0.0	0.5	0.9	0.3	0.0	7.0	4.3
DYRK1A 10µM	0.3	-0.4	0.4	-0.2	-0.5	-0.2	0.0	0.3	-0.2	-0.2	-0.2	9.0	8.0

Graph 44: Bar graph representation of DSF results for 2nd protocol analogues part 2.

In this second set of 11 compounds only one analogue showed some stabilization of DYRK2, **Graph 44**. **235** (**HTS12517**) had selectivity with T_m = 0.9 °C for DYRK2 and no stabilization for DYRK1A. It must be noted that error bars for analogues screened against DYRK1A were quite high and can be considered higly less accurate for certain derivatives.

Two possible hits have been found by running our second protocol, **Figure 153**.

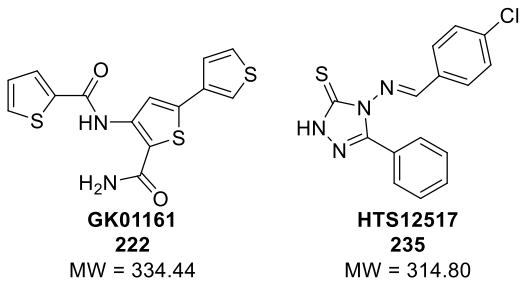

Figure 153: Two possible hits revealed by second protocol.

The first analogue **222** consisted of three thiophene rings linked together *via* a C-C bond and an amide bond. In addition, a primary amide was present on the central thiophene ring. The second analogue **235** had a trizaolethione core with a phenyl ring

as well as a benzylidene ring. Both these compounds showed chemical potential for chemical diversity as starting points for a SAR study.

We docked the compounds in the second putative allosteric pocket from the initial analysis, **Figure 154**.

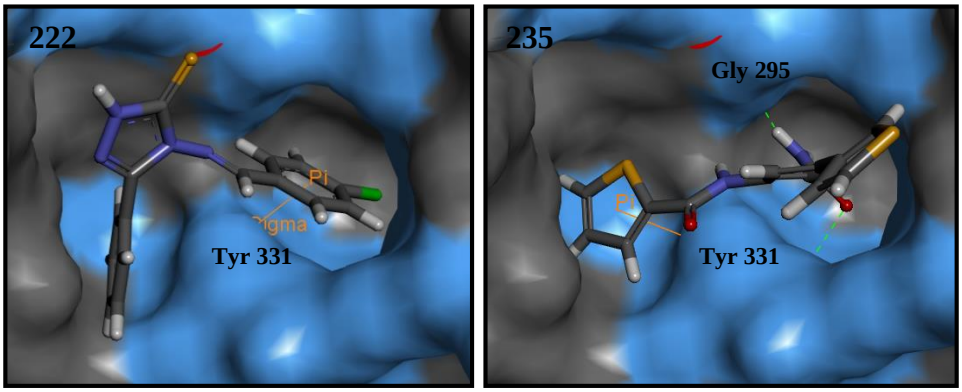

Figure 154: Predicted docked poses of the two DSF hits in second allosteric pocket.

Compound **222** was predicted to adopt a nice fit in the pocket with the chlorophenyl ring interacting with Tyr 331 through a π-σ bond. No other interactions were observed which may explain why the T_m was so low. The predicted docked pose of **235** in the pocket, which displayed less stabilization, was projected to sit such that two H-bonds interactions as well as a π-σ bond interactions were possible. The primary amide interacted with Gly 295 through the NH and through Tyr 331 with the carbonyl group. Finally, the thiophene ring was predicted to be involved in a π-σ bond interaction with Tyr 331. We were not entirely convinced that these compounds might bind to this pocket. Therefore, we also docked them in the ATP pocket, **Figure 155**.

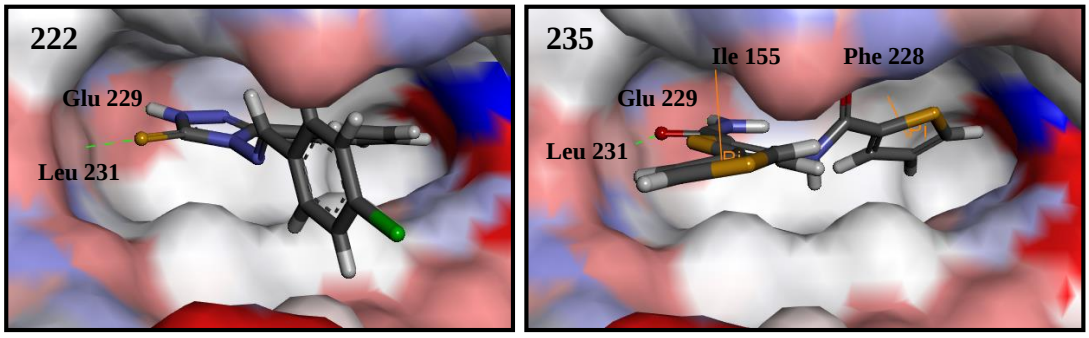

Figure 155: Predicted docked poses of the two DSF hits in ATP pocket.

In the ATP pocket, both compounds revealed predicted conformations where they were able to H-bond with the hinge region. Compound **222** displayed potential interaction with the hinge region through the triazole thione: the sulfur H-bonds to Leu 231 and the NH of the triazole to Glu 229. The chlorophenyl ring was exposed which could be a reason why the compound did not stabilize the protein significantly. For **235**, the primary amide was foreseen to be involved in H-bonding with the hinge region: the carbonyl group with Leu 231 and the NH with Glu 229. It was also involved in potential π-interactions: one thiophene ring interacted through a π-σ bond with Ile 155 and another ring with Phe 228 in a π-π interaction. One of the thiophene rings was predicted to be exposed to the solvent which could be a reason why the compound did not stabilize the protein to a significant extent.

IV. Conclusion

A new more refined model was developed in house by Tony Vassileiou and was applied to our test protein DYRK2, **Figure 156**.

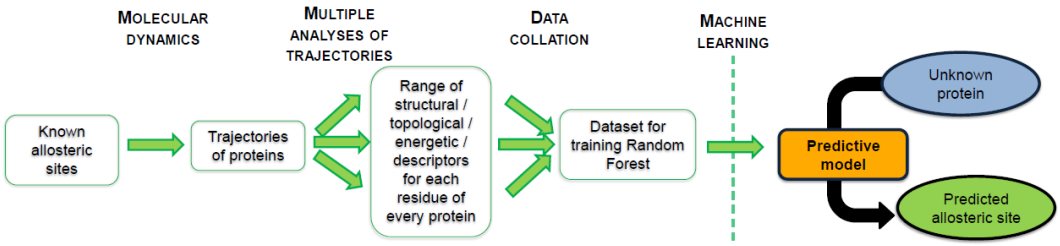

Figure 156: Schematic representation of how the model works.

The model began with a known set of allosteric sites of proteins on which molecular dynamics (MD) was carried out. This provided the trajectories of proteins on which multiple analyses were carried out, including SID analysis and hydrophobic surface area. This data was then used to train the model to detect allosteric sites. When the model was considered optimal it was then used on an unknown protein of interest. This predictive model then allowed the user to discover putative allosteric sites that could then be further analysed.

The model revealed a new potential allosteric site to be explored which was completely different to the site studied within this thesis.

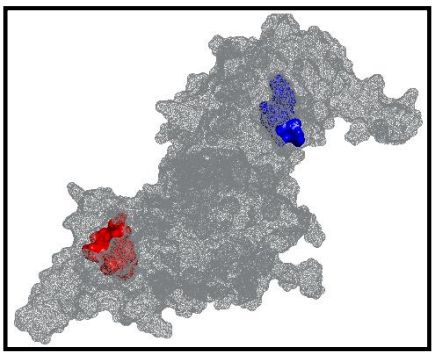

<u>Figure 157:</u> DYRK2 protein with two putative allosteric sites identified: blue with Al-Shar'i's model, red Vassileiou's model.

Figure 157 represents the two allosteric sites predicted: Al-Shar'i's pocket depicted in blue and Vassileiou's pocket in red. The blue pocket was in the *N*-lobe of the protein whereas the red site was in the *C*-lobe of the kinase. This model led us to explore the second pocket.

Pharmacophore generation and VS led us to a set of compounds that showed no stabilization of DYRK2. From this set two compounds showed stabilization for DYRK1A. No further analysis or evaluation of these compounds were attempted. In a second attempt to analyse the pocket, a library was directly screened in the pocket of interest. A protocol was generated to analyse the library and filter the data obtained. This led to a series of compounds that were tested and gave two potential hits: **GK01161** and **HTS12517**. No SAR was carried out on the two hits due to time limitations.

Chapter 6: Conclusion and future work

Allosteric modulators represent a significant potential for pharmaceutical companies to design new treatments for disease. No method currently exists to rationally define allosteric sites. Through the work of Al-Shar'i, a potential allosteric site was define for DYRK2. His method was unreported and experimental proof was sought to reinforce his findings.

The pocket was explored by generating a pharmacophore that was applied to a virtual screen. A hit compound, **C10**, was found which showed good stabilization of DYRK2 over DYRK1A in a DSF assay (T_m = 1.2 °C) as well as an IC_{50} = 3.22 µM in a Lanthascreen assay. This was the starting point for our SAR study.

With a range of compounds synthesized and evaluated, five compounds showed an increase in stabilization through the DSF assay as well as selectivity for DYRK2 over DYRK1A, **Figure 158**.

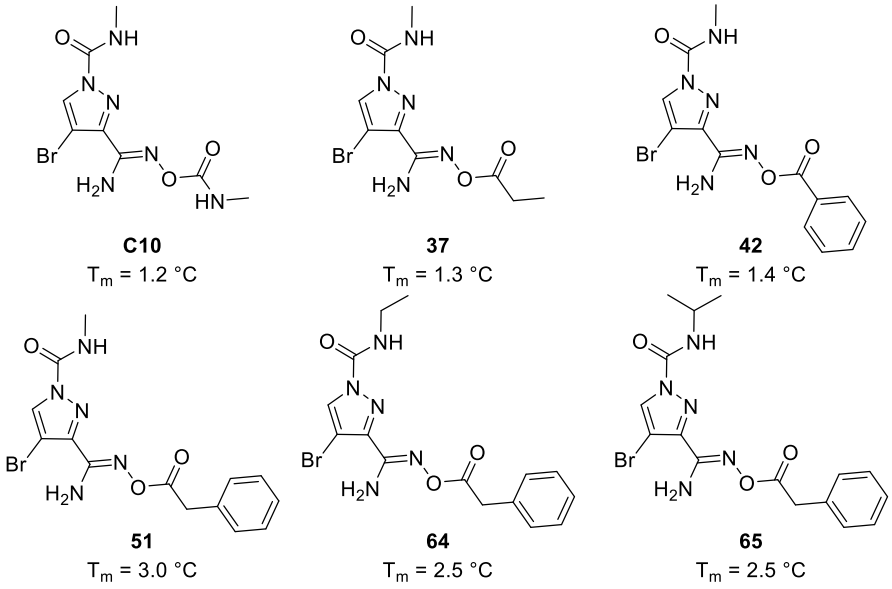

Figure 158: Oxyamidine analogues showing good stabilization.

From this study, it was observed that the NH of the urea functionality was important for stabilization. In addition, the carbamate NH was not necessary as analogues **37** and **42** showed a similar stabilization of DYRK2 to **C10**. Benzoyl analogues **51**, **64** and **65** each showed an important increase in stabilization. However, when **51** was screened

at a single point concentration in the Lanthascreen assay it was observed that it had a similar binding activity to initial hit **C10** (23% and 19% inhibition respectively).

All of these oxyamidine analogues involved a time consuming synthesis. For this reason we changed our focus into forming amide derivatives that were accessible in only four steps. The amide derivative **84** showed great potential (T_m = 1.9 °C) as a starting scaffold from which a SAR study was carried out, **Figure 159**.

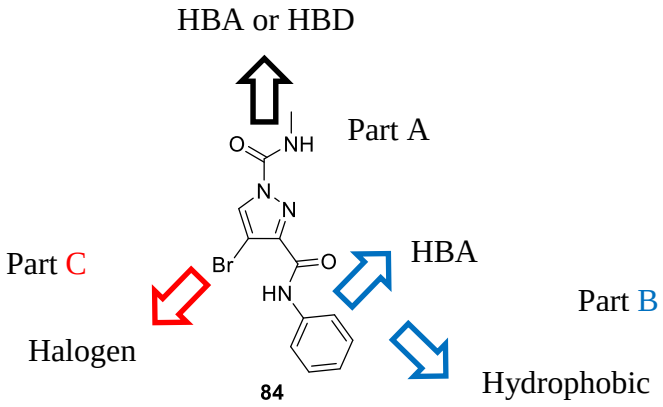

Figure 159: SAR study around analogue 84.

It was observed that an HBD or HBA was important in Part A either as a urea functionality or as a free pyrazole for activity. A halogen (bromine or chlorine) was necessary in order to increase activity in Part C of the molecule. Finally, the SAR of Part B revealed that an HBA in position 2 of an aromatic amide increased activity. Moreover, when a bicyclic core, such as benzimidazole, was present it led to our most active series of compounds.

During, this study, we were able to synthesize 10 analogues that showed good to excellent binding activity ($IC_{50} \leq 2.5$ µM), **Figure 160**. The initial hit for this scaffold was amide **84**, giving a binding activity of 15.5 µM. A 10 fold increase in activity was observed when a nitrophenol amide was present (**123**, IC_{50} = 1.45 µM). The presence of the nitro group was revealed to be of great importance for activity by lowering the pKa of the phenol and rendering it more like a phenoxide type analogue. Moreover, in the same series it was observed that the presence of a halogen in Part C of the molecule, was necessary for activity as unsubstituted analogue **167** showed an IC_{50} = 2.50 µM. When a chlorine was present, a small increase in activity was observed (IC_{50} = 1.11 µM) relative to **123**. Finally, in this series it was observed that the urea

functionality (**168**) was not deemed necessary as it displayed similar activity to **123** with an IC_{50} = 1.11 µM.

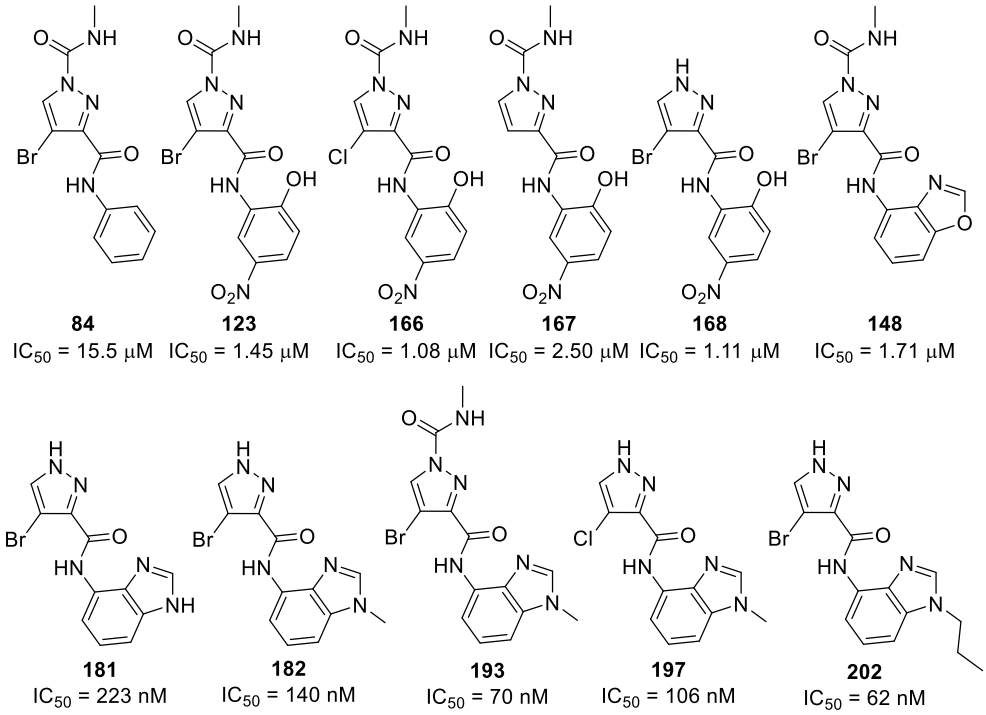

Figure 160: Active analogues with dose-response curves.

When a bicyclic core was introduced with a HBA still present in position 2 of the amide, analogue **148** (IC_{50} = 1.71 µM) revealed a similar activity to **123**. By changing the benzoxazole ring to a benzimidazole ring with **181** (IC_{50} = 223 nM) and **182** (IC_{50} = 140 nM) a 10 fold increase was observed. Finally, by extending the hydrophobic tail further with **202** (IC_{50} = 62 nM), we were able to prepare the most active compound in our set.

Analogue **202** was taken forward to determine its mode of inhibition by varying the concentration of ATP. The results revealed that **202** was a competitive inhibitor against DYRK2. Even though it was not the results anticipated for, **202** still showed high selectivity between the two DYRK isoforms. A kinase selectivity profile was carried out to determine potential off-targets by screening **202** at 1 µM against a panel of 40 kinases. Biological results revealed high selectivity over the kinases with only slight activity observed for CLK4 (32% inhibition) and Haspin (24% inhibition). Finally, co-crystallization of analogues **181** and **202** with DYRK2 revealed their binding pose

in the ATP pocket. These compounds will be submitted for cell-based studies to ensure that they are able to engage with DYRK2 in a cellular environment

A number of potential avenues of research exist for improving lead compound **202**. For example, preparation of the chlorine derivative **238** (**Figure 161**) would be sensible, as we have observed that having a chlorine atom on the pyrazole ring renders the molecule slightly more active. From the pictures provided of the docked pose it was not yet clear which interactions are made between **202** and the protein. This will become clearer as the crystal structure is refined. Nevertheless, a possible interaction that could be examined is between the end of the alkyl chain and a carbonyl functionality at the backbone level. This would involve adding a HBD at the end of the alkyl chain: an amine **241** or hydroxyl group **243** could be of interest as well as varying the length of this alkyl chain with these two groups **242** and **244**. Finally, a phenylalanine residue is pointing in the direction of the alkyl chain. Possible interactions between an alkene (**239**) or an alkyne (**240**) with this amino acid side-chain could help gain activity.

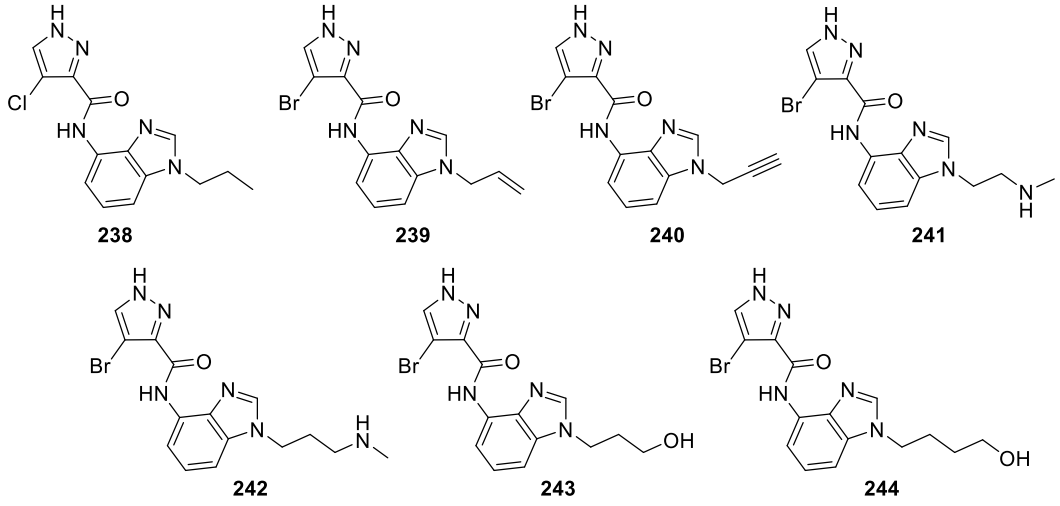

Figure 161: Potential analogues to further explore the orthosteric pocket.

A second allosteric pocket was proposed when the new predictive model by Vassileiou was used on DYRK2. This pocket was analysed through VS as well as docking of the HF library provided and led to two potential hits, **Figure 153**. A biochemical binding

assay should be carried on each of these scaffold to establish whether thermal melting data can be translated into actual binding affinity before an SAR is initiated.

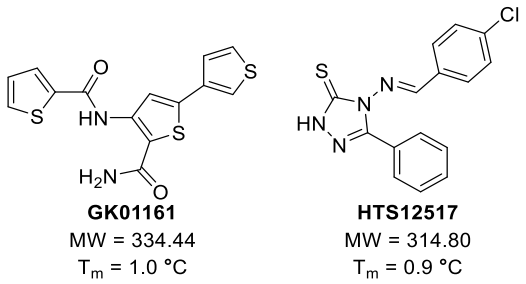

<u>Figure 162:</u> Two possible hits revealed by second protocol.

Another possibility would be to start from scratch and design a chemical probe for the pocket by analysing the amino acid residue present. One would need to determine the key interactions to be made in order for the probe to bind to this allosteric pocket.

Experimental

^{1}H, ^{13}C, NOESY NMR spectroscopy were carried out on a Bruker DPX-400 (or other NMR instruments such as DPX-500 and DPX-600) spectrometer at 20 °C unless otherwise stated with chemical shifts given in ppm (δ values), relative to the residual proton resonances in deuterated solvents for ^{1}H NMR and ^{13}C NMR. The ^{1}H NMR signals are reported by: m (multiplet), t (triplet), d (doublet), s (singlet), br (broad) and are recorded in Hz.

Chromatography was carried out using 200-400 mesh silica gel with eluent as stated.

Dry solvents were obtained by standard operating procedure for Innovative Technology Solvent Purification System. Anhydrous MeCN was obtained by drying it over 3 Å molecular sieves previously dried under vaccum at 150 °C.

All glassware, used in anhydrous reactions, was previously dried at 100 °C for 4 hours or more, left to cool under reduced pressure and then flushed with nitrogen prior to use. If flasks were not in oven they were dried under *vacuo* by flame drying them and then left to cool under inert atmosphere.

IR spectra were carried out on a SHIMADZU IRAFFINITY-1 spectrophotometer with a Perkin Elmer Universal ATR (attenuated total reflectance). Absorption frequncencies are reported in wavenumbers (cm^{-1}).

Melting points were masured on a Stuart automatic melting points apparatus, SMP40.

Microwave irradiation reactions were carried out in a Biotage initiator.

LC/MS analyses were carried out on Agilent technologies 1200 series with a 6130 quadrupole. The method used a 5−95% MeCN/Water ammonium acetate gradient. HPLC (Semiprep) analyses were carried out on Agilent technologies 1200 infinity series with a 6120 quadrupole. The method used a 5−95% MeCN/Water formic acid gradient. LRMS analyses were carried out on a Finnigan LC QDuo with methanol as the solvent. GC/MS analyses was done on an Agilent Technologies 7890A with chloroform as the solvent. HRMS were obtained courtesy of the EPSRC Mass Spectrometry Service at the University of Swansea. When bromine was present in a

molecule the mass has been reported as the ^{79}Br isotope, the bromine isotope pattern (^{79}Br and ^{81}Br) was observed in each case. Same applied to chlorine with ^{35}Cl.

Unfortunately not all analogues have complete analysis due to lack of sample (low mass recovery, used most for testing etc…)

I. General procedures

General procedure A for the synthesis of carbamate analogues 21, 22:

Oxyamidine **9** (1.0 equiv.) was dissolved in anhydrous THF (1.5 mL) in a microwave vial. The required isocyanate (3.0 equiv.) was then added and the reaction was stirred at room temperature for 24 h. The solvent was evaporated and the crude was purified either by column chromatography or by trituration.

General procedure B for the synthesis of carbonate, alkyl and aryl analogues 23–33:

In a dry flask, oxyamidine **9** (1.0 equiv.) was dissolved in anhydrous CH_2Cl_2 or anhydrous THF (3 mL). The solution was cooled to 0 °C before addition of Et_3N (2.4 equiv.) followed by an acyl chloride or chloroformate (2.4 equiv.). The reaction was left to stir for 2.5–4 h at room temperature. CH_2Cl_2 (5 mL) was added and the organic layer was washed with 1 M NaOH for acyl chloride (5 mL) or with 10% $NaHCO_3$ solution (5 mL) followed by H_2O (2 × 5 mL). The organic layer was dried over $MgSO_4$, filtered and concentrated *in vacuo*. The crude reaction mixture was purified by column chromatography.

General procedure C for the synthesis of analogues 38–40, 47−50:

In a microwave vial, oxyamidine **9** (1.0 equiv.) was added along with the carboxylic acid (1.0 equiv.) and PyBOP (1.0 equiv.). The vial was sealed and the reagents dissolved in anhydrous MeCN (1.5 mL). Hünig's base (0.17 mL, 0.96 mmol, 4.0 equiv.) was then added and the reaction left to stir at room temperature for 17 h.[111]

a. After this time, **12** (2.0 equiv.) and Et_3N (2.0 equiv.) were added. The reaction was stirred at 70 °C for 48 h.

b. After this time, **12** (4.0 equiv.) and Et_3N (4.0 equiv.) were added. The reaction was stirred at room temperature for 24 h.

To the reaction mixture EtOAc (15 mL) was added and the organic layer was washed with 1 M HCl (2 × 5 mL), H_2O (5 mL) and brine (5 mL). The organics were dried under $MgSO_4$, filtered and concentrated *in vacuo* to afford the crude product. It was then purified by column chromatography.

General procedure D for the synthesis of intermediates 42−45:[111]

In a microwave vial, oxyamidine **34** (1.0 equiv.) was dissolved in anhydrous CH_2Cl_2 (3 mL). The carboxylic acid (1.0 equiv.) was added followed by PyBOP (1.0 equiv.) and finally Hünig's base (4.0 equiv.). The reaction was left to stir at room temperature for 24 h. The solvent was evaporated *in vacuo* and the product dissolved in EtOAc (20 mL). The organic layer was washed with 1 M HCl (3 × 5 mL) and brine (10 mL). The organic layer was dried over $MgSO_4$, filtered and concentrated. The crude material was purified by flash chromatography.

General procedure E for the synthesis of analogues 75−93, 95−102, 105−111, 116−127, 134−136, 148−151, 154, 155, 158, 161, 164, 166−170, 173−175, 181, 182, 197, 202:

Carboxylic acid **6** (1.0 equiv.) was added to a vial followed by the addition of HATU (1.0 equiv.) and sealed. The reagents were dissolved in anhydrous MeCN (1.5 mL) and Hünig's base (2.0 equiv.) was added and left to stir for 5 minutes. The amine (1.0 equiv.) was then added and the reaction left to stir at room temperature for 17–24 h.

a. After this time, **12** (2.0 equiv.) and Et_3N (2.0 equiv.) were added. The reaction was stirred at 70 °C for 20 h.

b. After this time, **12** (4.0 equiv.) and Et_3N (4.0 equiv.) were added. The reaction was stirred at 70 °C for 20 h.

c. After this time, **12** (4.0 equiv.) and Et_3N (4.0 equiv.) were added. The reaction was stirred at room temperature for 20 h.

d. After this time, the desired isocyanate (1.2 equiv.) and Et_3N (1.2 equiv.) were added. The reaction was stirred at room temperature for 20 h.

e. After this time, the desired isocyanate (2.0 or 3.0 equiv.) and Et_3N (2.0 or 3.0 equiv.) were added. The reaction was stirred at room temperature for 20 h.

f. No acylation reagent was added and the reaction was worked up.

The mixture was left to cool to rt before adding EtOAc (15 mL). The organic layer was washed with H_2O (2 × 5 mL) and brine (5 mL). The organics were dried under $MgSO_4$, filtered and concentrated *in vacuo* to afford the crude product which was then purified by column chromatography.

General procedure F for the synthesis of derivatives 12, 60 and 61:

In a dry flask, under nitrogen, carbonyldiimidazole **13** (1.1 equiv.) and amine hydrochloride (1.0 equiv.) were dissolved in anhydrous DMF (1 mL) and anhydrous MeCN (3 ml). The reaction was stirred for 2.5 hours whereupon a stream of air was used to evaporate the solvent. The crude reaction was then purified by column chromatography.

General procedure G for the synthesis of analogues 41, 52−55:

In a microwave vial, oxyamidine **9** (1.0 equiv.) was dissolved in anhydrous MeCN (1.5 mL). The desired acyl chloride (0.8 equiv.) was added as well as Et_3N (0.8 equiv.). The reaction was left to stir for 1 h at room temperature before the addition of **12** (4.0 equiv.) and Et_3N (4.0 equiv.) and further stirred for 24 h at rt. To the mixture was added EtOAc (15 mL). The organic layer was washed with H_2O (2 × 5 mL) and brine (5 mL). The organics were dried under $MgSO_4$, filtered and concentrated *in vacuo* to afford the crude product which was then purified by column chromatography.

General procedure H for benzimidazole and benzoxazole 140−142, 177:[85]

In a microwave vial, to the desired nitro compound (1.0 equiv.), in toluene (2 mL) was added triethylorthoformate (3.0 equiv.) with a catalytic amount of *p*-toluenesulfonic acid monohydrate (5 mol%). The reaction mixture was heated in the microwave at 120 °C for 10 minutes followed by cooling to -10 °C in a salt ice bath. The precipitate

was filtered and dried under vacuum to give the desired compound that was used without further purification.

General procedure I for alkylation 184, 185, 200:

In a microwave vial, desired ester (1.0 equiv.) and K_2CO_3 (2.0 equiv.) were added before closing the vial. Anhydrous DMF (15 mL) was added followed by the alkylating reagent (1.5 equiv.). The reaction was left to stir overnight for 19 h. H_2O (30 mL) was added and the product was extracted with EtOAc (3 × 20 mL). The organic layer was washed with H_2O (6 × 20 mL), dried over $MgSO_4$, filtered and concentrated. The crude reaction mixture was purified by flash chromatography.

General procedure J for amide coupling 188−190, 196, 199:

In a microwave vial, desired acid (1.0 equiv.) and HATU (1.0 equiv.) were added followed by EtOAc (2 mL). Hünig's base (2.0 equiv.) was then added and the reaction stirred for 5 minutes before the addition of the desired amine. The reaction was stirred for 20 h at room temperature. The mixture was allowed to cool to rt before adding EtOAc (15 mL). The organic layer was washed with H_2O (2 × 5 mL) and brine (5 mL). The organics were dried under $MgSO_4$, filtered and concentrated to afford the crude product. It was then purified by column chromatography.

General procedure K hydrolysis of esters 186a, 186b, 187a, 187b, 195:

In a microwave vial, ester (1.0 equiv.) was dissolved in THF (3 mL) and H_2O (1.5 mL) and $LiOH{\cdot}H_2O$ (2.0 equiv.) was added. The reaction was stirred at room temperature for 20 h. The solvent was evaporated and H_2O (5 mL) was added to the residue which was acidified with 1 M HCl until pH = 2. The product was extracted with EtOAc (3 × 10 mL) and the organic layer washed with H_2O (5 mL). The organic layer was dried over $MgSO_4$, filtered and concentrated to give the desired acids that were used with no further purification.

General procedure L reduction of nitro compounds133, 172, 178, 180, 192, 201:

In a dry 3 neck flask under N_2, 10% activated Pd/C (10% mmol) was added followed by anhydrous MeOH or EtOH. The system was flushed three times (vacuum followed

by N_2) before addition of the desired nitro compound (1.0 equiv.). The system was again flushed three times (vacuum followed by N_2). A hydrogen balloon was added and the system was flushed three times again (vaccum followed by H_2). The reaction was left to stir between 1.5−5 h at room temperature. The solution was filtered through celite and washed with MeOH or EtOH and the solvent evaporated *in vacuo* to give the desired amine.

II. Oxyamidine hit series

1. C10 hit

1*H*-pyrazole-3-carboxylic acid 5:

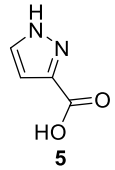

5

In a round bottom flask, $KMnO_4$ (19.1 g, 118.2 mmol, 2.0 equiv.) was dissolved in H_2O (250 mL) and stirred. In a separate round bottom flask, pyrazole **4** (4.9 mL, 59.1 mmol, 1.0 equiv.) was dissolved in H_2O (100 mL). The $KMnO_4$ solution was transferred to the pyrazole solution. As some residual $KMnO_4$ solid was left in the flask, the reaction mixture was transferred back to the $KMnO_4$ flask. The solution was heated to 100 ° C and stirred for 67 hours. The reaction mixture was cooled down and the black residue MnO_2 was filtered off. The water was evaporated till only 10 mL remained. The flask was put into ice and 1 M HCl was added until pH = 2 and a white precipitate formed. The product was filtered off to afford **5** as a white powder (2.96 g, 26.2 mmol, 51%). **IR (ATR)/cm^{-1}**: 3350, 1701; **^{1}H NMR** (400 MHz, DMSO-d_6): **δ** 13.04 (br s, 2H), 7.74 (d, 1H, *J* = 1.6 Hz), 6.71 (d, 1H, *J* = 1.6 Hz); **^{13}C NMR** (101 MHz, DMSO-d_6): **δ** 162.6, 140.7, 133.0, 107.8; **LRMS (ES-APCI)**: *m/z* = 111.1 $[M-H]^-$; **M.P.**: 210 °C (212 °C in lit)[112]

4-Bromo-1*H*-pyrazole-3-carboxylic acid 6:

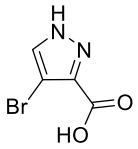

6

To a round bottom flask, pyrazole carboxylic acid **5** (4.34 g, 38.67 mmol, 1.0 equiv.) was dissolved in acetic acid (110 mL). Bromine (6.83 g, 42.54 mmol, 1.1 equiv.) in acetic acid (30 mL) was added drop-wise to the solution. The reaction mixture was left to stir at room temperature for 16 hours. H_2O (300 mL) was added and the product was extracted with diethyl ether (4 × 100 mL). The organic phase was washed with H_2O (100 mL), dried over $MgSO_4$, filtered and concentrated to afford a white/orange solid **6** (4.48 g, 23.46 mmol, 61%). **IR (ATR)/cm^{-1}:** 3320, 1691; **^{1}H NMR** (400 MHz, DMSO-d_6): **δ** 12.91 (br s, 2H), 7.92 (s, 1H); **^{13}C NMR** (101 MHz, DMSO-d_6): **δ** 161.0, 136.3, 136.2, 95.6; **LRMS (ES-APCI)**: *m/z* = 188.9 $[M-H]^-$; **HRMS**: found *m/z* = 190.9451, calculated for $C_4H_4Br_1N_2O_2$ *m/z* = 190.9451; **M.P.**: 238–240 °C (decomp) (240 °C decomp in lit)[113]

4-Bromo-1*H*-pyrazole-3-carboxamide 7:

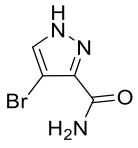

7

To a round bottom flask, pyrazole carboxylic acid **6** (4.53 g, 23.72 mmol, 1.0 equiv.) was added and cooled to 0 °C. Thionyl chloride (47 mL, 0.64 mmol, 0.4 M) was added drop-wise. The reaction was stirred for 3 hours at 90 °C. When cooled to rt the solvent was evaporated *in vacuo*. It was then treated with ammonia in THF at 0.4 M (286 mL, 114 mmol, 6.0 equiv.) and left to stir for 23 hours. The solvent was evaporated and afforded primary amide **7** as a beige solid (3.80 g, 20 mmol, 84%). It was used as is without further purification. **IR (ATR)/cm^{-1}**: 1650, 1580; **^{1}H NMR** (400 MHz, DMSO-d_6): **δ** 10.82 (br s, 1H), 7.99 (s, 1H), 7.45 (br s, 1H), 7.32 (br s, 1H); **^{13}C NMR** (101 MHz, DMSO-d_6): **δ** 167.2, 141.1, 132.9, 92.6;

LRMS (ES-APCI): *m/z* = 188.9 $[M]^-$; **HRMS**: found *m/z* = 189.9610, calculated for $C_4H_5BrN_3O_1$ *m/z* = 189.9611

4-Bromo-1*H*-pyrazole-3-carbonitrile 8:

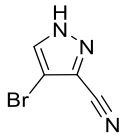

8

In a dry multineck flask under nitrogen, **7** (1.40 g, 7.13 mmol, 1 equiv.) was added and dissolved in anhydrous MeCN (12.5 mL). The solution was heated up to 80 °C before addition of NaCl (10.42 g, 178.3 mmol, 25 equiv.) and left to stir for 0.25 h. $POCl_3$ (0.4 mL, 4.28 mmol, 0.6 equiv.) was added and the reaction was stirred for 19 hours at 80 °C. The solution was left to cool down before filtration to remove the salt and washed with CH_2Cl_2. The filtrate was concentrated to afford a brown solid which was purified by column chromatography with 70:30 PE:acetone eluent. This gave nitrile **8** as a light brown solid (0.90 g, 5.23 mmol, 74%). **IR (ATR)/cm^{-1}:** 2254; **^{1}H NMR** (400 MHz, DMSO-d_6): **δ** 14.33 (br s, 1H), 8.34 (s, 1H); **^{13}C NMR** (101 MHz in DMSO-d_6): **δ** 131.7, 124.9, 112.9, 97.7; **LRMS (ES-APCI)**: *m/z* = 169.9 $[M-H]^-$; **M.P.**: 135 °C

(Z)-4-Bromo-*N*'-hydroxy-1*H*-pyrazole-3-carboximidamide 9:

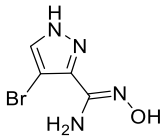

9

In a round bottom flask, nitrile **8** (0.20 g, 1.16 mmol, 1.0 equiv.) was dissolved while stirring in H_2O (2 mL). Hydroxylamine hydrochloride (0.16 g, 2.33 mmol, 2.0 equiv.) was then added followed by a solution of Na_2CO_3 (0.25 g, 2.33 mmol, 2.0 equiv.) in H_2O (1 mL). The reaction was heated and stirred for 22 hours at 70 °C. The solution was left to cool to rt and a saturated solution of brine (3 mL) was added. The product was extracted with EtOAc (3 × 5 mL). The recovered organic phase was dried over $MgSO_4$, filtered and concentrated to afford oxyamidine **9** as a pale orange solid (0.19 g, 0.93 mmol, 80%) without any further purification. **IR (ATR)/cm^{-1}:** 3460,

3340, 2968, 1651; **^{1}H NMR** (5:1 rotamers, minor rotamer*, 400 MHz, DMSO-d_6): **δ** 13.41* (br s, 1H), 13.34 (br s, 1H), 9.93* (s, 1H), 9.75 (s, 1H), 8.00 (s, 1H), 7.57* (s, 1H), 5.79* (br s, 2H), 5.50 (br s, 2H); **^{13}C NMR** (101 MHz, DMSO-d_6): **δ** 146.1, 141.8, 131.2, 89.9; **LRMS (ES-APCI)**: *m/z* = 205.1 $[M+H]^+$; **HRMS**: found *m/z* = 204.9719, calculated for $C_4H_6Br_1N_4O_1$ *m/z* = 204.9719; **M.P.**: 169 °C (decomp)

<u>*N*-Methyl-1*H*-imidazole-1-carboxamide 12:</u>[64]

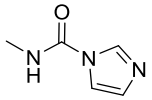

12

General procedure F was followed with CDI **13** (2.0 g, 12.0 mmol, 1.1 equiv.), methylamine hydrochloride (0.74 g, 10.9 mmol, 1.0 equiv.) in MeCN (6 mL) and DMF (2 mL). The crude reaction was purified by column chromatography with 95:5 CH_2Cl_2:MeOH eluent system to afford **12** as a white solid (1.32 g, 10.5 mmol, 88%). **IR (ATR)/cm^{-1}**: 3196, 2980, 1712; **^{1}H NMR** (400 MHz, $CDCl_3$): **δ** 8.21 (d, 1H, *J* = 1.2 Hz), 7.60 (br s, 1H), 7.48 (app t, 1H, *J* = 1.2 Hz), 7.03 (m, 1H), 3.00 (d, 3H, *J* = 4.8 Hz); **^{13}C NMR** (101 MHz, $CDCl_3$): **δ** 149.9, 136.0, 129.9, 116.7, 27.6; **M.P.**: 108 °C (109–111 °C in lit)[64]

<u>(*Z*)-4-Bromo-*N*-methyl-3-(*N*'-((methylcarbamoyl)oxy)carbamimidoyl)-1*H*-pyrazole-1-carboxamide C10:</u>

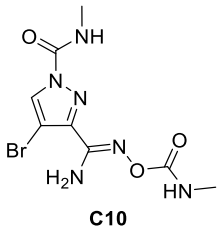

C10

In a dry two neck flask, oxyamidine **9** (175 mg, 0.85 mmol, 1.0 equiv.) was dissolved in anhydrous MeCN (6 mL). The isocyanate derivative **12** (214 mg, 1.71 mmol, 2.0 equiv.) was then added, followed by Et_3N (0.26 mL, 1.87 mmol, 2.2 equiv.). The reaction was stirred at 80 °C for 18 hours. The reaction was left to cool down before removal of the solvent *in vacuo*. The crude was purified by column chromatography with a 92:8 CH_2Cl_2:MeOH eluent. **C10** was isolated as a white solid (86 mg,

0.27 mmol, 32%). **IR (ATR)/cm^{-1}**: 3273, 2980, 1724; **^{1}H NMR** (400 MHz, DMSO-d_6): **δ** 8.64 (br s, 1H), 8.58 (s, 1H), 6.86 (br s, 3H), 2.84 (d, 3H, *J* = 4.8 Hz), 2.73 (d, 3H, *J* = 4.4 Hz); **^{13}C NMR** (101 MHz, $CDCl_3$): **δ** 155.7, 148.5, 147.6, 142.6, 130.8, 95.0, 27.4, 26.7; **LRMS (ES-APCI)**: *m/z* = 341.0 $[M+Na]^+$; **HRMS**: found *m/z* = 340.9970, calculated for $C_8H_{11}O_3N_6Br_1Na_1$ *m/z* = 340.9968; **M.P.**: 167 °C (decomp)

2. **Exploration Part C**

(*Z*)-*N*'-hydroxy-1*H*-pyrazole-3-carboximidamide 16:

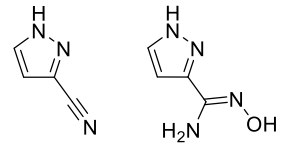

14 **16**

In a dry 2 necked round bottom flask under nitrogen, nitrile **8** (230 mg, 1.34 mmol, 1.0 equiv.) was dissolved in anhydrous THF (3 mL). The solution was cooled to -78 °C whereupon *n*-BuLi (1.7 mL, 2.94 mmol, 2.2 equiv.) at 2.5 M was added drop-wise. The reaction was left to stir for 3 hours at -78 °C. After that time, 2:3 MeOH: THF solution (10 mL) was added and the reaction was left to warm up to room temperature for 0.5 h before the solvent was removed *in vacuo*.[114] Product **14** was isolated as a brown/yellow solid and used as is in the next step. **^{1}H NMR** (400 MHz, DMSO-d_6): **δ** 8.01 (d, 1H, *J* = 2.4 Hz), 6.95 (d, 1H, *J* = 2.4 Hz); **^{13}C NMR** (101 MHz, DMSO-d_6): **δ** 131.1, 123.0, 115.2, 110.4.

In a round bottom flask, nitrile **14** (124 mg, 1.34 mmol, 1.0 equiv.) was dissolved in H_2O (10 mL) and stirred. Hydroxylamine hydrochloride (188 mg, 2.68 mmol, 2.0 equiv.) was then added followed by Na_2CO_3 (284 mg, 2.68 mmol, 2.0 equiv.). The reaction was heated and stirred for 24 hours at 70 °C. The solution was left to cool to rt and a saturated solution of brine (10 mL) was added. The product was extracted with EtOAc (3 × 10 mL). The recovered organic phase was dried over $MgSO_4$, filtered and concentrated to afford oxyamidine **16** as a light orange solid (130 mg, 1.03 mmol, 75%) and used without any further purification. **^{1}H NMR** (400 MHz, DMSO-d_6): **δ** 12,90 (br s, 1H), 9.45 (br s, 1H), 7.71 (br s, 1H), 6.40 (br s, 1H), 5.43, (br s, 2H);

^{13}C NMR (101 MHz, DMSO-d_6): **δ** 156.0, 130.0, 111.2, 106.7, **LRMS (ES-APCI)**: m/z = 127.1 $[M+H]^+$

(Z)-*N*-methyl-3-(*N'*-((methylcarbamoyl)oxy)carbamimidoyl)-1*H*-pyrazole-1-carboxamide 17:

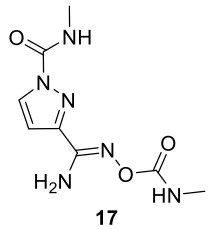

17

In a microwave vial oxyamidine **16** (122 mg, 0.97 mmol, 1.0 equiv.) and compound **12** (243 mg, 1.94 mmol, 2.0 equiv.) were added and the vial sealed. The solids were dissolved in anhydrous MeCN (1 mL) and Et_3N (0.3 mL, 2.13 mmol, 2.2 equiv.) was added. The reaction was stirred for 17 h at 70 °C. It was left to cool to rt before addition of CH_2Cl_2 (5 mL) and was washed with brine (5 mL). The organic phase was dried with $MgSO_4$, filtered and concentrated *in vacuo*. The crude product was purified by two column chromatographies (60:40 PE:acetone) and a recrystallization by vapour diffusion in MeOH and PE to afford derivative **17** as a white solid (60 mg, 0.25 mmol, 26%). **IR (ATR)/cm^{-1}**: 3469, 3369, 3269, 3124, 1699, 1656; **^{1}H NMR** (400 MHz, DMSO-d_6): **δ** 8.51 (br d, 1H, J = 4.8 Hz), 8.31 (d, 1H, J = 2.4 Hz), 7.33 (br d, 1H, J = 4.8 Hz), 6.88 (d, 1H, J = 2.4 Hz), 6.69 (br s, 1H), 2.85 (d, 3H, J = 4.4 Hz), 2.70 (d, 3H, J = 4.4 Hz); **^{13}C NMR** (101 MHz, DMSO-d_6): **δ** 155.8, 149.4, 147.8, 145.5, 129.9, 106.3, 27.3, 26.6; **M.P.**: 196 °C

4-phenyl-1*H*-pyrazole-3-carbonitrile 15:

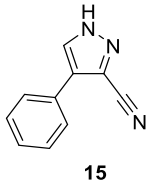

15

In a microwave vial, nitrile **8** (300 mg, 1.16 mmol, 1.0 equiv.), phenylboronic acid **18** (215 mg, 1.74 mmol, 1.5 equiv), Pd(dppf)Cl_2 (88 mg, 0.12 mmol, 10 mol%) and Na_2CO_3 (246 mg, 2.32 mmol, 2.2 equiv.) were added and the vial sealed. It was placed

under vacuum and then under a nitrogen flow before adding the solvent 2:1 dioxane:H_2O (12 mL). The reaction was stirred for 23 h at 120 °C. Left to cool to rt before adding EtOAc (20 mL) and washed with sat aq. $NaHCO_3$ solution (10 mL). The product was extracted with EtOAc (2 × 10 mL) and the organic phase was washed with brine (10 mL), dried over $MgSO_4$, filtered and concentrated *in vacuo*. The crude material was purified by column chromatography 70:30 PE:acetone to obtain **15** as a white solid (100 mg, 0.59 mmol, 51%). **^{1}H NMR** (400 MHz, DMSO-*d*$_6$): **δ** 14.11 (br s, 1H), 8.46 (s, 1H), 7.69–7.67 (m, 2H), 7.50–7.47 (m, 2H), 7.37 (tt, 1H, *J* = 1.2, 7.6 Hz); **^{13}C NMR** (101 MHz, CDCl3): **δ** 129.4, 129;3, 128.7, 127.8, 127.6, 127.1, 114.3; **LRMS (ES-APCI)**: *m/z* = 168.1 $[M-H]^-$; **M.P.**: 136-138 °C

<u>*N*-methyl-3-(*N'*-((methylcarbamoyl)oxy)carbamimidoyl)-4-phenyl-1*H*-pyrazole-1-carboxamide 20:</u>

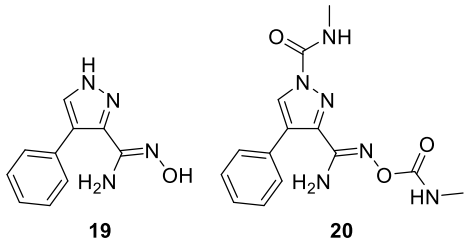

In a round bottom flask, nitrile **15** (100 mg, 0.59 mmol, 1.0 equiv.) was dissolved in H_2O (3mL). Hydroxyl amine hydrochloride (83 mg, 1.18 mmol, 2.0 equiv.) and Na_2CO_3 (125 mg, 1.18 mmol, 2.0 equiv.) were then added and the reaction left to stir at 70 °C for 19 h. The reaction was left to cool to rt and product extracted with EtOAc (3 × 10 mL). The organic layer was dried with $MgSO_4$, filtered and concentrated *in vacuo* to afford **19** (90 mg, 0.45 mmol, 76%) which was used without further purification. TLC revealed no trace of starting material.

In a microwave vial oxyamidine **19** (75 mg, 0.37 mmol, 1.0 equiv.) and compound **12** (93 mg, 0.74 mmol, 2.0 equiv.) were added and the vial sealed. The solids were dissolved in anhydrous MeCN (1 mL) and Et_3N (0.11 mL, 0.82 mmol, 2.2 equiv.) was added. The reaction was stirred for 17 h at 70 °C. The solvent was evaporated *in vacuo.* The crude product was purified by column chromatography with a 50:50 PE:acetone eluent followed by trituration with EtOAc and hexane to afford the hit derivative **20** as a white solid (30 mg, 0.10 mmol, 27%). X-ray structure obtained by vapour

diffusion in MeOH and PE. **IR (ATR)/cm^{-1}**: 3415, 3300, 1705, 1511; **^{1}H NMR** (400 MHz, $CDCl_3$): **δ** 8.26 (s, 1H), 7.42 (br s, 5H), 7.05 (br d, 1H, *J* = 3.6 Hz), 5.6 (br s, 1H), 5.44 (br s, 2H), 3.09 (d, 3H, *J* = 4.8 Hz), 2.65 (d, 3H, *J* = 4.8 Hz); **^{13}C NMR** (101 MHz, $CDCl_3$): **δ** 156.3, 149.6, 147.1, 142.6, 132.0, 129.9, 129.4, 128.2, 128.0, 124.3, 29.9, 27.3; **M.P.**: 190 °C

3. **Exploration Part A + B simultaneously**

a. **Carbamate**

(*Z*)-4-bromo-*N*-ethyl-3-(*N'*-((ethylcarbamoyl)oxy)carbamimidoyl)-1*H*-pyrazole-1-carboxamide 21:

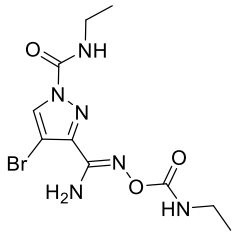

21

General procedure A was followed with oxyamidine **9** (50 mg, 0.24 mmol, 1.0 equiv.), ethylisocyanate (58 µL, 0.73 mmol, 3.0 equiv.) in THF (1.5 mL). The crude was triturated with EtOAc and PE to afford compound **21** as a white solid (34 mg, 0.1 mmol, 42%). **IR (ATR)/cm^{-1}**: 3153, 2972, 1691; **^{1}H NMR** (400 MHz, $CDCl_3$): **δ** 8.32 (s, 1H), 7.03 (br s, 1H), 6.76 (br s, 1H), 5.53 (br s, 2H), 3.50 (dq, 2H, J = 7.2, 6 Hz), 3.37 (dq, 2H, *J* = 7.2, 5.6 Hz), 1.30 (t, 3H, *J* = 7.6 Hz), 1.24 (t, 3H, *J* = 7.2 Hz); **^{13}C NMR** (101 MHz, $CDCl_3$): **δ** 155.7, 148.0, 146.7, 142.5, 131.9, 95.5, 36.4, 36.0, 15.3, 15.1; **LRMS (ES-APCI)**: *m/z* = 369.0 $[M+Na]^+$; **HRMS**: found *m/z* = 347.0468, calculated for $C_{10}H_{16}Br_1N_6O_3$ *m/z* = 347.0462; **M.P.**: 160 °C

(*Z*)-4-bromo-*N*-isopropyl-3-(*N'*-((isopropylcarbamoyl)oxy)carbamimidoyl)-1*H*-pyrazole-1-carboxamide 22:

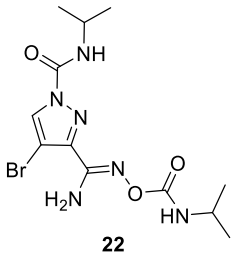

22

General procedure A was followed with oxyamidine **9** (50 mg, 0.24 mmol, 1.0 equiv.) and isopropylisocyanate (72 µL, 0.73 mmol, 3.0 equiv.) in THF (1.5 mL). The crude product was purified by column chromatography (90:10 PE:acetone) to afford compound **22** as a white solid (60 mg, 0.16 mmol, 67%). **IR (ATR)/cm^{-1}**: 3356, 2970, 1716, 1656; **^{1}H NMR** (400 MHz, $CDCl_3$): **δ** 8.31 (s, 1H), 6.84 (br d, 1H, *J* = 7.6 Hz), 6.70 (br d, 1H, *J* = 7.2 Hz), 5.56 (br s, 2H), 4.12 (dq, 1H, *J* = 8, 6.8 Hz), 3.93 (dq, 1H, *J* = 7.6, 6.8 Hz), 1.31 (d, 6H, *J* = 6.8 Hz), 1.24 (d, 6H, *J* = 6.8 Hz); **^{13}C NMR** (101 MHz, $CDCl_3$): **δ** 154.9, 147.2, 146.4, 142.3, 133.8, 95.3, 43.6, 43.5, 23.1, 22.8; **LRMS** (**ES-APCI)**: *m/z* = 375.0 $[M+H]^+$; **HRMS**: found *m/z* = 377.0774, calculated for $C_{12}H_{20}Br_1N_6O_3$ *m/z* = 377.0774; **M.P.**: 129–130 °C

(*Z*)-4-bromo-*N'*-((dimethylcarbamoyl)oxy)-1*H*-pyrazole-3-carboximidamide 23:

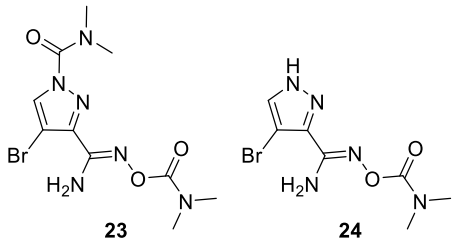

23 **24**

General procedure B was followed with oxyamidine **9** (80 mg, 0.39 mmol, 1.0 equiv.), Et_3N (0.13 mL, 0.94 mmol, 2.4 equiv.) and dimethyl carbamoyl chloride (88 µL, 0.94 mmol, 2.4 equiv.) in CH_2Cl_2 (3 mL). The crude was purified by column chromatography (60:40 PE:acetone). Two products were isolated: the mono **24** (16 mg, 0.06 mmol, 16 %) and disubstituted **23** (9 mg, 0.03 mmol, 8%) products. **23**: **IR (ATR)/cm^{-1}**: 3449, 3318, 1699, 1162 **^{1}H NMR** (400 MHz, $CDCl_3$): **δ** 8.15 (s, 1H), 5.18 (br s, 2H), 3.22 (br s, 6H), 3.03 (s, 6H); **^{13}C NMR** (101 MHz, $CDCl_3$): **δ** 154.7,

150.7, 149.2, 143.0, 134.3, 95.5, 39.3, 36.9; **LRMS (ES-APCI)**: *m/z* = 347.0 $[M+H]^+$; **HRMS**: found *m/z* = 369.0276, calculated for $C_{10}H_{15}Br_1N_6O_3Na_1$ *m/z* = 369.0281; **M.P.**: 176 °C; **24**: **IR (ATR)/cm^{-1}**: 3324, 3298, 3140, 2932, 1688, 1651; **^{1}H NMR** (400 MHz, $CDCl_3$): **δ** 8.17 (s, 1H), 5.16 (br s, 2H), 3.24 (br s, 6H); **^{13}C NMR** (101 MHz, $CDCl_3$): **δ** 150.9, 146.6, 143.3, 94.2, 39.3; **LRMS** (**ES-APCI)**: *m/z* = 276.0 $[M+H]^+$; **HRMS**: found *m/z* = 297.9912, calculated for $C_7H_{10}Br_1N_5O_2Na_1$ *m/z* = 297.9910; **M.P.**: 166 °C;

b. **Carbonate**

Methyl *(Z)*-4-bromo-3-(*N'*-((methoxycarbonyl)oxy)carbamimidoyl)-1*H*-pyrazole-1-carboxylate 25:

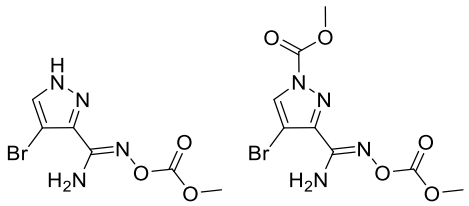

25a **25**

General procedure B was followed with oxyamidine **9** (80 mg, 0.39 mml, 1.0 equiv.), Et_3N (0.13 mL, 0.94 mmol, 2.4 equiv.) and methyl chloroformate (73 µL, 0.94 mmol, 2.4 equiv.) in CH_2Cl_2 (3 mL). The reaction was left to stir for 4 h at room temperature. Work up and ^{1}H NMR revealed monoester **25a** (60 mg, 0.23 mmol, 25%). **^{1}H NMR** (400 MHz, DMSO-d_6): **δ** 13.59 (br s, 1H), 8.09 (app d, 1H, *J* = 1.2 Hz), 6.65 (br s, 2H), 3.76 (s, 3H)

The monoacylated oxyamidine **25a** (41 mg, 0.16 mmol) was dissolved in anhydrous THF (0.5 mL). Et_3N (44 µL, 0.31 mmol, 2.0 equiv.) followed by methyl chloroformate (24 µL, 0.31 mmol, 2.0 equiv.) were added and the reaction was left to stir for 0.5 h at rt. Work up of **general procedure B** and then trituration with chloroform and PE gave **25** as a white solid (20 mg, 0.06 mmol, 40%). **IR (ATR)/cm^{-1}**: 3500, 3398, 3150, 1749, 1651; **^{1}H NMR** (400 MHz, $CDCl_3$): **δ** 8.21 (s, 1H), 5.48 (br s, 2H), 4.10 (s, 3H), 3.91 (s, 3H); **^{13}C NMR** (101 MHz, $CDCl_3$): **δ** 154.2, 149.3, 145.3, 133.6, 97.3, 55.9, 55.6; **LRMS (ES-APCI)**: *m/z* = 321.0 $[M+H]^+$; **HRMS**: found *m/z* = 342.9645, calculated for $C_8H_9Br_1N_4O_5Na$ *m/z* = 342.9649; **M.P.**: 135 °C

ethyl (*Z*)-4-bromo-3-(*N*'-((ethoxycarbonyl)oxy)carbamimidoyl)-1*H*-pyrazole-1-carboxylate 26:

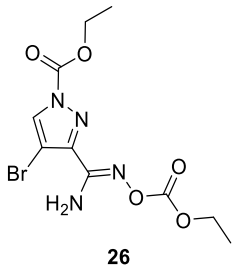

26

General procedure B was followed with oxyamidine **9** (80 mg, 0.39 mmol, 1.0 equiv.), Et_3N (0.13 mL, 0.94 mmol, 2.4 equiv.) and ethyl chloroformate (0.12 mL, 0.94 mmol, 2.4 equiv.) in CH_2Cl_2 (3 mL). The reaction was left to stir for 4 h at room temperature. The crude product was recrystallized by vapour diffusion with chloroform and PE to give compound **26** as a white solid (56 mg, 0.16 mmol, 42%). **IR (ATR)/cm $^{-1}$**: 3479, 3371, 3151, 1774, 1739, 1641; **^{1}H NMR** (400 MHz, $CDCl_3$): **δ** 8.21 (s, 1H), 5.50 (br s, 2H), 4.56 (q, 2H, *J* = 7.2 Hz), 4.35 (q, 2H, *J* = 6.8 Hz), 1.48 (t, 3H, *J* = 7.2 Hz), 1.38 (t, 3H, *J* = 6.8 Hz); **^{13}C NMR** (101 MHz, $CDCl_3$): **δ** 153.5, 149.3, 148.0, 145.1, 133.5, 97.1, 65.8, 65.0, 14.5, 14.4; **LRMS (ES-APCI)**: *m/z* = 349.0 $[M+H]^+$; **HRMS**: found *m/z* = 349.0141 $[M+H]^+$ calculated for $C_{10}H_{14}Br_1N_4O_5$ *m/z* = 349.0142; **M.P.**: 105–106 °C

phenyl (*Z*)-4-bromo-3-(*N*'-((phenoxycarbonyl)oxy)carbamimidoyl)-1*H*-pyrazole-1-carboxylate 27:

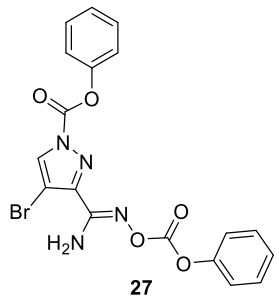

27

General procedure B was followed with oxyamidine **9** (80 mg, 0.39 mmol, 1.0 equiv.), Et_3N (0.13 mL, 0.94 mmol, 2.4 equiv.) and phenyl chloroformate (0.12 mL, 0.94 mmol, 2.4 equiv.) in CH_2Cl_2 (3 mL). The reaction was left to stir for 4 h at room temperature. The crude material was purified by column chromatography

(90:10 PE:acetone) to isolate **27** as a white solid (76 mg, 0.17 mmol, 45%). **^{1}H NMR** (400 MHz, $CDCl_3$): **δ** 8.38 (s, 1H), 7.53–7.48 (m, 2H), 7.44–7.36 (m, 3H), 7.32–7.26 (m, 5H), 5.65 (br s, 2H); **^{13}C NMR** (101 MHz, $CDCl_3$): **δ** 150.2, 149.7, 134.0, 130.2, 129.9, 128.8, 127.5, 126.4, 121.2, 121.1, 97.9; **LRMS (ES-APCI)**: *m/z* = 445.0 $[M+H]^+$; **M.P.**: 138 °C

benzyl (*Z*)-3-(*N*'-(((benzyloxy)carbonyl)oxy)carbamimidoyl)-4-bromo-1*H*-pyrazole-1-carboxylate 28:

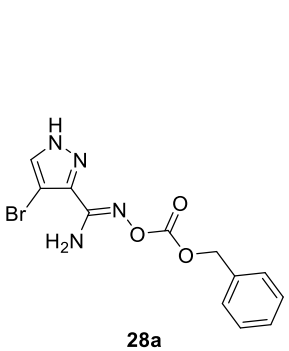

28a

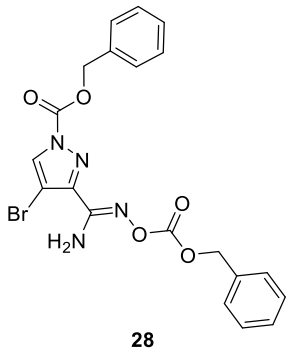

28

General procedure B was followed with oxyamidine **9** (80 mg, 0.39 mmol, 1.0 equiv.), Et_3N (0.13 mL, 0.94 mmol, 2.4 equiv.) and benzyl chloroformate (0.13 mL, 0.94 mmol, 2.4 equiv.) in CH_2Cl_2 (3 mL). The reaction was left to stir for 3 h at room temperature. The crude was triturated with chloroform and PE to afford monoacylated **28a** as a white solid (56 mg, 0.16 mmol, 31%). **^{1}H NMR** (400 MHz, $CDCl_3$): **δ** 7.64 (s, 1H), 7.45–7.37 (m, 5H), 5.69 (br s, 2H), 5.31 (s, 2H); **^{13}C NMR** (101 MHz, DMSO-*d*$_6$): **δ** 153.2, 151.4, 140.6, 135.6, 131.3, 128.4, 128.3, 128.2, 91.4, 68.9; **LRMS (ES-APCI)**: *m/z* = 339.0 $[M+H]^+$; **M.P.**: 140 °C

Monoacylated oxyamidine **28a** (50 mg, 0.15 mmol, 1.0 equiv.) was dissolved in anhydrous THF (1.0 mL). Et_3N (60 µL, 0.43 mmol, 2.4 equiv.) followed by benzyl chloroformate (61 µL, 0.43 mmol, 2.4 equiv.) were added and the reaction was left to stir for 0.5 h at room temperature. Same work up as **general procedure B** was followed and the crude was triturated with chloroform and PE to give **28** as a white solid (30 mg, 0.06 mmol, 40%). **IR (ATR)/cm^{-1}**: 2900, 1755, 1206; **^{1}H NMR** (400 MHz, $CDCl_3$): **δ** 8.19 (s, 1H), 7.48–7.35 (m, 10H), 5.48 (br s, 4H), 5.29 (s, 2H); **^{13}C NMR** (101 MHz, $CDCl_3$): **δ** 153.6, 149.5, 148.0, 145.3, 135.2, 133.9, 133.6, 129.7, 129.3, 129.2, 129.0, 128.9, 128.8, 97.3, 71.2, 70.6; **LRMS (ES-APCI)**:

m/z = 473.0 $[M+H]^+$; **HRMS**: found *m/z* = 473.0455 $[M+H]^+$, calculated for $C_{20}H_{18}Br_1N_4O_5$ *m/z* = 473.0453; **M.P.**: > 250 °C

c. Alkyl and aryl analogues

(*Z*)-*N*'-acetoxy-1-acetyl-4-bromo-1*H*-pyrazole-3-carboximidamide 29:

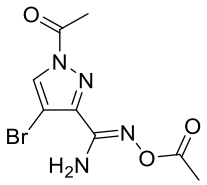

29

General procedure B was followed with oxyamidine **9** (80 mg, 0.39 mmol, 1.0 equiv.), Et_3N (0.13 mL, 0.94 mmol, 2.4 equiv.) and acyl chloride (67 µL, 0.94 mmol, 2.4 equiv.) in CH_2Cl_2 (3 mL). The reaction was left to stir for 4 h at room temperature. The crude material was purified by column chromatography (50:50 PE:acetone) to isolate compound **29** as a white solid (45 mg, 0.16 mmol, 42%). **IR (ATR)/cm^{-1}**: 3499, 3392, 1747, 1651; **^{1}H NMR** (400 MHz, $CDCl_3$): δ 8.34 (s, 1H), 5.43 (br s, 2H), 2.72 (s, 3H), 2.35 (s, 3H); **^{13}C NMR** (101 MHz, $CDCl_3$): δ 168.2, 148.6, 144.7, 131.2, 98.4, 21.3, 20.4; **LRMS (ES-APCI)**: *m/z* = 289.0 $[M+H]^+$; **HRMS**: found *m/z* = 268.9648, calculated for $C_6H_7Br_1N_4O_2Na_1$ *m/z* = 268.9642; **M.P.**: 141 °C

(*Z*)-4-bromo-1-propionyl-*N*'-(propionyloxy)-1*H*-pyrazole-3-carboximidamide 30:

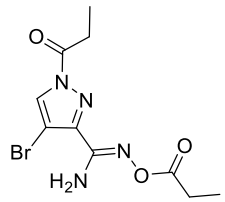

30

General procedure B was followed with oxyamidine **9** (80 mg, 0.39 mmol, 1.0 equiv.), Et_3N (0.13 mL, 0.94 mmol, 2.4 equiv.) and propionyl chloride (0.12 mL, 0.94 mmol, 2.4 equiv.) in CH_2Cl_2 (3 mL). The reaction was left to stir for 2.5 h at rt. Purification of the crude product by column chromatography (80:20 PE:acetone)

enabled the isolation of compound **30** as a white solid (53 mg, 0.17 mmol, 45%). **IR (ATR)/cm^{-1}**: 3450, 3352, 3132, 2978, 1747, 1730, 1647; **^{1}H NMR** (400 MHz, $CDCl_3$): **δ** 8.33 (s, 3H), 5.40 (br s, 2H), 3.15 (q, 2H, *J* = 7.2 Hz), 2.66 (q, 2H, *J* = 7.6 Hz), 1.31 (t, 3H, *J* = 7.6 Hz), 1.26 (t, 3H, *J* = 7.6 Hz); **^{13}C NMR** (101 MHz, $CDCl_3$): **δ** 173.3, 171.7, 148.8, 144.6, 131.3, 98.1, 27.1, 26.7, 9.4, 8.5; **HRMS**: found *m/z* = 260.9984, calculated for $C_7H_{10}Br_1N_4O_2$ *m/z* = 260.9982; **M.P.**: 113–114 °C

(*Z*)-1-benzoyl-*N*'-(benzoyloxy)-4-bromo-1*H*-pyrazole-3-carboximidamide 31:

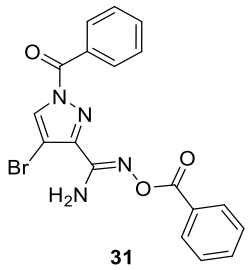

31

General procedure B was followed with oxyamidine **9** (80 mg, 0.39 mmol, 1.0 equiv.), Et_3N (0.13 mL, 0.94 mmol, 2.4 equiv.) and benzoyl chloride (0.11 mL, 0.94 mmol, 2.4 equiv.) in CH_2Cl_2 (3 mL). The reaction was left to stir for 4 h at t. Purification of crude material by column chromatography (75:25 PE:acetone) led to the isolation of compound **31** as a white solid (32 mg, 0.08 mmol, 21%). **IR (ATR)/cm^{-1}**: 3450, 3323, 3152, 1705,1622 ; **^{1}H NMR** (400 MHz, $CDCl_3$): **δ** 8.51 (s, 1H), 8.11–8.07 (m, 4H), 7.71–7.69 Hz (m, 1H), 7.64–7.59 (m, 1H), 7.57–7.53 (m, 2H), 7.52–7.48 (m, 2H), 5.44 (s, 2H); **^{13}C NMR** (101 MHz, $CDCl_3$): **δ** 165.1, 163.4, 150.4, 145.3, 134.1, 133.6, 133.5, 131.9, 130.3, 129.9, 129.7, 128.9, 128.7, 98.7; **LRMS (ES-APCI)**: *m/z* = 413.0 $[M+H]^+$; **M.P.**: 153 °C

(*Z*)-4-bromo-1-(cyclopropanecarbonyl)-*N*'-((cyclopropanecarbonyl)oxy)-1*H*-pyrazole-3-carboximidamide 32:

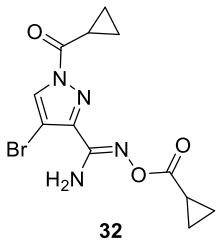

32

General procedure B was followed with oxyamidine **9** (80 mg, 0.39 mmol, 1.0 equiv.), Et_3N (0.13 mL, 0.94 mmol, 2.4 equiv.) and cyclopropane carbonyl chloride (85 µL, 0.94 mmol, 2.4 equiv.) in CH_2Cl_2 (3 mL). The reaction was left to stir for 3.5 h at room temperature. Purification of the crude material by flash chromatography (80:20 PE:acetone) enabled the isolation of compound **32** as a white solid (69 mg, 0.20 mmol, 51%). **IR (ATR)/cm^{-1}**: 3305, 3138, 1728, 1620; **^{1}H NMR** (400 MHz, $CDCl_3$): **δ** 8.32 (s, 1H), 5.48 (br s, 2H), 3.11−3.04 (m, 1H), 2.05−1.99 (m, 1H), 1.37–1.33 (m, 2H), 1.26–1.21 (m, 2H), 1.20–1.15 (m, 2H), 1.02–0.97 (m, 2H); **^{13}C NMR** (101 MHz, $CDCl_3$): **δ** 173.0, 171.7, 149.0, 144.6, 131.0, 98.1, 12.4, 11.7, 11.3, 9.5; **LRMS (ES-APCI)**: *m/z* = 341.0 $[M+H]^+$; **HRMS**: found *m/z* = 341.0244, calculated for $C_{12}H_{14}Br_1N_4O_3$ *m/z* = 341.0244; **M.P.**: 122 °C

(*Z*)-4-bromo-1-(cyclopentanecarbonyl)-*N*'-((cyclopentanecarbonyl)oxy)-1*H*-pyrazole-3-carboximidamide 33:

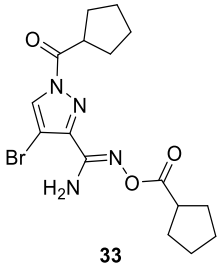

33

General procedure B was followed with oxyamidine **9** (80 mg, 0.39 mmol, 1.0 equiv.), Et_3N (0.13 mL, 0.94 mmol, 2.4 equiv.) and cyclopentane carbonyl chloride (0.11 mL, 0.94 mmol, 2.4 equiv.) in CH_2Cl_2 (3 mL). The reaction was left to stir for 2 h at room temperature. Recrystallization of the crude product by vapour diffusion in chloroform and PE gave **33** as a white solid (84 mg, 0.21 mmol, 54%).

IR (ATR)/cm^{-1}: 3493, 3369, 2954, 1737, 1616; **^{1}H NMR** (400 MHz, $CDCl_3$): **δ** 8.33 (s, 1H), 5.38 (br s, 2H), 3.94 (m, 1H), 3.09 (m, 1H), 2.1–1.88 (m, 8H), 1.86–1.61 (m, 8H); **^{13}C NMR** (101 MHz, $CDCl_3$): **δ** 174.6, 174.0, 149.0, 144.5, 131.4, 97.9, 42.4, 41.7, 30.7, 30.4, 26.4, 26.1; **LRMS (ES-APCI)**: *m/z* = 397.1 $[M+H]^+$; **HRMS**: found *m/z* = 419.0685, calculated for $C_{16}H_{21}Br_1N_4O_3Na_1$ *m/z* = 419.0688; **M.P.**: 149–150 °C

4. **Exploration of Part B**

4-bromo-3-cyano-*N*-methyl-1*H*-pyrazole-1-carboxamide 35:

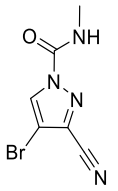

35

In a round bottom flask, nitrile **8** (1g, 5.81 mmol, 1.0 equiv.) was dissolved in anhydrous MeCN (15 mL). Isocyanate derivative **12** (1.45 g, 11.62 mmol, 2.0 equiv.) was added as well as Et_3N (1.62 mL, 11.62 mmol, 2.0 equiv.). The reaction was stirred for 20 h at 70 °C and then left to cool down. Solvent was evaporated *in vacuo* and the crude material was purified by column chromatography with 90:10 PE:acetone to afford desired product **35** as an off white solid (524 mg, 2.28 mmol, 39%). **IR (ATR)/cm^{-1}**: 3356, 3125, 2244, 2255, 1732; **^{1}H NMR** (400 MHz, DMSO-d_6): **δ** 8.92 (br app q, 1H, *J* = 4.0 Hz), 8.86 (s, 1H), 2.82 (d, 3H, *J* = 4.0 Hz); **^{13}C NMR** (101 MHz, DMSO-d_6): **δ** 147.5, 131.6, 127.5, 111.7, 100.4, 27.1; **LRMS (CI)**: *m/z* = 171.9 $[M+H-C_2H_3N_1O_1]^+$; **M.P.**: 170 °C

(*Z*)-4-bromo-3-(*N'*-hydroxycarbamimidoyl)-*N*-methyl-*1H*-pyrazole-1-carboxamide 34:

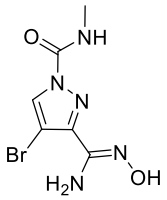

34

In a round bottom flask, nitrile **35** (351 mg, 1.53 mmol, 1.0 equiv.) was dissolved in MeOH (5 mL). Hydroxyl amine hydrochloride (117 mg, 1.69 mmol, 1.1 equiv.) and Na_2CO_3 (179 mg, 1.69 mmol, 1.1 equiv.) were added and the reaction was stirred at 60 °C for 0.6 h. The reaction mixture was left to cool to rt before addition of H_2O (10 mL) and extraction with EtOAc (3 × 10 mL). The organic layers were dried over $MgSO_4$, filtered and concentrated *in vacuo*. The crude product was purified by column chromatography 80:20 PE:acetone to give desired product **34** as white solid (190 mg, 0.72 mmol, 47%). **IR (ATR)/cm^{-1}**: 3367, 3274, 3131, 1721, 1660; **^{1}H NMR** (400 MHz, DMSO-d_6): **δ** 10.06 (s, 1H), 8.59 (br q, 1H, J = 4.0 Hz), 8.47 (s, 1H), 5.78 (br s, 2H), 2.84 (d, 3H, J = 4.8 Hz); **^{13}C NMR** (101 MHz in DMSO-d_6): **δ** 148.7, 145.2, 143.8, 130.7, 93.7, 26.6; **M.P.**: 162 °C

(*Z*)-4-bromo-3-(*N'*-((ethoxycarbonyl)oxy)carbamimidoyl)-*N*-methyl-1*H*-pyrazole-1-carboxamide 36:

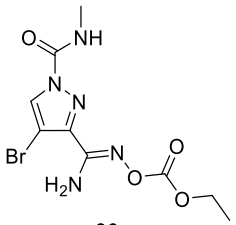

36

In a microwave vial, oxyamidine **34** (30 mg, 0.11 mmol, 1.0 equiv.) was dissolved in anhydrous THF (2 mL). Ethyl chloroformate (21 µL, 0.22 mmol, 2 .0 equiv.) was added followed by Et_3N (32 µL, 0.23 mmol, 2.0 equiv.). It was left to stir at room temperature for 3 hours. CH_2Cl_2 (5 mL) was added and the organic phase was washed with H_2O (5 mL) followed by 1 M NaOH (5 mL) and again H_2O (5 mL). The organic layer was dried over $MgSO_4$, filtered and concentrated *in vacuo* to afford the crude

reaction mixture. The product was triturated with EtOAc and PE to afford product **36** as a white solid (10 mg, 0.03 mmol, 27%). **IR (ATR)/cm^{-1}**: 3358, 1753, 1641; **^{1}H NMR** (400 MHz, $CDCl_3$): **δ** 8.29 (s, 1H), 7.06 (br s, 1H), 5.41 (br s, 2H), 4.34 (q, 2H, *J* = 7.2 Hz), 3.04 (d, 3H, *J* = 4.8 Hz), 1.38 (t, 3H, *J* = 7.2 Hz); **^{13}C NMR** (101 MHz, $CDCl_3$): **δ** 153.6, 149.3, 148.7, 142.9, 131.2, 96.1, 65.0, 27.2, 14.5; **LRMS** (**ES-APCI)**: *m/z* = 334.0 $[M+H]^+$; **HRMS**: found *m/z* = 334.0150, calculated for $C_9H_{13}O_4N_5Br_1$ *m/z* = 334.0145; **M.P.**: 145–146 °C

(*Z*)-4-bromo-*N*-methyl-3-(*N'*-(propionyloxy)carbamimidoyl)-1*H*-pyrazole-1-carboxamide 37:

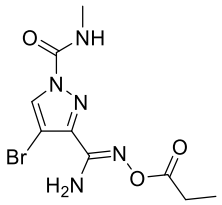

37

In a microwave vial, oxyamidine **34** (30 mg, 0.11 mmol, 1.0 equiv.) was dissolved in anhydrous THF (2 mL). Propionyl chloride (20 µL, 0.23 mmol, 2.0 equiv.) was added followed by Et_3N (32 µL, 0.23 mmol, 2.0 equiv.). It was left to stir at room temperature for 3 hours. CH_2Cl_2 (5 mL) was added and the organic phase was washed with H_2O (5 mL) followed by 1 M NaOH (5 mL) and again H_2O (5 mL). The organic layer was dried over $MgSO_4$, filtered and concentrated *in vacuo* to afford the crude reaction mixture. The product was triturated with EtOAc and PE to afford product **37** as a white solid (10 mg, 0.02 mmol, 27%). **IR (ATR)/cm^{-1}**: 3352, 2972, 1724, 1641; **^{1}H NMR** (400 MHz, $CDCl_3$): **δ** 8.28 (s, 1H), 7.09 (br s, 1H), 5.40 (br s, 2H), 3.03 (d, 3H, *J* = 4.8 Hz), 2.62 (q, 2H, *J* = 7.6 Hz), 1.24 (t, 3H, *J* = 7.6 Hz); **^{13}C NMR** (101 MHz, $CDCl_3$): **δ** 173.1, 148.8, 148.7, 143.1, 131.5, 96.0, 31.1, 27.2, 26.6, 9.2; **LRMS (ES-APCI)**: *m/z* = 318.1$[M+H]^+$; **HRMS**: found *m/z* = 318.0201, calculated for $C_9H_{13}O_3N_5Br_1$ *m/z* = 318.0196; **M.P.**: 125–126 °C

(*Z*)-4-bromo-*N*-methyl-3-(*N'*-((4-methylpentanoyl)oxy)carbamimidoyl)-1*H*-pyrazole-1-carboxamide 38:

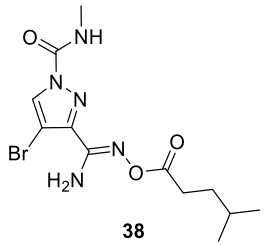

38

General procedure C.a. was followed with oxyamidine **9** (50 mg, 0.24 mmol, 1.0 equiv.), PyBOP (25 mg, 0.24 mmol, 1.0 equiv.), Hünig's base (0.17 mL, 0.98 mmol, 4.0 equiv.) and 4-methylvaleric acid (30 µL, 0.24 mmol, 1.0 equiv.) in MeCN (1.5 mL). Acylation was carried out with **12** (60 mg, 0.48 mmol, 2.0 equiv.) and Et_3N (70 µL, 0.48 mmol, 2.0 equiv.). The crude reaction mixture was purified by column chromatography with 90:10 PE:acetone eluent to afford **38** as a white solid (20 mg, 0.06 mmol, 25%). **IR (ATR)/cm^{-1}**: 3113, 2954, 1745, 1625; **^{1}H NMR** (400 MHz, $CDCl_3$): **δ** 8.31 (s, 1H), 7.01 (br s, 1H), 5.36 (br s, 2H), 3.05 (d, 3H, *J* = 4.8 Hz), 2.60 (app t, 2H, *J* = 7.2 Hz), 1.67–1.61 (m, 3H), 0.95 (d, 6H, *J* = 6 Hz); **^{13}C NMR** (101 MHz, $CDCl_3$): **δ** 172.4, 148.8, 143.2, 131.7, 96.2, 33.4, 31.3, 28.0, 27.3, 22.6;

(*Z*)-4-bromo-3-(*N'*-((3-methoxypropanoyl)oxy)carbamimidoyl)-*N*-methyl-1*H*-pyrazole-1-carboxamide 39:

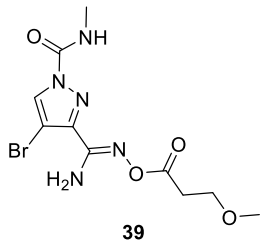

39

General procedure C.a. was followed oxyamidine **9** (50 mg, 0.24 mmol, 1.0 equiv.), PyBOP (25 mg, 0.24 mmol, 1.0 equiv.), Hünig's base (0.17 mL, 0.98 mmol, 4.0 equiv.) and 3-methoxypropionic acid (19 µL, 0.24 mmol, 1.0 equiv.) in MeCN (1.5 mL). Acylation was carried out with **12** (60 mg, 0.48 mmol, 2.0 equiv.) and Et_3N (70 µL, 0.48 mmol, 2.0 equiv.). The crude reaction mixture was purified by

column chromatography with 80:20 PE:acetone to afford **66** as a white solid (20 mg, 0.06 mmol, 25%). **^{1}H NMR** (400 MHz, $CDCl_3$): **δ** 8.40 (s, 1H), 7.32 (br s, 1H), 3.89 (t, 2H, *J* = 6.4 Hz), 3.40 (s, 3H), 3.30 (t, 2H, *J* = 6.4 Hz), 3.05 (d, 3H, *J* = 5.2 Hz); **^{13}C NMR** (101 MHz, $CDCl_3$): **δ** 178.5, 162.5, 148.9, 131.6, 97.3, 68.8, 59.2, 28.0, 27.2; **LRMS (ES-APCI)**: *m/z* = 425.0 $[M+NH_4+C_2H_3O_2+H]^+$; **HRMS**: found *m/z* = 330.0200, calculated for $C_{10}H_{13}O_3N_5Br_1Na_1$ *m/z* = 330.0196

(*Z*)-4-bromo-3-(*N'*-((cycloheptanecarbonyl)oxy)carbamimidoyl)-*N*-methyl-1*H*-pyrazole-1-carboxamide 40:

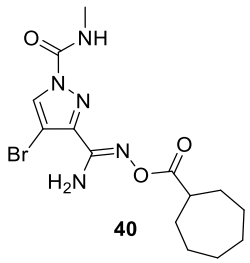

40

General procedure C.b. was followed oxyamidine **9** (50 mg, 0.24 mmol, 1.0 equiv.), PyBOP (25 mg, 0.24 mmol, 1.0 equiv.), Hünig's base (0.17 mL, 0.98 mmol, 4.0 equiv.) and cycloheptane carboxylic acid (27 µL, 0.24 mmol, 1.0 equiv.) in MeCN (1.5 mL). Acylation was carried out with **12** (120 mg, 0.96 mmol, 4.0 equiv.) and Et_3N (0.14 mL, 0.96 mmol, 4.0 equiv.). The crude was purified by column chromatography with 80:20 PE:acetone to isolate **40** as a white solid (80 mg, 0.19 mmol, 79%). **IR (ATR)/cm^{-1}**: 3454, 3344, 2962, 2935, 1722, 1620, 1257, 1016 ; **^{1}H NMR** (400 MHz, $CDCl_3$): **δ** 8.26 (s, 1H), 7.14 (br d, 1H, *J* = 3.6 Hz), 5.40 (br s, 2H), 3.01 (d, 3H, *J* = 5.2 Hz), 2.80–2.75 (m, 1H), 2.06–1.99 (m, 2H), 1.81–1.72 (m, 4H), 1.61–1.48 (m, 6H); **^{13}C NMR** (101 MHz, $CDCl_3$): **δ** 174.6, 149.3, 148.8, 143.1, 131.4, 96.0, 43.8, 31.2, 28.5, 27.2, 26.6; **LRMS (ES-APCI)**: *m/z* = 386.0 $[M+H]^+$; **HRMS**: found *m/z* = 386.0826, calculated for $C_{14}H_{21}O_3N_5Br_1$ *m/z* = 386.0822; **M.P.**: 152 °C

(*Z*)-4-bromo-3-(*N'*-((cyclohexanecarbonyl)oxy)carbamimidoyl)-*N*-methyl-1*H*-pyrazole-1-carboxamide 41:

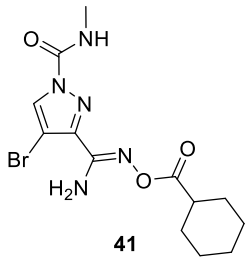

41

General procedure G was followed with oxyamidine **9** (50 mg, 0.24 mmol, 1.0 equiv.), Et_3N (28 µL, 0.20 mmol, 0.8 equiv.) and cyclohexane carbonyl chloride (27 µL, 0.20 mmol, 0.8 equiv.). Acylation was carried out with **12** (120 mg, 0.96 mmol, 4.0 equiv.) and Et_3N (0.14 mL, 0.96 mmol 4.0 equiv.). The crude product was purified by column chromatography with 70:30 PE:acetone and further triturated with chloroform and PE to isolate **41** as a white solid (30 mg, 0.08 mmol, 33%). **IR (ATR)/cm^{-1}**: 3454, 3344, 2962, 1722, 1257; **^{1}H NMR** (400 MHz, $CDCl_3$): **δ** 8.29 (s, 1H), 7.07 (br d, 1H, *J* = 4.4 Hz), 5.38 (br s, 2H), 3.03 (d, 3H, *J* = 5.2 Hz), 2.67−2.59 (m, 1H), 2.04−2.00 (m, 2H), 1.84−1.80 (m, 2H), 1.62−1.52 (m, 2H), 1.37−1.22 (m, 2H); **^{13}C NMR** (101 MHz, $CDCl_3$): **δ** 173.5, 149.2, 148.8, 143.1, 131.5, 96.0, 42.3, 29.4, 27.2, 25.9, 25.7; **LRMS (ES-APCI)**: *m/z* = 372.0 $[M+H]^+$; **HRMS**: found *m/z* = 372.0667, calculated for $C_{13}H_{19}O_3N_5Br_1$ *m/z* = 372.0666; **M.P.**: 151 °C

***Z*)-3-(*N'*-(benzoyloxy)carbamimidoyl)-4-bromo-*N*-methyl-1H-pyrazole-1-carboxamide 42:**[111]

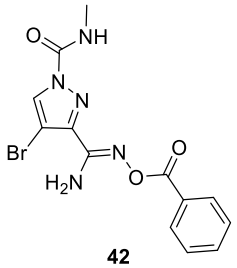

42

General procedure D was followed with oxyamidine **34** (30 mg, 0.11 mmol, 1.0 equiv.), PyBOP (60 mg, 0.11 mmol, 1.0 equiv.), benzoic acid (14 mg, 0.11 mmol, 1.0 equiv.), Hünig's base (80 µL, 0.46 mmol, 4.0 equiv.) and CH_2Cl_2 (1 mL). The crude material was purified by column chromatography with 60:40 PE:acetone to

afford compound **42** as an off white solid (14 mg, 0.04 mmol, 36%). **IR (ATR)/cm^{-1}**: 3478, 3309, 3121, 1716, 1640; **^{1}H NMR** (400 MHz, $CDCl_3$): **δ** 8.32 (s, 1H), 8.10 (dd, 2H, *J* = 1.2, 8.4 Hz), 7.62 (tt, 1H, *J* = 1.6, 7.2 Hz), 7.49 (app t, 2H, *J* = 8.0 Hz), 7.09 (br s, 1H), 5.45 (br s, 2H), 3.06 (d, 3H, *J* = 5.2 Hz); **^{13}C NMR** (101 MHz, $CDCl_3$): **δ** 163.7, 150.4, 148.8, 143.1, 133.5, 131.6, 129.8, 128.8, 96.3, 27.3; **LRMS (ES-APCI)**: *m/z* = 366.0 $[M+H]^+$; **HRMS**: found *m/z* = 366.0200, calculated for $C_{13}H_{13}O_3N_5Br_1$ *m/z* = 336.0196; **M.P.**: 164 °C (decomp)

(*Z*)-4-bromo-*N*-methyl-3-(*N'*-((2,4,6-trimethylbenzoyl)oxy)carbamimidoyl)-1H-pyrazole-1-carboxamide 43:

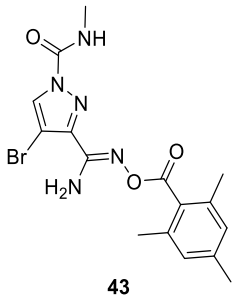

43

General procedure D was followed with oxyamidine **34** (33 mg, 0.13 mmol, 1.0 equiv.), PyBOP (68 mg, 0.13 mmol, 1.0 equiv.), 2,4,6-trimethylbenzoic acid (21 mg, 0.13 mmol, 1.0 equiv.) and Hünig's base (88 µL, 0.50 mmol, 4.0 equiv.) in CH_2Cl_2 (1 mL). The reaction was left to stir at room temperature for 48 h and then heated at 40 °C for 26 h. The solvent was evaporated *in vacuo* and the residue dissolved in EtOAc (10 mL). The crude product was purified by column chromatography with 80:20 PE:acetone to afford compound **43** as a white solid (19 mg, 0.04 mmol, 38%). **IR (ATR)/cm^{-1}**: 3466, 3331, 1726; **^{1}H NMR** (400 MHz, $CDCl_3$): **δ** 8.31 (s, 1H), 7.06 (br s, 1H), 6.91 (s, 2H), 5.38 (br s, 2H), 3.04 (d, 3H, *J* = 4.8 Hz), 2.38 (s, 6H), 2.32 (s, 3H); **^{13}C NMR** (101 MHz, $CDCl_3$): **δ** 149.6, 148.8, 143.1, 140.0, 135.9, 131.5, 129.9, 128.6, 96.3, 27.2, 21.4, 20.1; **LRMS (ES-APCI)**: *m/z* = 408.0 $[M+H]^+$; **HRMS**: found *m/z* = 408.0665, calculated for $C_{16}H_{19}O_3N_5Br_1$ *m/z* = 408.0666; **M.P.**: 175 °C (decomp)

(*Z*)-4-bromo-3-(*N'*-(2-(4-methoxyphenyl)acetoxy)carbamimidoyl)-*N*-methyl-1H-pyrazole-1-carboxamide 44:

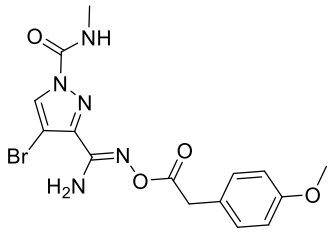

44

General procedure D was followed with oxyamidine **34** (30 mg, 0.11 mmol, 1.0 equiv.), PyBOP (60 mg, 0.11 mmol, 1.0 equiv.), Hünig's base (80 µL, 0.46 mmol, 4.0 equiv.) and *p*-Methoxyphenylacetic acid (18 mg, 0.11 mmol, 1.0 equiv.) in CH_2Cl_2 (1 mL). The crude product was purified by column chromatography with 70:30 PE:acetone to afford compound **44** as a white solid (26 mg, 0.06 mmol, 55%). **IR (ATR)/cm^{-1}**: 3448, 3313, 2990, 1737, 1622, 1512; **^{1}H NMR** (400 MHz, Acetone-d_6): **δ** 8.42 (s, 1H), 7.29 (d, 2H, *J* = 8.4 Hz), 6.98 (d, 2H, *J* = 8.4 Hz), 3.84 (s, 2H), 3.78 (s, 3H), 2.97 (s, 3H); **^{13}C NMR** (101 MHz, Acetone-d_6): **δ** 170.3, 159.7, 131.9, 131.4, 127.5, 114.6, 95.7, 55.5, 39.2, 27.0; **LRMS (ES-APCI)**: *m/z* = 409.9 $[M+H]^+$; **HRMS**: found *m/z* = 410.0459, calculated for $C_{15}H_{17}O_4N_5Br_1$ *m/z* = 410.0458; **M.P.**: 146 °C (decomp)

(*Z*)-4-bromo-3-(*N'*-((4-methoxybenzoyl)oxy)carbamimidoyl)-*N*-methyl-1H-pyrazole-1-carboxamide 45:

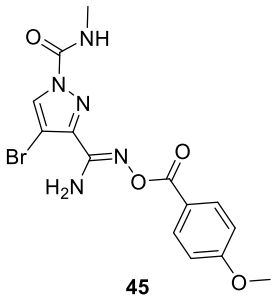

45

General procedure D was followed with oxyamidine **34** (32 mg, 0.12 mmol, 1.0 equiv.), PyBOP (62 mg, 0.12 mmol, 1.0 equiv.), Hünig's base (85 µL, 0.49 mmol, 4.0 equiv.) and *p*-Methoxybenzoic acid (18 mg, 0.12 mmol, 1.0 equiv.) in CH_2Cl_2 (1 mL). The crude material was purified by column chromatography with 60:40

PE:acetone to afford compound **45** as a white solid (26 mg, 0.07 mmol, 58%). **IR (ATR)/cm^{-1}**: 3356, 2960, 1726; **^{1}H NMR** (400 MHz, Acetone-d_6): **δ** 8.43 (s, 1H), 8.10 (dd, 2H, *J* = 8.8, 2.0 Hz), 7.04 (dd, 2H, *J* = 9.2, 2.4 Hz), 6.48 (br s, 1H), 3.90 (s, 3H), 2.98 (d, 3H, *J* = 4.8 Hz); **^{13}C NMR** (101 MHz, Acetone-d_6): **δ** 164.5, 163.6, 132.4, 131.9, 122.9, 114.7, 96.0, 56.0, 27.0 (3 carbons missing due to few number of scans and lack of enough material in sample); **LRMS (ES-APCI)**: *m/z* = 408.0 $[M+H]^+$; **HRMS**: found *m/z* = 396.0302, calculated for $C_{14}H_{15}O_4N_5Br_1$ *m/z* = 396.0302; **M.P.**: 168 °C

(*Z*)-4-bromo-*N*-methyl-3-(*N'*-(tosyloxy)carbamimidoyl)-1*H*-pyrazole-1-carboxamide 46:[115]

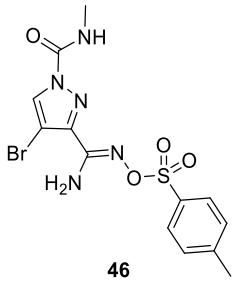

46

In a microwave vial, oxyamidine **34** (30 mg, 0.11 mmol, 1.0 equiv.) was dissolved in anhydrous THF (1 mL) and Et_3N (21 µL, 0.15 mmol, 1.4 equiv.) was added. The solution was left to stir for 10 min before slow addition of *p*-TsCl (23 mg, 0.12 mmol, 1.1 equiv.). The reaction was left to stir for 20 h at room temperature. The slurry was filtered and washed with a minimum amount of THF. The filtrate was removed *in vacuo*. The crude product was purified by trituration with chloroform and PE to give product **46** as an off yellow solid (20 mg, 0.04 mmol, 37%). **IR (ATR)/cm^{-1}**: 3367, 2972, 1745, 1728, 1641; **^{1}H NMR** (400 MHz, DMSO-d_6): **δ** 8.61 (br d, 1H, *J* = 4.4 Hz), 8.53 (s, 1H), 7.88 (d, 2H, *J* = 8.4 Hz), 7.44 (d, 2H, *J* = 8.0 Hz), 7.11 (br s, 2H), 2.82 (d, 3H, *J* = 4.8 Hz), 2.40 (s, 3H); **^{13}C NMR** (101 MHz, DMSO-d_6): **δ** 150.8, 148.3, 144.7, 141.9, 132.4, 131.0, 129.5, 128.6, 94.8, 26.6, 21.1; **LRMS (ES-APCI)**: *m/z* = 415.9 $[M+H]^+$; **HRMS**: found *m/z* = 416.0024, calculated for $C_{13}H_{15}Br_1N_5O_4S_1$ *m/z* = 416.0023; **M.P.**: 182 °C decomp

(*Z*)-4-bromo-*N*-methyl-3-(*N'*-((4-methylbenzoyl)oxy)carbamimidoyl)-1*H*-pyrazole-1-carboxamide 47:

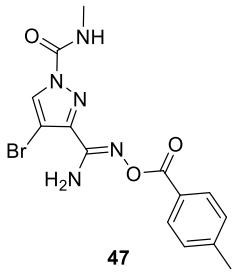

47

General procedure C.a. was followed with oxyamidine **9** (50 mg, 0.24 mmol, 1.0 equiv.), PyBOP (125 mg, 0.24 mmol, 1.0 equiv.), Hünig's base (0.17 mL, 0.96 mmol, 4.0 equiv.) and *p*-toluic acid (33 mg, 0.24 mmol, 1.0 equiv.). Acylation was carried out with **12** (60 mg, 0.48 mmol, 2.0 equiv.) and Et_3N (70 µL, 0.48 mmol, 2.0 equiv.). The crude reaction mixture was purified by column chromatography with 90:10 PE:acetone eluent to afford compound **47** as a white solid (50 mg, 0.12 mmol, 50%). **IR (ATR)/cm^{-1}**: 2918, 1749; **^{1}H NMR** (400 MHz, $CDCl_3$): **δ** 8.43 (s, 1H), 8.15 (d, 2H, *J* = 8.4 Hz), 7.38 (d, 2H, *J* = 8.4 Hz), 7.33 (br s, 1H), 3.07 (d, 3H, *J* = 5.2 Hz), 2.47 (s, 3H) ; **^{13}C NMR** (101 MHz, $CDCl_3$): **δ** 162.8, 148.9, 144.8, 144.4, 141.3, 131.4, 130.14, 128.6, 121.0, 97.4, 27.2, 22.0;

(*Z*)-4-bromo-3-(*N'*-(isonicotinoyloxy)carbamimidoyl)-*N*-methyl-1H-pyrazole-1-carboxamide 48:

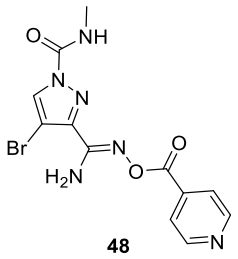

48

General procedure C was followed with oxyamidine **9** (50 mg, 0.24 mmol, 1.0 equiv.), PyBOP (125 mg, 0.24 mmol, 1.0 equiv.), Hünig's base (0.17 mL, 0.96 mmol, 4.0 equiv.) and isonicotinic acid (30 mg, 0.24 mmol, 1.0 equiv.). After addition of **12** (60 mg, 0.48 mmol, 2.0 equiv.) and Et_3N (70 µL, 0.48 mmol, 2.0 equiv.), the reaction mixture was stirred for 72 h at 70 °C. Precipitate was filtered and washed with a minimum amount of MeCN to afford compound **48** as a white solid (20 mg,

0.05 mmol, 21%). **IR (ATR)/cm^{-1}**: 3143, 2933, 2358, 2341, 1735, 1255; Compound was not soluble in deuterated solvent: $CDCl_3$, DMSO-d_6, CD_3CN, Acetone-d_6, CD_3OD were all attempted with no success; **LRMS (ES-APCI)**: *m/z* = 367.0 $[M+H]^+$; **HRMS**: on the way; **M.P.**: 230 °C

(*Z*)-4-bromo-*N*-methyl-3-(*N'*-(nicotinoyloxy)carbamimidoyl)-1H-pyrazole-1-carboxamide 49:

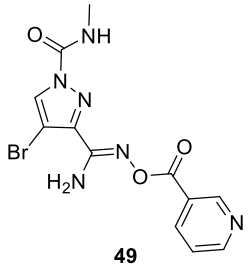

49

General procedure C followed with oxyamidine **9** (50 mg, 0.24 mmol, 1.0 equiv.), PyBOP (125 mg, 0.24 mmol, 1.0 equiv.), Hünig's base (0.17 mL, 0.96 mmol, 4.0 equiv.) and nicotinic acid (30 mg, 0.24 mmol, 1.0 equiv.). After addition of **12** (60 mg, 0.48 mmol, 2.0 equiv.) and Et_3N (70 µL, 0.48 mmol, 2.0 equiv.) the reaction mixture was stirred for 20 h at rt and 72 h at 70 °C. Precipitate was filtered and washed with a minimum amount of MeCN to afford compound **49** as a white solid (25 mg, 0.07 mmol, 29%). **IR (ATR)/cm^{-1}**: 3128, 2360, 2341, 1732, 1612; **^{1}H NMR** (400 MHz, DMSO-d_6): **δ** 9.34 (dd, 1H, *J* = 2.4, 0.8 Hz), 8.84 (dd, 1H, *J* = 4.8, 1.6 Hz), 8.70 (app q, 1H, *J* = 4 Hz), 8.63 (s, 1H), 8.51 (dt, 1H, *J* = 8.0, 2.0 Hz), 7.18 (br s, 2H), 2.85 (d, 3H, *J* = 4.8 Hz); **^{13}C NMR** (101 MHz, DMSO-d_6): **δ** 170.5, 153.6, 150.8, 150.4, 148.5, 143.4, 137.2, 131.0, 125.2, 123.8, 95.4, 26.8; **LRMS (ES-APCI)**: *m/z* = 367.0 $[M+H]^+$; **HRMS**: found *m/z* = 367.0151, calculated for $C_{12}H_{12}O_3N_6Br_1$ *m/z* = 367.0151; **M.P.**: 177 °C

(*Z*)-4-bromo-*N*-methyl-3-(*N'*-(picolinoyloxy)carbamimidoyl)-1*H*-pyrazole-1-carboxamide 50:

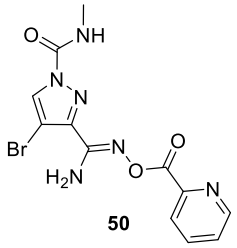

50

General procedure C.b. was followed with oxyamidine **9** (50 mg, 0.24 mmol, 1.0 equiv.), PyBOP (125 mg, 0.24 mmol, 1.0 equiv.), Hünig's base (0.17 mL, 0.96 mmol, 4.0 equiv.) and picolinic acid (30 mg, 0.24 mmol, 1.0 equiv.). Acylation was carried out with **12** (120 mg, 0.96 mmol, 4.0 equiv.) and Et_3N (0.14 mL, 0.96 mmol, 2.0 equiv.). The crude mixture was purified by column chromatography with 80:20 PE:acetone to isolate **50** as a white solid (15 mg, 0.04 mmol, 17%). **IR (ATR)/cm^{-1}**: 2970, 1745, 1253; **^{1}H NMR** (400 MHz, $CDCl_3$): **δ** 8.90 (ddd, 1H, *J* = 4.8, 1.6, 1.2 Hz), 8.43 (s, 1H), 8.35 (dt, 1H, *J* = 8.0, 1.2 Hz), 7.97 (td, 1H, *J* = 7.6, 1.6 Hz), 7.58 (ddd, 1H, *J* = 8.0, 4.8, 1.2 Hz), 7.33 (br s, 1H), 3.07 (d, 3H, *J* = 4.8 Hz); **^{13}C NMR** (101 MHz, $CDCl_3$): **δ** 164.8, 152.9, 141.0, 138.7, 132.9, 130.0, 128.9, 122.4, 118.0, 114.9, 86.6, 17.4; **HRMS**: on the way; **M.P.**: >250 °C

***Z*)-4-bromo-*N*-methyl-3-(*N*'-(2-phenylacetoxy)carbamimidoyl)-1*H*-pyrazole-1-carboxamide 51:**

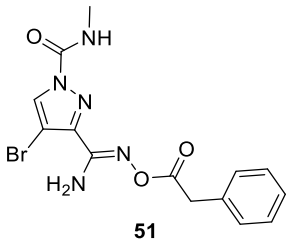

51

General procedure C.b. was followed with oxyamidine **9** (100 mg, 0.48 mmol, 1.0 equiv.), PyBOP (255 mg, 0.48 mmol, 1.0 equiv.), Hünig's base (0.34 mL, 1.95 mmol, 4.0 equiv.) and phenylacetic acid (67 mg, 0.49 mmol, 1.0 equiv.). Acylation was carried out with compound **12** (252 mg, 1.95 mmol, 4.0 equiv.) and

Et_3N (0.27 mL, 1.95 mmol, 4.0 equiv.). The crude reaction was purified by column chromatography with 70:30 PE:acetone eluent to give **51** as a white solid (70 mg, 0.18 mmol, 37%). **IR (ATR)/cm^{-1}**: 3355, 1761, 1736, 1629; **^{1}H NMR** (400 MHz, Acetone-d_6): **δ** 8.41 (s, 1H), 8.09 (br s, 1H), 7.39–7.31 (m, 4H), 7.28–7.24 (m, 1H), 6.40 (br s, 2H), 3.92 (s, 2H), 2.97 (d, 3H, *J* = 4.8 Hz); **^{13}C NMR** (101 MHz, DMSO-d_6): **δ** 169.1, 150.3, 148.5, 143.1, 134.5, 130.9, 129.5, 128.4, 126.8, 96.1, 26.7; **LRMS (ES-APCI)**: *m/z* = 380.0 $[M+H]^+$; **HRMS**: found *m/z* = 380.0356, calculated for $C_{14}H_{15}O_3N_5$ *m/z* = 380.0353; **M.P.**: 158 °C

(*Z*)-4-bromo-3-(*N*'-((2-fluorobenzoyl)oxy)carbamimidoyl)-*N*-methyl-1*H*-pyrazole-1-carboxamide 52:

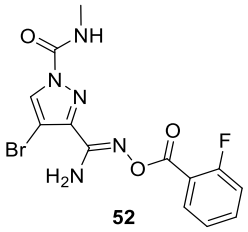

52

General procedure G was followed with oxyamidine **9** (50 mg, 0.24 mmol, 1.0 equiv.), Et_3N (28 µL, 0.20 mmol, 0.8 equiv.) and 2-fluorobenzoyl chloride (23 µL, 0.20 mmol, 0.8 equiv.). Acylation was carried out with **12** (120 mg, 0.96 mmol, 4.0 equiv.) and Et_3N (0.14 mL, 0.96 mmol, 4.0 equiv.). The crude product was purified by column chromatography with 80:20 PE:acetone to isolate **52** as a white solid (30 mg, 0.08 mmol, 33%). **IR (ATR)/cm^{-1}**: 3469, 3377, 3128, 2980, 1714, 1633; **^{1}H NMR** (400 MHz, $CDCl_3$): **δ** 8.32 (s, 1H), 8.10 (td, 1H, *J* = 7.6, 1.6 Hz, 7.61–7.55 (m, 1H), 7.31–7.27 (m, underneath $CHCl_3$ peak, 1H), 7.19 (ddd, 1H, *J* = 11.2, 8.4, 0.8 Hz), 7.09 (br s, 1H), 5.58 (br s, 2H), 3.05 (d, 3H, *J* = 4.8 Hz); **^{19}F NMR** (376 MHz, CDCl3): **δ** -108.8; **^{13}C NMR** (101 MHz, $CDCl_3$): **δ** 163.0 (d, *J* = 257.8 Hz), 161.9 (d, *J* = 4.0 Hz), 150.5, 148.8, 143.0, 135.1 (d, *J* = 9.3 Hz), 133.1, 131.5, 124.8 (d, *J* = 3.3 Hz), 117.8 (d, *J* = 11.6 Hz), 117.2 (d, *J* = 23.5 Hz), 96.3, 27.2 ; **LRMS (ES-APCI)**: *m/z* = 405.9 $[M+Na]^+$; **HRMS**: found *m/z* = 384.0106, calculated for $C_{13}H_{12}O_3N_5Br_1F_1$ *m/z* = 384.0102; **M.P.**: 163 °C

(*Z*)-4-bromo-3-(*N*'-((3-fluorobenzoyl)oxy)carbamimidoyl)-*N*-methyl-1*H*-pyrazole-1-carboxamide 53:

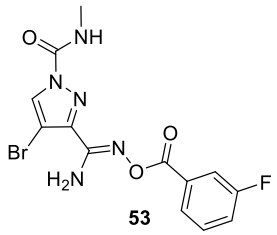

53

General procedure G was followed with oxyamidine **9** (50 mg, 0.24 mmol, 1.0 equiv.), Et_3N (28 µL, 0.20 mmol, 0.8 equiv.) and 3-fluorobenzoyl chloride (23 µL, 0.20 mmol, 0.8 equiv.). Acylation was carried out with **12** (120 mg, 0.96 mmol, 4.0 equiv.) and Et_3N (0.14 mL, 0.96 mmol, 4.0 equiv.). The crude product was purified by column chromatography with 80:20 PE:acetone and further triturated with EtOAc and PE to isolate **53** as a white solid (42 mg, 0.11 mmol, 46%). **IR (ATR)/cm^{-1}**: 3336, 3122, 1717, 1635, 1523; **^{1}H NMR** (400 MHz, $CDCl_3$): **δ** 8.32 (s, 1H), 7.90 (app dt, 1H, *J* = 7.6, 1.2 Hz), 7.77 (ddd, 1H, *J* = 9.2, 2.8, 1.6 Hz), 7.48 (td, 1H, *J* = 8.0, 5.6 Hz), 7.31 (tdd, 1H, *J* = 8.4, 2.4, 0.8 Hz), 7.07 (br s, 1H), 5.45 (br s, 2H), 3.06 (d, 3H, *J* = 5.2 Hz); **^{19}F NMR** (376 MHz, $CDCl_3$): **δ** -111.7; **^{13}C NMR** (101 MHz, $CDCl_3$): **δ** 162.2 (d, *J* = 3.0 Hz), 161.6, 150.5 (d, *J* = 177.0 Hz), 143.0, 131.6, 131.5, 130.6 (d, *J* = 8.0 Hz), 125.6 (d, *J* = 3.0 Hz), 120.7 (d, *J* = 21.3 Hz), 116.8 (d, *J* = 23.1 Hz), 96.3, 27.3; **LRMS (ES-APCI)**: *m/z* = 406.0 $[M+Na]^+$; **HRMS**: found *m/z* = 384.0106, calculated for $C_{13}H_{12}O_3N_5Br_1F_1$ *m/z* = 384.0102; **M.P.**: 182 °C

(*Z*)-4-bromo-*N*-methyl-3-(*N*'-((3-methylbenzoyl)oxy)carbamimidoyl)-1*H*-pyrazole-1-carboxamide 54:

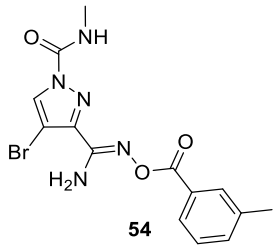

54

General procedure G was followed with oxyamidine **9** (50 mg, 0.24 mmol, 1.0 equiv.), Et_3N (28 µL, 0.20 mmol, 0.8 equiv.) and 3-toluoyl chloride (26 µL, 0.8 equiv.). Acylation was carried out with **12** (120 mg, 0.96 mmol, 4.0 equiv.) and

Et_3N (0.14 mL, 0.96 mmol, 4.0 equiv.). The crude product was purified by column chromatography with 70:30 PE:acetone to isolate **54** as a white solid (39 mg, 0.10 mmol, 42%). **IR (ATR)/cm^{-1}**: 3300, 3132, 1723, 1634, 1532; **^{1}H NMR** (400 MHz, $CDCl_3$): **δ** 8.30 (s, 1H), 7.90–7.87 (m, 2H), 7.43–7.34 (m, 2H), 7.17 (br d, 1H, *J* = 4.8 Hz), 5.47 (br s, 2H), 3.05 (d, 3H, *J* = 4.8 Hz), 2.43 (s, 3H); **^{13}C NMR** (101 MHz, $CDCl_3$): **δ** 164.1, 150.5, 148.9, 143.1, 138.8, 134.4, 131.6, 130.4, 129.4, 128.8, 126.9, 96.3, 27.4, 21.6; **LRMS (ES-APCI)**: *m/z* = 379.9 $[M+H]^+$; **HRMS**: found *m/z* = 380.0354, calculated for $C_{14}H_{15}O_3N_5Br_1$ *m/z* = 380.0353; **M.P.**: 150 °C

(*Z*)-4-bromo-*N*-methyl-3-(*N'*-((2-methylbenzoyl)oxy)carbamimidoyl)-1*H*-pyrazole-1-carboxamide 55:

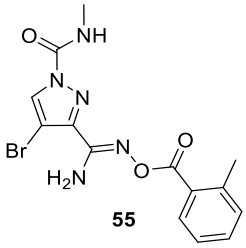

55

General procedure G was followed with oxyamidine **9** (50 mg, 0.24 mmol, 1.0 equiv.), Et_3N (28 µL, 0.20 mmol, 0.8 equiv.) and 2-toluoyl chloride (26 µL, 0.20 mmol, 0.8 equiv.). Acylation was carried out with **12** (120 mg, 0.96 mmol, 4.0 equiv.) and Et_3N (0.14 mL, 0.96 mmol, 4.0 equiv.). The crude was triturated with EtOAc and PE to isolate **55** as a white solid (30 mg, 0.08 mmol, 33%). **IR (ATR)/cm^{-1}**: 3325, 1720, 1618; **^{1}H NMR** (400 MHz, $CDCl_3$): **δ** 8.32 (s, 1H), 7.89 (dd, 1H, *J* = 8.0, 1.2 Hz), 7.45 (td, 1H, *J* = 7.6, 1.6 Hz), 7.32–7.26 (m, 2H), 7.13 (br d, *J* = 4 Hz), 5.46 (br s, 2H), 3.05 (d, 3H, *J* = 5.2 Hz), 2.65 (s, 3H); **^{13}C NMR** (101 MHz, $CDCl_3$): **δ** 164.7, 150.0, 148.7, 143.1, 140.3, 132.3, 132.0, 131.6, 130.2, 129.0, 126.0, 96.2, 27.2, 21.6; **LRMS (ES-APCI)**: *m/z* = 380.0 $[M+H]^+$; **HRMS**: found *m/z* = 380.0350, calculated for $C_{14}H_{15}O_3N_5Br_1$ *m/z* = 380.0353; **M.P.**: 148 °C

(*Z*)-4-bromo-*N'*-((ethylcarbamoyl)oxy)-1*H*-pyrazole-3-carboximidamide 56:

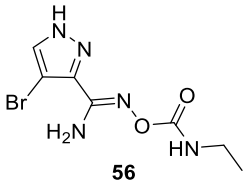

56

Oxyamidine **9** (100 mg, 0.49 mmol, 1.0 equiv.) was dissolved in anhydrous THF (1.5 mL) in a vial. Ethylisocyanate (39 µL, 0.49 mmol, 1.0 equiv.) was then added and the reaction was stirred at room temperature for 3 h. The solvent was evaporated and the crude material purified by column chromatography (gradient from 80:20 to 60:40 P.E:acetone) to afford compound **56** as a white solid (75 mg, 0.28 mmol, 57%). **IR (ATR)/cm^{-1}**: 3338, 3188, 2981, 1693 **^{1}H NMR** (400 MHz, DMSO-d_6): **δ** 13.61 (br s, 1H), 8.06 (br s, 1H), 6.96 (br , 1H), 6.61 (br s, 2H), 3.22–3.11 (m, 2H), 1.09 (t, 3H, *J* = 7.2 Hz); **LRMS (ES-APCI)**: *m/z* = 298.0 $[M+H]^+$; **HRMS**: found *m/z* = 276.0095 $[M+H]^+$ calculated for $C_7H_{11}Br_1N_5O_2$ *m/z* = 276.0091; **M.P.**: 198 °C

(*Z*)-4-bromo-*N'*-((isopropylcarbamoyl)oxy)-1*H*-pyrazole-3-carboximidamide 57:

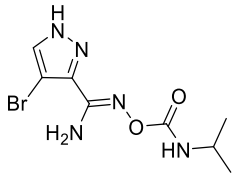

57

Oxyamidine **9** (100 mg, 0.49 mmol, 1.0 equiv.) was dissolved in anhydrous THF (2 mL) in a vial. Isopropylisocyanate (48 µL, 0.49 mmol, 1.0 equiv.) was then added and the reaction was stirred at room temperature for 1.5 h. The solvent was evaporated and the crude material purified by column chromatography with 90:10 PE:acetone eluent to afford compound **57** as a translucent oil (100 mg, 0.34 mmol, 69%). **IR (ATR)/cm^{-1}**: 3352, 3162, 2963, 1714; **^{1}H NMR** (400 MHz, $CDCl_3$): **δ** 13.65 (br s, 1H), 7.73 (s, 1H), 6.93 (br d, 1H, *J* = 7.6 Hz), 4.03–3.91 (m, 1H), 1.30 (d, 6H, *J* = 6.8 Hz); **^{13}C NMR** (101 MHz, $CDCl_3$): **δ** 157.3, 148.9, 139.6, 132.2, 92.2, 43.7, 23.1; **LRMS (ES-APCI)**: *m/z* = 312.0 $[M+Na]^+$; **HRMS**: found *m/z* = 290.0252, calculated for $C_8H_{13}Br_1N_5O_2$ *m/z* = 290.0247

(*Z*)-4-bromo-3-(*N'*-((ethylcarbamoyl)oxy)carbamimidoyl)-*N*-methyl-1*H*-pyrazole-1-carboxamide 58:

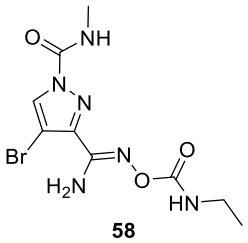

58

In a microwave vial, oxyamidine **56** (45 mg, 0.16 mmol, 1.0 equiv.) was dissolved in anhydrous MeCN (1.5 mL). Compound **12** (59 mg, 0.47 mmol, 3.0 equiv.) and Et_3N (65 µL, 0.47 mmol, 3.0 equiv.) were added and the reaction left to stir at 70 °C for 22 h. Reaction was cooled to room temperature before filtration of the white precipitate **58** (15 mg, 0.05 mmol, 31%). **IR (ATR)/cm^{-1}**: 3498, 3363, 3296, 1712, 1651; **^{1}H NMR** (400 MHz, $CDCl_3$): **δ** 8.34 (s, 1H), 6.92 (br s, 1H), 6.74 (br s, 1H), 5.46 (br s, 2H), 3.39 (qd, 2H, *J* = 7.2 Hz, 5.6 Hz), 3.07 (d, 3H, *J* = 4.8 Hz), 1.25 (t, 3H , *J* = 7.2 Hz); **^{13}C NMR** (101 MHz, DMSO-d_6): **δ** 159.4, 148.5, 147.4, 142.5, 130.9, 94.9, 35.3, 26.7, 15.0; **LRMS (ES-APCI)**: *m/z* = 355.0 $[M+Na]^+$; **HRMS**: found *m/z* = 333.0310, calculated for $C_9H_{14}O_3N_6Br_1$ *m/z* = 333.0305; **M.P.**: 174–176 °C decomp

(*Z*)-4-bromo-3-(*N'*-((isopropylcarbamoyl)oxy)carbamimidoyl)-*N*-methyl-1*H*-pyrazole-1-carboxamide 59:

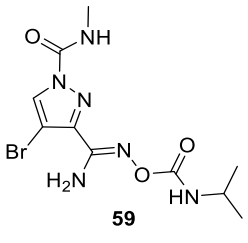

59

In a microwave vial, oxyamidine **57** (45 mg, 0.16 mmol, 1.0 equiv.) was dissolved in anhydrous MeCN (1.5 mL). Compound **12** (59 mg, 0.47 mmol, 3.0 equiv.) and Et_3N (65 µL, 0.47 mmol, 3.0 equiv.) were added and the reaction left to stir at 70 °C for 22 h. The solution was left to cool to rt before adding EtOAc (10 mL). The organic phase was washed with H_2O (2 × 5 mL) followed by brine (5 mL). It was then dried over $MgSO_4$, filtered and concentrated. The crude reaction was purified by column

chromatography with a 70:30 PE:acetone eluent. Compound **59** was isolated as a white solid (15 mg, 0.04 mmol, 25%). **IR (ATR)/cm^{-1}**: 3493, 3358, 3288, 1707, 1643; **^{1}H NMR** (400 MHz, $CDCl_3$): **δ** 8.34 (s, 1H), 6.94 (br d, 1H, *J* = 3.2 Hz), 6.69 (br d, 1H, *J* = 6.4 Hz), 5.46 (br s, 2H), 4.03–3.89 (m, 1H), 3.07 (d, 3H, *J* = 4.8 Hz), 1.26 (d, 6H , *J* = 6.4 Hz); **^{13}C NMR** (101 MHz, $CDCl_3$): **δ** 154.9, 148.7, 146.3, 131.8, 95.4, 43.5, 27.3, 23.1; **LRMS (ES-APCI)**: *m/z* = 347.0 $[M+H]^+$; **HRMS**: found *m/z* = 347.0467, calculated for $C_{10}H_{16}O_3N_6Br_1$ *m/z* = 347.0462;

<u>*N*-ethyl-1*H*-imidazole-1-carboxamide 60:</u>

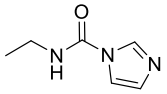

60

General procedure F followed with CDI **13** (3.3 g, 19.8 mmol, 1.1 equiv.) and ethylamine hydrochloride (1.5 g, 18.0 mmol, 1.0 equiv.) in DMF (5 mL) and MeCN (15 mL). Crude was purified by column chromatography with 95:5 CH_2Cl_2:MeOH to afford compound **74** as a white solid (1.94 g, 13.9 mmol, 77%). **IR (ATR)/cm^{-1}:** 3120, 2980, 1732; **^{1}H NMR** (400 MHz, DMSO-d_6): **δ** 8.51 (br s, 1H), 8.23 (s, 1H), 7.66 (app d, 1H, *J* = 1.2 Hz), 7.01 (s, 1H), 3.30–3.23 (m, 2H), 1.13 (td, 3H, *J* = 0.2, 7.2 Hz); **^{13}C NMR** (101 MHz, $CDCl_3$): **δ** 148.7, 136.0, 129.5, 116.6, 35.13, 14.6; **M.P.**: 50 °C

<u>*N*-isopropyl-1*H*-imidazole-1-carboxamide 61:</u>

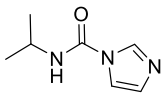

61

General procedure F followed with CDI **13** (2.5 g, 15.0 mmol, 1.1 equiv.) and ethylamine hydrochloride (1.3 g, 13.6 mmol, 1.0 equiv.) in DMF (4 mL) and MeCN (12 mL). Crude was purified by column chromatography with 97:3 CH_2Cl_2:MeOH to afford compound **61** as a white solid (1.40 g, 9.1 mmol, 67%). **IR (ATR)/cm^{-1}:** 3337, 3128, 2967, 1705; **^{1}H NMR** (2.:1 rotamers, minor rotamer*, 400 MHz, $CDCl_3$): **δ** 8.14 (br s, 1H), 7.69* (br s, 1H), 7.37 (br s, 1H), 7.12 (br s, 1H), 7.09* (br s, 2H), 6.03 (br s, 1H), 4.21–4.13 (m, 1H), 4.05* (br s, 1H), 3.88–3.73 (m, 1H), 1.31 (d, 6H, *J* = 6.4 Hz), 1.14* (d, 6H, *J* = 6.8 Hz); **^{13}C NMR** (3:1 rotamer, minor rotamer*,

101 MHz, DMSO-d_6): **δ** 148.0, 136.0, 135.2*, 129.4, 121.7*, 116.6, 42.7, 40.7*, 23.3*, 22.1; **M.P.**: 55 °C

(*Z*)-4-bromo-*N'*-(2-phenylacetoxy)-1*H*-pyrazole-3-carboximidamide 62:

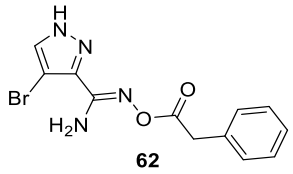

62

In a microwave vial, oxyamidine **9** (150 mg, 1.22 mmol, 1.0 equiv.) was dissolved in anhydrous CH_2Cl_2 (9 mL). Phenylacetic acid (166 mg, 1.22 mmol, 1.0 equiv.) was added followed by PyBOP (634 mg, 1.22 mmol, 1.0 equiv.) and finally Hünig's base (0.85 mL, 4.88 mmol, 4.0 equiv.). The reaction was left to stir at room temperature for 24 h. The solvent was evaporated *in vacuo* and the product dissolved in EtOAc (20 mL). The organic layer was washed with 1 M HCl (3 × 5 mL) and brine (10 mL). The organic layer was dried over $MgSO_4$, filtered and concentrated *in vacuo*. The crude material was purified by flash chromatography with 70:30 PE:acetone eluent followed by trituration with MeOH and PE to afford **62** as a white solid (148 mg, 0.44 mmol, 36%). **IR (ATR)/cm^{-1}**: 3450, 3307, 2980, 1732, 1614; **^{1}H NMR** (400 MHz, DMSO-d_6): **δ** 13.59 (br s, 1H), 8.08, (s, 1H), 7.34–7.35 (m, 4H), 7.30–7.25 (m, 1H), 6.66 (br s, 2H), 3.84 (s, 2H); **^{13}C NMR** (100 MHz, DMSO-d_6): **δ** 169.1, 151.5, 140.7, 134.6, 131.4, 129.5, 128.3, 126.7, 91.3, 39.2; **LRMS (ES-APCI)**: *m/z*= 324.1$[M+H]^+$; **HRMS**: found *m/z* = 323.0140, calculated for $C_{12}H_{12}Br_1N_4O_2$ *m/*z = 323.0138; **M.P.**: 155 °C

(*Z*)-4-bromo-*N'*-(2-(4-methoxyphenyl)acetoxy)-1*H*-pyrazole-3-carboximidamide 63:

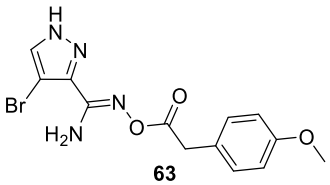

63

In a microwave vial, oxyamidine **9** (150 mg, 1.22 mmol, 1.0 equiv.) was dissolved in anhydrous CH_2Cl_2 (9 mL). *p*-Methoxyphenyl acetic acid (208 mg, 1.22 mmol,

1.0 equiv.) was added followed by PyBOP (634 mg, 1.22 mmol, 1.0 equiv.) and finally Hünig's base (0.85 mL, 4.88 mmol, 4.0 equiv.). The reaction was left to stir at room temperature for 24 h. The solvent was evaporated *in vacuo* and the product dissolved in EtOAc (20 mL). The organic layer was washed with 1 M HCl (3 × 5 mL) and brine (10 mL). The organic layer was dried over $MgSO_4$, filtered and concentrated *in vacuo*. The crude product was purified by column chromatography with a gradient eluent system from 80:20 to 60:40 PE:acetone to afford product **63** as a white solid (120 mg, 0.34 mmol, 29%). **IR (ATR)/cm^{-1}**: 3454, 3315, 1734, 1614; **^{1}H NMR** (400 MHz, DMSO-d_6): **δ** 13.58 (br s, 1H), 8.08 (app d, 1H, J = 1.2 Hz), 7.25 (d, 2H, J = 8.8 Hz), 6.89 (d, 2H, J = 8.8 Hz), 6.64, (br s, 2H), 3.76 (s, 2H), 3.74 (s, 3H); **^{13}C NMR** (101 MHz, DMSO-d_6): **δ** 169.3, 158.2, 151.4, 148.3, 140.8, 131.4, 130.5, 126.5, 113.8, 91.3, 55.0, 38.3; **LRMS (ES-APCI)**: m/z = 375.0 $[M+Na]^+$; **HRMS**: found m/z = 353.0244, calculated for $C_{13}H_{14}Br_1N_4O_3$ m/z = 353.0244; **M.P.**: 144–145 °C

(*Z*)-4-bromo-*N*-ethyl-3-(*N*'-(2-phenylacetoxy)carbamimidoyl)-1*H*-pyrazole-1-carboxamide 64:

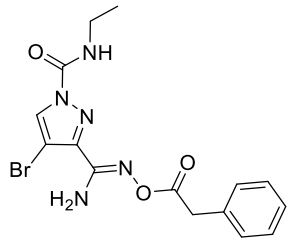

64

In a microwave vial, **62** (50 mg, 0.14 mmol, 1.0 equiv.) was dissolved in anhydrous MeCN (1.5 mL). Et_3N (40 µL, 0.42 mmol, 2.0 equiv.) and derivative **60** (39 mg, 0.28 mmol, 2.0 equiv.) were added. The reaction was stirred at room temperature for 66 h and 1.5 h at 40 °C. The solution was cooled to room temperature before adding EtOAc (10 mL). The organic phase was washed with 10% aq $NaHCO_3$ (5 mL), H_2O (5 mL) and brine (5 mL). The crude material was purified by column chromatography with 80:20 PE:acetone eluent. The product was recrystallized from chloroform to afford **64** as a white solid (10 mg, 0.03 mmol, 17%). **IR (ATR)/cm^{-1}**: 3317, 1732, 1620, 1514; **^{1}H NMR** (400 MHz, $CDCl_3$): **δ** 8.32 (s, 1H), 7.37 (app d, 4H, J = 4.4 Hz), 7.33−7.31 (m, 1H), 6.99 (br s, 1H), 5.29 (br s, 2H), 3.96 (s, 2H), 3.53−3.46 (m, 1H),

1.30 (t, 3H, *J* = 7.2 Hz); **^{13}C NMR** (101 MHz, CDCl3): **δ** 169.6, 149.3, 148.0, 142.9, 133.9, 131.6, 129.6, 128.9, 127.5, 96.0, 40.3, 35.9, 15.0; **LRMS (ES-APCI)**: *m/z* = 416.0 $[M+Na]^+$

(*Z*)-4-bromo-*N*-isopropyl-3-(*N*'-(2-phenylacetoxy)carbamimidoyl)-1*H*-pyrazole-1-carboxamide 65:

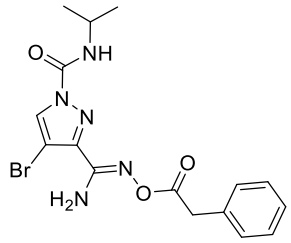

65

In a microwave vial, **62** (50 mg, 0.14 mmol, 1.0 equiv.) was dissolved in anhydrous MeCN (1.5 mL). Et_3N (40 µL, 0.42 mmol, 2.0 equiv.) and derivative **61** (43 mg, 0.28 mmol, 2.0 equiv.) were added. The reaction was stirred at room temperature for 66 h. The solution was cooled to room temperature before adding EtOAc (10 mL). The organic phase was washed with 10% aq $NaHCO_3$ (5 mL), H_2O (5 mL) and brine (5 mL). The crude material was purified by column chromatography with 80:20 PE:acetone eluent. The product was recrystallized from MeOH and PE by vapour diffusion to afford **65** as a white solid (20 mg, 0.05 mmol, 36%). **^{1}H NMR** (400 MHz, $CDCl_3$): **δ** 8.30 (s, 1H), 7.37−7.35 (m, 4H), 7.33−7.28 (m, 1H), 6.77 (app br d, 1H, *J* = 8.0 Hz), 5.26 (br s, 2H), 4.17−4.09 (m, 1H), 3.95 (s, 2H), 1.31 (d, 6H, *J* = 6.4 Hz); **^{13}C NMR** (400 MHz, $CDCl_3$): **δ** 149.3, 147.2, 133.9, 131.7, 129.7, 128.9, 127.5, 126.3, 96.1, 43.6, 40.3, 25.9; **LRMS (ES-APCI)**: *m/z* = 408.0 $[M+H]^+$

(*Z*)-4-bromo-*N*-ethyl-3-(*N'*-(2-(4-methoxyphenyl)acetoxy)carbamimidoyl)-1*H*-pyrazole-1-carboxamide 66:

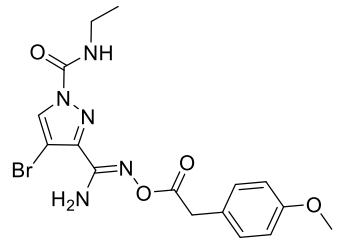

66

In a microwave vial, **63** (50 mg, 0.14 mmol, 1.0 equiv.) was dissolved in anhydrous MeCN (1.5 mL). Et_3N (59 µL, 0.42 mmol, 3.0 equiv.) and derivative **60** (43 mg, 0.28 mmol, 2.0 equiv.) were added. The reaction was stirred at room temperature for 66 h and 1.5 h at 40 °C. The solution was cooled to room temperature before adding EtOAc (10 mL). The organic phase was washed with 10% aq $NaHCO_3$ (5 mL), H_2O (5 mL) and brine (5 mL). The crude material was purified by column chromatography with 80:20 PE:acetone eluent. The product was further triturated with EtOAc and PE to afford **66** as a white solid (21 mg, 0.05 mmol, 36%). **IR (ATR)/cm^{-1}**: 3450, 3363, 3309, 1732, 1620; **^{1}H NMR** (400 MHz, $CDCl_3$): **δ** 8.30 (s, 1H), 7.27 (dd, 2H, *J* = 8.8, 2.0 Hz), 6.98 (br t, 1H, *J* = 5.2 Hz), 6.88 (dd, 2H, *J* = 8.4, 2.0 Hz), 5.27 (br s, 2H), 3.88 (s, 2H), 3.81 (br s, 3H), 3.52–3.45 (m, 2H), 1.29 (t, 3H, *J* = 7.2 Hz); **^{13}C NMR** (101 MHz, $CDCl_3$): **δ** 169.9, 159.0, 149.2, 148.0, 142.9, 131.6, 130.7, 125.9, 114.3, 96.1, 55.5, 39.4, 35.9, 15.0; **LRMS (ES-APCI)**: *m/z* = 424.0 $[M+H]^+$; **HRMS**: found *m/z* = 424.0612, calculated for $C_{16}H_{19}O_4N_5Br_1$ *m/z* = 438.0771; **M.P.**: 131 °C

(*Z*)-4-bromo-*N*-isopropyl-3-(*N'*-(2-(4-methoxyphenyl)acetoxy)carbamimidoyl)-1*H*-pyrazole-1-carboxamide 67:

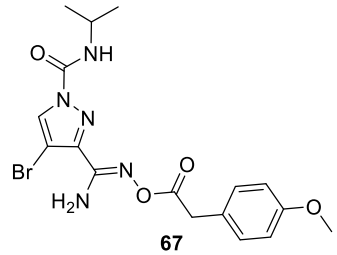

67

In a microwave vial, **63** (50 mg, 0.14 mmol, 1.0 equiv.) was dissolved in anhydrous MeCN (1.5 mL). Et_3N (59 µL, 0.42 mmol, 3.0 equiv.) and derivative **61** (43 mg,

0.28 mmol, 2.0 equiv.) were added. The reaction was stirred at room temperature for 66 h and 1.5 h at 40 °C. The solution was left to cool down before adding EtOAc (10 mL). The organic phase was treated with 10% aq $NaHCO_3$ (5 mL) than H_2O (5 mL) followed by brine (5 mL). The crude product was purified by column chromatography with 80:20 PE:acetone eluent. The product was further triturated with EtOAc and PE to afford product **67** as a white solid (15 mg, 0.03 mmol, 24%). **IR (ATR)/cm^{-1}**: 3448, 3315, 1735, 1618; **^{1}H NMR** (400 MHz, $CDCl_3$): **δ** 8.30 (s, 1H), 7.29–7.25 (m, 2H), 6.90–6.87 (m, 2H), 6.78 (br d, *J* = 8.0 Hz), 5.28 (br s, 2H), 4.17–4.08 (m, 1H), 3.88 (s, 2H), 3.81 (s, 3H), 1.31 (d, 6H, *J* = 6.4 Hz); **^{13}C NMR** (101 MHz, $CDCl_3$): **δ** 169.9, 159.0, 149.2, 147.2, 142.9, 131.6, 130.7, 125.9, 114.3, 96.0, 55.5, 43.6, 39.4, 22.8; **LRMS (ES-APCI)**: *m/z* = 438.0$[M+H]^+$, **HRMS**: found *m/z* = 438.0772, calculated for $C_{17}H_{21}O_4N_5Br_1$ *m/z* = 438.0771; **M.P.**: 122–124 °C

(*Z*)-4-bromo-*N*,N-dimethyl-3-(*N'*-(2-phenylacetoxy)carbamimidoyl)-1*H*-pyrazole-1-carboxamide 68:

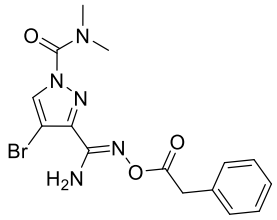

68

In a microwave vial, **62** (50 mg, 0.14 mmol, 1.0 equiv.) was dissolved in anhydrous MeCN (1.5 mL). Et_3N (59 µL, 0.42 mmol, 3.0 equiv.) and carbamoyl chloride (39 µL, 0.42 mmol, 3.0 equiv.) were added. The reaction was stirred at 40 °C for 18 h and the solvent was evaporated. The crude product was triturated with EtOAc and PE and filtrated to afford product **68** as a white solid (37 mg, 0.09 mmol, 60%). **IR (ATR)/cm^{-1}**: 3442, 3313, 3130, 2980, 1732, 1620; **^{1}H NMR** (400 MHz, $CDCl_3$): **δ** 8.18 (s, 1H), 7.39–7.36 (m, 4H), 7.32–7.30 (m ,1H), 5.26 (br s, 2H), 3.97 (s, 2H), 3.23 (br s, 6H); **^{13}C NMR** (100 MHz, $CDCl_3$): **δ** 169.8, 150.6, 149.5, 142.5, 134.6, 134.0, 129.7, 128.7, 127.4, 95.3, 40.3; **LRMS (ES-APCI)**: *m/z* = 394.0 $[M+H]^+$; **HRMS**: found *m/z* = 394.0509, calculated for $C_{15}H_{17}Br_1N_5O_3$ *m/z* = 394.0509; **M.P.**: 154 °C

(*Z*)-4-bromo-3-(*N'*-(2-(4-methoxyphenyl)acetoxy)carbamimidoyl)-*N*,*N*-dimethyl-1H-pyrazole-1-carboxamide 69:

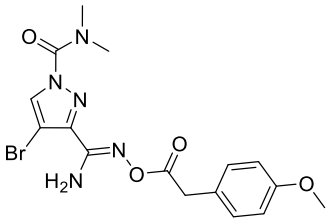

69

In a microwave vial, **63** (50 mg, 0.14 mmol, 1.0 equiv.) was dissolved in anhydrous MeCN (1.5 mL). Et_3N (59 µL, 0.42 mmol, 3.0 equiv.) and carbamoyl chloride (39 µL, 0.42 mmol, 3.0 equiv.) were added. The reaction was stirred at 40 °C for 18 h and the solvent was evaporated. The crude product was triturated with EtOAc and PE and filtrated to afford product **69** as a white solid (29 mg, 0.07 mmol, 50%). **IR (ATR)/cm^{-1}**: 3444, 3311, 3115, 2966, 1753, 1697; **^{1}H NMR** (400 MHz, $CDCl_3$): **δ** 8.17 (s, 1H), 7.29–7.25 (m, 2H), 6.90–6.96 (m, 2H), 5.26 (br s, 2H), 3.89 (s, 2H), 3.81 (s, 3H), 3.22 (br s, 6H); **^{13}C NMR** (100 MHz, $CDCl_3$): **δ** 170.2, 159.0, 150.6, 149.4, 142.5, 134.6, 130.7, 126.0, 114.3, 95.3, 55.5, 39.4; **LRMS (ES-APCI)**: *m/z* = 424.0 $[M+H]^+$; **HRMS**: found *m/z* = 424.0608, calculated for $C_{16}H_{19}Br_1N_5O_4$ *m/z* = 424.0615; **M.P.**: 151–152 °C

III. Amide analogues

1. **First set of compounds**

4-bromo-*N*-isopentyl-1*H*-pyrazole-3-carboxamide 71:

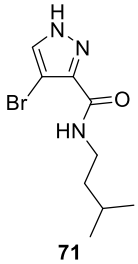

71

In a round bottom flask, acid **6** (135 mg, 0.71 mmol, 1.0 equiv.) was dissolved in CH_2Cl_2 (5 mL). HATU (270 mg, 0.71 mmol, 1.0 equiv.) was added followed by

Hünig's base (0.25 mL, 1.41 mmol, 2.0 equiv.). The reaction was left to stir for 5 min before addition of the amine (82 µL, 0.71 mmol, 1.0 equiv.). The reaction was left to stir at room temperature for 18 h. The solvent was evaporated before column chromatography with 60:40 PE:acetone eluent. This gave the desired compound as a white solid (85 mg, 0.37 mmol, 46%). **^{1}H NMR** (400 MHz, $CDCl_3$): **δ** 11.03 (br s, 1H), 7.73 (s, 1H), 6.97 (br t, 1H, *J* = 5.2 Hz), 3.53–3.48 (m, 2H), 1.75–1.65 (m, 1H), 1.56–1.51 (m, 2H), 0.96 (d, 6H, *J* = 6.4 Hz); **^{13}C NMR** (101 MHz, $CDCl_3$): **δ** 159.8, 138.2, 137.0, 93.0, 38.3, 38.1, 26.1, 22.6; **LRMS (ES-APCI)**: *m/z* = 260.0 $[M+H]^+$; **HRMS**: found *m/z* = 260.0393, calculated for $C_9H_{15}O_1N_3Br_1$ *m/z* = 260.0393

4-bromo-*N*^{3}-isopentyl-*N*^{1}-methyl-1*H*-pyrazole-1,3-dicarboxamide 73:

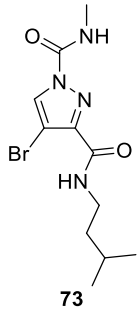

73

In a microwave vial, amide **71** (38 mg, 0.15 mmol, 1.0 equiv.) was dissolved in anhydrous MeCN (1.5 mL) before addition of **12** (75 mg, 0.60 mmol, 4.0 equiv.). Et_3N (84 µL, 0.60 mmol, 4.0 equiv.) was then added and the reaction left to stir for 24 h at 70 °C. The solvent was evaporated and the crude was purified by column chromatography with 70:30 PE:acetone eluent and further purified by vapour diffusion crystallization with MeOH and PE to give the desired compound **73** as a white solid (35 mg, 0.11 mmol, 73%). **^{1}H NMR** (400 MHz, $CDCl_3$): **δ** 8.29 (s, 1H), 7.00 (br s, 1H), 6.67 (br s, 1H), 3.50–3.44 (m, 2H), 3.06 (d, 3H, *J* = 4.8 Hz), 1.73–1.65 (m, 1H), 1.56–1.50 (m, 2H), 0.97 (d, 6H, *J* = 6.8 Hz) ; **^{13}C NMR** (101 MHz, $CDCl_3$): **δ** 160.0, 148.9, 145.0, 131.6, 97.1, 38.7, 38.1, 27.3, 26.2, 22.8; **LRMS (ES-APCI)**: *m/z* = 260.0 $[M+H-C_2H_4N_1O_1]^+$; **M.P.**: 103 °C

N^3-benzyl-4-bromo-N^1-methyl-1*H*-pyrazole-1,3-dicarboxamide 74:

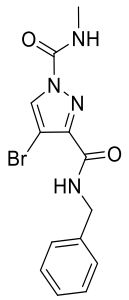

74

Carboxylic acid **6** (150 mg, 0.79 mmol, 1.0 equiv.) and HATU (300 mg, 0.79 mmol, 1.0 equiv.) were added to a vial and sealed. The reagents were dissolved in CH_2Cl_2 (5 mL) whereupon Hünig's base (0.27 mL, 1.57 mmol, 2.0 equiv.) was added and left to stir for 5 minutes. Benzylamine (86 µL, 0.79 mmol, 1.0 equiv.) was then added and the reaction left to stir over night at room temperature for 17 h. EtOAc (20 mL) was added and the organic washed with H_2O (2 × 20 mL) and brine (20 mL); The organic layer was dried over MgSO4, filtered and concentrated to get **72** which was used, as is, in the next step. **72** (70 mg, 0.25 mmol, 1.0 equiv.), was dissolved in anhydrous MeCN (2 mL) and **12** (63 mg, 0.50 mmol, 2.0 equiv.) following Et_3N (70 µL, 0.50 mmol, 2.0 equiv.) were added. The reaction was stirred at 70 °C for 22 h. The reaction was left to cool down before the solvent was evaporated *in vacuo*. The crude was purified by column chromatography with 80:20 PE:acetone eluent to afford product **74** as a translucent oil (45 mg, 0.13 mmol, 52%). **IR (ATR)/cm^{-1}**: 3296, 2921, 1727, 1660, 1511; **^{1}H NMR** (400 MHz, $CDCl_3$): **δ** 8.29 (s, 1H), 7.38 (app d, 4H, *J* = 4.0 Hz), 7.35–7.30 (m, 1H), 7.02 (br s, 1H), 6.97 (br s, 1H), 4.63 (d, 2H, *J* = 5.6 Hz), 3.02 (d, 2H, *J* = 5.2 Hz); **^{13}C NMR** (101 MHz, $CDCl_3$): **δ** 159.9, 148.8, 144.6, 138.0, 131.7, 129.1, 128.4, 128.1, 97.4, 43.7, 27.3; **LRMS (ES-APCI)**: *m/z* = 277.9 $[M-H-C_2H_1N_1O_1]^-$; **HRMS**: found *m/z* = 359.0105, calculated for $C_{13}H_{13}O_2N_4Br_1Na_1$ *m/z* = 359.0114

4-bromo-N^3-(cyclohexylmethyl)-N^1-methyl-1*H*-pyrazole-1,3-dicarboxamide 75:

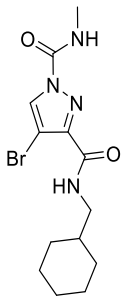

75

General procedure E.a. was followed acid **6** (50 mg, 0.26 mmol, 1.0 equiv.), HATU (100 mg, 0.26 mmol, 1.0 equiv.), Hünig's base (90 µL, 0.52 mmol, 2.0 equiv.) and cyclohexylmethylamine (34 µL, 0.26 mmol, 1.0 equiv.). Acylation was carried out with **12** (60 mg, 0.52 mmol, 2.0 equiv.) and Et_3N (73 µL, 0.52 mmol, 2.0 equiv.). The crude was purified by column chromatography with 80:20 PE:acetone to afford product **75** as a white solid (21 mg, 0.06 mmol, 23%). **IR (ATR)/cm^{-1}**: 3348, 2922, 1735, 1656; **^{1}H NMR** (400 MHz, $CDCl_3$): **δ** 8.50 (s, 1H), 7.19 (br s, 1H), 6.96 (br s, 1H), 3.50 (app t, 2H, *J* = 6.4 Hz), 3.26 (d, 3H, *J* = 5.2 Hz), 1.78 (app br t, 4H, *J* = 13.2 Hz), 1.71–1.66 (m, 1H), 1.64–1.58 (m, 1H), 1.32–1.16 (m, 3H), 1.06–0.96 (m, 2H); **^{13}C NMR** (101 MHz, $CDCl_3$): **δ** 160.1, 148.9, 145, 136.8, 131.6, 97.1, 46.0, 38.3, 27.3, 26.7, 26.1; **LRMS (ES-APCI)**: *m/z* = 365 $[M+Na]^+$; **HRMS**: found *m/z* = 343.0769, calculated for $C_{13}H_{20}O_2N_4Br_1$ *m/z* = 343.0764; **M.P.**: 132 °C

4-bromo-N^3-(2-methoxyethyl)-N^1-methyl-1*H*-pyrazole-1,3-dicarboxamide 76:

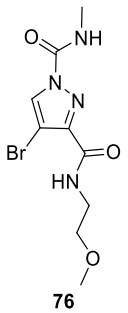

76

General procedure E.a. was followed with acid **6** (50 mg, 0.26 mmol, 1.0 equiv.), HATU (100 mg, 0.26 mmol, 1.0 equiv.), Hünig's base (90 µL, 0.52 mmol, 2.0 equiv.) and 2-methoxyethylamine (23 µL, 0.26 mmol, 1.0 equiv.). Acylation was carried out

with **12** (60 mg, 0.52 mmol, 2.0 equiv.) and Et_3N (73 µL, 0.52 mmol, 2.0 equiv.). The crude reaction mixture was purified by column chromatography with 80:20 PE:acetone as the eluent to afford **76** as a white solid (30 mg, 0.1 mmol, 38%). **IR (ATR)/cm^{-1}**: 3360, 2943, 1749, 1672; **^{1}H NMR** (400 MHz, $CDCl_3$): **δ** 8.29 (s, 1H), 7.09 (br s, 1H), 7.03 (br s, 1H), 3.67–3.63 (m, 2H), 3.60–3.56 (m, 2H), 3.41 (s, 3H), 3.06 (d, 3H, *J* = 5.2 Hz); **^{13}C NMR** (101 MHz, $CDCl_3$): **δ** 160.0, 148.8, 144.6, 131.5, 97.1, 71.3, 59.0, 39.2, 27.2; **LRMS (ES-APCI)**: *m/z* = 305.0 $[M+H]^+$; **HRMS**: found *m/z* = 305.0246, calculated for $C_9H_{14}O_3N_4Br_1$ *m/z* = 305.0244;

4-bromo-*N*^{3}-(2-(dimethylamino)ethyl)-*N*^{1}-methyl-1*H*-pyrazole-1,3-dicarboxamide 77:

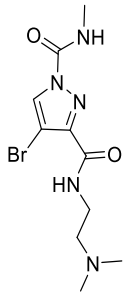

77

General procedure E.a. was followed acid **6** (50 mg, 0.26 mmol, 1.0 equiv.), HATU (100 mg, 0.26 mmol, 1.0 equiv.), Hünig's base (90 µL, 0.52 mmol, 2.0 equiv.) and dimethylethylamine (29 µL, 0.26 mmol, 1.0 equiv.). Acylation was carried out with **12** (60 mg, 0.52 mmol, 2.0 equiv.) and Et_3N (73 µL, 0.52 mmol, 2.0 equiv.). The crude material was purified by semiprep HPLC and afforded amide **77** as a light pink solid (10 mg, 0.03 mmol, 12%). **IR (ATR)/cm^{-1}**: 3390, 2924, 1730, 1672; **^{1}H NMR** (400 MHz, $CDCl_3$): **δ** 8.66 (br s, 1H), 8.24 (s, 1H), 7.93 (br s, 1H), 3.78 (dd, 2H, *J* = 10.8, 5.6 Hz), 3.11 (app br t, 2H, *J* = 5.6 Hz), 3.04 (d, 3H, *J* = 4.8 Hz), 2.71 (s, 6H); **^{13}C NMR** (101 MHz, $CDCl_3$): **δ** 161.0, 149.2, 143.3, 131.1, 97.0, 57.9, 44.0, 35.1, 27.2; **LRMS (ES-APCI)**: *m/z* = 318.0 $[M+H]^+$; **HRMS**: found *m/z* = 318.0566, calculated for $C_{10}H_{17}O_2N_5Br_1$ *m/z* = 318.0560, **M.P.**: 108 °C

4-bromo-N^1,N^3-dimethyl-1*H*-pyrazole-1,3-dicarboxamide 78:

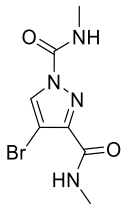

78

General procedure E.b. was followed with acid **6** (50 mg, 0.26 mmol, 1.0 equiv.), HATU (100 mg, 0.26 mmol, 1.0 equiv.), Hünig's base (90 µL, 0.52 mmol, 2.0 equiv.) and methylamine in THF at 2.0 M (0.2 ml, 0.39 mmol, 1.5 equiv.). Acylation was carried out with **12** (120 mg, 1.04 mmol, 4.0 equiv.) and Et_3N (0.14 mL, 1.04 mmol, 4.0 equiv.). The crude material was purified by column chromatography with 70:30 PE:acetone as the eluent. Desired product **78** was isolated as a white solid (35 mg, 0.13 mmol, 50%). **IR (ATR)/cm^{-1}**: 3294, 2926, 1714, 1656; **^{1}H NMR** (400 MHz, $CDCl_3$): **δ** 8.30 (s, 1H), 7.00 (br s, 1H), 6.72 (br s, 1H), 3.05 (d, 3H, *J* = 4.8 Hz), 3.02 (d, 3H, *J* = 5.2 Hz); **^{13}C NMR** (101 MHz, $CDCl_3$): **δ** 160.8, 148.9, 144.8, 131.5, 96.9, 27.3, 26.3; **LRMS (ES-APCI)**: *m/z* = 260.8 $[M+H]^+$; **HRMS**: found *m/z* = 282.9805, calculated for $C_7H_9O_2N_4Br_1Na_1$ *m/z* = 282.9801; **M.P.**: 131 °C

4-bromo-N^3-isopropyl-N^1-methyl-1*H*-pyrazole-1,3-dicarboxamide 79:

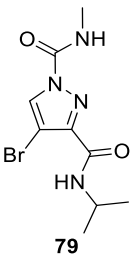

79

General procedure E.c. was followed with acid **6** (50 mg, 0.26 mmol, 1.0 equiv.), HATU (100 mg, 0.26 mmol, 1.0 equiv.), Hünig's base (90 µL, 0.52 mmol, 2.0 equiv.) and isopropylamine (22 µL, 0.26 mmol, 1.0 equiv.). Acylation was carried out with **12** (120 mg, 1.04 mmol, 4.0 equiv.) and Et_3N (0.14 mL, 1.04 mmol, 4.0 equiv.). The crude reaction mixture was purified by column chromatography with 80:20 PE:acetone eluent to give **79** as a white solid (60 mg, 0.21 mmol, 81%). **IR (ATR)/cm^{-1}**: 3336,

3126, 2974, 1737, 1651, 1544; **^{1}H NMR** (400 MHz, $CDCl_3$): **δ** 8.27 (s, 1H), 7.09 (br s, 1H), 6.58 (br d, 1H, *J* = 6.4 Hz), 4.30–4.22 (m, 1H), 3.04 (d, 3H, *J* = 6.8 Hz), 1.26 (d, 6H, *J* = 6.8 Hz); **^{13}C NMR** (101 MHz, $CDCl_3$): **δ** 159.1, 148.9, 144.8, 131.5, 96.9, 41.7, 27.2, 22.9; **LRMS (ES-APCI)**: *m/z* = 289.0 $[M+H]^+$; **HRMS**: found *m/z* = 311.0114, calculated for $C_9H_{13}O_2N_4Br_1Na_1$ *m/z* = 311.0114; **M.P.**: 148 °C

4-bromo-*N*^{3}-ethyl-*N*^{1}-methyl-1*H*-pyrazole-1,3-dicarboxamide 80:

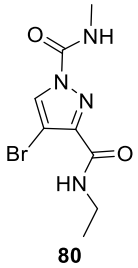

80

General procedure E.c. was followed with acid **6** (50 mg, 0.26 mmol, 1.0 equiv.), HATU (100 mg, 0.26 mmol, 1.0 equiv.), Hünig's base (90 µL, 0.52 mmol, 2.0 equiv.) and ethylamine hydrochloride (21 mg, 0.26 mmol, 1.0 equiv.). Acylation was carried out with **12** (120 mg, 1.04 mmol, 4.0 equiv.) and Et_3N (0.14 mL, 1.04 mmol, 4.0 equiv.). The crude reaction mixture was purified by column chromatography with 80:20 PE:acetone to afford **80** as a white solid (15 mg, 0.05 mmol, 19%). **IR (ATR)/cm^{-1}**: 3277, 2970, 1718, 1651, 1552, 1251; **^{1}H NMR** (400 MHz, $CDCl_3$): **δ** 8.28 (s, 1H), 7.08 (br s, 1H), 6.75 (br s, 1H), 3.51–3.41 (m, 2H), 3.03 (d, 3H, *J* = 5.2 Hz), 1.25 (t, 3H, *J* = 7.2 Hz); **^{13}C NMR** (101 MHz, $CDCl_3$): **δ** 159.9, 148.8, 144.8, 131.5, 96.9, 34.5, 27.2, 15.0; **LRMS (ES-APCI)**: *m/z* = 218.0 $[M+H-C_2H_3O_1N_1]^+$; **HRMS**: found *m/z* = 275.0137, calculated for $C_8H_{12}O_2N_4Br_1$ *m/z* = 275.0138; **M.P.**: 132 °C

4-bromo-N^3-isobutyl-N^1-methyl-1*H*-pyrazole-1,3-dicarboxamide 81:

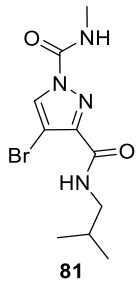

81

General procedure E.c. was followed with acid **6** (50 mg, 0.26 mmol, 1.0 equiv.), HATU (100 mg, 0.26 mmol, 1.0 equiv.), Hünig's base (90 µL, 0.52 mmol, 2.0 equiv.) and isobutylamine (26 µL, 0.26 mmol, 1.0 equiv.). Acylation was carried out with **12** (120 mg, 1.04 mmol, 4.0 equiv.) and Et_3N (0.14 mL, 1.04 mmol, 4.0 equiv.). The crude reaction mixture was purified by column chromatography with 80:20 PE:acetone to afford **81** as a white solid (18 mg, 0.06 mmol, 23%). **IR (ATR)/cm^{-1}**: 3323, 3130, 2958, 1743, 1653, 1556; **^{1}H NMR** (400 MHz, $CDCl_3$): **δ** 8.29 (s, 1H), 7.07 (br s, 1H), 6.80 (br s, 1H), 3.27 (app t, 2H, *J* = 6.4 Hz), 3.04 (d, 3H, *J* = 5.2 Hz), 1.95–1.85 (m, 1H), 0.98 (d, 6H, *J* = 6.8 Hz); **^{13}C NMR** (101 MHz, $CDCl_3$): **δ** 160.0, 148.8, 144.9, 131.5, 96.9, 46.9, 28.8, 27.2, 20.4; **LRMS (ES-APCI)**: *m/z*: 303.0 $[M+H]^+$; **HRMS**: found *m/z* = 325.0268, calculated for $C_{10}H_{15}O_2N_4Br_1Na_1$ *m/z* = 325.0271; **M.P.**: 137 °C

4-bromo-*N*-methyl-3-(morpholine-4-carbonyl)-1*H*-pyrazole-1-carboxamide 82:

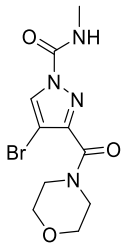

82

General procedure E.b. was followed with acid **6** (50 mg, 0.26 mmol, 1.0 equiv.), HATU (100 mg, 0.26 mmol, 1.0 equiv.), Hünig's base (90 µL, 0.52 mmol, 2.0 equiv.) and morpholine (23 µL, 0.26 mmol, 1.0 equiv.). Acylation was carried out with **12** (120 mg, 1.04 mmol, 4.0 equiv.) and Et_3N (0.14 mL, 1.04 mmol, 4.0 equiv.). The crude was purified by column chromatography with 70:30 PE:acetone as the eluent. The

product **82** was isolated as a white solid (40 mg, 0.13 mmol, 48%). **IR (ATR)/cm^{-1}**: 1745, 1625, 1109; **^{1}H NMR** (400 MHz, $CDCl_3$): **δ** 8.28, (s, 1H), 7.00 (br s, 1H), 3.84–3.78 (m, 4H), 3.71 (app br t, 2H, *J* = 4.8 Hz), 3.47 (app br t, 2H, *J* = 4.8 Hz), 3.02 (d, 3H, *J* = 5.2 Hz); **^{13}C NMR** (101 MHz, $CDCl_3$): **δ** 161.1, 149.0, 147.5, 130.2, 96.4, 67.3, 67.0, 47.7, 42.8, 27.3; **LRMS (ES-APCI)**: *m/z* = 317.0 $[M+H]^+$; **HRMS**: found *m/z* = 339.0061, calculated for $C_{10}H_{13}O_3N_4Br_1Na_1$ *m/z* = 339.0063; **M.P.**: 150 °C

4-bromo-*N*^{3}-cyclohexyl-*N*^{1}-methyl-1*H*-pyrazole-1,3-dicarboxamide 83:

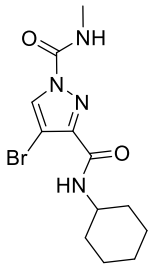

83

General procedure E.b. was followed acid **6** (50 mg, 0.26 mmol, 1.0 equiv.), HATU (100 mg, 0.26 mmol, 1.0 equiv.), Hünig's base (90 µL, 0.52 mmol, 2.0 equiv.) and cyclohexylamine (30 µL, 0.26 mmol, 1.0 equiv.). Acylation was carried out with **12** (120 mg, 1.04 mmol, 4.0 equiv.) and Et_3N (0.14 mL, 1.04 mmol, 4.0 equiv.). The crude material was purified by column chromatography with 90:10 PE:acetone eluent followed by trituration with chloroform and PE to afford **83** as a white solid (50 mg, 0.15 mmol, 58%). **IR (ATR)/cm^{-1}**: 3348, 2926, 1730, 1646; **^{1}H NMR** (400 MHz, $CDCl_3$): **δ** 8.29 (s, 1H), 7.01 (br s, 1H), 6.58 (br d, 1H, *J* = 7.2 Hz), 4.03–3.93 (m, 1H), 3.06 (d, 3H, *J* = 5.2 Hz), 2.04–2.01 (m, 2H), 1.78–1.75 (m, 2H), 1.68–1.61 (m, 1H), 1.48–1.39 (m, 2H), 1.32–1.21 (m, 3H); **^{13}C NMR** (101 MHz, $CDCl_3$): **δ** 159.0, 148.9, 145.0, 131.5, 97.0, 48.5, 33.2, 27.2, 25.8, 25.0; **LRMS (ES-APCI)**: *m/z* = 329.0 $[M+H]^+$; **HRMS**: found *m/z* = 329.0610, calculated for $C_{12}H_{18}O_2N_4Br_1$ *m/z* = 329.0608, **M.P.**: 128 °C

4-bromo-N^1-methyl-N^3-phenyl-1*H*-pyrazole-1,3-dicarboxamide 84:

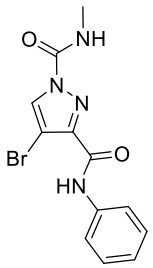

84

General procedure E.c. was followed with acid **6** (50 mg, 0.26 mmol, 1.0 equiv.), HATU (100 mg, 0.26 mmol, 1.0 equiv.), Hünig's base (90 µL, 0.52 mmol, 2.0 equiv.) and aniline (24 µL, 0.26 mmol 1.0 equiv.). Acylation was carried out with **12** (120 mg, 1.04 mmol, 4.0 equiv.) and Et_3N (0.14 mL, 1.04 mmol, 4.0 equiv.). The crude material was purified by column chromatography with 80:20 PE:acetone eluent to afford **84** as a white solid (25 mg, 0.08 mmol, 31%). **IR (ATR)/cm^{-1}**: 3442, 3319, 1730; **^{1}H NMR** (400 MHz, $CDCl_3$): **δ** 8.54 (br s, 1H), 8.30 (s, 1H), 7.64 (dd, 2H, *J* = 1.2, 8.8 Hz), 7.36–7.32 (m, 2H), 7.17–7.12 (m, 1H), 7.11 (br d, 1H, *J* = 4 Hz), 3.05 (d, 3H, *J* = 5.2 Hz) ; **^{13}C NMR** (101 MHz, $CDCl_3$): **δ** 157.8, 148.7, 144.5, 137.3, 132.1, 129.4, 125.1, 120.1, 97.6, 27.3; **LRMS (ES-APCI)**: *m/z* = 322.9 $[M+H]^+$; **HRMS**: found *m/z* = 323.0143, calculated for $C_{12}H_{12}O_2N_4Br_1$ *m/z* = 323.0138, **M.P.**: 160 °C

2. **SAR of analogue 84**

   a. **Part A**

4-bromo-N^1-ethyl-N^3-phenyl-1*H*-pyrazole-1,3-dicarboxamide 85 :

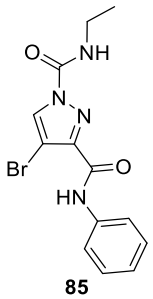

85

General procedure E.d. was followed with acid **6** (50 mg, 0.26 mmol, 1.0 equiv.), HATU (100 mg, 0.26 mmol, 1.0 equiv.), Hünig's base (90 µL, 0.52 mmol, 2.0 equiv.)

and aniline (24 µL, 0.26 mmol, 1.0 equiv.). Acylation was carried out with ethylisocyanate (25 µL, 0.31 mmol, 1.2 equiv.) and Et_3N (43 µL, 0.31 mmol, 1.2 equiv.). The crude reaction mixture was purified by column chromatography with 90:10 PE:acetone eluent to give **85** as a white solid (50 mg, 0.15 mmol, 58%). **IR (ATR)/cm^{-1}**: 3506, 2981, 1727, 1676, 1518, 1235; **^{1}H NMR** (400 MHz, $CDCl_3$): **δ** 8.53 (br s, 1H), 8.32 (s, 1H), 7.66 (dd, 2H, *J* = 8.8, 1.2 Hz), 7.35–7.33 (m, 2H), 7.17−7.13 (m, 1H), 7.11 (br t, 1H, *J* = 6.0 Hz), 3.51 (dq, 2H, *J* = 7.2, 6.0 Hz), 1.31 (t, 3H, *J* = 7.2 Hz); **^{13}C NMR** (101 MHz, $CDCl_3$): **δ** 158.0, 148.1, 144.5, 137.4, 132.1, 129.4, 125.1, 120.3, 97.6, 36.1, 15.1; **LRMS (ES-APCI)**: *m/z* = 383.0 $[M+H]^+$; **HRMS**: found *m/z* = 359.0114, calculated for $C_{13}H_{13}O_2N_4Br_1Na_1$ *m/z* = 359.0114; **M.P.**: 132 °C

4-bromo-*N*^{1}-isopropyl-*N*^{3}-phenyl-1*H*-pyrazole-1,3-dicarboxamide 86:

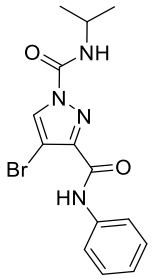

86

General procedure E.d. was followed with acid **6** (50 mg, 0.26 mmol, 1.0 equiv.), HATU (100 mg, 0.26 mmol, 1.0 equiv.), Hünig's base (90 µL, 0.52 mmol, 2.0 equiv.) and aniline (24 µL, 0.26 mmol, 1.0 equiv.). Acylation was carried out with isopropylisocyanate (31 µL, 0.31 mmol, 1.2 equiv.) and Et_3N (43 µL, 0.31 mmol, 1.2 equiv.). The crude reaction mixture was purified by column chromatography with 90:10 PE:acetone eluent to give **86** as a white solid (36 mg, 0.10 mmol, 38%). **IR (ATR)/cm^{-1}**: 3552, 3254, 2970, 1730, 1676, 1529, 1235; **^{1}H NMR** (400 MHz, $CDCl_3$): **δ** 8.48 (br s, 1H), 8.33 (s, 1H), 7.68 (dd, 2H, *J* = 8.4, 1.2 Hz), 7.39–7.34 (m, 2H), 7.19–7.15 (m, 1H), 6.85 (br d, 1H, *J* = 7.6 Hz), 4.21–4.12 (m, 1H), 1.35 (d, 6H, *J* = 6.8 Hz); **^{13}C NMR** (101 MHz, $CDCl_3$): **δ** 157.8, 147.2, 144.5, 137.3, 132.1, 129.3, 120.3, 97.5, 43.8, 22.8; **LRMS (ES-APCI)**: *m/z* = 265.9 $[M+H-C_4H_7N_1O_1]^+$; **HRMS**: found *m/z* = 351.0456, calculated for $C_{14}H_{16}O_2N_4Br_1$ *m/z* = 351.0451; **M.P.**: 122 °C

4-bromo-N^3-phenyl-N^1-propyl-1*H*-pyrazole-1,3-dicarboxamide 87:

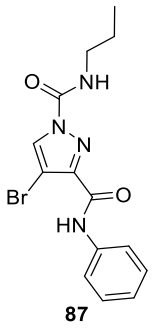

87

General procedure E.d. was followed with acid **6** (50 mg, 0.26 mmol, 1.0 equiv.), HATU (100 mg, 0.26 mmol, 1.0 equiv.), Hünig's base (90 µL, 0.52 mmol, 2.0 equiv.) and aniline (24 µL, 0.26 mmol, 1.0 equiv.). Acylation was carried out with propylisocyanate (30 µL, 0.31 mmol, 1.2 equiv.) and Et_3N (43 µL, 0.31 mmol, 1.2 equiv.). The crude was purified by column chromatography with 90:10 PE:acetone eluent followed by trituration with EtOAc and PE to give **87** as a white solid (20 mg, 0.06 mmol, 23%). **IR (ATR)/cm^{-1}**: 3335, 1744, 1504, 1188; **^{1}H NMR** (400 MHz, DMSO- d_6): **δ** 10.26 (br s, 1H), 8.74 (br s, 1H), 8.66 (s, 1H), 7.72 (br app d, 2H, J = 7.6 Hz), 7.39 (app t, 2H, J = 7.6 Hz), 7.14 (app t, 1H, J = 7.2 Hz), 3.26 (app q , 2H, J = 6.4 Hz), 1.59 (app q , 2H, J = 7.2 Hz), 0.91−0.89 (m, 3H); **^{13}C NMR** (101 MHz, DMSO-d_6): **δ** 158.3, 148.1, 144.7, 138.1, 131.4, 128.9, 124.2, 120.0, 96.8, 41.8, 22.3, 11.2; **LRMS (ES-APCI)**: m/z = 266.0 $[M–C_4H_7N_1O_1+H]^+$; **HRMS**: found m/z = 351.0458, calculated for $C_{14}H_{16}O_2N_4Br_1$ m/z = 351.0457; **M.P.**: 132 °C

4-bromo-N^1-butyl-N^3-phenyl-1*H*-pyrazole-1,3-dicarboxamide 88:

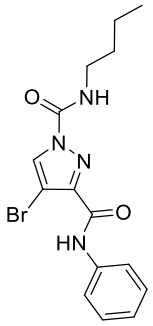

88

General procedure E.d. was followed with acid **6** (50 mg, 0.26 mmol, 1.0 equiv.), HATU (100 mg, 0.26 mmol, 1.0 equiv.), Hünig's base (90 µL, 0.52 mmol, 2.0 equiv.) and aniline (24 µL, 0.26 mmol, 1.0 equiv.). Acylation was carried out with butylisocyanate (35 µL, 0.31 mmol, 1.2 equiv.) and Et_3N (43 µL, 0.31 mmol, 1.2 equiv.). The crude was purified by flash chromatography with 85:25 PE:acetone eluent followed by trituration with chloroform and PE to give **88** as a white solid (43 mg, 0.12 mmol, 46%). **IR (ATR)/cm^{-1}**: 2972, 1745, 1535; **^{1}H NMR** (400 MHz, $CDCl_3$): **δ** 8.49 (br s, 1H), 8.34 (s, 1H), 7.59 (dd, 2H, *J* = 8.4, 1.2 Hz), 7.40–7.35 (m, 2H), 7.19–7.15 (m, 1H), 7.06 (app t, 1H, *J* = 5.2 Hz), 3.50–3.45 (m, 2H), 1.71–1.61 (m, 2H), 1.49–1.40 (m, 2H), 0.99 (t, 3H, *J* = 7.2 Hz); **^{13}C NMR** (101 MHz, $CDCl_3$): **δ** 157.8, 148.1, 144.5, 137.3, 132.1, 129.3, 125.1, 120.2, 97.6, 40.8, 31.8, 20.2, 13.9; **LRMS (ES-APCI)**: *m/z* = 266.0 $[M–C_5H_9N_1O_1+H]^+$; **HRMS**: found *m/z* = 365.0613, calculated for $C_{15}H_{18}O_2N_4Br_1$ *m/z* = 365.0608; **M.P.**: 119 °C

4-bromo-1-(butylcarbamothioyl)-*N*-phenyl-1*H*-pyrazole-3-carboxamide 89:

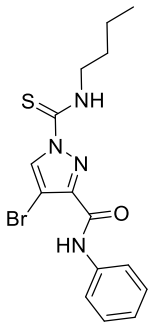

89

General procedure E.d. was followed with acid **6** (50 mg, 0.26 mmol, 1.0 equiv.), HATU (100 mg, 0.26 mmol, 1.0 equiv.), Hünig's base (90 µL, 0.52 mmol, 2.0 equiv.) and aniline (24 µL, 0.26 mmol, 1.0 equiv.). Acylation was carried out with butylisocyanate (30 µL, 0.31 mmol, 1.2 equiv.) and Et_3N (43 µL, 0.31 mmol, 1.2 equiv.). The crude reaction mixture was purified by column chromatography with a gradient eluent from 90:10 to 80:20 PE:acetone to afford **89** as a white solid (27 mg, 0.08 mmol, 31%). **IR (ATR)/cm^{-1}**: 3334, 3266, 1663, 1537, 1194; **^{1}H NMR** (400 MHz, $CDCl_3$): **δ** 8.81 (br s, 1H), 8.79 (s, 1H), 8.48 (br s, 1H), 7.67 (app dd, 2H, *J* = 8.4, 0.8 Hz), 7.40−7.35 (m, 2H), 7.20−7.16 (m, 1H), 3.82−3.77 (m, 2H), 1.82−1.74 (m, 2H), 1.52−1.43 (m, 2H), 1.01 (t, 3H, *J* = 7.2 Hz); **^{13}C NMR** (101 MHz, $CDCl_3$): **δ** 173.7, 167.8, 144.3, 137.2, 134.2, 129.4, 125.2, 120.3, 98.0, 45.9, 30.4, 20.4, 13.9; **LRMS (ES-APCI)**: *m/z* = 264.0 $[M–C_5H_9S_1O_1+H]^-$; **HRMS**: found *m/z* = 381.0382, calculated for $C_{15}H_{18}O_1N_2S_1Br_1$ *m/z* = 381.0379; **M.P.**: 150 °C

4-bromo-N^1,N^3-diphenyl-1*H*-pyrazole-1,3-dicarboxamide 90:

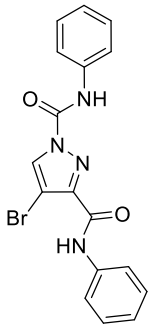

90

General procedure E.e. was followed with acid **6** (50 mg, 0.26 mmol, 1.0 equiv.), HATU (100 mg, 0.26 mmol, 1.0 equiv.), Hünig's base (90 µL, 0.52 mmol, 2.0 equiv.) and aniline (24 µL, 0.26 mmol, 1.0 equiv.). Acylation was carried out with phenylisocyanate (85 µL, 0.78 mmol, 3.0 equiv.) and Et_3N (0.11 mL, 0.31 mmol, 3.0 equiv.). The crude reaction mixture was purified by column chromatography with 90:10 PE:acetone eluent and further triturated with chloroform and PE to give **90** as a white solid (15 mg, 0.04 mmol, 15%). **IR (ATR)/cm^{-1}**: 3359, 3277, 3132, 1749, 1662, 1526, 1197; **^{1}H NMR** (400 MHz, $CDCl_3$): **δ** 8.84 (br s, 1H), 8.51 (br s, 1H), 8.43 (s, 1H), 7.70 (dd, 2H, *J* = 8.8, 1.2 Hz), 7.64 (dd, 2H, *J* = 8.4, 0.8 Hz), 7.45–7.42 (m, 2H), 7.42–7.36 (m, 2H),7.27–7.23 (m, 1H), 7.21–7.17 (m, 1H); **^{13}C NMR** (101 MHz, $CDCl_3$): **δ** 157.6, 145.3, 137.2, 135.8, 132.2, 129.6, 129.4, 125.9, 125.2, 120.4*, 120.4*, 120.3*, 98.3, *3 distinct peaks; **LRMS (ES-APCI)**: *m/z* = 264.0 $[M-H-C_7H_5N_1O_1]^-$; **HRMS**: found *m/z* = 385.0295, calculated for $C_{17}H_{14}O_2N_4Br_1$ *m/z* = 385.0295; **M.P.**: 167 °C

4-bromo-N^1-cyclohexyl-N^3-phenyl-1*H*-pyrazole-1,3-dicarboxamide 91:

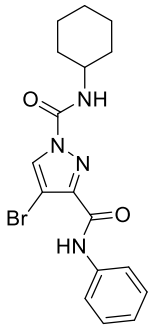

91

General procedure E.e. was followed with acid **6** (50 mg, 0.26 mmol, 1.0 equiv.), HATU (100 mg, 0.26 mmol, 1.0 equiv.), Hünig's base (90 µL, 0.52 mmol, 2.0 equiv.) and aniline (24 µL, 0.26 mmol, 1.0 equiv.). Acylation was carried out with cyclohexylisocyanate (66 µL, 0.52 mmol, 2.0 equiv.) and Et_3N (72 µL, 0.52 mmol, 2.0 equiv.). The crude reaction mixture was purified by column chromatography with 90:10 PE:Ace eluent and further triturated with chloroform and PE to give **91** as a white solid (25 mg, 0.06 mmol, 23%). **IR (ATR)/cm^{-1}**: 3307, 3157, 2932, 1740, 1662, 1524, 1219; **^{1}H NMR** (400 MHz, $CDCl_3$): **δ** 8.48 (br s, 1H), 8.34 (s, 1H), 7.69 (dd, 2H, *J* = 8.8, 1.2 Hz), 7.39–7.35 (m, 2H), 7.19–7.15 (m, 1H), 6.88 (br d, 1H, *J* = 8.0 Hz), 3.87–3.78 (m, 1H), 2.09–2.06 (m, 2H), 1.84–1.80 (m, 2H), 1.71–1.64 (m, 1H), 1.49–1.32 (m, 4H), 1.27–1.18 (m, 1H); **^{13}C NMR** (101 MHz, $CDCl_3$): **δ** 157.9, 147.2, 144.5, 137.3, 132.1, 129.3, 125.1, 120.3, 97.5, 50.9, 33.2, 25.9, 25.1; **LRMS (ES-APCI)**: *m/z* = 412.9 $[M+Na]^+$; **HRMS**: found *m/z* = 391.0766, calculated for $C_{17}H_{20}O_2N_4Br_1$ *m/z* = 391.0764; **M.P.**: 156 °C

N^1-allyl-4-bromo-N^3-phenyl-1*H*-pyrazole-1,3-dicarboxamide 92:

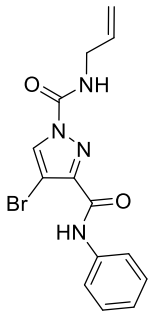

92

General procedure E.e. was followed with acid **6** (50 mg, 0.26 mmol, 1.0 equiv.), HATU (100 mg, 0.26 mmol, 1.0 equiv.), Hünig's base (90 µL, 0.52 mmol, 2.0 equiv.) and aniline (24 µL, 0.26 mmol, 1.0 equiv.). Acylation was carried out with allylisocyanate (46 µL, 0.52 mmol, 2.0 equiv.) and Et_3N (72 µL, 0.52 mmol, 2.0 equiv.). The crude reaction mixture was purified by column chromatography with 90:10 PE:acetone eluent (56 mg) and further triturated with chloroform and PE to give **92** as a white solid (11 mg, 0.03 mmol, 12%). **IR (ATR)/cm^{-1}**: 3352, 3322, 3132, 1740, 1675, 1539, 1504, 1188; **^{1}H NMR** (400 MHz, $CDCl_3$): **δ** 8.48 (br s, 1H), 8.36 (s, 1H), 7.69 (d, 1H, *J* = 7.6 Hz), 7.38 (t, 1H, *J* = 7.6 Hz), 7.17 (t, 1H, *J* = 7.6 Hz), 7.15 (br s, 1H), 5.99–5.90 (m, 1H), 4.12–4.09 (m, 2H); **^{13}C NMR** (101 MHz, $CDCl_3$): **δ** 157.7, 148.0, 144.7, 137.3, 132.9, 132.2, 129.4, 125.1, 120.2, 118.2, 97.8, 43.3; **LRMS (ES-APCI)**: *m/z* = 412.9 $[M+H-C_2H_4NO]^+$; **HRMS**: found *m/z* = 349.0300, calculated for $C_{14}H_{14}O_2N_4Br_1$ *m/z* = 349.0295; **M.P.**: 132 °C

4-bromo-N^1,N^1-dimethyl-N^3-phenyl-1*H*-pyrazole-1,3-dicarboxamide 93:

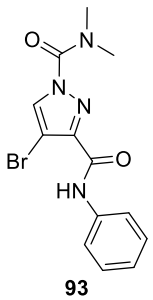

93

General procedure E was followed with acid **6** (50 mg, 0.26 mmol, 1.0 equiv.), HATU (100 mg, 0.26 mmol, 1.0 equiv.), Hünig's base (90 µL, 0.52 mmol, 2.0 equiv.)

and aniline (24 µL, 0.26 mmol, 1.0 equiv.). Dimethylcarbamoyl chloride (0.11 mL, 0.78 mmol, 3.0 equiv.) was then added followed by Et_3N (72 µL, 0.78 mmol, 3.0 equiv.) and stirred for 24 h at room temperature. EtOAc (15 mL) was added and the organic layer was washed with H_2O (2 × 5 mL) and brine (5 mL). The organics were dried under $MgSO_4$, filtered and concentrated to afford the crude product. It was then purified by flash chromatography with 90:10 PE:acetone to give **93** as an off-white solid (64 mg, 0.19 mmol, 73%). **IR (ATR)/cm^{-1}**: 3043, 2924, 1781, 1104; **^{1}H NMR** (400 MHz, $CDCl_3$): **δ** 8.52 (br s, 1H), 8.18 (s, 1H), 7.67 (dd, 2H, *J* = 8.4, 0.8 Hz), 7.40–7.35 (m, 2H), 7.17–7.14 (m, 1H), 3.26 (br s, 6H); **^{13}C NMR** (101 MHz, DMSO-d_6): **δ** 158.6, 150.4, 144.5, 138.3, 134.1, 128.7, 124.1, 120.4, 95.0, 37.9; **LRMS (ES-APCI)**: *m/z* = 263.9 $[M-H-C_3H_5N_1O_1]^-$; **HRMS**: found *m/z* = 337.0298, calculated for $C_{13}H_{14}O_2N_4Br_1$ *m/z* = 337.0295; **M.P.**: 112 °C

b. **Part B**

- Importance of amide NH

phenyl 4-bromo-1-(methylcarbamoyl)-1*H*-pyrazole-3-carboxylate 94:

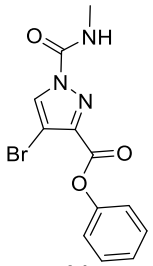

94

In a round bottom flask, acid **6** (150 mg, 0.79 mmol, 1.0 equiv.) was treated with thionyl chloride (4 mL, 0.2 M) and stirred at 90 °C for 3 hours. The solvent was evaporated and the crude material was dissolved in anhydrous CH_2Cl_2 (5 mL). Phenol (112 mg, 1.19 mmol, 1.5 equiv.) was added followed by Et_3N (0.17 mL, 1.19 mmol, 1.5 equiv.) and stirred at room temperature for 17 hours. No starting material was observed by LC/MS and compound **12** (395 mg, 3.16 mmol, 4.0 equiv.) was added with Et_3N (0.44 mL, 3.16 mmol, 4.0 equiv.) and stirred for 48 hours at room temperature. EtOAc (15 mL) was added and the organic layer was washed with H_2O (10 mL), saturated $NaHCO_3$ (10 mL), H_2O (10 mL) and brine (10 mL). The organic layer was dried over $MgSO_4$, filtered and concentrated. The crude product was purified

by column chromatography 90:10 PE:acetone and further recrystallized in EtOAc to afford ester **94** as a white solid (50 mg, 0.15 mmol, 19%). **IR (ATR)/cm^{-1}**: 3390, 1747, 1712, 1515, 1108; **^{1}H NMR** (400 MHz, $CDCl_3$): **δ** 8.39 (s, 1H), 7.47–7.42 (m, 2H), 7.33–7.29 (m, 1H), 7.28 (app d, 1H, *J* = 1.2 Hz), 7.26 (app t, 1H, *J* = 1.2 Hz), 7.23 (br s, 1H), 3.06 (d, 3H, *J* = 4.8 Hz); **^{13}C NMR** (101 MHz, $CDCl_3$): **δ** 158.4, 150.3, 148.7, 142.3, 131.6, 129.8, 126.6, 121.7, 99.3, 27.3; **LRMS (ES-APCI)**: *m/z* = 265.0 $[M-H-C_2H_3NO]^-$; **HRMS**: found *m/z* = 341.0248, calculated for $C_{12}H_{14}O_3N_4Br_1$ *m/z* = 341.0244; **M.P.**: 132 °C

4-bromo-*N*^{1},*N*^{3}-dimethyl-*N*^{3}-phenyl-1*H*-pyrazole-1,3-dicarboxamide 95:

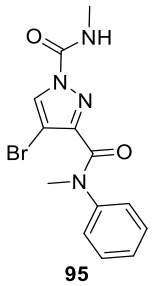

95

General procedure E.c. was followed with acid **6** (50 mg, 0.26 mmol, 1.0 equiv.), HATU (100 mg, 0.26 mmol, 1.0 equiv.), Hünig's base (90 µL, 0.52 mmol, 2.0 equiv.) and *N*-methylaniline (28 µL, 0.26 mmol, 1.0 equiv.). Acylation was carried out with **12** (120 mg, 1.04 mmol, 4.0 equiv.) and Et_3N (0.14 mL, 1.04 mmol, 4.0 equiv.). The crude reaction mixture was purified by column chromatography with 80:20 PE:acetone eluent to give **95** as a white solid (11 mg, 0.03 mmol, 12%). **IR (ATR)/cm^{-1}**: 3257, 3144, 2939, 1732, 1640, 1245; **^{13}C NMR** (101 MHz, $CDCl_3$): **δ** 162.0, 149.0, 148.1, 129.9, 129.2, 127.5, 127.1, 96.5, 37.8, 27.0; **LRMS (ES-APCI)**: *m/z* = 337.0 $[M+H]^+$; **HRMS**: found *m/z* = 337.0298, calculated for $C_{13}H_{14}O_2N_4Br_1$ *m/z* = 337.0295; **M.P.**: 72 °C

- Pyridine amides

4-bromo-*N*^{1}-methyl-*N*^{3}-(pyridin-4-yl)-1*H*-pyrazole-1,3-dicarboxamide 96:

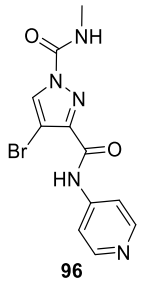

96

General procedure E.c. was followed with acid **6** (50 mg, 0.26 mmol, 1.0 equiv.), HATU (100 mg, 0.26 mmol, 1.0 equiv.), Hünig's base (90 μL, 0.52 mmol, 2.0 equiv.) and 4-aminopyridine (24 mg, 0.26 mmol, 1.0 equiv.). Acylation was carried out with **12** (120 mg, 1.04 mmol, 4.0 equiv.) and Et_3N (0.14 mL, 1.04 mmol, 4.0 equiv.). The crude reaction mixture was purified by column chromatography with 70:30 PE:acetone to give **96** as a white solid (15 mg, 0.05 mmol, 19%). **IR (ATR)/cm^{-1}**: 2994, 1707, 1509; **^{1}H NMR** (400 MHz, $CDCl_3$): **δ** 8.58 (dd, 2H, *J* = 4.8, 1.6 Hz), 8.55 (br s, 1H), 8.38 (s, 1H), 7.62 (dd, 2H, *J* = 4.8, 1.6 Hz), 7.01 (br s, 1H), 3.12 (d, 3H, *J* = 4.8 Hz); **^{13}C NMR** (101 MHz, DMSO-*d*$_6$): **δ** 159.1, 150.4, 148.4, 145.0, 143.9, 131.7, 113.8, 96.0, 26.8; **LRMS (ES-APCI)**: *m/z* = 323.9 $[M+H]^+$; **HRMS**: found *m/z* = 324.0096, calculated for $C_{11}H_{11}O_2N_5Br_1$ *m/z* = 324.0091; **M.P.**: 235 °C (decomp)

4-bromo-*N*^{1}-methyl-*N*^{3}-(pyridin-3-yl)-1*H*-pyrazole-1,3-dicarboxamide 97:

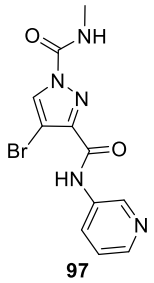

97

General procedure E.c. was followed with acid **6** (50 mg, 0.26 mmol, 1.0 equiv.), HATU (100 mg, 0.26 mmol, 1.0 equiv.), Hünig's base (90 μL, 0.52 mmol, 2.0 equiv.) and 3-aminopyridine (24 mg, 0.26 mmol, 1.0 equiv.). Acylation was carried out with **12** (120 mg, 1.04 mmol, 4.0 equiv.) and Et_3N (0.14 mL, 1.04 mmol, 4.0 equiv.). The

crude reaction mixture was purified by column chromatography with 60:40 PE:acetone and further triturated with chloroform and PE to give **97** as a white solid (32 mg, 0.10 mmol, 38%). **IR (ATR)/cm^{-1}**: 3118, 2980, 1747, 1722, 1537, 1055; **^{1}H NMR** (400 MHz, $CDCl_3$): **δ** 8.67 (app br d, 1H, *J* = 2.0 Hz), 8.60 (br s, 1H), 8.42–8.40 (m, 2H), 8.37 (s, 1H), 7.36–7.33 (m, 1H), 7.11, (br s, 1H), 3.10 (d, 3H, *J* = 4.8 Hz); **^{13}C NMR** (101 MHz, $CDCl_3$): **δ** 158.3, 148.6, 145.9, 143.9, 141.3, 134.4, 132.3, 127.6, 124.1, 97.8, 27.4; **LRMS (ES-APCI)**: *m/z* = 324.0 $[M+H]^+$; **HRMS**: found *m/z* = 324.0096, calculated for $C_{11}H_{11}O_2N_5Br_1$ *m/z* = 324.0091; **M.P.**: > 250 °C

4-bromo-*N*^{1}-methyl-*N*^{3}-(pyridin-2-yl)-1*H*-pyrazole-1,3-dicarboxamide 98:

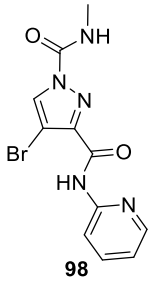

98

General procedure E.c. was followed with acid **6** (50 mg, 0.26 mmol, 1.0 equiv.), HATU (100 mg, 0.26 mmol, 1.0 equiv.), Hünig's base (90 μL, 0.52 mmol, 2.0 equiv.) and 2-aminopyridine (24 mg, 0.26 mmol, 1.0 equiv.). Acylation was carried out with **12** (120 mg, 1.04 mmol, 4.0 equiv.) and Et_3N (0.14 mL, 1.04 mmol, 4.0 equiv.). The crude reaction mixture was purified by column chromatography with 80:20 PE:acetone and further triturated with chloroform and PE to give **98** as a white solid (14 mg, 0.04 mmol, 17%). **IR (ATR)/cm^{-1}**: 3370, 3129, 2932, 1732, 1690; **^{1}H NMR** (400 MHz, $CDCl_3$): **δ** 9.22 (br s, 1H), 8.38–8.35 (m, 1H), 8.34 (s, 1H), 8.32 (app ddd, 1H, *J* = 4.8, 2.0, 0.8 Hz), 7.78–7.74 (m, 1H), 7.10 (br ddd, 2H, *J* = 7.6, 4.8, 0.8 Hz), 3.07 (d, 3H, *J* = 4.8 Hz); **^{13}C NMR** (101 MHz, $CDCl_3$): **δ** 158.0, 150.9, 148.6, 148.2, 143.7, 138.8, 132.1, 120.5, 114.4, 97.8, 27.3; **LRMS (ES-APCI)**: *m/z* = 324.0 $[M+H]^+$; **HRMS**: found *m/z* = 324.0093, calculated for $C_{11}H_{11}O_2N_5Br_1$ *m/z* = 324.0091; **M.P.**: 165 °C

- EWG on the phenyl ring

4-bromo-N^1-methyl-N^3-(4-(trifluoromethyl)phenyl)-1*H*-pyrazole-1,3-dicarboxamide 99:

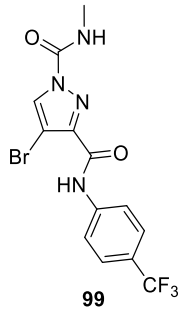

99

General procedure E.c. was followed with acid **6** (50 mg, 0.26 mmol, 1.0 equiv.), HATU (100 mg, 0.26 mmol, 1.0 equiv.), Hünig's base (90 µL, 0.52 mmol, 2.0 equiv.) and 4-(trifluoromethyl)aniline (33 µL, 0.26 mmol, 1.0 equiv.). Acylation was carried out with **12** (120 mg, 1.04 mmol, 4.0 equiv.) and Et_3N (0.14 mL, 1.04 mmol, 4.0 equiv.). The crude reaction mixture was purified by column chromatography with 70:30 PE:acetone eluent to give **99** as a white solid (20 mg, 0.04 mmol, 15%). **IR (ATR)/cm^{-1}**: 3425, 3336, 3142, 1762, 1681, 1531; **^{1}H NMR** (400 MHz, $CDCl_3$): **δ** 8.65 (br s, 1H), 8.36 (s, 1H), 7.81 (d, 2H, *J* = 8.4 Hz), 7.63 (d, 1H, *J* = 8.4 Hz), 7.06 (br s, 1H), 3.09 (d, 3H, *J* = 5.2 Hz); **^{13}C NMR** (101 MHz, DMSO-d_6): **δ** 158.7, 148.4, 144.2, 141.7, 131.5, 126.2 (q, *J* = 3.5 Hz), 125.6 (q, *J* = 272.7 Hz), 123.2 (q, *J* = 68.1 Hz), 119.8, 95.9, 26.8; **^{19}F NMR** (376 MHz, CDCl3): **δ** 62.2; **LRMS (ES-APCI)**: *m/z* = 336.0 $[M+H-C_2H_3N_1O_1]^+$; **HRMS**: found *m/z* = 412.9830, calculated for $C_{13}H_{10}O_2N_4Br_1F_3Na_1$ *m/z* = 412.9830; **M.P.**: 178 °C

4-bromo-N^1-methyl-N^3-(3-(trifluoromethyl)phenyl)-1H-pyrazole-1,3-dicarboxamide 100:

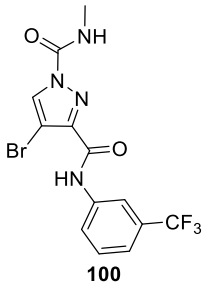

100

General procedure E.c. was followed with acid **6** (50 mg, 0.26 mmol, 1.0 equiv.), HATU (100 mg, 0.26 mmol, 1.0 equiv.), Hünig's base (90 µL, 0.52 mmol, 2.0 equiv.) and 3-(trifluoromethyl)aniline (33 µL, 0.26 mmol, 1.0 equiv.). Acylation was carried out with **12** (120 mg, 1.04 mmol, 4.0 equiv.) and Et_3N (0.14 mL, 1.04 mmol, 4.0 equiv.). The crude reaction mixture was purified by column chromatography with 80:20 PE:acetone and further triturated with chloroform and PE to give **100** as a white solid (20 mg, 0.05 mmol, 19%). **IR (ATR)/cm^{-1}**: 3257, 3168, 1723, 1675; 1331; **^{1}H NMR** (400 MHz, $CDCl_3$): **δ** 8.59 (br s, 1H), 8.37 (s, 1H), 7.95–7.92 (m, 2H), 7.50 (app t, 1H, *J* = 8.0 Hz), 7.43 (app d, 1H, *J* = 7.6 Hz), 7.01 (br s, 1H), 3.11 (d, 3H, *J* = 4.8 Hz); **^{13}C NMR** (101 MHz, DSMO-d_6): **δ** 158.6, 148.4, 144.0, 138.9, 131.6, 130.2, 129.6 (q, *J* = 32.1 Hz), 124.1 (q, *J* = 303.5 Hz), 123.4, 120.5 (q, *J* = 3.6 Hz), 115.9 (q, *J* = 9.1 Hz), 95.1, 26.8; **LRMS (ES-APCI)**: *m/z* = 390.9 $[M+H]^+$; **HRMS**: found *m/z* = 391.0010, calculated for $C_{13}H_{11}O_2N_4Br_1F_3$ *m/z* = 391.0012; **M.P.**: 150 °C

4-bromo-N^1-methyl-N^3-(4-nitrophenyl)-1*H*-pyrazole-1,3-dicarboxamide 101:

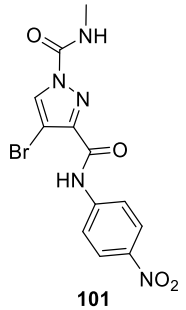

101

General procedure E.c. was followed with acid **6** (100 mg, 0.52 mmol, 1.0 equiv.), HATU (200 mg, 0.52 mmol, 1.0 equiv.), Hünig's base (0.18 mL, 1.04 mmol, 2.0 equiv.) and 4-nitroaniline (72 mg, 0.52 mmol, 1.0 equiv.). Acylation was carried out with **12** (240 mg, 2.08 mmol, 4.0 equiv.) and Et_3N (0.28 mL, 2.08 mmol, 4.0 equiv.). The reaction mixture was filtered and the solid washed with a minimum amount of cold MeCN. This gave compound **101** as a light yellow (30 mg, 0.08 mmol, 15%). **IR (ATR)/cm^{-1}**: 3413, 3259, 3136, 1731, 1504, 1232; **^{1}H NMR** (400 MHz, DMSO-d_6): **δ** 10.84 (br s, 1H), 8.72 (br s, 2H), 8.30 (d, 2H, J = 9.2 Hz), 8.00 (d, 2H, J = 9.2 Hz), 2.90 (d, 3H, J = 4.4 Hz); **^{13}C NMR** (101 MHz, DMSO-d_6): **δ** 158.9, 148.4, 144.3, 144.0, 142.9, 131.7, 125.1, 119.7, 96.1, 26.9; **LRMS (ES-APCI)**: m/z = 366.0 $[M-H]^-$; **HRMS**: found m/z = 367.9993, calculated for $C_{12}H_{11}O_4N_5Br_1$ m/z = 367.9989; **M.P.**: >250 °C

4-bromo-N^1-methyl-N^3-(3-nitrophenyl)-1*H*-pyrazole-1,3-dicarboxamide 102:

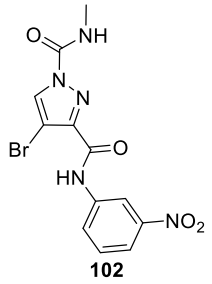

102

General procedure E.c. was followed with acid **6** (100 mg, 0.52 mmol, 1.0 equiv.), HATU (200 mg, 0.52 mmol, 1.0 equiv.), Hünig's base (0.18 mL, 1.04 mmol, 2.0 equiv.) and 3-nitroaniline (72 mg, 0.52 mmol, 1.0 equiv.). Acylation was carried out with **12** (240 mg, 2.08 mmol, 4.0 equiv.) and Et_3N (0.28 mL, 2.08 mmol,

4.0 equiv.). No work up was needed as the compound precipitated and was filtered to give **102** as a light yellow solid (50 mg, 0.14 mmol, 27%). **IR (ATR)/cm^{-1}**: 3398, 3367, 3119, 1745, 1537; **^{1}H NMR** (400 MHz, DMSO-*d*$_6$): **δ** 10.77 (br s, 1H), 8.73 (app t, 1H, *J* = 2.0 Hz), 8.72 (s, 1H), 8.70 (br app d, 1H, *J* = 4.8 Hz), 8.16–8.14 (m, 1H), 8.03–8.00 (m, 1H), 7.70 (t, 1H, *J* = 8.0 Hz), 2.92 (d, 3H, *J* = 4.8 Hz); **^{13}C NMR** (101 MHz, DMSO-*d*$_6$): **δ** 158.8, 148.4, 148.0, 144.0, 139.3, 131.7, 130.4, 125.8, 118.7, 114.0, 96.0, 26.9; **LRMS (ES-APCI)**: *m/z* = 368.0 $[M+H]^+$; **HRMS**: found *m/z* = 367.9994, calculated for $C_{12}H_{11}O_4N_5Br_1$ *m/z* = 367.9989; **M.P.**: 238 °C

- SEDG phenyl amide

4-methoxyaniline 104:

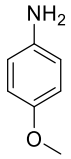

104

In a vial, NH_4Cl (200 mg, 1.31 mmol, 3.0 equiv.) was dissolved in H_2O (3 mL) and a spatula of iron was added. 4-nitroanisole **103** (200 mg, 1.31 mmol, 1.0 equiv.) in acetone (7 mL) was added to the solution. The reaction mixture was heated to 60 °C for 3 h. The reaction was left to cool to rt before filtration over celite and washed with acetone (20 mL). The solvent was removed and amine **104** (150 mg, 1.22 mmol, 93%) was isolated as a brownish solid and used as is in next step. **IR (ATR)/cm^{-1}**: 2919, 2850, 1504, 1234; **^{1}H NMR** (400 MHz, $CDCl_3$): **δ** 6.76 (d, 2H, *J* = 8.8 Hz), 6.65 (d, 2H, *J* = 8.4 Hz), 3.76 (s, 3H), 3.45 (br s, 2H); **^{13}C NMR** (101 MH, $CDCl_3$): **δ** 152.8, 140.1, 116.5, 114.9, 55.8;

4-bromo-N^3-(4-methoxyphenyl)-N^1-methyl-1*H*-pyrazole-1,3-dicarboxamide 105:

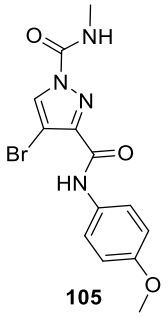

105

General procedure E.c. was followed with acid **6** (50 mg, 0.26 mmol, 1.0 equiv.), HATU (100 mg, 0.26 mmol, 1.0 equiv.), Hünig's base (90 µL, 0.52 mmol, 2.0 equiv.) and 4-aminoanisole (32 mg, 0.26 mmol, 1.0 equiv.). Acylation was carried out with **12** (120 mg, 1.04 mmol, 4.0 equiv.) and Et_3N (0.14 mL, 1.04 mmol, 4.0 equiv.). The crude reaction mixture was purified by column chromatography with 80:20 PE:acetone to give **105** as a white solid (40 mg, 0.11 mmol, 42%). **IR (ATR)/cm^{-1}**: 3333, 3144, 1727, 1673, 1247; **^{1}H NMR** (400 MHz, $CDCl_3$): **δ** 8.42 (br s, 1H), 8.33 (s, 1H), 7.60–7.56 (m, 2H), 7.09 (br s, 1H), 6.92–6.88 (m, 2H), 3.82 (s, 3H), 3.08 (d, 3H, J = 4.8 Hz); **^{13}C NMR** (101 MHz, $CDCl_3$): **δ** 157.6, 156.9, 148.7, 144.6, 131.9, 130.4, 121.8, 114.4, 97.5, 55.7, 27.3; **LRMS (ES-APCI)**: *m/z* = 353.0 $[M+H]^+$; **HRMS**: found *m/z* = 353.0243, calculated for $C_{13}H_{14}O_3N_4Br_1$ *m/z* = 353.0244; **M.P.**: 171 °C

4-bromo-N^3-(3-methoxyphenyl)-N^1-methyl-1*H*-pyrazole-1,3-dicarboxamide 106:

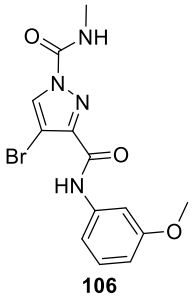

106

General procedure E.c. was followed with acid **6** (50 mg, 0.26 mmol, 1.0 equiv.), HATU (100 mg, 0.26 mmol, 1.0 equiv.), Hünig's base (90 µL, 0.52 mmol, 2.0 equiv.) and 3-anisidine (29 µL, 0.26 mmol, 1.0 equiv.). Acylation was carried out with **12** (120 mg, 1.04 mmol, 4.0 equiv.) and Et_3N (0.14 mL, 1.04 mmol, 4.0 equiv.). The crude

reaction mixture was purified by column chromatography with 85:25 PE:acetone eluent and further triturated with chloroform and PE to give **106** as a white solid (21 mg, 0.06 mmol, 23%). **IR (ATR)/cm^{-1}**: 3350, 3324, 3142, 2943, 1731, 1680, 1521; **^{1}H NMR** (400 MHz, $CDCl_3$): **δ** 8.49 (br s, 1H), 8.33 (s, 1H), 7.47 (app t, 1H, *J* = 2.0 Hz), 7.24 (t, 1H, *J* = 8.0 Hz), 7.10–7.06 (m, 2H), 6.73–6.70 (m, 1H), 3.83 (s, 3H), 3.08 (d, 3H, *J* = 4.8 Hz); **^{13}C NMR** (101 MHz, $CDCl_3$): **δ** 160.5, 157.8, 148.7, 144.4, 138.5, 132.1, 130.0, 112.1, 111.0, 105.7, 97.6, 55.6, 27.3; **LRMS (ES-APCI)**: *m/z* = 295.9 $[M+H-C_2H_3N_1O_1]^+$; **HRMS**: found *m/z* = 353.0247, calculated for $C_{13}H_{14}O_3N_4Br_1$ *m/z* = 353.0244; **M.P.**: 154 °C

4-bromo-*N*^{3}-(3,5-dimethoxyphenyl)-*N*^{1}-methyl-1*H*-pyrazole-1,3-dicarboxamide 107:

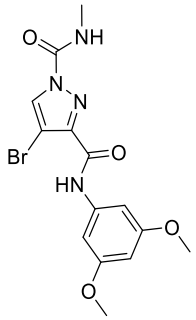

107

General procedure E.c. was followed with acid **6** (50 mg, 0.26 mmol, 1.0 equiv.), HATU (100 mg, 0.26 mmol, 1.0 equiv.), Hünig's base (90 µL, 0.52 mmol, 2.0 equiv.) and 3,5-dimethoxyaniline (40 mg, 0.26 mmol, 1.0 equiv.). Acylation was carried out with **12** (120 mg, 1.04 mmol, 4.0 equiv.) and Et_3N (0.14 mL, 1.04 mmol, 4.0 equiv.). The crude reaction mixture was purified by column chromatography with 90:10 PE:acetone eluent to give **107** as a beige solid (40 mg, 0.10 mmol, 38%). **IR (ATR)/cm^{-1}**: 3344, 3124, 2964, 1739, 1681, 1519; **^{1}H NMR** (400 MHz, $CDCl_3$): **δ** 8.44 (br s, 1H), 8.34 (s, 1H), 7.05 (br d, 1H, *J* = 4.0 Hz), 6.92 (d, 2H, *J* = 2.0 Hz), 6.29 (t, 1H, *J* = 2.4 Hz), 3.81 (s, 6H), 3.09 (d, 3H, *J* = 5.2 Hz); **^{13}C NMR** (101 MHz, $CDCl_3$): **δ** 161.4, 157.8, 148.6, 144.4, 139.1, 132.1, 98.3, 97.6, 55.7, 27.3; **LRMS (ES-APCI)**: *m/z* = 383.0 $[M+H]^+$; **HRMS**: found *m/z* = 383.0348, calculated for $C_{14}H_{16}O_4N_4Br_1$ *m/z* = 383.0349; **M.P.**: 182 °C

4-bromo-N^1-methyl-N^3-(3,4,5-trimethoxyphenyl)-1*H*-pyrazole-1,3-dicarboxamide 108:

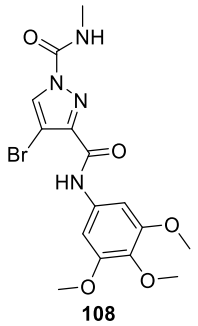

108

General procedure E.c. was followed with acid **6** (50 mg, 0.26 mmol, 1.0 equiv.), HATU (100 mg, 0.26 mmol, 1.0 equiv.), Hünig's base (90 µL, 0.52 mmol, 2.0 equiv.) and 3,4,5-trimethoxyaniline (48 mg, 0.26 mmol, 1.0 equiv.). Acylation was carried out with **12** (120 mg, 1.04 mmol, 4.0 equiv.) and Et_3N (0.14 mL, 1.04 mmol, 4.0 equiv.). The crude reaction mixture was purified by flash chromatography with 70:30 PE:acetone eluent followed by trituration with EtOAc and PE to give **108** as a white solid (11 mg, 0.03, 12%). **IR (ATR)/cm^{-1}**: 3540, 3281, 2937, 1732, 1508, 1128; **^{1}H NMR** (400 MHz, $CDCl_3$): **δ** 8.44 (br s, 1H), 8.38 (s, 1H), 7.07 (br s, 1H), 7.01 (s, 2H), 3.90 (s, 6H), 3.86 (s, 3H), 3.11 (d, 3H, *J* = 4.8 Hz); **^{13}C NMR** (101 MHz, $CDCl_3$): **δ** 157.7, 153.7, 148.6, 133.5, 132.2, 97.8, 61.2, 56.4, 27.4; **LRMS (ES-APCI)**: *m/z* = 356.0 $[M+H-C_2H_4NO]^+$; **HRMS**: found *m/z* = 413.0455, calculated for $C_{15}H_{18}O_5N_4Br_1$ *m/z* = 413.0455; **M.P.**: 84 °C

4-bromo-N^3-(4-hydroxyphenyl)-N^1-methyl-1H-pyrazole-1,3-dicarboxamide 109a:

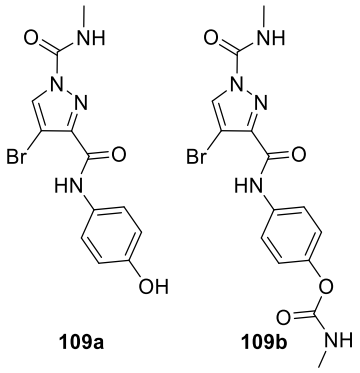

109a 109b

General procedure E.c. was followed with acid **6** (50 mg, 0.26 mmol, 1.0 equiv.), HATU (100 mg, 0.26 mmol, 1.0 equiv.), Hünig's base (90 µL, 0.52 mmol, 2.0 equiv.) and 4-aminophenol (28 mg, 0.26 mmol, 1.0 equiv.). Acylation was carried out with **12** (120 mg, 1.04 mmol, 4.0 equiv.) and Et_3N (0.14 mL, 1.04 mmol, 4.0 equiv.). The crude reaction mixture was purified by column chromatography with 80:20 to 70:30 PE:acetone eluent gave two compounds. **109a** was further triturated with chloroform and PE to give **109a** as a white solid (10 mg, 0.03 mmol, 12%) and **109b** as a white solid (5 mg , 0.01 mmol, 4%). **109a**: **IR (ATR)/cm^{-1}**: 3287 (br), 1731, 1515; **^{1}H NMR** (400 MHz, DMSO-d_6): **δ** 10.05 (br s, 1H), 9.34 (s, 1H), 8.70−8.67 (br m, 1H), 8.64 (s, 1H), 7.49 (d, 2H, *J* = 8.8 Hz), 6.76 (d, 2H, *J* = 8.8 Hz), 2.88 (d, 3H, *J* = 4.8 Hz); **^{13}C NMR** (101 MHz, DMSO-d_6): **δ** sample not concentrated enough and not enough scan to process; **LRMS (ES-APCI)**: *m/z* = 339.0 $[M+H]^+$; **HRMS**: found *m/z* = 339.0092, calculated for $C_{12}H_{12}O_3N_4Br_1$ *m/z* = 339.0087; **M.P.**: 162 °C; **109b**: **IR (ATR)/cm^{-1}**: 3287, 3132, 1740, 1712, 1673, 1506, 1214; **^{1}H NMR** (400 MHz, DMSO-d_6): **δ** 10.32 (br s, 1H), 8.71 (br d, 1H, *J* = 4.4 Hz), 8.67 (s, 1H), 7.70 (d, 2H, *J* = 8.8 Hz), 7.61 (br q, 1H, *J* = 4.0 Hz), 7.11 (d, 2H, *J* = 9.2 Hz), 2.88 (d, 3H, *J* = 4.8 Hz) , 2.66 (d, 3H, *J* = 4.4 Hz); **^{13}C NMR** (101 MHz, DMSO-d_6): **δ** sample not concentrated enough and not enough scan to process ; **LRMS (ES-APCI)**: *m/z* = 396.0 $[M+H]^+$; **HRMS**: found *m/z* = 396.0304, calculated for $C_{14}H_{15}O_4N_5Br_1$ *m/z* = 396.0302; **M.P.**: 174 °C

4-bromo-N^3-(3-hydroxyphenyl)-N^1-methyl-1*H*-pyrazole-1,3-dicarboxamide 110a:

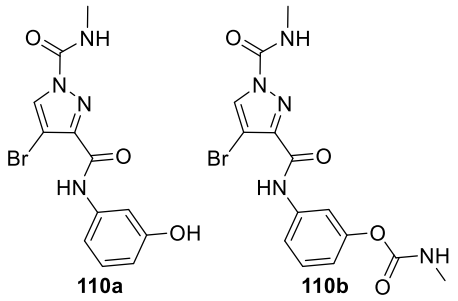

General procedure E.c. was followed with acid **6** (50 mg, 0.26 mmol, 1.0 equiv.), HATU (100 mg, 0.26 mmol, 1.0 equiv.), Hünig's base (90 μL, 0.52 mmol, 2.0 equiv.) and 3-aminophenol (28 mg, 0.26 mmol, 1.0 equiv.). Acylation was carried out with **12** (120 mg, 1.04 mmol, 4.0 equiv.) and Et_3N (0.14 mL, 1.04 mmol, 4.0 equiv.). The crude reaction mixture was purified by column chromatography with 70:30 PE:acetone eluent to give **110a** as a white solid (16 mg, 0.05 mmol, 19%) and **110b** (9 mg, 0.02 mmol, 8%). **110a**: **IR (ATR)/cm^{-1}**: 3389, 3324, 3264, 3114, 1732, 1662; **^{1}H NMR** (400 MHz, DMSO-d_6): **δ** 10.11 (br s, 1H), 9.50 (br s, 1H), 8.71 (br q, 1H, *J* = 4.4 Hz), 8.66 (s, 1H), 7.30 (app t, 1H, *J* = 2.4 Hz), 7.15 (app t, 1H, *J* = 8.0 Hz), 7.09–7.07 (m, 1H), 6.53 (ddd, 1H, *J* = 8.0, 2.4, 1.2 Hz), 2.88 (d, 3H, *J* = 4.8 Hz); **^{13}C NMR** (101 MHz, DMSO-d_6): **δ** 158.1, 157.7, 144.7, 139.1, 131.3, 129.6, 112.5, 111.3, 110.6, 107.0, 95.7, 26.8; **LRMS (ES-APCI)**: *m/z* = 339.0 $[M+H]^+$; **HRMS**: found *m/z* = 339.0088, calculated for $C_{12}H_{12}O_3N_4Br_1$ *m/z* = 339.0087; **M.P.**: 196 °C; **110b**: no analysis carried out

4-bromo-N^3-(2-hydroxyphenyl)-N^1-methyl-1*H*-pyrazole-1,3-dicarboxamide 111a:

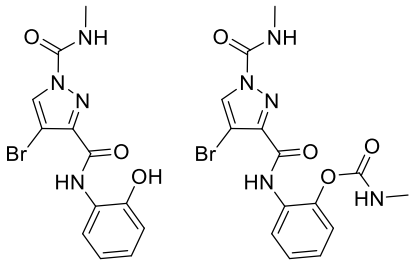

111a **111b**

General procedure E.c. was followed with acid **6** (50 mg, 0.26 mmol, 1.0 equiv.), HATU (100 mg, 0.26 mmol, 1.0 equiv.), Hünig's base (90 µL, 0.52 mmol, 2.0 equiv.) and 2-aminophenol (28 mg, 0.26 mmol, 1.0 equiv.). Acylation was carried out with **12** (120 mg, 1.04 mmol, 4.0 equiv.) and Et_3N (0.14 mL, 1.04 mmol, 4.0 equiv.). The crude reaction mixture was purified by column chromatography with 70:30 PE:acetone eluent to give **111a** as a white solid (10 mg, 0.03 mmol, 12%). **111a**: **^{1}H NMR** (400 MHz, DMSO-d_6): **δ** 10.06 (br s, 1H), 9.34 (br s, 1H), 8.78 (br app q, 1H, J = 4.8 Hz), 8.66 (s, 1H), 7.98 (dd, 1H, J = 8.0, 1.2 Hz), 7.03−6.99 (m, 1H), 6.95−6.92 (m, 1H), 6.85−6.81 (m, 1H), 2.86 (d, 3H, J = 4.8 Hz); **^{13}C NMR** (101 MHz, DMSO-d_6): **δ** sample not concentrated enough; **LRMS (ES-APCI)**: m/z = 279.8 $[M-H-C_2H_3N_1O_1]^-$; **HRMS**: found m/z = 339.0090, calculated for $C_{12}H_{12}O_3N_4Br_1$ m/z = 339.0087; **111b** no analysis carried out

N^3-(4-aminophenyl)-4-bromo-N^1-methyl-1*H*-pyrazole-1,3-dicarboxamide 112:

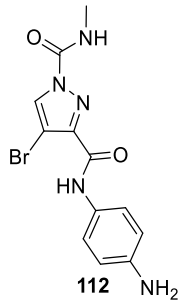

112

In a round bottom flask, NH_4Cl (41 mg, 0.76 mmol, 3.0 equiv.) was dissolved in H_2O (4 mL) and put under N_2. Fe (spatula) was added followed by nitro compound **101** (93 mg, 0.25 mmol, 1.0 equiv.) in acetone (8 mL). Reaction was stirred at 80 °C for 4

hours and left to cool down to room temperature. Product was extracted with EtOAc (3 × 10 mL) and the organic layer washed with sat aq. $NaHCO_3$ (10 mL) and with brine (10 mL). The organic layer was dried over $MgSO_4$, filtered and concentrated *in vacuo*. The crude reaction mixture was purified by column chromatography 0–1% MeOH in CH_2Cl_2 with 0.5% Et_3N. It was then further triturated with chloroform and PE to afford **112** as an off-white solid (23 mg, 0.07 mmol, 9%). **IR (ATR)/cm^{-1}**: 3488, 3439, 3357, 3214, 1716, 1651, 1515; **^{1}H NMR** (400 MHz, $CDCl_3$): **δ** 8.32 (br s, 2H), 7.43 (d, 2H, *J* = 8.8 Hz), 7.07 (br s, 1H), 6.68 (d, 2H, *J* = 8.4 Hz), 3.66 (br s, 2H), 3.07 (d, 3H, *J* = 5.2 Hz); **^{13}C NMR** (101 MHz, $CDCl_3$): **δ** 157.5, 148.8, 144.8, 143.9, 131.9, 128.6, 122.1, 115.6, 97.4, 27.3; **LRMS (ES-APCI)**: *m/z* = 360.0 $[M+Na]^+$; **HRMS**: found *m/z* = 360.0068, calculated for $C_{12}H_{12}O_2N_5Br_1Na_1$ *m/z* = 360.0067; **M.P.**: 110 °C

<u>*N*^{3}-(3-aminophenyl)-4-bromo-*N*^{1}-methyl-1*H*-pyrazole-1,3-dicarboxamide 113:</u>

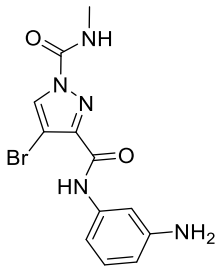

113

In a round bottom flask, NH_4Cl (44 mg, 0.81 mmol, 3.0 equiv.) was dissolved in H_2O (4 mL) and put under N_2. Fe (spatula) was added followed by nitro compound **102** (100 mg, 0.27 mmol, 1.0 equiv.) in acetone (8 mL). Reaction was stirred at 80 °C for 4 hours and left to cool down to room temperature. Product was extracted with EtOAc (3 × 10 mL) and the organic layer washed with sat aq. $NaHCO_3$ (10 mL) and with brine (10 mL). The organic layer was dried over $MgSO_4$, filtered and concentrated *in vaccuo*. The crude reaction mixture was purified by column chromatography with 80:20 PE:acetone and was further triturated with EtOAc and PE to give **113** as a white solid (40 mg, 0.12 mmol, 44%). **IR (ATR)/cm^{-1}**: 3367, 1736, 1550; **^{1}H NMR** (400 MHz, $CDCl_3$): **δ** 8.41 (br s, 1H), 8.31 (s, 1H), 7.32 (app t, 1H, *J* = 2.0 Hz), 7.10 (app t, 2H, *J* = 8.0 Hz), 6.78 (ddd, 1H, *J* = 8.0, 2.0, 0.8 Hz), 6.47 (ddd, 1H, *J* = 8.0, 2.4, 0.8 Hz), 3.74 (br s, 2H), 3.06 (d, 3H, *J* = 5.2 Hz); **^{13}C NMR** (101 MHz,

$CDCl_3$): **δ** 157.8, 148.7, 147.6, 144.4, 138.3, 131.9, 129.9, 111.7, 109.9, 106.8, 97.5, 27.3; **LRMS (ES-APCI)**: *m/z* = 337.9 $[M+H]^+$; **HRMS**: found *m/z* = 338.0251, calculated for $C_{12}H_{13}O_2N_5Br_1$ *m/z* = 338.0247; **M.P.**: 158 °C

- WEDG phenyl amides

[1,1'-biphenyl]-4-amine 465:[78]

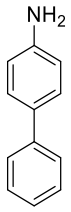

115

In a microwave vial, 4-bromoaniline **114** (172 mg, 1.00 mmol, 1.0 equiv.), and phenylboronic acid **18** (122 mg, 1.00 mmol, 1.0 equiv.) were dissolved in H_2O (2 mL). Na_2CO_3 (315 mg, 3.00 mmol, 3.0 equiv.) and $Pd(OAc)_2$ (1 mg, 0.4 mol%) were added followed by tetrabutylammonium bromide (322 mg, 1.00 mmol, 1.0 equiv.). The reaction was irradiated in the microwave for 5 minutes at 150 °C. The reaction mixture was allowed to cool to rt before pouring it into H_2O (20 mL). The product was extracted with diethyl ether (3 × 15 mL) and the organic layer was washed with brine (10 mL) before drying over $MgSO_4$, filtered and concentrated *in vacuo*. The crude was purified by flash chromatography with 90:10 PE:acetone eluent to give compound **115** as a light brown solid (100 mg, 0.59 mmol, 60%). **IR (ATR)/cm^{-1}**: 3423, 3389, 3292, 3194, 3028; **^{1}H NMR** (400 MHz, $CDCl_3$): **δ** 7.56 (app d, 2H, *J* = 8.0 Hz), 7.45–7.40 (m, 4H), 7.31–7.27 (m, 1H), 6.78 (d, 2H, *J* = 8.4 Hz), 3.74 (br s, 2H); **^{13}C NMR** (101 MHz, $CDCl_3$): **δ** 145.0, 141.4, 131.8, 128.9, 128.2, 126.6, 126.5, 115.6; **LRMS (ES-APCI)**: *m/z* = 170.3 $[M+H]^+$; **M.P.**: 65 °C (52–54 °C in lit)[116]

4-bromo-N^1-methyl-N^3-(*p*-tolyl)-1*H*-pyrazole-1,3-dicarboxamide 116:

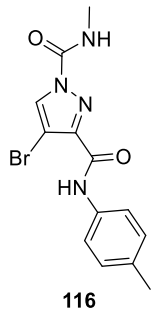

116

General procedure E.c. was followed with acid **6** (50 mg, 0.26 mmol, 1.0 equiv.), HATU (100 mg, 0.26 mmol, 1.0 equiv.), Hünig's base (90 µL, 0.52 mmol, 2.0 equiv.) and *p*-toluidine (28 mg, 0.26 mmol, 1.0 equiv.). Acylation was carried out with **12** (120 mg, 1.04 mmol, 4.0 equiv.) and Et_3N (0.14 mL, 1.04 mmol, 4.0 equiv.). The crude reaction mixture was purified by column chromatography with 80:20 PE:acetone to give **116** as a white solid (37 mg, 0.11 mmol, 42%). **IR (ATR)/cm^{-1}**: 339, 3298, 3142, 1729, 1675; **^{1}H NMR** (400 MHz, $CDCl_3$): **δ** 8.48 (br s, 1H), 8.29 (s, 1H), 7.52 (d, 2H, *J* = 8.4 Hz), 7.14 (d, 2H, *J* = 8.4 Hz), 7.11 (br s, 1H), 3.04 (d, 3H, *J* = 4.8 Hz), 2.33 (s, 3H); **^{13}C NMR** (101 MHz, $CDCl_3$): **δ** 157.7, 148.7, 144.5, 134.7, 131.9, 129.8, 120.1, 97.4, 22.3, 21.1; **LRMS (ES-APCI)**: *m/z* = 337.0 $[M+H]^+$; **HRMS**: found *m/z* = 337.0298, calculated for $C_{13}H_{14}O_2N_4Br_1$ *m/z* = 337.0295; **M.P.**: 180 °C

4-bromo-N^3-(3,5-dimethylphenyl)-N^1-methyl-1*H*-pyrazole-1,3-dicarboxamide 117:

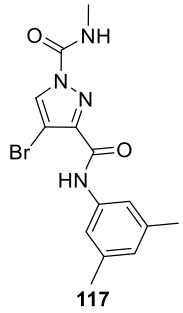

117

General procedure E.c. was followed with acid **6** (50 mg, 0.26 mmol, 1.0 equiv.), HATU (100 mg, 0.26 mmol, 1.0 equiv.), Hünig's base (90 µL, 0.52 mmol, 2.0 equiv.) and 3,5-dimethylaniline (32 µL, 0.26 mmol, 1.0 equiv.). Acylation was carried out with **12** (120 mg, 1.04 mmol, 4.0 equiv.) and Et_3N (0.14 mL, 1.04 mmol, 4.0 equiv.).

The crude reaction mixture was purified by column chromatography with 90:10 PE:acetone eluent to give **117** as a white solid (55 mg, 0.16 mmol, 62%). **IR (ATR)/cm^{-1}**: 3330, 2980, 1749, 1633, 1550; **^{1}H NMR** (400 MHz, $CDCl_3$): **δ** 8.40 (br s, 1H), 8.33 (s, 1H), 7.32 (br s, 1H), 7.05 (br app d, 1H, *J* = 4.0 Hz), 6.81 (br s, 1H), 3.09 (d, 3H, *J* = 5.2 Hz); **^{13}C NMR** (101 MHz, $CDCl_3$): **δ** 157.7, 148.7, 144.5, 139.1, 137.1, 132.0, 126.7, 117.8, 97.6, 27.3, 21.6; **LRMS (ES-APCI)**: *m/z* = 351.0 $[M+H]^+$; **HRMS**: found *m/z* = 351.0449, calculated for $C_{14}H_{16}O_2N_4Br_1$ *m/z* = 351.0451; **M.P.**: 162 °C

4-bromo-*N*^{1}-methyl-*N*^{3}-(4-vinylphenyl)-1*H*-pyrazole-1,3-dicarboxamide 118:

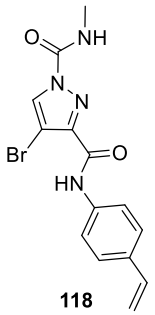

118

General procedure E.c. was followed with acid **6** (50 mg, 0.26 mmol, 1.0 equiv.), HATU (100 mg, 0.26 mmol, 1.0 equiv.), Hünig's base (90 µL, 0.52 mmol, 2.0 equiv.) and 4-vinylaniline (30 µL, 0.26 mmol, 1.0 equiv.). Acylation was carried out with **12** (120 mg, 1.04 mmol, 4.0 equiv.) and Et_3N (0.14 mL, 1.04 mmol, 4.0 equiv.). The crude reaction mixture was purified by column chromatography with 80:20 PE:acetone and further triturated with chloroform and PE to give **118** as a white solid (22 mg, 0.06 mmol, 24%). **IR (ATR)/cm^{-1}**: 3504, 3235, 3144, 1731, 1675; **^{1}H NMR** (400 MHz, $CDCl_3$): **δ** 8.48 (br s, 1H), 8.35 (s, 1H), 7.66 (d, 2H, *J* = 8.8 Hz), 7.42 (d, 2H, *J* = 8.4 Hz), 7.02 (br s, 1H), 6.70 (dd, 1H, *J* = 17.6, 10.8 Hz), 5.72 (dd, 1H, *J* = 17.6, 0.8 Hz), 5.24 (dd, 1H, *J* = 10.8, 0.4 Hz), 3.10 (d, 3H, *J* = 5.2 Hz); **^{13}C NMR** (101 MHz, $CDCl_3$): **δ** 157.6, 148.6, 144.4, 136.8, 136.2, 134.5, 132.1, 127.2, 120.0, 113.6, 97.7, 27.3; **LRMS (ES-APCI)**: *m/z* = 348.8 $[M+H]^+$; **HRMS**: found *m/z* = 348.0211, calculated for $C_{14}H_{13}O_2N_4Br_1$ *m/z* = 348.0216; **M.P.**: 86 °C

N^3-([1,1'-biphenyl]-4-yl)-4-bromo-N^1-methyl-1*H*-pyrazole-1,3-dicarboxamide 119:

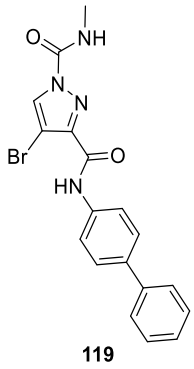

119

General procedure E.c. was followed with acid **6** (50 mg, 0.26 mmol, 1.0 equiv.), HATU (100 mg, 0.26 mmol, 1.0 equiv.), Hünig's base (90 μL, 0.52 mmol, 2.0 equiv.) and 4-aminobiphenyl (44 mg, 0.26 mmol, 1.0 equiv.). Acylation was carried out with **12** (120 mg, 1.04 mmol, 4.0 equiv.) and Et_3N (0.14 mL, 1.04 mmol, 4.0 equiv.). The crude reaction mixture was purified by trituration with EtOAc and PE to give **119** as a white solid (31 mg, 0.08 mmol, 31%). **IR (ATR)/cm^{-1}**: 3333, 3136, 1755, 1673, 1526; **^{1}H NMR** (400 MHz, $CDCl_3$): **δ** 8.61 (br s, 1H), 8.34 (s, 1H), 7.76 (app d, 2H, *J* = 8.4 Hz), 7.61–7.58 (m, 4H), 7.44 (app t, 2H, *J* = 7.2 Hz), 7.35 (app t, 1H, *J* = 7.6 Hz), 7.15 (app br d, 1H, *J* = 4.4 Hz), 3.09 (d, 3H, *J* = 4.8 Hz); **^{13}C NMR** (101 MHz, $CDCl_3$): **δ** 157.8, 148.7, 144.4, 140.5, 137.9, 136.6, 132.0, 129.0, 127.9, 127.5, 127.0, 120.4, 97.6, 27.3; **LRMS (ES-APCI)**: *m/z* = 421.0 $[M+Na]^+$; **HRMS**: found *m/z* = 399.0453, calculated for $C_{18}H_{16}O_2N_4Br_1$ *m/z* = 399.0451; **M.P.**: 200 °C (decomp)

- Halogen substitution on phenyl amide

4-bromo-N^3-(4-bromophenyl)-N^1-methyl-1*H*-pyrazole-1,3-dicarboxamide 120:

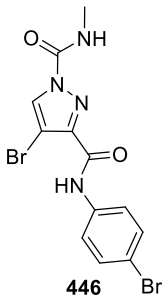

446

General procedure E.c. was followed with acid **6** (50 mg, 0.26 mmol, 1.0 equiv.), HATU (100 mg, 0.26 mmol, 1.0 equiv.), Hünig's base (90 µL, 0.52 mmol, 2.0 equiv.) and 4-bromoaniline (45 mg, 0.26 mmol, 1.0 equiv.). Acylation was carried out with **12** (120 mg, 1.04 mmol, 4.0 equiv.) and Et_3N (0.14 mL, 1.04 mmol, 4.0 equiv.). The crude reaction mixture was purified by column chromatography with 80:20 PE:acetone eluent to give **120** as an off-white solid (40 mg, 0.10 mmol, 38%). **IR (ATR)/cm^{-1}**: 3336, 3143, 2980, 1740, 1680; **^{1}H NMR** (400 MHz, $CDCl_3$): **δ** 8.47 (br s, 1H), 8.35 (s, 1H), 7.61–7.57 (m, 2H), 7.50–7.47 (m, 2H), 7.01 (br s, 1H), 3.09 (d, 3H, *J* = 4.8 Hz); **^{13}C NMR** (101 MHz, $CDCl_3$): **δ** 157.8, 148.7, 144.4, 136.5, 132.5, 132.3, 121.7, 117.8, 97.8, 27.5; **LRMS (ES-APCI)**: *m/z* = 400.9 $[M+H]^+$; **HRMS**: found *m/z* = 400.9243, calculated for $C_{12}H_{11}O_2N_4Br_2$ *m/z* = 400.9243; **M.P.**: > 250 °C

4-bromo-N^3-(4-fluorophenyl)-N^1-methyl-1*H*-pyrazole-1,3-dicarboxamide 121:

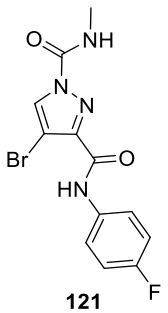

121

General procedure E.c. was followed with acid **6** (50 mg, 0.26 mmol, 1.0 equiv.), HATU (100 mg, 0.26 mmol, 1.0 equiv.), Hünig's base (90 µL, 0.52 mmol, 2.0 equiv.) and 4-fluoroaniline (25 µL, 0.26 mmol, 1.0 equiv.). Acylation was carried out with **12**

(120 mg, 1.04 mmol, 4.0 equiv.) and Et_3N (0.14 mL, 1.04 mmol, 4.0 equiv.). The crude reaction mixture was purified by column chromatography with 80:20 PE:acetone further triturated with chloroform and PE to give **121** as a white solid (32 mg, 0.09 mmol, 35%). **IR (ATR)/cm^{-1}**: 3423, 3311, 3129, 1760, 1667; **^{1}H NMR** (400 MHz, $CDCl_3$): **δ** 8.45 (br s, 1H), 8.35 (s, 1H), 7.65–7.62 (m, 2H), 7.09–7.06 (m, 3H), 3.09 (d, 3H, *J* = 5.2 Hz); **^{13}C NMR** (101 MHz, $CDCl_3$): **δ** 160.1 (d, *J* = 245.2 Hz), 157.8, 148.6, 144.4, 133.3 (d, *J* = 2.7 Hz), 132.1, 121.9 (d, *J* = 7.9 Hz), 116.0 (d, *J* = 22.6 Hz), 97.6, 27.3; **HRMS**: found *m/z* = 362.9864, calculated for $C_{12}H_{10}O_2N_4Br_1F_1$ *m/z* = 362.9863; **M.P.**: 175 °C

- Disubstituted phenyl amides

4-bromo-*N*^{3}-(4-chloro-2-methylphenyl)-*N*^{1}-methyl-1*H*-pyrazole-1,3-dicarboxamide 122:

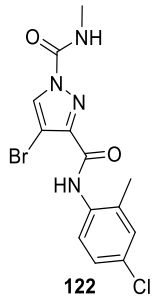

122

General procedure E.c. was followed with acid **6** (50 mg, 0.26 mmol, 1.0 equiv.), HATU (100 mg, 0.26 mmol, 1.0 equiv.), Hünig's base (90 µL, 0.52 mmol, 2.0 equiv.) and 4-chloro-2-methylaniline (31 µL, 0.26 mmol, 1.0 equiv.). Acylation was carried out with **12** (120 mg, 1.04 mmol, 4.0 equiv.) and Et_3N (0.14 mL, 1.04 mmol, 4.0 equiv.). The crude reaction mixture was purified by column chromatography with 80:20 PE:acetone and further triturated with chloroform and PE to give **122** as an off white solid (30 mg, 0.08 mmol, 31%). **IR (ATR)/cm^{-1}**: 3383, 3361, 3131, 1760, 1695, 1495, 338; **^{1}H NMR** (400 MHz, $CDCl_3$): **δ** 8.35 (s, 1H), 8.32 (br s, 1H), 7.96 (d, 1H, *J* = 9.6 Hz), 7.23–7.21 (m, 2H), 7.01 (br s, 1H), 3.08 (d, 3H, *J* = 5.2 Hz), 2.33 (s, 3H); **^{13}C NMR** (101 MHz, $CDCl_3$): **δ** 157.8, 148.6, 144.6, 133.7, 132.1, 130.8, 130.5, 127.1, 124.2, 97.4, 27.4, 18.0; **LRMS (ES-APCI)**: *m/z* = 371.0 $[M+H]^+$; **HRMS**: found *m/z* = 370.9907, calculated for $C_{13}H_{13}O_2N_4Br_1Cl_1$ *m/z* = 370.9905; **M.P.**: 161 °C

4-bromo-N^3-(2-hydroxy-5-nitrophenyl)-N^1-methyl-1*H*-pyrazole-1,3-dicarboxamide 123:

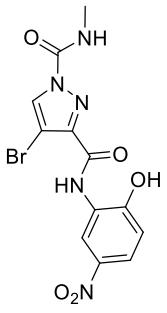

123

General procedure E.c. was followed with acid **6** (50 mg, 0.26 mmol, 1.0 equiv.), HATU (100 mg, 0.26 mmol, 1.0 equiv.), Hünig's base (90 µL, 0.52 mmol, 2.0 equiv.) and 2-amino-4-nitrophenol **138** (40 mg, 0.26 mmol, 1.0 equiv.). Acylation was carried out with **12** (120 mg, 1.04 mmol, 4.0 equiv.) and Et_3N (0.14 mL, 1.04 mmol, 4.0 equiv.). Stirred for 20 hours at room temperature before adding EtOAc and pouring it in water. Left in water layer overnight and precipitate was filtered off to afford compound **123** as a yellow solid that needed no further purification (35 mg, 0.09 mmol, 35%). **IR (ATR)/cm^{-1}**: 3382, 3147, 1757, 1517; **^{1}H NMR** (400 MHz, DMSO-d_6): **δ** 9.78 (br s, 1H), 8.91 (app d, 1H, *J* = 2.8 Hz), 8.72 (br q, 1H, *J* = 4.8 Hz), 8.64 (s, 1H), 7.74 (dd, 1H, *J* = 9.2, 3.2 Hz), 6.13 (d, 1H, *J* = 9.2 Hz), 2.85 (d, 3H, *J* = 4.8 Hz); **^{13}C NMR** (101 MHz, DMSO-d_6): **δ** 170.3, 157.0, 148.6, 144.5, 132.1, 127.6, 124.5, 115.4, 113.0, 95.9, 27.0; **LRMS (ES-APCI)**: *m/z* = 324.9 $[M-H-C_2H_3NO]^-$; **HRMS**: found *m/z* = 383.9936, calculated for $C_{12}H_{11}O_5N_5Br_1$ *m/z* = 383.9938; **M.P.**: > 250 °C

- Naphthalene and quinoline amides

4-bromo-N^1-methyl-N^3-(naphthalen-1-yl)-1*H*-pyrazole-1,3-dicarboxamide 124:

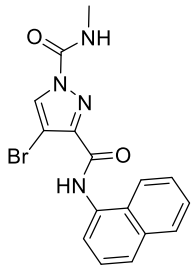

124

General procedure E.c. was followed with acid **6** (50 mg, 0.26 mmol, 1.0 equiv.), HATU (100 mg, 0.26 mmol, 1.0 equiv.), Hünig's base (90 µL, 0.52 mmol, 2.0 equiv.) and 1-naphtylamine (33 µL, 0.26 mmol, 1.0 equiv.). Acylation was carried out with **12** (120 mg, 1.04 mmol, 4.0 equiv.) and Et_3N (0.14 mL, 1.04 mmol, 4.0 equiv.). The crude reaction mixture was purified by column chromatography with 80:20 PE:acetone eluent and further triturated with chloroform and PE to give **124** as a white solid (20 mg, 0.05 mmol, 19%). **IR (ATR)/cm^{-1}**: 3423, 3385, 3341, 3131; 3075, 1736, 1679, 1519; **^{1}H NMR** (400 MHz, $CDCl_3$): **δ** 8.94 (br s, 1H), 8.32 (s, 1H), 8.04 (d, 1H, *J* = 7.6 Hz), 7.92–7.87 (m, 2H), 7.73 (d, 1H, *J* = 8.4 Hz), 7.54–7.47 (m, 3H), 7.21 (br d, 1H, *J* = 4.4 Hz), 3.06 (d, 3H, *J* = 4.8 Hz); **^{13}C NMR** (101 MHz, $CDCl_3$): **δ** 158.6, 148.7, 144.4, 134.2, 132.0, 131.5, 129.0, 127.3, 126.7, 126.5, 126.3, 125.9, 121.2, 120.8, 97.5, 27.3; **LRMS (ES-APCI)**: *m/z* = 394.7 $[M+Na]^+$; **HRMS**: found *m/z* = 373.0295, calculated for $C_{16}H_{14}O_2N_4Br_1$ *m/z* = 373.0295; **M.P.**: 174 °C

4-bromo-N^1-methyl-N^3-(quinolin-5-yl)-1*H*-pyrazole-1,3-dicarboxamide 125:

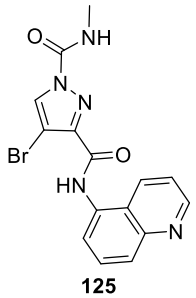

125

General procedure E.c. was followed with acid **6** (50 mg, 0.26 mmol, 1.0 equiv.), HATU (100 mg, 0.26 mmol, 1.0 equiv.), Hünig's base (90 µL, 0.52 mmol, 2.0 equiv.)

and 5-aminoquinoline (38 mg, 0.26 mmol, 1.0 equiv.). Acylation was carried out with **12** (120 mg, 1.04 mmol, 4.0 equiv.) and Et_3N (0.14 mL, 1.04 mmol, 4.0 equiv.). The crude reaction mixture was purified by column chromatography with 70:30 PE:acetone eluent to give **125** as a white solid (10 mg, 0.03 mmol, 12%). **IR (ATR)/cm^{-1}**: 3149, 1725, 1690, 1495, 1247; **^{1}H NMR** (400 MHz, DMSO-d_6): **δ** 10.52 (s, 1H), 8.97 (dd, 1H, *J* = 4.0, 1.6 Hz), 8.74 (br app q, 1H, *J* = 4.4 Hz), 8.71 (s, 1H), 8.49 (d, 1H, *J* = 8.4 Hz), 7.97 (app dd, 1H, *J* = 6.4, 3.2 Hz), 7.84–7.80 (m, 2H), 7.6 (dd, 1H, *J* = 8.8, 4.4 Hz), 2.91 (d, 3H, *J* = 4.8 Hz); **^{13}C NMR** (101 MHz, DMSO-d_6): **δ** 159.2, 150.7, 148.5, 148.1, 144.1, 132.7, 131.9, 131.4, 129.1, 127.2, 123.3, 122.7, 121.3, 96.0 26.8; **LRMS (ES-APCI)**: *m/z* = 374.0 $[M+H]^+$; **HRMS**: found *m/z* = 374.0245, calculated for $C_{15}H_{13}O_2N_4Br_1$ *m/z* = 374.0247;

4-bromo-*N*^{1}-methyl-*N*^{3}-(quinolin-3-yl)-1*H*-pyrazole-1,3-dicarboxamide 126:

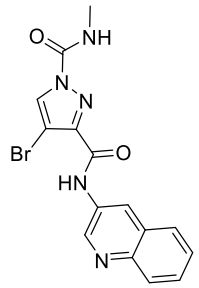

126

General procedure E.c. was followed with acid **6** (50 mg, 0.26 mmol, 1.0 equiv.), HATU (100 mg, 0.26 mmol, 1.0 equiv.), Hünig's base (90 µL, 0.52 mmol, 2.0 equiv.) and 3-aminoquinoline (38 mg, 0.26 mmol, 1.0 equiv.). Acylation was carried out with **12** (120 mg, 1.04 mmol, 4.0 equiv.) and Et_3N (0.14 mL, 1.04 mmol, 4.0 equiv.). The crude reaction mixture was purified by column chromatography with 70:30 PE:acetone eluent to give **126** as a white solid (47 mg, 0.13 mmol, 50%). **IR (ATR)/cm^{-1}**: 3514, 3266, 3134, 1744, 1556 ; **^{1}H NMR** (400 MHz, $CDCl_3$): **δ** 9.02 (app d, 1H, *J* = 2.4 Hz), 8.86 (br s, 1H), 8.85 (app d, 1H, *J* = 2.8 Hz), 8.39 (s, 1H), 8.04 (d, 1H, *J* = 8.0 Hz), 7.83 (dd, 1H, *J* = 8.0, 0.8 Hz), 7.69–7.65 (m, 1H), 7.59–7.55 (m, 1H), 7.17 (br s, 1H, *J* = 4.4 Hz), 3.11 (d, 3H, *J* = 4.8 Hz); **^{13}C NMR** (101 MHz, $CDCl_3$): **δ** 158.5, 148.6, 145.6, 143.8, 132.3, 131.0, 129.2, 128.9, 128.4, 128.2, 127.8, 124.4, 97.7, 27.4; **LRMS (ES-APCI)**: *m/z* = 374.1$[M+H]^+$;

HRMS: found *m/z* = 374.0250, calculated for $C_{15}H_{13}O_2N_5Br_1$ *m/z* = 374.0247; **M.P.**: 90 °C

4-bromo-*N*^{1}-methyl-*N*^{3}-(quinolin-6-yl)-1*H*-pyrazole-1,3-dicarboxamide 127:

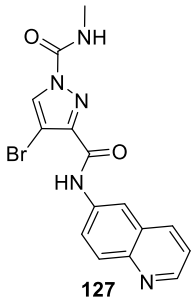

127

General procedure E.c. was followed with acid **6** (50 mg, 0.26 mmol, 1.0 equiv.), HATU (100 mg, 0.26 mmol, 1.0 equiv.), Hünig's base (90 µL, 0.52 mmol, 2.0 equiv.) and 6-aminoquinoline (37 mg, 0.26 mmol, 1.0 equiv.). Acylation was carried out with **12** (120 mg, 1.04 mmol, 4.0 equiv.) and Et_3N (0.14 mL, 1.04 mmol, 4.0 equiv.). The crude reaction mixture was purified by column chromatography with 85:25 PE:acetone eluent to give **127** as an off-white solid (10 mg, 0.03 mmol, 12%). **IR (ATR)/cm^{-1}**: 3341, 3140, 1725, 1679; **^{1}H NMR** (5 to 1 rotamers, minor rotamer*, 400 MHz, DMSO-d_6): **δ** 10.59 (br s, 1H), 10.5 (br s, 1H)*, 8.81 (dd, 1H, *J* = 4.4, 1.6 Hz), 8.80 (dd, 1H, *J* = 4.0, 1.6 Hz)*, 8.73 (br app d, H, *J* = 4.8 Hz), 8.72 (s, 1H), 2.90 (d, 3H, *J* = 4.8 Hz), 2.80 (d, 3H, *J* = 4.8 Hz)*; **^{13}C NMR** (101 MHz, DMSO-d_6): **δ** 158.6, 149.5, 148.5, 145.0, 144.4, 136.0, 135.7, 131.4, 129.7, 128.6, 123.6, 121.9, 116.1, 95.9, 26.8; **LRMS (ES-APCI)**: *m/z* = 374.0 $[M+H]^+$; **HRMS**: found *m/z* = 374.0249, calculated for $C_{12}H_{12}O_2N_5Br_1Na_1$ *m/z* = 374.0247; **M.P.**: > 250 °C (decomp)

- Indole amides

1*H*-indol-5-amine 131:[81]

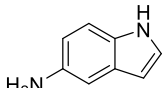

131

5-nitroindole **128** (200 mg, 1.23 mmol, 1.0 equiv.) was dissolved in EtOH (4 mL) and H_2O (1 mL) followed by addition of concentrated HCl (0.1 mL), NH_4Cl (658 mg, 12.3 mmol, 10.0 equiv.) and iron powder (344 mg, 6.16 mmol, 5.0 equiv.) were added under N_2. The reaction mixture was stirred under reflux for 2 hours and left to cool down before filtration. The filtrate was concentrated and then dissolved in H_2O. The mixture was basified with sat aq. Na_2CO_3 and extracted with CH_2Cl_2 (2 × 20 mL). The organic phase was dried over $MgSO_4$, filtered and concentrated to give product **131** as a brown solid (100 mg, 0.76 mmol, 62%). **IR (ATR)/cm^{-1}**: 3419, 3380, 3339, 3073; 1340; **^{1}H NMR** (400 MHz, $CDCl_3$): **δ** 7.91 (br s, 1H), 7.21 (d, 1H, *J* = 8.8 Hz), 7.14 (app t, 1H, *J* = 2.8 Hz), 6.96 (app d, 1H, *J* = 2.4 Hz), 6.68 (dd, 1H, *J* = 8.4, 2.4 Hz), 6.39–6.38 (m, 1H), 3.51 (br s, 2H); **^{13}C NMR** (101 MHz, $CDCl_3$): **δ** 139.8, 130.9, 129.1, 124.9, 113.2, 111.7, 105.8, 101.8; **LRMS (ES-APCI)**: *m/z* = 133.2 $[M+H]^+$; **M.P.**: 131 °C (130–132 °C in lit)[117]

1*H*-indol-6-amine 132:

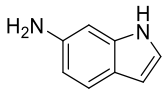

132

A mixture of 6-aminoindole **129** (150 mg, 0.93 mmol, 1.0 equiv.), iron powder (250 mg, 4.63 mmol, 5.0 equiv.), concentrated HCl (0.1 mL) with H_2O (0.5 mL) in EtOH (1.5 mL) was refluxed at 80 °C. After 2 hours, the reaction mixture was filtered through celite and the filtrate was concentrated *in vacuo*. The residue was diluted with cold H_2O (5 mL), basified with a 1 M NaOH solution to pH = 9 and extracted with EtOAc (2 × 10 mL). The organic layer was washed with brine, dried over $MgSO_4$, filtered and concentrated in vacuo. The crude brown product **132** (100 mg, 0.76 mmol, 82%) was used as is in next step.**^{1}H NMR** (400 MHz, DMSO-d_6): **δ** 10.42 (br s, 1H), 7.16 (d, 1H, *J* = 8.0 Hz), 6.95 (br app t, 1H, *J* = 2.4 Hz), 6.55 (br s, 1H), 6.37 (d, 1H,

J = 7.6 Hz), 4.68 (br s, 2H); **^{13}C NMR** (101 MHz, DMSO-d_6): **δ** 143.6, 137.5, 121.7, 120.0, 119.5, 109.7, 100.8, 95.2; **LRMS (ES-APCI)**: *m/z* = 133.2 $[M+H]^+$; **M.P.**: 66 °C (66−67 °C in lit)[118]

1*H*-indol-7-amine 133:[82]

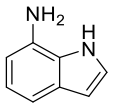

133

General procedure L was followed with Pd/C (170 mg, 0.16 mmol, 10 mol%), 7-nitroindole **130** (500 mg, 3.08 mmol, 1.0 equiv.) in MeOH (12 mL). The reaction was left to stir for 1.5 h at room temperature. The crude was triturated with chloroform and PE to give amine **133** as a dark gray solid (260 mg, 1.98 mmol, 64%). Low yield due to spillage. **IR (ATR)/cm^{-1}**: 3361, 3302, 3185, 1584, 1446; **^{1}H NMR** (500 MHz, $CDCl_3$): **δ** 8.02 (br s, 1H), 7.22 (d, 1H, *J* = 6.4 Hz), 7.13 (br s, 1H), 6.99 (app t, 1H, *J* = 6.4 Hz), 6.61 (d, 1H, *J* = 6.0 Hz), 6.55 (d, 1H, *J* = 2.2 Hz), 5.00 (br s, 2H); **^{13}C NMR** (101 MHz, DMSO-d_6): **δ** 133.7, 128.2, 125.7, 123.7, 119.9, 108.9, 104.5, 101.4; **LRMS (ES-APCI)**: *m/z* = 133.1 $[M+H]^+$; **M.P.**: 100 °C (94−95 °C in lit)[82]

4-bromo-*N*^{3}-(1H-indol-5-yl)-*N*^{1}-methyl-1*H*-pyrazole-1,3-dicarboxamide 134:

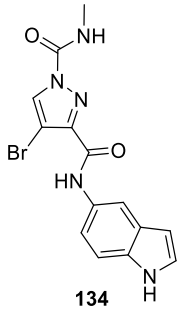

134

General procedure E.c. was followed with acid **6** (50 mg, 0.26 mmol, 1.0 equiv.), HATU (100 mg, 0.26 mmol, 1.0 equiv.), Hünig's base (90 µL, 0.52 mmol, 2.0 equiv.) and 5-aminoindole **131** (29 µL, 0.26 mmol, 1.0 equiv.). Acylation was carried out with **12** (120 mg, 1.04 mmol, 4.0 equiv.) and Et_3N (0.14 mL, 1.04 mmol, 4.0 equiv.). The crude reaction mixture was purified by column chromatography with 85:25 PE:acetone eluent and further triturated with chloroform and PE to give **134** as a white

solid (10 mg, 0.03 mmol, 12%). **IR (ATR)/cm^{-1}**: 3344 (br), 1727, 1658, 1537; **^{1}H NMR** (400 MHz, DMSO-*d*$_6$): **δ** 11.01 (br s, 1H), 10.06 (br s, 1H), 8.71 (br q, 1H, *J* = 4.4 Hz), 8.64 (s, 1H), 7.98 (app d, 1H, *J* = 2.0 Hz), 7.39–7.35 (m, 3H), 6.42–6.41 (m, 1H), 2.89 (d, 3H, *J* = 4.8 Hz); **^{13}C NMR** (101 MHz, DMSO-*d*$_6$): **δ** 157.8, 148.8, 145.0, 133.1, 131.2, 130.0, 127.5, 126.2, 115.2, 111.5, 111.3, 101.2, 95.6, 26.8; **LRMS (ES-APCI)**: *m/z* = 305.0 $[M+H-C_2H_3N_1O_1]^+$; **HRMS**: found *m/z* = 362.0252, calculated for $C_{14}H_{13}O_2N_5Br_1$ *m/z* = 362.0247; **M.P.**: 160 °C

4-bromo-*N*^{3}-(1*H*-indol-6-yl)-*N*^{1}-methyl-1*H*-pyrazole-1,3-dicarboxamide 135:

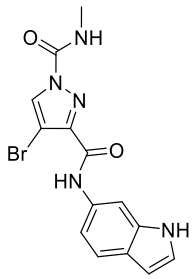

135

General procedure E.c. was followed with acid **6** (50 mg, 0.26 mmol, 1.0 equiv.), HATU (100 mg, 0.26 mmol, 1.0 equiv.), Hünig's base (90 μL, 0.52 mmol, 2.0 equiv.) and 6-aminoindole **132** (35 mg, 0.26 mmol, 1.0 equiv.). Acylation was carried out with **12** (120 mg, 1.04 mmol, 4.0 equiv.) and Et_3N (0.14 mL, 1.04 mmol, 4.0 equiv.). The crude reaction mixture was purified by column chromatography with 70:30 PE:acetone eluent and further triturated with EtOAc and PE to give **135** as a brownish solid (11 mg, 0.03 mmol, 12%). **IR (ATR)/cm^{-1}**: 3335, 3298; 1731, 1680, 1667; **^{1}H NMR** (400 MHz, DMSO-*d*$_6$): **δ** 10.26 (br s, 1H), 9.47 (br s, 1H), 8.46 (s, 1H), 8.22 (s, 1H), 8.14 (br s, 1H), 7.53 (d, 1H, *J* = 8.4 Hz), 7.32 (app t, 1H, *J* = 2.8 Hz), 7.16 (dd, 1H, *J* = 8.4, 2.0 Hz), 6.45 (1H, br s), 3.01 (d, 3H, *J* = 4.8 Hz); **^{13}C NMR** (101 MHz, DMSO-*d*$_6$): **δ** 157.8, 148.6, 145.0, 135.8, 132.1, 131.2, 125.4, 124.5, 119.9, 112.8, 102.9, 101.0, 95.6, 26.8; **LRMS (ES-APCI)**: *m/z* = 362.0 $[M+H]^+$; **HRMS**: found *m/z* = 362.0250, calculated for $C_{14}H_{13}O_2N_5Br_1$ *m/z* = 362.0247; **M.P.**: 178 °C (decomp)

4-bromo-N^3-(1H-indol-7-yl)-N^1-methyl-1*H*-pyrazole-1,3-dicarboxamide 136:

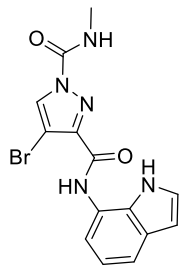

136

General procedure E.c. was followed with acid **6** (50 mg, 0.26 mmol, 1.0 equiv.), HATU (100 mg, 0.26 mmol, 1.0 equiv.), Hünig's base (90 µL, 0.52 mmol, 2.0 equiv.) and 7-aminoindole **133** (34 mg, 0.26 mmol, 1.0 equiv.). Acylation was carried out with **12** (120 mg, 1.04 mmol, 4.0 equiv.) and Et_3N (0.14 mL, 1.04 mmol, 4.0 equiv.). The crude mixture was purified by column chromatography with 70:30 PE:acetone eluent and further triturated with chloroform and PE to give **136** as a white solid (25 mg, 0.07 mmol, 29%). **IR (ATR)/cm^{-1}**: 3488, 3423, 1719, 1530, 1257; **^{1}H NMR** (400 MHz, $CDCl_3$): **δ** 10.12 (br s, 1H), 8.79 (br s, 1H), 8.40 (s, 1H), 7.55 (d, 1H, *J* = 7.6 Hz), 7.29 (app t, 1H, *J* = 2.8 Hz), 7.06 (app t, 1H, *J* = 7.6 Hz), 7.04 (br s, 1H), 6.88 (d, 1H, *J* = 7.2 Hz), 6.59 (dd, 1H, *J* = 3.2, 2.0 Hz), 3.12 (d, 3H, *J* = 5.2 Hz); **^{13}C NMR** (101 MHz, DMSO-d_6): **δ** 158.3, 148.6, 144.4, 131.3, 129.4, 129.1, 125.5, 122.0, 118.9, 117.7, 115.2, 101.6, 96.0, 26.8; **LRMS (ES-APCI)**: *m/z* = 362.0 $[M+H]^+$; **HRMS**: found *m/z* = 362.0251, calculated for $C_{14}H_{13}O_2N_5Br_1$ *m/z* = 362.0247; **M.P.**: 115 °C

- Benzoxazole amides

4-nitrobenzo[d]oxazole 140:

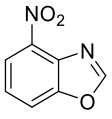

140

General procedure H was followed with 2-amino-3-nitrophenol **137** (150 mg, 0.97 mmol, 1.0 equiv.), triethylorthoformate (0.49 mL, 2.92 mmol, 3.0 equiv.) and *p*-toluenesulfonic acid monohydrate (9 mg, 0.05 mmol, 5 mol%) in toluene (2 mL). The precipitate was filtered and dried to give **140** as a light brown solid (102 mg,

0.62 mmol, 64%). **IR (ATR)/cm^{-1}**: 3118, 3077, 1504; **^{1}H NMR** (400 MHz, $CDCl_3$): **δ** 8.36 (br s, 1H), 8.25 (dd, 1H, *J* = 8.4, 0.8 Hz), 7.96 (dd, 1H, *J* = 8.0, 0.4 Hz), 7.58 (app t, 1H, *J* = 8.0 Hz); **^{13}C NMR** (101 MHz, DMSO-d_6): **δ** 157.5, 151.2, 138.9, 134.0, 125.8, 121.0, 118.2; **LRMS (ES-APCI)**: *m/z* = 165.1 $[M+H]^+$; **M.P.**: 129 °C

5-nitrobenzo[d]oxazole5-nitrobenzo[d]oxazole 141:

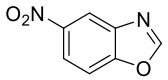

141

General procedure H was followed with 2-amino-4-nitrophenol **138** (150 mg, 0.97 mmol, 1.0 equiv.), triethylorthoformate (0.49 mL, 2.92 mmol, 3.0 equiv.) and *p*-toluenesulfonic acid monohydrate (9 mg, 0.05 mmol, 5 mol%) in toluene (2 mL).The precipitate was filtered and dried to give **141** as a light red solid (130 mg, 0.79 mmol, 81%). **IR (ATR)/cm^{-1}**: 3114, 3077, 1511; **^{1}H NMR** (400 MHz, $CDCl_3$): **δ** 8.72 (app d, 1H, *J* = 2.4 Hz), 8.39 (dd, 1H, *J* = 5.6 Hz), 8.28 (s, 1H), 7.73 (d, 1H, *J* = 8.8 Hz); **^{13}C NMR** (101 MHz, $CDCl_3$): **δ** 155.4, 153.7, 145.8, 140.7, 122.0, 117.4, 111.6; **LRMS (ES-APCI)**: *m/z* = 163.1 $[M-H]^-$; **M.P.**: 125 °C (127 °C in lit) [119]

6-nitrobenzo[d]oxazole 142:

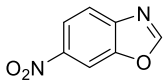

142

General procedure H was followed with 2-amino-5-nitrophenol **139** (150 mg, 0.97 mmol, 1.0 equiv.), triethylorthoformate (0.49 mL, 2.92 mmol, 3.0 equiv.) and *p*-toluenesulfonic acid monohydrate (9 mg, 0.05 mmol, 5 mol%) in toluene (2 mL). The precipitate was filtered and dried under vacuum to give **142** as a light solid (90 mg, 0.55 mmol, 57%). It was used as is in next step. **^{1}H NMR** (400 MHz, $CDCl_3$): **δ** 8.53 (app d, 1H, *J* = 2.4 Hz), 8.37–8.34 (m, 2H), 7.93 (d, 1H, *J* = 8.8 Hz); **^{13}C NMR** (101 MHz, $CDCl_3$): **δ** 156.7, 149.4, 146.1, 145.3, 121.0, 120.9, 108.0;

benzo[d]oxazol-4-amine 143:

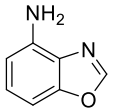

143

In a round bottom flask, NH_4Cl (68 mg, 1.28 mmol, 3.0 equiv.) was dissolved in H_2O (4 mL) whereupon Fe (spatula) was added. Nitro compound **140** (70 mg, 0.43 mmol, 1.0 equiv.) was dissolved in acetone (6 mL) and added to the reaction mixture which was heated at 90 °C for 3 hours. The reaction was left to cool down before extracting the product with EtOAc (3 × 15 mL). The organic layer was washed with a sat aq. $NaHCO_3$ solution (10 mL), followed by brine (10 mL) and dried over $MgSO_4$, filtered and concentrated *in vacuo*. The brown solid **143** (50 mg, 0.37 mmol, 88%) was used as is in next step. **IR (ATR)/cm^{-1}**: 3318, 3216, 3106, 2921, 1247; **^{1}H NMR** (400 MHz, $CDCl_3$): **δ** 7.97 (s, 1H), 7.16 (app t, 1H, *J* = 8.0 Hz), 6.95 (d, 1H, *J* = 8.0 Hz), 6.61 (d, 1H, *J* = 7.6 Hz); **^{13}C NMR** (101 MHz, $CDCl_3$): **δ** 151.3, 150.6, 139.5, 128.5, 126.6, 109.0, 100.6; **LRMS (ES-APCI)**: *m/z* = 135.1 $[M+H]^+$; **M.P.**: 76 °C

benzo[d]oxazol-5-amine 144:

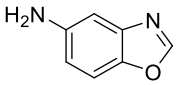

144

In a round bottom flask, NH_4Cl (96 mg, 1.79 mmol, 3.0 equiv.) was dissolved in H_2O (4 mL) whereupon Fe (spatula) was added. Nitro compound **141** (98 mg, 0.60 mmol, 1.0 equiv.) was dissolved in acetone (6 mL) and added to the reaction mixture which was heated at 90 °C for 3 hours. The reaction was left to cool down before extracting the product with EtOAc (3 × 15 mL). The organic layer was washed with a sat aq. $NaHCO_3$ solution (10 mL), followed by brine (10 mL) and dried over $MgSO_4$, filtered and concentrated *in vacuo*. The brown solid **144** (110 mg, 0.82 mmol, 46%) was used as is in next step. **IR (ATR)/cm^{-1}**: 3214, 2919, 1495; **^{1}H NMR** (400 MHz, $CDCl_3$): **δ** 8.00 (s, 1H), 7.35 (d, 1H, *J* = 8.8 Hz), 7.05 (d, 1H, *J* = 2.4 Hz), 6.74 (dd, 1H,

J = 8.8, 2.4 Hz), 3.27 (br s, 2H); **^{13}C NMR** (101 MHz, $CDCl_3$): **δ** 153.2, 144.1, 141.3, 125.7, 114.5, 111.2, 105.6; ; **LRMS (ES-APCI)**: *m/z* = 133.0 $[M-H]^-$; **M.P.**: 160 °C

benzo[d]oxazol-6-amine 145:

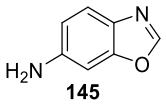

145

In a round bottom flask, NH_4Cl (68 mg, 1.28 mmol, 3.0 equiv.) was dissolved in H_2O (3 mL) whereupon Fe (spatula) was added. Nitro compound **142** (70 mg, 0.43 mmol, 1.0 equiv.) was dissolved in acetone (5 mL) and added to the reaction mixture which was heated at 90 °C for 3 hours. The reaction was left to cool down before extracting the product with EtOAc (3 × 15 mL). The organic layer was washed with a sat aq. $NaHCO_3$ solution (10 mL), followed by brine (10 mL) and dried over $MgSO_4$, filtered and concentrated *in vacuo*. The brown solid **145** (80 mg, 0.60 mmol, 47%) was used as is in next step. **IR (ATR)/cm^{-1}**: 3315, 3209, 2922, 1618, 1494; **^{1}H NMR** (400 MHz, DMSO-d_6): **δ** 8.31 (s, 1H), 7.38 (d, 1H, *J* = 8.4 Hz), 6.77 (app d, 1H, *J* = 2.0 Hz), 6.62 (dd, 1H, *J* = 8.4, 2.0 Hz), 5.34 (br s, 2H); **^{13}C NMR** (101 MHz, DMSO-d_6): **δ** 151.0, 150.8, 147.9, 129.9, 119.8, 112.4, 94.4; **LRMS (ES-APCI)**: *m/z* = 135.1 $[M+H]^+$; **M.P.**: 92 °C

2-methyl-4-nitrobenzo[d]oxazole 146:[86]

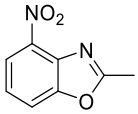

146

In a microwave vial, 2-amino-3-nitrophenol **137** (1.0 g, 6.49 mmol, 1.0 equiv.) was added and the vial sealed. Triethylorthoacetate (4.8 mL, 26 mmol, 4.0 equiv.) was added and the reaction stirred at 100 °C for 16 h. The crude was left to cool down and the precipitate was filtered and washed with hexane. This gave the desired benzoxazole **146** as a brown solid (1.0 g, 5.61 mmol, 86%). **IR (ATR)/cm^{-1}**: 3421, 3333, 1612, 1495; **^{1}H NMR** (400 MHz, DMSO-d_6): **δ** 8.14 (d, 2H, *J* = 8.4 Hz), 7.58 (t, 1H, *J* = 8.4 Hz), 2.73 (s, 3H); **^{13}C NMR** (101 MHz, DMSO-d_6): **δ** 168.0, 152.1, 137.9,

135.4, 124.5, 120.3, 117.1, 14.3; **LRMS (ES-APCI)**: *m/z* = 179.1 $[M+H]^+$; **M.P.**: 128 °C (124−125 °C in lit)[120]

2-methylbenzo[d]oxazol-4-amine 147:[86]

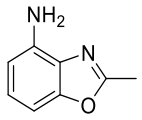

147

Nitro compound **146** (900 mg, 5.05 mmol, 1.0 equiv.) was dissolved in 1:1 EtOAc/10% AcOH (15 mL) and heated to 70 ° C. Fe powder (1.41 g, 25.30 mmol, 5.0 equiv.) was added portion wise and the reaction was stirred at 70 ° C for 3 h. After cooling, the mixture was filtered through celite and washed with EtOAc (30 mL). The organic layer was separated, washed with H_2O (3 × 20 mL), brine (10 mL), dried over $MgSO_4$, and concentrated *in vacuo* to give amine **147** as a light brown solid (500 mg, 3.37 mmol, 67%). **IR (ATR)/cm^{-1}**: 3423, 3333, 3250, 1634, 1240; **^{1}H NMR** (400 MHz, $CDCl_3$): **δ** 7.04 (app t, 1H, *J* = 7.6 Hz), 6.81 (d, 1H, *J* = 7.6 Hz), 6.53 (d, 1H, *J* =8.0 Hz), 5.76 (br s, 2H), 2.57 (s, 3H); **^{13}C NMR** (101 MHz, $CDCl_3$): **δ** 161.8, 151.9, 138.8, 128.8, 125.4, 109.0, 99.8, 14.2; **LRMS (ES-APCI)**: *m/z* = 149.1 $[M+H]^+$; **M.P.**: 170 °C (172 °C in lit)[120]

***N*^{3}-(benzo[d]oxazol-4-yl)-4-bromo-*N*^{1}-methyl-1*H*-pyrazole-1,3-dicarboxamide 148:**

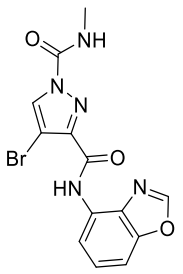

148

General procedure E.c. was followed with acid **6** (50 mg, 0.26 mmol 1.0 euiv.), HATU (100 mg, 0.26 mmol, 1.0 equiv.), Hünig's base (90 µL, 0.52 mmol, 2.0 equiv.) and aminobenzoxazole **143** (35 mg, 0.26 mmol, 1.0 equiv.). Acylation was carried out with **12** (120 mg, 1.04 mmol, 4.0 equiv.) and Et_3N (0.14 mL, 1.04 mmol,

4.0 equiv.). The crude reaction mixture was purified by column chromatography with 80:20 PE:acetone eluent and further crystallised by vapour diffusion with MeOH, CH2Cl2 and PE to give **148** was a light brown crystal (4 mg, 0.01 mmol, 4%). Only a crystal structure was obtained for this analogue

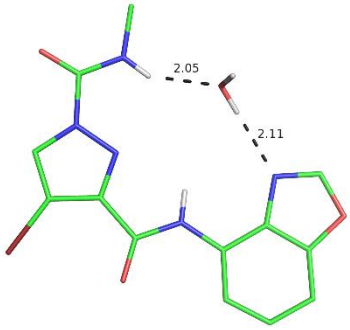

<u>*N*^{3}-(benzo[d]oxazol-5-yl)-4-bromo-*N*^{1}-methyl-1*H*-pyrazole-1,3-dicarboxamide 149:</u>

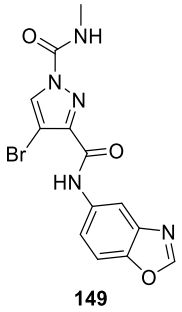

149

General procedure E.c. was followed with acid **6** (50 mg, 0.26 mmol, 1.0 equiv.), HATU (100 mg, 0.26 mmol, 1.0 equiv.), Hünig's base (90 µL, 0.52 mmol, 2.0 equiv.) and 5-aminobenzoxazole **144** (35 mg, 0.26 mmol, 1.0 equiv.). Acylation was carried out with **12** (120 mg, 1.04 mmol, 4.0 equiv.) and Et_3N (0.14 mL, 1.04 mmol, 4.0 equiv.). The crude reaction mixture was purified by column chromatography with 70:30 PE:acetone eluent, before trituration with EtOAc and PE to afford **149** as a pink solid (9 mg, 0.02 mmol, 7%) that still small traces of the analogue without the urea functionality. **^{1}H NMR** (400 MHz, DMSO-d_6): **δ** 10.47 (br s, 1H), 8.75 (s, 1H), 8.69 (br s, 1H), 8.68 (s, 1H), 8.24 (s, 1H), 7.79 (d, 1H, J = 8.8 Hz), 7.71 (d, 1H, J = 8.4 Hz), 2.90 (d, 3H, J = 4.4 Hz); **^{13}C NMR** (101 MHz, DMSO-d_6): **δ** 158.3, 155.1, 148.5, 146.0, 144.6, 139.9, 135.1, 131.4 , 118.5, 111.2, 111.1, 95.8, 26.8; **LRMS (ES-APCI)**:

m/z = 386.0 $[M+Na]^+$; **HRMS**: found *m/z* = 364.0038, calculated for $C_{13}H_{11}O_3N_5Br_1$ *m/z* = 364.0040

<u>*N*³-(benzo[*d*]oxazol-6-yl)-4-bromo-*N*¹-methyl-1*H*-pyrazole-1,3-dicarboxamide 150:</u>

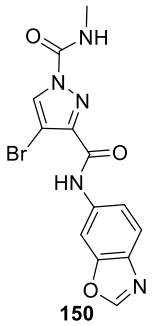

150

General procedure E.c. was followed with acid **6** (50 mg, 0.26 mmol, 1.0 equiv.), HATU (100 mg, 0.26 mmol, 1.0 equiv.), Hünig's base (90 µL, 0.52 mmol, 2.0 equiv.) and 6-aminobenzoxazole **145** (35 mg, 0.26 mmol, 1.0 equiv.). The crude reaction mixture was purified by column chromatography with 70:30 PE:acetone eluent to give **150** as an off-white solid (60 mg, 0.16 mmol, 62%). **IR (ATR)/cm^{-1}**: 3343, 3140, 1723, 1679, 1526, 1487; **^{1}H NMR** (400 MHz, $CDCl_3$): **δ** 8.67 (br s, 1H), 8.42 (app d, 1H, *J* = 1.2 Hz), 8.37 (s, 1H), 8.10 (s, 1H), 7.74 (d, 1H, *J* = 8.4 Hz), 7.32 (dd, 1H, *J* = 8.4, 2.0 Hz), 7.06 (br s, 1H), 3.10 (d, 3H, *J* = 4.8 Hz); **^{13}C NMR** (101 MHz, DMSO-d_6): **δ** 158.4, 154.2, 149.5, 148.5, 144.5, 136.1, 131.4, 120.1, 117.3, 102.5, 95.8, 26.8; **LRMS (ES-APCI)**: *m/z* = 305.0 $[M-H-C_2H_3NO]^-$; **HRMS**: found *m/z* = 364.0043, calculated for $C_{13}H_{11}O_3N_5Br_1Na_1$ *m/z* = 364.0040; **M.P.**: 245 °C

4-bromo-*N*^{1}-methyl-*N*^{3}-(2-methylbenzo[d]oxazol-4-yl)-1*H*-pyrazole-1,3-dicarboxamide 151:

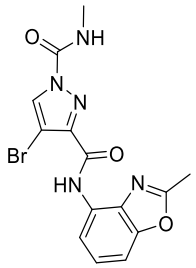

151

General procedure E.c. was followed with acid **6** (50 mg, 0.26 mmol, 1.0 equiv.), HATU (100 mg, 0.26 mmol, 1.0 equiv.), Hünig's base (90 µL, 0.52 mmol, 2.0 equiv.) and amine **147** (39 mg, 0.26 mmol, 1.0 equiv.). The reaction mixture was filtered and the precipitate washed with MeCN. Analogue **151** was isolated as an off-white solid (50 mg, 0.13 mmol, 50%). **IR (ATR)/cm^{-1}**: 3374, 3132, 1753, 1679, 1506; **^{1}H NMR** (400 MHz, DMSO-*d*$_6$, T = 50 °C): **δ** 9.87 (br s, 1H), 8.78 (br app q, 1H, *J* = 4.0 Hz), 8.63 (s, 1H), 7.99 (d, 1H, *J* = 8.0 Hz), 7.47 (dd, 1H, *J* = 8.0, 0.8 Hz), 7.37 (app t, 1H, *J* = 8.0 Hz), 2.90 (d, 3H, *J* = 4.8 Hz), 2.66 (s, 3H); **^{13}C NMR** (101 MHz, DMSO-*d*$_6$): **δ** 163.4, 158.2, 150.8, 148.5, 143.5, 131.9, 128.3, 124.9, 116.2, 106.8, 96.1, 26.8, 14.1; **LRMS (ES-APCI)**: *m/z* = 378.0 $[M+H]^+$; **HRMS**: found *m/z* = 378.0198, calculated for $C_{14}H_{13}O_3N_5Br_1$ *m/z* = 378.0196; **M.P.**: 215 °C

c. **Part C**

4-chloro-3-methyl-1*H*-pyrazole 152:[87]

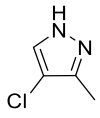

152

In a flask, pyrazole **4** (5.0 g, 73.4 mmol, 1.0 equiv.) was dissolved in glacial acetic acid (40 mL) and NaOCl (45 mL, 726 mmol, 10.0 equiv.) was then added. The reaction was left to stir at room temperature for 18 h, then neutralized with saturated aq. Na_2CO_3 solution. The product was extracted with CH_2Cl_2 (3 × 200 mL) and the solvent evaporated and then diluted with 1 M NaOH (50 mL) and further extracted with

CH_2Cl_2 (3 × 200 mL). The organic layer was dried over $MgSO_4$, filtered and concentrated to give **152** as a beige solid (3.61 g, 31.0 mmol, 42%). **IR (ATR)/cm^{-1}**: 3125, 2835, 1095; **^{1}H NMR** (400 MHz, $CDCl_3$): **δ** 10.64 (br s, 1H), 7.49 (s, 1H), 2.30 (s, 3H); **^{13}C NMR** (101 MHz, $CDCl_3$): **δ** 127.4, 111.8, 109.1, 9.8;

4-chloro-1*H*-pyrazole-3-carboxylic acid 153:

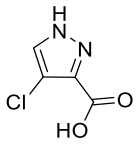

153

In a flask, pyrazole **153** (3.31 g, 28.4 mmol, 1.0 equiv.) and H_2O (150 mL) were added followed by portion wise addition over 1 hour of $KMNO_4$ (13.5 g, 85.2 mmol, 3.0 equiv.) whilst heating at 100 °C. The reaction was refluxed for 24 hours followed by 6 days at room temperature. MnO_2 was filtered off and the water evaporated until only 50 mL remained. The water layer was acidified with a 3 M HCl solution until pH = 2 whereupon a precipitate was formed. The precipitate was filtered and acid **153** was isolated as a white solid (1.69 g, 11.5 mmol, 41%). **IR (ATR)/cm^{-1}**: 3361, 2980, 1710; **^{1}H NMR** and **^{13}C NMR** have given weird spectra; **LRMS (ES-APCI)**: *m/z* = 144.9 $[M-H]^-$; **HRMS**: found *m/z* = 144.9813, calculated for $C_4H_2O_2N_2Cl_1$ *m/z* = 144.9810; **M.P.**: > 250 °C

4-chloro-*N*^{1}-ethyl-*N*^{3}-phenyl-1*H*-pyrazole-1,3-dicarboxamide 154:

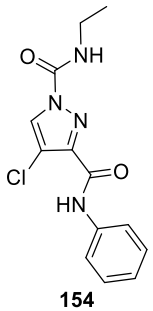

154

General procedure E.d. was followed with acid **153** (50 mg, 0.34 mmol, 1.0 equiv.), HATU (130 mg 0.34 mmol 1.0 equiv.), Hünig's base (0.12 mL, 0.68 mmol, 2.0 equiv.) as well as aniline (31 µL, 0.34 mmol, 1.0 equiv.). Ethylisocyanate (81 µL, 1.02 mmol, 3.0 equiv.) and Et_3N (0.14 mL, 1.02 mmol, 3.0 equiv.) were then added

after 20 h. The crude reaction mixture was purified by column chromatography with 80:20 PE:acetone eluent. The product was further triturated with EtOAc and PE to afford compound **154** as a white solid (50 mg, 0.17 mmol, 50%). **IR (ATR)/cm^{-1}**: 3504, 1730, 1678, 1523, 1236; **^{1}H NMR** (400 MHz, $CDCl_3$): **δ** 8.46 (br s, 1H), 8.31 (s, 1H), 7.69 (dd, 2H, *J* = 8.4, 0.8 Hz), 7.40–7.36 (m, 2H), 7.20–7.16 (m, 1H), 7.07 (br app t, 1H, *J* = 4 Hz), 3.53 (dq, 2H, *J* = 7.6, 6.4 Hz), 1.33 (t, 3H, *J* = 7.2 Hz); **^{13}C NMR** (101 MHz, $CDCl_3$): **δ** 157.6, 148.0, 143.3, 137.3, 129.5, 129.4, 125.1, 120.2, 114.3, 36.0, 15.0; **LRMS (ES-APCI)**: *m/z* = 222.0 $[M–C_3H_5N_1O_1+H]^+$; **HRMS**: found *m/z* = 293.0811, calculated for $C_{13}H_{14}O_2N_4Cl_1$ *m/z* = 293.0805; **M.P.**: 117 °C

<u>*N*^{1}-ethyl-*N*^{3}-phenyl-1*H*-pyrazole-1,3-dicarboxamide 155 :</u>

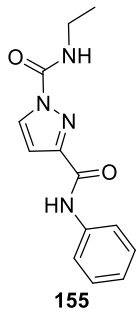

155

General procedure E.d. was followed with acid **5** (50 mg, 0.45 mmol, 1.0 equiv.), HATU (172 mg, 0.45 mmol, 1.0 equiv.), Hünig's base (0.16 mL, 0.84 mmol, 2.0 equiv.) with aniline (41 µL, 0.45 mmol, 1.0 equiv.) Ethylisocyanate (0.11 mL, 1.35 mmol, 3.0 equiv.) and Et_3N (0.19 mL, 1.35 mmol, 3.0 equiv.) were then added after 20 h. The crude material was purified by column chromatography with 80:20 PE:acetone eluent. The product was further triturated with EtOAc and PE to afford compound **155** as a white solid (42 mg, 0.16 mmol, 62%). **IR (ATR)/cm^{-1}**: 3290, 2973, 1732, 1500, 1229; **^{1}H NMR** (400 MHz, $CDCl_3$): **δ** 8.53 (br s, 1H), 8.30 (d, 1H, *J* = 2.4 Hz), 7.70 (dd, 2H, *J* = 8.8, 1.2 Hz), 7.42–7.37 (m, 2H), 7.20–7.15 (m, 1H), 7.07 (br s, 1H), 7.01 (d, 1H, *J* = 2.8 Hz), 3.55 (qd, 2H, *J* = 7.2, 6.0 Hz), 6.35 (t, 3H, *J* = 7.2 Hz); **^{13}C NMR** (101 MHz, $CDCl_3$): **δ** 158.9, 149.3, 148.9, 137.5, 131.0, 129.4, 124.9, 120.1, 109.1, 35.8, 15.1; **LRMS (ES-APCI)**: *m/z* = 188.1 $[M–C_3H_5N_1O_1+H]^+$; **HRMS**: found *m/z* = 259.1191, calculated for $C_{13}H_{15}O_2N_4$ *m/z* = 259.1190; **M.P.**: 108 °C

3. **Phenol and methoxy amide analogues**

2-aminopyridine-1-oxide 157:

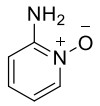

157

m-CPBA (606 mg, 3.51 mmol, 1.1 equiv.) was added to a solution of 2-aminopyridine **156** (300 mg, 3.19 mmol, 1.0 equiv.) at 0 °C in acetone (30 mL). The reaction mixture was stirred for 0.5 h at 0 °C and then warmed up to room temperature to stir for another 15 h. The reaction was concentrated *in vacuo* and the crude product purified my column chromatography with a gradient eluent 95:5 to 90:10 CH_2Cl_2:MeOH to give desired *N*-oxide **157** as an off-white solid (220 mg, 2.00 mmol, 63%). **IR (ATR)/cm^{-1}**: 2980, 1642, 1193; **^{1}H NMR** (400 MHz, DMSO-d_6): **δ** 8.00 (dd, 1H, J = 6.4 Hz), 7.09 (ddd, 1H, J = 8.4, 7.2, 1.2 Hz), 6.79 (dd, 1H), J = 8.8, 2.0 Hz), 6.78 (br s, 2H), 6.56 (ddd, 1H, J = 7.2, 6.8, 2.0 Hz) ; **^{13}C NMR** (101 MHz in DMSO-d_6): **δ** 150.7, 137.0, 126.9, 112.1, 109.0; **LRMS (ES-APCI)**: *m/z* = 111.1 $[M+H]^+$; **M.P.**: 164 °C (164−165 °C in lit)[121]

2-(4-bromo-1-(methylcarbamoyl)-1*H*-pyrazole-3-carboxamido)pyridine 1-oxide 158:

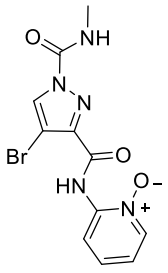

158

General procedure E.c. was followed with acid **6** (50 mg, 0.26 mmol, 1.0 equiv.), HATU (100 mg, 0.26 mmol, 1.0 equiv.), Hünig's base (90 µL, 0.52 mmol, 2.0 equiv.) and amine **157** (27 mg, 0.26 mmol, 1.0 equiv.). Compound **12** (124 mg, 1.04 mmol, 4.0 equiv.) and Et_3N (0.14 mL, 1.04 mmol, 4.0 equiv.) were added after 20 h. The reaction mixture was filtered and washed with MeCN. The light brown precipitate was isolated and analogue **158** did not need further purification (50 mg, 0.15 mmol, 58%).

IR (ATR)/cm^{-1}: 3250, 3067, 1736, 1710, 1504; difficult to obtain a clear NMR for this compound. Tried heating and cooling but unsuccessful; **LRMS (ES-APCI)**: *m/z* = 340.0 $[M+H]^+$; **HRMS**: found *m/z* = 340.0043, calculated for $C_{11}H_{11}O_3N_5Br_1$ *m/z* = 340.0040; **M.P.**: 210 °C (decomp)

benzyl 3-aminobenzoate 160:[122]

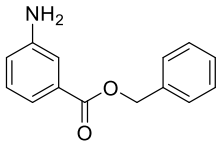

160

In a dry 3 neck, flask under inert atmosphere (N_2), 3-aminobenzoic acid **159** (500 mg, 3.65 mmol, 1.0 equiv.) was dissolved in anhydrous toluene (7 mL). Benzyl alcohol (0.42 mL, 4.01 mmol, 1.1 equiv.) and triphenylphosphine (1.15 g, 4.38 mmol, 1.2 equiv.) were added to the solution. DIAD (0.86 mL, 4.38 mmol, 1.2 equiv.) was added drop-wise and the reaction was stirred for 5.5 h at room temperature. The organic solvent was evaporated and the crude was purified by column chromatography with 80:20 PE:acetone eluent to afford **517** as a light yellow liquid (600 mg, 2.64 mmol, 72%). **IR (ATR)/cm^{-1}**: 3357, 1707, 1288, 1225; **^{1}H NMR** (400 MHz, $CDCl_3$): **δ** 7.49–7.36 (m, 7H), 7.22 (t, 1H, *J* = 7.6 Hz), 6.87 (ddd, 1H, *J* = 8.0, 2.4, 0.8 Hz), 5.35 (s, 2H), 3.77 (br s, 2H); **^{13}C NMR** (101 MHz, $CDCl_3$): **δ** 166.8, 146.7, 136.4, 131.3, 129.5, 128.8, 128.4, 128.4, 120.1, 119.7, 116.1, 66.8; **LRMS (ES-APCI)**: *m/z* = 228.1 $[M+H]^+$; **HRMS**: found *m/z* = 228.1018, calculated for $C_{14}H_{14}O_2N_1$ *m/z* = 228.1019;

benzyl 3-(4-bromo-1-(methylcarbamoyl)-1*H*-pyrazole-3-carboxamido)benzoate 161:

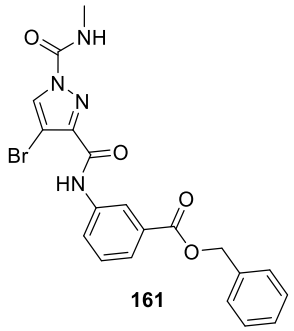

161

General procedure E.c. was followed with acid **6** (100 mg, 0.52 mmol, 1.0 equiv.), HATU (200 mg, 0.52 mmol, 1.0 equiv.), Hünig's base (0.18 mL, 1.04 mmol. 2.0 equiv.) and benzyl-3-aminobenzoate **160** (119 mg, 0.52 mmol, 1.0 equiv.). Acylation was carried out with **12** (240 mg, 2.08 mmol, 4.0 equiv.) and Et_3N (0.28 mL, 2.08 mmol, 4.0 equiv.). The precipitate was filtered and washed with a minimum amount of MeCN to afford **161** as a grey solid (110 mg, 0.24 mmol, 46%). **IR (ATR)/cm^{-1}**: 1719, 1676, 1535, 1274; **^{1}H NMR** (400 MHz, $CDCl_3$): **δ** 8.61 (br s 1H), 8.35 (s, 1H), 8.24 (dd, 1H, *J* = 8.4, 1.2 Hz), 8.05 (s, 1H), 7.87 (d, 1H, *J* = 7.6 Hz), 7.48–7.36 (m, 6H), 7.08 (br d, 1H, *J* = 4.0 Hz), 5.38 (s, 2H), 3.09 (d, 3H, *J* = 5.2 Hz); **^{13}C NMR** (101 MHz, $CDCl_3$): **δ** 166.1, 157.9, 148.6, 144.3, 137.7, 136.1, 132.2, 131.2, 129.7, 128.9, 128.7, 128.5, 126.1, 124.7, 120.8, 97.7, 67.2, 27.3; **LRMS (ES-APCI)**: *m/z* = 400.0 $[M–C_2H_3N_1O_1+H]^+$; **HRMS**: found *m/z* = 479.0315, calculated for $C_{20}H_{17}O_2N_4Br_1$ *m/z* = 479.0325; **M.P.**: 150 °C

ethyl 3-aminobenzoate 163:[89]

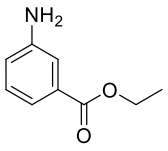

163

In a vial, 3-aminobenzoic acid **159** (500 mg, 3.65 mmol, 1.0 equiv.) was suspended in EtOH (8 mL) and concentrated H_2SO_4 (1 mL). The solution was refluxed for 12 h and the excess EtOH was evaporated *in vacuo*. H_2O (10 mL) was added to the residue and the solution was neutralized carefully with a saturated aq. $NaHCO_3$ solution. The

compound was extracted with EtOAc (2 × 25 mL) and the organic layer dried over $MgSO_4$, filtered and evaporated. This led to the isolation of amine **163** as a brown oil (550 mg, 3.33 mmol, 91%) that was used as is in the next step. **IR (ATR)/cm^{-1}**: 2971, 1702, 1234; **^{1}H NMR** (400 MHz, $CDCl_3$): **δ** 7.44 (app dt, 1H, *J* = 7.6, 1.2 Hz), 7.36 (app t, 1H, *J* = 2 Hz), 7.21 (t, 1H, *J* = 8.0 Hz), 6.86 (ddd, 1H, *J* = 8.0, 2.4, 0.8 Hz), 4.36 (q, 2H, *J* = 7.2 Hz), 3.76 (br s, 2H), 1.38 (t, 3H, *J* = 6.8 Hz); **^{13}C NMR** (101 MHz, $CDCl_3$): **δ** 167.0, 146.6, 132.7, 129.4, 119.9, 119.4, 115.9, 61.1, 14.5; **LRMS (ES-APCI)**: *m/z* = 166.1 $[M+H]^+$;

ethyl 3-(4-bromo-1*H*-pyrazole-3-carboxamido)benzoate 164:

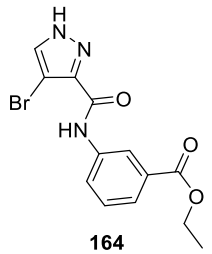

164

General procedure E.f. was followed with acid **6** (100 mg, 0.52 mmol, 1.0 equiv.), HATU (200 mg, 0.52 mmol, 1.0 equiv.), Hünig's base (0.18 mL, 1.05 mmol, 2.0 equiv.) and aniline **163** (86 mg, 0.52 mmol, 1.0 equiv.). The crude reaction mixture was purified by column chromatography with 70:30 PE:acetone eluent to give **164** as a white solid (75 mg, 0.22 mol, 42%). **IR (ATR)/cm^{-1}**: 3374, 3220, 1715, 1676, 1283; **^{1}H NMR** (400 MHz, DMSO-d_6): **δ** 13.81 (br s, 1H), 10.41 (s, 1H), 8.51 (s, 1H), 8.7 (br s, 1H), 8.01 (dd, 1H, *J* = 8.0, 0.8 Hz), 7.68 (d, 1H, *J* = 7.6 Hz), 7.47 (app t, 1H, *J* = 8.0 Hz), 4.33 (q, 2H, *J* = 7.2 Hz), 1.33 (t, 3H, *J* = 7.2 Hz); **^{13}C NMR** (101 MHz, DMSO-d_6): **δ** 165.6, 159.7, 142.2, 139.1, 132.1, 130.3, 129.0, 124.6, 124.2, 20.6, 93.1, 60.8, 14.2; **LRMS (E-APCI)**: *m/z* = 336.0 $[M-H]^-$; **HRMS**: found *m/z* = 338.0139, calculated for $C_{13}H_{13}O_3N_3Br_1$ *m/z* = 338.0135; **M.P.**: 177 °C

3-(4-bromo-1*H*-pyrazole-3-carboxamido)benzoic acid 165:[90]

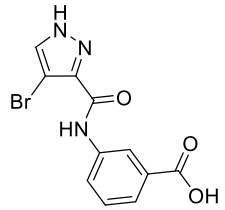

165

Ester **164** (70 mg, 0.21 mmol, 1.0 equiv.) was dissolved in H_2O:THF 2:1 solution (3 mL). 5 M NaOH (0.1 mL, 0.52 mmol, 2.5 equiv.) was added and the reaction mixture was stirred for 20 h at room temperature. The reaction was evaporated *in vacuo* and the residue was diluted with H_2O (5 mL) and washed with ether (2 × 10 mL). The aqueous layer was acidified with 3 M HCl until pH = 1. The compound was extracted with EtOAc (2 × 10 mL). The organic layer was dried over $MgSO_4$, filtered and concentrated. Recrystallization of the product was done with hot H_2O and filtered hot to give **165** as a white solid (36 mg, 0.12 mmol, 57%). **IR (ATR)/cm^{-1}**: 3212, 2982, 1666, 1617, 1249; **^{1}H NMR** (400 MHz, DMSO-d_6): **δ** 13.79 (br s, 1H), 12.94 (br s, 1H), 10.36 (s, 1H), 8.48 (s, 1H), 8.18 (s, 1H), 7.96 (d, 1H, *J* = 8.0 Hz), 7.66 (d, 1H, *J* = 7.6 Hz), 7.45 (t, 1H, *J* = 8.0 Hz); **^{13}C NMR** (101 MHz, DMSO-d_6): **δ** 167.2, 159.9, 138.9, 132.1, 131.2, 128.8, 124.4, 124.3, 120.9, 93.9; **LRMS (ES-APCI)**: *m/z* = 307.9 $[M-H]^-$; **HRMS**: found *m/z* = 307.9673, calculated for $C_{11}H_7O_3N_3Br_1$ *m/z* = 307.9676; **M.P.**: > 250 °C

4. **Nitrophenol amides**

4-chloro-*N*^{3}-(2-hydroxy-5-nitrophenyl)-*N*^{1}-methyl-1*H*-pyrazole-1,3-dicarboxamide 166:

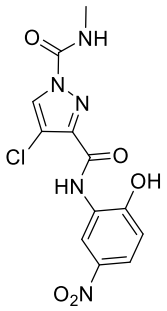

166

General procedure E.c. was followed with acid **153** (720 mg, 4.91 mmol, 1.0 equiv.), HATU (1.88 g, 4.91 mmol, 1.0 equiv.), Hünig's base (1.71 mL, 9.83 mmol, 2.0 equiv.) and 2-amino-4-nitrophenol **138** (757 mg, 4.91 mmol, 1.0 equiv.) in MeCN (25 mL). After the amide coupling, compound **12** (2.46 g, 19.64 mmol, 4.0 equiv.) and Et_3N (2.74 mL, 19.64 mmol, 4.0 equiv.) were added. To the reaction mixture was added H_2O (25 mL) and EtOAc (10 mL). A precipitate formed and was filtered and dried to give **166** as an orange solid (400 mg, 1.18 mmol, 24%). **IR (ATR)/cm^{-1}**: 3330, 3138, 2858, 1742, 1530,1221; **^{1}H NMR** (400 MHz, DMSO-d_6): **δ** 9.79 (br s, 1H), 8.92 (d, 1H, *J* = 2.8 Hz), 8.72 (br app q, 1H, *J* = 4.4 Hz), 8.65 (s, 1H), 7.75 (dd, 1H, *J* = 9.2, 2.8 Hz), 6.16 (d, 1H, *J* = 9.2 Hz), 2.86 (d, 3H, *J* = 4.8 Hz); **^{13}C NMR** (101 MHz, DMSO-d_6): **δ** 170.0, 166.7, 148.6, 143.2, 129.8, 127.5, 124.4, 115.4, 113.0, 111.9, 27.0; **LRMS (ES-APCI)**: *m/z* = 338.0 $[M–H]^–$; **HRMS**: found *m/z* = 362.0262, calculated for $C_{12}H_{10}O_5N_5Cl_1Na_1$ *m/z* = 362.0263; **M.P.**: >250 °C

N^3-(2-hydroxy-5-nitrophenyl)-N^1-methyl-1*H*-pyrazole-1,3-dicarboxamide 167:

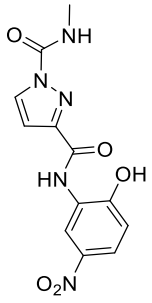

167

General procedure E.c. was followed with acid **5** (330 mg, 2.94 mmol, 1.0 equiv.), HATU (1.13 g, 2.94 mmol, 1.0 equiv.), Hünig's base (1.02 mL, 5.88 mmol, 2.0 equiv.) and 2-amino-4-nitrophenol **138** (453 mg, 2.94 mmol, 1.0 equiv.) in MeCN (25 mL). After the amide coupling, **12** (1.47 g, 11.76 mmol, 4.0 equiv.) and Et_3N (1.64 mL, 11.76 mmol, 4.0 equiv.) were added. To the reaction mixture was added H_2O (15 mL) and EtOAc (10 mL). A precipitate formed and was filtered and dried to give **167** as a brown-orange solid (160 mg, 0.52 mmol, 18%). **IR (ATR)/cm^{-1}**: 3348 (br), 3140 (br), 1715, 1532, 1223; **^{1}H NMR** (400 MHz, DMSO-d_6): **δ** 9.87 (br s, 1H), 8.93 (d, 1H, *J* = 2.8 Hz), 8.66 (br s, 1H), 8.38 (d, 1H, *J* = 2.4 Hz), 7.74 (ddd, 1H, *J* = 9.6, 3.2,0.8 Hz), 6.90 (d, 1H, *J* = 2.8 Hz), 6.16−6.12 (m, 1H), 2.87 (d, 3H, *J* = 4.8 Hz); **^{13}C NMR** (101 MHz, DMSO-d_6): **δ** 170.5, 157.9**,** 149.4, 149.2, 130.9, 127.7, 127.4, 124.3, 115.4, 112.9, 108.0, 26.9; **LRMS (ES-APCI)**: *m/z* = 305.0 $[M–C_3H_5N_1O_1–H]^–$; **HRMS**: found *m/z* = 306.0834, calculated for $C_{12}H_{12}O_5N_5$ *m/z* = 306.0833; **M.P.**: >250 °C

4-bromo-*N*-(2-hydroxy-5-nitrophenyl)-1*H*-pyrazole-3-carboxamide 168:

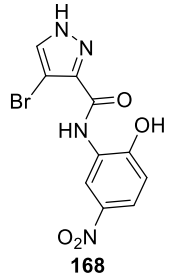

168

General procedure E.f. was followed with acid **6** (100 mg, 0.52 mmol, 1.0 equiv.), HATU (200 mg, 0.52 mmol, 1.0 equiv.), Hünig's base (0.18 mmol, 1.05 mmol,

2.0 equiv.) and 2-amino-4-nitrophenol **138** (39 mg, 0.52 mmol, 1.0 equiv.). The precipitate formed was filtered and washed with MeCN. This gave desired amide **168** as a brown solid (42 mg, 0.13 mmol, 25%). **IR (ATR)/cm^{-1}**: 3195 (br), 1670, 1531, 1336; **^{1}H NMR** (400 MHz, DMSO-d_6): **δ** 13.88 (br s, 1H), 9.61 (s, 1H), 9.11 (d, 1H, J = 2.8 Hz), 8.19 (s, 1H), 7.89 (dd, 1H, J = 9.2, 2.8 Hz), 6.81 (d, 1H, J = 8.8 Hz); **^{13}C NMR** (101 MHz, DMSO-d_6): **δ** 170.6, 158.0, 133.7, 133.6, 128.2, 127.3, 124.1, 115.0, 112.0, 92.3; **LRMS (ES-APCI)**: m/z = 324.9 $[M-H]^-$; **HRMS**: found m/z = 324.9576, calculated for $C_{10}H_6O_4N_4Br_1$ m/z = 324.9578; **M.P.**: 220 °C (decomp)

4-bromo-*N*-(2-methoxy-5-nitrophenyl)-1*H*-pyrazole-3-carboxamide 170:

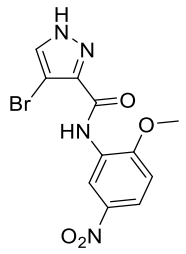

170

General procedure E.f. was followed with acid **6** (50 mg, 0.26 mmol, 1.0 equiv.), HATU (100 mg, 0.26 mmol, 1.0 equiv.), Hünig's base (90 μL, 0.52 mmol, 2.0 equiv.) and 2-methoxy-5-nitroaniline **169** (44 mg, 0.26 mmol, 1.0 equiv.). The crude material was purified by column chromatography with 70:30 PE:acetone eluent to afford **170** as a light yellow solid (21 mg, 0.06 mmol, 25%). **IR (ATR)/cm^{-1}**: 3221, 3211, 2962, 1672, 1531, 1336; **^{1}H NMR** (400 MHz, DMSO-d_6): **δ** 13.96 (br s, 1H), 9.50 (s, 1H), 9.20 (d, 1H, J = 2.8 Hz), 8.23 (br s, 1H), 8.07 (dd, 1H, J = 9.2, 2.8 Hz), 7.34 (d, 1H, J = 9.2 Hz), 4.06 (s, 3H); **^{13}C NMR** (101 MHz, DMSO-d_6): **δ** 158.6, 153.3, 140.6, 133.4, 133.3, 127.3, 120.2, 113.6, 111.0, 93.3, 57.1; **LRMS (ES-APCI)**: m/z = 338.8 $[M+H]^+$; **HRMS**: found m/z = 340.9886, calculated for $C_{11}H_{10}O_4N_4Br_1$ m/z = 340.9886; **M.P.**: > 250 °C (decomp)

2-amino-4-(trifluoromethyl)phenol 172:[92]

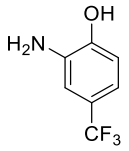

172

General procedure L was followed with 2-nitro-4-(trifluoromethyl)phenol **171** (500 mg, 2.41 mmol, 1.0 equiv.), Pd/C (250 mg, 0.24 mmol, 10 mol%) in EtOAc (6 mL). The reaction was stirred for 3 h at room temperature and the amine was isolated. The crude was triturated with chloroform and PE to give amine **172** as a light brown solid (320 mg, 1.80 mmol, 75%). **IR (ATR)/cm^{-1}**: 1326, 1094; **^{1}H NMR** (400 MHz, DMSO-*d*$_6$): **δ** 9.86 (br s, 1H), 6.88 (s, 1H), 6.77 (d, 1H, *J* = 8.0 Hz), 6.72 (d, 1H, *J* = 8.0 Hz), 4.96 (br s, 2H); **^{13}C NMR** (101 MHz, DMSO-*d*$_6$): **δ** 147.2, 137.3, 129.2–121.1 (q, *J* = 272.6 Hz), 120.6–119.7 (q, *J* = 31.1 Hz), 113.8, 113.3–113.2 (q, *J* = 4.0 Hz), 110.9–110.0 (q, *J* = 3 Hz); **LRMS (ES-APCI)**: *m/z* = 176.1 $[M-H]^-$; **M.P.**: 124 °C (121−122 °C in lit)[123]

4-bromo-*N*-(2-hydroxy-5-(trifluoromethyl)phenyl)-1*H*-pyrazole-3-carboxamide 173:

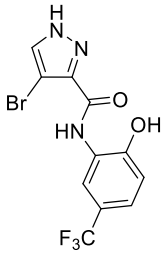

173

General procedure E.f. was followed with acid **6** (50 mg, 0.26 mmol, 1.0 equiv.), HATU (100 mg, 0.26 mmol, 1.0 equiv.), Hünig's base (90 µL, 0.52 mmol, 2.0 equiv.) and aniline **172** (46 mg, 0.26 mmol, 1.0 equiv.). The crude mixture was purified by column chromatography with a gradient eluent from 90:10 to 70:30 PE:acetone to give amide **173** as a white solid (40 mg, 0.11 mmol, 42%). **IR (ATR)/cm^{-1}**: 3305, 1645, 1450, 1330, 1105; **^{1}H NMR** (400 MHz, DMSO-d$_6$): **δ** 13.88 (br s, 1H), 11.25 (br s, 1H), 9.45 (s, 1H), 8.61 (s, 1H), 8.22 (s, 1H), 7.31 (d, 1H, *J* = 8.0 Hz), 7.08 (d, 1H, *J* = 8.4 Hz); **^{13}C NMR** (101 MHz, DMSO-d$_6$): **δ** 158.6, 149.4, 132.9, 126.0,

123.2, 121.0–120.9 (q, *J* = 6.1 Hz), 120.1–119.2 (q, *J* = 32.5 Hz), 115.6, 114.7, 93.2; **^{19}F NMR**(376 MHz, $CDCl_3$): **δ** −59.9, −69.2, −71.1; **LRMS (ES-APCI)**: *m/z* = 348.0 $[M-H]^-$; **HRMS**: found *m/z* = 349.9749, calculated for $C_{11}H_8O_2N_3Br_1F_3$ *m/z* = 349.9747; **M.P.**: 212 °C

5. **Fluoro phenyl amides and fluoropyridyl amides**

4-bromo-*N*-(2-fluoropyridin-3-yl)-1*H*-pyrazole-3-carboxamide 174:

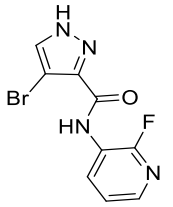

174

General procedure E.f. was followed with acid **6** (50 mg, 0.26 mmol, 1.0 equiv.), HATU (100 mg, 0.26 mmol, 1.0 equiv.), Hünig's base (90 µL, 0.52 mmol, 2.0 equiv.) and 2-fluoro-3-aminopyridine (19 µL, 0.26 mmol, 1.0 equiv.). The crude was purified by column chromatography with 70:30 PE:acetone eluent to give amide **174** as a light yellow solid (26 mg, 0.09 mmol, 15%). **IR (ATR)/cm^{-1}**: 3384, 3264, 1681, 1535; **^{1}H NMR** (400 MHz, DMSO-d_6): **δ** 11.89 (br s, 1H), 9.86 (s, 1H), 8.30 (ddd, 1H, *J* = 9.6, 7.6, 1.6 Hz), 8.19 (br s, 1H), 8.03 (dt, 1H, *J* = 4.8, 1.6 Hz), 7.39 (ddd, 1H, *J* = 7.6, 4.8, 1.2 H); **^{13}C NMR** (101 MHz, DMSO-d_6): **δ** 159.1, 156.6 (d, *J* = 237 Hz), 147.3, 142.5 (d, *J* = 14.1 Hz), 141.2, 134.9, 132.5, 122.2 (d, *J* = 4.0 Hz), 121.1 (d, *J* = 27.0 Hz), 93.3; **LRMS (ES-APCI)**: *m/z* = 283.0 $[M-H]^-$; **HRMS**: found *m/z* = 284.9784, calculated for $C_9H_7O_1N_4Br_1F_1$ *m/z* = 284.9782; **M.P.**: 245 °C (decomp)

4-bromo-*N*-(2-fluorophenyl)-1*H*-pyrazole-3-carboxamide 175:

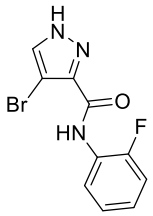

175

General procedure E.f. was followed with acid **6** (50 mg, 0.26 mmol, 1.0 equiv.), HATU (100 mg, 0.52 mmol, 1.0 equiv.), Hünig's base (90 µL, 0.52 mmol, 2.0 equiv.) and 2-fluoroaniline (25 µL, 0.26 mmol, 1.0 equiv.). The reaction was stirred for 44 h at room temperature and the crude material was purified by column chromatography with 80:20 PE:acetone eluent. This led to the isolation of **175** as an off-white solid (15 mg, 0.05 mmol, 19%); **IR (ATR)/cm^{-1}**: 3388, 3172, 3130, 1666, 1537, 1033; **^{1}H NMR** (400 MHz, DMSO-d_6): **δ** 9.67 (br s, 1H), 8.15 (s, 1H), 7.87−7.83 (m, 1H), 7.32 −7.26 (m, 1H), 7.23−7.19 (m, 2H); **^{13}C NMR** (101 MHz, DMSO-d_6): **δ** 159.0, 155.7 (d, J = 246.4 Hz), 141.1, 132.8 (d, J = 4.0 Hz), 126.0 (d, J = 8.1 Hz), 125.6 (d, J = 11.1 Hz), 124.8, 124.4 (d, J = 4.0 Hz), 115.6 (d, J = 20.2 Hz), 93.1; **LRMS (ES/APCI)**: *m/z* = 282.0 [M−H]$^{-}$; **HRMS**: found *m/z* = 305.9642, calculated for $C_{10}H_7O_1N_3Br_1F_1Na_1$ *m/z* = 305.9642; **M.P.**: 203 °C

6. **Benzoxazole amide analogues**

4-nitro-1*H*-benzo[*d*]imidazole 177:

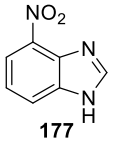

177

General procedure H was followed with 3-nitro-1,2-phenylenediamine **176** (150 mg, 0.97 mmol, 1.0 equiv.), triethylorthoformate (0.49 mL, 2.92 mmol, 3.0 equiv.) and *p*-toluenesulfonic acid monohydrate (9 mg, 0.05 mmol, 5 mol%) in toluene (2 mL). The reaction was filtered to give the desired benzimidazole **177** as a brown/yellow solid (130 mg, 0.80 mmol, 82%). **IR (ATR)/cm^{-1}**: 2963 (br), 1530, 1338, 1489; **^{1}H NMR** (400 MHz, DMSO-d_6): **δ** 8.51 (br s, 1H), 8.17 (dd, 2H, J = 8.0, 2.0 Hz), 7.44

(app t, 1H, *J* = 8.0 Hz); **^{13}C NMR** (101 MHz, DMSO-d_6): **δ** 145.2, 133.7, 127.8, 126.5, 125.5, 212.4, 119.0; **LRMS (ES-APCI)**: *m/z* = 164.1 $[M+H]^+$; **M.P.**: 238 °C (238–239 °C in lit)[124]

1*H*-benzo[*d*]imidazol-4-amine 178:

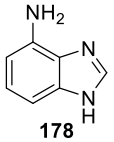

178

General procedure L was followed with nitrobenzimidazole **177** (150 mg, 0.92 mmol, 1.0 equiv.), Pd/C (96 mg, 0.09 mmol 10 mol%). The reaction was stirred for 5.5 h at room temperature followed by celite filtration. After solvent evaporation, this gave **178** as a mixture of regioisomers as a dark purple oil (120 mg, 0.90 mmol, 98%). **IR (ATR)/cm^{-1}**: 3159, 2980, 1614, 1600; **^{1}H NMR** (400 MHz, $CDCl_3$): **δ** 7.95 (s, 1H), 7.09 (app t, 1H, *J* = 7.6 Hz), 6.91 (d, 1H, *J* = 8.0 Hz), 6.56 (d, 1H, *J* = 7.6 Hz), 5.30 (br s, 2H); **^{13}C NMR** (101 MHz, $CDCl_3$): **δ** 138.8, 138.4, 134.4, 131.9, 124.6, 106.6, 102; **LRMS (ES-APCI)**: *m/z* = 134.0 $[M+H]^+$

1-methyl-1*H*-benzo[*d*]imidazol-4-amine 180:

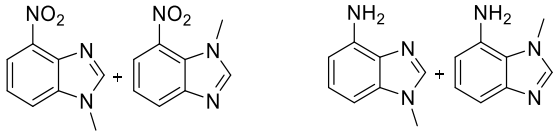

179

180

In a flask, powdered KOH (516 mg, 9.2 mmol, 5.0 equiv.) was added to a solution of nitro benzimidazole **177** (300 mg, 1.84 mmol, 1.0 equiv.) in acetone (10 mL) in an ice bath. The reaction was stirred for 0.5 h and MeI (0.17 mL, 2.76 mmol, 1.5 equiv.) was added and the reaction stirred for a further 4.5 h at room temperature. The solvent was evaporated to give a residue, to which H_2O (50 mL) and EtOAc (40 mL) were added. The organic layer was washed with H_2O (2 × 20 mL), dried over $MgSO_4$, filtered and concentrated to dryness. This led to the isolation of a mixture of regioisomers **179** as a brown solid (240 mg, 1.36 mmol, 74%).[94]

General procedure L was followed with the mixture of regioisomers **179** (230 mg, 1.30 mmol, 1.0 equiv.), Pd/C (140 mg, 0.13 mmol 10 mol%). The reaction was stirred

for 5 h at room temperature followed by celite filtration. After solvent evaporation, this gave **180** as a mixture of regioisomers in the form of a brown solid (150 mg, 1.03 mmol, 79%). **IR (ATR)/cm^{-1}**: 3321, 3211, 1591, 1487; **^{1}H NMR** (1.5:1 regioisomer with minor regioisomer*, 400 MHz, $CDCl_3$): **δ** 7.69 (s, 1H), 7.62 (s, 1H)*, 7.26 (d, 1H, *J* = 7.2 Hz)*, 7.10 (app t, 1H, *J* = 8.0 Hz), 7.02 (app t, 1H, *J* = 7.6 Hz)*, 6.75 (d, 1H, *J* = 8.0 Hz), 6.53 (d, 1H, *J* = 7.6 Hz) (both regioisomers), 4.27 (br s, 2H), 4.04 (s, 3H)*, 3.86 (br s, 2H)*, 3.74 (s, 3H); **^{13}C NMR** (1.5:1 regiosiomer with minor regioisomer*, 101 MHz, $CDCl_3$): **δ** 145.98, 144.18, 141.4, 139.1, 135.5, 132.9 (both regioisomers), 124.9, 124.2, 123.1*, 112.3*, 110.8*, 106.0, 99.3, 33.8*, 31.2; **LRMS (ES-APCI)**: *m/z* = 148.1 $[M+H]^+$

***N*-(1*H*-benzo[*d*]imidazol-4-yl)-4-bromo-1*H*-pyrazole-3-carboxamide 181:**

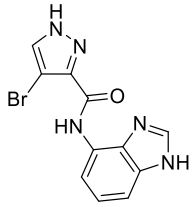

181

General procedure E.f. was followed with acid **6** (50 mg, 0.26 mmol, 1.0 equiv.), HATU (100 mg, 0.26 mmol 1.02 equiv.), Hünig's base (90 µL, 0.52 mmol, 2.0 equiv.) and benzimidazole **178** (35 mg, 0.26 mmol, 1.0 equiv.). The precipitate was filtered and washed with a minimum amount of MeCN. The precipitate was recrystallized with hot MeCN and analogue **181** was isolated as a brown solid (22 mg, 0.07 mmol, 27%). **IR (ATR)/cm^{-1}**: 3199, 3145, 2939, 1701, 1674; **^{1}H NMR** (400 MHz, DMSO-d_6): **δ** 14.29 (br s, 2H), 9.93 (br s, 1H), 9.14 (s, 1H), 8.36 (s, 1H), 8.31 (d, 1H, *J* = 8.0 Hz), , 7.95 (d, 1H, *J* = 8.0 Hz), 7.47 (app t, 1H, 8.0 Hz); **^{13}C NMR** (101 MHz, DMSO-d_6): **δ** sample not concentrated enough **LRMS (ES-APCI)**: *m/z* = 305.9 $[M+H]^+$; **HRMS**: found *m/z* = 305.9988, calculated for $C_{11}H_9O_1N_5Br_1$ *m/z* = 305.9985; **M.P.**: > 250 °C

4-bromo-*N*-(1-methyl-1*H*-benzo[*d*]imidazol-4-yl)-1*H*-pyrazole-3-carboxamide 182:

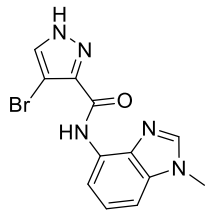

182

General procedure E.f. was followed with acid **6** (100 mg, 0.52 mmol, 1.0 equiv.), HATU (200 mg, 0.52 mmol 1.02 equiv.), Hünig's base (0.18 mL, 1.05 mmol, 2.0 equiv.) and benzimidazole **180** (76 mg, 0.52 mmol, 1.0 equiv.). The precipitate was filtered and washed with a minimum amount of MeCN. The precipitate was recrystallized in MeCN and analogue **182** was isolated as a brown solid (55 mg, 0.17 mmol, 33%). **IR (ATR)/cm^{-1}**: 3367, 3113, 2927, 1161, 1506; **^{1}H NMR** (400 MHz, DMSO-d_6): **δ** 13.90 (br s, 1H), 9.84 (s, 1H), 8.23 (s, 1H), 8.20 (s, 1H), 8.14 (d, 1H, J = 7.6 Hz), 7.33−7.24 (m, 2H), 3.86 (s, 3H); **^{13}C NMR** (101 MHz, DMSO-d_6): **δ** 143.7, 134.6, 133.8, 129.0, 122.9, 109.6, 106.7, 93.1, 30.9; **LRMS (ES-APCI)**: m/z = 319.9 $[M+H]^+$; **HRMS**: found m/z = 320.0133, calculated for $C_{12}H_{11}O_1N_5Br_1$ m/z = 320.0141; **M.P.**: > 250 °C

methyl 4-bromo-1*H*-pyrazole-3-carboxylate 183:[95]

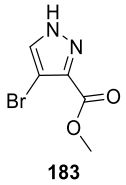

183

To a solution of pyrazole acid **6** (5 g, 26.2 mmol, 1.0 equiv.) in MeOH (44 mL), thionyl chloride (11 mL, 157 mmol, 6.0 equiv.) was added drop-wise at 0 °C. The reaction was then heated at reflux at 70 °C for 2 h. The reaction was concentrated and to the residue saturated aq. $NaHCO_3$ (50 mL) was added. The product was filtered to give title compound **183** as an off white solid (4.1 g, 20.0 mmol, 76%) that required no further purification. **IR (ATR)/cm^{-1}**: 3212, 3124, 1696, 1284; **^{1}H NMR** (500 MHz, DMSO-d_6): **δ** 8.02 (s, 1H), 3.81 (s, 3H); **^{13}C NMR** (101 MHz, DMSO-d_6): **δ** 160.6,

136.8, 134.9, 96.3, 51.7; **LRMS (ES-APCI)**: *m/z* = 202.9 $[M-H]^-$; **M.P.**: 203 °C (decomp)

methyl 4-bromo-1-(2-methoxyethyl)-1*H*-pyrazole-3-carboxylate 184a and methyl 4-bromo-1-(2-methoxyethyl)-1*H*-pyrazole-5-carboxylate 184b:

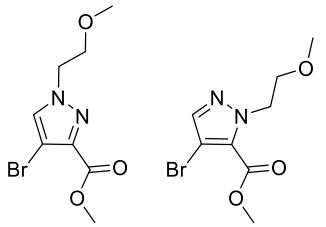

184a **184b**

General procedure I was followed with ester **183** (295 mg, 1.44 mmol, 1.0 equiv.), K_2CO_3 (398 mg, 2.88 mmol, 2.0 equiv.) and 2-bromoethylmethylether (0.20 mL, 2.16 mmol, 1.5 equiv.). The crude reaction was purified by column chromatography with a 90:10 to 80:20 PE:acetone eluent gradient to give two regioisomers **184a** (180 mg, 0.68 mmol, 47%) and **184b** (119 mg, 0.45 mmol, 31%) as oils determined by 2D NOESY experiment (**Appendix 1**). **184a**: **^{1}H NMR** (400 MHz, $CDCl_3$): **δ** 7.62 (s, 1H), 4.34 (app t, 2H, *J* = 4.8 Hz), 3.95 (s, 3H), 3.68 (app t, 2H, *J* = 5.2 Hz), 3.35 (s, 3H); **^{13}C NMR** (101 MHz, $CDCl_3$): **δ** 144.3, 133.4, 96.5, 70.8, 59.2, 53.9, 52.3; **LRMS (ES-APCI)**: *m/z* = 285.0 $[M+Na]^+$; **HRMS**: found *m/z* = 263.0028, calculated for $C_8H_{12}O_3N_2Br_1$ *m/z* = 263.0026; **184b**: **IR (ATR)/cm^{-1}**: 2929, 1720, 1267; **^{1}H NMR** (400 MHz, $CDCl_3$): **δ** 7.49 (s, 1H), 4.70 (app t, 2H, *J* = 4.8 Hz), 3.90 (s, 3H), 3.67 (app t, 2H, *J* = 5.2 Hz), 3.26 (s, 3H); **^{13}C NMR** (101 MHz, $CDCl_3$): **δ** 159.7, 140.7, 130.8, 99.2, 71.3, 58.9, 52.9, 52.3, ; **LRMS (ES-APCI)**: *m/z* = 263.1 $[M+H]^+$; **HRMS**: found *m/z* = 263.0029, calculated for $C_8H_{12}O_3N_2Br_1$ *m/z* = 263.0026;

methyl 4-bromo-1-propyl-1*H*-pyrazole-3-carboxylate 185a and methyl 4-bromo-1-propyl-1*H*-pyrazole-5-carboxylate 185b:

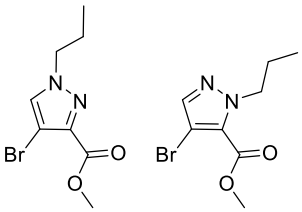

185a **185b**

General procedure I was followed with ester **183** (295 mg, 1.44 mmol, 1.0 equiv.), K_2CO_3 (398 mg, 2.88 mmol, 2.0 equiv.) and 1-bromopropane (0.20 mL, 2.16 mmol, 1.5 equiv.) in DMF (8 mL). The crude reaction mixture was purified by column chromatography with PE as the eluent to pack the column and a 90:10 PE:acetone eluent system. This lead to the isolation of two regioisomers **185a** (159 mg, 0.64 mmol, 44%) and **185b** (143 mg, 0.58 mmol, 40%) as oils determined by 2D NOESY experiment (**Appendix 2**). **185a**: **IR (ATR)/cm^{-1}**: 2964, 1722, 1226; **^{1}H NMR** (400 MHz, $CDCl_3$): **δ** 7.46 (s, 1H), 4.07 (app t, 2H, *J* = 7.2 Hz), 3.86 (s, 3H), 1.88–1.79 (m, 2H), 0.85 (t, 3H, *J* = 7.6 Hz); **^{13}C NMR** (101 MHz, $CDCl_3$): **δ** 161.4, 139.8, 132.0, 96.2, 55.3, 52.1, 23.5, 10.9; **HRMS**: on the way; **185b**: **^{1}H NMR** (400 MHz, $CDCl_3$): **δ** 7.45 (s, 1H), 4.44 (app t, 2H, *J* = 7.2 Hz), 3.89 (s, 3H), 1.80–1.74 (m, 2H), 0.85 (t, 3H, *J* = 7.2 Hz); **^{13}C NMR** (101 MHz, $CDCl_3$): **δ** 159.5, 140.1, 129.9, 99.1, 54.9, 52.1, 23.9, 11.0; **LRMS (ES-APCI)**: *m/z* = 247.0 $[M+H]^+$; **HRMS**: found *m/z* = 247.0079, calculated for $C_8H_{12}O_2N_2Br_1$ *m/z* = 247.0077;

4-bromo-1-(2-methoxyethyl)-1*H*-pyrazole-3-carboxylic acid 186a:

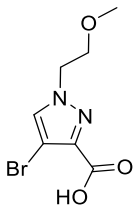

186a

General procedure K was followed with ester **184a** (140 mg, 0.53 mmol, 1.0 equiv.) and $LiOH \cdot H_2O$ (44 mg, 1.06 mmol, 2.0 equiv.) in THF (3 mL) an H_2O (1 mL). Acid **186a** was obtained as a white solid (100 mg, 0.40 mmol, 75%). **IR (ATR)/cm^{-1}**: 2908,

1691, 1251; **^{1}H NMR** (400 MHz, $CDCl_3$): **δ** 7.64 (s, 1H), 4.37 (t, 2H, *J* = 4.8 Hz), 3.75 (t, 2H, *J* = 5.2 Hz), 3.35 (s, 3H); **^{13}C NMR** (101 MHz, $CDCl_3$): **δ** 164.0, 139.8, 133.9, 97.0, 70.8, 59.3, 54.0; **LRMS (ES-APCI)**: *m/z* = 248.9 $[M+H]^+$; **HRMS**: found *m/z* = 248.9871, calculated for $C_7H_{10}O_3N_2Br_1$ *m/z* = 248.9869; **M.P.**: 86 °C

4-bromo-1-(2-methoxyethyl)-1*H*-pyrazole-5-carboxylic acid 186b:

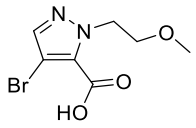

186b

General procedure K was followed with ester **184b** (100 mg, 0.38 mmol, 1.0 equiv.) and $LiOH \cdot H_2O$ (32 mg, 0.76 mmol, 2.0 equiv.) in THF (3 mL) ad H_2O (1 mL). Acid **186b** was obtained as a white solid (80 mg, 0.32 mmol, 84%). **IR (ATR)/cm^{-1}**: 2971, 1693, 1254, 1101; **^{1}H NMR** (400 MHz, $CDCl_3$): **δ** 7.59 (s, 1H), 4.79 (t, 2H, *J* = 5.2 Hz), 3.78 (t, 2H, *J* = 5.6 Hz), 3.33 (s, 3H); **^{13}C NMR** (101 MHz, $CDCl_3$): **δ** 162.5, 141.0, 130.7, 100.9, 71.4, 59.2, 52.7; **LRMS (ES-APCI)**: *m/z* = 203.0 $[M-CO_2-H]^-$; **HRMS**: found *m/z* = 248.9873, calculated for $C_7H_{10}O_3N_2Br_1$ *m/z* = 248.9869; **M.P.**: 94 °C

4-bromo-1-propyl-1*H*-pyrazole-3-carboxylic acid 187a:

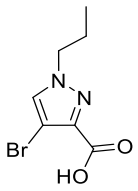

187a

General procedure K was followed with ester **185a** (130 mg, 0.53 mmol, 1.0 equiv.) and $LiOH \cdot H_2O$ (44 mg, 1.05 mmol, 2.0 equiv.) in THF (3 mL) and H_2O (1 mL). Acid **187a** was obtained as a white solid (10 mg, 0.47 mmol, 89%). **IR (ATR)/cm^{-1}**: 2968, 1693, 1500, 1257; **^{1}H NMR** (400 MHz, $CDCl_3$): **δ** 10.65 (br s, 1H), 7.50 (s, 1H), 4.15 (t, 2H, *J* = 6.8 Hz), 1.92−1.84 (m, 2H), 0.90 (t, 3H, *J* = 7.2 Hz); **^{13}C NMR** (101 MHz, $CDCl_3$): **δ** 165.3, 139.6, 132.4, 96.9, 55.5, 24.0, 11.0; **HRMS**: found *m/z* = 230.9775, calculated for $C_7H_8O_2N_2Br_1$ *m/z* = 230.9775; **M.P.**: 100 °C

4-bromo-1-propyl-1*H*-pyrazole-5-carboxylic acid 187b:

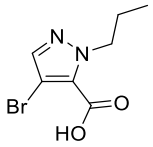

187b

General procedure K was followed with ester **185b** (110 mg, 0.45 mmol, 1.0 equiv.) and LiOH·H_2O (37 mg, 0.89 mmol, 2.0 equiv.) in THF (3 mL), an H_2O (1 mL). Acid **187b** was obtained as a white solid (50 mg, 0.21 mmol, 47%). **IR (ATR)/cm^{-1}**: 2968, 1705, 1247; **^{1}H NMR** (400 MHz, $CDCl_3$): **δ** 8.37 (br s, 1H), 7.54 (s, 1H), 4.50 (br s, 2H), 1.80 (br app q, 2H, *J* = 6.8 Hz), 0.83 (br app t, 3H, *J* = 6.4 Hz); **^{13}C NMR** (101 MHz, $CDCl_3$): **δ** 162.9, 139.4, 130.4, 98.9, 54.3, 23.4, 10.4; **LRMS (ES-APCI)**: *m/z* = 186.9 $[M-CO_2-H]^-$; **HRMS**: found *m/z* = 232.9932, calculated for $C_7H_{10}O_2N_2Br_1$ *m/z* = 232.9926; **M.P.**: 112 °C

***N*-(1*H*-benzo[*d*]imidazol-4-yl)-4-bromo-1-(2-methoxyethyl)-1*H*-pyrazole-3-carboxamide 188:**

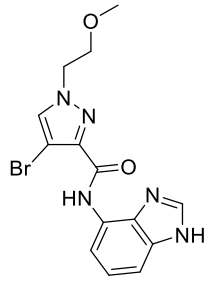

188

General procedure J was followed with acid **186a** (40 mg, 0.16 mmol, 1.0 equiv.), HATU (61 mg, 0.16 mmol, 1.0 equiv.), Hünig's base (56 µL, 0.32 mmol, 2.0 equiv.), and 4-aminobenzimidazole **178** (21 mg, 016 mmol, 1.0 equiv.). The crude was purified by column chromatography with 70:30 PE:acetone eluent to afford **188** as a greenish sticky oil (10 mg, 0.03 mmol, 19%). **IR (ATR)/cm^{-1}**: 2971, 1693, 1254; **^{1}H NMR** (400 MHz, $CDCl_3$): **δ** 8.99 (s, 1H), 7.76 (dd, 1H, *J* = 8.0, 0.4 Hz), 7.72 (s, 1H), 7.23 (t, 1H, *J* = 8.0 Hz), 6.69 (dd, 1H, *J* = 8.0, 0.8 Hz), 4.39 (app t, 2H, *J* = 4.8 Hz), 4.39 (br s, 1H) [overlap], 3.79 (app t, 2H, *J* = 5.2 Hz), 3.39 (s, 3H); **^{13}C NMR** (101 MHz, $CDCl_3$): **δ** 158.8, 142.0, 141.7, 138.9, 133.7, 132.2, 127.0, 109.9, 98.1,

70.6, 99.3, 54.1; **LRMS (ES-APCI)**: *m/z* = 364.0 $[M+H]^+$; **HRMS**: found *m/z* = 364.0408, calculated for $C_{14}H_{15}O_2N_5Br_1$ *m/z* = 364.0404

<u>*N*-(1*H*-benzo[*d*]imidazol-4-yl)-4-bromo-1-propyl-1*H*-pyrazole-3-carboxamide 189:</u>

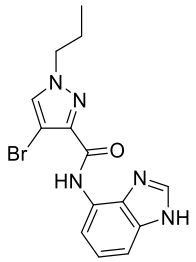

189

General procedure J followed with acid **187a** (45 mg, 0.19 mmol, 1.0 equiv.), HATU (72 mg, 0.19 mmol, 1.0 equiv.), Hünig's base (67 µL, 0.39 mmol, 2.0 equiv.), and 4-aminobenzimidazole **178** (25 mg, 0.19 mmol, 1.0 equiv.). The crude reaction mixture was purified by column chromatography with 70:30 PE:acetone eluent to afford **189** as a yellow solid (33 mg, 0.09 mmol, 47%). **IR (ATR)/cm^{-1}**: 3334, 3221, 1705, 1494, 1269; **^{1}H NMR** (400 MHz, $CDCl_3$): **δ** 9.02 (s, 1H), 7.77 (dd, 1H, *J* = 8.4, 0.8 Hz), 7.60 (s, 1H), 7.22 (t, 1H, *J* = 8.0 Hz), 6.69 (dd, 1H, *J* = 8.0, 0.8 Hz), 4.39 (br s, 2H), 4.19 (t, 2H, *J* = 6.8 Hz), 2.02–1.92 (m, 2H), 0.98 (t, 3H, *J* = 7.2 Hz); **^{13}C NMR** (101 MHz, $CDCl_3$): **δ** 158.8, 142.0, 141.4, 138.9, 133.3, 132.6, 132.2, 127.0, 109.9, 106.2, 98.1, 56.7, 23.6, 11.2; **LRMS (ES-APCI)**: *m/z* = 348.0 $[M+H]^+$; **HRMS**: found *m/z* = 348.0458, calculated for $C_{14}H_{15}O_1N_5Br_1$ *m/z* = 348.0454; **M.P.**: 152 °C

_N_-(1_H_-benzo[_d_]imidazol-4-yl)-4-bromo-1-(2-methoxyethyl)-1_H_-pyrazole-5-carboxamide 190:

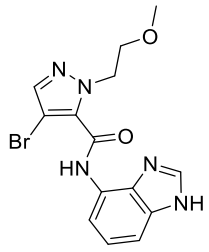

190

General procedure J followed with acid **187b** (30 mg, 0.12 mmol, 1.0 equiv.), HATU (46 mg, 0.12 mmol, 1.0 equiv.), Hünig's base (42 µL, 0.24 mmol, 2.0 equiv.), and 4-aminobenzimidazole **178** (16 mg, 0.12 mmol, 1.0 equiv.). The crude reaction mixture was purified by column chromatography with 70:30 PE:acetone eluent to afford **190** as a yellow solid (18 mg, 0.05 mmol, 42%). **IR (ATR)/cm^{-1}**: 3221, 1705, 1494, 1269; **^{1}H NMR** (400 MHz, $CDCl_3$): **δ** 7.96 (s, 1H), 7.62 (s, 1H), 7.55 (dd, 1H, *J* = 8.4, 0.8 Hz), 7.25 (app t, 1H, *J* = 8.0 Hz), 6.72 (dd, 1H, *J* = 7.6, 0.8 Hz), 4.59 (br s, 2H), 4.42 (br s, 2H), 3.57 (app t, 2H, *J* = 4.8 Hz), 3.01 (s, 3H); **^{13}C NMR** (101 MHz, $CDCl_3$): **δ** 158.2, 141.3, 140.3, 139.2, 135.2, 132.7, 132.2, 127.4, 110.4, 106.2, 96.5, 71.0, 58.9, 51.7; **LRMS (ES-APCI)**: *m/z* = 364.0 $[M+H]^+$; **HRMS**: found *m/z* = 364.0408, calculated for $C_{14}H_{15}O_2N_5Br_1$ *m/z* = 364.0404; **M.P.**: 156 °C

1-methyl-4-nitro-1_H_-benzo[_d_]imidazole 191:[96]

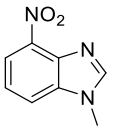

191

In a flask, 3-nitro-1,2-phenylenediamine **176** (1.0 g, 6.53 mmol, 1.0 equiv.) was dissolved in EtOH (20 mL) in the presence of concentrated HCl (5 mL). Aqueous formaldehyde 37% (0.97 mL, 13.06 mmol, 2.0 equiv.) was added and the reaction stirred for 20 h at 80 °C. The reaction was allowed to cool to rt before being neutralized with 10% aqueous NaOH. The solution was cooled to 0 °C, the precipitate was filtered and washed with cold H_2O. The crude material was recrystallized from a 2:1 toluene:hexane solution to give the desired regioisomer amine **191** as a yellow solid

(363 mg, 2.05 mmol, 31%). **IR (ATR)/cm^{-1}**: 1518, 1496, 1340, 1323; **^{1}H NMR** (400 MHz, $CDCl_3$): **δ** 8.18 (d, 1H, *J* = 8.0 Hz), 8.12 (s, 1H), 7.74 (d, 1H, *J* = 8.4 Hz), 7.43 (app t, 1H, *J* = 8.0 Hz), 3.96 (s, 3H); **^{13}C NMR** (101 MHz, $CDCl_3$): **δ** 147.0, 139.7, 137.4, 122.4, 119.6, 116.2, 31.8; **LRMS (ES-APCI)**: *m/z* = 178.1 $[M+H]^+$; **M.P.**: 169 °C (168−169 °C in lit)[125]

1-methyl-1*H*-benzo[*d*]imidazol-4-amine 192:

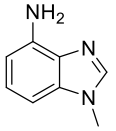

192

General procedure L was followed with Pd/C (432 mg, 0.41 mmol, 10 mol%), nitro benzimidazole **191** (720 mg, 4.06 mmol, 1.0 equiv.) in EtOH (18 mL). The reaction was stirred for 3 h at room temperature. Amine **192** was isolated as a brown solid (540 mg, 3.67 mmol, 90%). 2D NOESY experiment carried out to determine regioisomer (**Appendix 3**). **IR (ATR)/cm^{-1}**: 3373, 3307, 3176, 2989, 1598, 1494; **^{1}H NMR** (400 MHz, $CDCl_3$): **δ** 7.72 (s, 1H), 7.12 (t, 1H, *J* = 7.6 Hz), 6.77 (dd, 1H, *J* = 8.0, 0.8 Hz), 6.55 (dd, 1H, *J* = 7.6, 0.8 Hz), 4.38 (br s, 2H), 3.77 (s, 3H); **^{13}C NMR** (101 MHz, $CDCl_3$): **δ** 141.5, 139.1, 135.5, 133.1, 124.2, 106.0, 99.3, 31.3; **LRMS (ES-APCI)**: *m/z* = 148.1 $[M+H]^+$; **M.P.**: 148 °C

4-bromo-*N*^{1}-methyl-*N*^{3}-(1-methyl-1*H*-benzo[*d*]imidazol-4-yl)-1*H*-pyrazole-1,3-dicarboxamide 193:

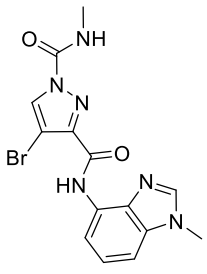

193

General procedure E.c. was followed with acid **6** (100 mg, 0.52 mmol, 1.0 equiv.), HATU (200 mg, 0.52 mmol, 1.0 equiv.), Hünig's base (0.18 mL, 1.04 mmol, 2.0 equiv.), amine **192** (77 mg, 0.52 mmol, 1.0 equiv.). Acylation was carried out with

12 (260 mg, 2.08 mmol, 4.0 equiv.) and Et_3N (0.29 mL, 2.08 mmol, 4.0 equiv.). The precipitate was filtered off and washed with a minimum amount of MeCN to give **193** as an off-pink solid (60 mg, 0.16 mmol, 31%). **IR (ATR)/cm^{-1}**: 3510, 3260, 3121, 1731, 1680, 1550, 1501; **^{1}H NMR** (400 MHz, DMSO-d_6): **δ** 9.85 (s, 1H), 8.88 (br app q, 1H, *J* = 4.4 Hz), 8.69 (s, 1H), 8.24 (s, 1H), 8.06 (d, 1H, *J* = 7.6 Hz), 7.38 (d, 1H, *J* = 8.0 Hz), 7.29 (app t, 1H, *J* = 8.0 Hz), 3.88 (s, 3H), 2.89 (d, 3H, *J* = 4.4 Hz); **^{13}C NMR** (101 MHz, DMSO-d_6): **δ** 157.8, 148.5, 143.8, 143.6, 134.9, 134.5, 128.4, 122.7, 111.6, 106.5, 96.1, 30.9, 26.9; **LRMS** (**ES-APCI**): *m/z* = 377.1 $[M+H]^+$; **HRMS**: found *m/z* = 377.0355, calculated for $C_{14}H_{14}O_2N_6Br_1$ *m/z* = 377.0356; **M.P.**: >250 °C

<u>methyl 4-bromo-1-methyl-1*H*-pyrazole-3-carboxylate 194a and methyl 4-bromo-1-methyl-1*H*-pyrazole-5-carboxylate 194b:</u>[97]

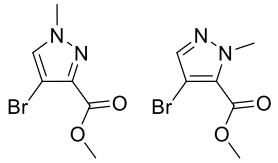

To ester **183** (590 mg, 2.88 mmol, 1.0 equiv.) was added MeCN (10 mL) and Cs_2CO_3 (2.3 g, 7.20 mmol, 2.5 equiv.) in a flask followed by MeI (0.21 mL, 3.31 mmol, 1.2 equiv.) and the reaction was left to stir for 20 h at room temperature. The solid was filtered and washed with EtOAc. The solvent was evaporated and the crude reaction was purified by column chromatography with a gradient eluent 90:10 to 70:30 PE:acetone. This lead to the isolation of two regioisomers **194a** (200 mg, 0.91 mmol, 32%) and **194b** (106 mg, 0.48 mmol, 17%) as white solids and determined by 2D NOESY experiment (**Appendix 4**). **194a**: **IR (ATR)/cm^{-1}**: 3203, 1718, 1477, 1224; **^{1}H NMR** (400 MHz, $CDCl_3$): **δ** 7.46 (s, 1H), 3.92 (s, 3H), 3.89 (s, 3H); **^{13}C NMR** (101 MHz, $CDCl_3$): **δ** 161.4, 140.1, 133.0, 96.5, 52.1, 40.3; **LRMS** (**ES-APCI**): *m/z* = 218.9 $[M+H]^+$; **HRMS**: found *m/z* = 240.9579, calculated for $C_6H_7O_2N_2Br_1Na_1$ *m/z* = 240.9583; **M.P.**: 79 °C; **194b**: **IR (ATR)/cm^{-1}**: 2958, 2930, 1718, 1452, 1263; **^{1}H NMR** (400 MHz, $CDCl_3$): **δ** 7.48 (s, 1H), 4.15 (s, 3H), 3.94 (s, 1H) ; **^{13}C NMR** (101 MHz, $CDCl_3$): **δ** 159.7, 140.1, 130.5, 99.3, 52.3, 41.4

4-bromo-1-methyl-1*H*-pyrazole-3-carboxylic acid 195:

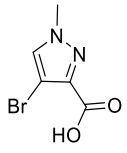

195

General procedure K was followed with ester **194a** (200 mg, 0.98 mmol, 1.0 equiv.), $LiOH \cdot H_2O$ (82 mg, 1.95 mmol, 2.0 equiv.) in THF (3 mL) and H_2O (1 mL). Acid **195** was obtained as an off-white solid (95 mg, 0.46 mmol, 47%). **IR (ATR)/cm^{-1}**: 3105, 2981, 2920, 1684, 1503, 1253; **^{1}H NMR** (400 MHz, Acetone-d_6): **δ** 7.88 (s, 1H), 3.97 (s, 3H); **^{13}C NMR** (101 MHz, Acetone-d_6): **δ** 162.1, 140.7, 134.4, 96.0, 40.3; **LRMS** (**ES-APCI**): *m/z* = 203.0 $[M-H]^-$; **HRMS**: found *m/z* = 204.9608, calculated for $C_5H_6O_2N_2Br_1$ *m/z* = 204.9607; **M.P.**: 190 °C

4-bromo-1-methyl-*N*-(1-methyl-1*H*-benzo[*d*]imidazol-4-yl)-1*H*-pyrazole-3-carboxamide 196:

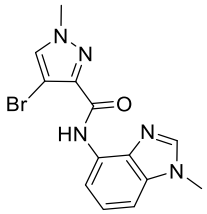

196

General procedure J was followed with acid **195** (23 mg, 0.11 mmol, 1.0 equiv.), HATU (40 mg, 0.11 mmol, 1.0 equiv.) Hünig's base (39 µL, 0.22 mmol, 2.0 equiv.), 4-nitro-*N*-methylbenzimidazole **192** (16 mg, 0.11 mmol, 1.0 equiv.) in MeCN (1.5 mL). The reaction was stirred for 20 h at room temperature. The crude product was triturated with EtOAc and PE to give **196** as an off white solid (20 mg, 0.06 mmol, 55%). **IR (ATR)/cm^{-1}**: 1684, 1534, 1493; **^{1}H NMR** (400 MHz, Acetone-d_6): **δ** 9.86 (br s, 1H), 8.31 (dd, 1H, *J* = 6.0, 2.8 Hz), 8.08 (s, 1H), 796 (s, 1H), 7.31−7.26 (m, 2H), 4.07 (s, 3H), 3.96 (s, 3H);); **^{13}C NMR** (101 MHz, DMSO-d_6): **δ** 157.9, 143.7, 140.8, 135.0, 134.6, 133.7, 128.9, 122.9, 109.5, 105.7, 93.1, 39.9, 30.9; **LRMS (ES-APCI)**: *m/z* = 334.0 $[M+H]^+$; **HRMS**: found *m/z* = 334.0302, calculated for $C_{13}H_{13}O_2N_5Br_1$ *m/z* = 334.0298; **M.P.**: 234 °C

4-chloro-*N*-(1-methyl-1*H*-benzo[*d*]imidazol-4-yl)-1*H*-pyrazole-3-carboxamide 197:

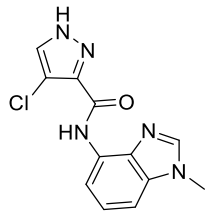

197

General procedure E.f. was followed with acid **153** (35 mg, 0.24 mmol, 1.0 equiv.), HATU (90 mg, 0.24 mmol, 1.0 equiv.), Hünig's base (80 µL, 0.48 mmol, 2.0 equiv.) and 4-nitro-*N*-methylbenzimidazole **192** (35 mg, 0.24 mmol, 1.0 equiv.). The crude material was purified by column chromatography with 100% acetone eluent to give **197** as a beige solid (14 mg, 0.05 mmol, 21%) **IR (ATR)/cm^{-1}**: 3369, 3122, 2907, 1672, 1507, 1329; **^{1}H NMR** (400 MHz, DMSO-d_6): **δ** 13.85 (br s, 1H), 9.81 (s, 1H), 8.21 (br s, 1H), 8.20 (s, 1H), 8.14 (d, 1H, J = 7.6 Hz), 7.33−7.25 (m, 2H), 3.86 (s, 3H); **^{13}C NMR** (101 MHz, DMSO-d_6): **δ** 158.2, 143.7, 140.0, 134.6, 133.8, 130.6, 128.9, 122.9, 109.6, 105.6, 30.9; **LRMS** (**ES-APCI**): *m/z* = 276.0 $[M+H]^+$; **HRMS**: found *m/z* = 276.0647, calculated for $C_{12}H_{11}O_1N_5Cl_1$ *m/z* = 276.0645; **M.P.**: > 250 °C

***N*-(1-methyl-1*H*-benzo[*d*]imidazol-4-yl)-1*H*-indazole-3-carboxamide 199:**

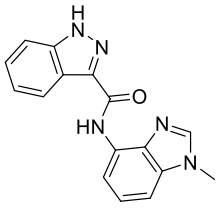

199

General procedure J was followed with indazole **198** (50 mg, 0.31 mmol, 1.0 equiv.), HATU (118 mg, 0.31 mmol, 1.0 equiv.), Hünig's base (0.11 mL, 0.62 mmol, 2.0 equiv.) and 4-nitro-*N*-methylbenzimidazole **192** (46 mg, 0.31 mmol, 1.0 equiv.). The reaction was stirred for 20 h at room temperature and the crude was purified by flash chromatography with 100% acetone followed by trituration with PE and acetone. This led to the isolation of **199** as a white solid (18 mg, 0.06 mmol, 19%). **IR (ATR)/cm^{-1}**: 2982, 1665, 1417; **^{1}H NMR** (400 MHz, Acetone-d_6): **δ** 12.87

(br s, 1H), 10.17 (br s, 1H), 8.42 (dd, 2H, *J* = 7.6, 1.6 Hz), 8.09 (s, 1H), 7.73 (d, 1H, *J* = 8.4 Hz), 7.52−7.48 (m, 1H), 7.37−7.27 (m, 3H), 3.96 (s, 3H); **^{13}C NMR** (101 MHz, DMSO-d_6): **δ** 160.1, 143.7, 141.6, 137.7, 134.7, 133.8, 129.2, 127.0, 123.0, 122.8, 121.35, 111.2, 109.6, 105.5, 31.0; **LRMS (ES-APCI)**: *m/z* = 292.1 $[M+H]^+$; **HRMS**: found *m/z* = 292.1188, calculated for $C_{16}H_{14}O_1N_5$ *m/z* = 292.1193; **M.P.**: 245 °C

4-nitro-1-propyl-1*H*-benzo[*d*]imidazole 200a and 7-nitro-1-propyl-1*H*-benzo[*d*]imidazole 200b:

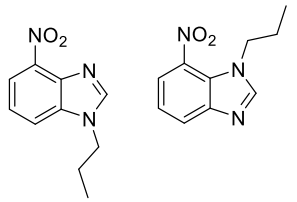

200a **200b**

General procedure I was followed with 4-nitrobenzimidazole **177** (350 mg, 2.15 mmol, 1.0 equiv.), K_2CO_3 (593 mg, 4.29 mmol, 2.0 equiv.), 1-bromopropane (0.29 mL, 3.22 mmol, 1.5 equiv.) in anhydrous DMF (8 mL). The reaction mixture was stirred for 20 h at room temperature. The crude reaction mixture was purified by column chromatography with a gradient of 70:30 to 10:90 PE:acetone to give two regioisomers as yellow oils: **200a** (225 mg, 1.10 mmol, 51%) and **200b** (100 mg, 0.49 mmol, 23%) determined by 2D NOESY (**Appendix 5**). **200a**: **IR (ATR)/cm^{-1}**: 2964, 11514, 1338; **^{1}H NMR** (400 MHz, $CDCl_3$): **δ** 8.14 (dd, 1H, *J* = 8.0, 1.2 Hz), 8.13 (s, 1H), 7.73 (dd, 1H, *J* = 8.0, 0.8 Hz), 7.39 (t, 1H, *J* = 8.0 Hz), 4.23 (t, 2H, *J* = 7.2 Hz), 1.99−1.90 (m, 2H), 0.97 (t, 3H, *J* = 7.2 Hz); **^{13}C NMR** (101 MHz, $CDCl_3$): **δ** 146.4, 139.9, 137.5, 136.8, 122.2 119.5, 116.5, 47.4, 23.4, 11.4; **LRMS (ES-APCI)**: *m/z* = 206.1 $[M+H]^+$; **200b**: **^{1}H NMR** (400 MHz, $CDCl_3$): **δ** 8.09 (dd, 1H, *J* = 8.0, 0.8 Hz), 8.01 (dd, 1H*J* = 8.0, 0.8 Hz), 7.98 (s, 1H), 7.35 (t, 1H, *J* = 8.0 Hz), 4.41 (app t, 2H, *J* = 7.2 Hz), 1.76−1.67 (m, 2H), 0.87 (t, 3H, *J* = 7.2 Hz); **^{13}C NMR** (101 MHz, $CDCl_3$): **δ** 148.2, 147.5, 127.4, 125.9, 121.5, 121.1, 50.6, 24.5, 11.1; **LRMS (ES-APCI)**: *m/z* = 206.1 $[M+H]^+$;

1-propyl-1*H*-benzo[*d*]imidazol-4-amine 201:

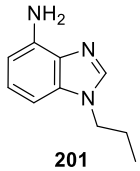

201

General procedure L was followed with Pd/C (96 mg, 0.09 mmol, 10 mol%), nitro compound **200a** (175 mg, 0.85 mmol, 1.0 equiv.), EtOH (10 mL) and was stirred for 5 h. This gave the desired amine **201** as a brown solid (145 mg, 0.83 mmol, 98%) and was used as is for the next step. **IR (ATR)/cm^{-1}**: 3310, 3171, 2965, 1610, 1492; **^{1}H NMR** (400 MHz, $CDCl_3$): **δ** 7.73 (s, 1H), 7.07 (t, 1H, *J* = 8.0 Hz), 6.75 (d, 1H, *J* = 8.0 Hz), 6.51 (d, 1H, *J* = 7.6 Hz), 4.33 (br s, 2H), 4.02 (t, 2H, *J* = 6.8 Hz), 1.89−1.80 (m, 2H,), 0.91 (t, 3H, *J* = 7.6 Hz); **^{13}C NMR** (101 MHz, $CDCl_3$): **δ** 140.8, 139.1, 134.6, 132.8, 124.0, 106.8, 99.5, 46.8, 23.1, 11.3; **LRMS (ES-APCI):** *m/z* = 176.1 $[M+H]^+$; **M.P.**: 74 °C

4-bromo-*N*-(1-propyl-1*H*-benzo[*d*]imidazol-4-yl)-1*H*-pyrazole-3-carboxamide 202:

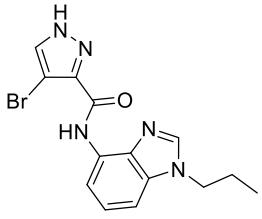

202

General procedure E.f. was followed with acid **6** (50 mg, 0.26 mmol, 1.0 equiv.), HATU (100 mg, 0.26 mmol, 1.0 equiv.), Hünig's base (90 µL, 0.52 mmol, 2.0 equiv.) and 4-amino-*N*-propylbenzimidazole **201** (46 mg, 0.26 mmol, 1.0 equiv.) in EtOAc (2 mL). The crude product was purified by column chromatography with 50:50 PE:acetone as the eluent and further recrystallized with EtOAc to give **202** as an off-white solid (25 mg, 0.07 mmol, 27%). **IR (ATR)/cm^{-1}**: 2981, 2882 1680, 1495, 1252; **^{1}H NMR** (400 MHz, DMSO-d_6): **δ** 13.90 (br s, 1H), 9.85 (s, 1H), 8.25 (s, 1H), 8.22 (br s, 1H), 8.12 (d, 1H, *J* = 7.6 Hz), 7.36 (app d, 1 H, *J* = 8.4 Hz), 7.25 (app t, 1H, *J* = 8.0 Hz), 4.23 (t, 2H, *J* = 6.8 Hz), 1.87−1.78 (m, 2H), 0.85 (t, 3H, *J* = 7.6 Hz);

^{13}C NMR (101 MHz, DMSO-d_6): **δ** 158.3, 143.2, 141.2, 133.9, 134.0, 129.1, 122.9, 109.5, 106.9, 93.1, 45.9, 22.8, 10.9; **LRMS (ES-APCI)**: *m/z* = 348.0 $[M+H]^+$; **HRMS**: found *m/z* = 348.0446, calculated for $C_{14}H_{15}O_1N_5Br_1$ *m/z* = 348.0454; **M.P.**: 228 °C

References

1. N. M. Goodey and S. J. Benkovic, *Nat. Chem. Biol.*, 2008, **4**, 474-482.
2. X. Li, Y. Chen, S. Lu, Z. Huang, X. Liu, Q. Wang, T. Shi and J. Zhang, *J. Mol. Graph. Model.*, 2013, **40**, 30-39.
3. Al-Shar'i, PhD Thesis, University of Strathclyde, 2012.
4. J. Berg, J. Tymoczko and L. Stryer, *Biochemistry* W H Freeman, New York, 5th edn., 2002.
5. classes.midlandstech.edu/carterp/Courses/bio225/chap02/225chap02.htm, February 2016.
6. boundless.com/biology/textbooks/boundless-biology-textbook/biological-macromolecules-3/proteins-56/protein-structure-304-11437/, Februaray 2016.
7. G. Manning, D. B. Whyte, R. Martinez, T. Hunter and S. Sudarsanam, *Science*, 2002, **298**, 1912-1934.
8. proteomicfx.com/scientific-philosophy, February 2016.
9. J. A. Ubersax and J. E. Ferrell Jr, *Nat. Rev. Mol. Cell Biol.*, 2007, **8**, 530-541.
10. N. Dhanasekaran and E. P. Reddy, *Oncogene*, 1998, **17**, 9.
11. M. A. Bogoyevitch and D. P. Fairlie, *Drug Discov. Today*, 2007, **12**, 622-633.
12. T. Tahtouh, J. M. Elkins, P. Filippakopoulos, M. Soundararajan, G. Burgy, E. Durieu, C. Cochet, R. S. Schmid, D. C. Lo, F. Delhommel, A. E. Oberholzer, L. H. Pearl, F. Carreaux, J.-P. Bazureau, S. Knapp and L. Meijer, *J. Med. Chem*, 2012, **55**, 9312-9330.
13. P. Wu, T. E. Nielsen and M. H. Clausen, *Trends Pharmacol. Sci.*, 2015, **36**, 422-439.
14. E. R. Wood, A. T. Truesdale, O. B. McDonald, D. Yuan, A. Hassell, S. H. Dickerson, B. Ellis, C. Pennisi, E. Horne, K. Lackey, K. J. Alligood, D. W. Rusnak, T. M. Gilmer and L. Shewchuk, *Cancer Res.*, 2004, **64**, 6652-6659.
15. J. Matsui, Y. Funahashi, T. Uenaka, T. Watanabe, A. Tsuruoka and M. Asada, *Clin. Cancer Res.*, 2008, **14**, 5459-5465.
16. D. Bossemeyer, *FEBS Lett.*, 1995, **369**, 57-61.
17. R. S. K. Vijayan, P. He, V. Modi, K. C. Duong-Ly, H. Ma, J. R. Peterson, R. L. Dunbrack and R. M. Levy, *J. Med. Chem*, 2015, **58**, 466-479.
18. J. A. Adams, *Biochemistry*, 2003, **42**, 601-607.
19. Y. Liu and N. S. Gray, *Nat. Chem. Biol.*, 2006, **2**, 358-364.
20. Q. Wang, M. Zheng, Z. Huang, X. Liu, H. Zhou, Y. Chen, T. Shi and J. Zhang, *J. Mol. Graph. Model.*, 2012, **38**, 324-333.
21. F. Jacob and J. Monod, *J. Mol. Biol.*, 1961, **3**, 318-356.
22. J. Monod, J. Wyman and J.-P. Changeux, *J. Mol. Biol.*, 1965, **12**, 88-118.
23. N. T. Burford, M. J. Clark, T. S. Wehrman, S. W. Gerritz, M. Banks, J. O'Connell, J. R. Traynor and A. Alt, *Proc. Natl. Acad. Sci. U.S.A.*, 2013, **110**, 10830-10835.
24. R. A. Laskowski, F. Gerick and J. M. Thornton, *FEBS Lett.*, 2009, **583**, 1692-1698.
25. R. Benesch and R. E. Benesch, *Biochem. Biophys. Res. Commun.*, 1967, **26**, 162.
26. D. E. Koshland, G. Némethy and D. Filmer, *Biochemistry (Mosc).* 1966, **5**, 365-385.
27. J.-P. Changeux and S. J. Edelstein, *Neuron*, 1998, **21**, 959-980.

28. K. Gunasekaran, B. Ma and R. Nussinov, *Proteins: Struct., Funct., Bioinf.*, 2004, **57**, 433-443.
29. V. J. Hilser, *Science*, 2010, **327**, 653-654.
30. M. Merdanovic, T. Mönig, M. Ehrmann and M. Kaiser, *ACS Chem. Biol.*, 2012, **8**, 19-26.
31. I. Bahar, C. Chennubhotla and D. Tobi, *Curr. Opin. Struct. Biol.*, 2007, **17**, 633-640.
32. C.-J. Tsai, A. del Sol and R. Nussinov, *J. Mol. Biol.*, 2008, **378**, 1-11.
33. Q. Shen, G. Wang, S. Li, X. Liu, S. Lu, Z. Chen, K. Song, J. Yan, L. Geng, Z. Huang, W. Huang, G. Chen and J. Zhang, *Nucleic Acids Res.*, 2015, DOI: 10.1093/nar/gkv902.
34. R. Eglen and T. Reisine, *Pharmacol. Ther.*, 2011, **130**, 144-156.
35. M. Epping-Jordan, E. Le Poul and J.-P. Rocher, *Allosteric Modulation: Novel Approach to Drug Discovery*, 2007.
36. I. Beis and E. A. Newsholme, *Biochem. J.*, 1975, **152**, 23-32.
37. J. A. Hardy and J. A. Wells, *Curr. Opin. Struct. Biol.*, 2004, **14**, 706-715.
38. G. J. P. van Westen, A. Gaulton and J. P. Overington, *PLoS Comput Biol*, 2014, **10**, e1003559.
39. S. Aranda, A. Laguna and S. de la Luna, *Faseb J.*, 2011, **25**, 449-462.
40. M. Soundararajan, Annette K. Roos, P. Savitsky, P. Filippakopoulos, Arminja N. Kettenbach, Jesper V. Olsen, Scott A. Gerber, J. Eswaran, S. Knapp and Jonathan M. Elkins, *Structure*, 2013, **21**, 986-996.
41. S.-I. Yamashita, M. Chujo, T. Moroga, K. Anami, K. Tokuishi, M. Miyawaki, Y. Kawano, S. Takeno, S. Yamamoto and K. Kawahara, *Anticancer Res.*, 2009, **29**, 2753-2757.
42. L. Pritchard, L. Cardle, S. Quinn and M. Dufton, *Protein Eng.*, 2003, **16**, 87-101.
43. B. Erman, *Phys. Bio.*, 2011, **8**, 056003.
44. GOLD, 5.2.2, Cambridge Crystallographic Data Centre.
45. maybridge.com, February 2016.
46. F. H. Niesen, H. Berglund and M. Vedadi, *Nat. Protoc.*, 2007, **2**, 2212-2221.
47. J. V. Rodrigues, V. Prosinecki, I. Marrucho, L. P. N. Rebelo and C. M. Gomes, *Phys. Chem. Chem. Phys.*, 2011, **13**, 13614-13616.
48. M. Vedadi, F. H. Niesen, A. Allali-Hassani, O. Y. Fedorov, P. J. Finerty, G. A. Wasney, R. Yeung, C. Arrowsmith, L. J. Ball, H. Berglund, R. Hui, B. D. Marsden, P. Nordlund, M. Sundstrom, J. Weigelt and A. M. Edwards, *Proc. Nat. Acad. Sci.*, 2006, **103**, 15835-15840.
49. ibhumanbiochemistry.wikispaces.com/C.7.2, Februaray 2016.
50. L. Michaelis and M. L. Menten, *Biochem. Z.*, 1913, **49**, 333-369.
51. K. A. Johnson and R. S. Goody, *Biochemistry*, 2011, **50**, 8264-8269.
52. H. Lineweaver and D. Burk, *J. Am. Chem. Soc*, 1934, **56**, 658-666.
53. en.wikipedia.org/wiki/Lineweaver%E2%80%93Burk_plot, February 2016.
54. guweb2.gonzaga.edu/faculty/cronk/CHEM440/images/inhibition_Lineweaver_Burk.gif, Februaray 2016.
55. G. L. Patrick, *An Introduction to Medicinal Chemistry*, Oxford University Press: Oxford, 2001.

56. C. E. Heise, J. Murray, K. E. Augustyn, B. Bravo, P. Chugha, F. Cohen, A. M. Giannetti, P. Gibbons, R. N. Hannoush, B. R. Hearn, P. Jaishankar, C. Q. Ly, K. Shah, K. Stanger, M. Steffek, Y. Y. Tang, X. R. Zhao, J. W. Lewcock, A. R. Renslo, J. Flygare and M. R. Arkin, *PLoS One*, 2012, **7**.
57. tools.thermofisher.com/content/sfs/brochures/O-091089_KBA_AppNote_TypeIII_Final.pdf, February 2016.
58. *Be and Es Pat.*, WO2012038438 A1, 2012.
59. M. G. Saulnier, D. B. Frennesson, M. D. Wittman, K. Zimmermann, U. Velaparthi, D. R. Langley, C. Struzynski, X. Sang, J. Carboni, A. Li, A. Greer, Z. Yang, P. Balimane, M. Gottardis, R. Attar and D. Vyas, *Bioorg. Med. Chem. Lett.*, 2008, **18**, 1702-1707.
60. *Se Pat.*, WO2006032851 A1, 2006.
61. *Se and Br Pat.*, WO2009053737 A2, 2009.
62. P. J. Skinner, M. C. Cherrier, P. J. Webb, Y.-J. Shin, T. Gharbaoui, A. Lindstrom, V. Hong, S. Y. Tamura, H. T. Dang, C. C. Pride, R. Chen, J. G. Richman, D. T. Connolly and G. Semple, *Bioorg. Med. Chem. Lett.*, 2007, **17**, 5620-5623.
63. *US Pat.*, WO2012129564 A3, 2012.
64. P. A. Duspara, M. S. Islam, A. J. Lough and R. A. Batey, *J. Org. Chem*, 2012, **77**, 10362-10368.
65. J. A. Grzyb, M. Shen, C. Yoshina-Ishii, W. Chi, R. S. Brown and R. A. Batey, *Tetrahedron*, 2005, **61**, 7153-7175.
66. M. W. Karaman, S. Herrgard, D. K. Treiber, P. Gallant, C. E. Atteridge, B. T. Campbell, K. W. Chan, P. Ciceri, M. I. Davis, P. T. Edeen, R. Faraoni, M. Floyd, J. P. Hunt, D. J. Lockhart, Z. V. Milanov, M. J. Morrison, G. Pallares, H. K. Patel, S. Pritchard, L. M. Wodicka and P. P. Zarrinkar, *Nat. Biotechnol.*, 2008, **26**, 127-132.
67. *US Pat.*, WO2012030922 A1, 2012.
68. *US Pat.*, US20120135977 A1, 2012.
69. E. P. Gillis, K. J. Eastman, M. D. Hill, D. J. Donnelly and N. A. Meanwell, *J. Med. Chem*, 2015, **58**, 8315-8359.
70. S. Purser, P. R. Moore, S. Swallow and V. Gouverneur, *Chem. Soc. Rev.*, 2008, **37**, 320-330.
71. H. G. Grimm, *Z. Elktrochem. Angew. P.*, 1925, **31**, 474-480.
72. H. G. Grimm, *Naturwissenschaften*, 1929, **17**, 557-564.
73. I. Langmuir, *J. Am. Chem. Soc*, 1919, **41**, 1543-1559.
74. H. Erlenmeyer and M. Leo, *Helv. Chim. Acta.*, 1932, **15**, 1171-1186.
75. G. A. Patani and E. J. LaVoie, *Chem. Rev.*, 1996, **96**, 3147-3176.
76. A. Burger, in *Progress in Drug Research / Fortschritte der Arzneimittelforschung / Progrès des recherches pharmaceutiques*, ed. E. Jucker, Birkhäuser Basel, 1991, vol. 37, ch. 7, pp. 287-371.
77. C. Bissantz, B. Kuhn and M. Stahl, *J. Med. Chem*, 2010, **53**, 5061-5084.
78. N. E. Leadbeater and M. Marco, *Org. Lett.*, 2002, **4**, 2973-2976.
79. R. Wilcken, M. O. Zimmermann, A. Lange, A. C. Joerger and F. M. Boeckler, *J. Med. Chem*, 2013, **56**, 1363-1388.
80. epoch.uky.edu/ace/public/pKa.jsp, February 2016.
81. *USA Pat.*, WO2010111483 A1, 2010.
82. T. Zieliński, P. Dydio and J. Jurczak, *Tetrahedron*, 2008, **64**, 568-574.

83. N. Kaushik, N. Kaushik, P. Attri, N. Kumar, C. Kim, A. Verma and E. Choi, *Molecules*, 2013, **18**, 6620.
84. P. Lokwani, B. P. Nagori, N. Batra, A. Goyal, S. Gupta and N. Singh, *J. Chem. Pharm. Res.*, 2011, **3**, 302-311.
85. A. Tanakit, M. Rouffet, D. P. Martin and S. M. Cohen, *Dalton Transactions*, 2012, **41**, 6507-6515.
86. *US Pat.*, US20040077605 A1, 2004.
87. *US Pat.*, US20040162282 A1 2004.
88. E. P. A. Talbot, M. Richardson, J. M. McKenna and F. D. Toste, *Adv. Synth. Catal.*, 2014, **356**, 687-691.
89. I. R. Greig, E. Coste, S. H. Ralston and R. J. van't Hof, *Bioorg. Med. Chem. Lett.*, 2013, **23**, 816-820.
90. *US Pat.*, WO2005108358 A2, 2005.
91. C. Ballatore, D. M. Huryn and A. B. Smith, *Chem. Med. Chem.*, 2013, **8**, 385-395.
92. *Jp Pat.*, WO2011049222 A1, 2011.
93. N. Nenajdenko, *Fluorine in Heterocyclic Chemistry*, Springer 2014.
94. *Br Pat.*, WO2006123145 A1, 2006.
95. *US Pat.*, WO2013120104 A3, 2014.
96. V. Milata and D. Ilavský, *Org. Prep. Proc. Int.*, 1993, **25**, 703-704.
97. *US Pat.*, US20140194443 A1, 2014.
98. G. Martiny-Baron, M. G. Kazanietz, H. Mischak, P. M. Blumberg, G. Kochs, H. Hug, D. Marmé and C. Schächtele, *J. Biol. Chem*, 1993, **268**, 9194-9197.
99. J. Qin, P. Dhondi, X. Huang, R. Aslanian, J. Fossetta, F. Tian, D. Lundell and A. Palani, *ACS Med. Chem. Lett.*, 2012, **3**, 100-105.
100. J. C. M. Uitdehaag, F. Verkaar, H. Alwan, J. de Man, R. C. Buijsman and G. J. R. Zaman, *Br. J. Pharmacol.*, 2012, **166**, 858-876.
101. G. D. Cuny, M. Robin, N. P. Ulyanova, D. Patnaik, V. Pique, G. Casano, J.-F. Liu, X. Lin, J. Xian, M. A. Glicksman, R. L. Stein and J. M. G. Higgins, *Bioorg. Med. Chem. Lett.*, 2010, **20**, 3491-3494.
102. W. Becker and W. Sippl, *FEBS Journal*, 2011, **278**, 246-256.
103. K. Rüben, A. Wurzlbauer, A. Walte, W. Sippl, F. Bracher and W. Becker, *PLoS One*, 2015, **10**, e0132453.
104. N. Rath and M. F. Olson, *EMBO Rep.*, 2012, **13**, 900-908.
105. S. McNeely, R. Beckmann and A. K. Bence Lin, *Pharmacol. Ther.*, 2014, **142**, 1-10.
106. R. Roskoski Jr, *Biochem. Biophys. Res. Commun.*, 2010, **399**, 313-317.
107. A. Y. Luhovy, A. Jaberi, J. Papillon, J. Guillemette and A. V. Cybulsky, *J. Biol. Chem*, 2012, **287**, 5446-5458.
108. D. Huertas, M. Soler, J. Moreto, A. Villanueva, A. Martinez, A. Vidal, M. Charlton, D. Moffat, S. Patel, J. McDermott, J. Owen, D. Brotherton, D. Krige, S. Cuthill and M. Esteller, *Oncogene*, 2012, **31**, 1408-1418.
109. L. Breiman, *Mach. Learn.*, 2001, **45**, 5-32.
110. A. Vassileiou, unpublished work.
111. T. P. Mathews, A. J. Kennedy, Y. Kharel, P. C. Kennedy, O. Nicoara, M. Sunkara, A. J. Morris, B. R. Wamhoff, K. R. Lynch and T. L. Macdonald, *J. Med. Chem*, 2010, **53**, 2766-2778.
112. M. S. Ermolenko, S. Guillou and Y. L. Janin, *Tetrahedron*, 2013, **69**, 257-263.

113. C. Musante, *Gazz. Chim. Ital.*, 1948, **78**, 178-191.
114. *US Pat.*, WO2012030922 A1, 2012.
115. A. Tam, I. S. Armstrong and T. E. La Cruz, *Org. Lett.*, 2013, **15**, 3586-3589.
116. Z. Du, W. Zhou, F. Wang and J.-X. Wang, *Tetrahedron*, 2011, **67**, 4914-4918.
117. A. K. Shil, D. Sharma, N. R. Guha and P. Das, *Tetrahedron Lett.*, 2012, **53**, 4858-4861.
118. R. K. Brown and N. A. Nelson, *J. Am. Chem. Soc*, 1954, **76**, 5149-5150.
119. R. Passerini, *J. Chem. Soc. (Resumed)*, 1954, DOI: 10.1039/JR9540002256, 2256-2261.
120. C. Sannie and H. Lapin, *Bull. Soc. Chim. Fr.*, 1952, 369-372.
121. R. Adams and S. Miyano, *J. Am. Chem. Soc*, 1954, **76**, 2785-2786.
122. J. Krauss, V. Knorr, V. Manhardt, S. Scheffels and F. Bracher, *Arch. Pharm.*, 2008, **341**, 386-392.
123. M. R. Pettit and J. C. Tatlow, *J. Chem. Soc. (Resumed)*, 1954, DOI: 10.1039/JR9540003852, 3852-3854.
124. G. M. van der Want, *Recl. Trav. Chim. Pays-Bas*, 1948, **67**, 45-51.
125. M. Bella and V. Milata, *J. Heterocyclic Chem.*, 2008, **45**, 425-427.

Appendices

I. Appendix 1: 182 analysis

- **182 ^{1}H NMR**

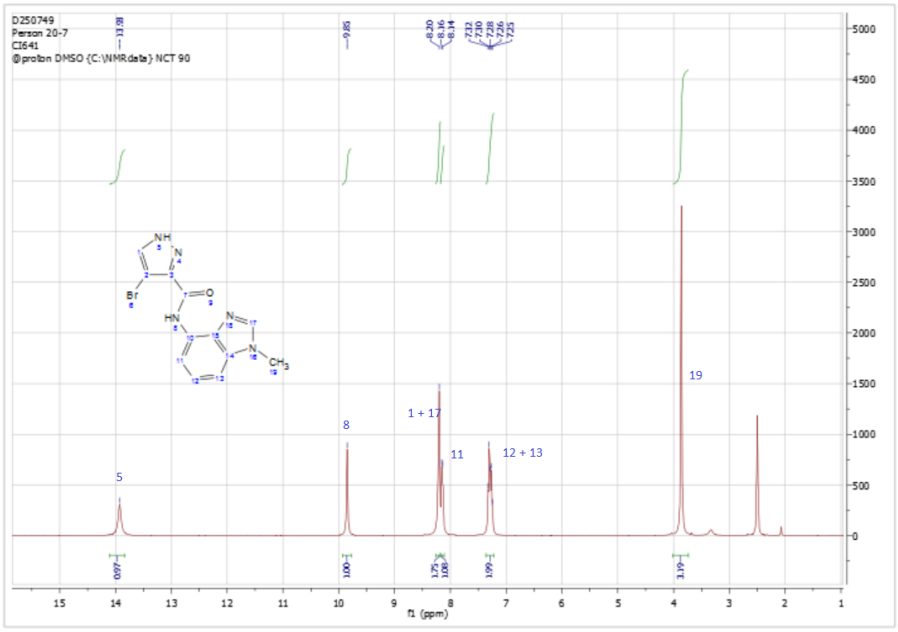

- **182 2D NOESY experiment**

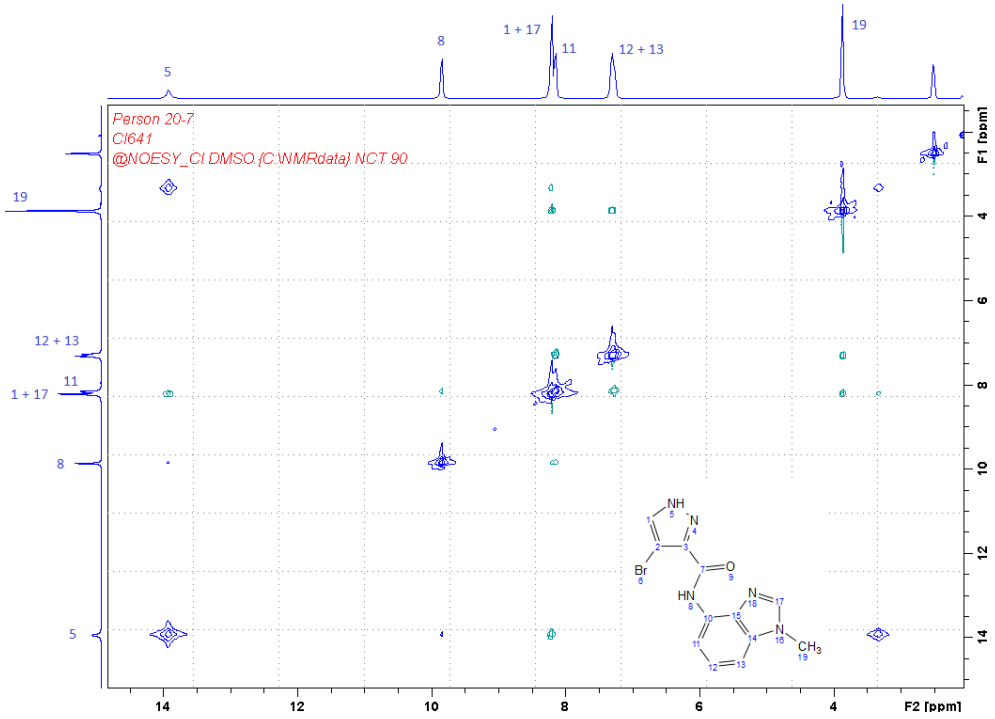

II. Appendix 2: 184 analysis

- **184a ^{1}H NMR**

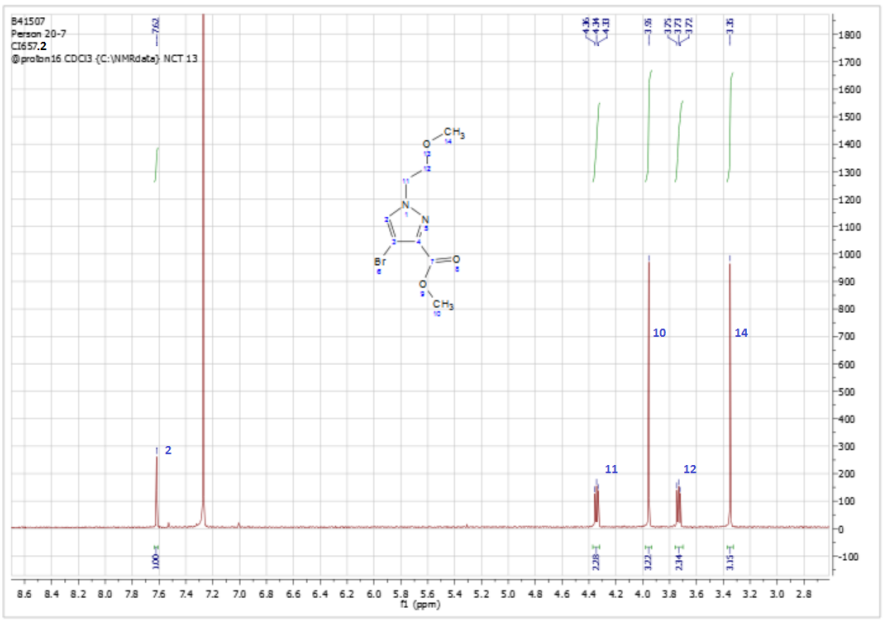

- **184a 2D NOESY experiment**

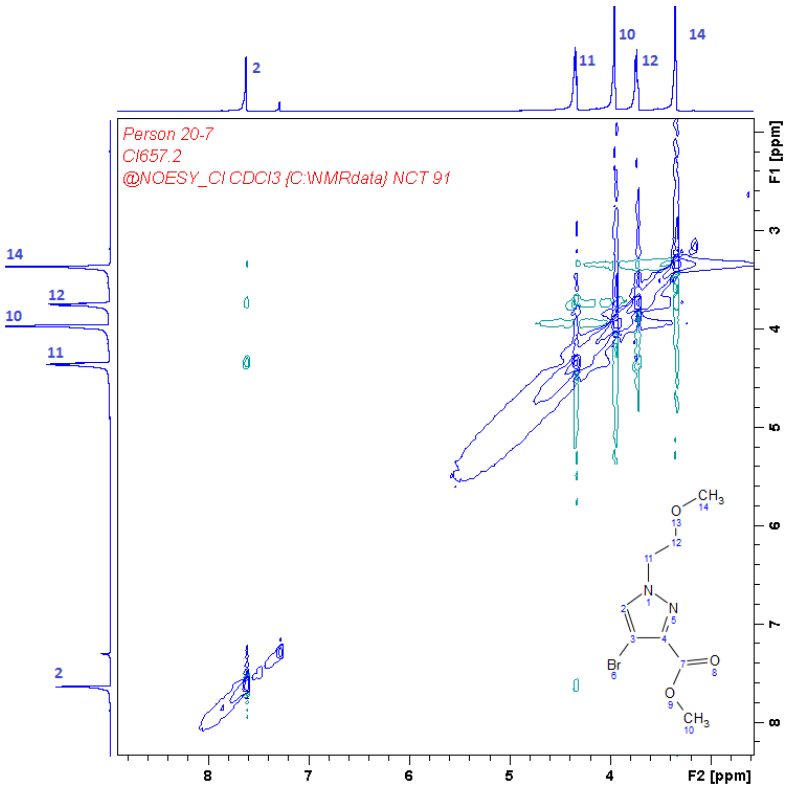

- **184b ^{1}H NMR**

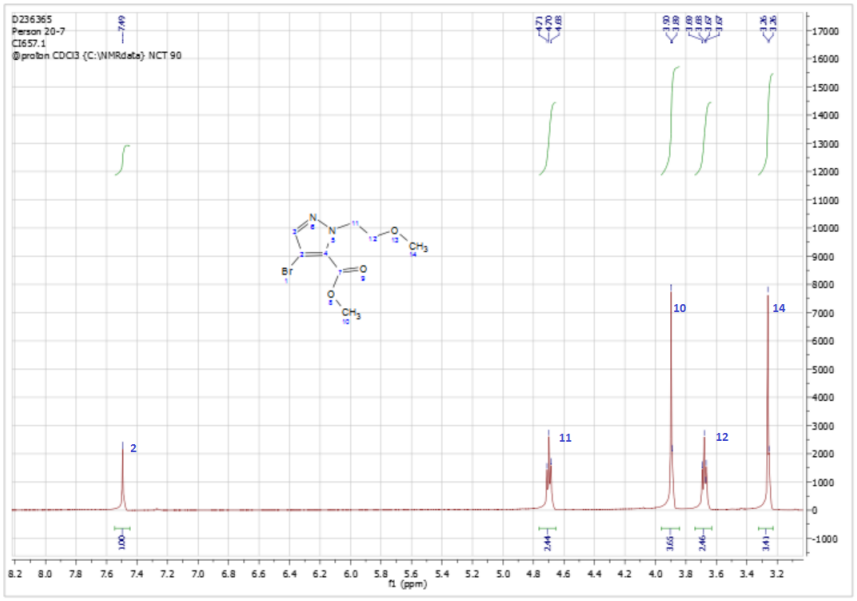

- **184b 2D NOESY experiment**

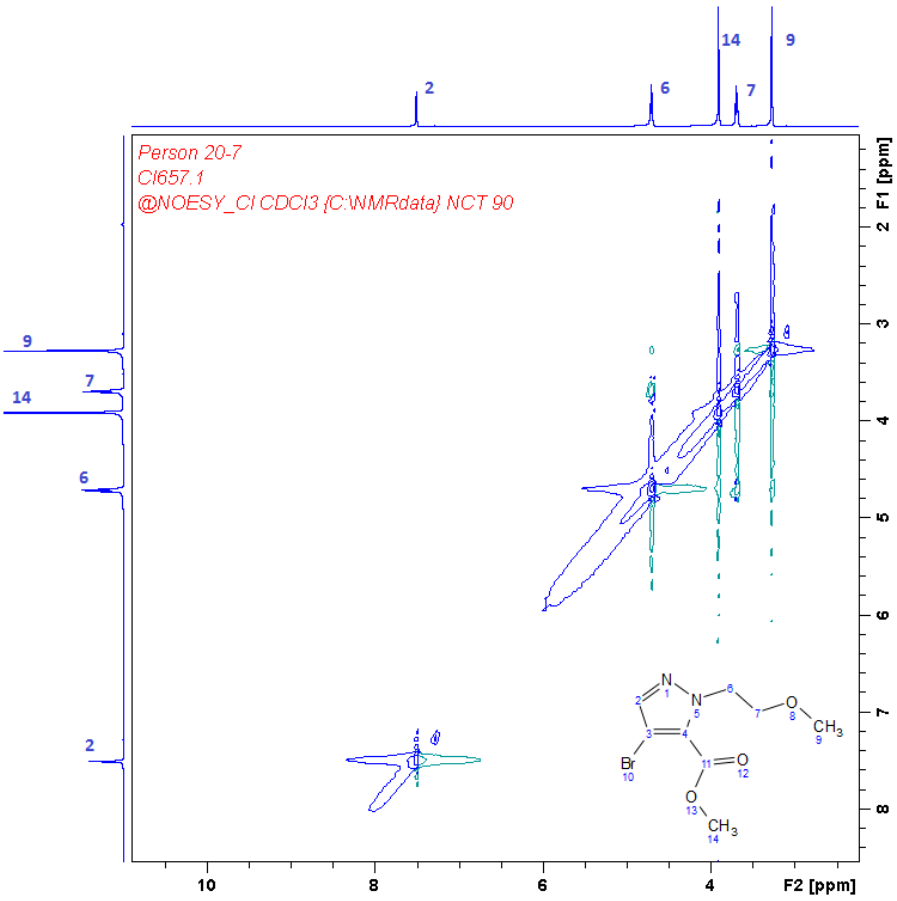

III. Appendix 3: 185 analysis

- **185a ^{1}H NMR**

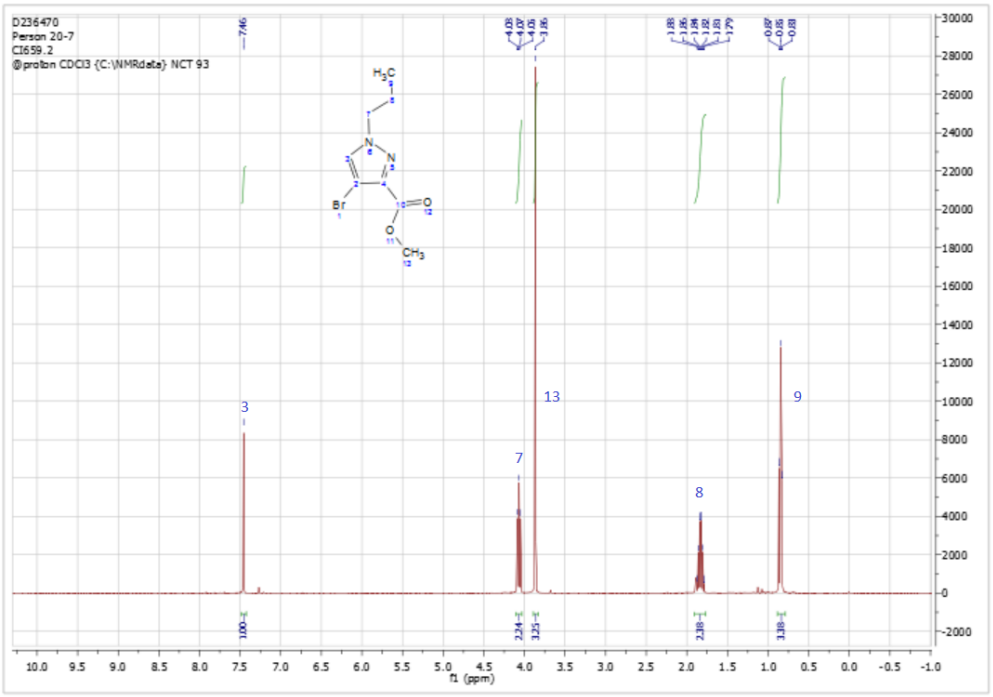

- **185a 2D NOESY experiment**

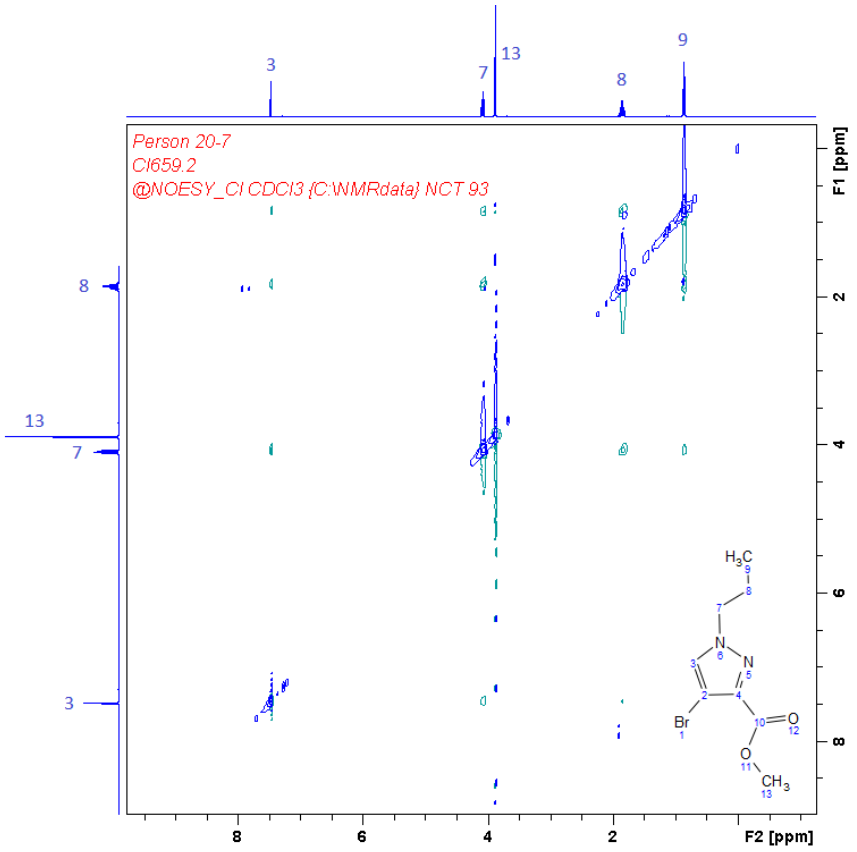

- **185b ^{1}H NMR**

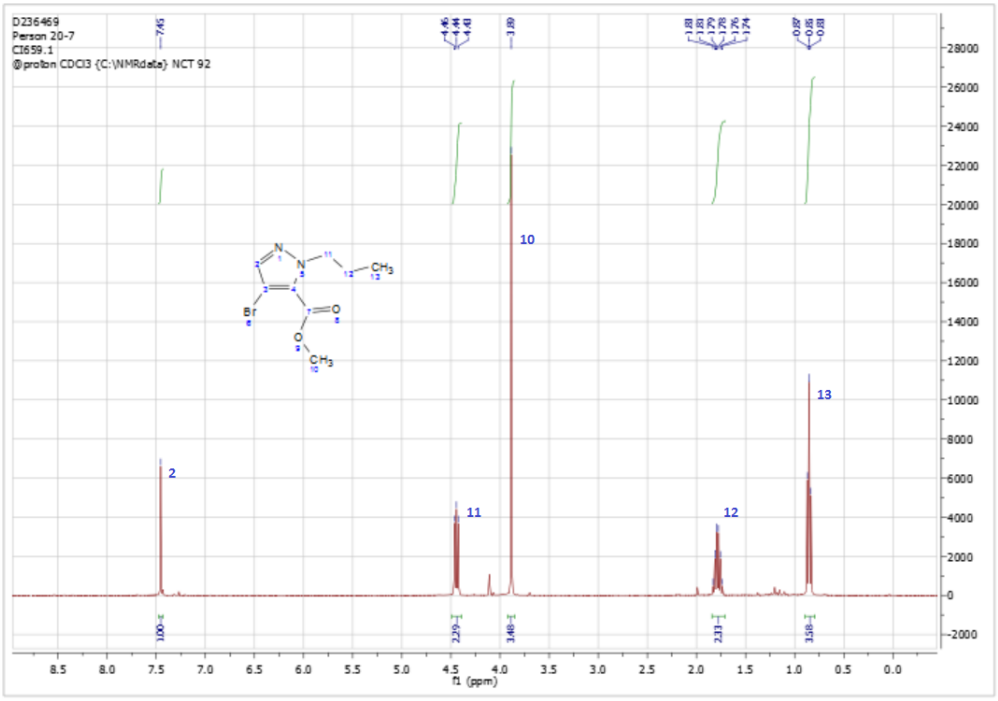

- **185b 2D NOESY experiment**

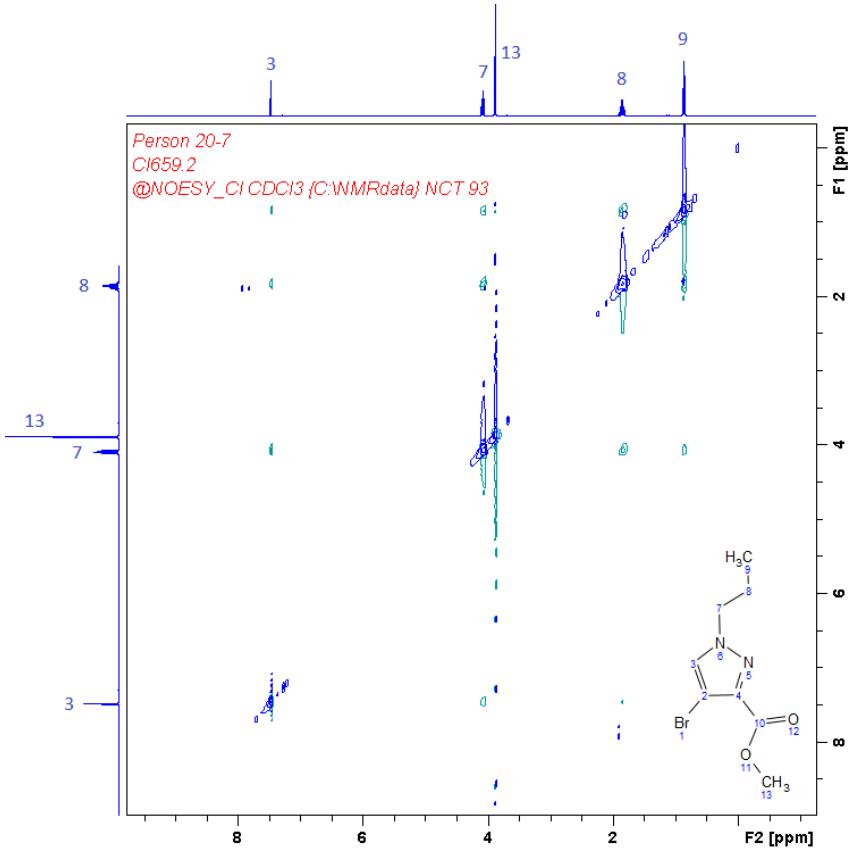

IV. Appendix 4: 192 analysis

- **192 ^{1}H NMR**

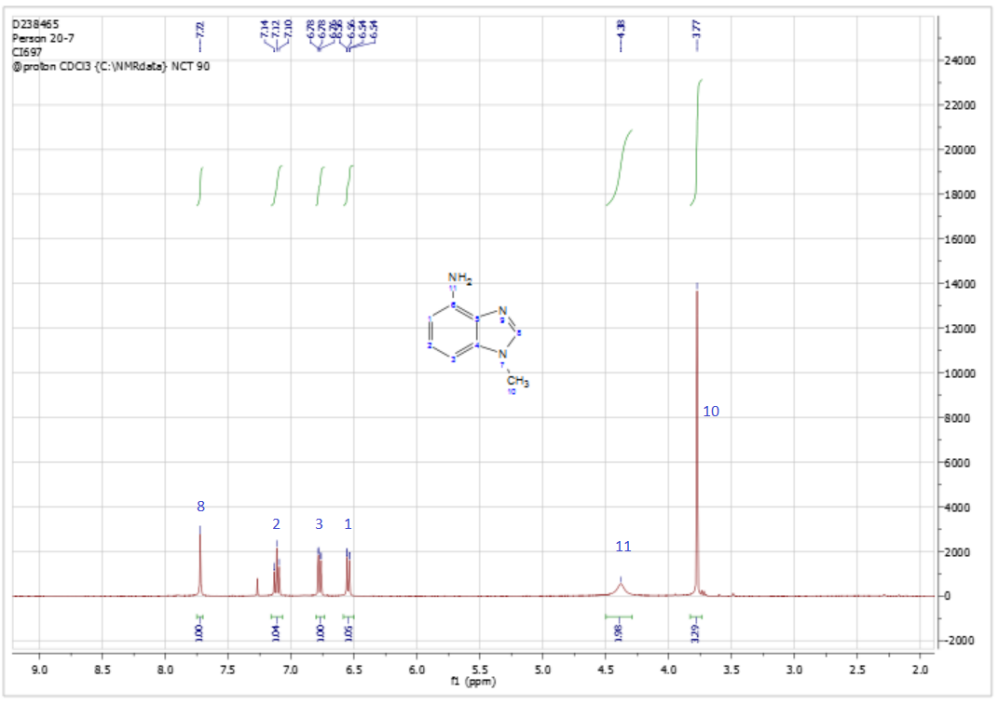

- **192 2D NOESY experiment**

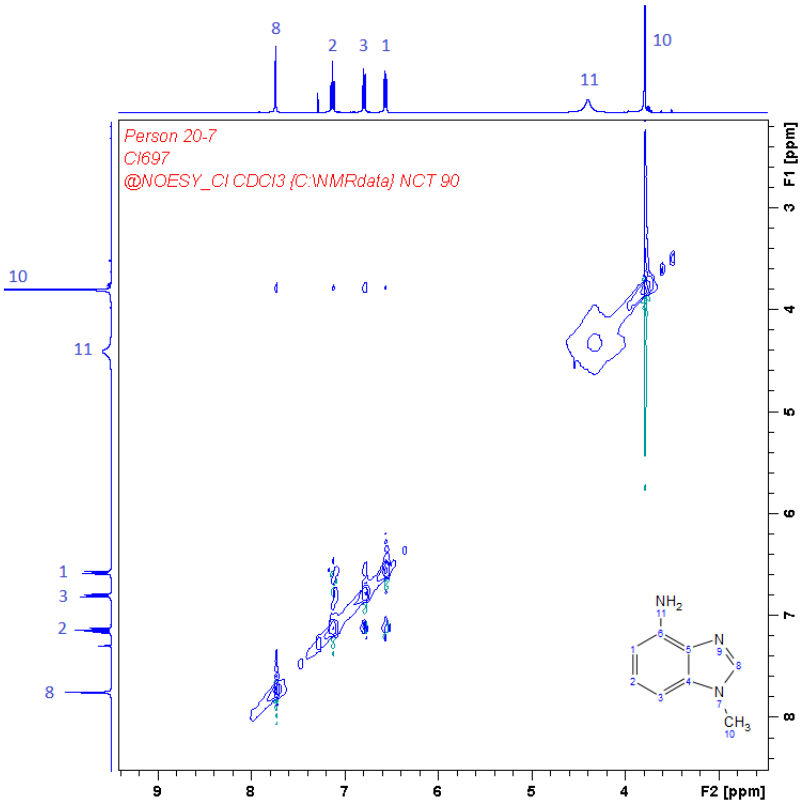

V. Appendix 5: 194 analysis

- **194a ^{1}H NMR**

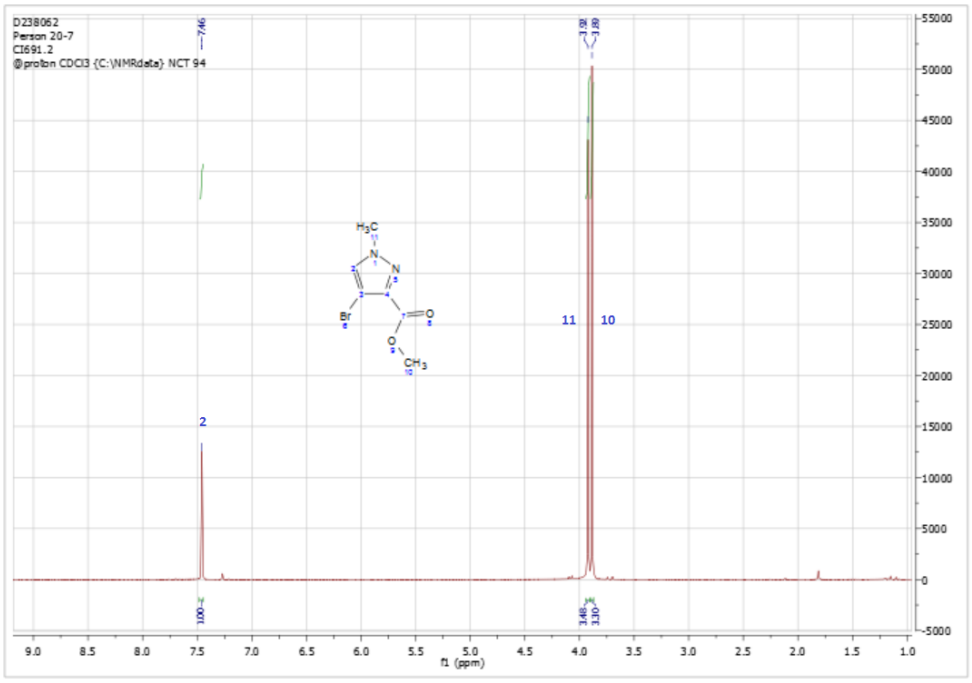

- **194a 2D NOESY experiment**

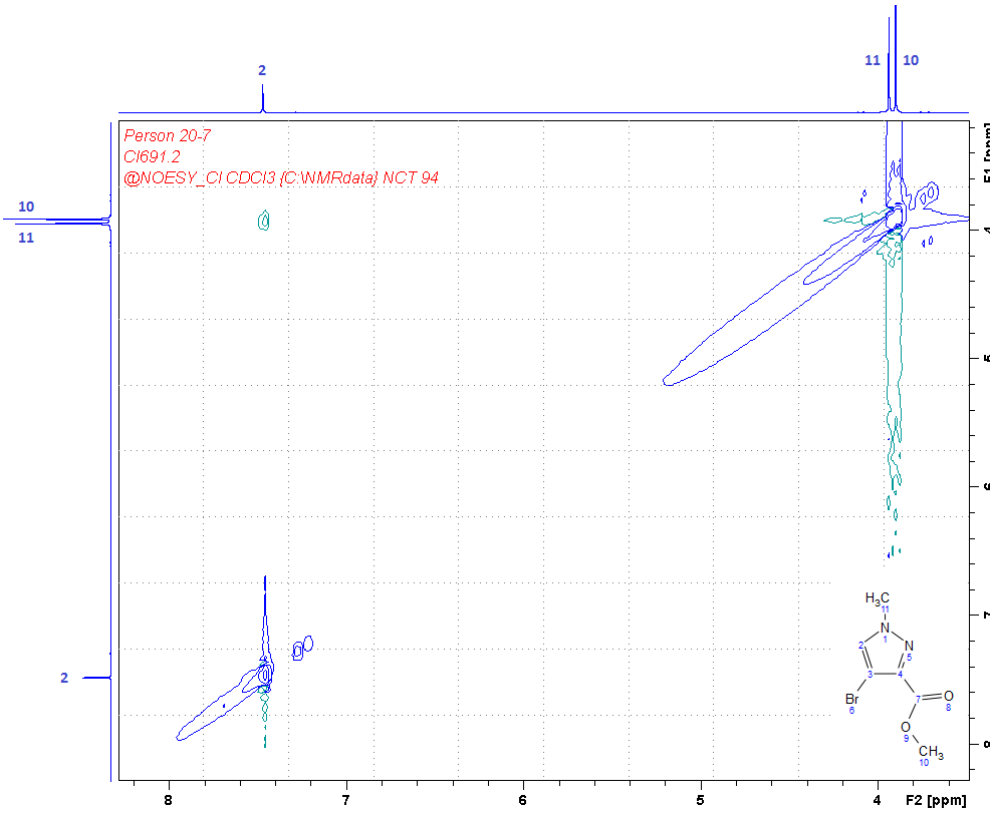

- **194b ^{1}H NMR**

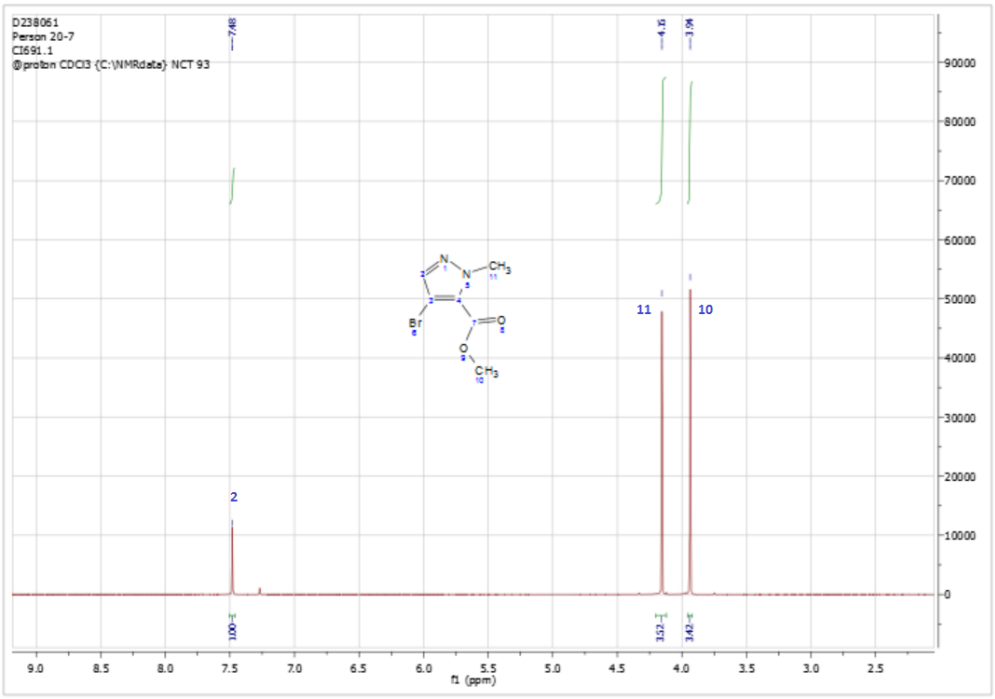

- **194b 2D NOESY experiment**

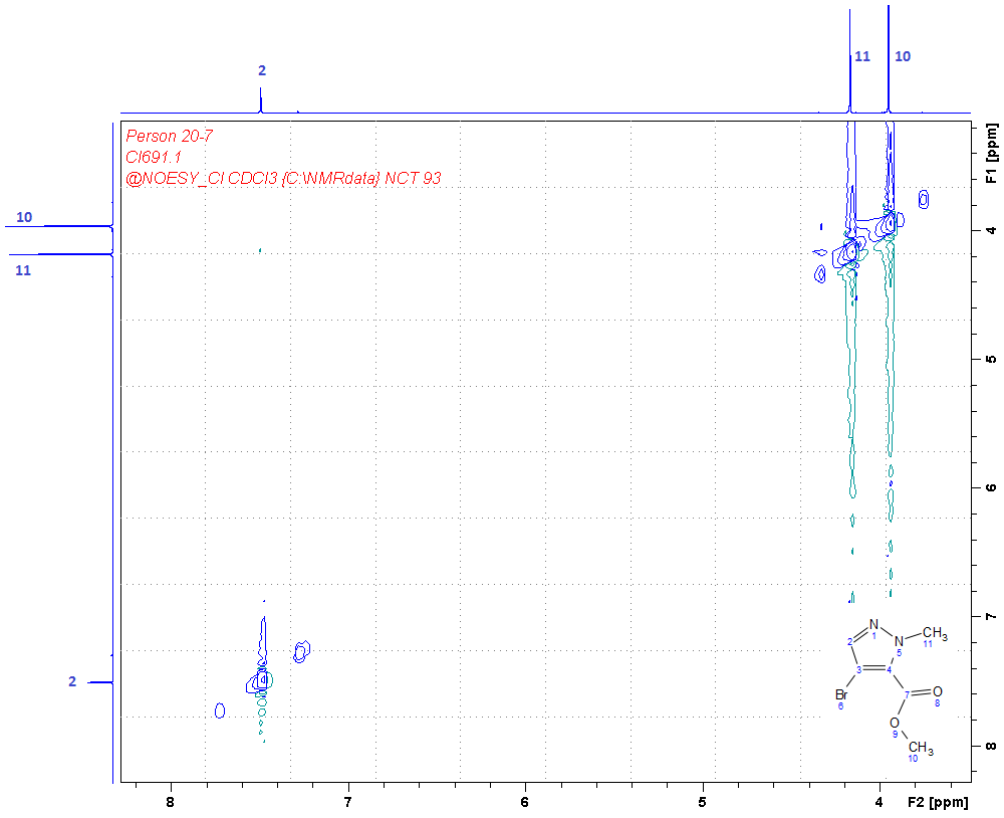

VI. Appendix 6: 200 analysis

- **200b ^{1}H NMR**

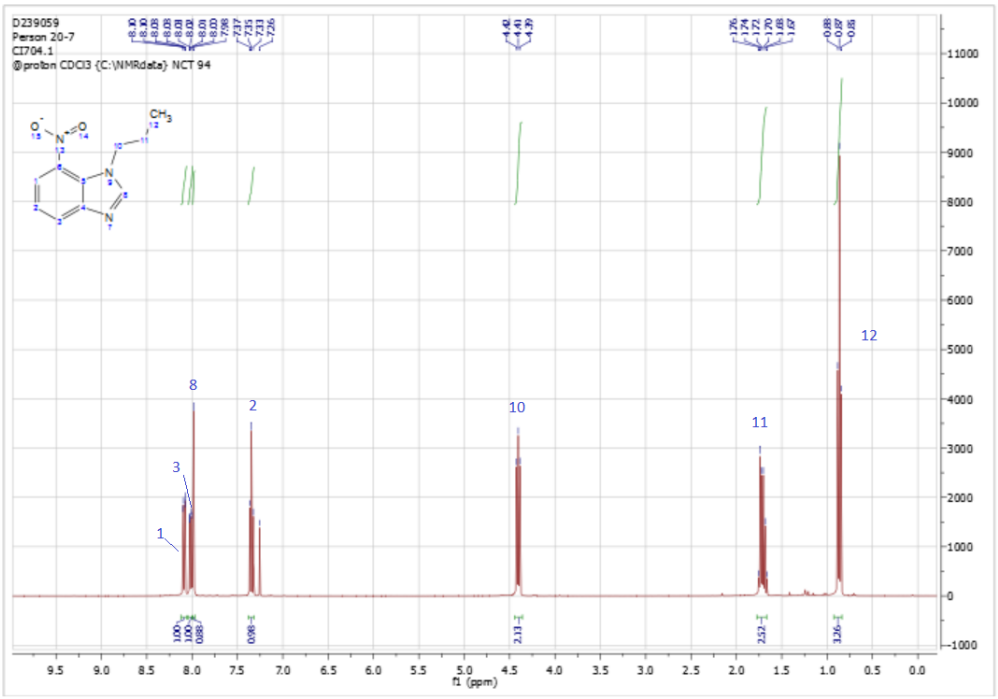

- **200b 2D NOESY experiment**

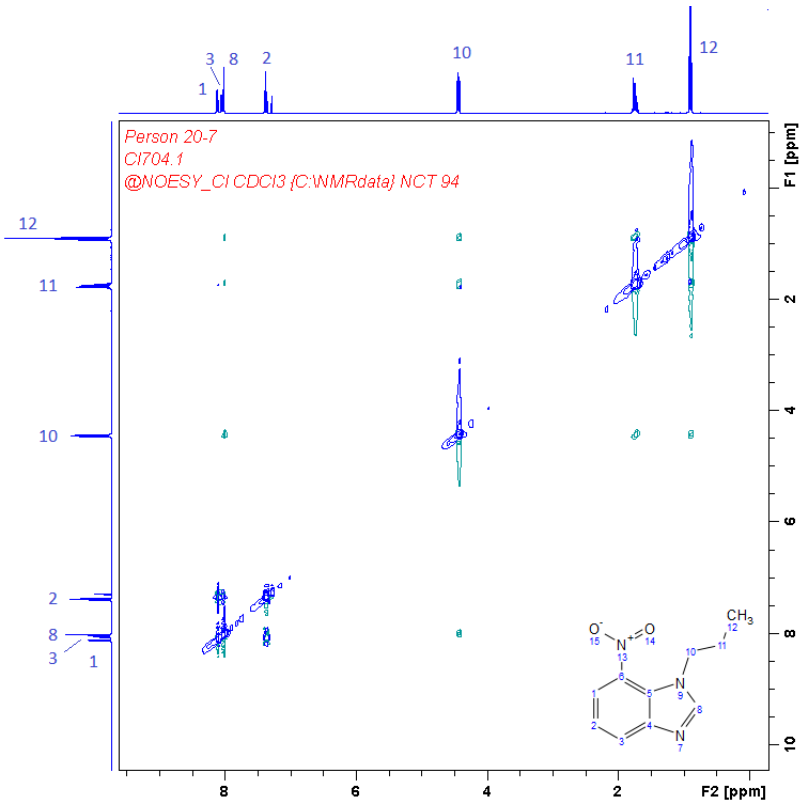

- **200a ^{1}H NMR**

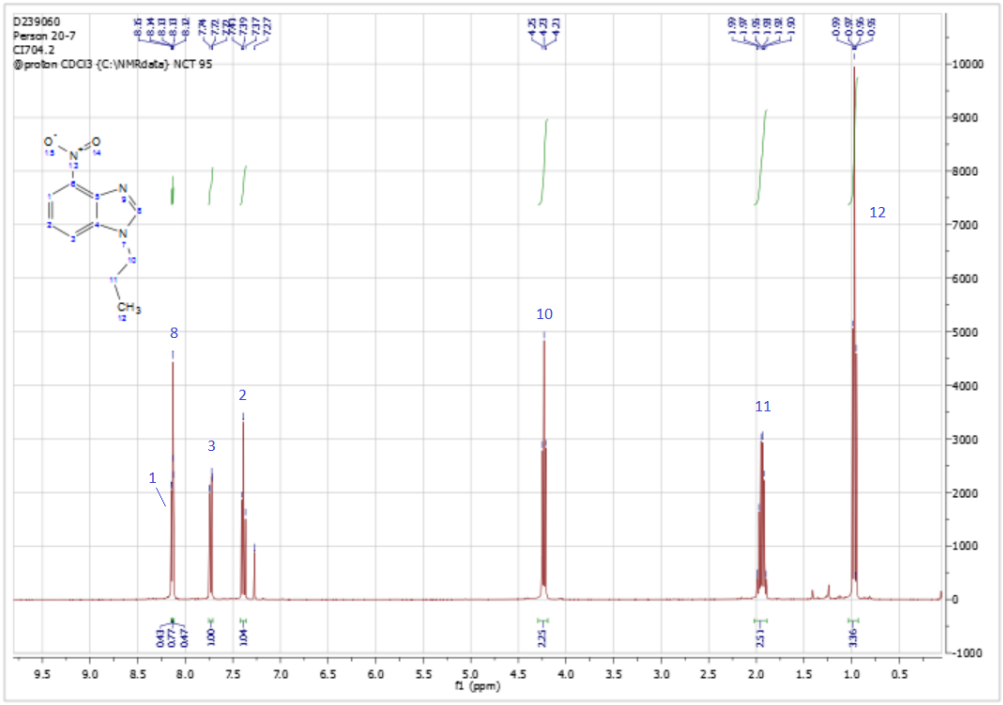

- **200a 2D NOESY experiment**